

INIS-mf--13113

# Hadron Structure '87

Proceedings  
Smolenice  
Czechoslovakia

Physics and  
Applications  
Vol. 14



# **Hadron Structure '87**

**Proceedings  
Smolenice  
Czechoslovakia  
November 16-20, 1987**

**Physics and  
Applications  
Vol. 14**

**Present volume of Physics and Applications contains most of the contributions delivered at the 1987 Hadron Structure Conference held in Smolenice, Czechoslovakia. The conference was devoted mainly to the nonperturbative methods in QCD, to the theory and experiment of high energy particle production and to the hadron-nucleus and heavy ion collisions.**

**The book is of interest to scientists working in the subnuclear physics research and to the senior research students.**

**CS922333A - 23378**

**INSTITUTE OF PHYSICS  
EPRC  
Slovak Academy of Sciences**

# **Slovak Academy of Sciences**

**Institute of Physics  
of the Electro-Physical  
Research Centre**

*Scientific Editor*

**Š. Luby**

*Distributed by:*

**Institute of Physics EPRC SASc.  
842 28 Bratislava  
Czechoslovakia**

# **Hadron Structure '87**

**Proceedings  
of the Conference  
Smolenice  
November 16—20, 1987**

**Physics and  
Applications  
Vol. 14**

**Edited by  
D. Krupa**

**INSTITUTE OF PHYSICS  
EPRC  
Slovak Academy of Sciences  
Bratislava 1988**



## Contents

### Lectures

W.Kummer: Status of Noncovariant Supergauges . . . . .	11
C.Cronström: Regularization of the Yang-Mills Action and Energy . . . . .	***
P.Hasenfratz: Singular Renormalization Group Transformation . . . . .	***
G.Tripiccione: Mass Spectrum of Glueballs in Lattice SU(3) QCD . . . . .	***
J.Greensite: Computer Measurements of the Yang-Mills Vacuum and String Wavefunctionals . . . . .	25
M.Campostrini: Monte Carlo Studies of Lattice QCD with Dynamical Quarks . . . . .	***
H.-C.Pauli: Discretized Light-Cone Quantization . . . . .	***
C.M.Bender: Nonperturbative Perturbation Theory . . . . .	40
A.V.Turbiner: Quasi-Exactly-Solvable Problems in Quantum Mechanics . . . . .	51
L.Ramello: Results on $^{16}\text{O}$ - and $^{32}\text{S}$ - Nucleus Collisions from the HELIOS Collaboration . . . . .	60
I.Derado: Results on Hadron Production in $^{16}\text{O}+\text{Au}$ at 200 GeV/Nucleon from NA35 Experiment . . . . .	***
R.Haroutunian: Results on $J/\psi$ Production in O-U Interactions at 200 GeV/Nucleon from the NA38 Experiment . . . . .	***
N.N.Nikolaev: Matter and Energy Density in Central Heavy Ion Collisions . . . . .	***
N.Pišútová, J.Pišút: Space-Time Evolution of Proton- Proton, Proton-Nucleus and Nucleus-Nucleus Collisions and the Dilepton Production . . . . .	70
<u>S.Yu.Shmakov</u> , V.V.Uzhinskii: New Realization of the Hadron-Hadron, Hadron-Nucleus and Nucleus- Nucleus Fragmentation Model . . . . .	85
<u>E.M.Levin</u> , M.G.Ryskin: Hadron Interactions at High Energy in QCD . . . . .	95

A.Bialas: Oscillations of the Quark-Gluon-Plasma . . . .	***
B.B.Levchenko: Correlation Phenomena in Particle Production on Nuclei . . . . .	118
M.Kutchera: Particle Production in Ultrarelativistic Proton-Proton and Proton-Nucleus Collisions in a Parton String Model . . . . .	123
A.V.Efremov: Nuclear Structure Functions and Cumulative Processes . . . . .	133
G.Ecker: Non-Leptonic Weak Interactions in Chiral Perturbation Theory . . . . .	145

Short Communications

<u>V.K.Petrov</u> , G.M.Zinoviev: Deconfinement Analysis in Exactly Solvable Model for Lattice QCD . . . .	158
C.B.Lang, <u>M.Salmhofer</u> : Optimization of Renormalization Group Transformations . . . . .	166
M.L.Laursen, <u>M.Müller-Preussker</u> : Monopole Excitations in the 3D Georgi-Glashow Model on Lattice. . .	171
M.Faber, <u>W.Feilmair</u> , H.Markum: Quark-Polarization Effects from Dynamical Quarks . . . . .	175
J.Wosiek: On the Space Structure of Confining Strings. .	***
S.G.Gorishny, <u>A.L.Kataev</u> , S.A.Larin: Next-Next-to- Leading $O(\alpha s^3)$ QCD Correlations to $\sigma_{tot}(e+e- \rightarrow \text{Hadrons})$ : Analytical Calculations and Estimation of the Parameter $\Lambda_{\overline{MS}}$ . . . . .	180
F.Schöberl: Influence of Strong Interactions on Electromagnetic Mass Differences . . . . .	192
L.Turko: Condensation of Hadronic Matter . . . . .	198
Z.Fodor: Infrared Asymptotics of the Quark Propagator in Gauge Theories . . . . .	202
G.V.Efimov, <u>M.A.Ivanov</u> : Confinement and Quark Structure of Hadrons . . . . .	210
P.Kolář: The QCD Sum Rules, their Validity and Applicability . . . . .	218
M.Schepkin: Masses of High Spin Hadrons . . . . .	223



<b>A.N.Ivanov: Physics of Low Energy Hadronic Interactions in the Quark Model of Superconductivity Type . . .</b>	<b>***</b>
<b><u>M.Nagy</u>, M.K.Volkov: Decay of Gluonium in the Gene- ralized Quark Model of Superconductivity Type . . . . .</b>	<b>235</b>
<b><u>H.J.Kaiser</u>, K.Scharnhorst, E.Wieczorek: Yang-Mills Propagators in Background Fields . . . . .</b>	<b>239</b>
<b>V.V.Bazhanov: Critical Exactly Solvable Models and Conformal Field Theory . . . . .</b>	<b>244</b>
<b><u>J.Dittrich</u>, P.Exner: A Non-Relativistic Model of Two- Particle Decay: Resonance and Bound States . .</b>	<b>247</b>
<b><u>M.Znojil</u>, M.F.Flynn, R.F.Bishop: The Triple Problem of Convergence in the Perturbation Expan- sions with Non-Diagonal Propagators . . . . .</b>	<b>252</b>
<b>M.Blažek: Remarks on Angular Distributions of Muon Pairs in High Energy Hadronic Collisions . . .</b>	<b>257</b>
<b><u>V.Šimák</u>, M.Šumbera, I.Zborovský: Entropy in the Multiparticle Production . . . . .</b>	<b>264</b>
<b><u>M.Plümer</u>, S.Raha, R.M.Weiner: Coherence, Chaos and Entropy Scaling in High Energy Collisions . .</b>	<b>272</b>
<b>P.Malecki: Long-Range Correlations in Hadron-Nucleus Interactions . . . . .</b>	<b>278</b>
<b>J.Ftáčnik: Transverse Energy Distribution in Hadron- Nucleus and Nucleus-Nucleus Collisions . . . . .</b>	<b>284</b>
<b>O.Pavlenko: Quark-Hadron Phase Transition in High Energy Hadronic and Nuclear Collisions . . . . .</b>	<b>***</b>
<b>P.Závada: Nuclear Response and Hadron Formation Length • in Hadron-Nucleus Interactions . . . . .</b>	<b>***</b>
<b>B.Řsman: Charged Particle Multiplicity Distributions at 200 GeV and 900 GeV . . . . .</b>	<b>289</b>
<b>W.Lohman: New Results on Proton Structure Functions from Deep Inelastic Muon Scattering at High <math>Q^2</math> . . . . .</b>	<b>294</b>
<b><u>D.Krupa</u>, V.A.Mashcheryakov, Yu.S.Surovtsev: Scalar Glueball Indication in Pion Scattering . . . .</b>	<b>299</b>

<u>D.S.Bagdasaryan</u> , <u>G.B.Kazaryan</u> , <u>H.G.Mkrtchyan</u> , I.A.Troshenkova: Investigation of $(e, e')$ Scattering on Electron Synchrotron at Yerevan Physics Institute . . . . .	305
<u>V.Kundrát</u> , M.Lokajíček, D.Krupa: High Energy Hadron Scattering in Forward Direction . . . . .	310
W.Grimus: A Model of Massive Neutrinos with a Conserved Lepton Number . . . . .	317
H.Neufeld: Spontaneous CP Violation and Neutral Flavour Conservation in $SU(2)_L \times U(1)^1$ . . . . .	324
H.Perlt: String Thermodynamics and Cosmology . . . . .	***
K.Lewin, <u>G.B.Motz</u> : On Quark Masses in $(Q\bar{Q})$ Potential Models . . . . .	329
M.Chaichian, <u>J.Fischer</u> : Unitarity Bounds for High Energy Scattering in Many Dimensions . . . . .	334
J.Szwed: The Square Root of the Dirac Equation within Supersymmetry . . . . .	***
A.R.Kereselidze, A.G.Liparteliani, <u>G.G.Volkov</u> : Superstring Inspired Left-Right Models . . . . .	339
P.Möbius: Nonlinear Field Equations and Infinite Dimensional Lie Algebras . . . . .	342
<u>H.Pérez-Rojas</u> , R.González: Phase Transitions of W-Condensation in the Hot Universe . . . . .	350
I.Lukáč: On the Geometry of Group Space of Group of Motion of Three-Dimensional Quadratic Form . . . . .	357
M.Bonesini: Prompt Gamma Physics: New Experimental Results . . . . .	362
Author Index . . . . .	369
List of Participants . . . . .	371

\*\*\* Oral presentation only.

The names of speakers are underlined.

## Preface

It became a good tradition that Czechoslovak physicists interested in elementary particle physics meet together with their colleagues from abroad at the Hadron Structure conferences every year. The present book represents the proceedings of the Hadron Structure '87 conference which was held in Smolenice Castle near Bratislava on November 16-20, this year.

The programme of the conference consisted of lectures and short communications. The main topics covered were:

- Nonperturbative calculations in field theory ( QCD in particular )
- Particle production in hadron-nucleus and nucleus-nucleus collisions and the quark-gluon plasma
- Recent experimental results.

The arrangement of papers follows closely chronology of talks as they were presented at the conference with the exception that lectures (presented during morning sessions) and short communications are grouped together separately.

In the contents we list all papers presented at the conference specifying those which were not made available for publication in the present volume.

The editors would like to thank all authors submitting their papers for printing in the camera ready form. We are also grateful to the Vela Publishing House for their interest to publish this proceedings and for their assistance.

Editor

9/10

# STATUS OF NONCOVARIANT SUPERGAUGES<sup>†</sup>

(Lecture at "Hadron Structure 1987" , 16. - 20.11.1987,  
Smolenice, CSSR)

W. KUMMER

Institut für Theoretische Physik  
der Technischen Universität Wien

## Abstract:

Supersymmetric gauge theories can be suitably quantized in non-supersymmetric gauges without abolishing the advantages of supergraph techniques. The state of the art now encompasses the proof of renormalization and of gauge-independence and supersymmetry for observable physical quantities.

---

Karlsplatz 13, A-1040 Wien

<sup>†</sup>Supported by "Fonds zur wissenschaftlichen Forschung",  
Proj. Nr. 5485

## 1. Introduction

The general superfield treatment of renormalization problem in supersymmetric gauge-theories [1] cannot evade the choice of a gauge which breaks supersymmetry, at least softly [2]. This suggests the study of general noncovariant supergauge which, on the other hand, allow the inclusion of celebrated gauges like the Wess-Zumino gauge [3,4,5] in a supergraph formalism.

## 2. Gauge-Superfield and Notation

The ordinary gauge-field  $v_m$  in supersymmetry becomes a component of a hermitian superfield [6,7]  $V = V^\dagger$

$$V(x, \theta, \bar{\theta}) = c + (\theta \sigma^m \bar{\theta}) v_m + \frac{1}{4} \theta^2 \bar{\theta}^2 \mathcal{D} + \left[ (\theta \chi) + \frac{1}{2} \theta^2 M + \frac{1}{2} \theta^2 (\bar{\theta} \lambda) + \text{h.c.} \right] \quad (2.1)$$

which contains powers of the Lorentz 2-spinor Grassmann-variables  $\theta_\alpha$  and  $\bar{\theta}_{\dot{\alpha}}$  ( $\alpha, \dot{\alpha} = 1, 2$ ). The basic anticommutator for the spinor charges  $Q_\alpha$  and  $\bar{Q}_{\dot{\alpha}}$  in supersymmetry reads ( $P_m$  is the generator of the translations)

$$\{Q_\alpha, \bar{Q}_{\dot{\alpha}}\} = 2P_{\alpha\dot{\alpha}} \quad (2.2)$$

Supersymmetric covariant derivatives ( $\partial_\alpha = \partial/\partial\theta^\alpha$ )

$$\begin{aligned} D_\alpha &= \partial_\alpha - i(\not{\theta}\bar{\theta})_\alpha \\ \bar{D}_{\dot{\alpha}} &= (\partial_{\dot{\alpha}})^\dagger = -\bar{\partial}_{\dot{\alpha}} + i(\theta\not{\theta})_{\dot{\alpha}} \end{aligned} \quad (2.3)$$

anticommute with  $Q_\alpha$  and  $\bar{Q}_{\dot{\alpha}}$ , but obey the same relation (2.2) with  $P_m = i\partial_m$ .

The supergraph-renormalization problem [2] is a consequence of the (mass-) dimension zero of  $V$  which in turn follows from

the dimension 1 of the vector-field  $v_m$  and from the dimension  $-\frac{1}{2}$  for  $\theta$ . The scalar component of  $V$  has dimension zero too and, for purely dimensional reasons, the c-propagator must behave like  $1/k^4$ . Thus a new type of infrared (IR) divergence appears, except the "unphysical" components of  $V$  are fixed appropriately. Only  $v_m$  and one spinor-field are physical degrees of freedom. Fixing the gauge in a way which does not break supersymmetry will not provide a solution of this problem. Sufficient for such a solution is the choice of the Wess-Zumino gauge [1] which eliminates all fields except  $v$ ,  $\lambda$  and  $\omega$ . Such a gauge clearly breaks supersymmetry. Nevertheless, in order to be able to still use the powerful modern versions of supergraphs [8] it is desirable to extend the latter method to such gauges.

### 3. Gauge Fixing in Supersymmetric Yang-Mills Theories

The supersymmetric Yang-Mills Lagrangian [6,7] is (the factor  $\rho/g^2$  depends on the convention for the component fields of  $V = T^i V^i$ ,  $\text{Tr} T^i T^j = \delta_{ij}$ )

$$\begin{aligned} \mathcal{L}_{\text{Y.M.}} &= \rho (16g^2)^{-1} \text{Tr} \int d^4x_+ W^\alpha W_\alpha \\ W_\alpha &= D^2 e^{-gV} D_\alpha e^{gV} \end{aligned} \quad (3.1)$$

with the "chiral" gauge-invariance ( $\Lambda_-^\dagger = \Lambda_+$ )

$$e^{gV'} = e^{-i\Lambda_+^\dagger} e^{gV} e^{i\Lambda_+} \quad (3.2)$$

For an infinitesimal change  $\delta\Lambda_+$ ,  $V' = V + \delta V$  one arrives at ( $L_x^\sim Y = [X, [X, \dots [X, Y]] \dots$ )

$$\begin{aligned} \delta V &= i L_{\frac{gV}{2}} \left\{ (\coth L_{\frac{gV}{2}}) (\delta\Lambda_+ - \delta\Lambda_+^\dagger) + \delta\Lambda_+ + \delta\Lambda_+^\dagger \right\} = \\ &= R(V) \delta\Lambda_+ + \bar{R}(V) \delta\Lambda_+^\dagger \end{aligned} \quad (3.3)$$

This implies for the vector component  $v_m$  of  $V$

$$\delta v_m = \partial_m (\Lambda_+ + \Lambda_+^\dagger) + \frac{i g}{2} [v_m, A_+ + \Lambda_+^\dagger] + O(g^2) \quad (3.4)$$

where  $\Lambda_+$  is the scalar component of the chiral superfield  $\delta \Lambda_+$ . From (3.4) we see that  $V$  contains a vector-gauge-field with proper gauge-transformation properties, embedded into a larger set of supersymmetric transformations involving also the other components of  $V$ . The gauge-function  $\Lambda_+$  has 8 degrees of freedom, allowing as many conditions for the components  $(c, \chi, M, v_m, \lambda, \mathcal{D})$  in  $V$ . E.g. in the celebrated Wess-Zumino gauge the 8 conditions are

$$c = \chi_\alpha = M = \ell^{k_2} v_m = 0 \quad (3.5)$$

where  $\ell$  is a fourvector which determines the (homogeneous) gauge of  $v_m$  ( $\ell_m = \partial_m$  for the Landau-gauge,  $\ell_m = n_m$  for the fixed fourvector in the homogeneous axial gauge etc.). This gauge clearly breaks the supersymmetry. The (homogeneous) covariant supergauge is given by

$$D^2 V = \bar{D}^2 V = 0 \quad (3.6)$$

yielding for the component field  $c$  the (spurious, but awkward) infrared singularity of covariant supergauges referred to above.

Because some sort of supersymmetry breaking cannot be avoided in the treatment of quantized superfields a general gauge-breaking Lagrangian [3]

$$\mathcal{L}_{g.b.} = \text{Tr} \int d^4x \left\{ (B K + \bar{B} \bar{K}) V - \alpha B \bar{B} \right\} \quad (3.7)$$

is considered, depending on a nonsupersymmetric operator  $K$  ( $\partial_m K = 0$ ) and on an auxiliary chiral field  $B$ . In the following we consider the special case  $\alpha = 0$  in (3.7) of homogeneous gauges [5]. This represents still a large gauge-family parameterized by  $K$  and it contains also e.g. the Wess-Zumino gauge (3.5). In that case alternative versions of (3.7) are

$$\begin{aligned} \mathcal{L}_{g.b.} &= \text{Tr} \int d^4x \, B \bar{D}^2 K V + \text{h.c.} = \\ &= \text{Tr} \int d^4x \, (B + \bar{B}) (K + \bar{K}) V \end{aligned} \quad (3.8)$$

The last equation follows from the vanishing of the cross-terms  $B\bar{K}_V$  and  $\bar{B}K_V$  in  $\int d^4x$ , because these expressions have fixed chirality. It shows that the longitudinal part as projected by  $P_L = P_+ + P_-$  is relevant for the determination whether  $K$  is admissible or not. (3.8) implies the gauge conditions

$$\bar{D}^2 K V = D^2 \bar{K} V = 0 \quad (3.9)$$

and hence by the standard argument the Faddeev-Popov Lagrangian ( $u'$  and  $u$  are chiral anticommuting superfields)

$$\begin{aligned} \mathcal{L}_{f.p.} &= \text{Tr} \int d^4x \, u' \bar{D}^2 K (\delta V)_{\epsilon \Lambda, ru} + \text{h.c.} = \\ &= \text{Tr} \int d^4x \, (u' K - \bar{u}' \bar{K}) (P_u + \bar{P} \bar{u}) \end{aligned} \quad (3.10)$$

(cf. (3.3)).

The total (bare) Lagrangian consisting of (3.1), (3.10), and (3.12) depends on the breaking of supersymmetry only through the explicit appearance of  $K$ . This is a strong reminder of the dependence on a fixed direction  $n_m$  in the axial gauge of ordinary gauge theory. Although  $n$  breaks the Lorentz-invariance, it is sufficient to carry it along in all expressions in order to maintain formal Lorentz-covariance [9]. In the case of supersymmetry with  $K$ , the situation is more complicated, because



(anti-) commuting  $K$  with the algebra of  $D$ -s and  $\bar{D}$ -s an enlarged algebra is produced, whose elements must be considered as well.

The subsequent derivations are greatly facilitated by a supersymmetric generalization of the elegant compact notation of deWitt [10]:

$$\begin{aligned}
 \int d^4x \ a^i(x) a^i(x) &\rightarrow a^i a^i \\
 \int d^4x \ a_i^\alpha a_i^\alpha &\rightarrow a_i^\alpha a_i^\alpha \\
 \int d^4x \ \bar{a}_i^{\dot{\alpha}} \bar{a}_i^{\dot{\alpha}} &\rightarrow a_i^{\dot{\alpha}} a_i^{\dot{\alpha}}
 \end{aligned}
 \tag{3.11}$$

Writing all fields (Yang-Mills-fields  $V^i$ , and matter fields  $\psi_+$  and  $\psi_-$ ) as components of one "vector"

$$\phi^A = (V^i, \psi_+^\alpha, \psi_-^{\dot{\alpha}}) = (V^i, \psi^S)
 \tag{3.12}$$

with

$$\delta \phi^A = R^{\Lambda\alpha} \delta \Lambda^\alpha + \bar{R}^{\Lambda\dot{\alpha}} \delta \Lambda^{\dot{\alpha}} = R^{\Lambda S} \delta \Lambda^S
 \tag{3.13}$$

and with the definitions

$$\begin{aligned}
 \bar{D}^i K &\rightarrow K^{\alpha i} \\
 D^i K &\rightarrow K^{\dot{\alpha} i}
 \end{aligned}
 \tag{3.14}$$

the total Lagrangian formally looks like the one in ordinary gauge theory

$$\mathcal{L} = \mathcal{L}_{inv} + B^S K^{\dot{\alpha} S} \phi^{\dot{\alpha}} + u_S^i K^{\dot{\alpha} S} R^{\Lambda\sigma} u^\sigma
 \tag{3.15}$$

the main difference being the nonpolynomial dependence  $R(V)$ . This notation is also well suited for the evaluation of the  $V$ -propagator. The (at most) quadratic part in  $V$  of (3.1) in (3.18) is

$$\mathcal{L} = \frac{R}{2} \phi^A (D P_T)_{AB} \phi^B + C^A K^B \phi^A \quad (3.16)$$

We take the propagator to be the negative inverse of  $\Gamma$ , the "matrix" in (3.16):

$$\Delta = -\Gamma^{-1} = \begin{pmatrix} \Delta_{WV} & \Delta_{VB} \\ \Delta_{BV} & \Delta_{BB} \end{pmatrix} \quad (3.17)$$

We now make the assumption that any admissible  $K$  must be such that  $(K P_L K^T)$  has an inverse. In this case  $\Delta \Gamma = -1$  yields

$$\Delta_{BB} = 0 \quad (3.18)$$

(no propagation of  $B$ !) and

$$\Delta_{VB} = P_L K^T U \quad (3.19)$$

with a matrix  $U^{\rho\sigma}$

$$U = U^T = - (K P_L K^T)^{-1} \quad (3.20)$$

and

$$\Delta^W = (\frac{1}{2} D)^{-1} (P_T + P_T K^T U K P_L + P_L K^T U K P_T + P_L K^T U K P_T K^T U K P_L) \quad (3.21)$$

Since the inversion (3.20) for  $U$  is relatively simple in practical cases, the full knowledge of the algebra enlarged by  $K$  is not required.

We now turn to a discussion of different choices for  $K$ . The simplest one is to make  $K$  a scalar superfield depending on  $\theta$  and  $\bar{\theta}$  only. E.g.

$$K = 1 - \frac{1}{2} \theta^2 \bar{\theta}^2 \quad (3.22)$$

has the property that (3.9) is the same as the covariant supergauge (3.6) with a change in the highest component of  $V$

$$V \rightarrow \tilde{V} = KV = V \Big|_{D \rightarrow D - \mu^2 c}$$

Thus the  $c$ -field in this case propagates with mass  $\mu$  and any mass-term for  $c$  is an artefact of gauge-fixing, a result also obtained in [2]. A "local" ansatz for  $K$  like (3.22) is not sufficient to produce a gauge like (3.5). We therefore consider the most general "bilocal"  $K = K(\theta, \bar{\theta}, \theta', \bar{\theta}')$ . It is straightforward but lengthy to write down this expression which in fact is just an  $N = 2$  scalar superfield. An alternative way to write  $K$  uses the derivative operator  $K = K(\theta, \bar{\theta}, \partial_\alpha, \bar{\partial}_{\dot{\alpha}})$ . It clearly has the same number of components and is, in fact, simply related to  $K$ :

$$K = \hat{K} \delta^4(\theta, \theta') \quad (3.23)$$

Historically, the first noncovariant supergauge was the " $N^{\perp}$  gauge" [3]. Defining ( $n_m$  is a fixed Lorentz-vector)

$$\begin{aligned} N_\alpha &= \partial_\alpha - i (n \bar{\theta})_\alpha \\ \hat{N}_\alpha &= \partial_\alpha + i (n \bar{\theta})_\alpha \end{aligned} \quad (3.24)$$

and  $K = N^2$ , the algebra of the covariant derivatives is enlarged in a very transparent manner. The superpropagator is rather complicated for this gauge but the  $c$ -field-component propagates with a mass  $n^2$  and  $n^m v_m = 0$  (axial gauge).

The advantage of the "FD-gauge" [4]

$$\begin{aligned} K &= F^\alpha D_\alpha \\ F_\alpha &= -i (\not{\partial} \theta)_\alpha \end{aligned} \quad (3.25)$$

is the simple set of new projection operators.

There are infinitely many choices of  $K$  yielding the Wess-Zumino gauge (3.5), but differing in the sector of the auxiliary field  $B$ . A very simple choice for  $K$  is [5]

$$K_{WZ} = \bar{\theta}^2 [1 + i \not{\partial} \bar{\theta}^2 (\theta \not{\partial} \theta)] \quad (3.26)$$

Recently, Johanson [11] has proposed a  $K$  of a general chiral type.

#### 4. BRS-Invariance, Identities, Remarks on Renormalization and Gauge-Independence

The similarity of (3.15) to the Lagrangian of ordinary gauge theories immediately allows the introduction of a BRS-transformation [12] with a special gauge transformation  $\delta\Lambda^P = iu^P\delta\lambda$  involving the Faddeev-Popov field and the anti-commuting quantity  $\delta\lambda$ :

$$\begin{aligned} \delta\phi^A &= i R^{A\beta} u^\beta \delta\lambda = s\phi^A \delta\lambda \\ \delta u^\beta &= -\frac{i}{2} f_{\rho\sigma\tau} u^\rho u^\sigma \delta\lambda = s u^\beta \delta\lambda \\ \delta u'^\rho &= -i B^\rho \delta\lambda = s u'^\rho \delta\lambda \\ \delta B^\rho &= 0 \end{aligned} \quad (4.1)$$

$f_{\alpha\beta\gamma} = f_{\alpha\beta\gamma}^-$  are the structure constants in our supercompact notation. The invariance of  $\mathcal{L}_{uv} + \mathcal{L}_{g^{\pm}} + \mathcal{L}_{F,F}$  under (4.1) follows from the validity of the "group relation"

$$\frac{\delta R^{A\rho}}{\delta \phi^B} R^{B\sigma} - (\rho \leftrightarrow \sigma) = g f_{\rho\sigma\tau} R^{A\tau} \quad (4.2)$$

Quantization proceeds through a generating functional with a path-integral of the fields

$$W(j, j', \xi, \xi', k, \ell) = \int \mathcal{D}\phi \mathcal{D}u \mathcal{D}u' \mathcal{D}B \exp i \mathcal{Z}_c = \int (d\phi du du' dB) \exp i (\mathcal{X} + \mathcal{X}_s) \quad (4.3)$$

where the sources are contained in

$$\mathcal{X}_s = \int^A \phi^A + j^B B^B + \xi^{\rho} u^{\rho} + \xi^{\rho'} u_{\rho'} + k^A R^{A\rho} u^{\rho} + \frac{g}{2} \ell^{\rho} f_{\rho\sigma\tau} u^{\sigma} u^{\tau} \quad (4.4)$$

As usual, additional sources are introduced for the "composite operators" in (4.1). The latter are BRS-invariant by themselves; therefore, only  $\mathcal{X}_s$  breaks the invariance (4.1). A change of variables (4.1) in (4.3) does not change  $W$ :

$$0 = -i \frac{\delta W}{\delta \lambda} = \xi^{\rho} \frac{\delta W}{\delta j^{\rho}} + \int^A \frac{\delta W}{\delta k^A} - \xi^{\rho} \frac{\delta W}{\delta \ell^{\rho}} \quad (4.5)$$

This "Slavnov-Taylor" identity does not depend explicitly on  $K$ . The second important identity obtains for the change  $B \rightarrow B + \delta B$  in (4.3):

$$0 = -i \frac{\delta W}{\delta \delta^{\rho}} = K^{\rho A} \frac{\delta W}{\delta j^A} + j^{\rho} W \quad (4.6)$$

and the third one for the transformation  $u' \rightarrow u' + \delta u'$

$$0 = - \sum_p \xi'_p W + K^{\rho A} \frac{\delta W}{i \delta k^A} \quad (4.7)$$

E.g. from (4.6) the "transversality" of all Green's functions with respect to K follows immediately

$$K^{\rho A} \left. \frac{\delta^n W}{\delta J^{\rho_1 A_1} \dots \delta J^{\rho_n A_n}} \right|_{J=0} = 0 \quad (4.8)$$

In a similar manner an identity for the change of W with respect to an infinitesimal variation of K is derived.

A Legendre-transformation

$$\Gamma = Z_c - J^A a^A - \dots \quad (4.9)$$

with  $a_A = \delta Z_c / \delta J^A$  etc., which does not involve k and l however, leads to the standard Lee-identity which is quadratic in the functional  $\Gamma$  of one-particle irreducible vertex functions:

$$S(\tilde{\Gamma}) = \frac{\delta \tilde{\Gamma}}{\delta \phi^A} \frac{\delta \tilde{\Gamma}}{\delta \eta^A} + \frac{\delta \tilde{\Gamma}}{\delta u_f} \frac{\delta \tilde{\Gamma}}{\delta l_f} = 0 \quad (4.10)$$

$$\tilde{\Gamma} = \Gamma - \mathcal{L}_{gk.}(a, l, \dots)$$

$$\eta^A = h^A + u^{\rho A} K^{\rho A} \phi^A$$

In order to make contact with previous proofs of renormalization [2] a crucial observation is that any K with bosonic gauge parameters  $N_{ij}$  (underlined indices mean no supercompact notation) may be written as [4]

$$K = \sum_{i\bar{j}} N_{i\bar{j}} G_i(D, \bar{D}, a) \theta^2 \theta^2 \bar{G}_{\bar{j}}(D, \bar{D}, a) \quad (4.11)$$

replacing formally

$$\theta^1 \bar{\theta}^1 \rightarrow w^1 = \theta^1 \bar{\theta}^1 + w \quad (4.12)$$

with an external gauge-singlet field  $w^1$ , the Ward-identity for an arbitrary supersymmetric quantity  $A$  ( $Q_\alpha$  is the generator)

$$Q_\alpha A = (Q_\alpha \phi^1) \frac{\delta A}{\delta \phi^1} \quad (4.13)$$

may be extended to the present broken case. If, for a "physical quantity"  $w$ -independence can be proved, supersymmetry follows.

The inclusion of the gauge-parameters  $N_{ij}$  into the BRS transformations (4.1) turns out to be very convenient:

$$\delta N_{ij} = M_{ij} \quad , \quad \delta M_{ij} = 0 \quad (4.14)$$

Further gauge parameters  $p_i$  appear in supersymmetric gauge theories because the dimensionless  $V$  may be redefined  $V \rightarrow F(V, p_i)$ . Writing  $sp_i = z_i$ ,  $sz_i = 0$  allows their inclusion in the extended BRS-transformation as well.

Similarly also  $w$  in (4.12) acquires a corresponding BRS-transformation  $v$ . Both terms may be summarized by  $N(i)$  in (4.14). An action which fulfills (4.1) and (4.14) is

$$\hat{\mathcal{L}} = \mathcal{L} - M_{ij} u'_f \frac{\partial K^f \phi^1}{\partial N_{ij}} - z_i \Delta_i(F) \quad (4.15)$$

where  $\Delta_i(F)$  can be given explicitly [5]. The generalization of (4.10) contains two further terms:

$$S(\hat{A}) + z_i \frac{\partial \mathcal{L}}{\partial p_i} + M_{ij} \frac{\partial \mathcal{L}}{\partial N_{ij}} = 0 \quad (4.16)$$

where  $\hat{\Gamma}$  is defined like  $L$  subtracting out  $L_{gb}$ . Then renormalization can be reduced to the solution of the cohomology problem of a nilpotent operator

$$\beta_Z = \frac{\delta Z}{\delta \phi} \frac{\delta}{\delta \eta} + \frac{\delta Z}{\delta \eta} \frac{\delta}{\delta \phi} + \frac{\delta Z}{\delta u} \frac{\delta}{\delta \bar{e}} + \frac{\delta Z}{\delta \bar{e}} \frac{\delta}{\delta u} + \gamma \frac{\delta}{\delta p} + M \frac{\delta}{\delta \lambda} \quad (4.17)$$

even in the absence of a supersymmetric regularisation scheme [5]. It can be shown that all gauge-dependent counter-terms are necessarily of the type  $B_L \Delta$ . The cohomology for the rest has been done (under certain technical assumptions, excluding anomalies) in ref. [2].

The proof of gauge-independence refers to an S-matrix-element, consisting of an amputated Green's function, decorated by "polarization vectors" and renormalization factors at external legs. The definition of "polarization vectors" (physical sources) is not without problems in supersymmetric theories [13]. Nevertheless, at least to the degree of rigour achieved in ordinary gauge theories, the proof can be carried through. The "extended" BRS transformation again is able to exhibit its superiority to other techniques. As a by-product also the covariance of the S-matrix with respect to (globally) supersymmetric transformations can be shown [13].



## REFERENCES:

- [1] J.Wess and B. Zumino, Phys.Lett. 49B (1974) 52;  
J.Wess and B. Zumino, Nucl.Phys. B87 (1974) 1,  
A. Salam and J. Strathdee, Phys.Lett. 51B (1974) 353,  
S. Ferrara and B. Zumino, Nucl.Phys. B71 (1974) 403
- [2] O.Piguet and K. Sibold, Nucl.Phys. B248 (1984) 336,  
*ibid.* B249 (1985) 396
- [3] W.Kummer and M. Schweda, Phys.Lett. 141B (1984) 363
- [4] T. Kreuzberger, W.Kummer, O.Piguet, A.Rebhan and  
M.Schweda, Phys.Lett. 167 (1986) 393
  
- [5] T.Kreuzberger, W. Kummer, H.Mistelberger, P.Schaller,  
M.Schweda, Nucl.Phys. B281 (1987) 411
  
- [6] S. Ferrara, J. Wess and B. Zumino, Phys.Lett. 51B (1974)  
239; A. Salam and J. Strathdee, Phys.Rev. D11 (1975) 1521
- [7] S. Ferrara and B. Zumino, Nucl.Phys. B79 (1974) 413;  
A. Salam and J. Strathdee, Phys.Lett. 51B (1974) 353;  
B. de Witt and D. Freedman, Phys.Rev. D12 (1975) 2286
- [8] M.T. Grisaru, W. Siegel and M. Rocek, Nucl.Phys. B159  
(1979) 429
- [9] W. Kummer, Acta Phys. Austr. 14 (1961) 149;  
R.L. Arnowitt and S.I. Fickler, Phys.Rev. 127 (1962) 182  
J. Schwinger, Phys.Rev. 130 (1963) 402;  
Y. P. Yao, Journal of Math.Phys. 5 (1964) 1319;  
E.S. Fradkin and I.V. Tyutin, Phys.Rev. D2 (1970) 2841;  
W. Kummer, Acta Phys. Austr. 41 (1975) 315;  
W. Konetschny and W. Kummer, Nucl.Phys. B100 (1975) 106
- [10] B.S. de Witt, Phys.Rev. 162 (1967) 1195
- [11] A.A. Johanson, Superfields in the noncovariant super-  
gauges, Leningrad prepr. 1985
- [12] C. Becchi, A. Rouet and R. Stora, Phys.Lett. 52B (1974)
- [13] W. Kummer, H.Mistelberger and P. Schaller, to be published

# COMPUTER MEASUREMENT OF THE YANG-MILLS VACUUM (AND STRING) WAVEFUNCTIONALS

J. Greensite\*

Physics and Astronomy Department  
San Francisco State University  
San Francisco, CA 94720 USA

## ABSTRACT

A Monte Carlo simulation of the exact path-integral representation of the Yang-Mills vacuum wavefunctional is carried out in three dimensions. The data for long-wavelength field configurations is accurately fit by the lattice version of

$$\Psi[A] = N \exp(-\mu \int d^2x \text{tr}\{F_{ij}^2\})$$

By insertion of Wilson lines into the path-integral representation it is also possible to measure the wavefunctional of a state containing heavy quark-antiquark charges. For large quark separations, this state represents the QCD string. Preliminary numerical results are consistent with the "gluon-chain" model of string formation.

\*Work supported by the U.S. Department of Energy under Contract No. DE-AC03-81ER40009.

The Hamiltonian formulation of quantum Yang-Mills theory is quite simple to express in temporal gauge; the problem is just to solve the Schrodinger wavefunctional equation

$$\frac{1}{2} \int d^3x \left[ -\frac{\delta^2}{\delta A_i^2} + \frac{1}{2} F_{ij}^2 \right] \Psi[A] = E \Psi[A] \quad (1)$$

subject to the Gauss law constraint that  $\Psi[A]$  be invariant under time-independent gauge transformations. Unfortunately, this equation is much easier to formulate than to solve. It would, however, be very interesting to know the solution of the equation for the QCD vacuum state, or for a meson state, or for an elongated string state. Presumably a lot of interesting physics is contained in the structure of the corresponding wavefunctionals.

For a theory of free photons (pure QED), the Schrodinger equation is soluble. The solution for the vacuum state is simply

$$\Psi[A] = \exp\left(-\frac{1}{8\pi^2} \int d^3x d^3y F_{ij}(x) F_{ij}(y) \frac{1}{(x-y)^2}\right) \quad (2)$$

but for QCD, the corresponding solution is unknown. Some years ago I argued that for long-wavelength field configurations (i.e. field configurations  $\Lambda(x)$  for which  $\text{Tr}(F^2)$  varies slowly compared to the confinement scale), the QCD vacuum should have the form [1]

$$\Psi[A] = \exp(-\mu \int d^3x \text{Tr}(F_{ij}^2)) \quad (3)$$

Note that the probability density  $\Psi^2$  looks like  $e^{-S}$  in one lower dimension ("dimensional reduction"). In fact, it is possible to prove that the QCD vacuum has precisely this form in strong-coupling lattice gauge theory, where [2]

$$\Psi[U] = \exp(\beta \sum_{\text{plaq}} \text{Tr}[UUU^{\dagger}U^{\dagger}]) + O(\beta^2)$$

is the ground state, and there is a systematic expansion for obtaining higher order terms in the exponent. But, of course, we are really interested in the structure of the vacuum at weak couplings.

One rather general argument in favor of eq.(3) is based on the concept of magnetic disorder. It is believed that confinement is associated with disorder in the field-strength  $F_{ij}$ . Wavefunctionals with the maximum possible disorder in the field strength must have the form

$$\Psi[A] = \prod_x \phi_x[\text{Tr}F^2(x), \text{Tr}F^4(x), \dots]$$

where  $\phi_x$  depends on  $F_{ij}$  only at the point  $x$ . Then the only correlation that exists between field strengths at different points is through the Bianchi identity. Such maximally disordered wavefunctionals can be rewritten as

$$\begin{aligned}
\Psi[A] &= \exp\left(\int dx \ln \phi_x\right) \\
&= \exp\left(-\int dx [-\ln \phi(0) - \frac{d\phi}{dT r F^2} \cdot T r(F^2) + O(F^4)]\right) \\
&\approx \text{const.} \times \exp\left(-\mu \int dx T r F^2\right)
\end{aligned}$$

for small amplitude fluctuations, in agreement with eq.(3).

However, this form cannot be completely correct. In particular, because of asymptotic freedom, we expect the QCD vacuum to resemble that of the free theory, eq.(2), at short distances. A simple interpolating form, which contains both eq.(2) and (3) as limiting cases, is

$$\Psi[A] = \exp\left(-\int d^3x d^3y T r [F_{ij}(x) V(x, y) F_{ij}(y) V(y, x)] \phi(x - y)\right) \quad (4)$$

where  $V(x, y)$  is a gauge connector (e.g. a Wilson line) between points  $x$  and  $y$ , and

$$\phi(x - y) \rightarrow \frac{1}{(x - y)^2} \text{ as } (x - y) \rightarrow 0$$

while  $\phi(x - y)$  damps exponentially to zero as  $|x - y|$  exceeds the confinement scale  $L$ . For field configurations  $A(x)$  which vary slowly compared to the confinement scale  $L$ , we then have

$$\Psi[A] = \exp\left(-\mu \int d^3x T r(F^2)\right) \quad (5)$$

where

$$\mu = \int d^3x \phi(x)$$

But, although I believe this reasoning is correct, it is obviously desirable to go beyond such heuristic arguments. I will now describe a method for actually measuring the relative values of  $\Psi^2[A]$  in an arbitrary (but finite) set of field configurations, by the Monte Carlo method. The method is based on the exact, path-integral representation of the ground state in temporal gauge

$$\Psi[A] = \int DA(t < 0) \delta[A_0] \exp\left(-\int_{-\infty}^0 dt L[A]\right)$$

Let  $\{^n A(x)\}$ ,  $n = 1, \dots, N$  be any set of field configurations on the time slice  $t=0$ . Then

$$\begin{aligned}
\Psi[^n A]^2 &= \int DA(x, t) \delta[A(x, 0) - ^n A] \delta[A_0] \exp\left(-\int_{-\infty}^{\infty} dt L[A]\right) \\
&= \int \sum_{m=1}^N D_m A \delta_{mn} e^{-S}
\end{aligned}$$

where

$$D_m A = DA \delta[A(x, 0) -^m A] \delta(A_0)$$

Now rescale the wavefunctionals as follows:

$$\Psi[n A] \Rightarrow \frac{\Psi[n A]}{[\sum_{m=1}^N \Psi^2[m A]]^{\frac{1}{2}}}$$

so that with this rescaling

$$\Psi[n A]^2 = \frac{\int \sum_m D_m A \delta_{mn} e^{-S}}{\int \sum_m D_m A e^{-S}}$$

This expression can now be latticized in the obvious way:

$$\Psi[n U]^2 = \frac{\int \sum_m D_m U \delta_{mn} \exp(\beta \sum \text{Tr}[UUU^t U^t])}{\int \sum_m D_m U \exp(\beta \sum \text{Tr}[UUU^t U^t])} \quad (6)$$

where

$$D_m U = \prod_{i,x} dU_i(x, t) \delta[U_i(x, 0) -^m U_i(x)] \delta[U_0 - 1]$$

Observe that the denominator of eq.(6)

$$Z = \int \sum_m D_m U \exp(\beta \sum \text{Tr}[UUU^t U^t])$$

is just the partition function of a lattice gauge theory with the fields on the  $t=0$  time-slice restricted to the finite set

$$U \in \{^m U, m = 1, \dots, N\}$$

It is clear that in this statistical system, the quantity  $\Psi^2[n U]$  just represents the probability that a random fluctuation selects  $U(x, 0) =^n U(x)$ . Therefore, in a Monte Carlo simulation of (6), we simply have

$$\Psi^2[n U] = \frac{N_n}{N_{it}}$$

where  $N_{it}$  is the total number of Monte Carlo iterations, and  $N_n$  is the number of iterations in which the  $n$ -th configuration  $^n U$  was selected by the Monte Carlo algorithm on the time-slice  $t=0$ . From this data, it is possible to check whether or not the vacuum wavefunctional fits the form

$$\Psi^2 = N \exp(\mu \sum \text{Tr}[UUU^t U^t]) \quad (7)$$

for small amplitude ( $U \approx 1$ ), slowly-varying link configurations.

The Monte Carlo calculation of eq.(6) was carried out on a microvax computer. In order to keep the computer time required within reasonable bounds ( $\approx 20 - 40$  hours cpu time for each coupling  $\beta$ ), some concessions were required: the computations were done in three dimensions, and on fairly small ( $4^3, 6^3, 8^3$ ) lattices. On lattices of this size, a "slowly-varying" configuration should have almost no variation over the length of the lattice, and in practice I have used only non-abelian constant configurations

$$\begin{aligned} {}^n U_1 &= (1 - a_n^2)^{\frac{1}{2}} 1 + i a_n \sigma_1 \\ {}^n U_2 &= (1 - a_n^2)^{\frac{1}{2}} 1 + i a_n \sigma_2 \end{aligned}$$

where

$$a_n = \frac{n S_\beta}{20 L^2}$$

and  $L =$  no. of sites/side. Then

$$\sum_{p1aq} (1 - \frac{1}{2} \text{Tr} [{}^n U_1^n U_2^n U_1^n U_2^n]) = \frac{n}{10} S_\beta$$

The constant  $S_\beta$  was chosen (by trial and error) so that  $N_1/N_{10} \approx 50$ .

From the data obtained in the Monte Carlo calculation, there are three things to check:

1) Does  $\Psi^2$  fall exponentially with  $\sum \text{Tr} [UUUU]$ ?

If this is true, then the parameter  $\mu(\beta)$  can be extracted from the data. If it is *not* true, then the form (7) is obviously false.

2) Is  $\mu(\beta)$  independent of lattice size?

This question is related to the long-distance behavior of  $\phi(x)$  in eq. (4). In deriving (5) from (4), it was assumed that  $\phi(x)$  damps exponentially to zero at large distances. If this assumption is not true, but rather

$$\mu = \int d^2 x \phi(x) \rightarrow \infty$$

in an infinite spatial volume, then  $\mu$  would increase as the lattice size increases, and again eq. (3) would be incorrect in the continuum limit.

3) Does  $\mu(\beta)$  scale correctly at weak couplings?

If eq.(3) is the continuum limit of (7), then as  $\beta \rightarrow \infty$  it is necessary that

$$\mu(\beta) = \text{const.} \times \beta^2$$

which is the correct weak-coupling scaling behavior in 3 dimensions (for strong-couplings,  $\mu = \beta$ ).

In ref. [3] it was found that weak-coupling scaling behavior for Wilson loops sets in around  $\beta = 5$  for SU(2) gauge theory in 3 dimensions. The data for  $\Psi^2$  as a function of  $\sum \text{Tr}[UUUU]$  at  $\beta = 5$  is shown in Fig. 1, on an  $8^3$  lattice. There is little doubt that this data accurately fits an exponential curve (straight-line on a semi-log plot), so  $\mu(\beta)$  can be accurately extracted from the slope.

In Fig. 2 the same data is shown for coupling  $\beta = 6$ , for three different lattice sizes ( $4^3, 6^3, 8^3$ ). Error bars (not shown) are roughly the same as corresponding points in Fig. 1. The data is almost independent of lattice size, which is good evidence that  $\mu(\beta)$  has a finite limit in infinite volume.

Fig. 3 is a plot of  $\mu(\beta)$  as a function of  $\beta$ . We see that the data in the strong-coupling region ( $0 < \beta < 2$ ) follows the strong-coupling curve  $\mu = \beta$ , while data in the weak-coupling region is closely fit by a parabola  $\mu = .405\beta^2$ , which is the correct weak-coupling scaling in 3 dimensions.

In summary, the Monte Carlo data obtained thus far supports eq.(3) as the QCD vacuum for long-wavelength field configurations in three dimensions. More work needs to be done, of course, using larger lattices with non-constant field configurations, and in four space-time dimensions.

Next we consider the QCD wavefunctional of states containing static quark-antiquark charges, i.e. "string" wavefunctionals. A state containing heavy quark-antiquark charges is given, in path-integral representation, by

$$\begin{aligned}\Psi_{ab}[A] &= \int DA(x, t < 0) W_{ab}[C_-] \delta[F[A]] \exp\left[-\int_{-\infty}^0 dt L[A]\right] \\ &= \Psi_R \delta_{ab} + i\Psi_I^c \sigma_{ab}^c = F_{ab}[A] \Psi_0\end{aligned}$$

where  $W_{ab}[C_-]$  is a path-ordered Wilson line, and  $C_-$  is the semi-rectangular path running from  $(x', t = 0)$  to  $(x', t = -T/2)$  to  $(x'', t = -T/2)$  to  $(x'', t = 0)$ . We then have

$$\begin{aligned}\langle \Psi_R | \Psi_R \rangle &= \frac{1}{2} \langle \text{Tr}W[C] + \text{Tr}[W[C_+]W^\dagger[C_-] \rangle \\ \langle \Psi_I | \Psi_I \rangle &= \frac{1}{2} \langle \text{Tr}W[C] - \text{Tr}[W[C_+]W^\dagger[C_-] \rangle\end{aligned}$$

where  $C_+$  is the semirectangular path from  $(x'', 0)$  to  $(x'', T/2)$  to  $(x', T/2)$  to  $(x', 0)$ , and  $\text{Tr}W[C]$  is the  $R \times T$  Wilson loop  $\text{Tr}W[C] = \text{Tr}W[C_+]W[C_-]$ .

It is important to note that the antihermitian part of the wavefunctional,  $\Psi_I^{ab} = \Psi^c \sigma_{ab}^c$  has a node at  $A = 0$ , i.e.

$$\Psi_I^{ab}[A = 0] = 0$$

which is implied by the fact that  $\text{Tr}\Psi_I = 0$ . The existence of nodes in the QCD string wavefunctional is crucial to the "gluon-chain" model of string formation [4,5], which I will now describe briefly.

The gluon-chain model is based on the idea that Nature does not tolerate charges of arbitrarily large magnitude, and that large charges tend to be screened, both in QED and QCD, by particle production. For example, it is impossible, in nuclear physics, to have a heavy nucleus of charge greater than some critical value  $Z_c \approx 170$ . If a nucleus has a charge greater than this value, it becomes energetically favorable to pull an electron-positron pair out of the vacuum. The electron is then captured by the heavy nucleus, reducing the nuclear charge below the critical value (Fig. 4a). Similarly, in QCD, as a quark-antiquark pair separates and the effective coupling increases, there is some critical separation  $R_c$  where it becomes energetically favorable to pop a light quark-antiquark pair out of the vacuum. The light quark binds to the antiquark, and the light antiquark to the quark, so that the original quark-antiquark charges are screened from one another (Fig. 4b). Again there is a natural limit to the growth of effective coupling.

Now consider the case of QCD with no light quarks (only in this idealized case is there a linear quark potential at arbitrarily large distances). In this case a type of charge screening is also possible. As massive quarks separate and the effective coupling grows, there is again a critical separation where it is energetically favorable to place a *gluon* in between the two quarks, as shown in Fig. 4c. From the point of view of the heavy quark (antiquark), the antiquark (quark) charge has moved to the position of the gluon, and therefore the average separation between color charges has been reduced. As the heavy quarks continue to move apart, an upper limit to the average charge separation is maintained by dragging out more gluons between the quarks. The eventual configuration of the confining QCD "string" is shown in Fig. 5; it consists of a chain of gluons between the quarks, with each gluon held in place by attraction to its nearest-neighbors in the chain (in the large  $N_{colors} \rightarrow \infty$  limit, there are only interactions between nearest neighbors). Let  $R_{av}$  be the average separation between neighboring gluons, and  $E(R_{av})$  the average (kinetic + interaction) energy per gluon,  $n_{gluons}$  the number of gluons in the chain, and  $L$  the distance between the heavy quarks. The total energy of the chain is then roughly

$$E_{chain} = n_{gluons} E(R_{av}) = \frac{E(R_{av})}{R_{av}} L = \sigma L$$

so that  $\sigma = E(R_{av})/R_{av}$  is the string tension (assuming  $n_{gluons} = L/R_{av}$ , which is an approximation that ignores roughening). This is the origin of the linear potential between quarks in the "gluon-chain" model of string formation.

The gluon-chain model is motivated in part by large- $N$  considerations. In the  $N_{colors} \rightarrow \infty$  limit, QCD has the rather striking property that the product of gauge-invariant quantities factorizes, e.g

$$\langle W[C_1]W[C_2] \rangle = \langle W[C_1] \rangle \langle W[C_2] \rangle$$

where  $W[C_{1,2}]$  are Wilson loops. This has the immediate consequence that adjoint (gluon) charge



are also confined by a linear potential, and that the relation between the string-tensions of adjoint and fundamental (quark) charges is simply

$$\sigma_{adjoint} = 2\sigma_{fundamental}$$

Simple relationships cry out for simple explanations. But models of confinement which are based on analogies to abelian theories (e.g. dual superconductors,  $Z_N$  fluxons), and depend on isolating some abelian subgroup of the full gauge group, find it difficult if not impossible to account for these conditions. In the gluon-chain model, on the other hand, factorization at large- $N$  is built in. In fact, suppose that large Wilson loops are dominated by very high (but finite) order planar Feynman diagrams. A time-slice of any such diagram (Fig. 6), in a physical gauge, reveals a state which is simply a chain of gluons with quarks at each end, as envisaged in the gluon-chain model.

Returning to the computer measurements, one would like to use these methods to test the model outlined above. Consider any excited state of the form

$$\Psi[A] = \sum_n \int d\mathbf{x}_1 \dots d\mathbf{x}_n f(\mathbf{x}_1 \dots \mathbf{x}_n) A(\mathbf{x}_1) \dots A(\mathbf{x}_n) \Psi_0[A]$$

This state contains constituent gluons in some spatial volume  $V$  if

$$\Psi[A] \neq 0$$

for any configuration  $A(\mathbf{x})$  such that  $A(\mathbf{x}) = 0$  for any  $\mathbf{x} \in V$ . For our purposes, a "constituent gluon" is just an  $A$ -field multiplying the true ground state.

In particular,  $\Psi_I$  contains at least one constituent gluon somewhere in space, since  $\Psi_I[0] = 0$ . This fact is useful, because it means that the ratio

$$\begin{aligned} \xi &= \frac{\langle \Psi_I | \Psi_I \rangle}{\langle \Psi | \Psi \rangle} \\ &= \frac{\langle \text{Tr}[W[C] - W[C_+]W^\dagger[C_-]] \rangle}{2 \langle \text{Tr}W[C] \rangle} \end{aligned}$$

is a lower bound to the probability that the QCD string state contains at least one constituent gluon. This is a quantity which can be readily measured by the Monte Carlo method.

The concept of gluons, of course, only makes sense in a fixed gauge. On the lattice, the gauge must be fixed well enough so that the link variables fluctuate around  $U = 1$ . The lattice Coulomb gauge, in which the quantity

$$\text{Re}(\text{Tr} \sum_{i=1}^2 [U_i(\mathbf{x}) + U_i^\dagger(\mathbf{x} - \mathbf{e}_i)])$$

is maximized at each site, is appropriate for this purpose. Monte Carlo calculations in Coulomb gauge can be readily carried out using the iterative gauge-fixing procedure of Mandula and Ogilvie [6].

Before proceeding to the non-abelian case, it is useful to know what is the expected behavior of  $\xi$  in an abelian theory. In the free abelian case, it is easy to show that  $\xi \rightarrow 0$  as  $T \rightarrow \infty$ , i.e. a state containing two static +/- electric charges contains no constituent photons. The reason is that, as  $T \rightarrow \infty$ , the state is dominated by instantaneous Coulomb interactions, which only contribute to the real part of the wavefunctional. The imaginary part of the wavefunctional is generated by transverse photons originating at  $t = -T/2$ , and propagating to  $t = 0$ . As  $T \rightarrow \infty$ , this contribution is suppressed. Another way of seeing this is to note that the ground state of the Schrodinger wavefunctional equation with static external charges, in Coulomb gauge, is identical to the vacuum state with *no* external charges, since the Coulombic part of the QED Hamiltonian is independent of the transverse A field.

The SU(2) data for  $\xi$  as a function of quark-separation R and loop-length T, in D=3 dimensions at a weak-coupling of  $\beta = 5.5$ , is shown in Fig. 7. It can be seen that there is very little probability for the state to contain a constituent gluon at small separations, but that the lower bound on this probability rises to roughly 70% at R=6 lattice spacings. Moreover, the tendency of  $\xi$  to fall as T increases does not seem very pronounced; and the evidence favors  $\xi \rightarrow \text{const.} \neq 0$  as  $T \rightarrow \infty$ . It appears that, for  $R \geq 6$ , the QCD string state contains at least one constituent gluon.

It is even possible to map, roughly, where this constituent gluon is on the lattice, although here my results are very preliminary. Define

$$\Gamma_V = \langle \Psi_I | \Psi_I \rangle_{(U(t \in V)=1)}$$

so that  $\Gamma_V = 0$  if there is a constituent gluon in volume V, and

$$r_V = \frac{\Gamma_V}{\Gamma_{V_0}}$$

As already noted, the antihermitian part of the wavefunctional  $\Psi_I$  contains at least one constituent gluon. I have measured the ratios  $r_V$  for a quark separation of R=3 (T=6) lattice spacings at  $\beta = 5.5$ , with V a strip at  $t=0$  one link in width. The values of  $r_V$ , for three inequivalent positions of the quarks relative to V, are shown in Fig. 8. From this data, it seems that the constituent gluon is most likely to be in the center region between the two quarks.

In summary, the data for  $\xi$  does seem to indicate that the QCD string contains at least one constituent gluon. To check the validity of the gluon-chain model, however, it would be highly desirable to detect more than one constituent gluon as quark separation increases. This could be done by the  $r_V$  calculations described above, which in principle could locate more than one node in

the wavefunctional in different regions of the string. Such calculations, however, at larger values of  $R$  and  $T$ , are extremely cpu-time intensive. Further work along these lines will require the use of a supercomputer.

#### References

1. J. Greensite, Nucl. Phys. **B158** (1979) 469.
2. J. Greensite, Nucl. Phys. **B166** (1980) 113.
3. J. Ambjørn, P. Olesen, and C. Peterson, Nucl. Phys. **B240** [FS12];  
E. D'Hoker, Nucl. Phys. **B180** [FS2] (1981) 341.
4. J. Greensite, Nucl. Phys. **B249** (1985) 263;  
J. Greensite and M. Halpern, Nucl. Phys. **B271** (1986) 379.
5. C. Thorn, Phys. Rev. **D19** (1979) 639.
6. J. Mandula and M. Ogilvie, Phys. Lett. **B 185** (1987) 127.

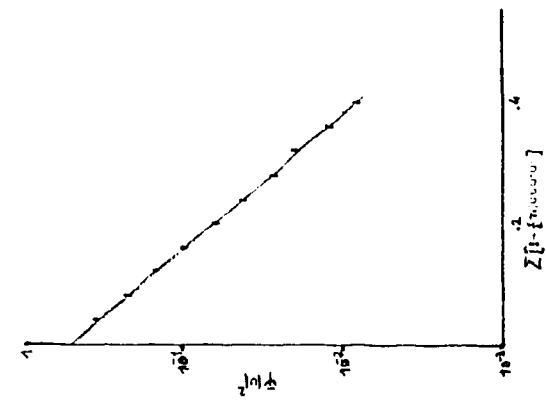


Fig. 1  
 Semilog plot of  $|\Psi(U)|^2$  vs  $Z[D-f_{max}(U)]$  for  $\beta=5$ , evaluated on an  $8^3$  lattice. The straight line is a least-squares fit through the 10 data points.

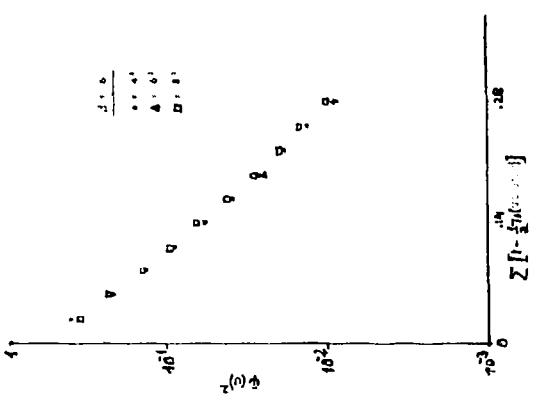


Fig. 2  
 Semilog plot of  $|\Psi(U)|^2$  vs  $Z[D-f_{max}(U)]$  for  $\beta=6.3$ , evaluated at 10 data points on  $4^3, 6^3$  and  $8^3$  lattices.

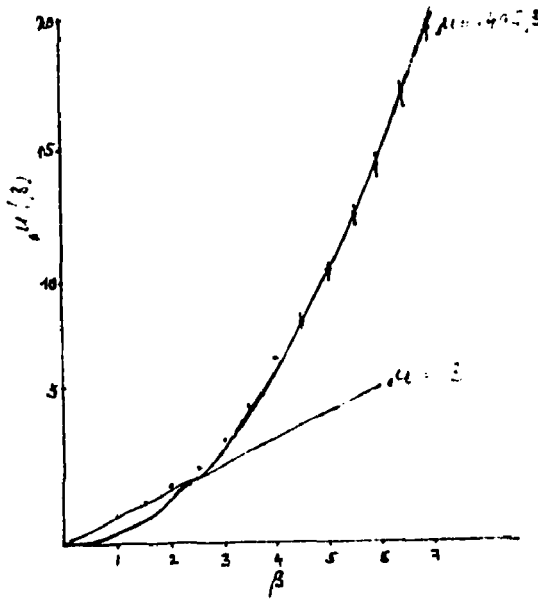


Fig.3

$\mu(\beta)$  vs  $\beta$  in the coupling region  $0 \leq \beta \leq 7$ . The straight line is the strong-coupling result  $\mu = \beta$ , while a fit to the parabolic curve  $\mu = .405\beta^2$ , shows the continuum scaling of  $\mu$  in the weak-coupling regime.

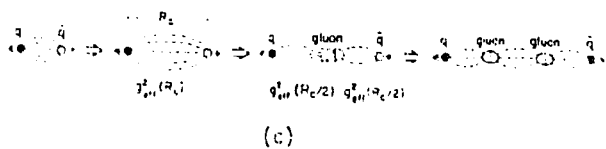
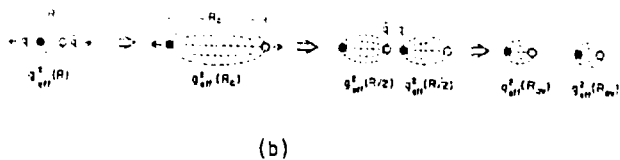
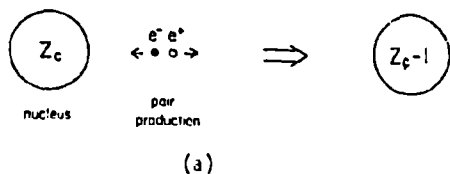


Figure 4: (a) Screening of nuclear charge by  $e^+e^-$  pair production; Screening of heavy quarks by (b)  $q\bar{q}$  pair-production, and (c) valence-gluon production

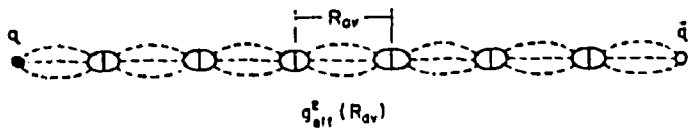


Figure 5 : Gluon-chain picture of the QCD string.

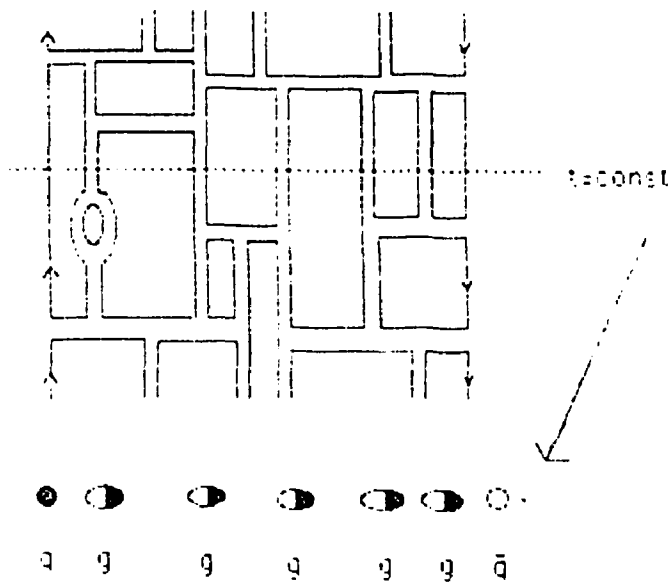


Figure 6: The gluon chain can be viewed as a time-slice of a high-order planar diagram.

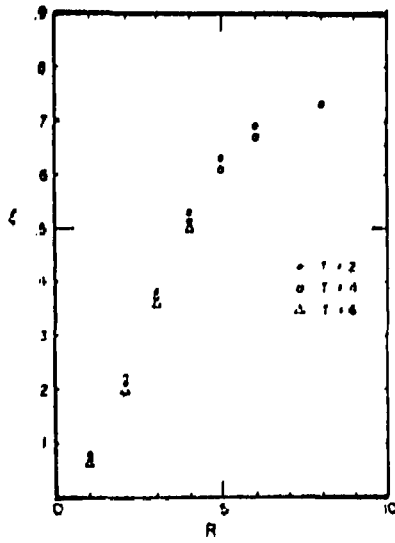


Fig. 7 : The ratio  $\zeta = \langle \Gamma \Psi | \Gamma \Psi \rangle / \langle \Psi | \Psi \rangle$  vs. quark separation  $R$ . This ratio is a lower limit to the probability that the state  $\Psi$  contains a constituent gluon

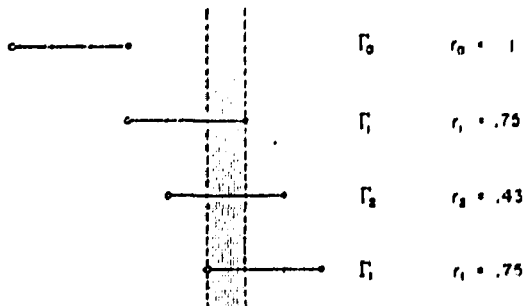


Fig. 8 : The  $r_i$  ratios for a quark-antiquark pair 3 lattice spacings apart. Links in the shaded region are frozen to  $U=1$ ; three inequivalent positions of the quark pair, relative to the shaded region, are shown. The Monte Carlo results for the  $r_i$  indicate that a constituent gluon is most likely to be found in the middle region between the quarks, rather than a region adjacent to one of the quarks. Statistical error for  $r_1, r_2$  is  $\approx 15\%$



## NONPERTURBATIVE PERTURBATION THEORY

Carl M. Bender  
Department of Physics  
Washington University  
St. Louis, MO 63130

In this talk we propose a new perturbative computational scheme for solving self-interacting scalar quantum field theories. To solve a  $\lambda\phi^4$  theory in  $d$ -dimensional space-time, we introduce a small parameter  $\delta$  and consider a  $\lambda(\phi^2)^{1+\delta}$  field theory. We show how to expand such a theory as a series in powers of  $\delta$ . The resulting perturbation series appears to have a finite radius of convergence and numerical results for low-dimensional models are good. We have computed the two-point and four-point Green's functions to second order in powers of  $\delta$  and the  $2n$ -point Green's functions ( $n>2$ ) to order  $\delta$ . We explain how to renormalize the theory and show that, to first order in powers of  $\delta$ , when  $\delta>0$  and  $d\geq 4$  the theory is free. This conclusion remains valid to second order in powers of  $\delta$ , and we believe that it remains valid to all orders in powers of  $\delta$ .

In two recent papers<sup>1,2</sup> a new perturbative technique was proposed for solving self-interacting scalar quantum field theories such as  $\lambda\phi^4$  theory. The technique consists of expanding the  $n$ -point Green's function  $G^{(n)}(x_1, x_2, \dots, x_n, \delta)$  for a  $\lambda(\phi^2)^{1+\delta}$  theory as a series in powers of  $\delta$ :

$$G^{(n)}(x_1, x_2, \dots, x_n, \delta) = \sum_{k=0}^{\infty} \delta^k g^{(n)}_k(x_1, x_2, \dots, x_n). \quad (1)$$

Diagrammatic rules were formulated for calculating the coefficient of  $\delta^k$  ( $k=0, 1, 2, \dots$ ) in this expansion for any (unrenormalized) Green's function in  $d$ -dimensional space-time. In the  $\delta$  expansion it is only the parameter  $\delta$  which is considered small. Thus, like the  $1/N$  expansion, the results are nonperturbative in the physical parameters such as the mass and the coupling constant.

Perturbation methods have played a central role in the quest for approximate numerical solutions to quantum-field-theory models. In this talk we distinguish between two different kinds of perturbation series: a *natural* expansion, which is a series in powers of a physical parameter that appears in the functional-integral representation of the theory, and an *artificial* expansion, which is a series in powers of a new parameter  $\delta$ , which has been introduced temporarily as an expansion parameter for computational purposes. Weak-coupling expansions in powers of the coupling constant  $\lambda$ , strong-coupling expansions in powers of  $1/\lambda$ , and semiclassical (loop) expansions in powers of Planck's constant are all natural perturbation expansions.

Unfortunately, natural perturbation expansions suffer a number of disadvantages. Weak-coupling series are divergent and may not even be asymptotic to the solution of the theory. Semiclassical approximations also give divergent series, are very difficult to obtain beyond leading orders, and therefore may give very poor numerical results. (For example, in a simple quantum-mechanical system with tunneling, when tunneling occurs rapidly because of a low barrier potential, the WKB method gives a very poor approximation to the tunneling amplitude.) The computation of strong-coupling series requires the introduction of a lattice and the subsequent taking of a continuum limit; such series are often very slowly converging with many terms being required to give a reasonable approximation. The principal difficulty with natural perturbation expansions is that the analytic dependence of the solution to the theory on the physical parameters is lost; by forcing the physical constants to play the role of expansion parameters they are no longer available to display adequately the true functional dependence of the physical theory on them. (For example, in electrodynamics the anomalous magnetic moment  $g-2$  is an unknown, but surely complicated function of  $\alpha$ . Its weak-coupling expansion,  $g-2=c_1\alpha+c_2\alpha^2+\dots$ , only makes sense in the limit  $\alpha\rightarrow 0$ . This expansion does not even begin to suggest how  $g-2$  depends on the parameter  $\alpha$  when  $\alpha$  is not small.)

The advantage of artificial perturbation expansions is that, if a parameter  $\delta$  is inserted in a clever way, the resulting series in powers of  $\delta$  may be easy to compute and rapidly convergent. Moreover, the terms in this expansion may exhibit a very nontrivial dependence on the physical parameters of the theory. One such perturbation scheme is the large- $N$  expansion, where  $N$  is the number of

components of a scalar field. In nonrelativistic quantum mechanics, large- $N$  expansions are surprisingly successful.<sup>3</sup> For a  $(\Phi^2)^p$  theory the very first term in the large- $N$  expansion gives a nontrivial and renormalizable quantum field theory.<sup>4</sup> Also, quantum chromodynamics at large  $N$  displays interesting theoretical and phenomenological features.<sup>5</sup>

We illustrate with a very simple example of an artificial perturbation expansion. Consider the problem of finding the (unique) real positive root of the fifth-degree polynomial

$$x^5 + x = 1 .$$

We introduce a small parameter  $\delta$ ,

$$x^5 + x\delta = 1 .$$

and seek a solution in the form of a series in powers of  $\delta$ . Such a series is very easy to find. The first few terms are

$$x(\delta) = 1 - \delta/5 - \delta^2/25 - \delta^3/125 \dots .$$

If we evaluate this series at  $\delta=1$  we get  $x(1)=0.752$ , an extremely good approximation to the exact root, which is at  $x=0.7549 \dots$ .

The problem of course is to find a method for expanding the Green's functions of a quantum field theory as perturbation series in powers of  $\delta$ . We are considering the Lagrangian

$$L = \frac{1}{2}(\partial\phi)^2 + \frac{1}{2}\mu^2\phi^2 + \lambda M^2\phi^2(\phi^2 M^{2-d})^\delta \quad (2)$$

in  $d$ -dimensional Euclidean space. In (2),  $\mu$  is the bare mass,  $\lambda$  is the *dimensionless* bare coupling constant, and  $M$  is a fixed mass parameter that allows the interaction to have the correct dimensions. The problem is that if we expand the Lagrangian in (2) as a series in powers of  $\delta$  using the identity

$$x^\delta = e^{\delta \ln x} = 1 + \delta \ln x + \frac{\delta^2}{2!}(\ln x)^2 + \frac{\delta^3}{3!}(\ln x)^3 + \dots .$$

we obtain a horrible-looking nonpolynomial Lagrangian:

$$L = \frac{1}{2}(\partial\phi)^2 + \frac{1}{2}(\mu^2 + 2\lambda M^2)\phi^2 + \delta\lambda\phi^2 M^2 \ln\left(\phi^2 M^{2-d}\right) + \frac{\delta^2}{2}\lambda\phi^2 M^2 \left[\ln\left(\phi^2 M^{2-d}\right)\right]^2 + \frac{\delta^3}{6}\lambda\phi^2 M^2 \left[\ln\left(\phi^2 M^{2-d}\right)\right]^3 + \dots . \quad (3)$$

We have devised a very simple and orderly procedure for calculating the  $n$ -point Green's function of the Lagrangian in (3) as series in powers of  $\delta$ . It consists of three steps:

- (i) Replace the Lagrangian  $L$  in (3) with a new Lagrangian  $L_{\text{whacko}}$  having *polynomial* interaction terms.
- (ii) Using  $L_{\text{whacko}}$ , compute the Green's function  $G^{(n)}_{\text{whacko}}$  using ordinary Feynman diagrams.

(iii) Apply a derivative operator  $D$  to  $G^{(n)}_{whacko}$  to get the delta expansion for  $G^{(n)}$ .

The new Lagrangian  $L_{whacko}$  and the derivative operator  $D$  depend on the number of terms in the  $\delta$  series that we intend to compute. For example, if we need one term in the  $\delta$  series we take

$$L_{whacko} = \frac{1}{2}(\partial\phi)^2 + \frac{1}{2}(\mu^2 + 2\lambda M^2)\phi^2 + \delta\lambda M^d \left(\phi^2 M^{2-d}\right)^{\gamma+1}.$$

Then we compute the n-point Green's function  $G^{(n)}_{whacko}$  to order  $\delta$ , apply

$$D = \frac{\partial}{\partial\alpha},$$

and set  $\alpha = 0$ .

Now suppose we need two terms in the  $\delta$  series expansion of  $G^{(n)}$ . We take

$$L_{whacko} = \frac{1}{2}(\partial\phi)^2 + \frac{1}{2}(\mu^2 + 2\lambda M^2)\phi^2 + (\delta + \delta^2)\lambda M^d \left(\phi^2 M^{2-d}\right)^{\gamma+1} + (-\delta + \delta^2)\lambda M^d \left(\phi^2 M^{2-d}\right)^{\gamma+1}.$$

Then we compute  $G^{(n)}_{whacko}$  to order  $\delta^2$ , apply

$$D = \frac{1}{2}\left(\frac{\partial}{\partial\alpha} - \frac{\partial}{\partial\beta}\right) + \frac{1}{4}\left(\frac{\partial^2}{\partial\alpha^2} + \frac{\partial^2}{\partial\beta^2}\right),$$

and set  $\alpha = \beta = 0$ .

For three terms in the  $\delta$  series expansion of  $G^{(n)}$ , we take

$$L_{whacko} = \frac{1}{2}(\partial\phi)^2 + \frac{1}{2}(\mu^2 + 2\lambda M^2)\phi^2 + \left[\delta + \frac{\delta^2}{2}(1 + \alpha) + \delta^3\right]\lambda M^d \left(\phi^2 M^{2-d}\right)^{\gamma+1} + \left[\delta\omega + \frac{\delta^2}{2}(\omega^2 + \beta) + \delta^3\right]\lambda M^d \left(\phi^2 M^{2-d}\right)^{\gamma+1} + \left[\delta\omega^2 + \frac{\delta^2}{2}(\omega + \gamma) + \delta^3\right]\lambda M^d \left(\phi^2 M^{2-d}\right)^{\gamma+1}.$$

As above, we compute  $G^{(n)}_{whacko}$  to order  $\delta^3$ , apply

$$D = \frac{1}{3}\left(\frac{\partial}{\partial\alpha} + \omega^2\frac{\partial}{\partial\beta} + \omega\frac{\partial}{\partial\gamma}\right) + \frac{1}{6}\left(\frac{\partial^2}{\partial\alpha^2} + \omega\frac{\partial^2}{\partial\alpha\beta} + \omega^2\frac{\partial^2}{\partial\gamma^2}\right) + \frac{1}{18}\left(\frac{\partial^3}{\partial\alpha^3} + \frac{\partial^3}{\partial\beta^3} + \frac{\partial^3}{\partial\gamma^3}\right),$$

and set  $\alpha = \beta = \gamma = 0$ .

If we need four terms in the delta expansion, we take

$$L_{whacko} = \frac{1}{2}(\partial\phi)^2 + \frac{1}{2}(\mu^2 + 2\lambda M^2)\phi^2 + \left[\delta + \delta^2\frac{2 + \alpha + \beta + \gamma + \nu + 3(\alpha^2 - i\beta^2 - \gamma^2 + i\nu^2)}{6} + \delta^3\frac{4 + 5\alpha}{9} + \delta^4\right]\lambda M^d \left(\phi^2 M^{2-d}\right)^{\gamma+1} + \left[i\delta + \delta^2\frac{-2 - i(\alpha + \beta + \gamma + \nu) + 3(i\alpha^2 + \beta^2 - i\gamma^2 - \nu^2)}{6} + \delta^3\frac{-4i + 5\beta}{9} + \delta^4\right]\lambda M^d \left(\phi^2 M^{2-d}\right)^{\gamma+1}$$

$$+[-\delta+\delta^2 \frac{2-\alpha-\beta-\gamma-\nu+3(-\alpha^2+l\beta^2+\gamma^2-l\nu^2)}{6}+\delta^3 \frac{-4+5\gamma}{9}+\delta^4] \lambda M^d \left( q^2 M^{2-d} \right)^{r+1}$$

$$+[-i\delta+\delta^2 \frac{-2+l(\alpha+\beta+\gamma+\nu)+3(-l\alpha^2-\beta^2+l\gamma^2+l\nu^2)}{6}+\delta^3 \frac{4l+5\nu}{9}+\delta^4] \lambda M^d \left( q^2 M^{2-d} \right)^{r+1}$$

We compute the Green's function  $G^{(n)}_{whacko}$  to order  $\delta^4$ , apply

$$D = \frac{1}{4} \left( \frac{\partial}{\partial \alpha} - i \frac{\partial}{\partial \beta} - \frac{\partial}{\partial \gamma} + i \frac{\partial}{\partial \nu} \right) + \frac{1}{8} \left( \frac{\partial^2}{\partial \alpha^2} - \frac{\partial^2}{\partial \beta^2} + \frac{\partial^2}{\partial \gamma^2} - \frac{\partial^2}{\partial \nu^2} \right)$$

$$+ \frac{1}{24} \left( \frac{\partial^3}{\partial \alpha^3} + i \frac{\partial^3}{\partial \beta^3} - \frac{\partial^3}{\partial \gamma^3} - i \frac{\partial^3}{\partial \nu^3} \right) + \frac{1}{96} \left( \frac{\partial^4}{\partial \alpha^4} + \frac{\partial^4}{\partial \beta^4} + \frac{\partial^4}{\partial \gamma^4} + \frac{\partial^4}{\partial \nu^4} \right),$$

and set  $\alpha=\beta=\gamma=\nu=0$ .

We do not have the general form of the Lagrangian  $L_{whacko}$  needed to obtain  $N$  terms in the delta series. However, we do have the form of the derivative operator  $D$ :

$$D = \frac{1}{N} \sum_{j=1}^N \sum_{k=1}^N \frac{e^{2\pi i(1-k)j/N}}{j!} \left( \frac{\partial}{\partial \alpha_k} \right)^j.$$

### Low-dimensional models

To examine the form of the delta expansion and to verify its numerical accuracy, we consider a zero-dimensional and a one dimensional field theory. The functional integral for the vacuum-vacuum amplitude  $Z$  of a  $\phi^4$  field theory in zero-dimensional space-time is an ordinary Riemann integral:

$$Z = \int_{-\infty}^{\infty} \frac{dx}{\pi^{1/2}} e^{-x^4}.$$

Now we insert the expansion parameter  $\delta$ :

$$Z = \int_{-\infty}^{\infty} \frac{dx}{\pi^{1/2}} e^{(x^2)^{1+\delta}}. \quad (4)$$

Recall that the ground-state energy  $E$  is given in terms of  $Z$ :

$$E(\delta) = -\ln Z.$$

For this simple theory we can, of course, evaluate directly the integral in (4):

$$E(\delta) = -\ln \left[ \frac{2}{\pi^{1/2}} \Gamma \left( \frac{2\delta+3}{2\delta+2} \right) \right]. \quad (5)$$

To find the delta series we merely expand the right side of (5) in a Taylor series in powers of  $\delta$ :

$$E(\delta) = \frac{\delta}{2} \psi \left( \frac{3}{2} \right) - \frac{\delta^2}{8} \left[ 4\psi \left( \frac{3}{2} \right) + \psi' \left( \frac{3}{2} \right) \right] + \frac{\delta^3}{48} \left[ 24\psi \left( \frac{3}{2} \right) + 12\psi' \left( \frac{3}{2} \right) + \psi'' \left( \frac{3}{2} \right) \right]$$

$$- \frac{\delta^4}{384} \left[ 192\psi \left( \frac{3}{2} \right) + 144\psi' \left( \frac{3}{2} \right) + 24\psi'' \left( \frac{3}{2} \right) + \psi''' \left( \frac{3}{2} \right) \right] + \dots \quad (6)$$

Notice that the structure of the delta series in (6) is rather strange in that the coefficients all depend on polygamma functions evaluated at  $3/2$ . The polygamma function  $\psi(x)$  is defined as the logarithmic derivative of a gamma function:

$$\psi(x) \equiv \frac{\Gamma'(x)}{\Gamma(x)} .$$

There is a general formula in terms of zeta functions for the  $n$ th derivative of a polygamma function evaluated at  $3/2$ :

$$\psi^{(n)}(3/2) = (-1)^n n! [(1-2^{n+1})\zeta(n+1) + 2^{n+1}] .$$

The first two polygamma functions are  $\psi(3/2) = 2 - \gamma - 2\ln 2$  and  $\psi'(3/2) = \frac{\pi^2}{2} - 4$ .

We list below the numerical values of the first few polygamma functions:

$$\begin{aligned} \psi(3/2) &= 0.0364899740; \\ \psi'(3/2) &= 0.9348022005; \\ \psi''(3/2) &= -0.8287966442; \\ \psi'''(3/2) &= 1.4090910340. \end{aligned}$$

It is crucial to determine for which  $\delta$  the series in (6) converges. Note that  $E(\delta)$  in (5) is singular whenever the argument of the gamma function vanishes. There are an infinite number of such singular points  $\delta_k$  in the complex- $\delta$  plane given by the formula

$$\delta_k = -\frac{2k+3}{2k+2}, \quad k=0,1,2,3,\dots$$

Each of these singular points is a logarithmic branch point. Note that these singular points form a monotone sequence on the negative- $\delta$  axis beginning at the point  $\delta = -3/2$  and converging to the point  $\delta = -1$ . We conclude that the delta series in (6) has a radius of convergence of 1.

A  $\phi^4$  theory corresponds to  $\delta = 1$ , which is situated on the circle of convergence. Thus, to compute the delta series with high numerical accuracy we use Padé summation. Here are the results: The exact value of the energy is  $E(1) = -0.0225104$ . Because we are on the circle of convergence we do not expect that a direct summation of the delta series will give a good result, and indeed it does not: ten terms in the power series give  $-0.367106$  and twenty terms in the power series give  $-0.517356$ . However, a (3,2) Padé gives  $-0.02252$  and a (5,4) Padé gives  $-0.0225103$ .

Now let us see how well the delta expansion works in one-dimensional field theory (quantum mechanics). Consider the Hamiltonian for the anharmonic oscillator:

$$H = -\frac{d^2}{2dx^2} + \frac{1}{2}x^4 .$$

Our strategy is to insert the parameter  $\delta$  in the  $x^4$  term:

$$H = -\frac{d^2}{2dx^2} + \frac{1}{2}(x^2)^{1+\delta} .$$

The ground-state energy  $E$  for this Hamiltonian has the delta expansion:

$$E(\delta) = \frac{1}{2} + \frac{\delta}{4} \psi\left(\frac{3}{2}\right) - \frac{\delta^2}{128} \left[ \psi'\left(\frac{3}{2}\right) + 8\psi\left(\frac{3}{2}\right) \ln 2 - 8\left[\psi\left(\frac{3}{2}\right)\right]^2 + 16\psi\left(\frac{3}{2}\right) - 32 + 32 \ln 2 \right] + \dots$$

This series is extremely accurate numerically. The exact value of  $E(1)$  is 0.530176, while the sum of the above series to order  $\delta^2$  is 0.534385. Notice that the form of the series is similar to that in (6); the coefficients are all constructed out of polygamma functions evaluated at  $3/2$ .

### Renormalization

We now consider the problem of how to renormalize the  $\delta$ -expansion. It was pointed out in Refs. 1 and 2 that when  $d \geq 2$  the coefficients of  $\delta^k$  in the expansions of the Green's functions are less divergent (as functions of the ultraviolet cutoff  $\Lambda$  in momentum space) than the terms in the conventional weak-coupling expansion in powers of  $\lambda$ . However, the coefficients  $g^{(n)}_k(x_1, x_2, \dots, x_n)$  in the  $\delta$  expansion are still divergent and it is necessary to use a renormalization procedure.

We will show how to regulate the theory by introducing a short distance cutoff  $a$  (which is equivalent to an ultraviolet cutoff  $\Lambda = 1/a$ ) and we compute the renormalized coupling constant  $G_R$  in terms of the bare mass  $\mu$  and the bare coupling constant  $\lambda$ . We then show that if we hold the renormalized mass  $M_R$  fixed at a finite value, then as the cutoff  $a$  is allowed to tend to 0 ( $\Lambda \rightarrow \infty$ ),  $G_R$  can remain finite and nonzero only when  $d < 4$ . When  $d \geq 4$ ,  $G_R \rightarrow 0$  as  $a \rightarrow 0$ . This result is the continuum analog of the numerical nonperturbative results already obtained in lattice Monte Carlo calculations.<sup>6</sup>

We have computed the  $d$ -dimensional two-point Euclidean Green's function  $G^{(2)}(p^2)$  to second order in powers of  $\delta$ . From  $G^{(2)}(p^2)$  we can obtain the wavefunction renormalization constant  $Z$  and the renormalized mass  $M_R$ . The conventional definitions are

$$Z^{-1} \equiv 1 + \frac{\partial}{\partial(p^2)} [G^{(2)}(p^2)]^{-1} \Big|_{p^2=0}, \quad (7)$$

and

$$M_R^2 \equiv Z [G^{(2)}(p^2)]^{-1} \Big|_{p^2=0}. \quad (8)$$

We have also computed  $G^{(4)}(p_1, p_2, p_3, p_4)$ , the connected  $d$ -dimensional Euclidean Green's function with its legs amputated, to second order in powers of  $\delta$ . From  $G^{(4)}$  we can obtain the dimensionless renormalized coupling constant  $G_R$  in the usual way:

$$G_R \equiv -Z^2 G^{(4)}(0, 0, 0, 0) M_R^{d-4}. \quad (9)$$

We do not discuss the calculations of  $G^{(2)}$ ,  $G^{(4)}$ , and the higher Green's functions such as  $G^{(6)}$  here; the calculation is long and detailed and it is presented

elsewhere.<sup>7</sup> It is sufficient to state that the calculation follows exactly the rules set down in Refs. 1 and 2. Here are the results for  $Z$ ,  $M_R^2$ , and  $G_R$  to first order in  $\delta$ :

$$Z=1+\mathbf{O}(\delta^2) \quad , \quad (10)$$

$$M_R^2=\mu^2+2\lambda M^2+2\lambda\delta M^2\left[1+\psi\left(\frac{3}{2}\right)+\ln[2\Delta(0)M^{2-d}]\right]+\mathbf{O}(\delta^2) \quad , \quad (11)$$

$$G_R=4\lambda\delta\frac{M^{d-2}}{\Delta(0)}+\mathbf{O}(\delta^2) \quad . \quad (12)$$

In (10)-(12),  $\Delta(x)$  represents the free propagator in  $d$ -dimensional coordinate space;  $\Delta(x)$  can be expressed as an associated Bessel function:

$$\begin{aligned} \Delta(x) &= (2\pi)^{-d} \int d^d p \frac{e^{ix \cdot p}}{p^2+m^2} \\ &= (2\pi)^{-d/2} (x/m)^{1-d/2} K_{1-d/2}(mx) \end{aligned} \quad (13)$$

where  $m^2=\mu^2+2\lambda M^2$ .

The function  $\Delta(x)$  is finite at  $x=0$  when  $d < 2$ :

$$\Delta(0)=2^{-d} \pi^{-d/2} m^{d-2} \Gamma(1-d/2) \quad . \quad (14)$$

However, we are concerned with quantum field theory, in which  $d \geq 2$ . For these values of  $d$ ,  $\Delta(0)=\infty$ , and it is clearly necessary to regulate the expressions for the renormalized quantities in (10)-(12) because of this divergence.

To regulate the theory we introduce a short-distance (ultraviolet) cutoff  $a$ ; to wit, we replace  $\Delta(0)$  in (11) and (12) with  $\Delta(a)$ , where

$$\Delta(a)=(2\pi)^{-d/2} (a/m)^{1-d/2} K_{1-d/2}(ma) \quad . \quad (15)$$

Apparently, there are three distinct cases which we must consider:

*Case 1:*  $am \ll 1$  ( $a \rightarrow 0$ ). Here we can approximate the Bessel function in (15) for small argument:

$$\Delta(a) \approx \frac{1}{4\pi} \Gamma\left(\frac{d}{2}-1\right) (\pi a^2)^{1-d/2} \quad . \quad (16)$$

*Case 2:*  $am = \mathbf{O}(1)$  ( $a \rightarrow 0$ ). Here,

$$\Delta(a) \approx (\text{constant}) m^{d-2} \quad . \quad (17)$$

*Case 3:*  $am \gg 1$  ( $a \rightarrow 0$ ). Here we can approximate the Bessel function in (15) for large argument:

$$\Delta(a) \approx \frac{1}{2m} \left(\frac{2\pi a}{m}\right)^{(1-d)/2} e^{-ma} \quad . \quad (18)$$



Now we consider each of these three cases in turn. In *case 1* we substitute (16) into (12) to obtain

$$\lambda\delta = (\text{constant}) G_R (aM)^{2-d} . \quad (19)$$

Then we use (19) to eliminate  $\lambda\delta$  from (11). The result is

$$M_R^2 = m^2 + (\text{constant}) [\text{logarithm term}] G_R M^2 (aM)^{2-d} . \quad (20)$$

It is necessary that the renormalized mass be finite. But as  $a \rightarrow 0$  the second term on the right side of (20) becomes infinite when  $d > 2$ . Thus, *both* terms on the right side of (20) must be infinite and must combine to produce a finite result. Hence they must be of the same order of magnitude as  $a \rightarrow 0$ :

$$(\text{constant}) [\text{logarithm term}] G_R M^2 (aM)^{2-d} \approx m^2 . \quad (21)$$

If we multiply (21) by  $a^2$  we obtain

$$(\text{constant}) [\text{logarithm term}] G_R (aM)^{4-d} \approx (am)^2 \ll 1 \quad (22)$$

by the assumption of *case 1*. Thus, when  $d < 4$ ,  $G_R$  can remain finite and nonzero as  $a \rightarrow 0$ , but when  $d \geq 4$ ,  $G_R \rightarrow 0$  as  $a \rightarrow 0$  and the theory is free.

Next, we consider *case 2*. We substitute (17) into (12) to obtain

$$\lambda\delta = (\text{constant}) G_R (m/M)^{d-2} . \quad (23)$$

We use (23) to eliminate  $\lambda\delta$  from (11) and obtain

$$M_R^2 = m^2 + (\text{constant}) \ln(m/M) G_R M^2 (m/M)^{d-2} . \quad (24)$$

As above, we argue that the left side of (24) must be finite so the two (infinite) terms on the right side of (24) must be of equal magnitude:

$$(\text{constant}) \ln(m/M) G_R M^2 (m/M)^{d-2} \approx m^2 . \quad (25)$$

We divide (25) by  $m^2$  and solve for  $G_R$ :

$$G_R = (\text{constant}) (m/M)^{4-d} / \ln(m/M) . \quad (26)$$

Again we observe that when  $d \geq 4$ ,  $G_R \rightarrow 0$  as  $m \rightarrow \infty$ .

Finally, we consider *case 3*. We substitute (18) into (12) to obtain

$$\lambda\delta = (\text{constant}) G_R (aM)^{(1-d)/2} (m/M)^{(d-3)/2} e^{-ma} . \quad (27)$$

We use (27) to eliminate  $\lambda\delta$  from (11) and obtain

$$M_R^2 = m^2 + \frac{[\text{logarithm term}]}{(\text{constant})} G_R M^2 (aM)^{(1-d)/2} (m/M)^{(d-3)/2} e^{-ma} . \quad (28)$$

Once again, we observe that the two terms on the right side of (28) are divergent and must be of the same magnitude:

$$\frac{[\text{logarithm term}]}{(\text{constant})} G_R M^2 (aM)^{(1-d)/2} (m/M)^{(d-3)/2} e^{-ma} \approx m^2 . \quad (29)$$

From (29) we then have

$$G_R \approx \frac{(\text{constant})}{[\text{logarithm term}]} e^{ma} (ma)^{(d-1)/2} (m/M)^{4-d} . \quad (30)$$

Thus, when  $d \leq 4$ ,  $G_R \rightarrow \infty$  as  $am \rightarrow \infty$ . Hence, case 3 may be excluded when  $d \leq 4$ . It is interesting that when  $d > 4$ ,  $G_R$  can remain finite as  $am \rightarrow \infty$  so long as  $m/M$  grows exponentially with  $am$ :

$$m/M \approx (\text{constant}) e^{ma/(d-4)} (am)^{(d-3)/(2d-8)}. \quad (31)$$

However, this possibility can be ruled out by computing the  $2n$ -point Green's functions  $G^{(2n)}$ . To order  $\delta$  we have

$$G^{(2n)}(0, 0, \dots, 0) = \delta \lambda (n-2)! M^{2n} [-\Delta(0)]^{1-n} + O(\delta^2). \quad (32)$$

If (31) holds, then (32) implies that for all  $n > 2$ ,  $G^{(2n)} \rightarrow 0$  as  $am \rightarrow \infty$  and the theory becomes trivial.

We have been able to generalize these arguments to second order in powers of  $\delta$ . However, we do not present the calculations here. We merely present for purposes of illustration the result for the renormalized mass to second order in delta:

$$\begin{aligned} M_R^2 = & \mu^2 + 2\lambda M^2 + 2\lambda \delta M^2 S + \delta^2 \{ \lambda M^2 [S^2 + 1 + \psi(3/2)] - 4\lambda^2 \Delta(0) M^4 S \int d^d x z \\ & - 4\lambda^2 \Delta(0) M^4 \int_0^1 d^d x \int dt \frac{\sqrt{1-t}}{t^2} [zt + \ln(1-zt)] \\ & + 4\lambda^2 \Delta(0) M^4 \int_0^1 d^d x \int dt \frac{\sqrt{z-zt}}{t} \ln(1-zt) \} + O(\delta^3), \end{aligned} \quad (33)$$

where  $S = \psi(3/2) + \ln[2\Delta(0)M^{2-d}] + 1$  and  $z = [\Delta(x)/\Delta(0)]^2$ . We cannot evaluate the integrals in (33) in closed form except in particular space-time dimensions; namely, when  $d=1$  and when  $d$  is even and negative semidefinite ( $d=0, -2, -4, -6, \dots$ ). For these special values of  $d$  we give the explicit evaluation of these integrals in Ref. 7.

Because the ideas presented in this talk are so new we cannot say at this point how useful these methods will ultimately be in quantum field theory. Much more research is required. However, it is already clear at this early stage that the delta expansion has very wide applicability. For example, the delta expansion is a natural tool for supersymmetric theories because global supersymmetry is preserved for all values of delta.

## REFERENCES

1. C. M. Bender, K. A. Milton, M. Moshe, S. S. Pinsky, and L. M. Simmons, Jr., *Phys. Rev. Lett.* **58**, 2615 (1987).
2. C. M. Bender, K. A. Milton, M. Moshe, S. S. Pinsky, and L. M. Simmons, Jr., to be published in *Phys. Rev.*
3. L. Yaffe, *Rev. Mod. Phys.* **54**, 407 (1982), and references therein; L. D. Mlodinow and N. Papanicolaou, *Ann. Phys.* **128**, 314 (1980), and **131**, 1 (1980); C. M. Bender, L. D. Mlodinow, and N. Papanicolaou, *Phys. Rev. A* **25**, 1305 (1982).
4. K. I. Wilson, *Phys. Rev. D* **7**, 2911 (1973). For a review, see S. Coleman, in *Pointlike Structures Inside and Outside of Hadrons*, edited by A. Zichichi (Plenum, New York, 1982).
5. G. 't Hooft, *Nucl. Phys.* **B72**, 461 (1974); G. Veneziano, *Nucl. Phys.* **B123**, 507 (1977); E. Witten, in *Quarks and Leptons*, edited by M. Levy and J.-L. Basevant (Plenum, New York, 1980).
6. B. Freedman, P. Smolensky, and D. Weingarten, *Phys. Lett.* **113B**, 481 (1982), and references therein.
7. C. M. Bender, H. F. Jones, K. A. Milton, S. S. Pinsky, and L. M. Simmons, Jr., to be published in *Phys. Rev.*

# QUASI-EXACTLY-SOLVABLE PROBLEMS IN QUANTUM MECHANICS

A.V. Turbiner

Institute for Theoretical and Experimental Physics

Moscow

There are no doubts about the importance of exactly-solvable problems in quantum mechanics. They serve as a basis for modelling different physical situations. As a matter of fact these models are quite rough and don't reproduce many essential properties of the phenomena considered. In this report we will describe so-called "quasi-exactly-solvable" quantum problems of two types: (1) when we know whole information about the first  $N$  eigenstates ( $N = 1, 2, 3, \dots$ ), which are related to each other by means of analytic continuation, and (2) there are  $N$  potentials of the same sort, which are different from each other in the magnitude of the potential parameter, with the same  $i$ -th eigenvalue of  $i$ -th potential; these potentials are related by analytic continuation. All the above problems are nontrivial and in the limit  $N \rightarrow \infty$  the well-known exactly-solvable problems in factorization method <sup>/1/</sup> are reproduced. It is worth emphasizing that their analytic properties are strongly different from analytic properties of exactly-solvable problems <sup>/2-4/</sup>. The calculation of the first  $N$  eigenvalues in quasi-exactly-solvable problems is equivalent to finding the eigenvalues of some  $N \times N$  Jacobi matrix.

A. One-dimensional case. Let's consider the Schrodinger equation

$$H \psi = E \psi \quad (1)$$

and make the substitution <sup>/5/</sup>

$$\psi(x) = p(x) \exp(-\varphi(x)) \quad (2)$$

in it where  $\rho(x)$  is a certain function containing the information about wave-function nodes in some minimal fashion (e.g. for the  $n$ -th excited state the simplest choice of the function  $\rho(x)$  is a polynomial of  $n$ -th power with  $n$  real roots. Letting  $y = \psi'$  and substituting Eq. (2) in (1), we obtain

$$y' - y^2 - \rho^{-1}[\rho'' - 2y\rho'] = E - V \quad (3)$$

Our purpose to choose the coefficients in the polynomials  $\rho$  and  $y$  in such a way that the ratio  $[\rho'' - 2y\rho'] / \rho$  is also a polynomial. Moreover, we will require it to be a two-term polynomial in certain variables. It's worth noting that in exactly-solvable problems the result is one-term polynomial.

Now, let's proceed to consideration of particular cases.

1. Generalized Morse potentials. Let's take as

$$y = -a e^{-\alpha x} + b + c e^{\alpha x}, \quad a \geq 0, \quad \alpha > 0 \quad (4)$$

and  $\rho = 1$ . Substituting eq. (4) to eq. (3), we obtain

$$V_0 = a^2 e^{-2\alpha x} - a(d+2b)e^{-\alpha x} + c(2b-d)e^{\alpha x} + c^2 e^{2\alpha x}, \quad E_0 = 2ac - b^2 \quad (5)$$

Thus, the potential (5) depends on the parameters  $a, b, c, d$  and we know the ground-state energy, which is single-valued analytic function in any variable  $a, b, c, \alpha$ . The potential (5) grows at  $|x| \rightarrow \infty$ , and the ground-state wave function decreases and is positive. Let  $\rho = e^{-\alpha x} + A$ . The parameter  $A$  will be sought by requiring the absence of singularities in the resulting potential (see eq. (3)) at real  $x$ . As a result the addition to potential (5) appears

$$V_1 = -2da e^{-\alpha x} \quad (6)$$

and

$$A_{\pm} = [d - 2b \pm \sqrt{(d+2b)^2 + 16ac}] / 4a$$

$$E_{0,1} = 2ac - b^2 - d[d + 2b \pm \sqrt{(d+2b)^2 + 16ac}] / 2$$

where plus corresponds to ground state (wave function is positive) and minus corresponds to the first excited state in the potential (5) + (6). Let's note that eigenvalues and eigenfunctions of the first two states in the potential (5) + (6) are plaited and two-sheet Riemann surface appears with square root branch points at  $(d+2b) = \pm 4i\sqrt{a_2}$ . Obviously, when  $p = e^{-dNx} + A_1 e^{-d(N-1)x} + \dots + A_N$  the cancellation condition in (3) leads to the potential addition  $V_N = -2daNe^{-dx}$ . In this potential the first  $N$  states arise from certain algebraic equation of  $(N+1)$ -th power which is a secular equation for certain Jacobi matrix of the size  $(N+1) \times (N+1)$ . They create the  $(N+1)$ -sheet Riemann surface. The limit  $N \rightarrow \infty$  corresponds to  $c=0$  under the suitable choice of the parameter dependence on  $N$ . In this case the spectral Riemann surface is unplaited and the exactly-solvable Morse potential appear.

There are two other families of quasi-exactly-solvable problems, which are associated with the Morse potential. It takes place when

$$y_2 = -c e^{-2dx} + a e^{-dx} + b, \quad c \geq 0, \alpha > 0 \quad (7)$$

$$y_3 = c e^{2dx} - b + a e^{dx}, \quad c \geq 0, \alpha > 0 \quad (8)$$

The both quasi-exactly-solvable problems turn out to be of the second-type unlike the quasi-exactly-solvable problem generated by (4). There exists plaiting of potentials in parameters  $a, b, c, \alpha$  at certain energy.

2. Generalized Föschl-Teller potential. Let's take

$$y_1 = a th dx + c sh^2 dx, \quad c \geq 0, \alpha > 0 \quad (9)$$

Substituting (9) to (3) at  $p = 1$ , we get

$$V_0 = -a(a+d)ch^{-2}dx - c(c+2d-2a)ch^2dx + c^2ch^4dx, \quad E_0 = 2ac - a^2 - \alpha c \quad (10)$$

and hence we know the ground state in potential (10), which is not plaited with the rest spectrum. If  $p = th dx$ , certain

addition to potential (10) arises

$$V_1 = -2d(a+d)ch^{-2}dx, \quad E_1 = 2ac - a^2 + dc \quad (11)$$

where  $E_1$  - is the energy of the first excited state in the potential (10)+(11). Hence, we know the energy of the first state in the potential (10)+(11). Due to the parity of the potentials under consideration, the Riemann surfaces of even and odd states are separated and they are not crossed. When  $p = th^2 dx + A$  (the sector of even states), then the addition to (10) equals to  $V_2 = -2d(2a+3d)ch^{-2}dx$  and

$$A_{\pm} = [-a-c-2d \pm \sqrt{(a+c+2d)^2 + 2(2a+3d)c}] / (2a+3d)$$

$$E_{0,2} = 2ac - a^2 - d[2a-c+2d \pm 2\sqrt{(a+c+2d)^2 + 2c(2a+3d)}]$$

If  $p = th dx (th^2 dx + A)$  (odd sector) the addition to (10) is  $V_3 = -6d(a+2d)ch^{-2}dx$  and

$$A_{\pm} = [-a-c-4d \pm \sqrt{(a+c+4d)^2 - 3d(2a+5d)}] / (2a+5d)$$

$$E_{1,3} = 2ac - a^2 - d[2a-5c+2d \pm \sqrt{(a+c+4d)^2 - 3d(2a+5d)}]$$

This situation is different from that which is described in section 1: the Riemann two-sheet surface is formed by the states of the same parity. In the general case, when  $p = th^k dx + A_1 th^{k-1} dx + \dots + A_k$ , the addition to (10) equals to  $V_k = -d k(dk+d+2a)ch^{-2}dx$ . In this potential the first  $N = [\frac{k}{2}] + 1$  states of parity  $(-1)^k$  are known. They plait forming N-sheet surface. In the limit  $N \rightarrow \infty$  the Riemann surface is unplaited, parameter  $c = 0$  and the exactly-solvable Poschl-Teller potential  $V \sim ch^{-2}dx$  arises. This quasi-exactly-solvable problem is the first-type one.

The other quasi-exactly-solvable problem of the second type associated with Poschl-Teller potential is generated by

$$V_2 = bth^3 dx + a th dx, \quad a > b, \quad d > 0 \quad (12)$$

The limit  $k \rightarrow \infty$  corresponds to  $b \rightarrow 0$ .

3. Generalized harmonic oscillator. Let's consider as in /4-7/

$$y = ax^3 + bx, \quad a \geq 0 \quad (13)$$

It's clear that the states of different parity form the separated Riemann surfaces. Let  $p = 1$ , then

$$V_0 = a^2x^6 + 2abx^4 + (b^2 - 3a)x^2, \quad E_0 = b \quad (14)$$

and at  $p=x$ , we get

$$V_1 = a^2x^6 + 2abx^4 + (b^2 - 5a)x^2, \quad E_1 = 3b \quad (15)$$

When  $p = x^2 + A$ , the addition to potential (14) equals  $\Delta V_2 = -4bx^2$  and  $A_{\pm} = [a \pm \sqrt{a^2 + 2b}]/2b$ ;  $E_{0,2} = 3a \pm 2(-\sqrt{a^2 + 2b})$ .  
 If  $p = x(x^2 + A)$ , the addition to (15) is  $\Delta V_2$  and  $A_{\pm} = [a \pm \sqrt{a^2 + 6b}]/2b$ ,  $E_{1,3} = 5a \pm 2(-\sqrt{a^2 + 6b})$ . Eigenvalues  $E_{0,2}$  ( $E_{1,3}$ ) form a two-sheet Riemann surface with branch points at  $b = \pm 2i\sqrt{a}$ ,  $b = \pm i\sqrt{6a}$ . As to  $p = x^k + A_1x^{k-1} + \dots + A_k$  the addition to (14) equals to  $\Delta V_k = -2akx^2$ ; in this potential it is known  $N = [k/2] + 1$  eigenstates of parity  $(-1)^k$ . Each eigenvalue  $E_i$  (eigenfunction  $\psi_i$ ) contains  $(N-1)$ -pairs of complex-conjugated square-root branch points in  $a$ . It corresponds to the crossing of the level under consideration with the rest levels of family given. It is worth noting that the different types of potential curves appear depending on various relations between parameters:  $b > 0, b^2 \geq a(2k+3)$  (single-well potential);  $b < 0, b^2 \geq a(2k+3)$  (triple-well potential);  $b^2 < a(2k+3)$  (double-well potential). If  $k \rightarrow \infty$ , then  $a \rightarrow 0$ , the spectrum is unplaited and potential  $V = b^2x^2$  appears.

B. Multidimensional case. The radial part of the d-dimensional Schrodinger equation with spherically-symmetric potential can be considered in an analogous manner

$$y' + r^{-1}(2\ell + d - 1)y - y^2 - p^{-1} \{p'' + [(2\ell + d - 1)r^{-1} - 2y]p'\} = E - V(r) \quad (16)$$

(compare (3)), where  $\ell$  is an angular quantum number.



4. Generalized multidimensional harmonic oscillator.

Apparently, the multidimensional analog (13) has the form

$$y = ar^3 + br + cr^{-1}, \quad a \geq 0, \quad c < \ell + d/2 \quad (17)$$

If  $p = 1$ , then we get

$$V_0 = c(c - 2\ell - d + 2)r^{-2} + [\beta^2 - a(2\ell + d + 2 - 2c)]r^2 + 2abr^{-4} + ar^6, \quad E_0 = \beta(2\ell + d - 2c) \quad (18)$$

for which the ground state is known. The addition to (18)

$\Delta V_N = -4Na r^2$  gives the potential with  $(N+1)$ -known levels. If  $N \rightarrow \infty$ , then  $a \rightarrow 0$ , the spectral Riemann surface is unplaited and the exactly-solvable problem appears (see e.g. /9/, p.158).

5. Generalized Coulomb problems. Let's take

$$y_1 = a + cr^{-1} + br, \quad b \geq 0, \quad c < \ell + d/2 \quad (19)$$

In the case of ground state ( $p = 1$ ), we have

$$V_0 = c(c - 2\ell - d + 2)r^{-2} - a(2\ell + d - 1 - 2c)r^{-1} + 2abr + br^2, \quad E_0 = \beta(2\ell + d - 2c) - a^2 \quad (20)$$

when  $p = r^N + A_1 r^{N-1} + \dots + A_N$ , there is the family of potentials which are related to each other by analytic continuation in parameters  $a, b, c$ ; the  $i$ -th state energy of the  $i$ -th potential has the value  $E_N = \beta(2N + 2\ell + d - 2c) - a^2$ . It is the quasi-exactly-solvable problem of the second type. At  $b=0$  unplaiting takes place and we get the exactly-solvable Kratzer potential (see e.g. /9/, p.157); it is the generalization of Coulomb problem to non-integer angular momentum.

Other generalization of Coulomb problem is generated by

$$y_2 = a + cr^{-1} + br^{-2}, \quad a > 0, \quad b \leq 0 \quad (21)$$

At  $b=0$  we get the Kratzer potential. It is worth noting, the case  $a=0$  was investigated by E.Korol /10/.

Now, let us give the list of the quasi-exactly-solvable problems of the first type with  $(N+1)$  known states;

$$V = a^2 e^{-2\alpha x} - a[2b + \alpha(2N+1)]e^{-\alpha x} + c(2b - \alpha)e^{\alpha x} + c^2 e^{2\alpha x}$$

$$\Psi = P_N(e^{-\alpha x}) \exp\left\{-\frac{a}{2}e^{-\alpha x} - bx - \frac{c}{2}e^{\alpha x}\right\}$$

$$V = -[a(a+\alpha) + \alpha k(\alpha + \alpha + 2a)]ch^{-2}\alpha x - c(c+2\alpha-2a)ch^2\alpha x + c^2 ch^4\alpha x$$

$$\Psi = P_k(th\alpha x)(ch\alpha x)^{-\alpha/\alpha} \exp\left\{-\frac{c}{4\alpha}ch2\alpha x\right\}$$

$$V = a^2 x^6 + 2abx^4 + [b^2 - (2k+3)a]x^2$$

$$\Psi = P_k(x) \exp\left\{-\frac{ax^4}{4} - \frac{bx^2}{2}\right\}$$

$$V = a^2 r^6 + 2abr^4 + [b^2 - (4N+2l+d+2-2c)a]r^2 + c(c-2l-d+2)r^{-2}$$

$$\Psi = P_N(r^2) r^{l-c} \exp\left(-\frac{ar^4}{4} - \frac{br^2}{2}\right)$$

and the list of the potentials of the second type (the  $i$ -th eigenvalue in the  $i$ -th potential equals  $E_N$ ):

$$V = b^2 r^2 + 2abr - [a(2l+d-1-2c) + \lambda]r^{-1} + c(c-2l-d+2)r^{-2}$$

$$E_N = b(2N+2l+d-2c) - a^2, \quad \Psi = P_N(r) r^{l-c} \exp\left(-\frac{br^2}{2} - ar\right)$$

$$V = b^2 r^{-4} + b(2c-2l-d+3)r^{-3} + [c(c-2l-d+2) + 2ab + \lambda]r^{-2} - a(2N+2l+d-1-2c)r^{-1}$$

$$E_N = -a^2, \quad \Psi = P_N(r) r^{l-c} \exp(-ar + br^{-1})$$

$$V = d^2 e^{-4\alpha x} + 2ade^{-3\alpha x} + (2bd + a^2 + 2\alpha d + 2N\alpha d)e^{-2\alpha x} + (2ab + \alpha a + \lambda)e^{-\alpha x}$$

$$E_N = -b^2, \quad \Psi = P_N(e^{-\alpha x}) \exp\left\{\frac{d}{2\alpha}e^{-2\alpha x} + \frac{a}{2}e^{-\alpha x} - bx\right\}$$

$$V = d^2 e^{4\alpha x} + 2ade^{3\alpha x} + (a^2 + 2bd - \lambda\alpha d)e^{2\alpha x} + (2ab - \alpha a + \lambda)e^{\alpha x}$$

$$E_N = -b^2 - \alpha k(\alpha + 2b), \quad \Psi = P_N(e^{-\alpha x}) \exp\left\{-\frac{d}{2\alpha}e^{2\alpha x} - \frac{a}{2}e^{\alpha x} - bx\right\}$$

$$V = -b^2 ch^6\alpha x + b[2a + 3b + \alpha(2k+3)]ch^{-4}\alpha x - [(a+3b)(a+b+\alpha) + 2k\alpha b + \lambda]ch^{-2}\alpha x$$

$$E_k = -(a+b)^2, \quad \Psi = P_k(th\alpha x)(ch\alpha x)^{-(a+b)/\alpha} \exp\left\{\frac{b}{2\alpha}th^2\alpha x\right\}$$

where  $N = [\frac{N}{2}] + 1$ . The eigenvalues  $E_i$  for (I)-(IV) and the values  $\lambda_i$  for (V)-(IX) (where  $i=1,2,\dots,N+1$ ) come from the roots of certain algebraic equations of the  $N$ -th power. One can prove that there are no potentials with the above properties at  $N > 0$  among polynomials in  $x, (r, r^{-1}), (ch^2 dx, ch^{-2} dx), (e^{dx}, e^{-dx})$ .

6. Generalized Mathieu problem. There is a quasi-exactly-solvable problem with a periodical potential. Let's take

$$y = a \sin dx \tag{22}$$

If  $a=1$ , then

$$V_0 = -a^2 \cos^2 dx - a \cos dx, \quad E_0 = -a^2 \tag{23}$$

for which the ground state is known. It's well-known that there are four types of solutions in a periodical potential: with period  $2\pi/a$  (even and odd) and with period  $4\pi/a$  (even and odd). In these cases per-exponential factor in eq. (2) is  $q(x) p(\cos dx)$ , where  $q(x) = 1, \sin dx, \cos dx/2, \sin dx/2$ , correspondently, and  $p(\cos dx)$  is polynomial in  $\cos dx$ . In general case we get

$$V_N = -a^2 \cos^2 dx - a N \cos dx, \quad \psi(x) = \begin{Bmatrix} 1 \\ \sin dx \\ \cos dx/2 \\ \sin dx/2 \end{Bmatrix} P(\cos dx) e^{-\frac{a}{2} \cos dx} \tag{X}$$

If  $N = 2k + 1$ ,  $k=0,1,\dots$  we know  $(k+1)$ -plaited levels of the first type and  $k$  plaited levels of the second one. If  $N = 2k$ ,  $k=1,2,\dots$ , it is known  $k$  plaited levels of the third type and  $k$  plaited levels of the fourth one. In the limit  $N \rightarrow \infty$  Mathieu potential emerges. Unfortunately, we could not obtain Brillouin zones appearing at non-zero Floke's index.

In a conclusion, it is worth noting that the above quasi-exactly-solvable problems (I)-(X) can be exploited as inputs in Hill determinant method (see e.g. /11/).

### References

1. L. Infeld, T.E. Hull. Rev.Mod.Phys. 23, 21 (1951)
2. C. Bender, T.T. Wu. Phys.Rev. 184, 1231 (1969)
3. B. Simon. Ann.Phys. 58, 76 (1970)
4. P.E. Stanley. Phys.Lett. A117, 161 (1986)
5. A.V. Turbiner. Uspekhi Fiz.Nauk 144, 36 (1984)
6. A.V. Turbiner, M.E. Gershenson. Yad.Fiz. 35, 1437 (1982)
7. A.V. Turbiner, A.G. Ushveridze. Preprint ITEP-55 (1987)
8. P.G.L. Leach. J.Math.Phys. 25, 974 (1984)
9. L.D. Landau, E.M. Lifshitz. "Quantum mechanics", Nauka, Moscow (1974)
10. E.N. Korol. Ukrainian Fiz.Zhurnal 18, 1890 (1973).
11. A. Hautot. Phys.Rev. D33, 437 (1986)

# Results on $^{16}\text{O}$ - and $^{32}\text{S}$ -nucleus collisions from the HELIOS Collaboration

*presented by Luciano Ramello  
Torino University and INFN*

## Introduction

The CERN heavy ion program consists of 6 large experiments and several emulsion exposures, all of which took data with 60 and 200 GeV/A  $^{16}\text{O}$  beams in December 1986 and with 200 GeV/A  $^{32}\text{S}$  beams in October 1987.

Its physics aim is the study of extremely dense, extremely hot nuclear matter over extended volumes. This should provide insight into non-perturbative QCD topics, and possibly lead to the formation of quark-gluon plasma, a macroscopic system of deconfined quarks.

The experiments must be able to handle complicated events with large multiplicity (several hundreds) and large energy deposition (several TeV).

## The HELIOS experimental setup

The components of the HELIOS setup which are relevant for the heavy ion experiment are calorimeters, multiplicity detectors, external spectrometer, muon spectrometer and emulsions. In the following the first three such components will be described in more detail.

### Calorimeters

A set of Uranium/scintillator, Uranium/Copper/scintillator and Iron/scintillator stacks surrounds the target at 120 cm distance (Fig. 1 and Ref. 1). They feature good granularity for  $-0.1 < \eta < 2.9$  and a coarser granularity in the forward region  $\eta > 2.9$  (this section was replaced in 1987 with a much more finely segmented Uranium-liquid Argon calorimeter).

The energy resolution is good, thanks to compensation, from moderate energies (Fig. 2) up to the full oxygen beam energy, where  $\sigma/E$  is 1.9 % (Fig. 3).

The ion beam composition can be clearly seen in the total energy spectrum, which shows very little contamination from breakups of the projectile occurring in the beam line (Fig. 4). These events are rejected by a  $dE/dx$  measurement in the beam counter.

### Multiplicity Detectors

These are finely segmented silicon detectors (400 elements each), located a few cm behind the target (Fig. 5). The ring counter has a geometry specially designed for  $dN/d\eta$  measurement, and provides a total multiplicity trigger. The silicon pad is used for the interaction trigger.

In 1987 the configuration was upgraded and contains now 3 ring counters.

### External spectrometer

A "slit" through the wall calorimeter, at  $0.9 < \eta < 2.0$  and  $3^\circ < \theta < 7^\circ$ , is equipped with momentum measurement, a time-of-flight and a Cherenkov system, forming the external spectrometer (Fig. 6).

Measurements of particle spectra, average  $p_T$  of different kinds of particles, rapidity distributions and 2-particle correlations are provided.

Photons are also measured with the help of a converter, sandwiched between two proportional chambers, which is placed in front of the spectrometer.

### Targets

The standard targets are thin discs (0.1 mm to 1 mm) of various materials (W, Ag, Al in the 1986 run). The same material with different thickness is used to unfold any target-thickness dependence of the measured quantities.

An "active" target, i.e. a drift chamber containing several thin Pt target wires, has also been used in 1987. Its purpose is to minimize (and tag) secondary interactions and still keep a substantial total thickness (4 % of an interaction length for  $^{32}\text{S}$  ions).

A special configuration with a movable emulsion stack is used to collect and measure completely "interesting" events, defined e.g. by high multiplicity or high transverse energy.

The results discussed in the following have been obtained with a set of thin disc targets (Ref. 2).

### What do we expect to observe ?

A generally accepted scenario for the time evolution of the quark-gluon plasma (QGP) is the following:

1. at sufficiently high energy density ( $\epsilon > 2.5 \text{ GeV}/\text{fm}^3$ ) the QGP exists as an ideal gas of massless quarks and gluons, imbedded in a colour-conductive perturbative vacuum
2. as the system cools down, there is a transition to a mixed phase, where deconfined quarks and gluons coexist with "blobs" of physical vacuum, containing hadrons
3. finally, after further expansion and cooling, the system becomes a gas of ordinary hadrons. Statistical QCD simulations predict a very sharp phase transition between QGP and the hadron gas at a temperature around 200 MeV.

The task of current experiments is then threefold:

- 1). demonstrate that a sufficient *initial energy density* has been achieved, at least in some of the collisions

- 2) show that a *thermalized state*, behaving like a fluid rather than a collection of independent particles, has been formed (thermodynamical calculations indicate a transverse expansion)
- 3) find *signatures of QGP* which are not easily affected from final state interactions, such as:
  - a) photons and lepton pairs,
  - b) strangeness production (reflecting the thermodynamical equilibrium of QGP),
  - c) dissolution of resonances ( $\rho$ ,  $J/\psi$ ,  $\psi'$ ) in the colour-conductive QGP.

### HELIOS results

#### Trigger and event selection

The highest energy densities are reached in *central collisions* of nuclei, where most of the nucleons participate to the reaction. Various methods to select central interactions, such as requiring little forward energy (i.e., the projectile is completely destroyed), high transverse energy or high multiplicity, have been found to be equivalent, as illustrated by a  $^{32}\text{S} \rightarrow \text{Ag}(\text{Br})$  central interaction (Fig. 7).

Our main trigger requires high  $E_T$  in the region  $-0.1 < \eta_{lab} < 2.9$ , which contains the highest  $dE_T/d\eta$  point at  $\eta_{lab} \simeq 2.4$ . Four different thresholds are used to cover the full  $E_T$  range. An interaction is required by asking  $\geq 10$  particles in the silicon pad.

Further offline selection consists of:

- i) requiring  $E_{TOT}$  and beam  $dE/dx$  consistent with a single incoming  $^{16}\text{O}$ ,
- ii) rejecting non-target interactions by using silicon pad and ring counter multiplicity,
- iii) subtracting the remaining non-target contamination, which is  $\leq 1\%$  at  $E_T > 50$  GeV, by using empty target data.

#### Energy flow

The measured  $E_T$  is related to the true  $E_T$  via a detailed Monte Carlo simulation, which uses realistic assumptions about particle composition and energy flow in  $\eta$ . The  $E_T$  resolution is found to be  $\sigma = 29\% \sqrt{E_T}$  ( $E_T$  in GeV), and the total systematic error on the  $E_T$  scale is 7.1%, of which 5.1% comes from the M.C. correction and 4% from the overall energy calibration uncertainty.

$E_T$  cross sections for 60 GeV/A and 200 GeV/A  $^{16}\text{O}$  on W, Ag and Al targets have been measured (Fig. 8). Values of  $E_T$  in the trigger region up to 200 GeV have been reached, which correspond to 280 GeV when the forward  $\eta$  region is included.

The kinematic limit for  $E_T$  can be evaluated assuming full stopping of the projectile and an isotropic distribution of the available energy in the center-of-mass system. For a central  $^{16}\text{O}$ -W collision at 200 GeV/A about 50 target nucleons participate,

$\sqrt{s}$  is 550 GeV and  $E_T^{max}$  is  $\pi/4 \times (\sqrt{s} - 66M_N) = 383$  GeV. The maximum observed  $E_T$  is then 73 % of the kinematic limit.

A simple geometrical scheme explains the shape of  $d\sigma/dE_T$  as a superposition of collisions with random impact parameter. A *geometrical model* (Ref. 3), postulating  $E_T$  production from  $N$  independent nucleon-nucleon collisions, with  $N$  given by the overlap integral of the nucleon densities, reproduces fairly well our data (Fig. 8).

The  $dE_T/d\eta$  distributions for the two beam energies, and for three  $E_T$  regions corresponding to the plateau of  $d\sigma/dE_T$ , to central collisions (defined as the  $E_T$  where the cross section is half the plateau value) and to the extreme tail, are shown in Fig. 9.

As  $E_T$  approaches the kinematical limit, the  $dE_T/d\eta$  distribution gets narrower, as would be expected from a spherical fireball in the center-of-mass system.

An estimate of the *energy density* can be done in the following way. The average  $^{16}\text{O}-\text{W}$  central collision involves 16 projectile and 50 target nucleons, in a cylindrical volume of  $\pi R_O^2 \times 2R_W \approx 320 \text{ fm}^3$ . In the "16+50" center-of-mass system the effective volume (contracted by a Lorentz factor  $\gamma_{cm}$  of 5.8) is  $55 \text{ fm}^3$ . The energy density is then  $\epsilon \approx E_T/V = 3.6 \text{ GeV/fm}^3$ , or alternatively, using the Bjorken model,  $\epsilon \approx (dE_T/d\eta)^{max}/(\pi R_O^2 c\tau) = 3.5 \text{ GeV/fm}^3$ .

This energy density is possibly over threshold for QGP formation, and certainly well above nuclear density (0.13) and hadronic density (0.5). A preliminary  $d\sigma/dE_T$  distribution for  $^{32}\text{S}-\text{W}$  collisions is shown in Fig. 10, reaching still higher  $E_T$ .

A comparison of our data with *absolute* predictions from the dual parton model IRIS (Ref. 4), whose parameters have been adjusted to fit pp and  $e^+e^-$  data, shows that the model qualitatively reproduces the  $d\sigma/dE_T$  (Fig. 11) but is systematically lower than data in the high  $E_T$  tail. However, it has to be noted that the  $E_T$  systematics is still  $\approx 10\%$ , and furthermore the model does not include cascading of hadrons in the nucleus, which could be important at backwards  $\eta$ . There is a good agreement between the IRIS prediction and the measured  $dE_T/d\eta$  distribution (Fig. 12).

### Multiplicity and particle spectra

A preliminary charged multiplicity distribution, measured with the ring counter and the silicon pad in the range  $0.9 < \eta < 5.0$ , is shown in Fig. 13. The general behaviour of  $d\sigma/dN_{ch}$  is similar to  $d\sigma/dE_T$ , with a plateau followed by a fall-off at high multiplicities, and similar geometrical considerations apply here.

The multiplicity flow ( $dN_{ch}/d\eta$ ) shows a shift towards lower  $\eta$  as  $E_T$ , and therefore the degree of "centrality" of the collision, is increased.

An estimate of the average  $p_T$  is given by  $\langle p_T \rangle \approx 0.55 E_T/N_{ch}$  for charged particles, where  $E_T$  and  $N_{ch}$  are measured in the same solid angle. The data show (Fig. 14) only a modest increase of  $\langle p_T \rangle$  as a function of  $E_T$  (one would expect a sudden rise above some threshold energy density, as in the JACEE collaboration events).



Charged-particle  $p_T$  spectra have been measured by the external spectrometer in the range  $1.0 < \eta < 2.0$ , both with p and  $^{16}\text{O}$  projectiles. The negative particle spectra show little difference between p and  $^{16}\text{O}$  (Fig. 15), although one might see an increase of the ratio  $^{16}\text{O}/\text{p}$  with increasing  $p_T$ .

There is a little but statistically significant increase of the  $\langle p_T \rangle$  of positive particles with  $E_T$  (Fig. 16). The photon  $p_T$  spectra (Fig. 17) do not show significant differences in slope between the p and  $^{16}\text{O}$  reactions.

### Figure captions

1. Layout of the calorimeters.
2. Energy resolution.
3. Measured total energy for identified  $^{16}\text{O}$  events.
4. Total energy spectrum for all events.
5. Multiplicity detectors.
6. External spectrometer.
7. A  $^{32}\text{S}-\text{Ag}(\text{Br})$  central collision at 200 GeV/A.
8.  $d\sigma/dE_T$  for 60 and 200 GeV/A  $^{16}\text{O}$ -nucleus collisions. The curves are a geometrical model fit to the data.
9. Normalized  $dE_T/d\eta$  distributions.
10. Preliminary  $d\sigma/dE_T$  for 200 GeV/A  $^{32}\text{S}-\text{W}$  collisions (1987 data) compared to that for  $^{16}\text{O}-\text{W}$  collisions (1986 data).
11.  $d\sigma/dE_T$  for 200 GeV/A  $^{16}\text{O}$  compared to the IRIS model.
12.  $dE_T/d\eta$  compared to the IRIS model.
13. Preliminary  $d\sigma/dN_{ch}$  for 200 GeV/A  $^{16}\text{O}-\text{W}$  collisions.
14. Preliminary  $\langle p_T \rangle$  of charged particles vs.  $E_T$  for 200 GeV/A  $^{16}\text{O}-\text{W}$  collisions.
15. Preliminary  $p_T$  spectra of negative particles for p-W and  $^{16}\text{O}-\text{W}$  collisions.
16. Preliminary  $\langle p_T \rangle$  of positive and negative particles for  $^{16}\text{O}-\text{W}$  collisions.
17. Preliminary  $p_T$  spectra of photons produced in p-W and  $^{16}\text{O}-\text{W}$  collisions.

### References

1. T. Akesson *et al.*, preprint CERN-EP/87-111, 24 June 1987, submitted to Nucl. Instr. Methods
2. T. Akesson *et al.*, preprint CERN-EP/87-176, 29 September 1987, submitted to Z. Phys. C
3. A.D. Jackson and H. Bøggild, Nucl. Phys. **A470** (1987) 669
4. J.P. Pansart, Nucl. Phys. **A461** (1987) 521c

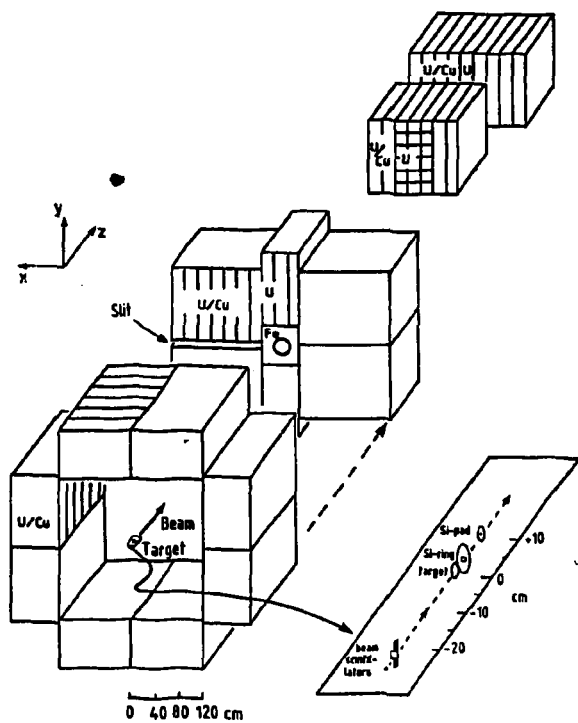


Fig. 1

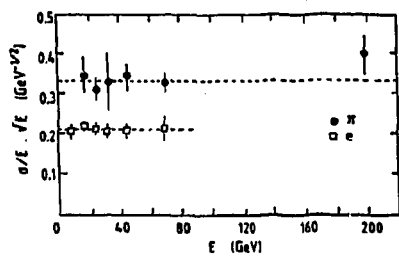


Fig. 2

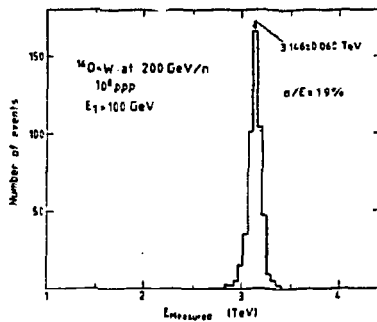


Fig. 3

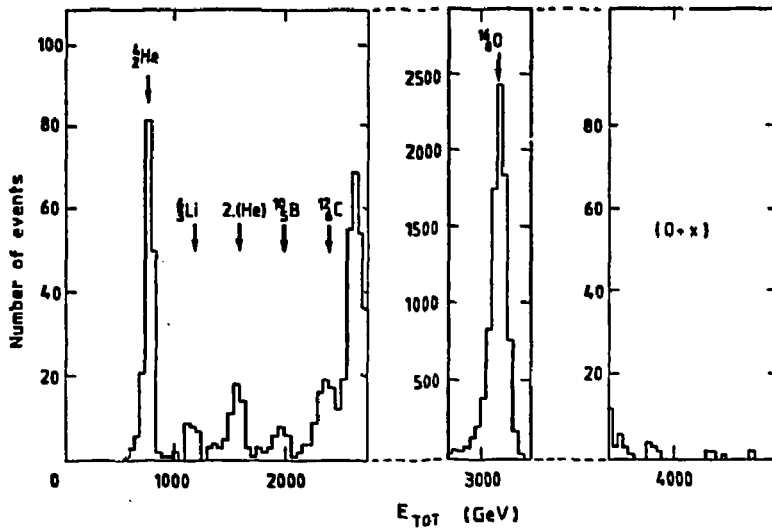


Fig. 4

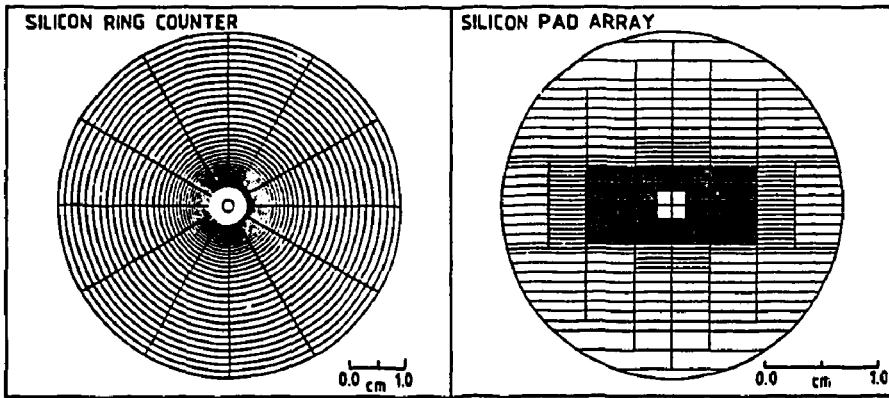


Fig. 5

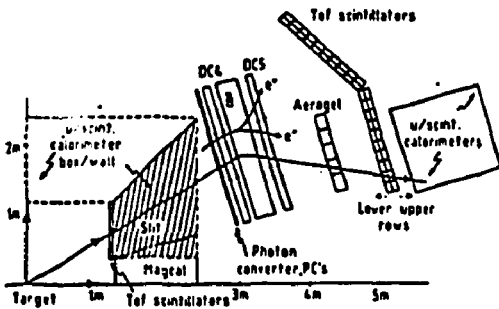


Fig. 6

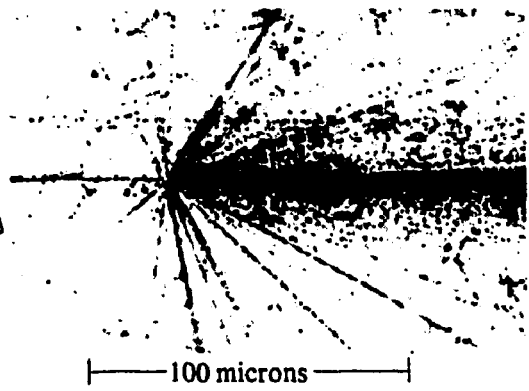


Fig. 7

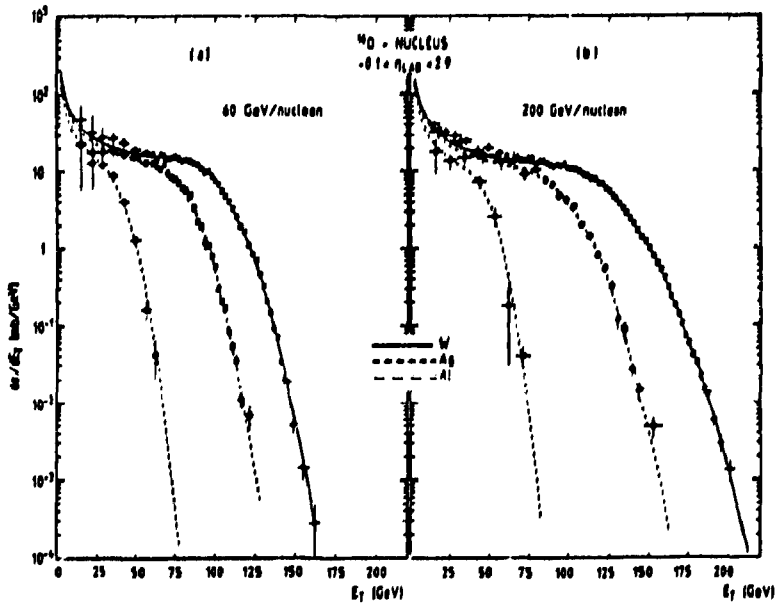


Fig. 8

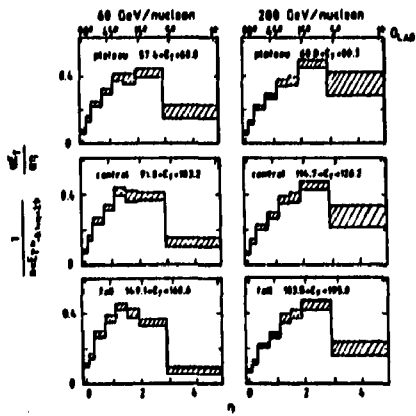


Fig. 9

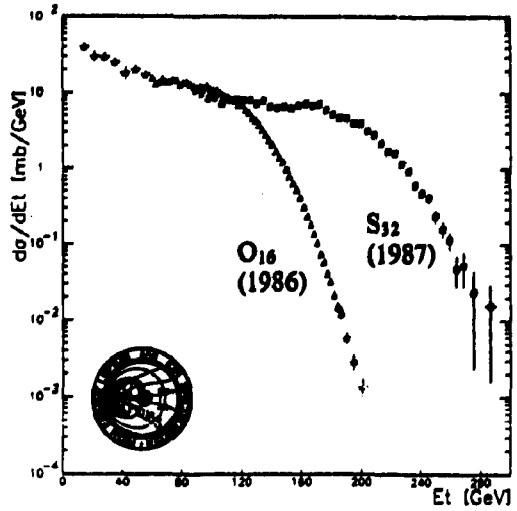


Fig. 10

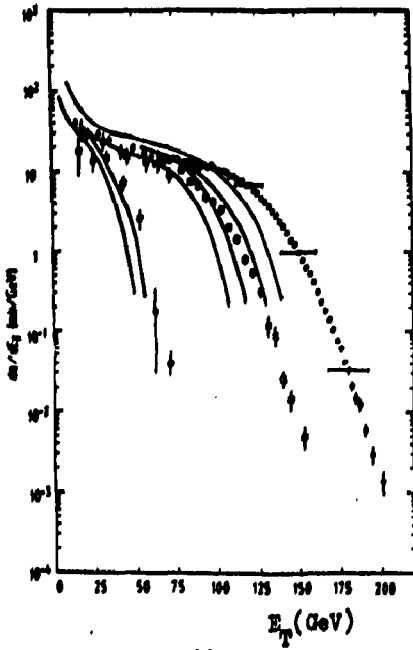


Fig. 11

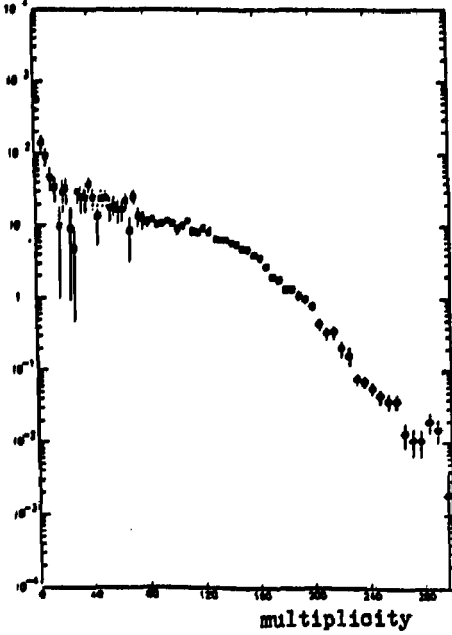


Fig. 13

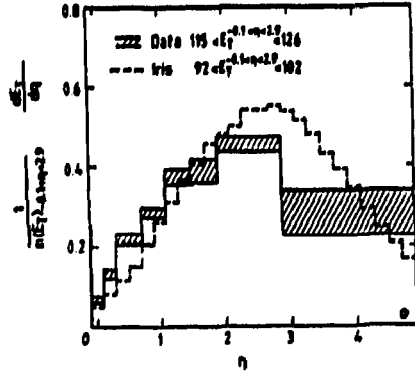


Fig. 12

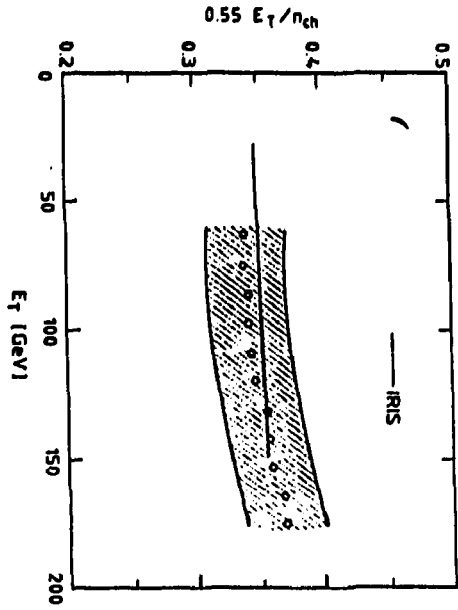


Fig. 14

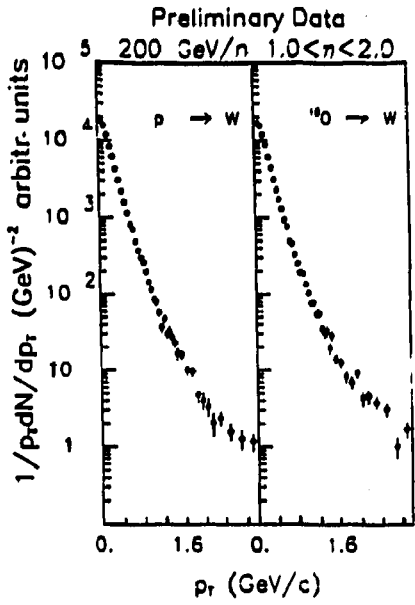


Fig. 15

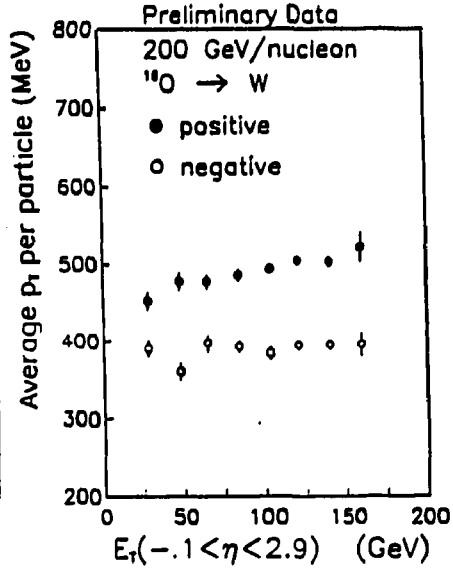


Fig. 16

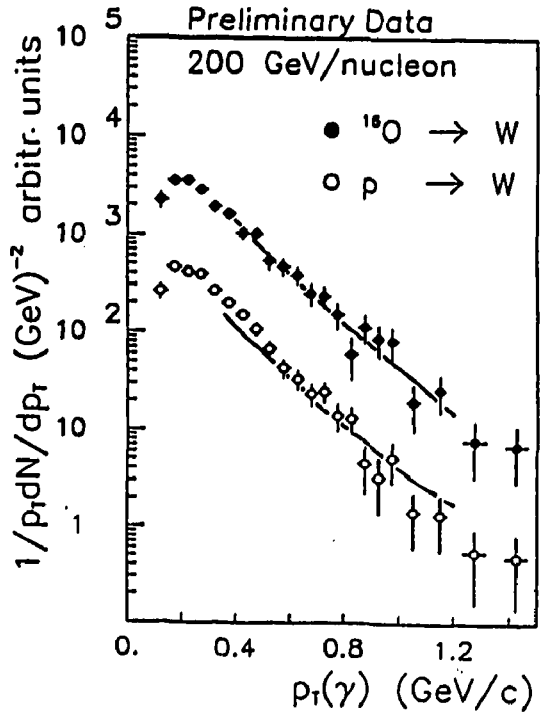


Fig. 17

SPACE-TIME EVOLUTION OF PROTON-PROTON, PROTON-NUCLEUS AND  
NUCLEUS-NUCLEUS COLLISIONS AND THE DILEPTON PRODUCTION

N. Pišútová<sup>2)</sup> and J. Pišút<sup>1)</sup>

<sup>1)</sup> Department of Theoretical Physics, Comenius University,  
842 15 Bratislava, Czechoslovakia

<sup>2)</sup> Department of Nuclear Physics, Comenius University

A review of our recent calculations of dilepton production in pp, pA and AB collisions, performed partly in collaboration with J. Ftáčnik and P. Lichard is presented. The emphasis is put upon the connection between the space-time evolution of the collision and dilepton production. We discuss also less understood aspects of the problem and try to point out possible ways to separate signatures of the quark-gluon plasma from other, more prosaic, mechanisms of the dilepton production.

Space-time evolution of pp collision and the dilepton production.

The picture of the space-time evolution of hadronic collisions within the framework of the parton model has been described in classic papers by Bjorken [1] and V. Gribov [2]. The amendments taking into account the QCD are discussed in Ref. [3]. For a proton-proton collision considered in the c.m.s. the production of secondary hadrons proceeds via the inside-outside cascade consistent with the boost invariance of the process. At the moment of collision wee partons of both protons interact and this spoils the coherence of wave functions of both protons. After time  $\tau_c$  the coherence is lost and current quarks ( $q$ 's), antiquarks ( $\bar{q}$ 's) and gluons ( $g$ 's) start their transformation to final state hadrons. Details of this

transition are unknown, since the process is governed by QCD at low momentum transfer. One of the possibilities [4,5] proceeds as follows.

The gluons are converted in time  $\tau_1$  into pairs of quarks and antiquarks which dress themselves into constituent quarks (Q's) and antiquarks ( $\bar{Q}$ 's) and recombine to mesons in time  $\tau_2$ . The time order is given below

- $\tau_1$  - coherence of  $q, \bar{q}, g$  lost
- $\tau_2$  - gluons convert to current quarks and antiquarks, which change to constituent quarks
- $\tau_3$  - constituent quarks and antiquarks recombine to mesons.

All this happens in the proper time (at  $y^* = 0$  in the c.m.s.). Due to the Lorentz invariance of the space-time evolution the same sequence of events happens at any rapidity at the same proper time. The "co-moving" or "space-time" rapidity  $\eta$  is defined as

$$\eta = \frac{1}{2} \ln \frac{t+x}{t-x} \quad (2)$$

where  $x$  is the longitudinal distance from the point of the pp collision in the c.m.s. The proper time  $\tau$  is related to  $t$  and  $x$  by the standard relation

$$\tau = \sqrt{t^2 - x^2} \quad (3)$$

From (1) and (2) we obtain useful formulae

$$t = \tau \operatorname{ch} \eta, \quad x = \tau \operatorname{sh} \eta$$

Lines corresponding to a fixed value of  $\eta$  are given as

$$x/t = \operatorname{th} \eta$$

The space-time evolution of the pp collision is shown in Fig.1.



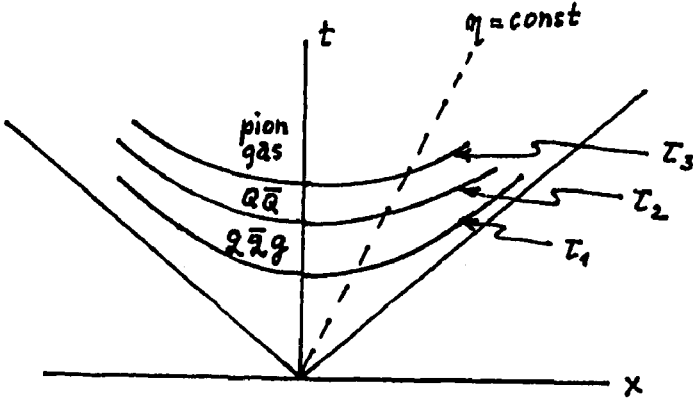


Fig.1

The three regions denoted as "q $\bar{q}$ g", "Q $\bar{Q}$ " and "pion gas" correspond respectively to the system of current q's,  $\bar{q}$ 's and gluons, constituent Q's and  $\bar{Q}$ 's before the recombination and pion gas.

As mentioned above the picture is rather uncertain in details, it is e.g. not clear whether the current quarks are not dressed into the constituent ones only after pions has been formed.

An interesting and perhaps important fact noted in [4,5] is that the number of current quarks and antiquarks obtained after the conversion of gluons from the incident protons is roughly the same as is the number of constituent quarks and antiquarks present in final state pions. This indicates that the density of constituent quarks in the "Q $\bar{Q}$ " stage is about the same as the number of final state pions

$$\frac{dN_Q}{dy} = \frac{dN_{\bar{Q}}}{dy} = \frac{dN_{\pi}}{dy} \quad (4)$$

In discussing the dilepton production we have to discriminate between two mechanisms. The former produces dileptons from interaction of constituents created during the space-time evolution of the collision [4,5] and contributes predominantly to low mass,  $M < 1$  GeV, dileptons. The latter is a fast process occurring at the moment of the collision and contributes mainly to large mass dileptons. A typical representant of this process is the Drell-Yan annihilation  $q\bar{q} \rightarrow e^+e^-$ .

We shall start with discussing the former process. At any value of  $\eta$  all of the three stages namely  $q\bar{q}g$ ,  $Q\bar{Q}$ , and pion gas can contribute to the low mass dilepton production via diagrams shown in Fig.2.

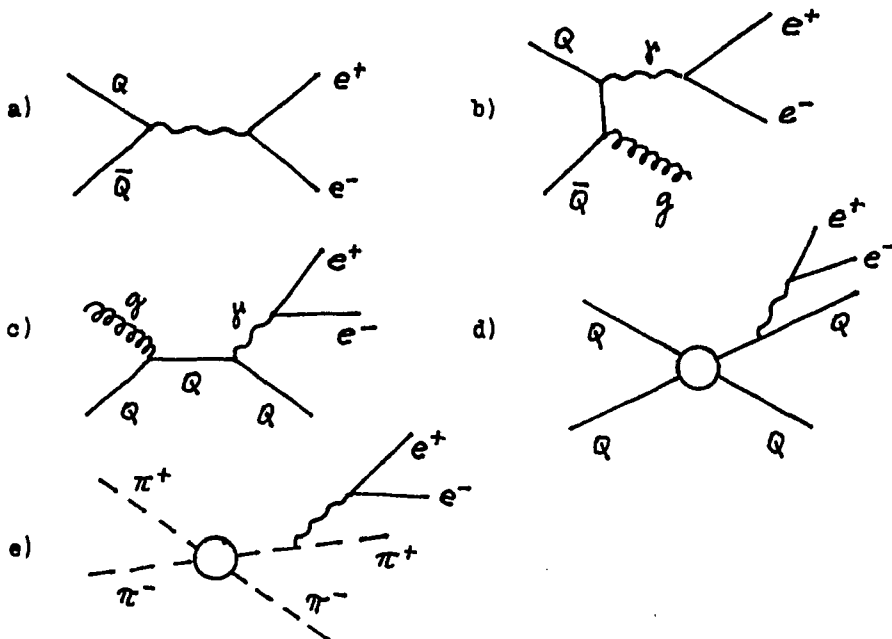


Fig.2 Some of possible subprocesses contributing to  $e^+e^-$  production during the space-time evolution of pp collision.

Some information about the relative importance of various subprocesses can be obtained from the data on  $d\sigma/dM^2$  obtained in numerous experiments, in particular by the AFS collabora-

tion at CERN. Such an analysis has not been performed so far, but it is most desirable.

As pointed out in Ref.[5] interactions of constituents created during the collision yield only low mass dileptons. At any value of time  $t$ , the constituents are "excited" only in a specified region of co-moving rapidity  $\eta$ . This can be seen from Fig.3 where we plot the line  $t=\text{const}$  and two lines  $\eta_1$  and  $\eta_2$  corresponding to the "Q $\bar{Q}$ " region excited at this time.

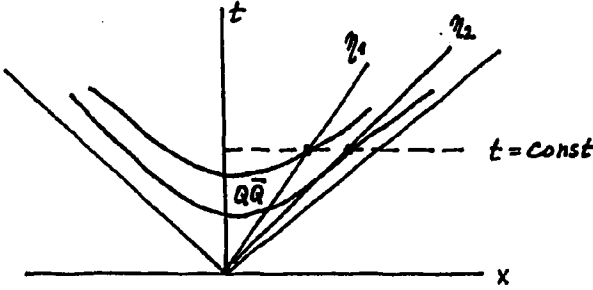


Fig.3

The interaction of constituents with a small rapidity difference can produce only low mass dileptons. To see this in more detail, suppose that  $\rho(t, x, p_{\parallel}, p_{\perp})$  denotes the excitation intensity of constituents with  $p_{\parallel}$  and  $p_{\perp}$  in the space-time region  $x, t$ . The excitation function can be rewritten into variables  $\tau, \eta$  and  $y = (1/2)\ln[(E+p_{\parallel})/(E-p_{\parallel})]$  and  $p_{\perp}$ . Because of the Lorentz invariance the excitation function can depend only on  $\tau, y-\eta$  and  $p_{\perp}$ :  $\rho = \rho(\tau, y-\eta, p_{\perp})$ . The dilepton yield is proportional to the integral of the product

$$\int \rho(\tau, y_1 - \eta, p_{\perp 1}) \int \bar{\rho}(\tau, y_2 - \eta, p_{\perp 2}) \text{ over } dx dt = \tau d\tau d\eta$$

At any value of  $\eta$  only interactions with a small rapidity difference  $y_1 - y_2$  are possible and these give only low mass dileptons.

The calculations in the soft annihilation model are very similar to quark-gluon plasma calculations in what con-

cerns the Lorentz invariance of the space-time evolution, the difference is in the density of excitation which is taken from the thermal equilibrium in one case and from the density of final state pions in another case.

We have to stress further that by using diagrams like those in Fig.2 for constituents separated by a small rapidity gap we can obtain only a rough estimate of the dilepton yield, since we are, in fact, using perturbative arguments in the region where perturbative expansion is not applicable.

This implies also that more general statements, independent of detailed properties of various diagrams, are probably of more value than specific results. A general statement of this kind concerns the dependence of low mass dilepton production on the rapidity density of produced pions [6]. The argument is simple. Assume that the  $Q\bar{Q}$  stage dominates the low mass dilepton production. The dilepton yield is proportional to the product  $(dN_Q/dy) \cdot (dN_{\bar{Q}}/dy)$ . Because of Eq.(4) this product is proportional to  $(dN_T/dy)^2$ . This quadratic dependence has been recently observed by the AFS collaboration [7,8]. It is interesting to note that the same quadratic dependence is predicted also by the model with quark-gluon plasma formation [9]. The constant in front of the quadratic dependence is, of course, different [10] and with increasing pion multiplicity one expects the transition between the two different quadratic dependences [11].

The available soft annihilation model [5,12] of low mass dilepton production takes into account only the  $Q\bar{Q}$  stage of the evolution of the collision and includes only diagrams 2a) and 2b).

The state of matter from which low mass dileptons were produced in pp collisions is not yet known, it can be somewhat elucidated by

- studying the shape of  $d\sigma/dM_{e^+e^-}$  spectrum and looking for subprocesses which might give agreement with the data. The soft annihilation model [5,12] should be extended to include also the diagram 2d) in the  $Q\bar{Q}$  stage and other diagrams in other stages of the evolution.

- The soft annihilation model should be reformulated in a way as close as possible to the thermal equilibrium models.
- Comparing detailed models of the space-time evolution of the pp collision with data extending to as high as possible  $dN_T/dy$ .

The trouble with pp collisions lies in the fact that the evolution is rather short. The transverse dimension of the system is about 1 fm and because of that the whole time of the evolution is only 1 fm/c. Still, observation and theoretical understanding of a change of the slope of the quadratic dependence would bring an important information.

Large mass dileptons ( $M > 1-2$  GeV) are produced almost exclusively by the Drell-Yan process which is much better understood than the mechanism of low mass dilepton production. Any excess of the large mass dilepton production over the Drell-Yan contribution would be an indication of high temperatures reached during the collision. Such an excess should be also proportional to the square of  $dN_T/dy$ :

- a more detailed studies of correlations between  $dN_T/dy$  and large mass dileptons are desirable both from experimental and theoretical side.

#### Space-time evolution of proton-nucleus collision and the dilepton production

The soft annihilation model described above is a preequilibrium model, the plasma is not formed because the excited system exists only during a time interval of about 1 fm/c. In proton-nucleus collisions higher energy densities can be formed and with higher densities of constituents the mean free path becomes smaller and the time over which the excitation exists could increase.

The basic question is whether the energy released in subsequent collisions of the incident protons with nucleons in the nucleus can be accumulated in the same space-time region. To introduce the problem consider the proton-deuteron collision in the rest frame of the deuteron (Fig.4) in

the configuration when proton collides with both nucleons. The first collision occurs at  $x=0, t=0$  the second one at  $x=d$

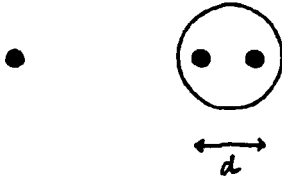


Fig.4

and  $t=d/v$ , where  $v$  is the velocity of the incident proton.

The space-time evolution of both collisions is shown in Fig.5. The two excitation functions can be described as

$$\begin{aligned} \rho_1(x, t, P_H, P_T) &= \rho_1(\tau, y-\eta, P_T) \\ \rho_2(x, t, P_H, P_T) &= \rho_2(\tau', y-\eta', P_T) \end{aligned} \quad (5)$$

where

$$\tau' = \sqrt{\left(t - \frac{d}{v}\right)^2 - (x-d)^2}, \quad \eta' = \frac{1}{2} \ln \frac{(t-d/v) + (x-d)}{(t-d/v) - (x-d)}$$

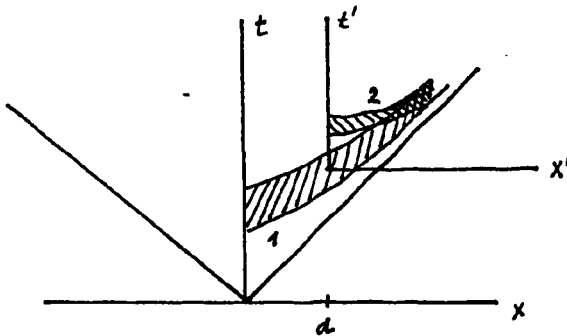


Fig.4. The excitation region of the first (1) and second (2) proton-nucleon collision

As seen in Fig.5 both excitation regions overlap for larger rapidities. This is also natural. If the collision is considered in the proton-nucleon c.m.s. the nucleus is Lorentz contracted to a pancake with width of 1 fm (due to wee partons) and the centres of both nucleons are separated by a small  $\Delta x$ . So for rapidities near  $y^* = 0$  we can expect a more or less complete overlap of the excited regions, whereas in the nucleus fragmentation region the overlap will be small.

The low mass dilepton production is given by the total quark and antiquark densities

$$\rho(t, x, p_q, p_T) = \rho_1(t, x, p_q, p_T) + \rho_2(t, x, p_q, p_T)$$

which enters the expression

$$n_{e^+e^-} = \int \rho_q \rho_{\bar{q}} v \delta(QQ \rightarrow e^+e^- + X) dV dt \quad (6)$$

With a complete overlap in the central rapidity region we expect qualitatively

$$n_{e^+e^-}^{pd} = 4 n_{e^+e^-}^{pp} \sim \left( \frac{dN^{pd}}{dy} \right)^2 \quad (7)$$

and for no overlap in the deuteron fragmentation region

$$n_{e^+e^-}^{pd} = 2 n_{e^+e^-}^{pp} \sim \frac{1}{2} \left( \frac{dN^{pd}}{dy} \right)^2 \quad (8)$$

The difference between (7) and (8) is due to the fact that, in the former case  $\rho_q \rho_{\bar{q}}$  in Eq.(6) is effectively equal to  $4 \rho_1 \rho_1$ , whereas in the latter case it is equal to  $\rho_1 \rho_1 + \rho_2 \rho_2 = 2 \rho_1 \rho_1$ .

For collisions of a pion with heavier nuclei we argue in the same way. In the central rapidity region the density of excitation is the sum of all densities produced in subsequent proton-nucleon collisions. In this way we have

$$n^{e^+e^-} \sim (\beta_1 + \beta_2 + \dots + \beta_m)^2 \sim \left( \frac{dN_\pi}{dy} \right)^2 \sim E_T^2 \quad (9)$$

where  $dN_\pi/dy$  is the total rapidity density of pions in the final state. Assuming that each of pions has about the same transverse energy  $E_T$  (per pion)  $\sim 0.5$  GeV we have also  $dN_\pi/dy \sim E_T$  and this gives the last term in Eq.(9).

More details can be found in the recent CERN preprint by Peter Lichard [13] and in Ref. [14].

- A really deep analysis would probably require an ansatz on the form of the excitation function containing a few free parameters, determination of these parameters from low mass dilepton production in collisions of protons with lighter nuclei and analysis of interactions of protons with heavier nuclei using these parameters. Such calculations has not been attempted so far.

- The production of large mass dileptons is given by the Drell-Yan mechanism. This process is fast and occurs prior to the space-time evolution of the collision. The cross-section for the Drell-Yan production in proton-nucleus collisions is proportional to the number of proton-nucleon collision and that means roughly proportional to the transverse energy released in a specified rapidity window in the central region. Detailed calculations of this correlation has not been performed so far. Apart of understanding how the incident proton releases transverse energy in subsequent collisions with nucleon, it would also require understanding of the mechanism of fluctuations of energy released in individual proton-nucleon collisions.

#### space-time evolution of nucleus-nucleus collisions and the dilepton production

In ion-ion collision, especially with heavy ions, the quark-gluon plasma may be formed and the dilepton production is one of the most promising signatures of its formation.



The transition from the quark-gluon plasma to pion gas is not yet well understood. The most popular, though very simplified model used the idea of the first order transition: at sufficiently high energy density the QGP is formed, during its expansion the temperature and energy density of the QGP decreases and the mixed phase (of QGP and pion gas) is formed, finally, when the temperature decreases below  $T_C$  the whole mixed phase goes into the pion gas [10,15].

Another option proposed [16] and advocated by Shuryak [17] assumes that the transition goes in two steps. In the first one the QGP goes (via a mixed phase) into the gas of constituent quarks and in the second step this goes (again via a mixed phase) into the pion gas. Note that the latter scenario is closed to the soft annihilation model, at least so far, as the energy density is just sufficient to produce the constituent quark gas with energy slightly above  $T_C$ . In the proton-proton collision small transverse dimensions of the system prevent longer existence of the gas of constituent quarks, whereas in heavy ion collision the system can live for time which is sufficient for the properties of the system to be manifested.

The data on production of both low mass and large mass dileptons produced in  $^{16}\text{O-U}$  and  $^{32}\text{S-U}$  interactions will soon become available from the NA-38 collaboration [18] at CERN. The first basic information to be obtained from these data concerns the question whether there is any other source of dileptons different from what one would expect if a heavy ion collision were a simple sum of nucleon-nucleon collisions.

We shall now describe our predictions for this minimal dilepton production.

For low mass dilepton production in the central rapidity region we consider the collision in the nucleon-nucleon c.m.s. Both nuclei are Lorentz contracted to pancakes with a longitudinal dimension of about 1 fm. The transverse area of the nuclei is divided into small areas of  $\Delta S = \sigma$  where  $\sigma$  is the nucleon-nucleon cross-section; behind each of these areas there is a "tube" containing  $m_1$  nucleons in  $^{16}\text{O}$

and  $n_1$  nucleons in  $^{238}\text{U}$ . The  $i$ -th tube thus leads to  $m_1 n_1$  nucleon-nucleon collisions (see Fig.6). Assuming that in each of the nucleon-nucleon collisions the same amount of constituent quarks is produced as in a  $pp$  collision and assuming that in each collision only the soft annihilation mechanism works we find that the number of low mass  $e^+e^-$  pairs produ-

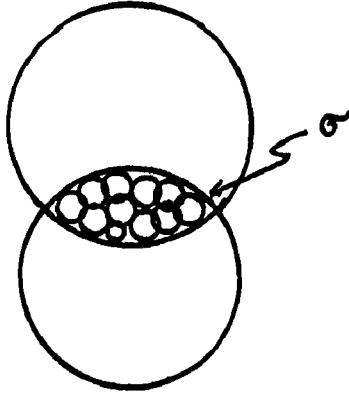


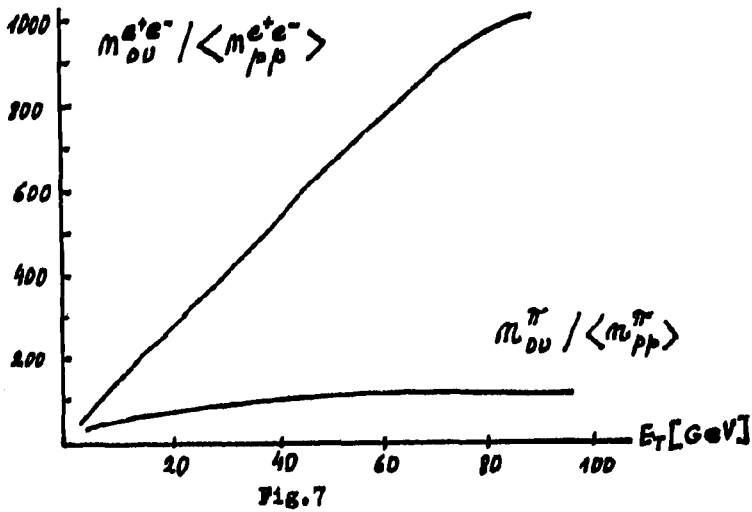
Fig.6

ced in a collision at a given impact parameter  $b$  is

$$n^{e^+e^-}(b) \approx \sum_{\text{tubes}} \sum_{m_1 n_1} (m_1 n_1)^2 P_A(n_1) P_B(m_1) \langle n_{pp}^{e^+e^-} \rangle \quad (10)$$

where  $P_A(n_1)$  is the probability to find  $n_1$  nucleons in the  $i$ -th tube in the  $A$ -nucleus,  $P_B(m_1)$  denotes the same for  $B$ -nucleus and  $\langle n_{pp}^{e^+e^-} \rangle$  is the  $e^+e^-$  production in proton-proton collision. It is easy to calculate also the transverse energy released at a given value of  $b$  and plot the dependence of the  $e^+e^-$  production versus  $E_T$  in a given rapidity window. Values of  $n_{OU}^{e^+e^-} / \langle n_{pp}^{e^+e^-} \rangle$  are plotted versus  $E_T$  released in a central rapidity region of length  $\Delta y = 2$  in Fig.7.

We plot also the average multiplicity of pions at a given value of the transverse energy. It is seen that the



ratio of  $e^+e^-/\pi^+$  is about 10 times as high as in an average pp collision. The number of  $e^+e^-$  pairs is also seen to be roughly proportional to  $E_T$  up to the highest values of  $E_T$ . More details can be found in Ref. [14].

It is <sup>to be</sup> stressed that this is the minimal rate of the low mass lepton pair production, any further increase would be due to some collective effects, most probably thermalization of excitations of neighbouring tubes and this would be the way to plasma formation. If such an excess is observed, its further study may hopefully lead to understanding also the type of the thermalized matter.

The minimal large mass dilepton production has been studied in Ref. [15]. We have assumed that the  $^{16}\text{O-U}$  collision can be viewed as a sum of nucleon-nucleon collisions and that in each of these collisions the Drell-Yan mechanism is the only source of large mass dileptons. Each of nucleon-nucleon collisions is also assumed to contribute to a specified rapidity window in the central region about the same amount of transverse energy. This leads to the linear dependence of the large mass dilepton production on the total transverse energy. We understand that the results con-

tained in Refs. [14,19] should be considered as preliminary qualitative studies and that more detailed calculations including

- energy losses in subsequent nucleon-nucleon collisions
  - estimates of possible contributions from plasma formation
  - specific calculations taking into account realistic conditions in the NA-38 experiment
- should be performed.

We are indebted to J.Ftáčnik and P.Lichard for collaboration on these topics and to V.Černý, A.Nogová, O.Pavlenko, C.Fabjan, E.Levin, M.Ryskin and K.Kajantie for discussions and correspondence.

### References

- [1] J.D.Bjorken, Current Induced Reactions, Lecture Notes in Physics, Vol.56, p.93, Springer Verlag 1976, ed.J.Körner, G.Kramer and D.Schildknecht, and Proc.of the Summer Institute on Particle Physics, SLAC-Report-167(1973), ed.M.Zipf.
- [2] V.N.Gribov, Elementary Particles, Vol.I., p.65, First ITEP School on Theoretical Physics, Atomizdat, Moscow 1973.
- [3] L.V.Gribov, E.M.Levin and M.G.Ryskin, Phys.Reports 100 (1983)1.
- [4] J.D.Bjorken and H.Weisberg, Phys.Rev. D13(1976)1405.
- [5] V.Černý, P.Lichard and J.Pišút, Acta Phys.Pol. B9(1978)901.
- [6] V.Černý, P.Lichard and J.Pišút, Zeit.f.Phys. C31(1986)163.
- [7] T.Akesson et al., Phys.Lett. B122(1987)463.
- [8] V.Hedberg, Production of positrons with low  $p_T$  and low mass  $e^+e^-$  pairs in pp collisions at a c.m.s. energy of 63 GeV, Thesis, University of Lund, LUNDFD6/(NFFL-7037)/1987.
- [9] R.Hwa and K.Kajantie, Phys.Rev. D32(1985)1109.
- [10] M.I.Gorenstein and O.P.Pavlenko: Correlations between dilepton emission and hadronic multiplicity in ultrarelativistic nuclear collisions as the signal of deconfinement phase transition, Kiev preprint, ITP-87-3E.

- [11] O.P.Pavlenko and J.Pišút, Low  $p_T$  lept n and low mass dilepton production in pp collisions as signatures of thermalization of hadronic matter. Bratislava preprint 1987.
- [12] V.Černý, P.Lichard and J.Pišút, Phys.Rev.D24(1981)652.
- [13] P.Lichard, Non-plasma approach to the soft dilepton production in hA and AA interactions, CERN-TH-4805/87, to be published in Zeit.f.Phys.C.
- [14] N.Pišútová and J.Pišút, Low mass dilepton production in heavy ion collisions - a signature of the onset of plasma formation, Bratislava preprint, Sept.1987.
- [15] B.L.Friman, K.Kajantie, P.V.Ruuskanen, Converting mixed phase into hadrons, Helsinki preprint, HU-TFT-85-21.
- [16] E.V.Shuryak, Non-perturbative phenomena in QCD vacuum,... CERN yellow 83-01.
- [17] E.V.Shuryak, Phys.Lett. 72B,477(1978).
- [18] A.Haratounian, Talk presented at this meeting.
- [19] J.Ptáček, M.Mojžiš and J.Pišút, Phys.Lett.196B(1987)387.

NEW REALIZATION OF THE HADRON-HADRON, HADRON-NUCLEUS  
AND NUCLEUS-NUCLEUS FRAGMENTATION MODEL

S.Yu. Shmakov, V.V. Uzhinski

Joint Institute for Nuclear Research, Dubna, USSR

Abstract

A new Monte-Carlo realization of the dual parton model is suggested. The code takes into account high and low mass diffraction dissociation processes, transverse momenta of quarks, Fermi-motion of nuclear nucleons. The code operation results in an exclusive state satisfying the energy-momentum, baryonic and electric charges, strangeness etc. conservation laws.

Authors of Monte-Carlo codes realizing the main assumptions of the dual parton model <sup>/1/</sup> must solve the following problems

1. How to avoid the low mass string creation.
2. How to describe the decay of hadrons into quark subsystems.
3. How to satisfy the energy-momentum conservation law, especially in the case of hadron-nucleus and nucleus-nucleus interactions.

Since questions like this arise in different approaches at the description of various reactions, we think it reasonable to give a solution we used when developing the new realization of the dual parton model.

The main idea we were guided with was the uncertainty principle according to which mass, energy of particles, strings etc. can't be determined with an accuracy  $\Delta M \sim \hbar/\tau$  during the time interaction  $\tau$ . So, at the interactions time  $\tau$  one can "ascribe" masses different from the table ones to initial hadrons. Besides, during this time one may not worry about low mass string creation. What matters is all final hadrons were on the mass shell. To consider the main features of the algorithm realizing this ideas let us take a simple

example, namely the diffraction dissociation of hadrons to the low mass states, e.g. in nucleon-nucleon interactions.

In the Born approximation of QCD the diffraction dissociation process is described by a set of graphs (fig. 1). Let us suppose that the creation and decay of the string are the final state interactions. Then at the intermediate stage we have a system: the baryon, the quark and the diquark of the dissociating hadron. Due to the energy-momentum conservation law an exclusive state of this system is completely characterized by one independent kinematic variable  $x$ , the transverse momenta neglected. Let this variable ratio of the longitudinal quark momentum to the sum of the quark and diquark longitudinal momenta. At a given value of  $x$  the kinematic characteristics of all particles defined as

$$\begin{aligned} P_B &= (\sqrt{m_B^2 + p_B^2}, p_B, \vec{0}^{\perp}) \\ P_q &= (\sqrt{m_q^2 + x^2 p^2}, xp, \vec{0}^{\perp}) \\ P_{qq} &= (\sqrt{m_{qq}^2 + (1-x)^2 p^2}, (1-x)p, \vec{0}^{\perp}) \end{aligned} \quad (1)$$

Here  $m_B, m_q, m_{qq}$  are the masses of the baryon, quark and diquark respectively;  $p_B$  and  $p$  are the solutions of the equation system

$$\begin{cases} p_B + p = p_0 \\ E_B + E_q + E_{qq} = E_0 \end{cases} \quad (2)$$

where  $E_0$  and  $p_0$  are the total energy and momentum respectively. It is easy to see that the primary hadron "mass"  $(P_q + P_{qq})^2$ , defined in this way, is different from the table value  $m_B$ .

Supposing that the value of  $x$  is distributed according to the rule

$$f(x) \sim \frac{1}{\sqrt{x}} (1-x)^{1.5+2.5} \quad (3)$$

and calculating the  $p_{\perp}$  dependence of the process amplitude by the graphs of fig. 1, one can obtain (see fig. 2) various characteristics of the diffraction dissociation process. One can easily formulate a similar algorithm for the description of hadron decays into a greater number of subsystems.

An independent "simulation" of quark, antiquark and diquark momenta followed by determination of kinematic charac-

teristics of strings created between various hadron subsystems may face the occurrence of low mass strings. We interpret them as off-shell hadrons and formulate the "putting-onto-the mass-shell" algorithm as follows.

Let a set of particle characteristics is given

$$\mathcal{P}_i = (E_i, p_{\parallel i}, \vec{p}_{\perp i}), m_{\alpha_i}, 1 \leq i \leq N \quad (4)$$

For some particles  $m_{\alpha_i}^2 \neq E_i^2 - p_{\parallel i}^2 - p_{\perp i}^2$ . Solving the system of equation for the unknown variables  $C_1$  and  $C_2$

$$\sum_{i=1}^N p_{\parallel i} [C_1 \theta(p_{\parallel i}) + C_2 \theta(-p_{\parallel i})] = p_0$$

$$\sum_{i=1}^N [\sqrt{m_{\alpha_i}^2 + C_1^2 p_{\parallel i}^2 + p_{\perp i}^2} \theta(p_{\parallel i}) + \sqrt{m_{\alpha_i}^2 + C_2^2 p_{\parallel i}^2 + p_{\perp i}^2} \theta(-p_{\parallel i})] = E_0 \quad (5)$$

we determine the particle characteristics in the final state

$$\mathcal{P}_i' = \left( \sqrt{m_{\alpha_i}^2 + C_1^2 p_{\parallel i}^2 + p_{\perp i}^2} \theta(p_{\parallel i}) + \sqrt{m_{\alpha_i}^2 + C_2^2 p_{\parallel i}^2 + p_{\perp i}^2} \theta(-p_{\parallel i}), \right. \\ \left. C_1 p_{\parallel i} \theta(p_{\parallel i}) + C_2 p_{\parallel i} \theta(-p_{\parallel i}), p_{\perp i} \right). \quad (6)$$

Here  $m_{\alpha_i}$  are the table values of hadron masses. So, we have an opportunity to avoid rejecting events with low strings created, which in its turn allows an increase in the code operation rate. We also have an opportunity to satisfy the energy momentum conservation law with computer accuracy, to take into account the transverse momenta of the constituents, the binding energy, etc. when simulating interactions of composite systems.

In the case of nucleus-nucleus collisions an additional problem of simulation of inelastic configurations of interacting nucleons arises. A large number of elementary interactions aggravates the problem of creation of low mass chains. Our earlier algorithm for the configuration choosing <sup>/3/</sup> realized in the code DIAGEN <sup>/4/</sup> together with the "putting-onto-the mass-shell" algorithm allow one to solve these problems without violating Glauber's relations between cross sections of various processes <sup>\*)</sup> and without losing the code operation

---

\*) These relations are violated in the existing realization <sup>/5,6/</sup>.



efficiency. In this case no simplifying assumptions on the elastic NN scattering amplitude are required.

In figs. 3-5 one can see various characteristics of proton-proton interactions calculated by us with allowance for the processes of diffraction dissociation both to the low-mass and high-mass states. Fig. 6 shows the rapidity distributions of secondary particles in hadron-nucleus collisions calculated without violation of the energy-momentum conservation law with allowance for Fermi-motion of nuclear nucleons. In figs. 7,8 characteristics of  $\alpha$ -particle interactions at  $\sqrt{s_{tot}} = 126$  GeV are given. In fig. 9 transverse energy spectra for h-A and A-A collisions are represented.

For all calculations we used the string fragmentation code BAMJET /15/. As is seen our calculations are in satisfactory agreement with the experimental data.

Thus, our realization of the dual parton model describes the available experimental data well enough and permits one to analyse more subtle characteristics of h-A and A-A interactions thanks to allowance for the energy momentum conservation law, the structure of elastic A-A scattering and the diffraction dissociation processes.

#### References

1. A.Capella et al. Phys.Lett., 1979, v. 81B, p. 68; A.Capella et al. Zeit.fur Phys., 1980, v. C3, p. 329; A.Capella, J. Tran Thanh Van. Phys.Lett., 1980, v. 93B, p. 146; A.Capella et al. Phys.Lett., 1982, v. 108B, p. 347; A.Capella, C.Pajares, A.V.Ramallo. Nucl.Phys., 1984, v. B241, p. 75.
2. C.V.Mukhin, V.A.Tharev. In: Particles and Nuclei. v. 8, Moscow, Energoizdat, 1977, p. 989.
3. A.M.Zadorozhnyj et al. Yad.Fiz., 1984, v. 39, p. 1155.
4. A.M.Zadorozhnyj et al. JINR, B1-2-86-858, Dubna, 1986.
5. J.Ranft, S.Ritter. Zeit.fur Phys., 1983, v. C20, p. 347; 1985, v. C27, p. 314; 1985, v. C27, p. 469. H.J.Mohring et al. Zeit.fur Phys., 1985, v. C27, p. 419.

6. N.S.Amelin. JINR, P2-86-837, Dubna, 1986; P2-86-836, Dubna, 1986; P2-86-802, Dubna, 1986.
7. V.V.Amosov et al. Phys.Lett., 1972, v. 42B, p. 519; H.Bialkowski et al. Nucl.Phys., 1976, v. B110, p. 300; C.Bromberg et al. Phys.Rev.Lett., 1973, v. 31, p. 1569; W.M.Morss et al. Phys.Rev., 1977, v. D15, p. 66; J.Whitmore. Phys.Rep., 1974, v. 10C, p. 274; J.Erwin. Phys.Rev.Lett., 1974, v. 32, p. 537; C.Bromberg. Nucl.Phys., 1976, v. B107, p. 82; S.Barish et al. Phys.Rev., 1974, v. D9, p. 2689; A.Firestone et al., Phys.Rev., 1974, v. D10, p. 2080, J.W.Chapman. Phys.Rev.Lett., 1974, v. 32, p.257.
8. W.Thome et al. Nucl.Phys., 1977, v. B129, p. 365.
9. W.Bell et al. Zeit.fur Phys., 1985, v. C27, p. 191.
10. De Marzo et al. Phys.Rev., 1982, v. D26, p. 1019.
11. Yu.M.Shabelskii, LIYaF, preprint No 1224, Leningrad, 1986.
12. M.A.Faessler. Phys.Rep., 1984, v. 115, p. 1.
13. H.C.Pugh et al. CA 94120, Berkeley, 1987.
14. L.V.Gribov, E.M.Levin, M.G.Ryskin. Phys.Rep., 1982, v. 100, p. 1.
15. S.Ritter. Comp.Phys.Comm., 1984, v. 31, p. 397.

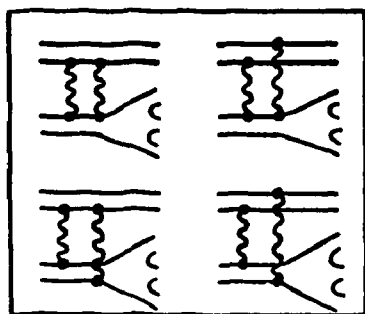


Fig.1

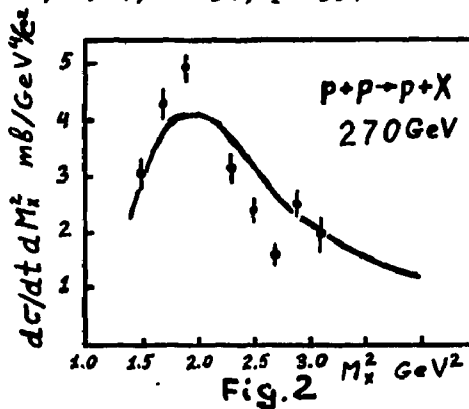


Fig.2

Fig. 1. Diffraction dissociation to the low mass state in the Born approximation of QCD,

Fig. 2. Created system mass distribution in the process  $p+p \rightarrow p+X$ . The curve is the calculation, the points are the experimental data <sup>1/2</sup>.

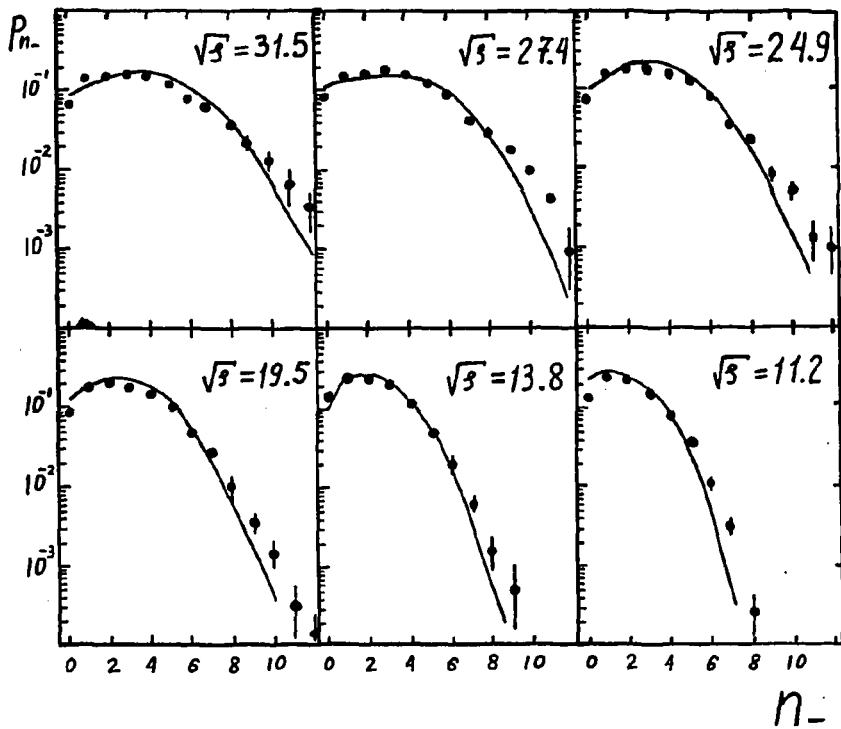


Fig. 3. Negative particle multiplicity distribution in pp-interactions. Curves are the calculations, the points are the experimental data [7].

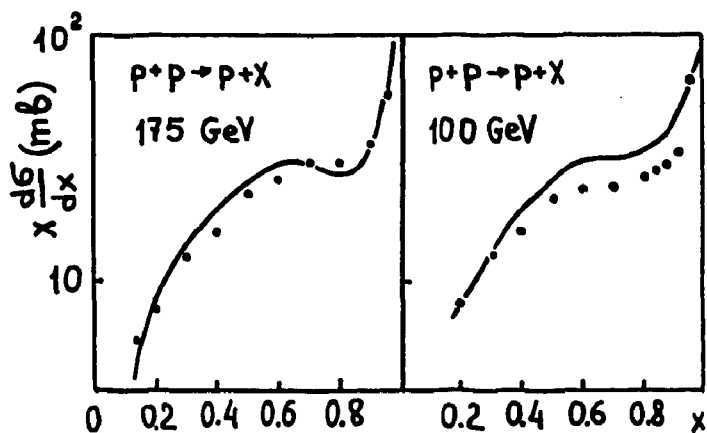


Fig. 4. Inclusive spectra of protons in pp-interactions. The points are the data <sup>/8/</sup>.

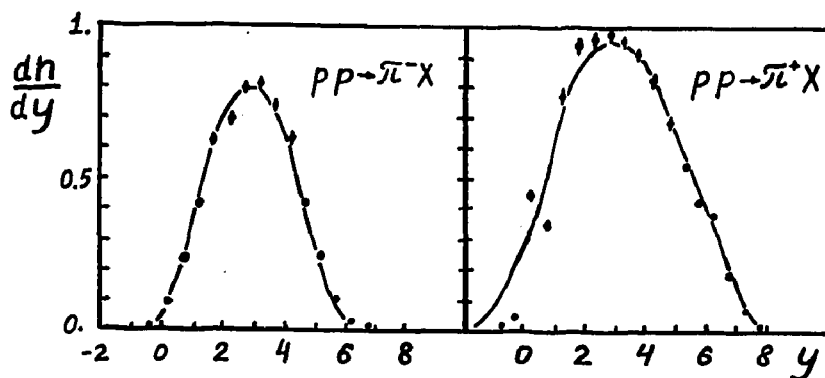


Fig. 5. Rapidity distribution of secondary particles in pp-interactions. The points are the data <sup>/9/</sup>.

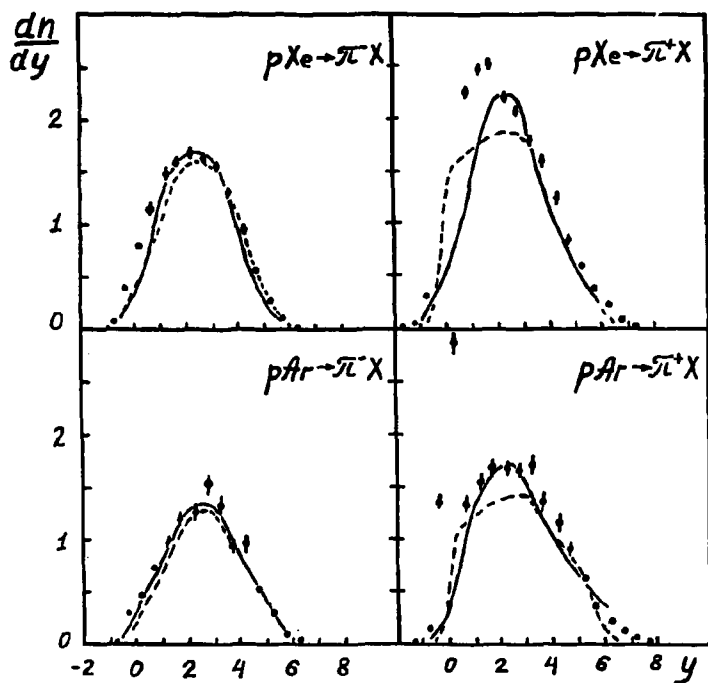


Fig. 6. Rapidity distribution of secondary particles in pA interactions. The points are the data /10/. The dashed lines are the calculations /11/. The solid lines are our calculations.

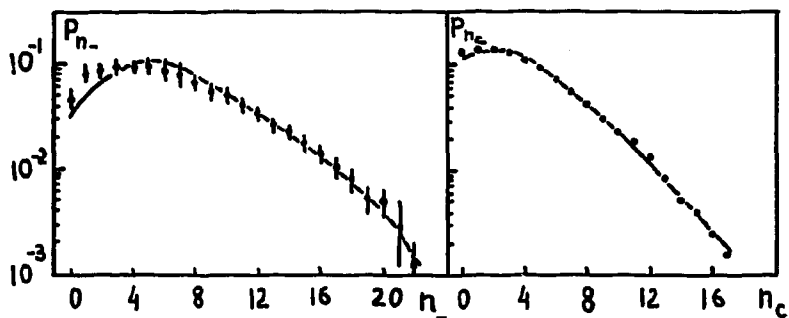


Fig. 7. a) Negative particle multiplicity distribution in  $\alpha\alpha$ -interactions at  $\sqrt{s_{\alpha\alpha}} = 126$  GeV.  
 b) Multiplicity distribution of charged particles produced in the central region. The points are the data /12/.

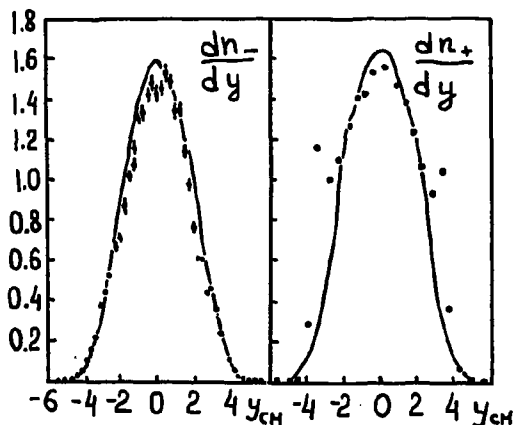


Fig. 8. Rapidity distributions of negative and positive particles in  $\alpha\alpha$ -collisions (figs. 8a and 8b respectively). The points are the data /12/.

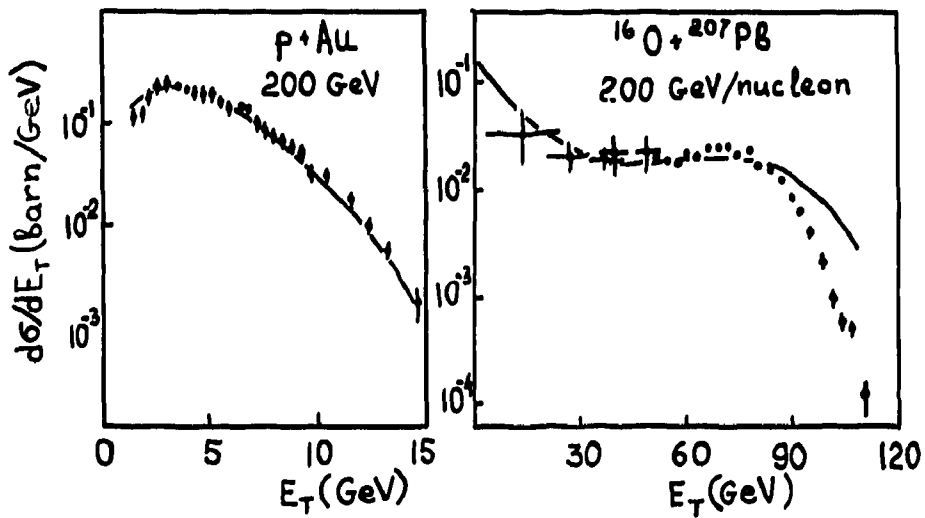


FIG. 9. Transverse energy spectra in hadron-nucleus and nucleus-nucleus interactions. The points are the data /13/.

# HADRON INTERACTION AT HIGH ENERGY IN QCD

E.M. Levin and M.G. Ryskin

Academy of Sciences of the USSR  
Leningrad Nuclear Physics Institute

## A b s t r a c t

It is shown that the perturbative QCD allows one to understand the main properties of the hadron interaction at high energy. Developed on the basis of the leading logarithmic approximation in perturbative QCD and the reggeon diagram technique, our approach successfully describes the inclusive spectra of the secondary hadrons including small transverse momenta  $p_t \sim 300$  MeV, and the multiplicity distribution in a wide region of energy  $s = 50-900$  GeV, using only three phenomenological parameters. It turns out that the main source of the secondary hadrons is the production and the fragmentation of the gluon minijets with transverse momentum  $q_t \sim q_0$ , where  $q_0 = 2.5$  GeV at  $s = 0.5$  TeV, and  $q_0 = 7$  GeV for  $s = 40$  TeV. Our approach predicts a rapid increase of the total multiplicity  $N \sim q_0^2 \sim \exp(2.5 \ln s)$ , the total cross section  $\sigma_t \sim \ln^2 s$  and a comparatively slow increase of the diffraction dissociation cross section  $\sigma_D \sim \ln s$ .

## 1. INTRODUCTION

It is well known that the typical hadronic interactions at high energy are soft processes that occur at large distances (or small transferred momenta) where the mysterious confinement forces should be acted. For this reason, discussing these processes in framework of QCD, we are to use some models that contain our qualitative improvization utilizing rather the QCD terminology (quark and gluon degrees of freedom) /1-3/, than the explicit form of QCD interaction.



Here, we advocate a quite different view point, namely, the leading logarithmic approximation (LLA) of perturbative QCD is a sufficiently good basis for the description of high energy physics. We are trying to demonstrate below, that we can achieve the full and self-consistent understanding of the main properties of high energy collisions on this way including both the processes with small and large transverse momenta ( $q_t$ ). We predict i) the logarithmical increase of the interaction radius  $R_0 \sim \ln s$  (the diffraction slope  $B \sim \ln^2 s$  and of the total cross section  $G_t \sim \ln^2 s$ , ii) the specified behaviour of the diffraction dissociation  $d\sigma^D/d_M^2 \sim \ln s/M^2 (\ln M^2)^{-3/2}$  at high energy, iii) the rapid increase of the mean transverse momentum of the secondary hadrons or jets, namely  $q_{t,jet} \sim \exp(a \sqrt{\ln s})$  and their multiplicity  $N \sim \bar{q}_{t,jet}^2$  for typical inelastic event.

In our approach we prove the s and t channel unitarity and can easily show that our formulas have a usual limit of the perturbative QCD at large  $q_t$ . The main reason why we can discuss so conventional soft phenomena as total cross section is the significantly large mean transverse momentum for typical inelastic event, that, as predicted, rapidly grows with energy ( $q_t^2 = q_0^2 \sim \exp(2.5 \sqrt{\ln s})$ ). Such a large  $q_t^2$  reveals itself in small coupling constant of QCD  $\alpha_s(q_t^2) = 4\pi/b \cdot \ln q_t^2/\Lambda^2$ , which smallness controls the accuracy of our calculation in perturbative QCD. We see some experimental support of the above ideas even in the energy behaviour of the slope of the diffraction peak <sup>14/</sup>.

$$B(p,p) = (10.9 - 0.08 \ln s + 0.043 \ln^2 s) \text{ GeV}^{-2} \quad (1)$$

It is easy to see from eq. (1) that the factor  $\ln^2 s$ , being proportional to  $p_t^{-2}$ , where  $p_t$  is the parton peripheral transverse momentum, is extremely small and corresponding to  $p_t \sim 1-2$  GeV since  $0.043 \sim (\alpha_s/p_t)^2$ .

Even at not high energy, i.e.  $\sqrt{s} = 10 - 60$  GeV the slope of pomeron trajectory  $\alpha' (B = B_0 + 2\alpha' \ln s)$  only slightly

exceeds the minimal value permitted by t-channel unitarity for  $t = 4m^2$  /5/.

$$\alpha'_{\min} = \frac{3}{2} \frac{\sigma_{\text{tot}}}{32\pi^2} \ln 4m^2 / m_p^2 = 0.08 \text{ GeV}^{-2}$$

Experimentally /6/  $\alpha' = 0.13 \pm 0.02 \text{ GeV}^{-2}$ . Thus, the experimental value of  $\alpha'$  is connected with comparatively rare events of the pion production on the periphery of a hadron, while the typical transverse momenta of a parton in the fast hadron is sufficiently large ( $> 1 \text{ GeV}$ ) to provide the application of the perturbative QCD. Thus, we claim that the original lagrangian of QCD allows us to build the picture for hadron interaction at high energy on the same level of our understanding of the high energy dynamics as has been reached in quantum electrodynamics. In our approach, that is based on the LLA of perturbative QCD and taking into account the rescattering of partons /7/, we can describe the main properties of the inelastic nucleon interaction for

$\sqrt{s} = 50\text{-}900 \text{ GeV}$  such as i) the rapidity distribution  $d\sigma/d\eta$ , ii) the  $p_t$  spectra  $d\sigma/dp_t^2$  in the wide range of  $p_t$  from 300 MeV to 10 GeV, iii) the multiplicity distribution  $\sigma_N$ , and iv) the increase of the mean transverse momentum  $\langle p_{t\text{th}} \rangle$  versus  $N$ . Fitting experimental data we use only three parameters that cannot be calculated in perturbative QCD and their values have been extracted from experiments. At the same value of these parameters we reproduce the energy dependence of the slope of the diffractive peak  $B = a^2 \ln^2 s$  and the total cross section  $\sigma_t = 8\pi a^2 \ln^2 s$ , and also the inclusive cross section with large transverse energy  $E_t$  for proton-nucleus interaction  $(d\sigma(p, \text{Pb})/dE_t)^+$ . As in QCD we can develop the regular procedure for the calculations of small corrections to our approach.

Thus, we have discussed briefly only the positive aspects of our approach, which is based on the well developed LLA of QCD /8/ and the reggeon diagram technique /9,10/. Now let us consider our difficulties. First of all, it is the low

practical precision of the IIA calculations. Even in such simple process as the heavy lepton pair production, the IIA formula gives the value of the cross section  $\sigma(\mu^+ \mu^-)$  twice larger than experimental one. Of course, we know how to calculate the corrections to IIA but unfortunately such calculations are extremely complicated. The second difficulty is typical for all many body interactions. Although the probability of the rescattering of each pair of partons is not large, in the central rapidity region where there are many partons we face the usual problems for the many body interaction, and are obliged to use more or less reasonable approximations for real calculations. Unfortunately, the accuracy of such approximations is not good. At least, all calculations are related to quark and gluons, and we can take from experiment the phenomenological structure function for gluon (quark) distribution in initial hadrons and the hadron fragmentation function for producing quark and gluon jets. Fortunately, all qualitative features and the most part of the quantitative calculations, at least for the central region depend very weakly on the details of the used structure functions and even on the way how we take into account the parton-parton interactions ++).

-----  
 +) Let us note that the discussed approach /7-10/ allows us to solve the problem of screening corrections for the deep inelastic scattering /11/.

++) It occurs because the parton density grows with energy and reaches its maximal value permitted by unitarity.

## 2. PARTON WAVE FUNCTION OF A FAST HADRON

1. First of all let us outline two important peculiarities of QCD.

A. Due to the spin of a gluon being equal to the unity we get the constant cross section even in Born approximation of QCD at high energy from the two gluon exchange (see fig. 1a). The radiation of intermediate gluons shown in fig. 1b leads to the increase of the total cross section, namely  $\sigma_{t,LLA} \sim \alpha_s^2 \langle r_1^2 \rangle s^{0.08}$ . Thus, some chance appears to study the processes with rising cross sections already in perturbative QCD at small  $\alpha_s$ .

B. In QCD a gluon, gradually slowing down in the ladder diagram of fig. 1b is taking part in two random movements simultaneously. One from them is a usual diffusion in the impact parameters ( $b_t$ ) which is typical for any reggeon exchange <sup>/12/</sup>. At each gluon emission "i" the parton that loses its energy shifts its position in  $b_t$  on the value  $\Delta b_t \sim 1/q_t$ . Such diffusion provides the increase of the interaction radius with energy <sup>/12/</sup>. The second diffusion that was firstly considered in ref. <sup>/8/</sup>, is the random changing in  $\log q_t$ . Since the QCD coupling constant is dimensionless, all integrals over any transverse momentum  $q_{t,i}$  are logarithmical looking like  $\int \alpha_s(q_{t,i}) dq_{t,i}^2 / q_t^2$  and converge at  $q_{t,i} = q_{t,i+1}$  or  $q_{t,i} = q_{t,i-1}$ . In other words, at each step of the diffusion (for each radiation)  $\ln q_t^2$  changes by the value of the order of unity. As a result of such a diffusion the mean transverse momentum of the particles rapidly grows and the main contribution for multiparticle generation results from the fragmentation of the gluon jet with  $q_t = q_0 = \Lambda \exp(1.26 \sqrt{\ln s})$ .

2. Let us consider in details the development of the quark-gluon cascade that forms the wave function of low partons in a hadron <sup>+</sup>). We would like to emphasize, that the summation of the simplest ladder diagrams that has been carried out in the LLA of QCD (see fig. 1b) in fact means that the developed cascade of gluons is taken into account since each

produced parton decays into a whole cascade of slowed partons as shown in fig. 1c. The probability to emit a gluon with the fraction  $x$  of the hadron momentum  $p$  is proportional to  $dw \propto \alpha_s dx/x$ , and, thus, the multiplicity of the partons ( $N$ )  $N = N_0 \exp(c \alpha_s \ln 1/x)$  since  $dN/N = dw = \frac{c \alpha_s dx}{x}$ . The cross section is determined by the product of the  $N$  for the slowest partons and the parton-parton cross section ( $\sigma_0$ )  $\sigma_t \propto \sigma_0 N(\ln 1/x = \ln \sqrt{s})$  so the increase of multiplicity  $N$  provides  $\sigma_t = \sigma_0 \cdot s^{c \alpha_s}$ . The question arises, what is the distribution of the partons in  $b_t$  and  $q_t$  ++). Let us consider two extreme situations. 1) For each gluon radiation,  $\log$  of its  $q_t$  grows,  $\Delta \log q_t = +1$ . The transverse momentum in such ladders (shown in fig. 1d by vertical lines) increases with the growing number of diffusion steps - "  $m$  ". The thickness of the lines in fig. 1d reflects the increase of  $\log q_t = m$  \*. Each step of the diffusion occupies the rapidity interval  $\Delta y = \Delta \ln 1/x \sim 1/\alpha_s (q_t^2)$ , since  $w \propto \alpha_s \ln 1/x \sim 1$ . The coupling constant  $\alpha_s \sim 1/\ln q_t^2$ , so the characteristic value of  $\ln q_t$  grows as  $\ln q_t \sim \alpha_s dy$  and

$$\ln \langle q_t \rangle \propto \sqrt{y}, \quad \langle q_t \rangle = \Lambda \exp c \sqrt{y}, \quad y = \ln 1/x \quad (3)$$

At the first sight it seems unnatural that from diffusion with equal probability for increasing and decreasing  $\log q_t$  some grows of  $q_t$  follows.

+) The gluons play the most important role in this formation and for this reason here we restrict ourselves to gluon ladders only although in practical calculations we have involved the quark production as a well.

++) Strictly speaking, in quantum mechanics it is impossible to fix the coordinate and momentum ( $b_t$  and  $q_t$ ) simultaneously. Such a situation is in contradiction with uncertainty relation, but in our case we can use  $q_t$  and  $b_t$  with semiclassical accuracy since the number of partons is extremely large.

Let us present a very simple estimation to confirm this statement. Let us suppose that the  $\ln q_t$  distribution has the usual diffusion form /8/, namely

$$\frac{1}{\sqrt{4\pi m}} \exp\left(-\frac{\ln^2 q_t}{m}\right) d \ln q_t .$$

The mean transverse momentum can be found from a simple expression

$$\langle q_t \rangle = \frac{\Lambda}{m} \int_0^\infty \left( \ln \frac{q_t}{\Lambda} - \ln^2 \frac{q_t}{\Lambda} \cdot \frac{1}{m} \right) d \ln q_t = \exp \frac{m}{4}$$

If we put  $m \approx \alpha_s y \approx y / \ln q_t^2$  in the above equation, we get eq. (3) for  $q_t$ . It is easy to understand that such ladder can not shift its position in impact parameters  $b_t$ ; since such a shift is about  $1/q_t$  ( $\Delta b_t \sim 1/q_t$ ) and exponentially falls down (eq. (3)) with rapidity  $y$ . 1) The opposite example, the transverse momentum only weakly changes in a ladder,  $q_t \sim Q_0$ . We can reach such a situation in the  $\log q_t$  diffusion if on each step  $\ln q_t = +1$  or  $-1$ , successively.

In such a ladder the parton can move in  $b_t$  up to  $b_t = m \Delta b_t \approx m/Q_0 \approx \alpha_s(Q_0) y/Q_0$ , and these movements provide the increase of the interaction radius  $R = \alpha' \ln s$  where  $\alpha' \approx \alpha_s/Q_0$  and  $y = \ln s/Q_0^2$ .

3. Of course in full parton cascade all situations can be realized that are intermediate between the two above, but since the total parton multiplicity grows as a power with energy ( $N \approx S^{\alpha_s}$ ), in any case such branch of the cascade can be found, where the transverse momentum ( $\ln q_t$ ) monotonically increases or the branch where the parton gradually shifts its position further and further from the center of the initial hadron (the last branch is presented in fig. 1d by sloping wave lines). For example, fig. 1d shows the two steps of the diffusion ( $m = 2$ ) when the initial parton decays in four gluons from which two increase their  $\ln q_t$  in average, while from the two others with smaller  $q_t$  one shifts to the right ( $\Delta b_t \sim 1/q_t$ ) and another to the left further and further from the disc centre  $b_t = 0$ . Thus, the total multi-

plicity of slow partons increases and becomes so large that the gluons within a unit of rapidity must begin to overlap in space of the thin disc which they occupy. At the distances  $b_t = R = ay$  apart from the disc centre at least one parton at  $x = e^{-y}$  can be found with the probability ( $W$ ) of the order of the unity, but inside the disc ( $b_t \leq ay$ ) the parton always exists (with  $W \sim 1$ ) with the transverse momentum  $q_t = q_0(y, b_t)$  that used the rapidity interval  $y = y - b_t / a$  for the increase  $\ln q_t$ . Thus,

$$q_0^2(y, b_t) = q_0^2 + \Lambda^2 \exp(3.56 \sqrt{y - b_t/a}) \quad (4)$$

In eq. (4) we substitute the value of the constant  $c = 1.78^{7/7}$  in eq. (3) and the preasymptotic term  $Q_0$  is added, that determines the initial virtuality. It is useful to introduce the kinematical variables  $r = \ln q_t$  and  $y = \ln 1/x$ , which are given in fig. 2. The solid line shows the equation  $q_t = q_0(y, b_t)$  which is the condition that in the point  $b_t, q_t$  and  $y$  at least one gluon can be found with the probability  $W \sim 1$ . To the right of this curve in the region of large  $q_t \gg q_0$  the probability to find a gluon or a quark is small. In this region the parton distribution is calculated by Lipatov-Altarelli-Parisi evolution equations, but the initial condition for the evolution equation should be the gluon density along the boundary (4). However, in the IIA where the smallness of  $\alpha_s$  is compensated by large  $\log^2$  of the energy  $\alpha_s \ln s \rightarrow O(1)$  ( $\sum C_n (\alpha_s \ln \frac{1}{x})^n$ ) the calculation of the parton density along the boundary of eq. (4) has been successful only for small  $x$ , while on the first vertical part of the solid curve in fig. 2 we are to use some phenomenological initial structure function  $D(x, Q_0)$ . The particular value of the function  $D$  is very essential for the calculations in the region of large  $q^2$  and not small  $x$  (see point 1 in fig. 2) and almost negligible for small  $x$  (see point 2 in fig. 2), when the initial condition for Lipatov-Altarelli-Parisi equation is entirely determined by the parton

<sup>7)</sup>In the language of the reggeon field theory the time interval  $y = it$ .

density on the boundary (4). To the left of the boundary (4) the most of the slow partons are concentrated. Their number rapidly grows  $N \sim S^{\alpha_s}$  without the parton-parton interaction. This power-like increase is closely related to the logarithmically large probability to emit a gluon in the parton cascade:

In space the variable  $\log E$  corresponds to the logarithmical integration over the time of the coherent emission of the gluon "1":  $dw_1 = \alpha_s d\tau/\tau_1$ . The total formation time  $\tau_1$  is equal to  $E_1/q_1^2$  ( $\tau_1 = E_1/q_{1t}^2$ ), but the parton can use this time  $\tau_1$  only if the parton-parton interaction is negligible. Indeed, any collisions that require a small time interval  $\Delta\tau_1 \sim 1/q_{1t}$  for example the one gluon exchange violates the condition of the coherent emission changing the colour and the momentum of the parent parton. Therefore, to the left of the boundary (4), where the number of collision is very large <sup>+) the LLA conditions are violated and, calculating the structure function in this region (region C in fig. 2) we can restrict our ourselves by the lowest order diagrams in  $\alpha_s$  that is to calculate the simplest two gluon exchange between the parton of interest (point 3 in fig. 2) and gluons on the solid curve in fig. 2.</sup>

4. Now let us write the equation /8/ that describes the behaviour of the total cross section from  $q^2$  and  $\ln x = y$  in LLA of QCD (in  $\log x$ ). Introducing  $\phi(q^2, y)$  which is the cross section of the gluon interaction under condition that the transverse momentum of the fast gluon  $q_t^2$  equals to  $q^2$  in the upper cell of the ladder, we can reproduce the equation of ref. /8/ in the form

$$\frac{\partial \phi}{\partial y} = \int K(q, q') \phi(q', y) \frac{N_c}{\pi} \alpha_s(q'^2) dq'^2 \epsilon \quad (6)$$

<sup>+) On the boundary (see eq. (4)) the probability of the parton rescattering is of the order of the unit.</sup>



$$\phi(q^2, y) \sim D(q^2, x = e^{-y}) \cdot x/q^2 \quad (6)$$

$N_0 = 3$  is the number of colours, and the factor  $g$  that is introduced for the description of the effectiveness of the gluon radiation, is equal to 1 for LLA

$$K(q, q') \phi(q') = \frac{\phi(q')}{(q' - q)_+^2} - \frac{q_+^2 \phi(q)}{(q' - q)_+^2 (q'^2 + (q - q')_+^2)}$$

(see ref. 8).

For the function  $\phi_f \sim q^{2(f-1)}$

$$\int K(q, q') \phi_f(q') dq'^2 = \chi(f) \phi_f(q)$$

where the eigenvalue  $\chi(f) = 2\Psi(1) - \Psi(f) - \Psi(1-f)$  and  $\Psi(f) = d \ln \Gamma(f)/df$ ,  $\Gamma(f)$  is the gamma function. The integral over  $q'$  is convergent of values of  $q' \sim q$  and in the case when  $\phi \sim 1/\sqrt{q^2}$  the dominant  $\ln q'_+$  differs from  $\ln q_+$  by  $\pm 1$ . Let us note that  $\phi = 1/\sqrt{q^2}$  gives the fastest possible increase of the total cross section /8/ with energy

$\phi_{\frac{1}{2}}(y) \sim \exp(4 \ln 2 N_0 \alpha_s y/T)$ . To include the parton-parton interactions in eq. (5), for the region to the right of the solid curve in fig. 2, it is enough to take into account the semienhanced "fan" diagrams of fig. 3a type. The equation that sums to these diagrams looks like eq. (5) with

$$\epsilon = 1 - \alpha_s \phi(q^2, y) / \phi_0 \quad (7)$$

instead of  $\epsilon = 1$  as in LLA. Such a modified equation gives us the following answer. With the increase of energy the function  $\phi(q^2, y)$  exponentially grows ( $\phi \sim e^{y\chi - N_0}$ ) up to  $\phi(q^2, y) = \phi_0 = \text{Const}$  at  $q^2 = q_0^2(y) = q_0^2 + \Lambda^2 \exp(3.56 \sqrt{y})$ . For larger  $y$  the increase of  $\phi$  slows down and its value tends to the unitarity limit that is  $\phi_{\text{max}} = \phi_0 / \alpha_s (q^2) (\phi \rightarrow \phi)^+$ . Now let us generalize eq. (5),

including  $b_t$  and assuming (with a semiclassical accuracy) that for each emission the probability for the parton to change its position in  $b_t$  should be describe by function  $\exp(-\Delta B t^2 q'^2/4)$ . The new equation has a form

$$\frac{\partial \phi(b_t, q, y)}{\partial y} = \int K(q, q') \phi(b_t', q', y) \cdot$$

$$\cdot \frac{(b - b_t')^2 q'^2}{4} \alpha_s(q'^2) \frac{N_0}{4\pi} q_t'^2 d^2 b_t' d^2 q_t' \cdot$$

$$\cdot [1 - \alpha_s \phi(b, q, y) / \phi_0] \quad (q > Q_0) \quad (8)$$

As seen from eq.(8),  $\phi$  monotonously increases with  $y$  going to  $\phi_{\max}$  ( $\phi \rightarrow \phi_m$ ).

In the disc centre ( $b_t = 0$ ) the value of  $\phi$  is  $\phi(0, q_t, y) = \phi_0$  reached at  $q = q_0(y)$ . The maximal value in the periphery should be for  $\phi = \phi(b, Q_0, y)$  since  $\Delta b_t$  falls down with the rise of  $q_t$ .  $\phi(b_t, Q_0, y) = \phi_0$  for  $b_t = ay$ , where

$$a = \frac{\chi N_0 \alpha_s(Q_0^2)}{Q_0} = 0.40 \text{ GeV}^{-1}$$

$$\text{at } Q_0^2 = 2 \text{ GeV}^2.$$

Therefore from the parton view point the fast hadron is nothing more than the almost black disc with  $R = ay$ . The blackness inside the disc grows as a result of the increase of the parton density for large  $q_t$ , since  $\phi(b, q, y)$  is very close to  $\phi_{\max}$  up to  $q_t = q_0(y, b_t)$  (see eq. (41)). The momentum  $q_t \sim q_0$  gives the main contribution in the processes of the multiparticle production, since the inclusive cross section is equal to the following expression (see fig.4)

-----  
 +) The right hand side of eq. (5) is positive and the function  $\phi(q, y)$  grows with  $y$ , but at  $\phi > \phi_{02}$   $\phi$  changes its sign,  $\partial \phi / \partial y$  becomes negative and  $\phi(q^2, y)$  falls down.

$$\frac{d\sigma}{d\eta} = \frac{d\sigma}{d\eta d q_t^2} dq_t^2 \rightsquigarrow \int \phi(q_t, y) \phi(q_t, y_2) \alpha_s dq_t^2 \rightsquigarrow$$

$$\rightsquigarrow \phi_0^2 q_0^2 \quad (10)$$

The multiplicity  $N$  grows proportionally to the whole permitted phase space, namely  $N \rightsquigarrow q_0^2 \rightsquigarrow \exp(2.52 \sqrt{\ln s})$ . We would like to emphasize that eq. (8) allows us to calculate the structure functions with a good accuracy that is controlled by a smallness of the QCD coupling constant  $\alpha_s$  only in the kinematical regions, where the parton density has not been large yet and the value of  $\phi$  does not exceed  $\phi_0 = \text{const}$ . The above condition is satisfied either to the right of the boundary  $q_t > q_0(y, b_t)$  or at the disc edge  $b_t > ay$ . For  $q_t < q_0(y, b)$  we have to use some hypothesis, but the uncertainty arising here is not large, since  $\phi$  becomes already equal to  $\phi_0$  on the boundary  $q_t = q_0(y, b_t)$  and its further increase is restricted by the unitary condition, namely  $\phi < \phi_{\text{max}} = \phi_0 / \alpha_s$ . We can get this inequality using Kancheli-Mueller rules [13]. Nevertheless, we would like to draw your attention that for the whole region to the left of the boundary we need some model for  $\phi$ . Our assumption is  $\phi = \phi_0$  for  $q_t \leq q_0(y, b_t)$ . The above picture is in a good agreement with the available experimental data. As was discussed in ref. [14], the so called BEL-effect was observed experimentally for energies from  $\sqrt{s} = 50 \text{ GeV}$  (ISR) to  $\sqrt{s} = 540 \text{ GeV}$  (Sp $\bar{p}$ S-collider). The proton becomes Blacker, its Border Edgier, and its radius larger. In other words the proton turns into the black disc with a sufficiently sharp border, as expected in our approach. Experimentally,  $dR/dy = a = 0.42 \text{ GeV}^{-1}$  in our picture for  $Q_0^2 = 2 \text{ GeV}^2$ , that was extracted from the inclusive production at Sp $\bar{p}$ S energy [7],  $a = 0.40 \text{ GeV}^{-1}$ . The contribution of pions, that can be emitted rarely from the border of the disc, is in 10 times smaller. Of course, this contribution ( $a = 0.04 \text{ GeV}$ ) can not be

calculated in the perturbative QCD but we can develop its own perturbative theory for such a small correction taking into account all rare peripheral pions. Thus, the energy behaviour of the total cross section is in agreement with the experiment.

As for multiparticle production, we claim that its main source is the fragmentation of gluon minijets with  $q_t \sim q_0$ . The  $q_0$  value for the central rapidity region  $\eta = 0$  is  $q_0 = 2.5$  GeV ( $\sqrt{s} = 540$  GeV, SpP̄S),  $q_0 = 4.5$  GeV ( $\sqrt{s} = 6$  TeV, UNK), and  $q_0 = 7$  GeV ( $\sqrt{s} = 40$  TeV, SSC). Experimentally, the cross section for the hadron jet with  $p_t > 5$  GeV is sufficiently large. About 40% of the events at  $\sqrt{s} = 900$  GeV contain at least one jet with  $q_t > 5$  GeV for  $|\eta| < 3$ . The observed value for

$$\frac{d\sigma^{\text{jet}}}{d\eta dq_t} \quad \begin{array}{l} q_t = 5 \text{ GeV} \\ \eta = 0 \\ \sqrt{s} = 540 \text{ GeV} \end{array}$$

$= 0.4 \pm 0.15$  mb/GeV that is in a good agreement with the predicted magnitude  $d\sigma^{\text{jet}}/d\eta dq_t = 0.55$  mb/GeV.

### 3. MULTIPARTICLE PRODUCTION

Let us briefly discuss the inclusive hadron cross sections. Using eq. (4) for  $q_0(y)$  and the formulae of the review<sup>/7/</sup>, we have been able to describe the experimental data on  $d\sigma/dq_t^2$  and  $d\sigma/d\eta$  in the wide range of energies ( $\sqrt{s}$ ) from 50 to 900 GeV and the transverse momentum ( $q_t$ ) from 300 MeV to 10 GeV, assuming that all secondary hadrons (even with  $q_t \sim 300$  MeV) originate from fragmentation of the gluon jets<sup>/15,16/</sup>. The corresponding curves are given in fig. 5<sup>/16/</sup>. Fitting the observed data the two free parameters (which cannot be fixed in LLA) have been extracted directly from experiments. The value  $Q_0^2 = 2 \text{ GeV}^2$  determines the initial virtuality of the parton, the scale of the cross section  $\sigma \sim 1/Q_0^2$  and, simultaneously, the increase of the total

cross section with energy (the factor "a" in  $R = ay$ ,  $\sigma_t = 2 \pi R^2$ ) and for the inclusive one,  $d\sigma(a)/d\eta$ , presented in fig. 5. The second parameter  $\Lambda$ , sets the scale on  $q_t$  axis and the value of the coupling constant  $\alpha_s = 4\pi/b \ln q^2/\Lambda^2$ . The obtained value  $\Lambda = 52 \text{ MeV}$  is in agreement with the value of  $\alpha_s$ , observed in ref.<sup>/17/</sup>, namely,  $\alpha_s = 0.16 \pm 0.01$  at  $q^2 = 22.5 \text{ GeV}^2$ .

It is interesting that the mean transverse momentum for the inelastic event increases with the multiplicity  $N$ <sup>/16/</sup>. Indeed, the increase of  $N$  can be reached either 1) as the result of a more frequent radiation of gluons, i.e. the increase in the number of the diffusion step "m" in the rapidity interval  $y$ . Since  $\langle \ln q_t \rangle \approx m$ , this mechanism directly leads to the large transverse momentum, or ii) due to creation of several branches of the cascades that can be described by diagrams responsible for the exchanges by many reggeons in the reggeon diagram technique (see fig. 6). However, in these diagrams the additional logarithmical integration over the transverse reggeon (ladder) momenta  $Q_i$  arise generating each its own diffusion in  $\log Q_{it}$ . Since momentum  $Q_i$  plays the role of the initial virtuality  $Q_0$  for its own ladder, the mean  $q_t$  becomes larger when the number "n" of the ladders increases<sup>/16/</sup> (see fig. 7). The multiplicity distribution also can be described in our approach in agreement with the experimental data<sup>/16/</sup> (see fig. 8), but we are to introduce one more parameter  $g = 0.37$ , that characterizes the probability to create additional branches of the cascade  $P_n \approx g^n$ . It is important to note that the values of all three parameters turn out to be very reasonable, natural and coinciding to 20-30% accuracy with the estimations from the calculations of the lowest order diagrams in perturbative QCD. It turns out that our results are very close to the quark-gluon plasma (QGP) approach, although all our calculations were sufficiently apart from the thermodynamical ones. The energy density in the unit volume rapidly increases.  $\epsilon \approx q_0^3/\epsilon_3 \approx \exp(3.8 \sqrt{\ln s})$  reaches the

value  $3 \text{ GeV}/\text{fm}^3$  at Sp̄p̄S energy ( $\sqrt{s} = 0,54 \text{ TeV}$ ) and  $17 \text{ GeV}/\text{fm}^3$  at the UNK-energy ( $\sqrt{s} = 6 \text{ TeV}$ ) /16/. The effective temperature or the mean kinetic energy of the gluon tends to be the large value about 1.5-2 GeV for  $\sqrt{s} = 6 \text{ TeV}$ . At that high temperature the production of heavy hadrons as charmed, strange, beauty, and so on, rises, and because of the parton collisions with  $q_t < q_0$  a kind of the equilibrium distribution in the transverse space is organized. But the system as a whole is quite far from the equilibrium. Firstly, the particles with  $q_t > q_0$  has a too small cross section and can freely come out of the system, creating the hadron sets with the power-like tails of the momentum contributions  $d\sigma/dq_t^2 \propto q_t^{-4}$  at  $q_t \gg q_0$ . Thus, such a jet emission is the permanent source of the evaporation processes in our system which is opened. Secondly, we have not reason for the equilibrium in the longitudinal momentum because of the lack of time in the hadron collision. Our picture leads to large fluctuations in the multiplicity or the number of the ladders " n ", and in the transverse momentum because of the diffusion in  $\ln q_t$ . Thus, the event that we are going to interpret as the plasma production can be only a large fluctuation in the typical hadronic multiparticle production. Even the increase in the mean  $\langle q_t \rangle$  versus the multiplicity that was considered frequently as the indication for the production of the plasma in our approach gets very natural explanation (see fig. 8) /16/.

#### 4. CONCLUSION

In conclusion we would like to emphasize that we are understanding now quite well principle properties of the dynamics at high energy hadron interaction. We have explained the main features of the multiparticle productions and elucidated the reason for the energy increase of the total cross sections directly from QCD Lagrangian, using the perturbative theory. We also have demonstrated in simple model with only three parameters, how all available experimental data

can be described in our approach. +)

For small  $q_t \ll q_0(b_t, y)$  the logarithmically large corrections are absent and the value of the total cross section for  $\sqrt{s} = 20$  GeV can be reproduced by the two gluon exchange /19/, and the observed increase of the total cross section with energy is provided by the parameter  $Q_0$ , that determines also the scale of the inclusive multiparticle production.

Now let us discuss the value of the parameter  $Q_0$ . As discussed, we have extracted  $Q_0 = 1.4$  GeV from experiments, and this value seems unnatural for many our colleagues /20,21/. Indeed, formally speaking,  $Q_0$  is the transverse momentum of the "reggeon" (ladder) in the semienhanced diagram in fig. 3. It looks natural that such momentum should be cut off by the hadronic electromagnetic radius and equal to 400 MeV. Of course, it is correct for the diagram of fig. 9, where the two ladders are influenced by two different valence quarks in a hadron. The contribution of a such diagram is proportional to  $I_a = (n_q^2 - n_q) Q_{0,a}^2 \approx n_q^2 / \langle r_p^2 \rangle$ , where  $n_q$  is the number of quarks, and  $r_p$  is the proton radius. However if the both ladders interact with the single valence quark, as shown in fig. 9b, the corresponding  $Q_0$  is closely related to the size ( $r_q$ ) of the constituent quark, namely  $I_b = n_q Q_{0,b}^2 = n_q / \langle r_q^2 \rangle$ . Although the number of the diagrams of fig. 9b type is  $(n_q - 1)$  times smaller than the number of fig. 9a graphs, the contribution of such diagrams can be large because of the large value  $Q_{0,b}^2$ . The most important contribution comes from enhanced diagrams of fig. 3b type (see fig. 9c), from which we have started the discussion of the screening corrections /7/.

-----  
+) In any case up to now we have not faced the certain observed quantity, that is in contradiction with the discussed approach. Even the  $E_t$  distributions for hadron nucleus collisions can be described without new parameters /18/.

These graphs also have large  $Q_0^2$ . One more argument for the large value of  $Q_0$  ( $Q_0 = 1-2$  GeV) comes from the small radius of the triple pomeron vertex,  $r_{3p} \sim 1/1$  GeV, as observed experimentally. In our approach  $r_{3p} = 2/Q_0$  and, as discussed above,  $Q_0 = 1.4$  GeV allows us to describe the inclusive cross section of the diffraction dissociation  $pp \rightarrow p + X$  in the triple reggeon region. Of course, strictly speaking, we cannot discuss the value of  $Q_0$  in LLA. The only thing that we must do is to verify whether we could describe the large body of the experimental data with the same value of  $Q_0$ . Up to now we have been lucky in this business. We would like to claim that we do not know any experiment, which would contradict our approach (with  $Q_0 = 1.4$  GeV) and have no theoretical or phenomenological arguments against the large value of  $Q_0$ . For this reason, we believe, that our approach can be a good guide for the understanding of high energy physics at new generation of the accelerators. It can be used for simulation of the multiparticle production at higher energies, including SSC energy ( $\sqrt{s} = 40$  GeV) and for estimation of the background from typical inelastic production for rare event for production of heavy fermions, Higgs bosons, and other exotics. All these typical processes, that have been discussed as soft ones before, should be considered as semihard now, since the typical transverse momentum of the gluon sets in the central rapidity region ( $\eta = 0$ ), reaches a large value about  $q_t = 7$  GeV, at  $\sqrt{s} = 40$  TeV.

To our opinion during the last few years the situation in high energy physics has been essentially elucidated and now we have sufficiently transparent and selfconsistent picture for the high energy interactions. This is a good starting point for the full understanding of the problem.

#### REFERENCES

- 1 Kaidalov A.B., Ter-Martirosyan K.A., Yad.Fiz., 1984, 39, 1545, 40 211.
- 2 Gershtein S.S., Logunov A.A., Yad.Fiz., 1984, 39, 1514.



- 3 Kaidalov A.B., Phys. Lett., 1982, 116B, 459;  
Capella A. Staar A., Tran Thunh, Phys. Rev., 1985  
D32, 2933.
- 4 Block M.M., Cahn R.N., Phys. Lett., 1986, 168B, 151.
- 5 Anselm A.A., Gribov V.N., Phys. Lett., 1972, 40B, 487.
- 6 Burg J.P. et al., Phys. Lett., 1982, 109B, 124;  
Nucl. Phys. 1983, B217, 285.
- 7 Gribov L.V., Levin E.M., Ryskin M.G., Phys. Rep.,  
1983, 100, p.1.
- 8 Kuraev E.A., Lipatov L.N., Fadin V.S., JETP. 1976,  
72, 377.
- 9 Gribov V.N., JETP, 1967, 53, 654.
- 10 Abramovsky V.A., Gribov V.N., Kancheli O.V., Yad. Fiz.  
1973, 18, 595.
- 11 Levin E.M., Ryskin M.G., Yad. Fiz., 1985, 41, 472.
- 12 Feinberg E.L., Chernavsky D.S., Usp. Fiz. Nauk, 1964,  
82, 41.  
Gribov V.N., Yad. Fiz., 1969, 9, 640.
- 13 Kancheli O.V., Pis'ma v JETP 1970, 11, 397;  
Mueller A.H., Phys. Rev. 1970, D2, 2963.
- 14 Henzi K., Valin P., Phys. Lett, 1985, 160B, 167.
- 15 Gribov L.V., Levin E.M., Ryskin M.G., Phys. Lett.,  
1983, 121B, 65.
- 16 Ryskin M.G., Yad. Fiz., (in print).
- 17 Aubert J.J., et al., Nucl. Phys., 1986, B272, 58.
- 18 Levin E.M., Ryskin M.G., Preprint LNPI-1276, Lenin-  
grad, 1987.
- 19 Levin E.M., Ryskin M.G., Yad. Fiz. 1981, 31 1114.
- 20 Mueller A.H., Qiu J., Nucl. Phys., 1985, B268. 127.
- 21 Kwiecinski J. Talk at the VIII Int. Seminar of High  
Energy Physics Problems, Dubna 19-24 June 1986;  
preprint 1928/Th Inst. of Nucl. Phys.,  
Krakow Z., Phys., 1985, 29, 147

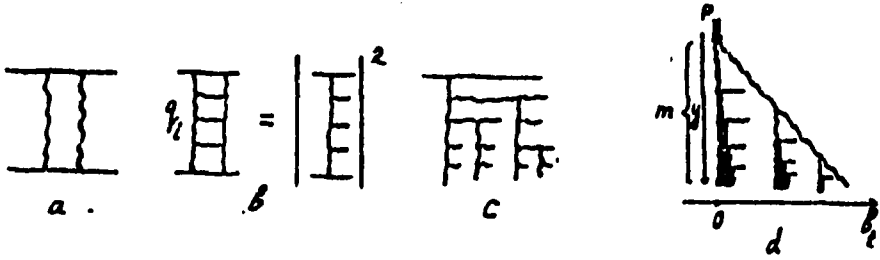


Fig. 1. The diagrams for hadron interaction at high energies. The increase of the thickness of the lines in fig. 1d reflects the growth of the characteristic transverse momenta.

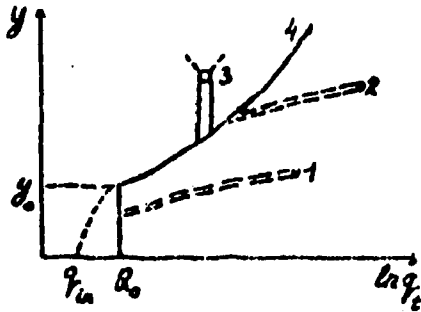


Fig. 2.

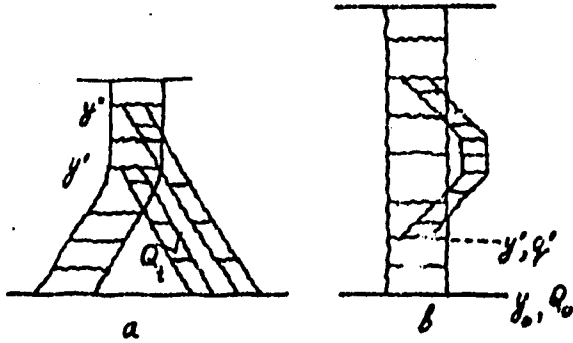


Fig. 3.

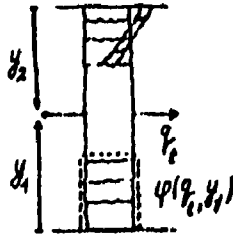


Fig. 4.

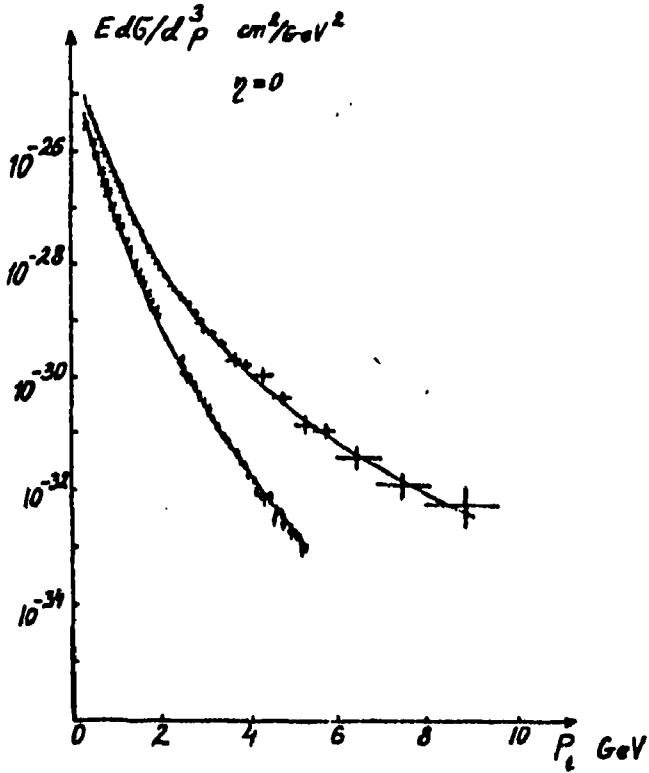


Fig. 5a. The dependence of the inclusive cross sections for the secondary hadron production on  
 a) the transverse momentum ( $\eta = 0$ )

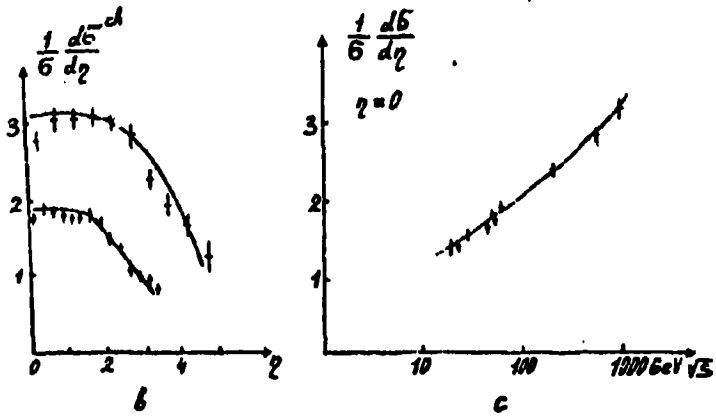


Fig. 5b.c. The dependence of the inclusive cross sections for the secondary hadron production on  
 b) the rapidity, c) the initial energy  
 ( $\eta = 0$ )

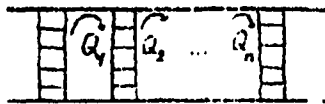


Fig. 6

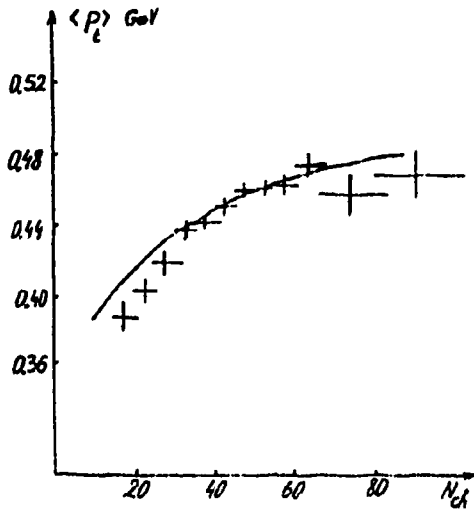


Fig. 7. The mean transverse momentum  $p_t$  of charged hadrons versus the multiplicity in the event.

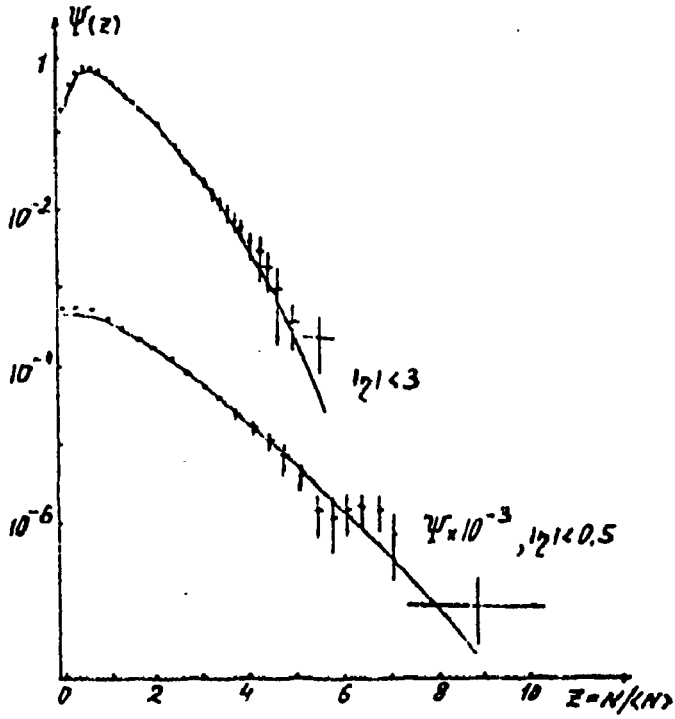


Fig. 8. KNO distribution in the charged hadron multiplicity (N).

$$G_N = G_{in} \Psi(z) / \langle N \rangle ; z = \frac{N}{\langle N \rangle}$$

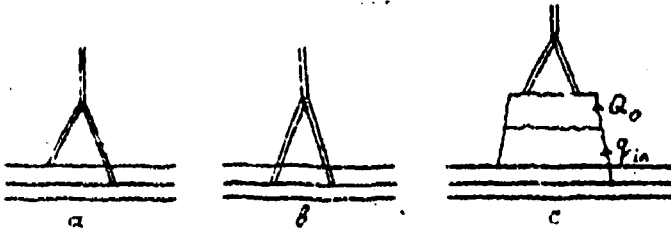


Fig. 9.

CORRELATION PHENOMENA IN PARTICLE PRODUCTION  
ON NUCLEI

B. B. Levchenko

Nuclear Physics Institute, Moscow State University  
Moscow, USSR

The necessary condition for creation of the QGP in the nuclear collisions is a high density of matter exceeding certain critical density. This density can be evaluated one knows the dimensions of the particle production region. These dimensions can be inferred from measurements of the identical particle correlations [1]. Namely, one has to measure the correlation function

$$C(\vec{p}_1, \vec{p}_2) = P(\vec{p}_1, \vec{p}_2) / (P(\vec{p}_1) \cdot P(\vec{p}_2)) \quad (1)$$

where  $P(\vec{p}_1, \dots, \vec{p}_n)$  is the probability of observing the particles  $\vec{p}_1$  through  $\vec{p}_n$  all in the same event. The calculations (1) showed that for uncorrelated sources of particles  $\vec{p}_1$  and  $\vec{p}_2$

$$C(\vec{p}_1, \vec{p}_2) = 1 + e^{-q^2 L^2} / (1 + q_0^2 \tau^2), \quad (2)$$

where  $q = p_1 - p_2$ ,  $q_0 = \epsilon_1 - \epsilon_2$ ,  $p = (\epsilon, \vec{p})$ ,  $L$  is linear dimension of the particle production region,  $\tau$  is the life time of the source.

On the other side, for many years in particles physics one has studied the two particle correlation function

$$R_2(\alpha_1, \alpha_2) = \frac{(1, 2)}{(1)(2)} - 1 \quad (3)$$

where  $(i) = \frac{d\sigma}{\sigma_{in} d\alpha_i}$ ,  $(i,K) = \frac{1}{\sigma_{in}} \frac{d\sigma}{d\alpha_i d\alpha_K}$ ,  $\alpha = (\eta, y, x, \vec{P}_1, \dots)$ .

In Fig. 1 we present, for example,  $R_2(y_1^*, y_2^*)$  for charge particles produced in nucleon-nucleon (NN), nucleon-nucleus (NB), and nucleus-nucleus (AB) (expected form) interactions at few hundred GeV.

From definitions (1) and (3) it follows that the two correlation functions are practically the same function. Therefore, if one could compute  $R_1$  for NN, NB, AB interactions in the framework of some multiproduction model, then the function (2) or its like would allow one to determine the particle source size and its A-dependence. Moreover, in the Glauber type models one can relate to each other  $R_2$  for all the three types of collisions and relate the particle source sizes  $R_2(y_1^*, y_2^*)$  in NN, NB and AB collisions.

Using the Glauber multiple scattering model the following equation relates the correlation function  $R_2^{NB}$  and  $R_2^{NN}$  for the production on nuclei and nucleons may be obtained [2]:

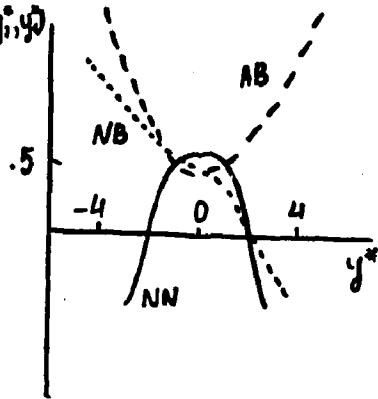


Fig. 1

$$R_2^{NB}(\vec{P}_1, \vec{P}_2) = \frac{\langle V^2 \rangle - \langle V \rangle^2}{\langle V \rangle^2} + \frac{1}{\langle V \rangle} R_2^{NN}(\vec{P}_1, \vec{P}_2). \quad (4)$$

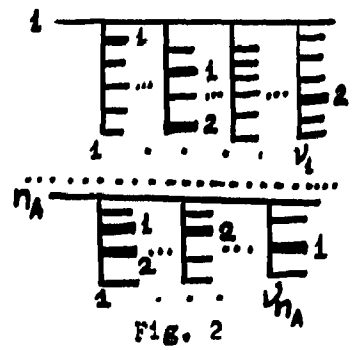
Here  $V$  stand for the number of inelastic collisions of the incident fast nucleon with the nucleons of the nucleus (the number of wounded nucleons).

Now we calculate the function  $R_2^{AB}$  following the



method [2] and using the multiple-scattering formalism [3] used for the calculation different kinds of the cross-sections in framework of the optical approximation to the Glauber model.

In Fig.2 we present multiscattering diagram an AB interaction. Let us call  $G^{n_A, n_B, \{v_i^A\}}$  ( $i = 1, \dots, n_A$ ) the probability that  $n_A$  ( $n_B$ ) nucleons of A(B) are wounded and the  $i$ -th nucleon of A collides with  $v_i^A$  of these nucleons of B. Then the single particle inclusive spectrum (see Fig.2) is



$$(1)_{AB} = \frac{1}{\sigma_{AB}} \sum_{n_A=1}^A \sum_{n_B=1}^B \sum_{\{v_i^A\}} \sigma^{n_A, n_B, \{v_i^A\}} v_i^A (1)_{NN}$$

$$= \frac{1}{\sigma_{AB}} \sum_{v=1}^B \sum_{n_A=1}^A \sigma^{n_A, v} n_A \cdot v \cdot (1)_{NN} = \langle n_A \cdot v \rangle \cdot (1)_{NN} \quad (5)$$

here

$$\sigma^{n_A, v}(b) = \binom{A}{n_A} [\sigma_{NB}(b)]^{n_A-1} [1 - \sigma_{NB}(b)]^{A-n_A} \binom{B}{v} [\sigma_{TA}(b)]^v [1 - \sigma_{TA}(b)]^{B-v} \quad (6)$$

and  $\sigma_{NB}(b)$  is the nucleon-nucleus B profile function, given by

$$\sigma_{NB}(b) = (1 - (1 - \sigma_{TA}(b))^B)$$

Using eq. (6) from eq.(5) can be obtained

$$\langle n_A v \rangle = A \cdot B \cdot \sigma / \sigma_{AB}$$

The two particle inclusive spectrum as it following from Fig. 2, is

$$(1,2)_{AB} = \frac{1}{\sigma_{AB}} \sum_{n_A=1}^A \sum_{n_B=1}^B \sum_{\{v_i^A\}; \{v_j^B\}} \sigma^{n_A, n_B, \{v_i^A\}, \{v_j^B\}} [v_i^A (v_i^A - 1) (1)_{NN} (2)_{NN} + v_j^B (1,2)_{NN}]$$

$$+ v_i v_j (1)_{NN} (2)_{NN}] = [\langle n_A v^2 \rangle + \langle n_A (n_A - 1) v_i v_j \rangle + \langle n_A v \rangle R_2^{NN}]. \quad (7)$$

Integrating the eq.(5) and (7) over the impact parameter  $b$  we obtain

$$R_2^{AB} = \frac{\langle n_A (n_A - 1) v_i v_j \rangle - \langle n_A v \rangle^2 + \langle n_A v^2 \rangle}{\langle n_A v \rangle^2} + \frac{R_2^{NN}}{\langle n_A v \rangle} \quad (8)$$

The equations (4) and (8) enable one to connect the functions  $R_2^{AB}$  and  $R_2^{NB}$ . In order to do so we use the fact that eq.(6) for  $G^{n_A, v}$  factorizes as a function of variables  $n_A$  and  $v$  and therefore

$$\langle n_A^k \cdot v^l \rangle = \langle n_A^k \rangle \langle v^l \rangle$$

It results in :

$$R_2^{AB} = \frac{\langle n_A (n_A - 1) v_i v_j \rangle - \langle n_A v \rangle \langle n_A v \rangle}{\langle n_A v \rangle^2} + \frac{R_2^{NB}}{\langle n_A v \rangle} \quad (9)$$

Equations (2), (4), (8) and (9) enable one to relate the linear dimensions of the particle source in the three type reactions:

$$\lambda_{AB} e^{-q^2 L_{AB}^2} = \Delta R_{NB} + \frac{\lambda_{NB} e^{-q^2 L_{NB}^2}}{\langle n_A \rangle} = \Delta R_{NN} + \frac{\lambda_{NN} e^{-q^2 L_{NN}^2}}{\langle n_A v \rangle} \quad (10)$$

where  $\lambda = 1 / (1 + q_0^2 \tau^2)$  and  $\Delta R$  is the first terms on the right side of eq. (8) - (9) correspond to the long range piece of the correlation function.

Using the same method one can obtain the relations between the Wroblewski's ratio  $D/\langle N \rangle$  for the particle multiplicity in AB, NB and NN collisions.

So

$$\left(\frac{D}{\langle NN \rangle}\right)_{AB}^2 = \Delta R_{NB} + \frac{I}{\langle n_A \rangle} \left(\frac{D}{\langle NN \rangle}\right)_{NB}^2 = \Delta R_{NN} + \frac{I}{\langle n_A \rangle} \left(\frac{D}{\langle NN \rangle}\right)_{NN}^2 \quad (\text{II})$$

In conclusion one must note that relations (5) and (7) correspond to an asymptotical energy and at present energy must take into account the energy-momentum corrections. Yet in the relationship (3) the major part of the finite energy corrections are cancelled.

More consistent calculations of the correlation functions (4) should rely upon models which do explicitly incorporate energy-momentum conservation. The principal conclusions on the A-dependence of  $R_2$  are preserved, though the counterparts of simple and self-explanatory formulae (10) are fairly complicated ones.

I would like to thank the Institute of Physics Slovak Academy of Sciences for hospitality during the conference and Prof. J. Pišut and Š. Olejník. I thank to N.N. Nikolaev for discussions.

#### R e f e r e n c e s

- [1] G.I. Kopylov, M.I. Podgoretsky, *Yad. Fis.* 19 1974 434;  
R. Lednicky, M.I. Podgoretsky, *Yad. Fis.*, 30 1979 837;  
R. Lednicky, V.L. Lyuboshits, M.I. Podgoretsky, *Yad. Fis.*  
38 1983 251
- [2] E.M. Levin, N.N. Nikolaev, M.G. Ryskin, *Z. Physik* 05 1980  
285
- [3] C. Pajares, A.V. Ramallo, *Phys. Rev.* D31 1980 2800;  
A. Capella et al. *Z. Physik* C33 1987 541
- [4] B.B. Levchenko, to be published

# PARTICLE PRODUCTION IN ULTRARELATIVISTIC PROTON-PROTON AND PROTON-NUCLEUS COLLISIONS IN A PARTON-STRING MODEL

M. Kutschera  
Institute of Nuclear Physics  
ul. Radzikowskiego 152  
31-342 Kraków, Poland

## Introduction

A successful detection of a quark-gluon plasma phase in ultrarelativistic heavy ion collisions will require an answer to the question how different is the normal production of particles from the production resulting from a collective behaviour of the plasma phase. Our aim here is to present a model of normal production of particles in pp and pA collisions, which is a first step in this direction. Since in the area of soft processes QCD does not yet provide quantitative predictions, one has to rely on phenomenological models, which are compatible with QCD, and implement as many measured quantities as possible.

In my talk I shall discuss a model<sup>1,2,3)</sup>, which was developed by K. Werner, J. Hüfner, O. Nachtmann and myself in Heidelberg. The model is a specific realization of the parton model ideas, and is most closely related to the Dual Parton Model of Capella et al.<sup>4)</sup> Presently K. Werner at BNL is working on the Monte-Carlo version of the model with the aim to construct an event generator for ultrarelativistic heavy ion reactions, which would fully account for the normal production of particles.

The physical picture of a pA collision is as follows: When the projectile proton traverses the nucleus, one or more collisions with target nucleons take place. These collisions are assumed to proceed by a colour exchange between quarks, antiquarks and gluons of the projectile and the appropriate partons of the target nucleon. Alternatively, one can view this

process as stripping quarks, antiquarks and gluons off the projectile<sup>2)</sup>. As a result, a number of colour strings are produced, which later on hadronize into observed particles. The dynamics of soft collisions cannot at the moment be calculated from QCD. Instead, for description of inclusive hadron-hadron collisions we shall employ the parton distribution functions in nucleons and the fragmentation functions of the colour strings, as measured in  $e p$ ,  $\mu p$ ,  $\nu p$  and  $e^+ e^-$  reactions. An essential assumption is that these functions are somehow universal, i.e. can be measured in lepton scattering off nucleons.

### Proton-proton scattering

When colour is exchanged between projectile and target protons, Fig. 1, the space-time structure of colour singlets is changed. Now the singlet is formed by partons moving in opposite directions. In Fig.1 there are two such states after the collision takes place. These are the colour strings, which, as virtual objects, have to decay into hadrons. Leading particles in this case are products of hadronization of a diquark (by diquark we always mean a remnant,  $N-q$ , after removing a parton  $q$  from the nucleon). We sometimes refer to this process as quark removal. The diagram a of Fig.1 is supposed to be mainly responsible for the inelastic production at small  $x$ . The other basic process, giving the diffractive peak in  $pp$  scattering, is the removal of a colour-neutral  $q\bar{q}$  pair from the projectile. In principle the quark can be a valence quark or a sea quark, and the remaining three quark system ( $B=1$ ) can be excited. In Fig.1 and Fig.3 the arrows indicate the colour exchange.

Longitudinal momentum distributions of hadrons  $h$  produced in a  $pp$  collision,  $f^{ph}(x, p_T)$ , are measured as inclusive cross sections for given value of  $p_T$  :

$$f^{ph}(x, p_T) = x \frac{d^3 \sigma_{pp \rightarrow hX}}{dx d^2 p_T} \frac{1}{\sigma_{in}^{pp}} \quad (1)$$

where  $x$  is the momentum fraction of the observed hadron  $h$  relative to the projectile momentum  $p_0$ ,  $x = p_h/p_0$ . The functions  $f^{ph}(x, p_T)$  contain the dynamics of the process.

To calculate longitudinal momentum distributions for various hadrons we evaluate the diagrams schematically shown in Fig.1. To do so for hadrons  $h$  originating from the proton remnant  $N-q$ , we have to specify both the momentum distribution of this remnant,  $\rho_{qq}(x)$ , and the function  $D_{qq}^h(z)$ , describing the distribution of momenta of hadrons  $h$ , which were produced by fragmentation of the remnant  $N-q$  ( $\equiv qq$ ). The contribution of diagram a of Fig.1 is then:

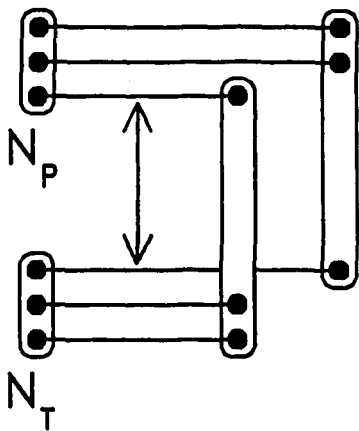
$$f_a^{ph}(x, p_T) = x \int \frac{dy}{y} \rho_{qq}(y) D_{qq}^h\left(\frac{x}{y}, p_T\right). \quad (2)$$

As the diquark distribution function,  $\rho_{qq}(z)$ , we take the measured quark distribution function,  $q(z)$ , calculated at the complementary momentum  $1-z$ :  $\rho_{qq}(z) = q(1-z)$ . In the actual computations we take care of flavours, which we suppress here for simplicity of notation. Similarly, to evaluate the diagram b of Fig.1, we need the momentum distribution of the remnant  $N-q\bar{q} \equiv qq\bar{q}$  (a triquark), for which we take a convolution of measured quark and antiquark structure functions at  $1-z$ :  $\rho_{qq\bar{q}}(z) = q\bar{q}(1-z)$ .

We take fragmentation functions of the projectile remnants into observed hadrons, if only possible, from measurements in lepton-nucleon scattering. The diquark fragmentation functions,  $D_{qq}^h$ , are well measured for various final hadrons<sup>3)</sup>, whereas no such measurements are available for the triquark fragmentation function  $D_{qq\bar{q}}^h$ . We choose this function somewhat arbitrarily to be  $D_{qq\bar{q}}^h(z) = \delta_{hp} \delta(1-z)$ . By this choice we do not allow for excitation of the projectile proton by the  $q\bar{q}$  pair removal. This also means that the diagram b of Fig.1 gives a contribution to  $f^{ph}(x, p_T)$  only when the observed hadron is the same as the projectile, which reads

$$f_b^{ph}(x, p_T) = x \int \frac{dy}{y} q\bar{q}(1-y) D_{qq\bar{q}}^h\left(\frac{x}{y}, p_T\right). \quad (3)$$

a)



b)

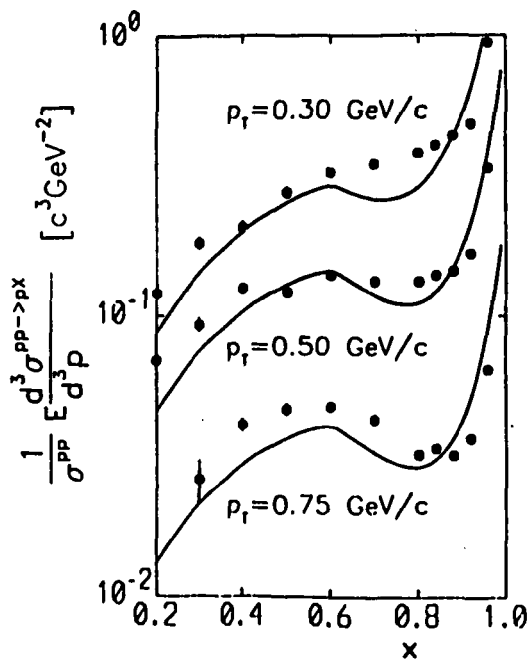
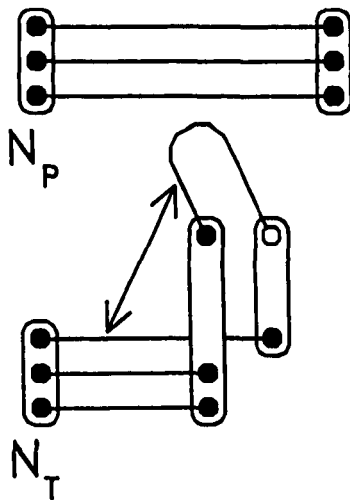


Fig.1 Two basic processes of the model: quark removal (a) and quark-antiquark pair removal (b).  $N_P$  is the projectile nucleus,  $N_T$  is the target nucleus.

Fig.2 The longitudinal momentum distribution of protons in a pp collision for different values of  $p_t$ , data ref. 6. For large  $p_t$  the two contributions: q-removal, Fig.1a, and  $q\bar{q}$  pair removal, Fig.1b, are clearly distinguishable.

In cases, when the detected hadron  $h$  is not the same as the projectile, only the diagram a of Fig.1 contributes, as we have neglected excitation of the triquark in Fig.1b. When the detected and incident hadrons are identical, both contributions, eqs. (2) and (3), are present.

We have identified<sup>1)</sup> the  $q\bar{q}$ -pair removal with the diffractive target excitation. This contribution gives a peak at  $x \rightarrow 1$ , as it is proportional to  $q\bar{q}(1-x)$ , which in this limit varies as  $1/(1-x)$ . To account quantitatively for the diffractive events we have to weight appropriately the two contributions,  $f_a^{ph}$  and  $f_b^{ph}$ :

$$f^{ph}(x, p_T) = (1-w)f_a^{ph} + wf_b^{ph}. \quad (4)$$

Parameter  $w$  can be identified with the ratio of the diffractive production cross section to the total inelastic  $pp$  cross section:  $w = \sigma_d^{pp}/\sigma_{in}^{pp}$ . Data from ref<sup>5)</sup> show, that  $w = 0.2$  for  $pp$  and  $w = 0.15$  for  $n^+p$ .

Fig.2 shows the inclusive cross section for the reaction  $pp \rightarrow pX$ . The data points are from ref<sup>6)</sup> at 100 GeV. In ref<sup>1)</sup> the detailed description of the structure and fragmentation functions used, is given. One can also find there the discussion of the transverse momentum dependence of the inclusive cross section. Our model agrees with the data reasonably well.

#### Proton-nucleus collisions

To generalize the above ideas to the case of  $pA$  scattering, we consider first the second collision. In the Dual Parton Model of Capella et al.<sup>4)</sup>, the leading diquark, which is formed in the first collision, does not change its nature in subsequent collisions. This corresponds, in the language of Fig.1b, to  $q\bar{q}$ -pair stripping off the leading diquark in the second, third, etc...., collisions. We have developed an alternative view in ref<sup>2)</sup>, namely we have considered stripping of a quark also in the second collision. We thus allow for diquark breaking. It was shown<sup>2)</sup> that inclusive pion spectra



from measurement by Barton et al.<sup>7)</sup> of proton-nucleus collisions suggest that this really happens. We have used the characteristic difference between fragmentation functions of diquark and quark into pions to identify the leading parton after two collisions.

Typical diagrams for two inelastic collisions are shown in Fig.3. We allow for stripping a quark off the projectile with probability  $1-w$ , and a  $q\bar{q}$ -pair with probability  $w$ . Fig.3c shows the double stripping of quarks, what produces the single leading quark after two collisions. For higher number of collisions,  $\nu \geq 3$ , we will limit ourselves to the two basic processes mentioned above, with the restriction, that the leading parton cannot be in a zero- or negative baryon number state.

Longitudinal momentum distributions of hadrons  $h$  originating from the leading parton after exactly  $\nu$  collisions,  $f_{\nu}^{ph}(x, p_T)$ , is thus given by a formula:

$$f_{\nu}^{ph}(x, p_T) = \sum_{m \geq 1} A_{\nu}^{(m)} \int dy \frac{x}{y} \rho_{\nu}^{(m)}(y) D_{qm}^h\left(\frac{x}{y}, p_T\right), \quad (5)$$

where  $A_{\nu}^{(m)}$  is the probability for the projectile remnant to contain  $m$  valence quarks,  $\rho_{\nu}^{(m)}(x)$  is the momentum distribution function of the leading projectile remnant, and  $D_{qm}^h(z)$  is its fragmentation function into hadrons  $h$ . Formula (5) says, that this leading object contains at least one valence quark. The fragmentation functions of a quark and diquark are taken from measurements of the lepton-induced reactions. For triquark fragmentation we use the function described above. The remnant momentum distributions,  $\rho_{\nu}^{(m)}$ , are calculated as suitable many-fold convolutions of quark and antiquark structure functions.

The inclusive cross section to observe hadron  $h'$  as a product of the collision of hadron  $h$  with the nucleus  $A$  is expressed by functions  $f_{\nu}^{hh'}$  according to the formula:

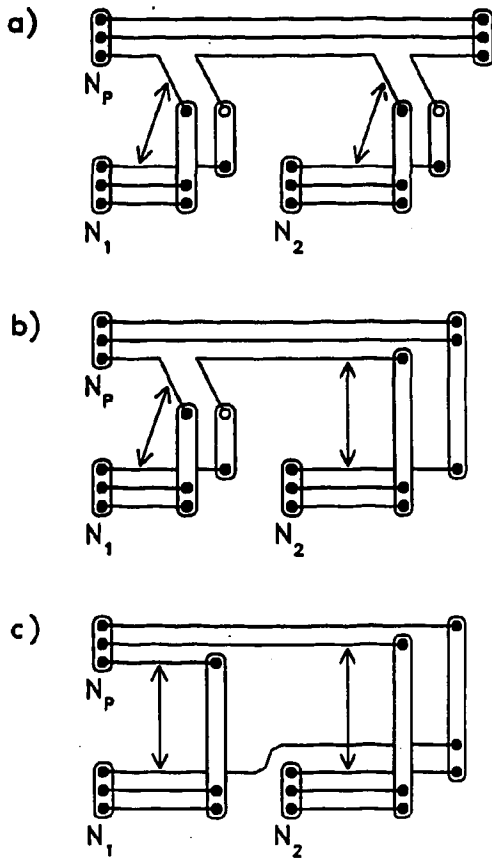


Fig.3 The interaction of the projectile nucleus  $N_p$  with two target nucleons. (a): the removal of two  $q\bar{q}$  pairs, (b): the removal of one  $q\bar{q}$  pair and one quark, (c): double quark stripping.

$$x \frac{d^3 \sigma_{hA \rightarrow h'A}}{dx d^2 p_T} = \sum_{\nu \geq 1} \sigma_{\nu}^{hA} f_{\nu}^{hh'}(x, p_T) \quad (6)$$

where  $\sigma_{\nu}^{hA}$  are the geometrical cross sections for exactly  $\nu$  inelastic collisions of hadron  $h$  on nucleus  $A$ . These are calculated using the Glauber formula:

$$\sigma_{\nu}^{hA} = \int d^2 b T^{\nu}(b) e^{-T(b)} \frac{1}{\nu!} \quad (7)$$

The thickness function

$$T(b) = \sigma_{in}^{hN} \int dz n(b, z) \quad (8)$$

is calculated using the inelastic hadron-nucleon cross section  $\sigma_{in}^{hN}$  and the nuclear matter density  $n(r)$  of the target nucleus ( $\int n(r) d^3 r = A$ ).

#### Results and discussion

Fig.4 shows the results of our calculations of the absolute values of the inclusive cross sections for the reaction  $pA \rightarrow hX$ , where  $h = p, \pi^{\pm}$ . The data are from Barton et al.<sup>7)</sup> at 100 GeV. For protons the data stop at a too low  $x$  to see the peak near  $x=1$ , which is present in Fig.2. The  $\pi^+$  spectra exhibit a peculiar behaviour: for  $x \rightarrow 1$  the cross section for  $pp \rightarrow \pi^+X$  drops faster than that for  $p^{12}C \rightarrow \pi^+X$ . This cannot be explained by the energy loss of the projectile proton, since the energy loss is larger in a collision on carbon nucleus, and from such an argument one would expect the cross section to drop faster for  $p^{12}C$  than for  $pp$ . The qualitative agreement of our calculation with the data is due to quark fragmentation in the case of  $p^{12}C$  collision. The quark fragmentation into  $\pi^+$  produces a harder spectrum than that of the diquark. For  $pp$  collision the fragmenting leading parton is a diquark, while in  $p^{12}C$  collision we also have a leading quark, producing harder pions.

As many other authors<sup>4,8)</sup> we have treated quarks and gluons

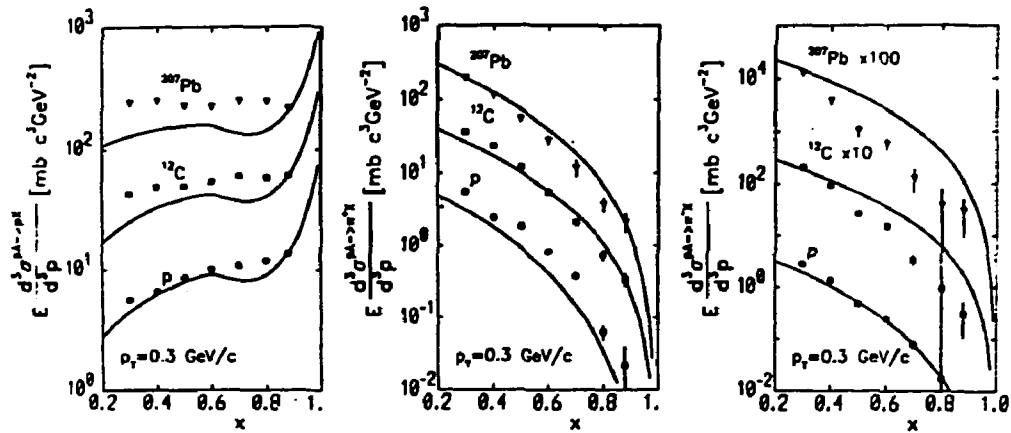


Fig. 4 Experimental and calculated cross sections for the reactions  $pA \rightarrow hX$ . The observed hadron is a proton (left), a  $\pi^+$  (middle) and a  $\pi^-$  (right), respectively. The solid lines are the results of the calculations. The data are from Barton et al.<sup>7)</sup>

very differently. Colour exchange in our model occurs only between quarks, while the gluons are treated as spectators. The gluon contribution is accounted for partially by employing the measured fragmentation functions. To estimate the influence of including the dynamical gluons, we have calculated a diagram corresponding to the Fig.1a, i.e. the gluon removal<sup>3)</sup>. In case of gluon removal the leading parton is a triquark in a colour-octet state. Making the same assumption for its fragmentation function as for the colour-neutral triquark, and using the gluon structure function of ref.<sup>9)</sup>, we find the inclusive pp scattering with single quark and gluon removal to be qualitatively similar to the case of q and qq-pair removal<sup>3)</sup>. Discrepancies between the predictions and the data in this case are probably due to our oversimplified assumptions about fragmentation of triquark.

The author is grateful to K. Werner, J. Hüfner and O. Nachtmann for creating an enjoyable and stimulating atmosphere during our work in Heidelberg. He would also like to thank the organizers of the Smolenice conference for invitation and warm hospitality and Wojciech Broniowski for reading the manuscript.

#### References

- 1) K. Werner and M. Kutschera, Phys. Lett. B183, 385 (1987)
- 2) K. Werner, J. Hüfner, M. Kutschera and O. Nachtmann, Phys. Rev. Lett. 57, 1684 (1986)
- 3) K. Werner, J. Hüfner, M. Kutschera and O. Nachtmann, Heidelberg University preprint HD-IVP-87-4
- 4) A. Capella and J. Tran Thanh Van, Z. Phys. C10, 249 (1981)
- 5) A. Wróblewski, in Proceedings of the XIV International Symposium on Multiparticle Dynamics, Granlibakken 1983, P. Yager and J. F. Gunion (Eds.), World Scientific Publ. Comp.
- 6) A. E. Brenner et al., Phys. Rev. D26, 1497 (1982)
- 7) D. S. Barton et al., Phys. Rev. D27, 2580 (1983)
- 8) V. V. Anisovich, Yu. M. Shabelsky and V. M. Shekhter, Nucl. Phys. B133, 477 (1978)
- 9) D. W. Duke and J. F. Owens, Phys. Rev. D30, 49 (1984)  
J. F. Owens, Phys. Rev. D30, 943 (1984)

NUCLEAR STRUCTURE FUNCTIONS AND CUMULATIVE  
PROCESSES

Efremov A.V. - JINR, Dubna

**Abstract**

The author's point of view on nuclear quark structure is presented. Different models for explaining the EMC effect are reviewed. It is also shown that cumulative production data can be used to improve our understanding of the EMC effect and to give evidence for its multiquark nature.

Discovery of the EMC-effect<sup>/1/</sup> has drawn attention of the world-wide community of physicists to the problem of quark structure of nuclei, and to its irreducibility to the quark structure of constituent nucleons only<sup>/2/</sup>. Stream of theoretical papers followed the discovery of EMC suggesting a whole spectrum of possibilities for understanding the phenomena<sup>/3/</sup>. However, many of the suggestions met with difficulties after a change of experimental data on  $F_A/F_D$  in the region of small  $X$ <sup>/4,5/</sup>. Nowadays, when all suggestions seem to be made, one can try to analyze them on a general basis and to estimate to what extent the nuclear quark structure is understood and what is still unclear.

**1. CONNECTION OF NUCLEUS AND NUCLEAR QUARK STRUCTURE**

Probably G. West first noticed that QCD evolution equations results in a simple convolution relation of nonsinglet quark distribution functions (the valence quarks) of nucleus and nucleon\*

$$x F_{3A} \approx \bar{V}_A(x, Q^2) = \int T_A^{NS}(\alpha) \bar{V}_N\left(\frac{x}{\alpha}, Q^2\right) d\alpha, \quad (1a)$$

where the function  $T_A^{NS}(\alpha)$  satisfies the baryon number sum rule

$$\int_0^A T_A^{NS}(\alpha) d\alpha = 1 \quad (1b)$$

(all nuclear functions are here divided by  $A$ ). Due to this, one can consider  $T^{NS}$  as an effective valence nucleon's distribution function over a fraction of momenta  $\alpha$  (in spite of the impossibility of expressing it through the one-nucleon wave function). The problem is as follows: does it describe a process that defines the distribution  $T^{NS}$  (e.g. the stripping of a nucleon)?

A similar relation can be written for the doublet channel as well<sup>7,8)</sup> which mixes the singlet quark,  $\Sigma(x, Q^2) = \sum_f x(q_f, u, Q^2) + q_f(u, u^c) = k_2$ , and gluon distributions functions

$$\Sigma_A(x, Q^2) = \int_0^A T_A^S(\alpha) \Sigma_N(\frac{x}{\alpha}, Q^2) d\alpha \quad (2a)$$

$$G_A(x, Q^2) = \int_0^A T_A^S(\alpha) G_N(\frac{x}{\alpha}, Q^2) d\alpha \quad (2b)$$

where, in general,  $T_A^S \neq T^{NS}$  and  $T^S$  satisfies the energy-momentum sum rule

$$\int_0^A T_A^S(\alpha) d\alpha = M_A / A M_N \simeq 1 \quad (2c)$$

Really, diagonalizing the system of two linear evolution equations for the moments  $\Sigma(n, Q^2)$  and  $G(n, Q^2)$ , one can obtain the relation for two eigenfunctions  $f_A^\pm(n, Q^2) = \Sigma_A(n, Q^2) \cdot C_n^\pm(n, Q^2) / G(n, Q^2)$  ( $C_n^\pm$  are some diagonalizing coefficients depending on anomalous-dimension matrix):

$$f_A^\pm(n, Q^2) = T_A^\pm(n) f_N^\pm(n, Q^2) \quad (3)$$

Now, let us take into account the fact that both nucleons and nucleus are bound states of quarks and gluons. Due to this quark (and gluon) propagator  $\langle P | \bar{q}(0) q(\bar{z}) | P \rangle$  must satisfy a homogeneous Bethe-Salpeter equation (Fig.1) whose eigenvalues determine the effective mass (the binding energy) of the quarks. The quark distribution function is expressed through the limit of this propagator when  $\bar{z} \rightarrow 0$ , regularized with the help of an ultraviolet cutoff parameter  $Q^2$ . In the approximation of leading twist, i.e. disregarding  $1/Q^2$  corrections, the equation of Fig.1 become algebraic: there is no  $Q^2$  dependence and, consequently, the mass-independent coefficients are the same for the nucleus and nucleon

$$\Sigma(n, Q^2) = K_{qq}(n)\Sigma(n, Q^2) + K_{q_0}(n)G(n, Q^2).$$

For this reason,

$$\left( \frac{\Sigma(n, Q^2)}{G(n, Q^2)} \right)_A = \left( \frac{\Sigma(n, Q^2)}{G(n, Q^2)} \right)_N = (1 - K_{qq})^{-1} K_{q_0}(n),$$

and  $T'_A = T'_A \equiv T'_A$ , which give, together with (3) relations (2).

An immediate consequence of relations (2) is the equality of average momenta fractions of gluons and quarks and antiquarks in the nucleus and nucleon

$$\frac{\langle xq \rangle_A}{\langle xq \rangle_N} = \frac{\langle xG \rangle_A}{\langle xG \rangle_N} = 1 \quad (4)$$

This relation is in good agreement with EMDMS<sup>14/</sup> data which are the most precise nowadays:  $(\langle x \rangle_{N_A} / \langle x \rangle_{01} - 1) = (0.7 \pm 1.7 \pm 1.0)\%$ . (The old EMD-data<sup>11/</sup> give for the quantity  $(7.1 \pm 1.0 \pm 3.0)\%$ ).

The relation (4) clearly contradicts the rescaling hypothesis<sup>12/</sup> in explanation of the EMC-effect. In fact, the passage from nucleon to nucleus in these models is equivalent to the growth of  $Q^2$  for which, according to<sup>13/</sup>,  $\langle xq \rangle$  increases and  $\langle xG \rangle$  decreases.

In conclusion of this section let us stress once more that QCD evolution equations just as relation (3) are results of the leading twist approximation. So, the relations (1) and (2) do not include the nuclear screening which is formally a high-twist effect<sup>10,11/</sup>.

## 2. THE EMC-EFFECT

Let us see now what the EMC-effect means in the frame of our approach. Let us assume that the functions  $T'_A$  determine an effective distribution of nucleons in nucleus, at least approximately, and therefore they are mostly concentrated in the region of  $\alpha \approx 1$  (i.e. in the region of zero internal momentum of the nucleon). Expanding  $F_N(\frac{x}{A})$  in (1) and (2) around  $\alpha = 1$ , it is easy to obtain for not very large  $x$



$$R = \frac{F_A}{F_N} \approx \langle T_N \rangle + \langle (1-x) T_N \rangle \times \frac{F_N'(\alpha)}{F_N(\alpha)} + \frac{1}{2} \langle (1-x)^2 T_N \rangle \times \left( x \frac{F_N''}{F_N} + 2 \frac{F_N'}{F_N} \right) + \dots \quad (5)$$

where  $\langle \rangle$  means integration over interval  $[0, A]$ . If one accept that  $F_N \sim (1-x)^\kappa$  and  $\kappa \approx 3$ , then  $x$ -dependences of the second and the third term are the factors  $-Kx/(1-x)$  and  $Kx(1-x) \left[ \frac{K(1-x)}{(1-x)} - 2 \right]$  respectively. In the region of  $x \approx 0.5$  the second term is close to zero and to obtain the depletion in the region one should have

$$\langle T_A^S \rangle - 1 = \Delta_A > 0 \quad \text{or} \quad \int_0^A (T_A^S(\alpha) - T_A^{NS}(\alpha)) d\alpha = \Delta_A > 0 \quad (6)$$

for the ratio  $R_2$  of the structure functions  $F_2 \approx \Sigma$  and

$$1 - \langle \alpha T_A^{NS} \rangle = \delta_A > 0 \quad \text{or} \quad \int_0^A \alpha (T_A^S(\alpha) - T_A^{NS}(\alpha)) d\alpha = \delta_A > 0 \quad (7)$$

for the ratio  $R_3$  of the structure functions of  $x F_3^*$ .

In addition, in the region  $x \approx 0.5$  the sea quarks are practically absent; therefore one can expect that and

$$\delta_A \approx \Delta_A \quad (\text{more exactly } 2/3 \Delta_A) \quad (8)$$

The relations (8) and (7), mean that the number of "effective nucleons" in a nucleus have to be more than  $A$ , and valence nucleons have to carry only a part of the total nucleus momentum. In other words, there is a repumping over of part of momentum from valence quarks to sea quarks, in the nucleus in comparison with free nucleons.

Notice that the shock produced by the discovery EMC was due to the prejudice that a nucleus is made of  $A$  nucleons and so the condition  $\Delta_A = 0$  has to be imposed on the distribution  $T$ , which unavoidably results in  $R_2(x \approx 0.5) = 1$ , independent of the form of  $T$ . In this sense, the difference between  $T^S$  and  $T^{NS}$  (necessary to explain the EMC-effect) leads to the irreducibility of nuclear quark structure to the quark structure of free nucleons.

\* For a more accurate proof of this result see <sup>16/</sup>.

In spite of its generality, this approach allows to draw a number of interesting conclusions:

i) It immediately follows from (6) that the ratio

$$R_2(x=0) = \int_0^A T_A^S(\alpha) d\alpha = 1 + \Delta_A > 1 \quad (9)$$

ii) The most accurate measurement of BCDMS<sup>4/</sup> shows a small ( $\approx 5\%$ ) but definite excess of the ratio over 1 in the region of small, i.e. the same value as the loss of momenta of the valence nucleons  $\bar{\delta}_A$ . This means a small number of particles of the nonnucleon component. However, they have to be heavy enough to supply the 5% pumping over of the momentum ( $\rho$ -mesons, NN-pairs or pions far off the mass shell). So, in addition to the internucleon sea there is a small ( $\approx \Delta_A$ ), but hard enough "collective sea" of quark-antiquark pairs in nuclei.

Using (1) and (2) it is easy to obtain for the sea

$$O_A(x) = \sum_A -V_A = \int_x^A T_A^{NS}(\alpha) O_N(\frac{x}{\alpha}) d\alpha + \int_x^A (T_A^S(\alpha) - T_A^{NS}(\alpha)) \sum_N(\frac{x}{\alpha}) d\alpha \quad (10)$$

where the first term comes from the internucleon sea, which rapidly decreases with increasing  $X$ , and the second term comes from the hard collective sea  $O_A'$ , because its center of gravity is

$$\bar{\alpha}_{O'} = \langle \alpha (T_A^S - T_A^{NS}) \rangle / \langle T_A^S - T_A^{NS} \rangle = \bar{\delta}_A / \Delta_A \approx 1 \quad (11)$$

For pions on the mass shell this number is  $m_\pi / M_N \approx 1/7$ . That is the reason why the pumping over into the pions<sup>12/</sup> gives no satisfactory description of new data in the region of small  $X$  (too many pions are needed to supply the 5% pumping over).

iii) The place of intersection  $R(x_0) = 1$  does not depend on the sort of nucleus and is at  $x_0 \approx 0.3$ . Really, if there are no screening and light particles in nuclei,  $T_A^S(\alpha)$  has to be smooth enough in the region of small  $\alpha$ . Using then the first two terms of (5) it is easy to find

$$3 \frac{x_0}{1-x_0} \approx \left( 1 - \int_0^{x_0} \alpha T_A^S(\alpha) d\alpha / \int_0^{x_0} T_A^S(\alpha) d\alpha \right)^{-1}$$

The ratio of integrals in the right-hand side is in the interval  $[0, x_0]$  and thus  $0.28 < x_0 < 1/3$ . This feature of the ratio seems confirmed experimentally.

Now, what about the proposed models? Different models are in fact different suggestions of the pumping over mechanisms. Not all of them seem satisfactory from our viewpoint. We have mentioned the rescaling

models<sup>/9/</sup> where part of the pumping-over comes into gluon component. However, the main drawback of these models is the softness of the gluon and the sea component in nucleon. This leads to a too big value of  $R_2(x \approx 0)$  after the 5% pumping over. (Although the authors deny the applicability of their model to the region of small  $X$ ). As it was noticed, models with pumping-over of moments into the mass shell pions<sup>/12/</sup> have the same disadvantage.

Other models can be divided into three big categories:

i) Models with pumping over of the momentum either into massive meson component<sup>/13/</sup> ( $\rho, \omega$ , off the mass-shell pions) or into nucleon-antinucleon pairs<sup>/8/</sup>. A component like that is probably related to the core of nuclear force at small distances. However, it is hard to believe that the nucleon can conserve at such small distances its individual quark structure without converting it into multiquark states;

ii) Pumping inside each nucleon<sup>/14/</sup>, i.e. change of its quark structure due to the influence of the internuclear field. Transition of part of nucleons into  $\Delta$ -isobars<sup>/15/</sup> also belongs to this class. We do not see, however, how it is possible to obtain the hard sea here.

iii) Pumping over inside a multiquark-fluctuation<sup>/16/</sup>. By this we mean not only a bound state of two or more nucleons with interaction of their quarks, as proposed in<sup>/10/</sup>, or an exchange quark interaction in the final state considered in<sup>/17/</sup>. That kind of interactions is inevitable in any theory with a composite nucleon. However, the calculation of the quark structure of states like that seems as difficult as the calculation of the quark structure of nucleus.

It is necessary to stress the important difference between a multiquark state and few-nucleon correlation (FNC)<sup>/18/</sup>. The losses of momenta of the valence quarks for the latter are the same as averaged over the nucleus,  $\Delta_{FNC} = \Delta_A$ , due to a change of structure of each nucleon. For the multiquark, however, it has to be much larger

$$\Delta_{69} > \Delta_A \quad (12)$$

e.g. if there is no pumping-over inside the nucleons, then  $\Delta_A \approx P \Delta_{69}$  where  $P$  is a probability of multiquark states. In fact, the relation (12) can be considered as a definition of the multiquark state. A statistical realization of the hard antiquark sea is known (see Kondratyuk paper<sup>/16/</sup>).

It seems that structure-function measurements cannot distinguish between these models. So, new sources of information are necessary.

One of them is deep-inelastic scattering with measurement of hadrons in a final state. Production of  $\rho$ - and  $\Delta$ -resonances and also  $K^-$ -mesons and antiprotons which carry the information about the collective sea is especially interesting for evident reasons. The published data of the EMC-collaboration give evidence in favour of the enlarged yield of antiprotons from the deuterium in comparison with the hydrogen<sup>/19/</sup>. They also give an argument in favour of an enlarged content of  $\bar{N}N$ -pairs in nuclei<sup>/8/</sup>. However, the excess of antiprotons is so large that seems improbable. In the region of  $X \approx 0.025$  it is about 100%. (It is a new discovery if it is not an error!) Except that, the data on cumulative production of antiprotons, as we see below, give no evidence in favour of this explanation of the EMC-effect.

### 3. CUMULATIVE PARTICLES PRODUCTION

Another source of information is cumulative particle production. Especially, the production of  $K^-$ -meson and antiprotons on nuclei in the region  $X \gtrsim 1$ , because of the peculiarity of the nuclear quark structure mentioned before\*.

However, a question arises: to what extent is the cumulative production cross section determined by the nuclear structure functions  $F_A(x)$ ? Until now there have been no quite reliable data for nuclear deep-inelastic scattering in the region  $X \gtrsim 1$ , though there are some indications of similarity of the cumulative mesons spectra and structure function  $F_2(x)$  in this region<sup>/20/</sup>.

There exist two points of view on the physics of cumulative production<sup>/2/</sup>: (a) "Hot models", in which massive clusters in nuclei (which are necessary to produce a cumulative particle) are formed by an incoming hadron, either by a sort of compression of the nuclear matter and heavy fireball formation or multiple rescattering; (b) "cold models", in which formations of that sort already exist in nuclei because of Blokhintsev's fluctuations of density<sup>/21/</sup> either in a form of multiquark states or in a form of a few-nucleon correlation, resulting in the high-momentum Fermi motion. This reflects in the structure functions of the nucleus. A common property of these models is the independence of type of the nucleus of the nuclear parton fragmentation. This allows us to write down the cross section of the process in the form<sup>/22/</sup>

\*Formally, they can be presented as valence quarks in antinucleons.

$$\frac{E}{A} \frac{dG}{dP} \equiv \rho_{A \rightarrow h}(x, y, P_T) = \int_x^A F_A(x) f_h\left(\frac{x}{A}, y, P_T\right) \frac{d\alpha}{\alpha} \quad (13)$$

where  $x = -u/s$ ,  $y = -t/s$  and the function  $f_h$  does not depend on  $A$ , i.e. it is the same for a nucleus and for a free nucleon. Combining (13) with (1,2), it is easy to obtain a natural expression (illustrated in fig. 2a):

$$\rho_{A \rightarrow h}(x, y, P_T) = \int_x^A N_A(x) \rho_{N \rightarrow h}\left(\frac{x}{A}, y, P_T\right) + \int_x^A \tilde{N}_A(x) \rho_{\tilde{N} \rightarrow h}\left(\frac{x}{A}, y, P_T\right) \quad (14a)$$

where we use the notation

$$N_A = \frac{1}{2} (T_A^S + T_A^{NS}), \quad \tilde{N}_A = \frac{1}{2} (T_A^S - T_A^{NS}) \quad (14b)$$

The first expression can be considered approximately, due to smallness of the EMC-effect, as a distribution of nucleons over fractions of the momentum. For cumulative and stripping protons it is necessary to add to (14a) a term proportional to  $N_A(x)$  which takes into account dissociation of the nucleus (Fig. 2b). Moreover, just this term gives the main contribution when  $P_T \approx 0$  <sup>/23/</sup>. Parametrizing the form of the spectrum of stripped and cumulative protons with  $P_T \approx 0$  (with normalisation  $\langle N_A \rangle = 1 + \Delta_A/2$ ,  $\langle \tilde{N}_A \rangle = 1 - \tilde{\Delta}_A/2$  and using the experimental cross section for  $\rho_{N \rightarrow \pi}$ , we obtain the cross section of cumulative-pion production without any new parameter. (The second term in (14a) naturally gives a small correction). This programme for deuterium (to minimize possible secondary nuclear effects) has recently been made in work <sup>/22/</sup> and shows a good agreement with experiment. Also, the ratio  $K^+/\pi^+$  agrees with experiment. This agreement confirms the independence of fragmentation of the kind of a nucleus (at least, for light nuclei), which is the base of (14) and means also that the valence mesons carry the same information on the nuclear quark structure as the cumulative protons <sup>/24/</sup>. However, the peculiarity of the nuclear quark structure is hidden here.

Interpretation of  $\tilde{N}_A$  in (14) depends on the mechanism of pumping over and, due to the second term in (14a), dominates for "sea particles" ( $K^-, \bar{p}$ ) in the region  $x \gtrsim 1$ . They are just sensitive to the peculiarity of the nuclear quark structure. For the ratio of  $K^+ | K^-$  yields in the region, we have

$$r = \frac{K^+}{K^-} = \frac{\int_x^A N_A(x) P_{N \rightarrow K^+}(\frac{x}{\alpha}) d\alpha}{\int_x^A \tilde{N}(x) P_{N \rightarrow K^+}(\frac{x}{\alpha}) d\alpha} \quad (15)$$

where the approximation  $\int_x^A \tilde{N} \rightarrow K^- \approx \int_x^A P_{N \rightarrow K^+}$  is used. It is well-known experimentally<sup>/25/</sup> that the ratio  $r$  for aluminium and lead is constant, to experimental accuracy, in the region  $1 < X < 2.3$  (Fig.3). Therefore, the functions  $N_A$  and  $\tilde{N}_A$  in this region may only differ by a coefficient. Due to different normalization conditions for these functions  $\langle \tilde{N} \rangle \approx \langle N \rangle \approx \Delta_A/2$  one can expect that for the models of type i) and ii)  $r \approx 2(1+A/2)/\Delta_A$ . Using the parametrization<sup>/B/</sup> of the SLCA-data<sup>/26/</sup> for the EMC-effect one finds  $r_{AL} \approx 65$  ( $\Delta_{AL} \approx 0,036$ ) and  $r_{Pb} \approx 45$  ( $\Delta_{Pb} \approx 0,058$ ) which is significantly higher than the experimental ratio, especially for the aluminium ( $r_{AL}^{exp} \approx 10$ ). For the pumping over inside multiquark states, which have to determine the cumulative cross sections in this region of  $X$ , the pumping over  $\Delta_{6q} \approx \Delta_A/P_A$  has to be higher (due to a small  $P_A$ ) and  $r \approx 2(1+\Delta_{6q}/2)/\Delta_{6q}$  has to be lower. The experimental ratio  $r_{AL}$  corresponds to  $\Delta_{6q} \approx 0.22$  and  $P_{AL} \approx 16\%$ . This can be considered as an indication of the multiquark mechanism in the cumulative phenomena as well as in the EMC-effect.

Let us turn now to the cumulative antiprotons. Naturally, they are sensitive to the  $N\tilde{N}$ -pair pumping-over mechanism<sup>/B/</sup>. The ratio of  $p/\tilde{p}$ -yields for  $90^\circ$  in the nuclear rest frame is determined by an expression of type (15) and is of the order of  $2/\Delta_A \approx 10^2$ . The experimental bound for this ratio is<sup>/25/</sup>  $> 10^4$ , which seems to reject the above mechanism<sup>/24/</sup>. On the other hand, if there is no packing of the collective sea into  $NN$ -pairs and cumulative  $\tilde{p}$  results in fragmentation of  $\tilde{q} \rightarrow \tilde{p}$  (just as  $K^-$ ), then the ratio  $\tilde{p}/K^-$  has to be  $\approx 0.3$  (suppression by an order of magnitude due to fragmentation  $\tilde{q} \rightarrow \tilde{p}$  and a growth due to a smaller transverse momentum of  $\tilde{p}$  at the same  $X$ ), which is not far from the experimental limit  $\tilde{p}/K^- < 1$ . However, this conclusion contradicts the conclusion made from the EMC-data<sup>/19/</sup>. So, a more accurate investigation of the antiproton yield seems necessary.

It is necessary to stress also that secondary nuclear effects can be significant for the intermediate and heavy nuclei we have considered. Indications of these effects come, for example, from the

enlarged A-dependence of cumulative proton and  $\bar{K}^-$ -productions and from a depletion of 4-5 times from unity of  $\rho_{A \rightarrow \pi} / \rho_{D \rightarrow \pi}$  in the region  $X \approx 0.6$  as compared to that for deep inelastic scattering. (One should mention also that the ratio of cumulative cross sections  $H_e/D$  shows even an anti-EMC effect in this region). For these reasons it would be desirable to obtain accurate data on the kaon and antiproton production off deuterium.

The conclusive headlines are:

- i) The cause of the EMC-effect is the pumping over of the valence-quark momentum to a collective sea of quark-antiquark pairs.
- ii) Small excess of the  $A/D$  ratio in the  $X \approx 0$  region points to hardness of the collective sea or to a big value of a nonnucleon component in nuclei.
- iii) Many popular models are in trouble due to i) and ii).
- iv) The ratio of  $\bar{K}^-/K^-$  cumulative cross sections supports the multiquark mechanism in the EMC-effect and in the cumulative process.
- v) The production of antiprotons is very intriguing but the data seem controversial.

### References

1. EMC, J.J.Aubert et al. Phys.Lett., 123B (1983) 275.
2. Baldin A.M. PANIC X-th Int.Conf., Heidelberg (1984) p. J11; Progress Part. Nucl.Phys., 4 (1980) 95, Pergamon Press. Stavinski V.S. Elem.Part. and Nucl. (EPAN) 11 (1980) 571. Efremov A.V. EPAN, 13 (1982) 613; Blokhintzev D.I.Proc. of 19-th Int.Conf. on HEP, Tokyo, 1978, p. 475.
3. Krzywicki A., Nucl.Phys. A446 (1985) 135.
4. BGDMS, Benvenuti A.C. et al., Phys.Lett., B189 (1987) 483.
5. Norton P.R. Proc. of 23-th Int.Conf. on HEP, Berkley, 1986.
6. West G.B. Los Alamos Prepr. LA-UR, 84-2072 (1984).
7. Efremov A.V. Yad.Fiz., 44 (1986) 776.
8. Efremov A.V. Phys.Lett., B174 (1986) 219.
9. Close F.E., Roberts R.G., Ross G.G. Phys. Lett., 129B (1983) 346;

- Close F.E., Jaffe R.L., Roberts R.G., Ross G.G., Phys.Rev., D31 (1985) 1004.
- Nachtmann O., Pirner H.J. Z.Phys., G21 (1984) 277.
10. Levin E.M., Ryskin M.G., Yad.Fiz., 41 (1985) 1622.
11. Mueller A.H., Jianwei Qiu, Colamb. Univ. Prepr. CU-TP-322, 361 (1987).
12. Llewellyn Smith C.H.Phys.Lett., 128B (1983) 107;  
Ericson M., Thomas A.W. Phys.Lett., 128B (1983) 112;  
Titov A.I. Yad.Fiz., 40 (1984) 76.  
Akulinichev et al., Phys.Lett., B158 (1985) 485;  
Pisma JETP 42 (1985) 105; Phys.Rev.Lett., 55 (1985) 2239;  
Birbrair et al., Phys.Lett., B166 (1986) 119.  
Saperstein E.E., Shmatikov M. Zh.Pisma JETP, 41 (1985) 44.
13. Morley P.D., Schmidt I. Phys.Rev., D34 (1986) 1305;  
Berger E.L., Coester P., Wiringa R.B. Phys.Rev., D29 (1984) 398.
14. Frankfurt L.L., Strinkman M.I. Nucl.Phys., B148 (1982) 107.
15. Szwed J. Phys.Lett., 128B (1983) 245.
16. Jaffe R.L. Phys.Rev.Lett., 50 (1983) 228.  
Date S. Progr. Theor.Phys., 70 (1983) 1682;  
Carlson C.E., Havens T.Y., Phys.Lett., 51 (1983) 261;  
Titov A.I.Yad.Fiz., 40 (1984) 76;  
Zotov N.P., Saleev V.A., Tearev V.A., Pis'ma JETP 40 (1984) 200;  
Yad.Fiz., 45 (1987) 561; Chemo  
Chentob M., Peschansky R. J.Phys., G 10 (1984), 599;  
Dias de Deus J., Varela M., Phys.Rev., D30 (1984) 697;  
Bondarchenko E.A., Efremov A.V. Prepr. JINR, E2-84-124;  
Kondratyuk L.A., Shmatikov M., Zh., Z.Phys., A321 (1985) 301;  
Yad.Phys., 41 (1985) 222;  
Clark B.C. et al. Phys.Rev., D31 (1985) 617;  
Nguyen Q.B. et al. Acta Phys.Austr., 57 (1985) 277.
17. Hoodbhoy P., Jaffe R.L., Phys.Rev., D35 (1987) 113.
18. Frankfurt L.L., Strikman M.I. EPAN 11 (1980) 571; Phys.Rep., 76 (1981) 215.
19. EMC, Arneodo et al. Z.Phys., G35 (1987) 433.
20. Savin I.A. Proc. 22-nd Intern.Conf. on HEP, Leipzig, 1984, p.251.  
Proc. 6-th Intern. Seminar on Problems of HEP, Dubna, 1981, JINR, D1, 2-81-728, p.223.
21. Blokhitzev D.I. JETP 33 (1957) 1295.
22. Efremov A.V., Kaidalov A.B., Kim V.T., Lykasov G.I., Slavin N.V., Preprint JINR, E2-87-355 (1987).



23. Ashgirey L.S. et al., JINR Prepr., P1-86-728 (1986); *Yad.Fiz.*, **46** (1987) N9.
24. Leksin G.A. Proc. of 8-th Int.Sem., on HEP, JINR D1,2-86-668, 1986, 259.
25. Baldin A.M. et al. JINR Communication E1-82-472, 1982.
26. Arnold et al., *Phys.Rev.Lett.*, **52** (1984) 727; SLAC-PUB-3257 (1984).

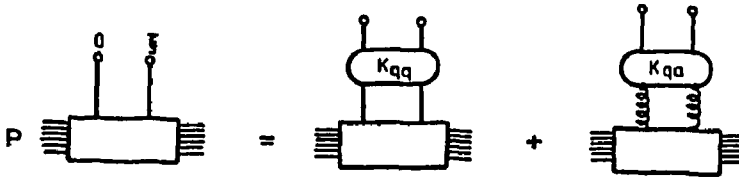


Fig.1

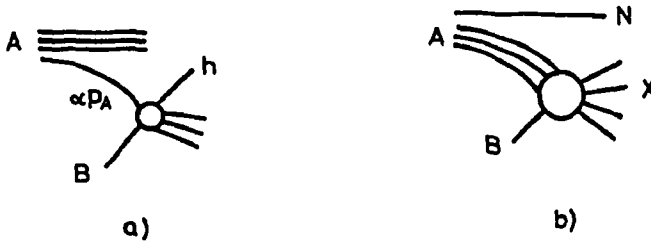


Fig.2

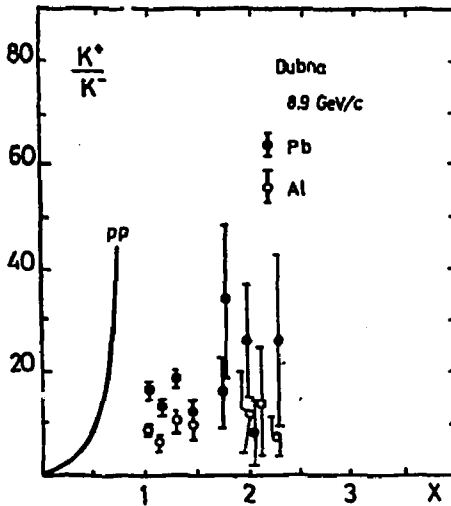


Fig.3

# NON-LEPTONIC WEAK INTERACTIONS IN CHIRAL PERTURBATION THEORY<sup>1</sup>

Gerhard Ecker

Institut für Theoretische Physik, Universität Wien

## Abstract

Prospects for testing QCD in non-leptonic weak decays are analyzed in the framework of the effective chiral Lagrangian of the Standard Model.

## 1. MOTIVATION

Quantitative tests of the Standard Model (SM) [1] in non-leptonic weak interactions are rendered difficult by our limited understanding of QCD at low energies (long-distance effects). There are nevertheless several good reasons for detailed theoretical investigations of non-leptonic weak decays:

- i) A new round of high-precision experiments on rare  $K$  decays is already under way at BNL [2]. Compared to the present state, the sensitivity of these experiments will allow for improvements of several orders of magnitude in the branching ratios, reaching down as low as  $10^{-12}$  in some cases.
- ii) In the purely electroweak sector, clarifying the structure of CP violation is of paramount importance. After the recent experimental indication of CP violation in the  $K^0 \rightarrow 2\pi$  decay amplitudes [3], as distinguished from the well-established CP non-invariance in the neutral kaon mass matrix, it becomes even more urgent to confront the SM with different manifestations of this still mysterious symmetry breaking [4]. Although non-leptonic weak decays are very promising in this respect [4,5] in view of the forthcoming high-statistics experiments, I shall in accordance with the main topic of this conference concentrate in this talk on the QCD aspects of the problem.
- iii) Instead of regarding the strong interactions as an unavoidable evil blurring our view of the electroweak interactions, we may try to extract information on QCD itself from non-leptonic weak decays.

The standard approach to non-leptonic weak interactions makes use of the operator product expansion [6]. The dominant terms in the effective weak Hamiltonian are four-fermion operators of light quark fields with Wilson coefficients which are calculable in QCD (short-distance structure). The problem arises in the calculation of hadronic matrix elements of these quark operators where the long-distance structure of QCD enters in an essential way. Most of the methods proposed for calculating such matrix elements can at best be called QCD-inspired. The problem is especially acute for radiative decays which will be my main concern later in this

<sup>1</sup>To be published in the Proc. of "Hadron Structure '87", Smolenice, ČSSR, Nov. 1987.

talk. To calculate hadronic matrix elements to all orders in the strong interactions and to the relevant order in  $\alpha_{em}$  is simply beyond our present capabilities.

A possible alternative to the standard approach is provided by chiral perturbation theory (CHPT), an effective field theory at the hadronic level which incorporates the softly broken chiral symmetry of QCD. The effective chiral Lagrangian contains certain coupling constants which are not restricted by chiral symmetry alone. It is important to realize that the chiral Lagrangian is not just another QCD-inspired model, but it is really the SM itself at the hadronic level, with a few constants left undetermined a priori. Further theoretical progress in QCD cannot change the structure of this Lagrangian without completely upsetting our notions of how chiral symmetry is realized, but it can only give information on the coupling constants in the chiral Lagrangian. Based on recent work with Antonio Pich and Eduardo de Rafael [5,7,8] I shall try to convince you that the chiral approach is certainly complementary [9] and in some cases such as radiative  $K$  decays definitely superior to the standard approach.

This talk is organized as follows. In Sect. 2 CHPT for the strong and electromagnetic interactions of pseudoscalar mesons is briefly reviewed. Sect. 3 is devoted to a discussion of how to incorporate the non-leptonic weak interactions in the chiral Lagrangian. The main emphasis will be on Sect. 4 where radiative  $K$  decays are analyzed in the chiral approach. Specific ways to test QCD in different decay channels are investigated. Conclusions are summarized in Sect. 5.

## 2. CHIRAL PERTURBATION THEORY

QCD with massless quarks  $u, d, s$  exhibits a global chiral symmetry  $SU(3)_L \times SU(3)_R$ . All experimental and theoretical evidence points to the spontaneous breaking of this chiral symmetry to the diagonal vectorial subgroup  $SU(3)_V$ . This spontaneous symmetry breaking entails the existence of eight Goldstone bosons to be identified with the octet of pseudoscalar mesons. The Goldstone fields  $\varphi^i(x)$  ( $i = 1, \dots, 8$ ) parametrize the coset space  $SU(3)_L \times SU(3)_R / SU(3)_V$  and carry a non-linear realization of the chiral group [10]

$$U(\varphi) \xrightarrow{SU(3)_L \times SU(3)_R} g_L U(\varphi) g_R^\dagger. \quad (2.1)$$

$U(\varphi)$  may be parametrized using the fundamental representation of  $SU(3)$ , i.e.

$$U(\varphi) = \exp(i\sqrt{2}\Phi/f_\pi)$$

$$\Phi = \frac{\lambda_i \varphi^i}{\sqrt{2}} = \begin{pmatrix} \frac{\pi^0}{\sqrt{2}} + \frac{\eta}{\sqrt{6}} & \pi^+ & K^+ \\ \pi^- & -\frac{\pi^0}{\sqrt{2}} + \frac{\eta}{\sqrt{6}} & K^0 \\ K^- & \bar{K}^0 & -\frac{2\eta}{\sqrt{6}} \end{pmatrix}. \quad (2.2)$$

The unique chiral invariant Lagrangian with the minimal number of derivatives is given by the non-linear  $\sigma$  model

$$\mathcal{L}_0 = \frac{f_\pi^2}{4} \text{tr}(\partial_\mu U \partial^\mu U^\dagger) = \frac{f_\pi^2}{4} g_{ij}(\varphi) \partial_\mu \varphi^i \partial^\mu \varphi^j \quad (2.3)$$

with the invariant metric

$$g_{ij}(\varphi) = \text{tr}(\partial_i U \partial_j U^\dagger). \quad (2.4)$$

For later use we record the  $V \pm A$  Noether currents

$$\begin{aligned} L_\mu &= i f_\pi^2 U \partial_\mu U^\dagger & (V - A) \\ R_\mu &= i f_\pi^2 U^\dagger \partial_\mu U & (V + A) \end{aligned} \quad (2.5)$$

allowing in particular the identification of the coupling constant  $f_\pi$  with the pion decay constant ( $f_\pi \simeq 93 \text{ MeV}$ ) to lowest order in (2.3).

Following Gasser and Leutwyler [11], we now couple the quarks  $q = (u, d, s)$  to  $SU(3)$ -valued hermitian external fields  $S, P, v_\mu, a_\mu$ :

$$\mathcal{L} = \mathcal{L}_{QCD} + \bar{q} \gamma^\mu (v_\mu + a_\mu \gamma_5) q - \bar{q} (S - iP \gamma_5) q. \quad (2.6)$$

Actually, we shall only be interested in the external electromagnetic field  $A_\mu$  appearing in

$$v_\mu = e Q A_\mu \quad (2.7)$$

with the  $3 \times 3$  quark charge matrix  $Q$  and in the scalar field  $S$  which gives rise to non-zero quark masses upon spontaneous symmetry breaking:

$$\langle S(x) \rangle_{vac} = \mathcal{M} = \text{diag}(m_u, m_d, m_s). \quad (2.8)$$

Because of the additional chiral invariant  $\text{tr} [(S + iP)U]$  of lowest dimension, the Lagrangian (2.3) gets replaced by

$$\mathcal{L}_{ch} = \frac{f_\pi^2}{4} \text{tr}(D_\mu U D^\mu U^\dagger) + v \text{tr}(\mathcal{M}U + U^\dagger \mathcal{M}) \quad (2.9)$$

with the covariant derivative

$$D_\mu U = \partial_\mu U - ie A_\mu [Q, U] \quad (2.10)$$

and

$$\frac{2v}{f_\pi^2} = \frac{m_{K^+}^2}{m_u + m_d} = \frac{M_{K^+}^2}{m_u + m_s} = \frac{M_{K^0}^2}{m_d + m_s} \quad (2.11)$$

to lowest order in CHPT.

The chiral Lagrangian (2.9) is non-renormalizable. The loop expansion for (2.9) corresponds to a derivative expansion where some derivatives may be replaced by external fields. At the one-loop level, the Lagrangian (2.9) must be supplemented with the most general chiral invariant Lagrangian of fourth order in derivatives and/or external fields [11].

Instead of writing down the complete list, of which we shall only need two terms later on, I would like to dwell on the interpretation of the corresponding dimensionless coupling constants. These constants originate in the process of integrating out quarks and gluons and they receive in general both long- and short-distance contributions. The long-distance parts comprise in particular the effect of higher hadronic states (resonances) which do not appear as fundamental fields in the theory. Many,

but not all of the coupling constants in the fourth-order Lagrangian will be scale dependent corresponding to divergences in the one-loop functional. Therefore, they will sometimes generically be called counterterm coupling constants. In order to appreciate the generality of CHPT it is crucial to realize that to the order we shall be working the complete dynamical structure of QCD, long- and short-distance, is contained in  $f_\pi$ ,  $v$  and the ten coupling constants of Gasser and Leutwyler. If these constants are determined by comparison with experiment [11], we get the complete effective chiral Lagrangian to one-loop accuracy as

$$\mathcal{L}_{ch} + \mathcal{L}_{counter} + \mathcal{L}_{WZW} \quad (2.12)$$

including the anomalous Wess-Zumino-Witten term  $\mathcal{L}_{WZW}$  [12].

### 3. CHIRAL REALIZATION OF NON-LEPTONIC WEAK INTERACTIONS

The effective  $\Delta S = 1$  Lagrangian for light quarks

$$\mathcal{L}_{\Delta S=1} = \frac{G_F}{\sqrt{2}} s_1 c_1 c_3 \delta \gamma_\mu (1 - \gamma_5) u \bar{u} \gamma^\mu (1 - \gamma_5) d + h.c. \quad (3.1)$$

is modified in the presence of strong interactions. From the operator product expansion one derives [6] the QCD-corrected Lagrangian

$$\mathcal{L}_{\Delta S=1}^{QCD} = \frac{G_F}{\sqrt{2}} s_1 c_1 c_3 \sum_{i=1}^6 C_i(\mu^2) Q_i + h.c. \quad (3.2)$$

Neither the explicit form of the 4-quark operators  $Q_i$  nor of the scale dependent Wilson coefficients  $C_i(\mu^2)$  will be needed. For the effective chiral realization of (3.2) the only important observation is that (3.2) transforms as

$$(8_L, 1_R) + (27_L, 1_R) \quad (3.3)$$

under the chiral group. The most prominent feature of  $\Delta S = 1$  non-leptonic weak interactions is the pronounced dominance of the octet part of (3.3) whenever it can contribute at all. The chiral approach cannot explain this octet dominance ( $\Delta I = 1/2$  rule), but it can provide consistency checks for the assumption that QCD fully accounts for this enhancement, as we shall soon see.

Neglecting the 27-plet from now on, we are led to the unique effective chiral realization of (3.2) to lowest order in the derivative expansion [13]

$$\mathcal{L}_{\Delta S=1}^{eff} = \frac{G_F}{2\sqrt{2}} s_1 c_1 c_3 g_8 \text{tr}(\lambda_{6-17} L_\mu L^\mu) + h.c. \quad (3.4)$$

in terms of the V - A current  $L_\mu$ . The dimensionless octet coupling constant  $g_8$  is determined from  $K \rightarrow 2\pi$  decays as

$$|g_8| \simeq 5.1. \quad (3.5)$$

Including the electromagnetic field is now straightforward and yields [7]

$$\mathcal{L}_{\Delta S=1}^{eff} = \frac{G_F}{2\sqrt{2}} s_1 c_1 c_3 g_8 \text{tr}(\lambda_{6-17} \mathcal{L}_\mu \mathcal{L}^\mu) + h.c. \quad (3.6)$$

with a "covariant"  $V - A$  current

$$\mathcal{L}_\mu = if_\pi^2 U D_\mu U^\dagger. \quad (3.7)$$

To evaluate decay amplitudes consistently to one-loop accuracy, we must add to (3.6) as in the purely strong and electromagnetic case all possible terms of fourth order in derivatives and/or external fields allowed by chiral symmetry. Taking into account a discrete symmetry of (3.1) and (3.2) called CPS [14], one finds [5,7,8] for the fourth-order  $\Delta S = 1$  effective Lagrangian

$$\begin{aligned} \mathcal{L}_{\Delta S=1,em}^{(4)} = & -\frac{ieG_8}{2f_\pi^2} F^{\mu\nu} \{w_1 \text{tr}(Q\lambda_{6-i7}\mathcal{L}_\mu\mathcal{L}_\nu) + w_2 \text{tr}(Q\mathcal{L}_\mu\lambda_{6-i7}\mathcal{L}_\nu)\} + \\ & + \frac{e^2 f_\pi^2 G_8 w_4}{2} F^{\mu\nu} F_{\mu\nu} \text{tr}(\lambda_{6-i7} Q U Q U^\dagger) + h.c. \end{aligned} \quad (3.8)$$

$$G_8 = \frac{G_F}{\sqrt{2}} s_1 c_1 c_3 g_8$$

where I have only included terms which are relevant for radiative  $K$  decays with at most one pion in the final state to be discussed subsequently.  $w_1$ ,  $w_2$  and  $w_4$  are a priori undetermined dimensionless coupling constants. At this point, I also list the two relevant terms in the strong + electromagnetic counterterm Lagrangian  $\mathcal{L}_{counter}$  in (2.12) as given in Ref. [11]:

$$\mathcal{L}_{em}^{(4)} = -ieL_9 F^{\mu\nu} \text{tr}(Q D_\mu U D_\nu U^\dagger + Q D_\mu U^\dagger D_\nu U) + e^2 L_{10} F^{\mu\nu} F_{\mu\nu} \text{tr}(U Q U^\dagger Q) \quad (3.9)$$

with two further constants  $L_9$ ,  $L_{10}$ . Finally, we shall also need the anomalous WZW terms in (2.12) linear in meson fields with the familiar form [15]

$$\mathcal{L}_{WZW} = \frac{\alpha}{8\pi f_\pi} \epsilon_{\mu\nu\rho\sigma} F^{\mu\nu} F^{\rho\sigma} (\pi^0 + \eta/\sqrt{3}). \quad (3.10)$$

The stage is now set for a complete calculation of radiative  $K$  decays (with at most one pion in the final state) to one-loop accuracy.

#### 4. RADIATIVE $K$ DECAYS

Rare  $K$  decays are ideally suited for a treatment in CHPT for mainly two reasons:

- i) All hadrons in the initial and final state are pseudoscalar mesons.
- ii) The natural expansion parameter of CHPT is  $q^2/(4\pi f_\pi)^2$  for a generic momentum  $q$  which is at most

$$\frac{M_K^2}{16\pi^2 f_\pi^2} = 0.18 \quad (4.1)$$

for  $K$  decays.

Starting to calculate amplitudes for radiative  $K$  decays one soon makes an observation which can be phrased as a general theorem [5]: the amplitude for any radiative  $K$  decay with at most one pion in the final state vanishes to lowest order in CHPT. This theorem can be traced back to a mismatch between the minimum number of powers of external momenta required by gauge invariance and the powers of momenta that the lowest order chiral Lagrangian can provide [7,8].

We must therefore pass on to the next order of CHPT. A natural classification of decay channels is provided by the convergence properties of the corresponding loop amplitudes:

- a) The fourth-order couplings in (3.8) and (3.9) do not contribute. Consequently, chiral symmetry forces the corresponding loop integrals to converge.
- b) The loop amplitude converges although there is a counterterm contribution. The counterterm amplitude must be scale independent in this case.
- c) The loop amplitude diverges so that chiral symmetry must allow for a scale dependent counterterm amplitude.

#### 4a. $K^0 \rightarrow (\pi^0)\gamma\gamma$

In the so-called diagonal basis of pseudoscalar fields [5,8] the relevant loop diagrams are given in Fig. 1 where the  $\pi^0$  is to be omitted in the final state for  $K^0 \rightarrow \gamma\gamma$ . The complete loop amplitude must be finite because there are no contributions from the counterterm Lagrangians (3.8) and (3.9). With CP conserved, the loop amplitudes only contribute to  $K_S \rightarrow \gamma\gamma$  and  $K_L \rightarrow \pi^0\gamma\gamma$ .

The final results for  $\Gamma(K_S \rightarrow 2\gamma)$  are [16]

$$\Gamma(K_S \rightarrow 2\gamma) = \frac{\alpha^2 M_K^3 G_8^2 f_\pi^2 (1 - \tau_\pi^2)^2}{2(2\pi)^3} |F(\frac{1}{r_\pi^2})|^2 \quad (4.2)$$

with  $\tau_\pi = \frac{m_\pi^2}{M_K^2}$  and for the differential decay rate  $d\Gamma(K_L \rightarrow \pi^0\gamma\gamma)/dz$  [8,17]

$$\frac{d\Gamma(K_L \rightarrow \pi^0\gamma\gamma)}{dz} = \frac{\alpha^2 M_K^3 G_8^2}{(4\pi)^6} \lambda^{1/2}(1, z, \tau_\pi^2) \left| \underbrace{(z - \tau_\pi^2)F(\frac{z}{\tau_\pi^2})}_{\pi\text{-loop}} + \underbrace{(1 - \tau_\pi^2 - z)F(z)}_{K\text{-loop}} \right|^2 \quad (4.3)$$

$$z = \frac{m_\pi^2}{M_K^2}, \quad 0 \leq z \leq (1 - \tau_\pi^2)^2 = 0.52, \quad \lambda(a, b, c) = a^2 + b^2 + c^2 - 2(ab + bc + ca), \quad (4.4)$$

where  $F$  is a certain loop function [8]. With

$$|G_8| \simeq 9.1 \cdot 10^{-6} \text{ GeV}^{-2} \quad (4.5)$$

one obtains a branching ratio

$$B(K_S \rightarrow 2\gamma) = 2.0 \cdot 10^{-6} \quad (4.6)$$

to be compared with a recent measurement at CERN by the NA31 collaboration [18]:

$$B(K_S \rightarrow 2\gamma) = (2.4 \pm 1.2) \cdot 10^{-6}. \quad (4.7)$$

From (4.2) and (4.4) we get the parameter free prediction

$$\frac{\Gamma(K_L \rightarrow \pi^0 \gamma \gamma)}{\Gamma(K_S \rightarrow 2\gamma)} = 5.9 \cdot 10^{-4}. \quad (4.8)$$

Here, we are in the fortunate position that the rates are unambiguously given in terms of only the octet coupling  $g_8$  due to the absence of counterterm contributions. The prediction (4.8) will serve as a non-trivial test of the octet enhancement in QCD.

The spectrum (4.4) is dominated by the pion-loop contribution and has a very characteristic shape shown in Fig. 2. The specific  $z$ -dependence in (4.4) is in principle a direct test of the chiral structure of vertices implied by QCD.

The two-photon amplitudes can, of course, also be calculated for off-shell photons. As an example, the normalized spectrum for  $K_S \rightarrow \gamma \mu^+ \mu^-$  is shown in Fig. 3. For all details, including a comparison with an earlier dispersion theoretic analysis of Sehgal [19], I refer to Ref. [5].

The decays  $K_L \rightarrow 2\gamma$  and  $K_S \rightarrow \pi^0 \gamma \gamma$  proceed via the diagram in Fig. 4 (for  $K_S \rightarrow \pi^0 \gamma \gamma$ ) involving the anomaly (3.10). Without the final  $\pi^0$ , the  $\pi^0$  and  $\eta$  contributions exactly cancel to lowest order in CHPT for  $K_L \rightarrow 2\gamma$ . A complete calculation to the next order in CHPT (sixth order in the derivative expansion) does not yet exist. On the other hand, the amplitude for  $K_S \rightarrow \pi^0 \gamma \gamma$  due to the diagram in Fig. 4 is non-vanishing. Away from the pion pole in the  $\gamma\gamma$ -invariant mass, the chiral structure of the weak cubic vertex can again be tested in the spectrum [8].

#### 4b. $K^+ \rightarrow \pi^+ \gamma \gamma$

To lowest non-trivial order, the amplitude for  $K^+ \rightarrow \pi^+ \gamma \gamma$  derives from three different sources: loop diagrams similar to Fig. 1, the counterterm Lagrangians (3.8) and (3.9) and the anomaly (3.10). Altogether, the differential decay rate comes out to be

$$\frac{d\Gamma(K^+ \rightarrow \pi^+ \gamma \gamma)}{dz} = \frac{M_K^5}{2(8\pi)^3} \lambda^{1/2}(1, z, r_\pi^2) z^2 \{ |A(z)|^2 + |C(z)|^2 \} \quad (4.9)$$

where the anomalous contribution  $C(z)$  can be found in Ref. [5] and with

$$\begin{aligned} A(z) &= \frac{G_8 \alpha}{2\pi z} \left[ (r_\pi^2 - 1 - z) F\left(\frac{z}{r_\pi^2}\right) + (1 - z - r_\pi^2) F(z) + \hat{c} z \right] \\ \hat{c} &= 32\pi^2 [4(L_9 + L_{10}) - \frac{1}{3}(w_1 + 2w_2 + 2w_4)]. \end{aligned} \quad (4.10)$$

It is quite remarkable that as in the case of  $K_L \rightarrow \pi^0 \gamma \gamma$  the loop amplitude is again convergent although there is now also a counterterm amplitude proportional to  $\hat{c}$ . The total rate is shown in Fig. 5 as a function of  $\hat{c}$ . The spectrum (4.9) has again a very characteristic shape [5].

What can we say about the magnitude of the scale independent constant  $\hat{c}$ ? From the analysis of Gaillard and Lee [20] one infers that there is no leading short-distance contribution to  $\hat{c}$ . From what we know about the separate coupling constants appearing in  $\hat{c}$  we estimate [5]  $\hat{c} = O(1)$ .



From Fig. 5 we obtain a lower bound for the rate

$$\Gamma(K^+ \rightarrow \pi^+ \gamma \gamma) \geq 2 \cdot 10^{-23} \text{ GeV} \quad (4.11)$$

corresponding to a branching ratio

$$B(K^+ \rightarrow \pi^+ \gamma \gamma) \geq 4 \cdot 10^{-7}. \quad (4.12)$$

With the estimate  $\tilde{c} = O(1)$  we conclude from Fig. 5 that a branching ratio significantly larger than  $10^{-6}$  could hardly be consistent with QCD [21].

#### 4c. $K \rightarrow \pi \ell^+ \ell^-$

It is instructive to compare the decays  $K^+ \rightarrow \pi^+ \ell^+ \ell^-$  with the semileptonic decays  $K^+ \rightarrow \pi^0 \ell^+ \nu_\ell$ . If the transition  $K^+ \rightarrow \pi^+ \gamma^*$  would proceed in lowest order we would expect

$$\frac{\Gamma(K^+ \rightarrow \pi^+ \ell^+ \ell^-)}{\Gamma(K^+ \rightarrow \pi^0 \ell^+ \nu_\ell)} = \left( \frac{e^2 f_\pi^2 g_{NL}}{M_K^2} \right)^2 = g_{NL}^2 \cdot 10^{-8} \quad (4.13)$$

where  $g_{NL}$  is a non-leptonic enhancement factor. However, experimentally this ratio is [22]

$$\frac{\Gamma(K^+ \rightarrow \pi^+ e^+ e^-)}{\Gamma(K^+ \rightarrow \pi^0 e^+ \nu_e)} = (5.6 \pm 1.1) \cdot 10^{-6} \quad (4.14)$$

for the electronic mode. In other words, the non-leptonic enhancement is more than compensated by some suppression mechanism. This suppression requires rather delicate cancellations in the standard approach [23]. In CHPT the transition  $K^+ \rightarrow \pi^+ \gamma^*$  vanishes in lowest order in view of the general theorem discussed earlier. A more realistic estimate is therefore

$$\frac{\Gamma(K^+ \rightarrow \pi^+ e^+ e^-)}{\Gamma(K^+ \rightarrow \pi^0 e^+ \nu_e)} = \left( \frac{e^2 g_{NL}}{16\pi^2} \right)^2 = 3.4 g_{NL}^2 \cdot 10^{-7} \quad (4.15)$$

in accordance with the experimental value (4.14).

The loop amplitudes are divergent for both  $K^+ \rightarrow \pi^+ \gamma^*$  and  $K_S \rightarrow \pi^0 \gamma^*$  (in the limit of CP invariance  $K_L \rightarrow \pi^0 \gamma^*$  is exactly zero). Thus, the counterterm amplitudes depending on  $w_1$ ,  $w_2$  and  $L_9$  must contribute in this case and they are necessarily scale dependent. With an additional assumption (absence of exotics) [7]  $w_2$  can be related to  $L_9$  which in turn is determined by the pion charge radius [11]. Fixing the remaining constant  $w_1$  with the measured rate [22] for  $K^+ \rightarrow \pi^+ e^+ e^-$ , all other rates and spectra are uniquely predicted up to a twofold ambiguity [7].

## 5. CONCLUSIONS

In summarizing the advantages of CHPT as applied to rare  $K$  decays the difficulties of the standard approach in distinguishing between genuine predictions of the SM and additional more or less plausible assumptions concerning the long-distance dynamics should be kept in mind.

- i) CHPT as the Lagrangian formulation of softly broken chiral symmetry is a direct consequence of QCD.
- ii) Chiral invariance and electromagnetic gauge invariance together imply strong restrictions for radiative decay amplitudes (e.g., vanishing amplitudes in lowest order for a whole class of radiative  $K$  decays).
- iii) In spite of higher order counterterms, CHPT as a non-renormalizable field theory can give rise to precise predictions.
- iv) CHPT is a systematic expansion in momenta and meson masses especially well suited for  $K$  decays with a natural expansion parameter of usually much than  $M_K^2/(4\pi f_\pi)^2 = 0.18$ .
- v) In favourable cases like  $K_S \rightarrow \gamma\gamma$  and  $K_L \rightarrow \pi^0\gamma\gamma$  the rates are unambiguously calculable at the one-loop level. Comparison with experiment can test the underlying assumption that QCD fully accommodates the  $\Delta I = 1/2$  rule.
- vi) For 3-body decays the differential decay rates are either directly predicted or given in terms of the total rates. The shapes of the distributions test the chiral structure of vertices dictated by QCD.

Despite the complicated interplay between strong and electroweak interactions in non-leptonic weak decays precision tests in this field will become possible in the near future.

#### Acknowledgements

It is a great pleasure to thank Toni Pich and Eduardo de Rafael for a very enjoyable and rewarding collaboration.

## References

- [1] S.L. Glashow, Nucl. Phys. **22** (1961) 579;  
S. Weinberg, Phys. Rev. Lett. **19** (1967) 1264;  
A. Salam, Proc. 8th Nobel Symposium, Aspenåsgården, 1968, ed. N. Svartholm, Almqvist and Wiksell, Stockholm:
- [2] Brookhaven Nat. Lab. experiments E777, E780, E787 and E791.
- [3] I. Mannelli, Int. Symposium on Lepton and Photon Interactions at High Energies, Hamburg, 1987, CERN preprint CERN-EP/87-177.
- [4] For recent reviews, see e.g.  
J.F. Donoghue, B.R. Holstein and G. Valencia, Univ. of Mass. preprint UMHEP-272 (1987), to be publ. in J. Mod. Phys. A;  
W. Grimus, Univ. Wien preprint UWThPh-1987-10, to be publ. in Forts. Phys.;  
G. Ecker, Univ. Wien preprint UWThPh-1987-33, to be publ. in Proc. Phenomenology of High Energy Physics, Trieste, July 1987, eds. J.C. Pati and Q. Shafi, World Scient. Publ. Co., Singapore.
- [5] G. Ecker, A. Pich and E. de Rafael, CERN and Univ. Wien preprint CERN-TH.4853/87, UWThPh-1987-31.
- [6] F.J. Gilman and M.B. Wise, Phys. Rev. **D20** (1979) 2392.
- [7] G. Ecker, A. Pich and E. de Rafael, Nucl. Phys. **B291** (1987) 692.
- [8] G. Ecker, A. Pich and E. de Rafael, Phys. Lett. **B189** (1987) 363.
- [9] W. Bardeen, A.J. Buras and J.-M. Gérard, Phys. Lett. **B180** (1986) 133; Nucl. Phys. **B293** (1987) 25; Phys. Lett. **B192** (1987) 138.
- [10] S. Coleman, J. Wess and B. Zumino, Phys. Rev. **177** (1969) 2239;  
C. Callan, S. Coleman, J. Wess and B. Zumino, Phys. Rev. **177** (1969) 2247.
- [11] J. Gasser and H. Leutwyler, Ann. of Phys. **158** (1984) 142; Nucl. Phys. **B250** (1985) 465, 517, 539.
- [12] J. Wess and B. Zumino, Phys. Lett. **37B** (1971) 95;  
E. Witten, Nucl. Phys. **B223** (1983) 422, 433.
- [13] J.A. Cronin, Phys. Rev. **161** (1967) 1483.
- [14] C. Bernard et al., Phys. Rev. **D32** (1985) 2343.
- [15] S. L. Adler, Phys. Rev. **177** (1969) 2426;  
J.S. Bell and R. Jackiw, Nuovo Cimento **60A** (1969) 47.
- [16] G. D'Ambrosio and D. Espriu, Phys. Lett. **B175** (1986) 237;  
J.L. Goity, Z. Phys. **C34** (1987) 341.

- [17] L. Cappiello and G. D'Ambrosio, INFN-Napoli preprint (June 1987).
- [18] H. Burkhardt et al., CERN preprint CERN/EP 87-146.
- [19] L.M. Sehgal, Phys. Rev. D7 (1973) 3303.
- [20] M.K. Gaillard and B.W. Lee, Phys. Rev. D10 (1974) 897.
- [21] J.O. Eeg, Nucl. Phys. B289 (1987) 673.
- [22] P. Bloch et al., Phys. Lett. 56B (1975) 201.
- [23] A. I. Vainshtein, V.I. Zakharov, L.B. Okun and M.A. Shifman, Yad. Fiz. 24 (1976) 820 [Sov. J. Nucl. Phys. 24 (1976) 427].

**Figure Captions**

- Fig. 1 One-loop diagrams for  $K^0 \rightarrow \pi^0 \gamma \gamma$  in the diagonal basis of pseudoscalar fields [8].
- Fig. 2 Normalized  $z$ -distribution for  $K_L \rightarrow \pi^0 \gamma \gamma$  (full curve) compared with phase space (dashed curve).
- Fig. 3 Normalized  $q_2^2$ -distribution ( $q_2^2 = m_{\mu^+ \mu^-}^2$ ) for  $K_S \rightarrow \gamma \mu^+ \mu^-$  (full curve) compared with phase space (dashed curve).
- Fig. 4 Tree diagram for  $K_S \rightarrow \pi^0 \gamma \gamma$ .
- Fig. 5 Total rate for  $K^+ \rightarrow \pi^+ \gamma \gamma$  (full curve) as a function of  $\hat{c}$  defined in (4.10).

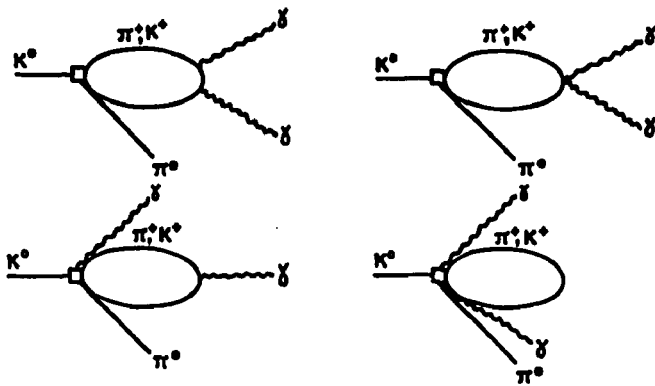


Fig.1

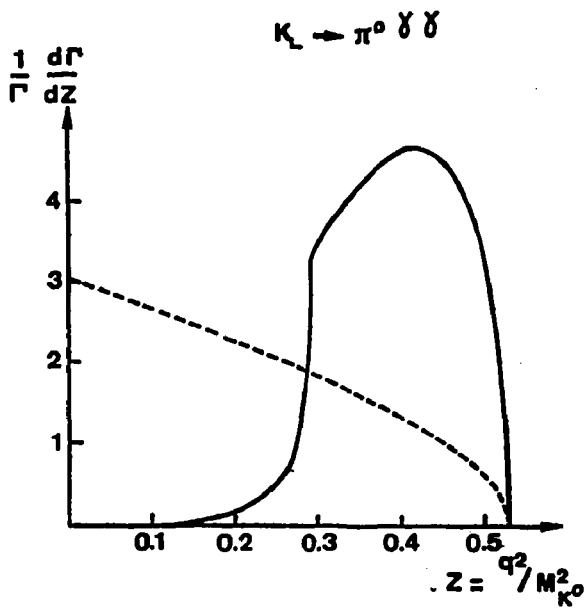


Fig.2

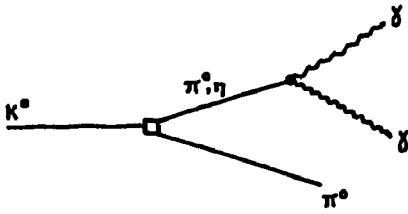
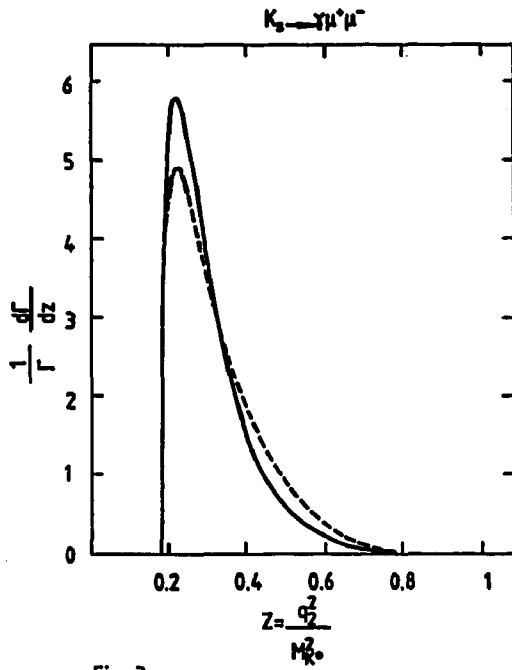
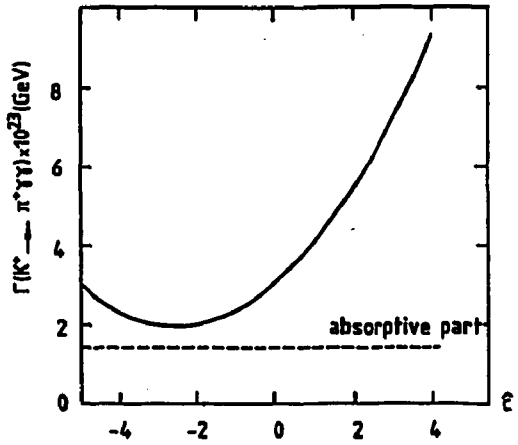


Fig. 4



DECONFINEMENT ANALYSIS IN EXACTLY  
SOLVABLE MODEL FOR LATTICE QCD

V.K.Petrov, G.M.Zinovjev

INSTITUTE FOR THEORETICAL PHYSICS  
ACADEMY OF SCIENCES OF UKRAINIAN SSR  
252130, Kiev 130, USSR

On the whole it is now an established fact at high temperatures the quarks and gluons are practically liberated and chiral symmetry is restored but at low temperatures it is spontaneously broken and the constituents are confined [1]. The Monte-Carlo numerical experiments have made it possible to ascertain the temperature and order of appropriate phase transitions (though there are some contradictions between results of different groups) however, the physics underlying the closeness of both temperatures and at any rate the intuitively apparent interrelation existing between them is still rather unclear [2]. Experience teaches us (if only through the example of Landau-Ginzburg effective theory in superconductivity) that at the present stage of theoretical development any attempts are extremely important to construct an effective model theory allowing us to promote essentially the analytical methods of investigating phase transition problem in gauge theories.

Specifically deeper analysis of deconfinement phase transition nature comes from the constructive idea about the dual-like correspondence between  $d+1$  - dimension finite temperature pure gauge theories and  $d$ -dimension spin systems with local interaction [3]. However the Monte-Carlo analysis of the lattice QCD with dynamical quarks has shown that this transition may disappear in the real world of interacting quarks and gluons. Although in this case the calculations

are not so irreproachable, since nobody has succeeded in inventing the relevant order parameter, nevertheless these circumstances have given rise to the opinion in a number of papers that the confinement can be no more than a qualitative conception in such theories.

In the present note we develop an approach to analyze the deconfinement phase transition which, as a matter of fact, demonstrates the origin of universality arguments [3], at any rate, in the strong coupling approximation. We find it to be a valuable suggestion as a detailed investigation of the critical region can be fulfilled analytically. This approach is based on the so-called spherical model [4] arising as an approximation to solve the Ising model and so far remaining to be one of a few (if not a unique one) ferromagnetic models allowing an exact solution and discovering the phase transition for a three-dimension lattice. Moreover, it is known [5] that the singularities of the thermodynamical functions take the form of power laws with the critical indices close to those in the Ising model

In order to make the essence of our suggestion more transparent we first consider SU(2)-lattice pure gluodynamics. We employ the Hamiltonian formulation (in  $A_0 = 0$  gauge) in the strong coupling regime and then include the quarks following the recipes of Ref. [6]. The corresponding partition function takes the form

$$\mathcal{Z} = \int \prod_x \frac{d\psi_x}{2\pi} \sin^2 \frac{\psi_x}{2} \prod_{\mu, \nu} F(\gamma, \psi_x, \psi_{x+\mu}) ; \mu=1, \dots, d \quad (1)$$

where

$$F(\gamma, \psi_x, \psi_{x+\mu}) = \sum_{n=0}^{\infty} e^{-n(n+1)\gamma} \frac{\sin(n+1)\frac{\psi_x}{2} \sin(n+1)\frac{\psi_{x+\mu}}{2}}{\sin \frac{\psi_x}{2} \sin \frac{\psi_{x+\mu}}{2}} \quad (2)$$

and  $\gamma = \beta g^2 / 2a$ ,  $a$  is the lattice spacing,  $d$  is the space dimension,  $N^d$  is the number of lattice sites. Knowing the low-temperature ( $\gamma \gg 1$ ) and high-temperature ( $\gamma \ll 1$ ) asymptotic behaviours of Eq.(2), [7,8] it is not difficult to realize that the function  $F(\gamma, \psi_x, \psi_{x+\mu})$  could suitably be approximated by

$$F(\gamma, \psi_x, \psi_{x+\mu}) = \exp \left\{ \tilde{I}(\gamma) \cos \frac{\psi_x}{2} \cos \frac{\psi_{x+\mu}}{2} + \tilde{I}(\gamma) \sin \frac{\psi_x}{2} \sin \frac{\psi_{x+\mu}}{2} + K(\gamma) \right\} \quad (3)$$

The functions  $I$ ,  $\tilde{I}$  and  $K$  are some smooth functions of  $\gamma$  (however, there is the condition  $I > \tilde{I}$ ) and these reproduce the corresponding asymptotic behaviours of the function  $F(\gamma, \psi_x, \psi_{x+\mu})$ .



The computations have shown that the accuracy of this approach is about two percents in the whole region of  $\gamma, \gamma_x$  and  $\gamma_x'$  variables.

Now introducing two-dimensional unit vectors  $\vec{\delta}_x = \{\delta_x, \tilde{\delta}_x\} = \{\cos \frac{\gamma_x}{2}, \sin \frac{\gamma_x}{2}\}$  in each site of  $d$ -dimensional space and noticing that  $\sin^2 \frac{\gamma_x}{2} d\gamma_x = \delta(\delta_x^2 + \tilde{\delta}_x^2 - 1) \delta_x^2 d\tilde{\delta}_x d\delta_x$  we have for the partition function

$$\mathcal{Z} \sim e^{K(N)N^d} \int \prod_x d\tilde{\delta}_x^2 \delta(\delta_x^2 + \tilde{\delta}_x^2 - 1) \exp\left\{I(\gamma) \sum_{\langle x, y \rangle} \delta_x \delta_{x+y} + \tilde{I}(\gamma) \sum_{\langle x, y \rangle} \tilde{\delta}_x \tilde{\delta}_{x+y}\right\} \quad (4)$$

Thus the proposed approximation makes it possible to reduce the initial partition function Eq.(1) to the effective one Eq.(4), displaying the generalization of the well-known classical Heisenberg model to the asymmetric interaction  $I(\gamma) \neq \tilde{I}(\gamma)$ . The critical behaviour of this system can be studied by the powerful methods in spin system theory. The situation is quite relevant to the universality arguments [3] and furthermore, in a sense, it illuminates the nature of their origin.

Investigating the phase transition character and an appearance of corresponding singularities of the thermodynamic quantities we utilize the spherical model [4]. The crucial point is to prove a replacement of the condition  $\delta_x^2 = \tilde{\delta}_x^2 = 1$  by weaker condition

$$\frac{1}{N^d} \left( \sum_x \delta_x^2 + \sum_x \tilde{\delta}_x^2 \right) = 1 \quad (5)$$

is equivalent for Eq.(4) to replace

$$\mathcal{Z} \sim \int_{c-i\infty}^{c+i\infty} d\lambda e^{\frac{\lambda}{2} N^d} \int \prod_x d\delta_x d\tilde{\delta}_x \delta_x^2 \exp\left\{-\frac{1}{2}(\delta_x \tilde{A} \tilde{\delta}_x) - \frac{1}{2}(\tilde{\delta}_x A \delta_x)\right\} \quad (6)$$

The constant  $c$  is chosen here in such a way as to ensure the legitimacy of interchanging the integration order after putting Eq.(6) into Eq.(4). It means that  $c$  is a line to the right of all  $\lambda$ -singularities of the integrand. It will be clear from what follows that it is enough  $c > d$ .

As to the inclusion of the matter fields, following Ref. [9], we have to add the factor which in the present notation is equivalent to the following substitution

$$\prod_x d\delta_x \rightarrow \text{const} \prod_x (1 + \delta_x) d\delta_x$$

In Ref. [10], the model of the gluodynamics with a gas of the probe charges has been developed and we has shown that the partition function takes an additional factor of a more general

(than at Ref.[6]) form. For the present consideration this will be

$$\prod_x (1 + \lambda \delta_x) d\delta_x \quad (7)$$

where  $\lambda$  is the fugacity regulating the contribution of colour-charged particles and colourless ones. It is evident taking  $\lambda = 1$  that we reproduce the result of Ref.[6]. Then the partition function of this QCD model can be written in the spherical model approximation as

$$\mathcal{Z} \sim \int_{c-i\infty}^{c+i\infty} d\lambda e^{\frac{dI\lambda}{2}} \int \prod_x d\delta_x (1 + \lambda \delta_x) d\tilde{\delta}_x \tilde{\delta}_x^2 \exp\left\{-\frac{1}{2}(\delta_x \lambda^2) - \frac{1}{2}(\tilde{\delta}_x \tilde{\lambda}^2)\right\} \quad (8)$$

where

$$A = dI(r) \left( \delta_x^{x'} - \frac{1}{d} \sum_{\mu=1}^d \delta_{x+\mu}^{x'} \right), \quad \tilde{A} = dI(r) \left( \tilde{\delta}_x^{x'} - \frac{1}{p} \sum_{\mu=1}^p \tilde{\delta}_{x+\mu}^{x'} \right), \quad \rho = \frac{dI}{I} \quad (9)$$

In order to obtain the integrals over  $\delta$  and  $\tilde{\delta}$  in Eq.(8) in the Gaussian forms, it is convenient to perform those as

$$\mathcal{Z} \sim \int_{c-i\infty}^{c+i\infty} d\lambda e^{\frac{dI\lambda}{2}} \left\{ \prod_x \frac{\partial^2}{\partial \eta_x} (1 + \lambda \frac{\partial}{\partial \eta_x}) \int d\delta_x d\tilde{\delta}_x \exp\left[-\frac{1}{2}(\delta_x \lambda^2) - \frac{1}{2}(\tilde{\delta}_x \tilde{\lambda}^2) + \eta_x \delta_x + \tilde{\eta}_x \tilde{\delta}_x\right] \right\} \quad (10)$$

Making use the fact that

$$\prod_x (1 + \lambda \frac{\partial}{\partial \eta_x}) = \sum_n \lambda^n \sum_{\{x\}} \prod_{k=1}^n \frac{\partial}{\partial \eta_{x_k}}$$

where the summation  $\sum_{\{x\}}$  is running over all unequal  $x_{k_1}, \dots, x_{k_n}$  from the whole set  $x_1, \dots, x_{N^d}$  we can reduce Eq.(10) to the calculation of the following integrals

$$\begin{aligned} & \int \exp\left\{-\frac{1}{2}(\delta_x \lambda^2)\right\} \delta_i^{m_1} d\delta_1 \dots \delta_n^{m_n} d\delta_n = (2\pi)^{\frac{n}{2}} (-1)^{\frac{1}{2} \sum_k m_k} (\text{Det} A)^{-\frac{1}{2}} \prod_k \frac{\partial}{\partial \eta_{x_k}} \left. \exp\left\{\frac{1}{2}(\eta_x \lambda^2)\right\} \right|_{\eta_x=0} \\ & = (2\pi)^{\frac{n}{2}} (-1)^{\frac{1}{2} \sum_k m_k} (\text{Det} A)^{-\frac{1}{2}} G_{m_1, \dots, m_n}(i\eta_1, \dots, i\eta_n) \Big|_{\eta_x=0} \end{aligned} \quad (11)$$

where  $G_{m_1, \dots, m_n}(\xi_1, \dots, \xi_n)$  is the generalization of the Hermitian polynomial to n-dimensions. In order to determine  $G_m(0)$  in Eq.(11) we take into account following [11] that

$$\sum_{\{m_j\}} \delta(m - \sum_{k=1}^n m_k) G_{m_1, \dots, m_n}(\xi_1, \dots, \xi_n) \prod_j \frac{x_j^{m_j}}{(m_j)!} = \frac{(x A^{-1} x)^{m/2}}{m! 2^{m/2}} H_m\left(\frac{(x A^{-1} x)}{\sqrt{2(x A^{-1} x)}}\right), \quad m = \sum_{k=1}^n m_k \quad (12)$$

where  $H_m(y)$  has already been normal Hermitian polynomial for which we have

$$H_m(0) = \begin{cases} (-1)^{m/2} \cdot \frac{m!}{(m/2)!} & m \text{ is even} \\ 0 & m \text{ is odd} \end{cases} \quad (13)$$

These give finally for the integral Eq.(14)

$$\int e^{-\frac{1}{2} \xi A \xi} d\xi_1 d\xi_2 \dots d\xi_n = \begin{cases} (2\pi)^{n/2} (\det A)^{-1/2} \prod_{k=1}^n \frac{\xi_k^{m_k}}{\sqrt{2\pi} (m_k)!} \Big|_{x=0} & (14) \\ \text{when } m \text{ is odd} \end{cases}$$

Integrating over  $\xi$  and  $\tilde{\xi}$  we have the partition function Eq.(10) in the form

$$\mathcal{Z} \sim \int_{c-i\infty}^{c+i\infty} d\lambda \exp\left[\frac{1}{2} I(\lambda) N^d\right] \text{Per } \tilde{A}^{-1} (\det A \det \tilde{A})^{-1/2} \mathcal{Q} \quad (15)$$

here the result of the integration over  $d\tilde{\xi}$  is given as

$$(\det \tilde{A})^{-1/2} \prod_{x'} \int \frac{d\tilde{\xi}_x}{\sqrt{2\pi}} \exp\left[-\frac{1}{2} \tilde{\xi}_x \tilde{A}^{-1} \tilde{\xi}_x\right] = (\det \tilde{A})^{-1/2} \text{Per } \tilde{A}^{-1} = (\det \tilde{A})^{-1/2} \prod_{x'} (\tilde{A}^{-1})_{xx} \quad (16)$$

and  $\prod_{x'}'$  means that the summation is taken over all  $x_j$  unequal to each other (over permutations). As to the integration over  $d\delta$  its result is

$$(\det A)^{-1/2} \sum_n \lambda^{2n} \sum_{\{x\}} \prod_{x'} \frac{\lambda}{\sqrt{2\pi}} \left(\frac{\lambda A^{-1}}{2}\right)^n \frac{1}{n!} = \mathcal{Q} = \sum_{\{x\}} \sum_{m=0}^{\infty} \frac{\lambda^{2m}}{2^m m!} \prod_{x'} (A^{-1})_{x_2 x_1}^{k_{2m+1}} \quad (17)$$

Calculating  $\text{Per}(1/A)$  we have by definition that

$$\frac{1}{\mathcal{K}} = \frac{1}{\rho! I(\rho)} \sum_n \frac{(\sum \tilde{J}_v)^n}{\rho^n}; \quad (\tilde{J}_v)_{x'} \equiv (\tilde{J}_v)_{x_1 \dots x_d} = \delta_{x_1 x_1}^{x'_1} \dots \delta_{x_1 x_d}^{x'_d} \prod_{\mu, \nu} \delta_{x_\mu}^{x'_\nu}; \quad \delta_{x'}^{x'_1 \dots x'_d} = \delta_{x'}^{x'_1} \quad (18)$$

Using the explicit form of  $\tilde{J}_v$  we find approximately up to the  $\rho^{-N}$  terms ( $\rho > d, N \gg 1$ )

$$1/\mathcal{K}_{x_1 \dots x_d}^{x'_1 \dots x'_d} = \frac{1}{\rho! I(\rho)} \frac{(\sum m_\nu)!}{\rho^{2m_\nu} \prod m_\nu!}; \quad m_\nu \equiv m_\nu(x_\nu, x'_\nu) = x_\nu x'_\nu + N \theta(x'_\nu - x_\nu) \quad (19)$$

Now admitting the numbers  $m_{\nu}$  to be independent in the definition of  $\text{Per}(1/A)$  for all matrices  $1/A = \begin{matrix} x_1 & \dots & x_n \\ \dots & \dots & \dots \\ x_n & \dots & x_n \end{matrix}$  i.e. ignoring restriction  $(x_1, \dots, x_n) \neq (x_1, \dots, x_n)$  and extending the summation to all  $x_{\nu}$  (all  $m_{\nu} > 0$ ) we obtain

$$\text{Per} \frac{1}{A} = \frac{1}{[P]I(n)} N^d \sum_{\{m_{\nu}\}} \prod_{s=1}^n \frac{(z \frac{m_{\nu}}{2})!}{\rho \frac{z m_{\nu}}{2} \prod_{\nu} m_{\nu}!} = e^{-N^d \ln [d-d \frac{I(n)}{I(n)}]} \quad (20)$$

Remind now that  $I(n) > I(n)$  we conclude  $\text{Per}(1/A)$  is the regular function of  $\lambda$  in the region  $\lambda > d$ .

To calculate  $\mathcal{Q}$  we notice that

$$\frac{1}{2 \cdot 1!} \sum_{\{x_i\}} B_{x_i}^{x_i} = \frac{1}{2} \left[ \frac{1}{(\lambda-d)I(n)} - 1 \right], \quad B_{x_i}^{x_i} = (A^{-1})_{x_i}^{x_i} \quad (21)$$

$$\frac{1}{2 \cdot 2!} \sum_{\{x_i\}} B_{x_i}^{x_i} B_{x_i}^{x_i} = \frac{1}{2} \left( \frac{1}{2} - 1 \right) \left[ \frac{1}{(\lambda-d)I(n)} - 1 \right]^2 \left( 1 + \mathcal{O}\left(\frac{1}{\lambda}\right) \right)$$

etc. We believe the suitable approximation for  $\mathcal{Q}$  is as follows

$$\mathcal{Q} \approx \sum_n \binom{\lambda}{n} \lambda^{2n} \left[ \frac{1}{(\lambda-d)I(n)} - 1 \right]^n \equiv e^{N^d f_{\mathcal{Q}}(\lambda, d)} \quad (22)$$

where

$$f_{\mathcal{Q}}(\lambda, d) = \frac{1}{2} \ln \left\{ 1 + \lambda^2 \left[ \frac{1}{(\lambda-d)I(n)} - 1 \right] \right\} \quad (23)$$

Indeed the precision of approximation is slightly getting worse with  $n$  increasing but if we are interested in not so large  $\lambda$  the deviation for high orders does not tell practically on the general result. The correction calculated elsewhere which is not testifies to the infinite values of exact function  $f_{\mathcal{Q}}(\lambda, d)$  and its derivative at  $\lambda = d$ . Substituting the obtained expressions of  $\text{Per} A^{-1}$  and  $\mathcal{Q}$  into Eq.(15) we find for the partition function

$$\mathcal{Z} \sim \int_{c-i\infty}^{c+i\infty} d\lambda \exp \{ N^d \Phi(\lambda, d) \} \quad (24)$$

where

$$\Phi(\lambda, d) = \frac{1}{2} I(n) + f_{\mathcal{Q}}(\lambda, d) - \ln \lambda - \frac{1}{2N^d} \left[ \ln \text{Det} A + \ln \text{Det} \tilde{A} \right] \quad (25)$$

We can show that

$$\frac{1}{N^d} \ln \text{Det} A \equiv g(\lambda-d) = \text{const} + \int_0^{\infty} \frac{dt}{t} \left[ I_0(t) \right]^d e^{-\lambda t} \quad (26)$$

but

$$\frac{1}{N_d} \ln \det \tilde{A} = g \left( \alpha \frac{I}{T} - d \right)$$

and since the behaviour of  $g(z)$  is well studied (see, for instance Ref. [12]) the integral Eq. (15) can be calculated by the method of steepest descent. The saddle point  $\alpha = \alpha_0$  is defined by the condition  $\int_{\alpha_0} \Phi(\alpha, \lambda) = 0$

$$g'(\alpha_0 - d) + \frac{I}{T} g' \left( \alpha_0 \frac{I}{T} - d \right) + 2 \ln \left( \frac{\alpha_0 - d}{\alpha_0} \right) = I + 2 \int_{\alpha_0} (\alpha, \lambda) \quad (27)$$

It can be solved graphically and depicted in the figure.

The curves 0, 1, 2 correspond to the values of the function  $I + 2 \int_{\alpha} (\alpha, \lambda)$  at  $\lambda = 0, \lambda_1, \lambda_2$  respectively moreover  $\lambda_2 > \lambda_1 > 0$ . The curve 3 corresponds to the function

$$G(\alpha) = g'(\alpha - d) + \frac{I}{T} g' \left( \alpha \frac{I}{T} - d \right) + 2 \ln \left( \alpha - d \frac{I}{T} \right)$$

Its singular point at  $\alpha = d$  is denoted by asterisk. The saddle points are expressed via the opened circles and their positions are defined by the point of intersections between the curves 0, 1, 2 and curve 3.

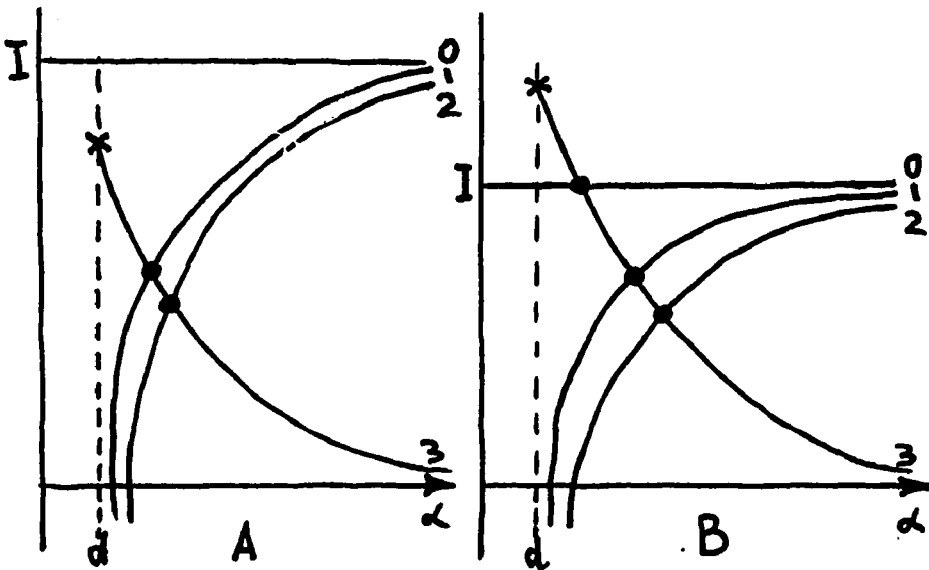
It is evident from the figure that the saddle point is present at all  $\lambda > 0$  (the curves 1 and 2) and at any  $I(\gamma)$  (figs. A and B); then the free energy  $\Phi(\lambda, \alpha_0(\lambda))$  is a smooth function of temperature  $\beta^{-1}$  (more exactly, the smooth function of  $I(\gamma)$ ) that signals the absence of the temperature phase transition. When the matter fields are absent ( $\lambda = 0$ , and hence  $\int_{\alpha} (\alpha, 0) = 0$ ) the curve 0 at the figure, the saddle point does exist at not all values of  $I(\gamma)$  (fig. A) and the phase transition is restored. The value of  $I$  at which the phase transition takes place is defined by the equation

$$G(\alpha = d) = I(\gamma)$$

#### References

1. B. Svetitsky. Status of lattice gauge theory, MIT preprint CTP # 1374 (1986).
2. F. Karsch. QCD at finite temperature and baryon number density, preprint ILL-(TH)-86 # 9 (1986).

3. B.Svetitsky, L.Yaffe. Phys.Rev. D26 (1982) 963;  
Nucl.Phys. B210 (1982) 423.
4. T.H.Berlin, M.Kac. Phys.Rev. 86 (1952) 821.
5. H.E.Stanley. Introduction to phase transitions and critical phenomena, (Clarendon Press, Oxford, 1971).
6. T.Banks, A.Ukawa. Nucl.Phys. B225 (1983) 145.
7. A.M.Polyakov. Phys.Lett. 72B (1978) 477.
8. L.Susskind. Phys.Rev. 20D (1979) 2610.
9. L.Susskind. Quark confinement in gauge theories of strong interactions, Lectures given at the Bonn summer school, 1974.
10. O.A.Borisenko, V.K.Petrov, G.M.Zinovjev. Teor.Mat.Fiz. 73 (1987) 351.
11. A.Erdelyi. Higher transcendental functions, vol.2, (McGraw Hill Book Co., New York, 1953).
12. G.S.Joyce. in: Phase transitions and critical phenomena, vol.2, eds. C.Domb and M.Green (Acad.Press, London, New York, 1972).



# Optimization of Renormalization Group Transformations

C.B. Lang and M. Salmhofer<sup>†</sup>

Institut für Theoretische Physik  
Universität Graz  
A-8010 Graz, AUSTRIA

## ABSTRACT

We discuss the dependence of the renormalization group flow on the choice of the renormalization group transformation (RGT). An optimal choice of the transformation's parameters should lead to a renormalized trajectory close to a few parameter action. We apply a recently developed method to determine an optimal RGT to SU(2) lattice gauge theory and discuss the achieved improvement.

The lattice provides a gauge invariant regularization for field theories and quantization amounts to the determination of expectation values over the ensemble of field configurations in equilibrium. The construction of a continuum quantum field theory requires the investigation of such a system of statistical mechanics at criticality, where the correlation length diverges. In this region of coupling space the lattice system is scale invariant (the characteristic length being infinite); renormalization group transformations (RGT), which perform changes of the length scale of the system and corresponding changes of the action, are then symmetry transformations. The critical exponents that determine the continuum theory can be calculated from eigenvalues of the linearized transformation at a fixed point (FP) of the transformation, a scale invariant action  $S^*$ , and it is also possible to determine universality classes as domains of attraction of  $S^*$ .<sup>1</sup>

Real Space RGTs for a lattice system with fields  $U$  and action  $S$  are introduced by defining a transition probability  $P(U', U) \geq 0$ ,  $\text{tr}_{U'}(P(U', U)) = 1$ , where  $U'$  denotes the configurations on a smaller lattice and  $\text{tr}_{U'}(\cdot)$  the integral over all of such configurations. The renormalized action is then

$$S'(U') = \log \text{tr}_U \left( P(U', U) e^{S(U)} \right). \quad (1)$$

For most systems of interest this integral cannot be calculated in closed form and approximations have to be applied. Monte Carlo Renormalization Group (MCRG) has emerged as an efficient procedure to obtain informations about the critical structure.<sup>2</sup>

Wilson<sup>3</sup> has proposed a gauge invariant action; for the non-abelian  $SU(N)$  gauge theories in four space-time dimensions the critical value of the Wilson coupling  $K_F = \frac{2N}{g^2}$  is infinite. MCRG studies of systems of that kind have concentrated on the non-perturbative  $\beta$ -function of the theory by calculating the change of  $K_F$  under a change of scale. This can be done with a single RGT step under the assumption that  $S'$  is again

---

<sup>†</sup> Contribution presented by M.Salmhofer at the conference "Hadron Structure 87", Smolenice, CSSR, Nov.18-20, 1987

of the simple Wilson form.<sup>4</sup> The effective renormalized coupling can be determined by comparison of the expectation values derived from the blocked lattice with expectation values determined in a simulation of the system with this simple action. More trustworthy are operator matching procedures<sup>5</sup>; they rely on the fact that for any starting action the sequence of renormalized actions will, after sufficiently many blocking steps, be attracted by the renormalized trajectory (RT), the line connecting the critical and the trivial FP. However, for an arbitrary chosen RGT the initial action may be quite far from the RT and thus "sufficiently many" often enough may require simulation on very large lattices even if observables are compared on the smallest ones possible.

This problem can be overcome by "improvement" of the starting action by including more complicated interaction terms which place it in the vicinity of the RT of a given RGT<sup>6</sup>. On the other hand, there is a great variety of functions  $P(U', U)$  satisfying the rather general conditions mentioned above; each of them should be equally well suited to determine scaling behaviour. Since the position of the RT may depend on the specific RGT one can as well try to move the RT into a few-parameter subspace by adjusting the weight factor  $P(U', U)$ <sup>7</sup>.

The aim of the work reported here<sup>8</sup> was to find a transition probability  $P(U', U)$  for  $SU(2)$ -lattice gauge theory such that  $S'$  has Wilson's form if  $S$  does, that is to make  $S'$  lie in the subspace where only  $K_F$  is nonzero. Whereas such an optimization clearly reduces the problems mentioned above and even does away with the ever-lurking menace of truncation errors<sup>6</sup> in the calculation of the critical exponents, its main problem is whether a restriction as strong as that is possible at all. This question arises because globally and exactly keeping the RT in a certain subspace would move the FP into this subspace as well, which is, of course, desirable, but need not be possible. Provided the RGTs applied are nonsingular, the FP can be moved only in redundant directions<sup>9</sup> along which no non-analytic corrections to scaling appear. Some recent studies<sup>10</sup> indicate that perfect optimization might be possible using a nonlocal  $P(U', U)$  only and that there might arise problems in the sector of odd couplings<sup>6</sup>. Swendsen concluded<sup>11</sup> that the RGT's used are singular since his optimization seems to move the FP successfully not only in redundant directions. A dependence of the RG flow on the specific form of the RGT has also been demonstrated in  $d=4$   $\Phi^4$ -theory.<sup>12</sup> As concerns the work presented here we find definite improvement but we also find that complete optimization in the above mentioned sense is not possible in our case. The RT can be moved closer to the one parameter subspace but there are still further couplings contributing to the renormalized action.

The transformation investigated has scale factor 2, the transition probability is

$$P(\rho, U', U) = \prod_{z', \mu} \delta(U'_{z', \mu}, V_{z', \mu}(U)), \quad (2)$$

where each block link  $V$  is constructed from a sum  $W$  over paths of length 2 and 4 on the larger lattice,

$$W_{z', \mu}(U) = \rho_1 U_{z, \mu} U_{z+\mu, \mu} + \rho_2 \sum_{\nu \perp \mu} U_{z, \nu} U_{z+\nu, \mu} U_{z+\nu+\mu, \mu} U_{z+2\mu, \nu}^\dagger + \rho_3 \sum_{\nu \perp \mu} (U_{z, \nu} U_{z+\nu, \mu} U_{z+\mu, \nu}^\dagger U_{z+\mu, \mu} + U_{z, \mu} U_{z+\mu, \nu} U_{z+\nu+\mu, \mu} U_{z+2\mu, \nu}^\dagger), \quad (3)$$

normalized to unit determinant. The transformation is local, nonlinear and preserves gauge invariance; a RGT of this kind was first introduced by Swendsen.<sup>13</sup> Due to the



normalization one of the parameters may be put to a constant and we fix  $\rho_1 = 1$ . Any reasonable choice of the parameters should, in principle, be sufficient for the determination of scaling behaviour and the transformations  $(\rho_1, \rho_2, \rho_3) = (1, 1, 0)$  and  $(1, 1, 1)$  have already been used in other studies.<sup>4,14</sup>

The optimization can be carried out without calculating the renormalized couplings or taking  $S'$  to be of any special form. If the actions of two ensembles of configurations agree (up to a constant that has no influence on the statistical behaviour of the system) so will the observables. The Wilson line in coupling space thus corresponds to a curve (denoted by WT) in observable space, and the optimization consists of finding values  $\rho_i^*$  such that the euclidean distance of  $S'(\rho_i^*)$  to WT is minimal. Of course, we have to restrict ourselves to a tractable number of observables: we considered plaquette, planar, bent and twisted bent double plaquette in fundamental and adjoint representation only. These eight observables are sufficiently local to make sense on the lattice sizes we used.

Due to the normalization one finds that the variation of one parameter, keeping the others fixed, leads to closed curves of the observables of the blocked system in the corresponding space, as demonstrated in Fig.1 in  $O_1$ - $O_3$ -projection. Similar figures may be produced for any combination of observables. The amount of variation of results of possible RGTs is surprising.

At the optimal point  $\rho = (1, -0.70, -0.18)$  the average distance per observable is 0.003 with a statistical error of the order of 0.0003 in the determination of the observable, which is about 4 times closer to the Wilson line (in operator space) than the naive value  $(1, 1, 1)$  and a factor of 4.2 better than the choice  $(1, 1, 0)$ . The minimal valley is very flat with regard to  $\rho_2$ , however, and even values like  $(1, -6.00, -0.18)$  are clearly better than the naive choice. Repeating the optimization for  $K_F = 2.4$  leads to compatible values of RGT parameters. It was not possible to find zero distance for any value of the RGT parameters. This implies that the renormalized action necessarily will contain further couplings to interaction terms beyond the simple Wilson form.

There are various possibilities to check on the possible improvement due to the optimized RGT. One is the determination of the renormalized couplings; this was subsequently done within a SU(2) gauge-Higgs system study by Reusch<sup>15</sup> and the results indicate that the projection of the RT into the plane of the fundamental and adjoint plaquette couplings,  $K_F$  and  $K_A$ , lies below the Wilson line, roughly a factor of 4 closer to it than e.g. the Migdal-Kadanoff RT<sup>16</sup> or the RT with<sup>17-18</sup>  $\rho = (1, 1, 1)$ .

The evidence that the optimized RGT has a RT much closer to the Wilson line than the conventional choice for RGTs is further supported by an operator matching study. We simulated the theory at various values of  $K_F$  between 2 and 3 for lattice sizes  $16^4$  and  $8^4$  and performed up to 3 (on  $16^4$ ) or 2 (on  $8^4$ ) RGTs of (A) the optimal values for  $\rho = (1, -0.70, -0.18)$  and (B) the naive choice  $(1, 1, 1)$ . Up to values of  $K_F \approx 2.6$  we observed consistently good matching of all the operators already after 1 RGT for (A), i.e. comparing expectation values on  $8^4$ , whereas one needed at least 2 RGT's until good matching was obtained for (B). At larger values of  $K_F$  one noticed a clear deviation from the Wilson line.

The only way to avoid spurious results in that domain is to perform sufficiently many RGTs to make sure that one has arrived at the RT. One way to confirm that is to check the saturation of the observed value of  $K'_F$  after sufficiently many blocking steps. For the optimal parameter choice (A) this saturation was observed for  $K_F \leq 2.5$  in the second RGT step, for  $K_F \leq 2.6$  in the third step and for larger value of  $K_F$  not at all (cf. fig. 1). For the parameter set (B) saturation required three steps even below  $K_F = 2.5$ . The  $\beta$ -function we got<sup>8</sup> essentially agrees with other determinations<sup>18</sup>.

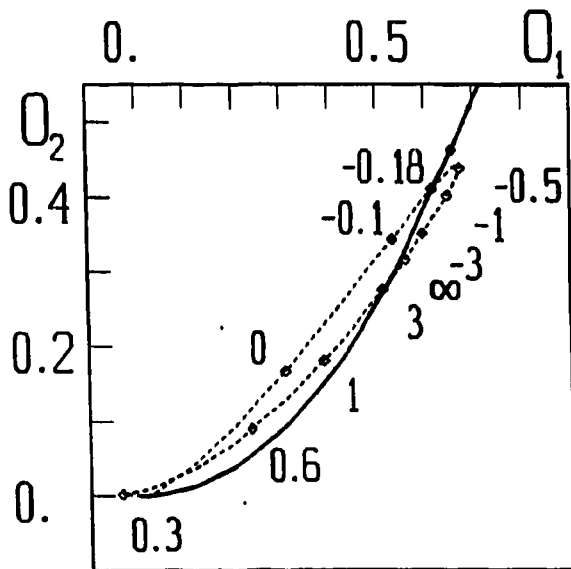


Figure 1: The full curve gives WT in operator space for observables  $O_1$  and  $O_2$  (as determined on  $4^4$ ), the full circle shows the point of simulation on an  $8^4$  lattice at  $K_F = 2.5$  and the dashed curve gives the results of BSTs with  $\rho_1 = 1, \rho_2 = -0.65$  and  $\rho_3$  varying continuously. In this projection two points appear to be close to the Wilson line, however, only one of them has minimal distance in the complete space.

In conclusion we may say that the operator oriented optimization allows a modification of the RT such as to bring it closer to a few parameter action. Since the RT is often used only as a technical means to obtain information on the renormalization behaviour along e.g. the Wilson line, one may well use different optimizations at different points in coupling space. However, it became clear that at least for the model and the parameterization studied it is not possible to obtain an overlap of the RT with the Wilson line. It may be possible to study this behaviour at weak coupling with perturbation theory. The net gain in comparison to a non-optimized RGT approach amounts to roughly one blocking step less in the operator matching approach, which in  $d=4$  correspond to a factor of 16 in computer resources.

**Acknowledgment:** We want to thank H.J. Reusch for communicating his results and R. Baier, H. Gausterer and P. Hasenfratz for many discussions. The calculations have been done on the VAX 785 of the EDV-Zentrum der Universität Graz and on the CYBER 205 at the Supercomputer Computations Research Institute of Florida State University, which is partially funded by the U.S. Dept. of Energy through Contract DE-FC05-85ER250000. The work was partially supported by Fonds zur Förderung der Wissenschaftlichen Forschung in Österreich, project P5965.

## REFERENCES

1. W. Burkhardt and J.M.J. van Leeuwen (eds.), *Real Space Renormalization*, Springer Topics In Current Physics 1982.
2. R.H. Swendsen., in ref.1.
3. K.G. Wilson, *Phys. Rev. D* **10**, 2445 (1974).
4. D.J.E. Callaway and R. Petronzio, *Nucl. Phys.* **B267** (1986)253.
5. S.H. Shenker and J. Tobochnik, *Phys. Rev. B* **22**, 4462 (1980); J.E. Hirsch and S.H. Shenker, *Phys. Rev. B* **27**, 1736 (1983); A. Hasenfratz et al., *Phys. Lett.* **140B**, 76 (1984); K.C. Bowler et al., *Nucl. Phys.* **B257**, 155 (1985).
6. R. Gupta, preprint LAUR-86-3618 (1986)and references therein.
7. R.H. Swendsen, *Phys. Rev. Lett.* **52**, 746 (1984); H. Gausterer and C.B. Lang, *Phys. Lett.* **186B**, 103 (1987).
8. C.B. Lang and M. Salmhofer, UNIGRAZ-UTP-04/87.
9. M.E. Fisher and M. Randeria, *Phys. Rev. Lett.* **56**, 2332 (1986).
10. A. Bennett, Edinburgh preprint 87/389 (1987).
11. R.H. Swendsen, *Phys. Rev. Lett.* **56**, 2333 (1986).
12. T.L. Bell and K.G. Wilson, *Phys. Rev. B* **11**, 3431 (1975); C.B. Lang, *Phys. Lett.* **155B**, 399 (1985); *Nucl. Phys.* **B265**, 630 (1986).
13. R.H. Swendsen, *Phys. Rev. Lett.* **47** (1981)1775.
14. K.C. Bowler et al.,in Ref. 2; P.B. Mackensie,*Proc. of the ANL Workshop Gauge Theory on a Lattice: 1984*, 1 (1984).
15. H.J. Reusch, private communication.
16. K.M. Bitar, S. Gottlieb and C.K. Zachos, *Phys. Rev. D* **26**, 2853 (1982).
17. K.M. Bitar, *Phys. Rev. D* **34**, 2462 (1986).
18. R. Gupta and A. Patel, *Phys. Rev. Lett.* **53**, 531 (1984); A. Patel et al., *Phys. Rev. Lett.* **53**, 527 (1984); A. Patel and R. Gupta, *Nucl. Phys.* **B251**, 789 (1985); *Advances in Lattice Gauge Theory*, Ed. D. Duke and J.F. Owens, World Scientific; 206 (1985).

Monopole Excitations in the 3D Georgi-Glashow Model  
on the Lattice

M.L. Laursen <sup>+) ,</sup> M. Müller-Preußker <sup>++)</sup>

<sup>+) Niels-Bohr-Institute, Copenhagen, Denmark  
<sup>++) Humboldt-Universität zu Berlin, Sektion Physik, GDR</sup></sup>

1. In this talk we present results of a numerical investigation concerning the vacuum structure of the Georgi-Glashow model (GGM) defined on a three-dimensional lattice with periodic boundary conditions <sup>/1/</sup>. By an appropriate relaxation procedure quantum fluctuations of Monte Carlo (MC) generated equilibrium configurations are frozen out in order to study the typical underlying background fields. This method already proved to be suited for studies of the vacuum structure of pure 4D Yang-Mills theory, where at  $T \lesssim T_c$  (multi-) instantons <sup>/2/</sup> and at  $T \gtrsim T_c$  monopoles <sup>/3/</sup> were found to be relevant ( $T_c$  being the critical temperature of the deconfinement transition). A similar (multi-) vortex investigation has been carried out for the 2D Abelian Higgs model, too <sup>/4/</sup>. The 3D GGM is studied here in order to establish the existence of 't Hooft-Polyakov monopole solutions in the quantized vacuum and to show that these background configurations play an important role in the Higgs phase transition ( a first exploratory study has been done in Ref. <sup>/5/</sup>). We take this as a preparation for an investigation of the more complicated 4D case. In the latter case recent measurements of magnetic fluxes out of elementary 3D cubes for MC equilibrium configurations showed that loops of monopole-anti-monopole pairs ( $m\bar{m}$ ) seem to condense in the confinement phase and to form a dilute gas in the Higgs and deconfinement phases ( see Refs. <sup>/6/</sup>).

2. We consider the SU(2) gauge Higgs model with the Higgs field  $\phi^a$ ,  $a=1,2,3$  in the adjoint representation

$$S = \beta_G \sum_{n,\mu,\nu} (1 - \frac{1}{2} \text{tr} U_{n\mu\nu}) + \frac{\beta_H}{2} \sum_{n,\mu} \text{tr} (\phi_n \phi_n^\dagger - \phi_n U_{n\mu} \phi_{n+\hat{\mu}}^\dagger U_{n\mu}^\dagger) \quad (1)$$

$$+ \beta_R \sum_n \left[ \frac{1}{2} \text{tr} (\phi_n \phi_n^\dagger) - V \right]^2,$$

where  $\phi_n = i\sigma^a \phi_n^a$ ,  $V = 1 + (\beta_H - 1)/2\beta_R$ .  $U_{n\mu\nu}$  denotes the standard plaquette variable. Due to superrenormalizability the continuum limit of this 3D model corresponds to  $\beta_G \rightarrow \infty$  and  $\beta_R/\beta_H^2 \rightarrow 0$ . Mostly we have chosen the unitary gauge  $\phi_n = iR_n \sigma^3$  for all sites  $n$ . Equilibrium fields were generated by a standard Metropolis algorithm, which allowed the radial Higgs mode  $R_n$  to fluctuate. The lattice size was  $8^3$ . We concentrated on a region at fixed  $\beta_R = 0.1$ ,  $\beta_G = 5.0$  and varying  $\beta_H$  ( $0.4 \leq \beta_H \leq 0.8$ ). By measuring  $\langle \text{tr} \hat{\phi}_n^\dagger U_{n\mu} \hat{\phi}_{n+\hat{\mu}} U_{n\mu}^\dagger \rangle$  as an order parameter we have found there a narrow crossover related to the transition between the confinement and Higgs phases in the 4D case <sup>/6,7/</sup>. In order to detect monopole excitations we measured the magnetic flux through plaquettes perpendicular to the  $\mu$ -direction

$$f_{n\mu} = \frac{1}{8\pi} \epsilon_{\mu\nu\lambda} \left( \text{tr} (\hat{\phi}_n U_{n\nu\lambda}) + \frac{1}{2} \text{tr} (\hat{\phi}_n U_{n\nu} \hat{\phi}_{n+\hat{\nu}}^\dagger U_{n\nu}^\dagger U_{n\lambda} \hat{\phi}_{n+\hat{\lambda}}^\dagger U_{n\lambda}^\dagger) \right) \quad (2)$$

( $\hat{\phi} \equiv \phi/|\phi|$ ) and the magnetic charge inside cubes at sites  $n$

$$m_n = \sum_{\mu} (f_{n\mu} - f_{n+\hat{\mu},\mu}). \quad (3)$$

In the continuum limit the manifestly gauge invariant expression (2) corresponds to the magnetic field invented by 't Hooft <sup>/8/</sup>.

Starting from MC generated equilibrium configurations we have iteratively minimized the action for each of them by applying a Langevin type relaxation procedure (without noise term) symbolically written as

$$\chi_{N+1} = \chi_N - \Delta\tau \left. \frac{\delta S}{\delta \chi} \right|_N, \quad \chi = (U_{n\mu}, R_n) \quad (4)$$

The time step was taken to  $\Delta\tau = 0.15$ .

3. The results are the following. Only for those configurations produced within a rather narrow 'window' for the gauge-Higgs coupling  $0.45 \lesssim \beta_H \lesssim 0.55$  we observe non-trivial plateaus developing during the cooling process. We have found two types of plateaus: mostly unstable ones roughly at action values  $S_1^{\overline{m}\overline{m}} \approx 1.40$ ,  $i=1,2$  and absolutely stable ones at  $S_1^{DS} = 1.12.4$ ,  $i=1,2$ . Unstable plateaus finally decay either into the  $S^{DS}$  ones or into the trivial configuration ( $S = 0$ ). The configurations we arrived with on a plateau, where the classical field equations are satisfied approximately, have been thoroughly investigated by plotting out the spatial distribution of the action density acc. to Eq. (1), the magnetic charge distribution (Eqs. (2,3)) and the spatial behaviour of the Higgs field modulus  $R_n$ .

It turns out that the  $S_1^{\overline{m}\overline{m}}$  - plateaus correspond to 1 pairs of well-separated and localized (anti-) monopoles of the 't Hooft-Polyakov type with zeros of the Higgs field at their centres. These  $\overline{m}\overline{m}$  -pairs can stabilize their positions due the periodic boundary conditions. The magnetic charge of elementary cubes belonging to a single local excitation sums up to  $\pm 1$  with good accuracy.

Furthermore, we see the stable plateaus at  $S_1^{DS} = 1.12.4$  to correspond to Dirac string configurations. They occur, when a monopole and the corresponding anti-monopole leave the finite volume in opposite directions and thereby annihilating due to spatial periodicity. If this happens, the only leftover is the magnetic flux directed from  $m$  to  $\overline{m}$ . This flux spreads until each plaquette perpendicular to the  $\overline{m}\overline{m}$  -axis is carrying the same amount  $f_p$  (acc. to definition (2)). The total flux is topologically quantized. The  $S_1^{DS}$  - plateaus contain pure Abelian gauge fields with all links along the flux direction equal to one. Thus, the observed  $S_1^{DS}$  - value is easily understood for our lattice of size  $8^3$ . Since  $f_p = 1/8^2 = \sin \varphi_p / 2\pi$  ( $\varphi_p$  denoting the U(1) plaquette angle), each of these plaquettes contribute  $1 - \cos \varphi_p$  to the action yielding finally  $S_1^{DS} = \beta_G \cdot 8^3 \cdot (1 - \cos \varphi_p) \approx 12.4$ . By writing out the  $\varphi_p$  - values for all plaquettes we convinced us that in each slice

perpendicular to the flux direction there is a distinct plaquette with  $\varphi_p$  differing by  $2\pi$  from all the others. This is the manner the Dirac string singularity well-known from continuum considerations is showing up on the lattice.

### References

- /1/ M.L. Laursen, M. Müller-Preussker, 't Hooft-Polyakov Monopoles and Dirac Strings in the 3D Georgi-Glashow Model: A Lattice Investigation, NBI-preprint October 1987.
- /2/ Y. Iwasaki, T. Yoshie, Phys. Lett. 131B(1983)159;  
M. Teper, Phys. Lett. 162B(1985)357;  
E.-M. Ilgenfritz, M.L. Laursen, M. Müller-Preussker,  
G. Schierholz, H. Schiller, Nucl. Phys. B268(1986)693;  
J. Hoek, Phys. Lett. 166B(1986)199;  
M.I. Polikarpov, A.I. Veselov, Pis'ma v ZhETF 45(1987)113;  
ITEP preprint 41 (1987).
- /3/ M.L. Laursen, G. Schierholz, DESY report 87-061 (1987).
- /4/ S. Grunewald, E.-M. Ilgenfritz, M. Müller-Preussker,  
Z. f. Phys. C33(1987)561.
- /5/ J. Seixas, Phys. Lett. 171B(1986)95.
- /6/ A.S. Kronfeld, G. Schierholz, U.-J. Wiese, DESY report  
87-023 (1987);  
A.S. Kronfeld, M.L. Laursen, G. Schierholz, U.-J. Wiese,  
DESY report 87-073 (1987);  
V.K. Mitriushkin, M. Müller-Preussker, A.M. Zadorozhny,  
JINR preprint E2-87-555 (1987).
- /7/ V.K. Mitriushkin, A.M. Zadorozhny, Phys. Lett. 161B  
(1986)111.
- /8/ G. 't Hooft, Nucl. Phys. B79(1974)276.

# QUARK-POLARIZATION EFFECTS FROM DYNAMICAL QUARKS<sup>†</sup>

M.Faber, W.Feilmair, H.Markum

Institut für Kernphysik, Techn.Universität Wien  
Wiedner Hauptstraße 8-10, A-1040 Wien  
Austria

The linear gluonic potential between a static quark-antiquark pair becomes screened in the presence of the dynamical quark sea. This is usually explained by polarization effects from virtual quark-antiquark pairs. We investigate the polarization cloud around a static quark charge. We find that the correlation  $\langle L(0)\bar{\Psi}(r)\Psi(r) \rangle$  between a static quark and the fermion condensate increases with increasing distance.

## INTRODUCTION

Lattice QCD has proven to be an extreme powerful method to investigate non-perturbative phenomena in QCD. In the last years even the effects of virtual light quark loops have been taken into account in numerical investigations. The inherent fermionic determinant in the partition function became manageable by new algorithms and new computer power in a satisfactory way /1,2,3/.

In this frame the potential between a static quark-antiquark source has been investigated for Kogut-Susskind fermions and Wilson-fermions /4,5/. The main result was that there is no longer a linearly rising confinement potential but the confinement potential becomes bounded. This is an effect due to the dynamical quarks. It can be explained as a screening of the static sources by virtual quark-antiquark pairs similar to the polarization of an electron by virtual electron-positron pairs in QED. But one has to be careful with such a comparison because QED is an abelian theory and QCD is not.

This has for example a dramatic effect on the running coupling constant. Results of renormalization group theory indicate that a single quark is surrounded by virtual gluons which carry the same color charge as the quark. Therefore, the coupling constant decreases when the distance to the quark source goes to zero and the momentum transfer to infinity. One reaches the region of asymptotic freedom /6/. In this picture it would be interesting to investigate polarization effects in QCD. This paper presents first results.

---

<sup>†</sup>Supported in part by "Fonds zur Förderung der wissenschaftlichen Forschung" under Contract No. P5501.



## THEORY

We investigate the behavior of a static quark within full lattice-QCD which in Wilson-Polyakov theory can be described by a thermal loop

$$L(\vec{r}) = \frac{1}{3} \text{tr} \prod_{k=1}^{N_t} U_{x=(\vec{r},k),\mu=0}$$

where  $N_t$  is the temporal extension of the lattice with spacing  $a$  and  $U_{x\mu}$  are the link variables of the gauge field. To measure the polarization cloud around the single static quark we decided to evaluate the correlation function between the Polyakov loop  $L(r=0)$  and the local fermion condensate  $\bar{\Psi}(r)\Psi(r)$ . The last operator also can be interpreted as the occupation number of virtual fermions per spatial lattice site // . So we have to evaluate the path integral

$$\langle L(0) \bar{\Psi}(r) \Psi(r) \rangle = \frac{\int D[U, \bar{\Psi}, \Psi] L(0) \bar{\Psi}(r) \Psi(r) e^{-(S_G + S_F)}}{\int D[U, \bar{\Psi}, \Psi] e^{-(S_G + S_F)}} \quad (1)$$

on an Euclidean lattice by means of Monte Carlo simulations.  $S_G$  is the gluonic action in Wilson formulation and  $S_F$  is the fermionic action in Kogut-Susskind formulation

$$S_F = \frac{n_f}{4} a^3 \left\{ \sum_{x,\mu} \frac{1}{2} \Gamma_{x,\mu} (\bar{\Psi}_x U_{x\mu}^\dagger \Psi_{x+\mu} - \Psi_{x+\mu} U_{x\mu} \bar{\Psi}_x) + m \sum_x \bar{\Psi}_x \Psi_x \right\} =$$

$$= \sum_{xx'} \bar{\Psi}_x (D(U) + m)_{xx'} \Psi_{x'}$$

where  $n_f$  is the number of flavors,  $m$  is the mass of the virtual quarks and  $\bar{\Psi}_x$  and  $\Psi_x$  are one-component Kogut-Susskind spinors carrying also color indices. The factor  $\frac{1}{4}$  takes the fermion doubling into account. Eq.(1) can be integrated analytically over  $\bar{\Psi}_x$  and  $\Psi_x$  applying the formula of Matthews-Salam

$$\langle L(0) \bar{\Psi}(r) \Psi(r) \rangle = \frac{\int D[U] L(0) \text{tr}(D(U)+m)^{-1} e^{-(S_G + \frac{n_f}{4} \text{Tr} \ln(D+m))}}{\int D[U] e^{-(S_G + \frac{n_f}{4} \text{Tr} \ln(D+m))}} =$$

$$=: \langle L(0) \text{tr}(D(U)+m)^{-1} \rangle_U$$

where  $\text{tr}$  stands for the trace in color space and  $\text{Tr}$  is the trace over the fermionic matrix and the subscript  $U$  denotes the remaining evaluation of the integral over the gauge fields. As a result of the above integration (2)  $\bar{\Psi}(r)\Psi(r)$  has to be replaced by  $\text{tr}(D(U)+m)^{-1}$ . This

represents a pointlike propagator. In hopping parameter expansion this propagator is a sum of closed virtual loops. This we define as our measurer for the polarization effects.

## RESULTS

For the evaluation of expression (2) we used a  $8^3 \times 4$  lattice with periodic boundary conditions for the gauge fields and antiperiodic boundary conditions for the fermion fields. The number of flavors  $n_f$  was set to 3 and the inverse coupling  $\beta = 5.2$  was taken below the phase transition to deconfinement. The mass  $m$  of the dynamical quarks is 0.1. We performed 300 Monte Carlo iterations with the Metropolis algorithm for the gauge field and the fermionic determinant and fermion propagator  $\text{tr}(D(U)+m)^{-1}$  were approximated by the pseudo-fermion method using a heat-bath algorithm with 50 fermionic steps per gauge field.

The correlation function  $\langle L(0)\bar{\Psi}(r)\Psi(r) \rangle$  is displayed in fig.1. We find the surprising result that the correlations increase with increasing distance  $r$ . This means that polarization effects in the near surrounding of the quark are suppressed. This is the opposite effect to QED in regard to fermionic vacuum polarization. The horizontal line in fig.1 is the cluster value  $\langle L \rangle \langle \bar{\Psi}\Psi \rangle$  for  $\langle L\bar{\Psi}\Psi \rangle$  for  $r \rightarrow \infty$ . For distances greater than  $r=3$  the correlations reach the cluster value. Beyond this distance the two operators do not feel each other.

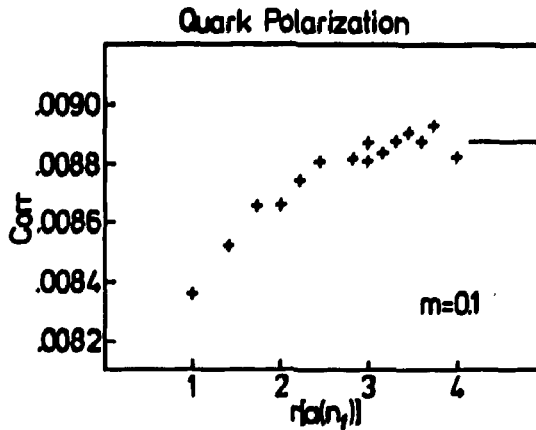


Fig.1: Correlation  $\langle L(0)\bar{\Psi}(r)\Psi(r) \rangle$  between the Polyakov loop of a static quark and the fermion condensate. The horizontal line gives the value expected from the cluster theorem.

## DISCUSSION

How can the behavior of the correlations be explained? The main question is why the bare vacuum fluctuations seem to be suppressed near the quark. Maybe this can be solved in analogy to a spin system. If we insert a fixed local spin in a magnetized spin system the presence of the fixed spin will influence the neighboring ones. When the fixed spin is not parallel to the other spins the local magnetization in its surrounding is lowered. The correlations between the fixed spin and the local magnetization will increase with distance  $r/\lambda$ . In QCD  $\langle\bar{\Psi}\Psi\rangle$  acts as an order parameter for the chiral symmetry. It has a phase transition at the same  $\beta_{\text{crit}}$  as the gluon field. For  $\beta < \beta_{\text{crit}}$  the chiral symmetry is broken spontaneously. The chiral condensate is unequal zero because there is an ordering in the system with regard of fermionic vacuum fluctuations. This becomes plausible if one imagines that the virtual quark-antiquark pair creation leads to the formation of colored dipoles pointing in a certain direction. Now the external static quark disturbs this ordering because it induces a repolarization of the virtual quark-antiquark pairs towards the charge. Thus the chiral condensate as an order parameter has a smaller value near the quark.

This leads to another explanation interpreting  $\langle\bar{\Psi}\Psi\rangle$  as occupation number density. Near the quark source it is energetically disadvantageous to create polarized virtual fermionic pairs having a finite mass. Therefore, the system tries to become colorless by means of virtual gluons which are massless. This gluons carry the color charge away from the static quark and will end in virtual quark-antiquark pairs outside of the near surrounding of the quark.

## CONCLUSION

To summarize we found the remarkable result that the vacuum polarization seems to decrease in the vicinity of an external quark source compared to vacuum fluctuations of the quark sea in empty space. At a first sight this might seem to be in disagreement with the idea of the running coupling constant but one should bear in mind that in a system with static quarks the momentum transfer is zero.

## OUTLOOK

As next work one should try to study this feature by strong coupling expansion. From our data we have a hint that the chiral condensate can be written as a function of  $L/\beta$ . It would be also very desirable to distinguish in the virtual quark-antiquark production the parts stemming from virtual quarks and antiquarks, respectively. To get further information we are going to extend our calculations for different dynamical quark masses and different  $\beta$ -values,

eventually also in the deconfinement region. In a recently started work we are trying to investigate a static quark-antiquark with regard of polarization effects from dynamical quarks.

#### **REFERENCES**

- /1/ F.Fucito,E.Marinari,G.Parisi,C.Rebbi, Nucl.Phys. B180 (1981) 369**
- /2/ H.W.Hamber,E.Marinari,G.Parisi,C.Rebbi, Phys.Lett. 124 B (1983) 99**
- /3/ Ph.deForcrand,H.Haraguchi,H.C.Hege,V.Linke,A.Nakamura,I.O.Stamatescu, Phys.Rev.Lett. 58 (1987) 2011**
- /4/ H.Markum, Phys.Lett. B173 (1986) 337**
- /5/ M.Faber,Ph.deForcrand,H.Markum,M.Meinhart,I.O.Stamatescu, Phys.Lett.B, in print**
- /6/ P.Becher,M.Böhm,H.Joos: Eichtheorien der starken und elektroschwachen Wechselwirkung, B.G.Teubner, Stuttgart 1983**
- /7/ J.Potvin, Phys.Rev. D32 (1985) 2070, D33 (1986) 2388**
- /8/ J.Kostlinek,H.Markum,H.Rauch, Phys.stat.sol. 112 (1982) 417**

Next-next-to-leading  $O(\alpha_s^3)$   
 QCD corrections to  $\sigma_{\text{tot}}(e^+e^- \rightarrow \text{hadrons})$ :  
 analytical calculations and estimation of the  
 parameter  $\Lambda_{\overline{MS}}$ .

S.G.Gorishny

Joint Institute for Nuclear Research, Dubna

A.L.Kataev, S.A.Larin

Institute for Nuclear Research, Academy  
 of Sciences of the USSR, Moscow

### Abstract.

We have calculated next-next-to-leading  $O(\alpha_s^3)$  QCD correction to  $\sigma_{\text{tot}}(e^+e^- \rightarrow \text{hadrons})$ . Taking into account this correction in the fit of the combined PETRA and PEP data at  $\sqrt{s} = 34$  GeV decreases the value of  $\Lambda_{\overline{MS}}$  in twice.

### 1. Introduction

The process  $e^+e^-$  annihilation into hadrons is one of the most informative processes in elementary particle physics. Both theoretical and experimental analysis of the behaviour of its basic characteristic  $R(s) = \sigma_{\text{tot}}(e^+e^- \rightarrow \text{hadrons}) / \sigma(e^+e^- \rightarrow \mu^+\mu^-)$  allows us to obtain important information about the properties of hadrons and their constituents i.e. quarks and gluons. In particular, the comparison of the QCD prediction for  $R(s)$  with the experimental data above the thresholds of  $J/\psi$ -system allowed to observe before the experimental discovery of the b-quark that it is highly desirable to introduce in the theory the fifth heavy quark with the charge  $Q_b = -1/3$  [1].

The zeroth order perturbation theory (PT) QCD prediction  $R(s) = 3 \sum_f Q_f^2$  is in qualitative agreement with experiment. However, in order to perform quantitative examination of the QCD theoretical prediction it is necessary to take into account the effects of higher PT corrections. The QCD expression for  $R(s)$  up to next-to-leading order  $O(\alpha_s^2)$  has been

calculated in [2]. In this work we present the results of calculations of the next-next-to-leading  $O(\alpha_s^3)$  corrections to  $R(s)$  and obtain the new estimates of the parameter  $\Lambda_{\overline{MS}}$  based on the analysis of the combined PETRA and PEP results [3].

## 2. The outline of calculations.

Throughout this work we shall follow the calculational Program outlined in refs. [4,5] and use  $\alpha$  introduced there notations. In course of calculations it is convenient to use the quantity

$$D(Q^2) = -\frac{3}{4} Q^2 \frac{d}{dQ^2} \Pi(Q^2) = Q^2 \int_0^1 \frac{R(s)}{(s+Q^2)^2} ds \quad (2.1)$$

where  $Q^2$  is the euclidian transferred momentum and  $\Pi(Q^2)$  is the hadronic vacuum polarization function. It can be shown, that in order to calculate the next-next-to-leading  $O(\alpha_s^3)$  corrections to the D-function it is necessary to use the two-loop approximation of the bare charge  $g_0 = \left(\frac{\alpha_s}{\pi}\right)_0$ , to calculate the three-loop approximation of the bare expression  $\Pi_B(g_0)$  of the hadronic vacuum polarization function and find the four-loop approximation of the photon wave function renormalization constant  $Z_3$ . At this level over 100 diagrams contribute to  $Z_3$ . All the calculations have been done within the dimensional regularization in  $D=4-2\epsilon$  space-time dimensions and the minimal subtractions (MS) scheme. The application of methods of infrared rearrangement [6,5] and the infrared  $R^*$  - operation [7] allows us to reduce the calculation of the four-loop approximation of  $Z_3$  to the evaluation of the three-loop massless propogator-type integrals up to  $O(\epsilon^0)$  -terms. These integrals as well as the three-loop approximation of  $\Pi_B(g_0)$  have been calculated with the help of the integration by parts algorithm [8]. Some basic scalar integrals used in the calculations has been calculated with the help of the Gegenbauer polynomial x-space technique [5]. The methods of calculations have been briefly discussed in the review [9]. All analytical calculations have been done with the help of the SCHOONSCHIP program [10]. The whole running time at the CDC-6500 computer totals about 200 hours.

### 3. The byproduct of calculations: the four-loop approximation for the $\beta$ -function in QED.

All calculations have been done at two stages. At the first stage we have found the counteterms of 58 diagrams which contribute to  $Z_3$  in QED. As the result the four-loop approximations of the  $\beta$ -function of QED in the MS and MOM (momentum subtractions) schemes have been calculated [11]. For QED with  $N=1$  types of fermions the result for  $\beta$ -function in the MS-scheme reads:

$$\frac{1}{4\pi} \mu^2 \frac{\partial \alpha}{\partial \mu^2} = \beta_{MS}(\alpha) = \frac{4}{3} \left(\frac{\alpha}{4\pi}\right)^2 + 4 \left(\frac{\alpha}{4\pi}\right)^3 - \frac{62}{9} \left(\frac{\alpha}{4\pi}\right)^4 + \left(\frac{16301003}{7776} + \frac{18368}{9} \zeta(3) - 3200 \zeta(5)\right) \left(\frac{\alpha}{4\pi}\right)^5 \quad (3.1)$$

After the transformation of (3.1) to the MOM-scheme, defined by performing subtractions in the photon propagator at the euclidian point  $q^2 = -\lambda^2$ , the last two coefficients of the  $\beta$ -function change their values. The correspondent approximation of the Gell-Mann-Low function of QED takes the form

$$\begin{aligned} \psi(\alpha_{MOM}) = \beta_{MOM}(\alpha_{MOM}) &= \frac{\partial \alpha_{MOM}}{\partial \alpha_{MS}} \beta_{MS}(\alpha_{MS}) = \\ &= \frac{4}{3} \left(\frac{\alpha}{4\pi}\right)^2 + 4 \left(\frac{\alpha}{4\pi}\right)^3 + \left(\frac{64}{3} \zeta(3) - \frac{202}{9}\right) \left(\frac{\alpha}{4\pi}\right)^4 + \\ &+ \left(\frac{1991731}{864} + \frac{6656}{3} \zeta(3) - \frac{10880}{3} \zeta(5)\right) \left(\frac{\alpha}{4\pi}\right)^5 \end{aligned} \quad (3.2)$$

where  $\alpha = \alpha_{MOM}$ . Using the numerical values of Riemann  $\zeta$ -functions  $\zeta(3)=1.20205\dots$ ,  $\zeta(5)=1.03692\dots$  and presenting the results (3.1), (3.2) in the numerical form we obtain

$$\begin{aligned} \beta_{MS}(\alpha) &= 0.0833 \left(\frac{\alpha}{\pi}\right)^2 + 0.0625 \left(\frac{\alpha}{\pi}\right)^3 - 0.0269 \left(\frac{\alpha}{\pi}\right)^4 + \\ &\quad + 1.2025 \left(\frac{\alpha}{\pi}\right)^5 \quad (3.3) \\ \psi(\alpha) &= 0.0833 \left(\frac{\alpha}{\pi}\right)^2 + 0.0625 \left(\frac{\alpha}{\pi}\right)^3 + 0.0124 \left(\frac{\alpha}{\pi}\right)^4 + \\ &\quad + 1.1832 \left(\frac{\alpha}{\pi}\right)^5 \end{aligned}$$

Notice positivity and relatively large numerical values of both four-loop coefficients. Thus in the region of application of PT there are no indications on the existence of ultraviolet fixed point in QED. Other discussions of the obtained results can be found in [11].

#### 4. The QCD results.

At the second stage of the calculations the QCD result for the D-function has been obtained. However, to compare the theoretical results obtained in the euclidian region  $Q^2 > 0$  it is necessary to transform them into the physical region of energies by means of the following representation:

$$R^{\text{th}}(s) = \frac{1}{2\pi i} \int_{-s-i\epsilon}^{-s+i\epsilon} d\sigma \frac{D(\sigma)}{\sigma} \quad (4.1)$$

It can be shown that taking into account of eq.(4.1) leads to the appearance of the additional scheme independant corrections in the PT order we are interested in:

$$R^{\text{th}}(s) = D(s, a) - 3 \sum_f Q_f^2 \pi^2 \frac{\beta_0^2}{3} a^3 + D(a^4) \quad (4.2)$$

where  $a = \frac{\alpha_s}{\pi}$  and  $\beta_0$  is the first coefficient of the QCD  $\beta$ -function which has been calculated in [12] in the MS-scheme at the three-loop level:

$$\begin{aligned} \frac{1}{\pi} \mu^2 \frac{\partial \alpha_s}{\partial \mu^2} &= \mu^2 \frac{\partial a}{\partial \mu^2} = \beta(a) = -\beta_0 a^2 - \beta_1 a^3 - \beta_2 a^4 \\ &= -\beta_0 a^2 (1 + c_1 a + c_2 a^2) \\ \beta_0 &= (11 - \frac{2}{3}f) \frac{1}{4} \quad \beta_1 = (102 - \frac{38}{3}f) \frac{1}{16} \\ \beta_2 &= (2857 + \frac{5083}{18}f + \frac{325}{54}f^2) \frac{1}{64} \end{aligned} \quad (4.3)$$

The additional contribution to  $R(s)$  in eq. (4.2) appears after taking into account the effects of analytical continuation in the terms  $\ln^3(a^2/\mu^2) \rightarrow (\ln(s/\mu^2) + i\pi)^3$ . These effects have been discussed earlier in the case of  $e^+e^- \rightarrow$  annihilation [3, 14] and  $\gamma^*(V) \rightarrow g \rightarrow$  hadrons process [15]. The analogous correction also appeared in calculations of the next-next-to-leading order corrections to the total hadronic decay width of the heavy Higgs boson of the standard theory [16].

As well as in the case [16] taking into account of the  $\pi^2 a^3$  terms decreases the numerical value of the analysed PT coefficients. Thus we will not redefine the expansion parameter is



the space-like region in contrast to the proposals of refs. [13,14].

Solving renormalization group equation we obtain the following analytical expression for  $R(s)$  in the  $\overline{MS}$ -scheme in QCD:

$$\begin{aligned}
 R^{\overline{MS}}(s) = & 3 \sum Q_f^2 \left\{ 1 + \bar{\alpha} + \left[ \left( \frac{730}{3} - 176 \gamma(s) \right) - \left( \frac{44}{3} - \frac{32}{3} \gamma(s) \right) f \right] \frac{1}{16} \bar{\alpha}^2 \right. \\
 & + \left[ \left( \frac{3503881}{144} - \frac{473774}{27} \gamma(s) + \frac{25120}{9} \gamma(s)^2 \right) + \right. \\
 & + \left( \frac{62776}{27} - \frac{16768}{9} \gamma(s) + \frac{1600}{9} \gamma(s)^2 \right) f + \left( \frac{4832}{81} - \frac{1216}{27} \gamma(s) \right) f^2 \\
 & \left. - \pi^2 \left( 11 - \frac{2}{3} f \right)^2 \frac{4}{3} \right] \frac{1}{64} \bar{\alpha}^3 \left. \right\} - \left( \sum Q_f \right)^2 \left( \frac{560}{27} - \frac{8}{3} \gamma(s) \right) \bar{\alpha}^3 \quad (4.4)
 \end{aligned}$$

In the numerical form eq. (4.4) reads:

$$\begin{aligned}
 R^{\overline{MS}}(s) = & 3 \sum Q_f^2 \left\{ 1 + \bar{\alpha} + (1.986 - 0.115f) \bar{\alpha}^2 + \right. \\
 & \left. + (70.985 - 1.200f - 0.005f^2) \bar{\alpha}^3 \right\} - \left( \sum Q_f \right)^2 0.840 \bar{\alpha}^3 \quad (4.5)
 \end{aligned}$$

The last term, which does not appear in the previous orders of PT appears from the QCD analogs of the QED light-by-light diagrams with  $SU(N)$ -group factors proportional to  $d^{abc} d^{abc}$  and is scheme independent. However, other coefficients do depend on the subtraction scheme used. We have obtained the results in the  $\overline{MS}$ -scheme and the  $\mathcal{G}$ -scheme [4,5] which is very convenient modification of the  $\overline{MS}$ -scheme. The results shows that as well as in the case of other physical quantities (see e.g. [16,17]) in the  $\mathcal{G}$ -scheme the values of the scheme-dependant coefficients are smaller. The transformation to the MOM-scheme is not so straightforward. However, the corresponding result can be in principal obtained after using the information about the third coefficient of the  $\beta$ -function in the MOM-scheme [18, 19].

### 5. Discussions of the results and determination of the parameter $\Lambda_{\overline{MS}}$ .

We have obtained that the coefficients of the  $O(\bar{\alpha}^3)$  corrections to  $R(s)$  are large in the  $\mathcal{G}$ ,  $\overline{MS}$  and  $\overline{MS}$ -schemes. Thus the question arises: at which energies is it

necessary to involve  $O(\bar{\alpha}^3)$ -terms to determine the correct value of the parameter  $\Lambda_{\overline{MS}}$  from the fit of experimental data for  $R(s)$ ? Indeed, it is known that PT series of quantum field theory are asymptotic ones, see e.g. the reviews [20]. In QCD they have sign constant character in contrast with e.g.  $g^4$ -theory and QED. Thus, they should be truncated in some way for correct comparison with experiment. However, it would be very strange if asymptotic character of PT series would begin to manifest itself at the level of the next-next-to-leading corrections. Indeed at the model  $g^4$  theory the asymptotic n! growth has not been observed even at the five-loop level [21]. Therefore we will include the calculated corrections in the analysis of the experimental data.

We shall use the data obtained at PETRA and PEP colliders far above the thresholds of production of b-quarks. The recent analysis of these data by means of the method  $R_{(s)}^{exp} = R^{th}(s)$  with taking into account the  $O(\bar{\alpha}^2)$  corrections in the  $\overline{MS}$ -scheme gives [3] :  $\bar{\alpha}_s(34^2 \text{Gev}^2) = 0.169 \pm 0.025$ ,  $\bar{a}_{ne} = \frac{\alpha_s}{\pi} = 0.054 \pm 0.008$  where index ne means that the next-to-leading order corrections have been taken into account.

Let us now take into account the calculated next-next-to-leading corrections and find the corresponding value of the parameter  $\Lambda_{\overline{MS}}$ . The analysis will be made by two different ways: (I) the direct analysis in the  $\overline{MS}$ -scheme and (II) the analysis in the framework of the invariant charges approach [22] known in the literature as the fastest apparent convergence (FAC) criterion (this approach has been also discussed in [23]). We will call it "the effective scheme approach". Substituting  $f=5$  into eq. (4.5) and introducing the index nnl to indicate the next-next-to-leading PT order and index eff for the effective scheme results we obtain:

$$R^{\overline{MS}}(s) = 3 \sum_{j=0}^{\infty} \alpha_s^j [1 + \bar{a}_{nne} + r_1 \bar{a}_{nne}^2 + r_2 \bar{a}_{nne}^3 + \dots] \quad (5.1)$$

$$= 3 \sum_{j=0}^{\infty} \alpha_s^j [1 + \bar{a}_{eff}^{(j)}]$$

$$r_1 = 1.411 \quad r_2 = 64.835$$

From the result for  $\bar{\alpha}_s$  we have that  $\bar{\alpha}_{eff}^{(2)} = \bar{\alpha}_{ne}(1 + r_1 \bar{\alpha}_{ne}) = 0.058 \pm 0.009$ . Solving now numerically the equation  $\bar{\alpha}_{eff}^{(3)} = \bar{\alpha}_{eff}^{(2)}$  we obtain the new corrected value of  $\bar{\alpha}_s(34^2 \text{ GeV}^2)$  in the  $\overline{\text{MS}}$ -scheme:  $\bar{\alpha}_{ne} = 0.048 \pm \frac{0.005}{0.006}$ .  $\bar{\alpha}_s(34^2 \text{ GeV}^2) = 0.151 \pm \frac{0.016}{0.019}$ . The corresponding numerical form of the PT series for  $R(s)$  in the  $\overline{\text{MS}}$ -scheme reads:

$$R^{\overline{\text{MS}}}(s) = 3 \sum_{j=1}^{\infty} Q_s^2 \left\{ \begin{array}{l} 1 + 0.053 + 0.004 + 0.010 + \dots \\ 1 + 0.048 + 0.003 + 0.007 + \dots \\ + 0.042 + 0.002 + 0.005 + \dots \end{array} \right\} \quad (5.2)$$

Thus at  $\sqrt{s} = 34 \text{ GeV}$  the contributions of the next-next-to-leading order correction is 2.5 times as large as the previous  $O(\bar{\alpha}^2)$  - corrections.

There are several methods of extracting the estimates of  $\Lambda_{\overline{\text{MS}}}$  from the numerical values of  $\bar{\alpha}$ . The first of them is based on the exact solution of RG equation (4.3). Let us introduce the following designations:

$$\Psi_{ne}(a) = \frac{1}{\beta_0 a} + \frac{c_1}{\beta_0} \ln \frac{c_1 a}{1 + c_1 a} \quad (5.3)$$

$$\Psi_{nne}(a, c_2) = \Psi_{ne}(a) + \frac{c_1}{\beta_0} \ln \frac{(1 + c_1 a)^2}{1 + c_1 a + c_2 a^2} + \frac{2c_2 - c_1^2}{\sqrt{\Delta} \beta_0} \left[ \text{arctg} \frac{c_1 + 2c_2 a}{\sqrt{\Delta}} - \text{arctg} \frac{c_1}{\sqrt{\Delta}} \right]$$

where  $\Delta = 4c_2 - c_1^2$ .

In the next-to-leading order the solutions of (4.3) in the  $\overline{\text{MS}}$  - and effective schemes are:

$$\ln \frac{s}{\Lambda_{\overline{\text{MS}}}^2} \Big|_{\sqrt{s}=34 \text{ GeV}} = \Psi_{ne}(\bar{\alpha}_{ne}); \quad \ln \frac{s}{\Lambda_{eff}^2} \Big|_{\sqrt{s}=34 \text{ GeV}} = \Psi_{ne}(\bar{\alpha}_{eff}^{(2)}) \quad (5.4a)$$

The parameter  $\Lambda_{\overline{\text{MS}}}$  is connected with  $\tilde{\Lambda}_{\overline{\text{MS}}}$  and  $\tilde{\Lambda}_{eff}$  by the following ways  $\Lambda_{\overline{\text{MS}}}^2 = \tilde{\Lambda}_{\overline{\text{MS}}}^2 (c_1/\beta_0)^{c_1/\beta_0}$

$$\Lambda_{\overline{\text{MS}}}^2 = \Lambda_{eff}^2 \exp(r_1/\beta_0) = \tilde{\Lambda}_{eff}^2 \exp(r_1/\beta_0) (c_1/\beta_0)^{c_1/\beta_0}$$

Solving eqs. (5.4) we obtain the the corresponding estimates:

$$(\Lambda_{\overline{MS}})_{ne} = 585_{-320}^{+481} \text{ MeV} \quad (\Lambda_{\overline{MS}})_{ne} = 533_{-298}^{+415} \text{ MeV} \quad (5.5a)$$

In order to take into account the next-next-to-leading PT corrections both to  $R(s)$  and the  $\beta$ -function one should solve the following equations:

$$\ln \frac{s}{\Lambda_{\overline{MS}}^2} \Big|_{\sqrt{s}=34 \text{ GeV}} = \Psi_{nne}(\bar{a}_{nne}, c_2); \quad \ln \frac{s}{\Lambda_{\text{eff}}^2} \Big|_{\sqrt{s}=34 \text{ GeV}} = \Psi_{nne}(\bar{a}_{\text{eff}}^{(n)}, \tilde{c}_2) \quad (5.6)$$

where  $\tilde{c}_2$  can be found from the property that the quantity  $\beta_2 = c_2 + r_2 - c_1 r_1 - r_1^2$  is the scheme invariant [24-26]. In the effective scheme  $r_1 = r_2 = 0$ , thus we have that  $c_2 = \beta_2$ . Hence we have from (5.6) in the  $\overline{MS}$ -scheme directly and the effective scheme approaches:

$$(\Lambda_{\overline{MS}})_{nne} = 326_{-169}^{+201} \text{ MeV} \quad (\Lambda_{\overline{MS}})_{nne} = 241_{-117}^{+139} \text{ MeV} \quad (5.7)$$

Let us now find the values of  $\Lambda_{\overline{MS}}$  in the framework of the second method which presupposes the expansions of the solution of RG equation (4.3) in powers of  $1/\ln(s/\Lambda^2)$ . The corresponding representations for the running coupling constants can be expressed in terms of the following functions

$$\Psi_{ne}(\Lambda) = \frac{1}{\beta_0 \ln(s/\Lambda^2)} - \frac{c_1}{\beta_0} \frac{\ln \ln(s/\Lambda^2)}{\ln^2(s/\Lambda^2)} \quad (5.8)$$

$$\Psi_{nne}(\Lambda, c_2) = \Psi_{ne}(\Lambda) + \frac{1}{\beta_0 \ln^2(s/\Lambda^2)} (c_1^2 \ln^2 \ln(s/\Lambda^2) - c_1^2 \ln \ln(s/\Lambda^2) + c_2 - c_1^2)$$

In the next-to-leading PT order we have  $\bar{a}_{ne} = \Psi_{ne}(\Lambda_{\overline{MS}}) \Big|_{\sqrt{s}=34 \text{ GeV}}$  from which we obtain  $\bar{a}_{\text{eff}}^{(2)} = \Psi_{ne}(\Lambda_{\text{eff}}) \Big|_{\sqrt{s}=34 \text{ GeV}}$  in the following estimates

$$(\Lambda_{\overline{MS}})_{ne} = 600_{-320}^{+460} \text{ MeV} \quad (\Lambda_{\overline{MS}})_{ne} = 560_{-297}^{+423} \text{ MeV} \quad (5.9)$$

After using the information about the next-next-to-leading order corrections we obtain  $\bar{a}_{nne} = \Psi_{nne}(\Lambda_{\overline{MS}}, c_2)$

$\bar{a}_{\text{eff}}^{(a)} = \Psi_{nne}(\Lambda_{\text{eff}}, \tilde{c}_2)$ , from which we obtain

$$(\Lambda_{\overline{MS}})_{nne} = 325_{-170}^{+200} \text{ MeV} \quad (\Lambda_{\overline{MS}})_{nne} = 211_{-104}^{+135} \text{ MeV} \quad (5.10)$$

Thus the values of  $\Lambda_{\overline{MS}}$  do depend on both the method of representing the solutions of RG equations and the ways of extracting the numerical values of the  $\Lambda_{\overline{MS}}$ -parameter. Nevertheless we arrive at the definite conclusion that taking into account of the calculated  $O(\overline{\alpha}^3)$  next-next-to-leading corrections decreases the values of  $\Lambda_{\overline{MS}}$  in twice. The numerical results (5.7), (5.10) are in better agreement with the values of  $\Lambda_{\overline{MS}}$  extracted from other processes [27] then the results (5.5), (5.9). This better agreement can indicate that in the presently available region of energies of PEP and TRISTAN the corrections calculated by us are experimentally sensible and thus they should be included in the procedures of analysing  $e^+e^-$  data not only at the present machines, but at the future ones, say LEP. It should be noted that this interpretation presumes that both the unknown  $O(\overline{\alpha}^4)$  corrections to  $R(s)$  and the next-next-to-leading PT corrections to other observable physical quantities are small. Thus from the point of view of studying the region of applicability of the asymptotic PT predictions of as the whole it is highly desirable (i) to decrease the experimental error of  $e^+e^-$ - data and (ii) to analyse the effects of the next-next-to-leading order corrections to other physical quantities, say the Gross-Llewelyn-Smith sum rule for deep inelastic lepton-hadron scattering where the next-to-leading corrections have been calculated in ref. [28].

### 6. Conclusion.

We have calculated the next-next-to-leading  $O(\alpha_s^3)$  QCD corrections to  $R(s) = \sigma_{\text{tot}}(e^+e^- \rightarrow \text{hadrons}) / \sigma(e^+e^- \rightarrow \mu^+\mu^-)$ . The obtained corrections are large e.g. in the  $\overline{MS}$ -scheme at  $\sqrt{s}=34$  GeV they are over two times larger than the previous next-to-leading correction. Of course it is possible that the asymptotic nature of the PT series manifests itself at the level of the next-next-to-leading cor-

rections. However, it can not be ruled out that some contributions of the lower PT corrections are accidentally small. That is why we include the  $O(\alpha_s^3)$  corrections in the procedure of fitting PEP and PETRA data. As the result taking into account of these corrections drastically (in twice) decreases the value of  $\Lambda_{\overline{MS}}$ . For example, for the fit in the  $\overline{MS}$ -scheme we obtain  $\Lambda_{\overline{MS}} = 326^{+201}_{-109}$  MeV which is in better agreement with the estimates of the same parameter obtained in other processes.

We are grateful to V.A.Matveev, D.V.Shirkov and A.N.Tavkhelidze for interest in the work, constant support and useful discussions. It is pleasure to thank K.G.Chetyrkin, D.I.Kazakov, N.V.Krasnikov, S.A.Kulagin, A.A.Pivovarov, O.V.Tarasov, F.V.Tkachov, M.E.Shaposhnikov and other researchers of the theoretical divisions of both INR and JINR for useful discussions at different stages of the work. One of us (A.L.K.) is grateful to the organizers of the Hadrons Structure-87 conference for hospitality.

#### References.

1. Chetyrkin K.G., Krasnikov N.V., Tavkhelidze A.N. in Proc. of the Hadron Structure-77 Conference, edited by S. Dubnicka, VEDA, Bratislava 1979, 185.  
Chetyrkin K.G., Krasnikov N.V., Tavkhelidze A.N. Phys. Lett., 1978, 76 B, 83.
2. Chetyrkin K.G., Kataev A.L., Tkachov F.V. Phys. Lett., 1979, 85B, 277.  
Dine M., Saperstein J. Phys. Rev. Lett., 1979, 43, 668.  
Celmaster W., Gonsales R. Phys. Rev. Lett., 1980, 44, 560.
3. Behrend H.J. et al. CELLO collaborations. Phys. Lett., 1987, 183B, 400.
4. Chetyrkin K.G., Kataev A.L., Tkachov F.V. Preprint INR, P-0170, 1980.
5. Chetyrkin K.G., Kataev A.L., Tkachov F.V. Nucl. Phys., 1980, B174, 345.

6. Vladimirov A.A. Teor. Mat. Fiz., 1980, 43, 210.
7. Chetyrkin K.G., Tkachov F.V. Phys. Lett., 1982, 114B, 340.  
Chetyrkin K.G., Smirnov V.A. Phys. Lett., 1984, 144B, 419.
8. Tkachov F.V. Phys. Lett., 1981, 100B, 65.  
Chetyrkin K.G., Tkachov F.V. Nucl. Phys., 1981, B192, 159.
9. Chetyrkin K.G., Kataev A.L., Tkachov F.V. in Proc. of  
the Hadron Structure-80 Conference edited by A.Nogova,  
VEDA, Bratislava, 1982.
10. Gorishny S.G., Larin S.A., Tkachov F.V. Preprint INR  
P-0330, 1984.
11. Gorishny S.G., Kataev A.L., Larin S.A. Phys. Lett., 1987,  
194B, 429.
12. Tarasov O.V., Vladimirov A.A., Zharkov A.Yn. Phys. Lett.,  
1980, 93B, 429.
13. Pennington M.R., Ross G.G. Phys. Lett., 1981, 102B, 167.
14. Radyushkin A.V. Preprint JINR E2-82-159, 1982.
15. Krasnikov N.V., Pivovarov A.A. Phys. Lett., 1982, 116B,  
168.
16. Gorishny K.G., Kataev A.L., Larin S.A., Yad. Fiz., 1984,  
40, 517, Erratum Yad. Fiz., 1985, 42, 1312.
17. Gorishny K.G., Kataev A.L., Larin S.A. Nuovo Cim., 1986,  
92A, 116.
18. Hagiwara K., Yoshino T. Preprint MAD/PH /39, TUMP-HEL-  
8202, 1982; Phys. Rev., 1983, ser. D.
19. Tarasov O.V. Talk at the Seminar on QCD high energy  
processes, Novorossisk, october 1982.
20. Kazakov D.I., Shirkov D.V. Fortsch. Phys., 1980, 28,  
465.  
Bogomolny E.B., Fateev V.A., Lipatov L.N. in Soviet  
Scientific Reviews, sect A, Phys. Rev., 1980, 2, 247.
21. Chetyrkin K.G., Gorishny S.G., Larin S.A., Tkachov F.V.  
Phys. Lett., 1983, 132B, 351.

22. Grunberg G. Phys. Lett., 1980, 93B, 70.
23. Krasnikov N.V. Phys. Lett., 1981, 105B, 212.  
Kataev A.V., Krasnikov N.V., Pivovarov A.A.  
Nucl. Phys., 1982, B198, 508.
24. Stevenson P.M. Phys. Rev., 1984, D23, 2916.
25. Dhar A. Phys. Lett., 1983, 128B, 407.
26. Kazakov D.I., Shirkov D.V. Yad. Fiz., 1985, 42, 768.
27. Duke D.W., Roberts R.G. Phys. Rep., 1980, 120, 275.
28. Gorishny S.G., Larin S.A. Phys. Lett., 1986, 172B, 109.  
Gorishny S.G., Larin S.A. Nucl. Phys., 1987, B283, 452.



# INFLUENCE OF STRONG INTERACTIONS ON ELECTROMAGNETIC MASS DIFFERENCES

F. Schöberl

Institut für Theoretische Physik der Universität Wien  
Boltzmannngasse 5 A-1090 Wien

## Abstract

*Calculating the electromagnetic mass differences of mesons in the framework of a non-relativistic potential model we find in contrast to experiment that  $B^0 - B^+ < 0$ . The reason is that the influence of the  $m_d - m_u$  mass difference to the strong interaction can be larger than the electromagnetic effect. In other words, the  $q\bar{q}$ -bound state containing the lighter quark may be heavier than the  $q\bar{q}$ -bound state containing the heavier quark. A general condition for this problem is given.*

The success of nonrelativistic potential models, being guided by QCD is remarkable, even in the case where a nonrelativistic treatment is questionable (for a discussion of potential models and various references see e.g. Ref.[1,2,3]). However nonrelativistic potential models have also been applied to light quark-bound-states and the predicted spectrum and decay properties of hadrons are in rather good agreement with experiment [3,4,5,6]. One of the latter potential models has also been used for the calculation of the quark core contribution to the electric polarizability of hadrons [7]. Other interesting quantities are the electromagnetic mass differences of hadrons which have been discussed from different point of views in the literature (for a list of references see [6]). I will use here an explicit nonrelativistic potential model to calculate the electromagnetic mass differences of mesons. One finds in contrast to experiment, that  $B^0 - B^+ < 0$ . Since the  $B^0$  contains the heavier quark (the d-quark) compared to the  $B^+$  (which contains the u-quark) this result looks rather peculiar, because the contribution of the electromagnetic interaction is smaller than the  $m_d - m_u$  mass difference. I will discuss this effect in some detail later. First let me review the potential model under consideration [6].

This model should, as usually, be guided by QCD. It should have a Coulomb like part for the short-range behaviour and a confinement part for the long-range behaviour. Concerning the light mesons a perturbative treatment of the spin-spin interaction is not allowed since the spin-spin interaction is of the same order of magnitude as the mass itself. On the other hand the spin-spin interaction arising from the Coulomb interaction is proportional to the  $\delta$ -function which cannot be treated nonperturbatively. A nonperturbative treatment of the  $\delta$ -function would lead to an unbounded Hamiltonian. One should note that the  $\delta$ -function appearing in the Breit-Fermi Hamiltonian is simply an approximation, resulting from the nonrelativistic reduction. One can overcome this problem by regularizing the Coulomb potential which physically is justified by the fact, that at very short distances various relativistic effects such as quark pair creation arise, and the original Coulomb like behaviour will be distorted.

In addition, the physical justification of a nonrelativistic treatment of light quark-

bound states, is questionable. These bound states should be highly relativistic. However Rosenstein [8] argues that the Schrödinger equation with a linear potential and the zero-mass Klein-Gordon equation with a quadratic potential transform to each other by a duality transformation. The first equation describes the main features of the potential models, while the second describes the main features of the spectra of the MIT bag-model. This is the reason that one obtains the same spectra even for light hadrons from the two very different models. From this point of view the nonrelativistic treatment of light hadrons in the framework of potential models seem to be justified.

Having all this in mind we use a phenomenological potential with a Coulomb short-range behaviour regularized in the simplest possible way plus a confinement part.

$$V = -\frac{4}{3} \frac{\alpha_s}{(r+r_0)^n} + a \cdot r^p + V_0 \quad (1)$$

Usually the Coulombic part is purely of vector type while the confinement part is purely of scalar type. We allow both parts to have vector as well as a scalar contributions.

Thus we split the potential into two parts, a vector part

$$V_V = -\frac{4}{3} \frac{\alpha_s}{(r+r_0)^n} \cdot (1-c) + a \cdot r^p \cdot (1-d) \quad (2)$$

and a scalar part

$$V_S = -\frac{\alpha_s}{(r+r_0)^n} \cdot c + a \cdot r^p \cdot d \quad (3)$$

with  $r_0 = k_1(2\mu)^{-k_2}$  and  $V = V_V + V_S$ .

All parameters are obtained by solving the Schrödinger equation numerically [9] and performing a  $\chi^2$  best fit. The obtained parameters and quark masses are:

$$\begin{aligned} \alpha_s &= 0.740, & n &= 1.107, & c &= 0.421 \\ a &= 0.222 \text{ GeV}^{1.91}, & p &= 0.910, & d &= 0.752 \\ V_0 &= 0.856 \text{ GeV}, & k_1 &= 0.617, & k_2 &= 0.040 \\ m_u &= 0.340 \text{ GeV}, & m_s &= 0.553 \text{ GeV}, & m_c &= 1.825 \text{ GeV} \\ & & m_b &= 5.195 \text{ GeV} \end{aligned} \quad (4)$$

Using these parameters we have calculated the meson spectrum for  $L=0$  and  $L \neq 0$  heavy and light quark-bound-states. Also the leptonic decay width of light and heavy vector mesons have been calculated and are in very good agreement with experiment. Since I restrict myself to electromagnetic mass differences I do not give the above predictions here (these predictions can be found in Ref. [6])

The electromagnetic interaction in which we are interested here is given by the Breit-Fermi-Hamiltonian and reads

$$V_{elm} = \alpha \frac{Q_1 Q_2}{r} - \alpha Q_1 Q_2 \frac{2\pi \vec{\sigma}_1 \cdot \vec{\sigma}_2}{3 m_1 m_2} \delta^3(r) \quad (5)$$

where  $Q_1, Q_2$  are the quark charges and  $\alpha$  is Sommerfeld's finestructure constant.

In Eq. 5 we have omitted the Darwin term since its contribution is negligible, at least in our potential model. The expectation value of Eq. 5 is given by

$$\langle V_{elm} \rangle_0 = \alpha \langle Q_1 Q_2 \rangle \left\{ \left\langle \frac{1}{r} \right\rangle + \frac{1}{2m_1 m_2} |R(0)|^2 \right\}$$

$$\langle V_{elm} \rangle_1 = \alpha \langle Q_1 Q_2 \rangle \left\{ \left\langle \frac{1}{r} \right\rangle - \frac{1}{6m_1 m_2} |R(0)|^2 \right\} \quad (6)$$

$\langle Q_1 Q_2 \rangle$  is e.g. for  $\pi^+$ ,  $2/9$  and for  $\pi^0$ ,  $-5/18$ .

In the naive nonrelativistic quark model the mass difference of e.g.  $K^0$  and  $K^+$  would be

$$K^0 - K^+ = m_d - m_u - \frac{\alpha}{3} \left\{ \left\langle \frac{1}{r} \right\rangle + \frac{1}{2m_S m_u} |R(0)|^2 \right\} \quad (7)$$

Experimentally we know that  $K^0 - K^+$  is positive, thus from Eq. 7 one sees that  $m_d$  is larger than  $m_u$ . However Eq. 7 is too naive since the contribution of the strong interaction to the mass difference is important. In fact, it turns out that the latter may be larger than the contribution of the electromagnetic mass difference itself.

Thus we split the mass difference into two parts, one part  $\Delta M_S$  originating from the strong (gluonic) interaction and one part  $\Delta M_{elm}$  originating from the electromagnetic interaction Eq. 5. The total mass difference is then given by

$$\Delta M_{tot} = \Delta M_S + \Delta M_{elm} \quad (8)$$

$\Delta M_S$  is the analog to  $\Delta M_{elm}$  just replacing  $\alpha Q_1 Q_2 / r$  in Eq.5 by our potential Eq.1 and replacing in the second contribution  $\alpha Q_1 Q_2 \delta^3(r)$  by the Laplacian of the potential  $V_V$  from Eq.2. Following our discussion that the  $\delta$  function is simply an approximation and that, in fact, taking into account relativistic effects it would be a "smeared" function. We assume that relativistic effects are incorporated if one replaces  $R(0)$  in Eq. 6 and Eq. 7 by  $R(1/2\mu)$  i. e. the wave function at the Compton wave length with  $\mu$  the reduced quark mass.

With the wave function obtained from our potential model and from Eq. 7 we find the quark mass difference

$$m_d - m_u = 6MeV \quad (9)$$

We now choose the quark masses to be

$$m_d = 0.343 GeV, \quad m_u = 0.337 GeV \quad (10)$$

and calculate the mass differences  $\Delta M_S$  and  $\Delta M_{elm}$  which are displayed and compared with other predictions in Table 1.

Particle	$\Delta M_S$	$\Delta M_{elm}$	$\Delta M_{tot}$	$\Delta M_{exp}$	Ref.[10]	Ref.[11]	Ref.[12]
$\pi^\pm - \pi^0$	0.	3.1	3.1	$4.6043 \pm 0.0037$	3.2	-	1.61
$\rho^\pm - \rho^0$	0.	1.1	1.1	$-0.3 \pm 2.2$	1.6	-0.6	0.94
$K^0 - K^+$	6.0	-1.8	4.2	$4.05 \pm 0.07$	4.07	6.0	1.62
$K^{*0} - K^{*+}$	1.0	-0.8	0.2	$6.7 \pm 1.2$	0.27	2.7	1.11
$D^+ - D^0$	0.7	2.9	3.6	$4.7 \pm 0.3$	1.37	6.0	-
$D^{*+} - D^{*0}$	$\sim 0.$	2.0	2.0	$2.9 \pm 1.3$	0.57	4.6	-
$B^0 - B^+$	-0.2	-1.3	-1.5	$4.0 \pm 3.4$	-	-	-
$B^{*0} - B^{*+}$	-0.4	-1.1	-1.5	-	-	-	-

Table 1. Comparison of the predicted electromagnetic mass differences with experiment and other predictions. The units are MeV.  $\Delta M_S$  is the contribution of the strong interaction and  $\Delta M_{elm}$  the contribution of the electromagnetic interaction.

As one can see most of the results obtained are similar to the results obtained by Gelmaster [10] and that in fact the contribution of the strong interaction is larger than the contribution of the electromagnetic interaction itself, except for  $\pi$  and  $\rho$  where the strong interaction contribution cancels because of the same content of u and d quarks in the charged and neutral particle.

In the case of the B meson the strong interaction even overcompensates the  $m_d - m_u$  mass difference. This looks rather peculiar [10,13] but in fact this effect appears, and depends strongly on the detailed form of the potential and its parameters. This is easily demonstrated using a simple example.

Let us assume a potential of the form  $V(r) = ar$ . We know from the scaling behaviour of the Schrödinger equation that the bound state energy is given by

$$E = \left(\frac{a^2}{2\mu}\right)^{1/3} \epsilon + m_1 + m_2 \quad (11)$$

where  $\epsilon$  are the zeros of the Airy function. Introducing the ratio of the masses  $\lambda = m_1/m_2$ , one obtains

$$E = \left(\frac{1}{m_2} \frac{\lambda + 1}{\lambda} \frac{a^2}{2}\right)^{1/3} \epsilon + m_2(\lambda + 1) \quad (12)$$

The equation for the critical  $\lambda_c$  (where the derivative of the energy with respect to  $\lambda$  is zero) is

$$\lambda_c^4(1 + \lambda_c)^2 - \left(\frac{\epsilon}{3}\right)^3 \cdot \frac{a^2}{2m_2^4} = 0 \quad (13)$$

In order to treat this problem more generally, we shall deal with the derivative  $\partial E/\partial m_1$  and see if it is negative or not [16]. First let us make clear about our notations and footings. We are dealing with the following equation:

$$\left(-\frac{\Delta}{2\mu} + V + m_1 + m_2\right)\Psi = E\Psi \quad (14)$$

where  $\mu$  is the reduced mass,  $V$  is the spherical symmetric potential which does not depend on the mass,  $E$  is the energy eigenvalue and  $\Psi$  the normalized wave function respectively. We rewrite Eq.14 to

$$\left(-\frac{\Delta}{2\mu} + V\right)\Psi = \bar{E}\Psi \quad (15)$$

where  $\bar{E} = E - m_1 - m_2$ . By definition one gets the following relation

$$\frac{\partial E}{\partial m_1} = \frac{d\bar{E}}{d\mu} \cdot \frac{m_2^2}{(m_1 + m_2)^2} + 1 \quad (16)$$

Following the way of deriving the Feynman-Hellmann theorem [14,15], we get

$$-\frac{d\bar{E}(\mu)}{d\mu} = \frac{1}{2\mu} (\bar{G}\bar{\Psi}, \bar{\Psi})n(\mu)^{-1} \quad (17)$$

where

$$\bar{\Psi}(y) \equiv \Psi((2\mu)^{-1/2}y), \quad \bar{G}(y) \equiv G((2\mu)^{-1/2}y), \quad G(r) \equiv r \frac{dV}{dr}, \quad n(\mu) \equiv (2\mu)^{3/2}$$

Now we are ready to state our result. Let the potential satisfy the following condition (C):  $r dV/dr$  has a global positive minimum  $C_0$ , then

$$\frac{d\bar{E}}{d\mu} \leq -\frac{C_0}{2\mu} \quad (18)$$

and

$$\frac{\partial E}{\partial m_1} \leq -\frac{C_0}{2} \cdot \frac{m_2}{m_1} \cdot \frac{1}{m_1 + m_2} + 1 \quad (19)$$

As one can see from inequality 19, there are always masses which make the derivative  $\partial E/\partial m_1$  negative.

Examples of potentials which satisfy condition (C) are shown below:

1)

$$V(r) = -\frac{a}{r^\ell} + br^k \quad (20)$$

$$\begin{aligned} a &> 0, & b &> 0 \\ 0 < \ell < 2, & & k &> 0 \end{aligned}$$

2)

$$V(r) = a \log r + b, \quad a > 0 \quad (21)$$

In this case the right hand side of Eq.19 is equal to the left hand side. That is

$$\frac{\partial E}{\partial m_1} = -\frac{a m_2}{2 m_1} \frac{1}{m_1 + m_2} + 1$$

i.e.  $a = C_0$ .

At this point I would like to mention that a number of inequalities and equalities among the masses of ground-state hadrons in the framework of potential models have been derived by D.B. Lichtenberg [17].

Summarizing one finds that considering energy eigenvalues  $E(m_1, m_2)$  with respect to two particles whose masses are  $m_1, m_2$ , respectively, one would expect that if  $M > m$  then  $E(M, m_2) > E(m, m_2)$ , but actually the opposite can happen if one solves the Schrödinger equation. In other words the derivative  $\partial E/\partial m_1$  can be negative. This means, the quark bound state containing the lighter quark can be heavier than the quarkbound state containing the heavier quark. Exactly this happens in our potential model, the strong interaction overcompensates the  $m_d - m_u$  mass difference and thus  $B^0 - B^+ < 0$ .

## References

- [1] D.Flamm, F.Schöberl: Introduction to the quark-model of elementary particles Vol.I, Gordon and Breach, New York 1982.
- [2] B.Dieckmann: CERN Preprint CERN-EP/86-112.
- [3] F.Schöberl: Il Nuovo Cimento 94A(1986)79.
- [4] S.Ono, F.Schöberl: Phys.Lett.118B(1982)419.
- [5] F.Schöberl, P.Falkensteiner, S.Ono: Phys.Rev D30(1984)603.
- [6] D.Flamm, F.Schöberl, H.Uematsu: Il Nuovo Cimento (in print) UWThPh-1987-7
- [7] F.Schöberl, H.Leeb: Phys.Lett. 166B(1986)355.
- [8] B.Rosenstein: Phys.Rev D33(1986)813.
- [9] P.Falkensteiner, H.Grosse, F.Schöberl, P.Hertel: Computer Physics Communication 34(1985)287.
- [10] W.Celmaster: Phys.Rev.Lett 37(1976)1042.
- [11] N.Isgur: Phys.Rev D21(1980)779.
- [12] R.P.Bickestaff, A.W.Thomas: D25(1982)1869.
- [13] J.M.Richard, P.Taxil: Z.Phys. 26C(1984)421.
- [14] H.Hellmann: Acta Physicochimica URSS, 16(1935)913; IV2(1936)225; Einführung in die Quantenchemie (F. Deuticke, Leipzig and Vienna, 1937) p. 286.
- [15] R.P. Feynman: Phys.Rev.Lett. 34(1975)364.
- [16] D.Flamm, F.Schöberl, H.Uematsu: Phys.Rev. D36(1987)2176.
- [17] D.B.Lichtenberg: Phys.Rev. D35(1987)2183.

# CONDENSATION OF HADRONIC MATTER<sup>†</sup>

Ludwik Turko

Institute of Theoretical Physics

University of Wrocław, ul. Cybulskiego 36

50-205 Wrocław, Poland

**ABSTRACT:** A particle number conservation should be taken into account even if other chemical potentials related to the internal symmetries were introduced. The condensation of pions is taken as an example.

It is believed that in the case of relativistic particles with internal symmetry one should not introduce a chemical potential related to a particle number conservation [1,2,3]. A simple example of noninteracting pions will show that this is not the case. Let us consider an ideal gas of pions. We write the partition function as [1]

$$1/\log Z = -V \int \frac{d^3k}{(2\pi)^3} [\log(1 - e^{-\beta(\omega - \mu)}) + \log(1 - e^{-\beta\omega}) + \log(1 - e^{-\beta(\omega + \mu)})]$$

The first term corresponds to  $\pi^+$ , the second one to  $\pi^0$  and the last one to  $\pi^-$ . In the case of pions the isospin conservation is equivalent to the charge conservation.

Densities of pions are given by

$$1/2a) \langle \pi^+ \rangle = \int \frac{d^3k}{(2\pi)^3} \frac{1}{\exp[\beta(\omega - \mu)] - 1}$$

$$1/2b) \langle \pi^0 \rangle = \int \frac{d^3k}{(2\pi)^3} \frac{1}{\exp(\beta\omega) - 1}$$

$$1/2c) \langle \pi^- \rangle = \int \frac{d^3k}{(2\pi)^3} \frac{1}{\exp[\beta(\omega + \mu)] - 1}$$

---

<sup>†</sup> Work supported by the government research project CPBP

In the uncondensed phase  $|\mu| < m$  and the condensation corresponds to the values  $\mu = \pm m$

We have for the charge density

$$/3/ \quad \langle q \rangle = \int \frac{d^3k}{(2\pi)^3} \left[ \frac{1}{e^{\beta(\omega - \mu)} - 1} - \frac{1}{e^{\beta(\omega + \mu)} - 1} \right]$$

We can notice from the Eqs. /2a,b,c/ the exceptional situation of  $\pi^0$ . The corresponding density is a function of a temperature and we would have an almost diminishing density of  $\pi^0$  except for the temperature of the order  $10^{12}$  K. This pathology does not appear if we consider only a doublet of particles or we restrict ourselves to the charge density [2,3]. In the theory of free particles there is no physical reason for such an exceptional behaviour of neutral pions. Let us introduce also a subsidiary chemical potential related to the conservation of the global number of pions. This will provide a consistent treatment of a condensation phenomena and it preserves the isotopic symmetry because a common potential is introduced for all kinds of pions.

The improved partition function has a form

$$/4/ \quad \log Z = -V \int \frac{d^3k}{(2\pi)^3} \left[ \log (1 - e^{-\beta(\omega - \mu_1 - \mu_2)}) + \log (1 - e^{-\beta(\omega - \mu_2)}) + \log (1 - e^{-\beta(\omega + \mu_1 - \mu_2)}) \right]$$

where  $\mu_1$  is a chemical potential related to the charge conservation

$\mu_2$  is a chemical potential related to the particle number conservation

The physical range of chemical potentials is given by the inequalities

$$/5/ \quad \mu_1 + \mu_2 < m \qquad \mu_2 - \mu_1 < m$$

There are two condensation lines

$$/6/ \quad \mu_1 + \mu_2 = m \qquad \mu_2 - \mu_1 = m$$



It is immediately seen that the state equations obtained from the partition functions /1/ and /4/ are different. The densities of pions have a form

$$/7a/ \quad \langle \pi^+ \rangle = \int \frac{d^3k}{(2\pi)^3} \frac{1}{e^{\beta(\omega - \mu_1 - \mu_2)} - 1}$$

$$/7b/ \quad \langle \pi^0 \rangle = \int \frac{d^3k}{(2\pi)^3} \frac{1}{e^{\beta(\omega - \mu_2)} - 1}$$

$$/7c/ \quad \langle \pi^- \rangle = \int \frac{d^3k}{(2\pi)^3} \frac{1}{e^{\beta(\omega + \mu_1 - \mu_2)} - 1}$$

The charge density is

$$/8/ \quad \langle q \rangle = \langle \pi^+ \rangle - \langle \pi^- \rangle$$

Expanding the Eqs. /7,8/ we get from the density of pions

$$/9/ \quad \langle n \rangle = \frac{m^3}{2\pi^2} \sum_{n=1}^{\infty} \frac{1}{mn\beta} K_2(mn\beta) [e^{\beta n(\mu_1 + \mu_2)} + e^{\beta n\mu_2} + e^{\beta n(\mu_2 - \mu_1)}]$$

and for the charge density

$$/10/ \quad \langle q \rangle = \frac{m^3}{2\pi^2} \sum_{n=1}^{\infty} \frac{1}{mn\beta} K_2(mn\beta) [e^{\beta n(\mu_1 + \mu_2)} - e^{\beta n(\mu_2 - \mu_1)}]$$

where  $K_2$  is a modified Bessel function.

In the low temperature limit  $\beta m \gg 1$  we have

$$/11/ \quad \langle n \rangle = \left(\frac{m}{2\pi\beta}\right)^{3/2} \sum_{n=1}^{\infty} \frac{1}{n^{3/2}} [e^{\beta n(\mu_1 + \mu_2 - m)} + e^{\beta n(\mu_2 - m)} + e^{\beta n(\mu_2 - \mu_1 - m)}]$$

$$/12/ \quad \langle q \rangle = \left(\frac{m}{2\pi\beta}\right)^{3/2} \sum_{n=1}^{\infty} \frac{1}{n^{3/2}} [e^{\beta n(\mu_1 + \mu_2 - m)} - e^{\beta n(\mu_2 - \mu_1 - m)}]$$

Let us consider a behaviour of the system on the condensation line  $\mu_1 + \mu_2 = m$ .

We obtain a set of two equations for the critical temperature

$$/13/ \quad \langle n \rangle = \left( \frac{m}{2\pi\beta} \right)^{3/2} \sum_{n=1}^{\infty} \frac{1}{n^{3/2}} \left[ 1 + e^{-\beta n(m-\mu_2)} + e^{-2\beta n(m-\mu_2)} \right]$$

$$/14/ \quad \langle q \rangle = \left( \frac{m}{2\pi\beta} \right)^{3/2} \sum_{n=1}^{\infty} \frac{1}{n^{3/2}} \left[ 1 - e^{-2\beta n(m-\mu_2)} \right]$$

We can directly obtain the critical temperature only in the case of zeroth net background charge what corresponds to the value  $\mu_2 = m$ . Then

$$/15/ \quad T_c = \frac{2\pi}{m} \left[ \frac{\langle n \rangle}{3 \zeta(3/2)} \right]^{2/3}$$

We have in general a nontrivial dependence on  $\mu_2$ , i.e. the critical temperature will depend on the charge density and on the pions density /or on the pressure/.

Using the asymptotic formula for  $x = 0^+$

$$/16/ \quad \sum_{n=1}^{\infty} \frac{e^{-nx}}{n^{3/2}} = \zeta\left(\frac{3}{2}\right) - 2\sqrt{\pi x} + O(x)$$

we can approximately solve the Eqs./13,14/ for  $\mu_2 = m$ . Such a choice of parameters gives  $\langle n \rangle \gg \langle q \rangle = 0^+$ .

We have after simple algebraic manipulations the result:

$$/17/ \quad T_c = \frac{2\pi}{m} \left[ \frac{\langle n \rangle + \frac{1+\sqrt{2}}{\sqrt{2}} \langle q \rangle}{3 \zeta\left(\frac{3}{2}\right)} \right]^{2/3}$$

Concluding, we can say that the subsidiary chemical potential:  
a/ is needed to unify particles belonging to the same multiplet

b/ modifies the equation of state

c/ modifies properties of the condensate

More details will be given in the subsequent publication.

- REFERENCES: [1] L. Turko Phys.Lett. 104B, 153, /1981/  
[2] J.I. Kapusta P.R. D24, 426, /1981/  
[3] H.E. Haber and H.A. Weldon Phys.Rev.Lett. 46  
1497, /1981/

# INFRARED ASYMPTOTICS OF THE QUARK PROPAGATOR IN GAUGE THEORIES

ZOLTAN FODOR

INSTITUTE FOR THEORETICAL PHYSICS

ROLAND EOTVOS UNIVERSITY, BUDAPEST

The well known problem of quark confinement is, why do not we see free quarks in final states. The question is rather critical, because the quarks behave approximately like free particles and their masses are pretty small.

The absolute confinement of quarks can manifest itself in the lack of singularities of the quark propagator in the infrared limit.

As it is well-known in QED the fermion propagator is:

$$S_F(p) = \text{const.} \frac{-\hat{p} + m}{p^2 + m^2 - i\epsilon} (1 + p^2/m^2)^{-\beta} \quad , (1)$$

where

$$\beta = (3-a)d/2\pi \quad ; \quad p^2 \text{ near } m^2 \quad , (2)$$

and

$$D_{\mu\nu} = \frac{\delta_{\mu\nu}}{k^2 - i\epsilon} - (1-a) \frac{k_\mu k_\nu}{(k^2 - i\epsilon)^2} \quad . (3)$$

$S_F(p)$  has a branch point in the infrared region.

In QCD the problem is far more complicated. If we use for the gluon propagator a  $k^{-2}$  term, then it gives a non-confining quark propagator and a nonconfining potential proportional to  $|\mathbf{x}|^{-1}$ , while for a gluon propagator  $D_F \sim k^{-4}$  we will get a confining static potential in  $\mathbf{x}$  space, namely  $V(\mathbf{x}) \sim |\mathbf{x}|$ . That is the famous linearly confining potential. The case of  $D_F \sim k^{-4}$  has been studied solving the Dyson-Schwinger equations

$$1 = (\hat{p} - m) S'(p) + ig_0^2 \frac{4}{3} \frac{1}{(2\pi)^4} \int d^4k \gamma_\mu D_F^{\mu\nu}(k) \Lambda_\nu(p-k, p), \quad (4)$$

where

$$\Lambda_\nu(p-k, p) = S'(p-k) \Gamma_\nu(p-k, p) S'(p) \quad . \quad (5)$$

Most of the considerations use an approximation, namely on the one hand one can determine  $\Gamma_\nu$  using  $S'(k)$  and the Ward identity, but on the other hand they neglect the transverse part of  $\Gamma_\nu$ . In various gauges and approximations there have been shown that the quark propagator vanishes on the mass shell [e.g. 1-5] while in other approaches the quark propagator is the free one in the infrared region [6,7]. All these considerations have not said anything about the case when  $D_F \sim k^{-L}$ , but  $L \neq 4$ .

A similar treatment is a resummation of quark lines with many dressed gluon propagators, both ends of which are attached to the quark line. This calculation has been done for  $L=4$  in this paper, and shown that for  $L \geq 3$  the mass shell singularities of the quark propagator are cancelled. These

values of  $L$  correspond to confining static potentials.

We are working in axial gauges  $n^2 \neq 0$  where ghost loops are absent. In the infrared limit effects of quark loops are neglected. The quark propagator can be expressed by functional derivatives in the following form

$$S_F(x-y) = N \left[ G(x,y) \left( \frac{\delta}{\delta J} \right) Z(J) \right]_{J=0} \quad (6)$$

where

$$Z(J) = \exp \left[ \int d^4x L_I \left( \frac{\delta}{\delta J} \right) \right] \exp \left[ -\frac{1}{2} \int d^4y \int d^4y J_{\mu a}(x) G_{0ab}^{\mu\nu}(x-y) J_{\nu b}(y) \right] \quad (7)$$

and

$$N^{-1} = Z(J) \Big|_{J=0} \quad (8)$$

The Lagrangian  $L_I$  contains the self-couplings of gluons,  $J_a^\mu(x)$  is an external colour current,  $G_{0ab}^{\mu\nu}(x-y)$  is the free gluon propagator in axial gauge, and  $G(x,y|A)$  means the Green's function of the quark moving in the external gluon field  $A$ . The dressed gluon Green's functions are given by the functional derivatives of  $Z(J)$  at  $J=0$  multiplied by  $N$ . The Green's function  $G(x,y|A)$  satisfies the equation

$$\left[ i\gamma_\mu \left( \partial_x^\mu - ig \frac{\lambda^a}{2} A^{a\mu}(x) \right) - m \right] G(x,y|A) = \delta^4(x-y) \quad (9)$$

$m$  means the mass parameter of the quark,  $\lambda^a$  is the colour matrix. Let us introduce the functional  $H(x,y|A)$  by the definition

$$[i\gamma_\mu\{\partial_x^\mu - ig\frac{\lambda^a}{2}A^{a\mu}(x)\} + m]H(x, y|A) = G(x, y|A) \quad . \quad (10)$$

The Fourier transform of  $H(x, y|A)$ ,  $\tilde{H}(p, q|A)$  determines the quark propagator in momentum space as follows

$$(2\pi)^4 S_F(p) \delta^4(p-q) = S^I + S^{II} \quad ,$$

$$S^I = (\gamma_\mu p^\mu + m) [\tilde{H}(p, q|A) NZ(J)]_{J=0} \quad , \quad (11)$$

$$S^{II} = \frac{g}{2(2\pi)^4} \gamma_\mu \lambda^a \left[ \int d^4 q' \tilde{A}^{a\mu}(q') \tilde{H}(p-q', q|A) NZ(J) \right] \quad ,$$

here  $\tilde{A}^{a\mu}(q')$  is the Fourier transform of  $A^{a\mu}(x)$ .

Following the fifth parameter method of Fock we represent  $\tilde{H}(p, q|A)$  as the integral

$$\tilde{H}(p, q|A) = -i \int d\nu U(p, q; \nu|A) e^{i\nu(p^2 - m^2 + i\epsilon)} \quad , \quad (12)$$

where the new functional obeys the normalisation

$$U(p, q; 0|A) = (2\pi)^4 \delta^4(p-q) \quad . \quad (13)$$

Substituting (12) into the definition equation of  $\tilde{H}$ , using (13), leads to the definition equation of  $U(p, q; \nu|A)$ . For the infrared limit one could get

$$i \frac{d}{d\nu} U(p, q; \nu|A) + g\lambda^a p^\mu A_\mu^a(2p\nu) U(p, q; \nu|A) = 0 \quad . \quad (14)$$

(14) has the usual time ordered solution which, making use of (11), (12) and (13) yields

$$S^I = -(2\pi)^4 i s^4 (p-q) (\gamma_\mu p^\mu + m)$$

$$\int d\nu e^{i\nu(p^2 - m^2 + i\epsilon)} \left[ 1 + \sum_{n=1}^{\infty} (ig)^n \prod_{i=1}^n \lambda^{a_i} p^{\mu_i} \right] \quad (15)$$

$$\int_0^\nu d\nu_1 \dots \int_0^{\nu_{n-1}} d\nu_n \langle T A_{\mu_1}^{a_1}(2p\nu_1) \dots A_{\mu_n}^{a_n}(2p\nu_n) \rangle_0$$

$$S^{II} = -\frac{ig}{2} \int d^4x \gamma^\mu \lambda^{a_1} e^{ix(p-q)}$$

$$\int d\nu e^{i\nu(p^2 - m^2 + i\epsilon)} \left[ \langle A_{\mu}^a(x) \rangle_0 + \sum_{n=1}^{\infty} (ig)^n \prod_{i=1}^n \lambda^{a_i} p^{\mu_i} \right] \quad (16)$$

$$\int_0^\nu d\nu_1 \dots \int_0^{\nu_{n-1}} d\nu_n \langle T A_{\mu}^a(x) A_{\mu_1}^{a_1}(2p\nu_1) \dots A_{\mu_n}^{a_n}(2p\nu_n) \rangle_0$$

Now we calculate (15) and (16) in such an approximation where gluons starting from the quark line are absorbed by the same line corresponding to keeping the gluon propagator in the dressed gluon Green's functions in (15), (16). /This is the only possibility in QED/ The summation of the remaining colour factor is extremely complicated even for SU(2) gauge group in case of arbitrary L, therefore we confine ourselves to an Abelian gauge group. Hence

$$\begin{aligned} \frac{1}{(2\pi)^4} \int d^4q S^I = & -i(\gamma_\mu p^\mu + m) \int_0^\infty d\nu \exp[i\nu(p^2 - m^2 + i\epsilon)] \\ & - ig^2 \int_0^\nu d\nu_1 \int_0^{\nu_1} d\nu_2 f(\nu_1 - \nu_2) \end{aligned} \quad (17)$$

$$\frac{1}{(2\pi)^4} \int d^4 q S^{II} = \frac{1}{2} \int_0^\infty d\nu \int_0^\nu \gamma^\mu p^\nu G_{\mu\nu}(2p\nu_0) d\nu_0 \exp[i\nu(p^2 - m^2 + i\epsilon)] \\ - \frac{1}{2} g^2 \int_0^\nu d\nu_1 \int_0^{\nu_1} d\nu_2 f(\nu_1 - \nu_2) \quad (18)$$

where  $f(\nu_1 - \nu_2) = p_\alpha p_\beta G_0^{\alpha\beta}[2p(\nu_1 - \nu_2)]$ .

A similar type of exponential  $\nu$  dependence has been shown with a dipole gluon field too [9].

In covariant and axial gauges one has for  $G_0^{\alpha\beta}(k)$  in  $d$  dimensions

$$G_{0G}^{\alpha\beta}(k) = - \frac{\Omega^{L-2}}{k^L} \left[ g^{\alpha\beta} - \frac{k^\alpha k^\beta}{k^2} + \alpha \frac{k^\alpha k^\beta}{k^2} \right] \quad (19)$$

$$G_{0A}^{\alpha\beta} = - \frac{\Omega^{L-2}}{k^L} \left[ g^{\alpha\beta} - \frac{k^\alpha n^\beta + k^\beta n^\alpha}{(kn)} + \frac{k^\alpha k^\beta n^2}{(kn)^2} \right. \\ \left. + (1+\delta)(4-d) \left( g^{\alpha\beta} - \frac{n^\alpha n^\beta}{n^2} \right) \right] \quad (20)$$

where  $iG_0^{\alpha\beta}(x-y) = \langle T A^\alpha(x) A^\beta(y) \rangle_0$ ;  $\alpha=0$  (1) corresponds to the Landau (Feynmann) gauge.  $\Omega$  is a constant and  $\delta$  is a parameter. The choice  $\delta=0$  is used in [7],  $\delta=-1$  reproduces the usual axial gauge. Fourier transforming (19) and (20) one can calculate  $f(\nu_1 - \nu_2)$  in general covariant  $/f_G/$  and axial  $/f_A/$  gauges. Substituting  $f_G$  and  $f_A$  into (15) and (16) we get  $S^I$  and  $S^{II}$ .

In the above approximation  $S^I$  and  $S^{II}$  become entire functions of  $p^2$  in the infrared region if  $2\Omega L - d + 2 > 0$  in



covariant and  $3 > L-d+2 > 0$  in axial gauges ( $d=4+\epsilon$ ). The upper bounds come from the existence of (17) and (18). For instance in covariant gauges the violation of  $0 < L-d$  can induce both regular (vanishing or nonvanishing) and singular  $S_F^2$  depending on the value of  $L$ .

In covariant gauges at  $d \rightarrow 4$   $S_F^2 = 0$  for  $L=3,4$ ; otherwise for  $4 > L > 2$   $S_F^2$  is nonvanishing and regular.

For these values of  $d$  and  $L$  the infrared singularities of the quark propagator are cancelled, thus no quark can appear asymptotically.

A static potential can be defined from the gluon propagator  $-\frac{\Omega^{L-2}}{k^L}$  by the equation

$$V(\mathbf{x}) = \int_{-\infty}^{\infty} dx_0 \int d^d k e^{-ikx} \left[ -\frac{\Omega^{L-2}}{k^L} \right] \quad (21)$$

One can carry out the integrations and gets for  $d-L-1 \neq 0$

$$V(\mathbf{x}) = \Omega^{L-2} \pi^{\frac{d}{2}} \frac{\Gamma(L/2 - d/2 + 1/2) \Gamma(d/2 - L/2 - 1/2) \Gamma(d-L)}{\Gamma(L/2) \Gamma(d/2 - L/2) |\mathbf{x}|^{d-L-1}} \quad (22)$$

and  $V(\mathbf{x})$  is proportional to  $\ln(\mathbf{x})$  if  $d-L-1=0$ . Hence  $L-d+1$  leads to confining static potential.

In four dimensions and in axial (covariant) gauges  $5 > L \geq 3$  ( $4 > L \geq 3$ )  $S_F^2$  is regular in the infrared region so it corresponds to confining static potentials. In both gauges for  $3 > L > 2$  (nonconfining static potentials) the singularities

of  $S_{\vec{p}}$  are verified to depend on the regularization chosen. For  $L=2$  one obtains the well-known results of QED, independently of the regularization. For  $L < 2$   $S_{\vec{p}}$  is singular and these  $L$ 's lead to nonconfining potentials.

#### References

1. H.Pagels: Phys.Rev. D14, 2747 (1976)
2. J.S.Ball and F.Zachariassen: Phys.Lett. 106B, 133 (1981)
3. K.Harada: Progr.Theor.Phys. 68,1324 (1982)
4. G.Pocsik and T.Torma: ITP Budapest Report, No.429, February 1985; Acta Phys.Hung. (in print)
5. G.Pocsik and T.Torma: ITP Budapest Report, No.431, July 1986; Acta Phys.Hung. (in print)
6. R.L.Stuller: Phys.Rev. D13, 513 (1978)
7. B.A.Arbuzov: Phys.Lett. 125B, 497 (1983)
8. W.Kummer: Acta Phys.Austriaca 41, 315 (1975)
9. E.d'Emilio and M.Mintchev: Phys.Rev. D17, 1840 (1983)

# CONFINEMENT AND QUARK STRUCTURE OF HADRONS

Efimov G.V. and Ivanov M.A.

Joint Institute for Nuclear Research, Dubna

## I. Introduction

At present considerable efforts are made to describe physical processes occurring in the quark-confinement region on the basis of the fundamental representations of QCD [1]. However, QCD is not directly applicable to low-energy physics due to the mathematical problems associated with a nonperturbative theory. Therefore, various models and approaches originated from QCD are developed to obtain quantitative results for definite low-energy processes by means of different assumptions and hypotheses. An approach may be considered quite reasonable if it contains a few free parameters and the hypotheses have a clear physical meaning.

We have developed [2,3] the quark confinement model (QCM) based on a definite representation about the hadronization and quark confinement. First, hadrons are treated as collective colourless excitations of quark-gluon interactions. Second, the quark confinement is realized as averaging over the vacuum gluon fields for the quark diagrams. Strong, weak and electromagnetic hadron interactions can be described in the QCM from a unique point of view. The preliminary calculations [2,3] of the meson and baryon processes have shown that the model reproduces the quark structure of hadrons quite correctly.

## II. Hadronization and Confinement Hypotheses

A starting point of the QCM is the Lagrangian of interaction between the hadron field  $H$  with quantum numbers  $J^{PC}$

and the quark current  $Q_H$

$$\mathcal{L}_I^H = \frac{g_H}{\sqrt{2}} H \cdot Q_H$$

For example,

$$H = M(P, V, S, A) \quad Q_M = \bar{q}_\alpha \Gamma_M \lambda^M q_\alpha,$$

$$H = B(N, \Delta) \quad Q_B = R_{\alpha_1 \alpha_2 \alpha_3} q_{\alpha_1} q_{\alpha_2} q_{\alpha_3}.$$

where  $\Gamma, \lambda, R$  are Dirac and Gell-Mann matrices.

The hadron interaction is described by the S-matrix

$$S = \int d\sigma_{VAC} T \exp \left\{ i \int dx \mathcal{L}_I^H \right\}.$$

The quark propagator has the following form

$$\begin{aligned} S(x_1, x_2 | B_{VAC}) &= \langle 0 | T(q(x_1) \bar{q}(x_2)) | 0 \rangle = \\ &= (m_q - \hat{p} - \hat{B}_{VAC})^{-1} \delta(x_1 - x_2). \end{aligned}$$

Here  $m_q$  is the quark mass,  $B_{VAC}$  is the vacuum gluon field,  $\int d\sigma_{VAC}$  is the indefinite integration measure over the gluon field.

The measure  $d\sigma_{VAC}$  is defined so as to provide the quark confinement, that is the singularities of the S-matrix elements which correspond to quarks in the observable hadron spectrum must be absent.

The confinement ansatz is that the integration over  $d\sigma_{VAC}$  can be changed by the integral

$$\begin{aligned} \int d\sigma_{VAC} \frac{1}{m_q - \hat{p} + \hat{B}_{VAC}} &= \int d\sigma_\lambda \frac{1}{m_q - \hat{p} + \lambda \Lambda_q} = \\ &= \frac{1}{\Lambda_q} G\left(\frac{m_q - \hat{p}}{\Lambda_q}\right) = \frac{1}{\Lambda_q} \left[ a\left(-\frac{p^2}{\Lambda_q^2}, \frac{m_q}{\Lambda_q}\right) + \frac{\hat{p}}{\Lambda_q} b\left(-\frac{p^2}{\Lambda_q^2}, \frac{m_q}{\Lambda_q}\right) \right], \end{aligned}$$

where the parameter  $\Lambda_q$  characterizes the confinement range.

The confinement function is an entire analytical function on the  $\bar{z}$  -plane which decreases faster than any degree of  $\bar{z}$ . The analytical structure of quark diagrams is expressed in terms of  $a(\bar{z}^2, \frac{m}{\Lambda})$  and  $b(\bar{z}^2, m/\Lambda)$ .

We used the following functions for the numerical calculations of physical quantities

$$a(u) = 2.12 \exp[-u^2 - 1.2 u],$$

$$b(u) = 2 \cdot \exp[-u^2 + 0.4 u].$$

The coupling constants  $g_H$  are defined from the compositeness condition by which the renormalization constant of the hadron wave function is equal to zero

$$Z_H = 1 - g_H^2 \cdot \tilde{\Pi}'(m_H) = 0.$$

Here  $\tilde{\Pi}(p)$  is the hadron mass operator.

### III. The Fundamental Meson Processes

We define our single free dimensional parameter  $\Lambda_q$  by fitting the main meson decays:

1.  $\pi \rightarrow \mu \nu$ . This decay is defined by  $f_\pi$  that is the basic parameter of the chiral theory.



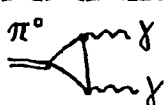
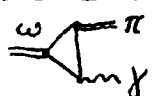

2.  $\rho^0 \rightarrow e^+ e^-$ . This decay is defined by  $g_{\rho\gamma}$ , the basic parameter of the vector dominance model.

3.  $\pi^0 \rightarrow \gamma\gamma$ ,  $\omega \rightarrow \pi\gamma$ . These decays are defined by the Adler anomaly.

4.  $\rho \rightarrow \pi\pi$ . This is the strong  $\rho$ -meson decay.

In the QCM these decays are described by quark diagrams (see Table I). The best agreement with experiment is achieved for  $\Lambda_q = 480$  MeV that corresponds to  $m_q = \Lambda_q / a(0) = 226$  MeV. One can see that there is a good agreement with experimental data [4].

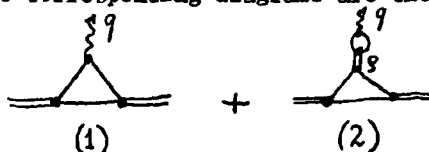
Table I

Coupling constants	$\lambda = \left(\frac{g}{4\pi}\right)^2 = \begin{cases} 0.0722 & \pi \\ 0.0675 & \rho \\ 0.0671 & \omega \end{cases}$	
	$f_{\pi} = 134 \text{ MeV}$	$f_{\pi}^{\text{expt}} = 132 \text{ MeV}$
	$g_{\rho\pi\gamma} = 0.20$	$g_{\rho\pi\gamma}^{\text{expt}} = 0.18$
	$g_{\omega\pi\gamma} = 0.27 \text{ GeV}^{-1}$	$g_{\omega\pi\gamma}^{\text{expt}} = 0.276 \text{ GeV}^{-1}$
	$g_{\omega\pi\gamma} = 2.25 \text{ GeV}^{-1}$	$g_{\omega\pi\gamma}^{\text{expt}} = 2.54 \text{ GeV}^{-1}$
	$g_{\rho\pi\pi} = 5.9$	$g_{\rho\pi\pi}^{\text{expt}} = 6.1$

It is essential that the OCM allows us to calculate not only integral characteristics, like decay width, but also the momentum dependences of physical matrix elements.

For example, let us consider the electromagnetic pion form factor.

The corresponding diagrams are shown below:



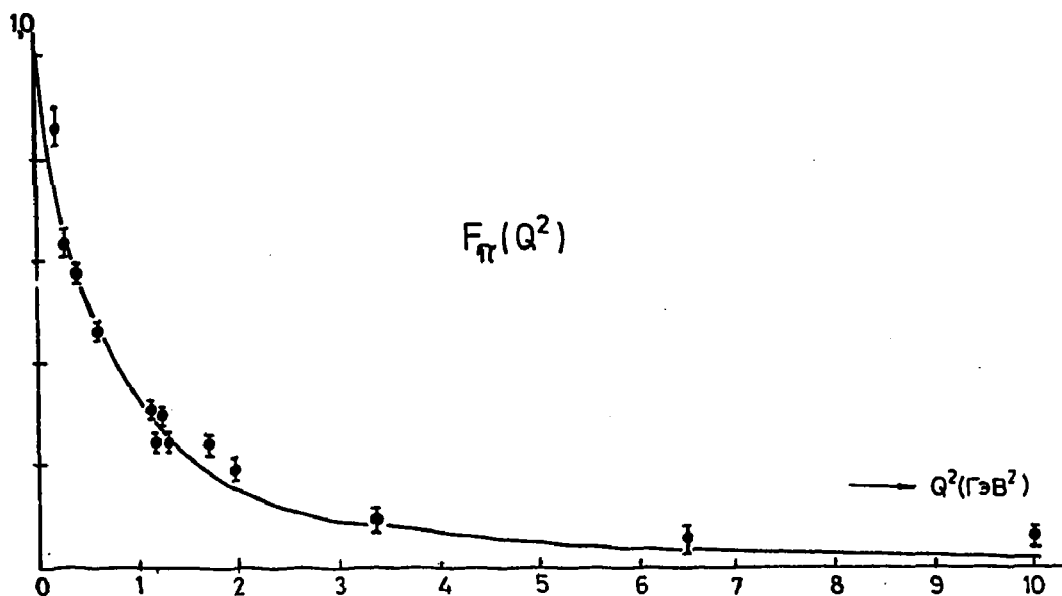
For the spacelike momenta  $q^2 = -Q^2 \leq 0$  the pion form factor  $F_{\pi}^+(Q^2)$  can be represented in the form

$$F_{\pi}(Q^2) = \frac{F_{\rho\pi\pi}(Q^2)}{F_{\rho\pi\pi}(0)} \cdot \frac{m_{\rho}^2 F_{\rho\gamma}(-\frac{m_{\rho}^2}{\Lambda^2})}{m_{\rho}^2 F_{\rho\gamma}(-\frac{m_{\rho}^2}{\Lambda^2}) + Q^2 F_{\rho\gamma}(Q^2/\Lambda^2)}$$

where

$$F_{\rho\pi\pi}(z) = \int_{z/4}^{\infty} du b(u) + \frac{z}{4} \int_0^1 du b(u \cdot \frac{z}{4}) [1 - \sqrt{1-u}],$$

$$F_{\rho\gamma}(z) = \int_{z/4}^{\infty} du b(u) + \frac{z}{4} \int_0^1 du b(u \cdot \frac{z}{4}) [1 - \sqrt{1-u} (1 + \frac{u}{2})].$$



Good agreement with experimental data [5] is observed.

#### IV. The Electromagnetic and Strong Nucleon Form Factors

In paper [3] we have calculated electromagnetic and strong nucleon form factors. Static electromagnetic characteristics (magnetic moments, the ratio  $G_A/G_V$ , etc.) and the

strong meson-nucleon coupling constants were calculated too.

The experimental data on electromagnetic nucleon form-factors are described quite accurately by the empirical dipole formula. Our results are shown below.

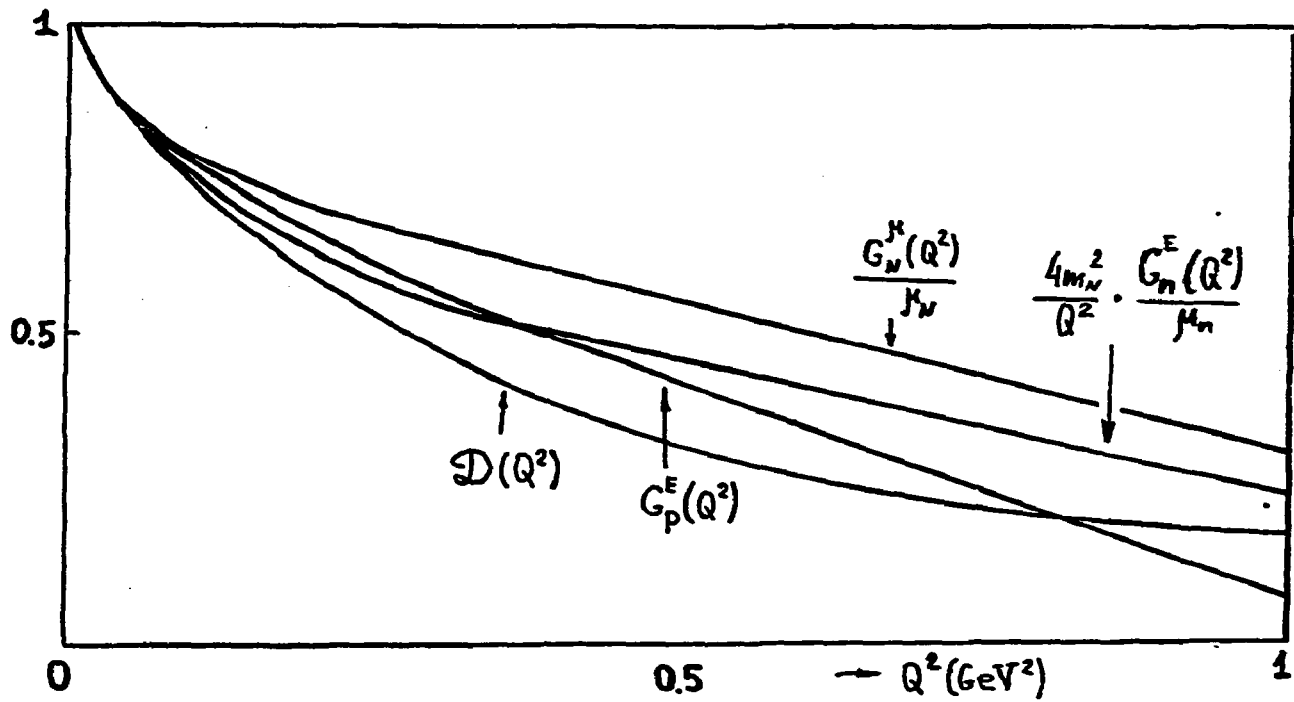
One can see a qualitative agreement only with the dipole formula for  $Q^2 \leq 2 \text{ GeV}^2$ .

The meson-nucleon form factors play a fundamental role for the description of NN-interaction [6]. They are introduced phenomenologically and are chosen from the best description of the experimental NN-scattering data. In the QCM these form factors are calculated in a standard manner without any assumptions. Their behaviour is shown below. The obtained results are in agreement with phenomenological curves [6]. In future we plan to calculate the NN-scattering phase shifts.

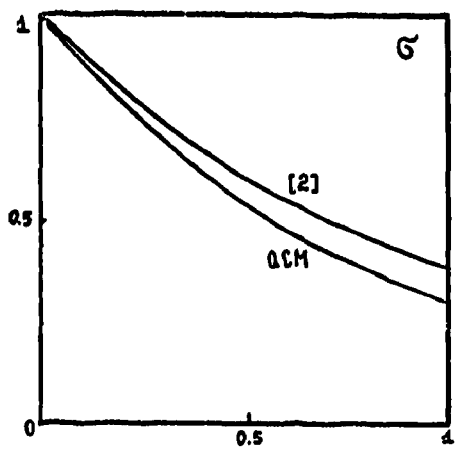
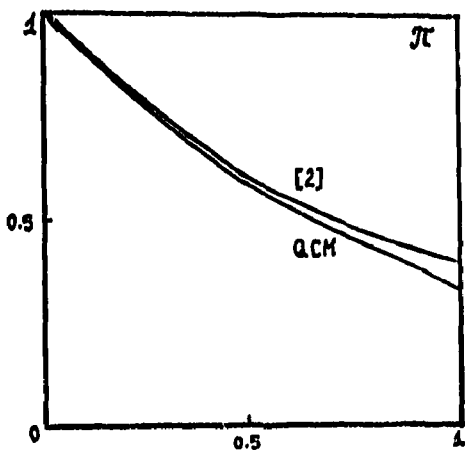
#### References

1. Yndurain F.J. "Quantum Chromodynamics", Springer-Verlag; New York, Berlin, Heidelberg, Tokyo, 1983; Shifman M., Vainshtein A., Zakharov V., Nucl.Phys. B147, p.385, 1979.
2. Efimov G.V., Ivanov M.A., Lubovitskij V.E. JINR P2-87-384, 1987.  
Avakyan E.Z. et al. JINR E2-87-630, 1987.
3. Efimov G.V., Ivanov M.A., Lubovitskij V.E. JINR P2-87-776, 1987.
4. Particle Data group, Phys.Lett., B170, 1986.
5. Bebek C. et al. Phys.Rev., D17, p.1693, 1978.
6. Machleidt R., Hollinde K., Elster Ch. Phys.Rep. 149, p.1, 1987.

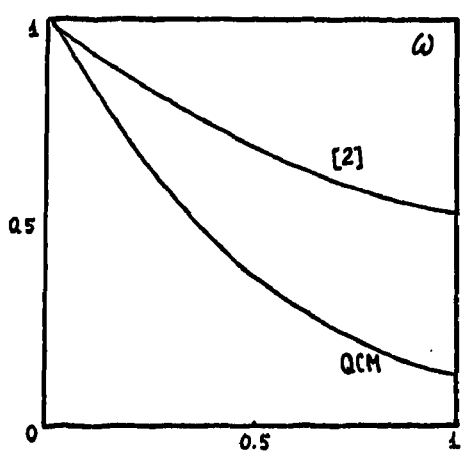
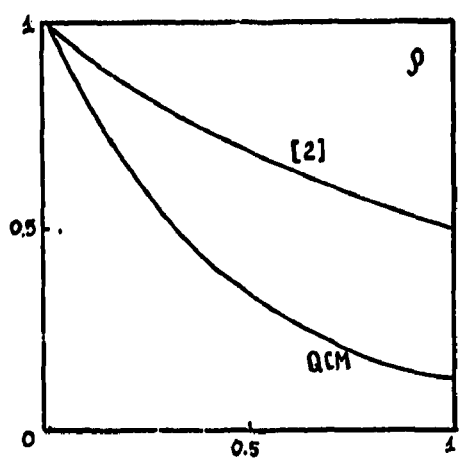




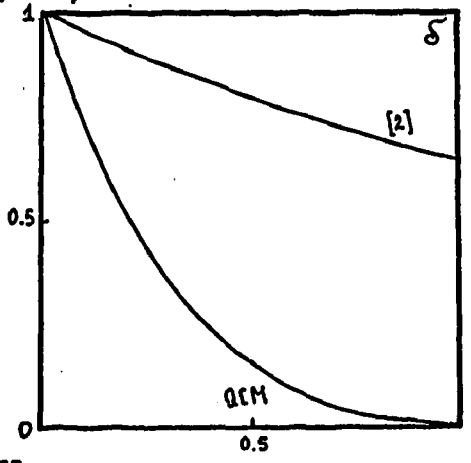
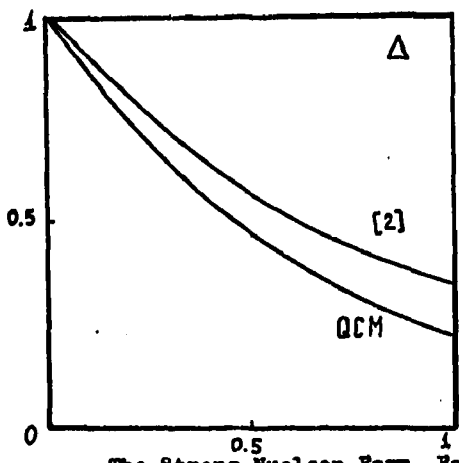
The Electromagnetic Nucleon Form Factors



→  $Q^2$  ( $\text{GeV}^2$ )



→  $Q^2$  ( $\text{GeV}^2$ )



The Strong Nucleon Form Factors

# The QCD sum rules, their validity and applicability

P. Kolář

Institute of Physics ČSAV, Prague

## ABSTRACT

Modifications of the QCD sum rules are investigated. It is shown that, for practical applications with the present knowledge of condensates, the standard Borel sum rules are the most convenient ones out of the modifications considered.

### 1. Introduction

The method of the QCD sum rules is very successful in applications to the low energy resonance parameters. Nevertheless, there are some problems which prevent us from obtaining the needed accuracy. In the case of light quark systems the form of sum rules (SR) is given by the relation

$$\int_0^R w(s) \ln \Pi(s) ds = \frac{i}{2} \oint_{C_R} w(s) \Pi(s) ds \quad (1)$$

where  $\Pi(s)$  is the polarization function,  $w(s)$  is an weight function and  $C_R$  is the circle with the radius  $R$ . We choose  $w(s)$  to be an entire function in  $s$ . Retaining  $R$  finite we get the Finite Energy Sum Rules (FESR) while the limit  $R \rightarrow \infty$  leads to the SR of Shifman, Vainstein and Zakharov [1]. The choice  $w(s) = \frac{1}{M^2} e^{-s/M^2}$  exactly coincides with the Borel sum rules. In the following we restrict ourselves to the case of  $\rho$ -meson generated by

the current  $j_c = \frac{1}{2}(\bar{\psi}\gamma_5\psi - \bar{\psi}\gamma_5\psi)$  We mostly parametrize  $\text{Im } \Pi(s)$  by the  $\delta$ -function and the step function:

$$\text{Im } \Pi(s) = \frac{\pi m^2 \delta(s-m^2)}{g^2} + \frac{2}{\beta_0} \left(1 + \frac{\alpha_s}{\pi}\right) \theta(s-s_0) \quad (2)$$

where  $s_0$  is the starting point of the continuum.

The practical use of the QCD sum rules can be difficult due to the following facts:

- (i) the continuum contribution is known only at high energies;
- (ii) the condensates corresponding to higher-dimensional operators are, in general, unknown;
- (iii) the effective parameter  $s_0$  is not directly measurable quantity; the correct value of  $s_0$  is not known;
- (iv) the correct parametrizations of resonance and continuum is also unknown.

In practical applications  $s_0$  is considered as a parameter and a consequence of (i) and (ii) is the necessity to introduce the fiducial interval [1] in which our ignorance of higher condensates and of continuum does not change the predictions of SR within reasonable limits. It was proposed in [2] that the fiducial interval should be estimated directly in the quantity to be extracted from the SR. Thus, the practical problems of QCD sum rules are: the correct determination of the fiducial interval and the correct determination of  $S_0$ . Can any modification of SR improve the situation?

The modification of the QCD sum rules can be under-

stood as a choice of the weight function. We shall consider three classes of the QCD sum rules for light quark systems.

## 2. Modifications of the QCD sum rules

### a) The Gaussian sum rules.

It was proposed by Bertlmann et al. [3] to choose

$$W_G(s-\bar{s}^2) = \frac{1}{\sqrt{4\bar{s}^2}} \exp\left(-\frac{(s-\bar{s}^2)^2}{4\bar{s}^2}\right) \quad (3)$$

This choice of the weight function can, in principle, serve as a formulation of the local duality ( $\tilde{\nu} \rightarrow 0$ ). The detailed inspection of the corresponding sum rule shows that the suppression of higher condensates is weaker in comparison with the Borel sum rule.

### b) The weight functions

$$W_k(s, M^2) = \frac{k \cdot s^{k-1}}{\pi(M^2)^k} e^{-\left(\frac{s}{M^2}\right)^k} \quad (4)$$

were considered in [2]. The corresponding modification of SR provides another formulation of local duality ( $k \rightarrow \infty$ ). Note that the both approaches to local duality requires the knowledge of higher condensates.

The Borel sum rules represents the special case of eq. (4) for  $k=1$  and are the most suitable ones out of the class (4) in practical applications. The reason is the weak suppression of higher condensates for  $k > 1$ .

### c) Finite energy sum rules.

We shall define the FESR with nonpositive weight function by generalizing the approach of Kremer et al. [4] (this approach is called as analytic continuation by duality). We denote the condensate contributions as  $h_i$  (see [2]).

The equation (1) can be rewritten into the form

$$-\frac{1}{\pi} \int_0^{s_R} w(s) \operatorname{Im} \Gamma(s) ds - \Delta(s_R, R) = \frac{1}{2\pi i} \oint_{C_R} w(s) \Gamma(s) ds \quad (5)$$

The contribution

$$\Delta(s_R, R) = \frac{1}{\pi} \int_{s_R}^R w(s) \operatorname{Im} \Gamma(s) ds$$

is, in general, unknown and should be minimized. We define

$s_R$  as the last point of the first resonance and the weight function  $w(s)$  can be chosen in the form

$$w(s) = f(s) - P_N(s) \quad (6)$$

where  $P_N(s)$  is a polynomial in  $s$ ; the function  $f(s)$  is an entire function. The simple examples are  $f = e^{\beta s}$  and  $f = s^N$ . The coefficients of the polynomial are determined by the least square fit and are dependent on

$R$ . To illustrate this kind of FESR we choose two weight function

$$w_1(s) = s^{k+2} - a_0 - a_1 s - \dots - a_{k+1} s^{k+1}$$

and

$$w_2(s) = s \cdot w_1(s) \quad ; \quad a_{k+2} = -1 \quad (7)$$

Using the parametrization (2) we get from (5)

$$-\frac{m^2 w_i(m^2)}{g^2} = \frac{1}{2\pi i} \oint \Gamma(s) w_i(s) ds + \Delta_i(s_R, R) \quad (8)$$

Hence

$$m^2 = \frac{\Delta_2 + \sum_{n=2}^{k+3} a_{n-1} \left\{ \frac{1}{g^2} \left( 1 + \frac{d_i(R)}{s} \right) \frac{R^{n+1}}{n+1} + (-1)^n \frac{h_{n+1}}{n+1} \right\}}{\Delta_1 + \sum_{n=0}^{k+2} a_n \left\{ \frac{1}{g^2} \left( 1 + \frac{d_i(R)}{s} \right) \frac{R^{n+1}}{n+1} + (-1)^n \frac{h_{n+1}}{n+1} \right\}} \quad (9)$$

where we have neglected higher perturbative corrections.

To determine  $k$  we require

$$\int_{s_R}^R w_i(s) \cdot P_k(s) ds = 0$$

for any polynomial  $P_k$  of order  $k$ . As a consequence  $k$  is the order of polynomial which approximates  $\operatorname{Im} \Gamma(s)$  sufficiently well. The formula (9) contains the con-

condensates up to the dimension  $2(k+4)$ .

The resulting SR are very sensitive to the values of condensates and to  $s_R$ . The practical applications are restricted only to the values  $k=0$  and  $k=1$  where the experimental mass can be reproduced sufficiently well. It should be stressed that the sum rules with a positively indefinite weight function have the problem in the estimate of fiducial interval. Nevertheless, the SR proposed above can be useful in the determination of the condensates from the experimental data.

### 3. Conclusion

The modification of the QCD sum rules considered here can not significantly improve the results of the standard Borel sum rules. They could be used, in principle, for consistency tests of the QCD.

### References

- [1] M.A.Shifman, A.I.Vainshtein and V.I.Zakharov, Nucl.Phys. B147,385 and 448 (1979).
- [2] J.Fischer and P.Kolář, Z.Phys. C34,375 (1987).
- [3] R.A.Bertlman,G.Launer and E. de Rafael, Nucl.Phys. B250,61 (1985).
- [4] M.Kremer,N.F.Nasrallah,N.A.Papadopoulos,K.Schilcher, Phys.Rev. D34,2127 (1986).

## Masses of High Spin Hadrons

M. Schepkin  
ITEP, Moscow

This report is devoted to the problem of spin effects in spectrum of orbitally excited hadrons. We will consider rather high orbital angular momenta for which spin effects look as spin-orbit interaction its sign and strength being defined by character of forces between quarks at large distances.

There exists widely accepted point of view according to which hadron with high spin looks as rotating string with quarks at the ends /1-3/. The string is understood as a flux-tube of chromo-electric field with the amplitude defined by color charges at the ends. In the simplest version, when quarks are massless, the model predicts linear Regge trajectories with the slope  $\alpha' = (2\pi V)^{-1}$ , where  $V$  is the string tension. In reality, however, quarks localized at the string ends, acquire effective masses, and velocities of the string ends become less than speed of light.

For the application of the model to real hadrons it is necessary to take into consideration quark spins /4-6/. This gives rise to the problem of spin-orbit coupling /6/. It is clear, that the only source of ls-coupling is Thomas precession because in the co-moving frame the gluon field is pure electric. The frequency of Thomas precession of spin of particle moving along the given trajectory is equal to

$$\vec{R}_T = -(\gamma - 1) \frac{[\vec{v}, \dot{\vec{v}}]}{v^2}, \quad (1)$$

where  $\vec{v}$  - velocity of the particle,  $\dot{\vec{v}} = d\vec{v}/dt$ ,  
 $\gamma = 1/\sqrt{1-v^2}$ . For circular motion  $[\vec{v}, \dot{\vec{v}}] = \vec{\omega} v^2$ ,



where  $\omega$  is rotation frequency. Hence, Thomas correction to hadron mass is equal to

$$\Delta E_T = - \vec{\omega} (\vec{S}_1 + \vec{S}_2) (\gamma - 1). \quad (2)$$

For high orbital excitations when the system can be treated quasiclassically the relation between the mass and total angular momentum (spin) of the string is given by following equations :

$$\begin{aligned} M &= \frac{2\mathcal{V}}{\omega} \left( \arccos \sin \nu + \frac{1}{\gamma} \right) + \Delta E_T, \\ J &= S_1 \omega + S_2 \omega + \frac{\mathcal{V}}{\omega^2} \left( \arccos \sin \nu + \frac{\nu}{\gamma} \right), \\ m \nu \omega \gamma^2 &= \mathcal{V}. \end{aligned} \quad (3)$$

The last equation follows from the equilibrium condition for the quark at the string end. Effective quark mass  $m$  and string tension  $\mathcal{V}$  are parameters of the model.

The correction  $\Delta E_T$  is negative for spins parallel to the rotation axis. Thus for high orbital excitations the model predicts the inverse order of levels with different sign of  $\vec{1S}$  as compared to that in electrodynamics. This is due to the fact, that for the motion in vector field there exists nonzero magnetic field in co-moving frame; its contribution to the spin precession is larger than Thomas effect in magnitude and opposite in sign. In the flux-tube model magnetic field in co-moving frame is absent. Hence, inspite of the vector nature of gluon field, the spin at the end of the string behaves like spin of particle confined in scalar potential. This analogy can be used to reproduce quasiclassical result (2) from quantum mechanics in the limit of high orbital excitations /7/. Consider Dirac particle in scalar potential  $m(r)$  :

$$(\hat{p} - m(r)) \psi = 0.$$

Let us calculate the matrix element of Hamiltonian squared  $\langle H^2 \rangle = \int \psi^\dagger H^2 \psi d\vec{r}$ . For Dirac particle  $H = \vec{\alpha} \vec{p} + \beta m$ , therefore

$$H^2 = \vec{p}^2 + m^2 + i m' (\vec{n} \cdot \vec{\gamma}), \quad \vec{n} = \vec{r}/r, \quad m' = \gamma m / \partial r. \quad (4)$$

The expression for  $\varepsilon^2 = \langle H^2 \rangle$  can be presented as a series /7/

$$\begin{aligned} \varepsilon^2 = \langle \vec{p}^2 + m^2 \rangle &= \int \psi^+ \frac{m}{2\varepsilon^2} \left[ m^{(2)} - \frac{m^{(4)}}{4\varepsilon^2} + \frac{m^{(6)}}{(4\varepsilon^2)^2} - \dots \right] \psi d\vec{r}^3 \\ &+ \int \psi^+ \frac{\gamma}{\varepsilon r} \left[ m' - \frac{m^{(3)}}{4\varepsilon^2} + \frac{m^{(5)}}{(4\varepsilon^2)^2} - \dots \right] \psi d\vec{r}^3. \end{aligned} \quad (5)$$

where  $m^{(n)} = \partial^n m / \partial r^n$ ,  $\gamma = -(1 + \vec{\ell} \cdot \vec{\sigma})$ . For high orbital excitations  $\psi$ -function is different from zero in the vicinity of the point of classical motion  $r_0$ . In that case ls-splitting is approximately equal to

$$\Delta \varepsilon_{\gamma} \approx \frac{\gamma}{2\varepsilon^2 r_0} \left[ m'(r_0) - \frac{m^{(3)}(r_0)}{4\varepsilon^2} + \dots \right] \quad (6)$$

For relativistic rotation in the potential  $m \sim r^n$  the main contribution to  $\Delta \varepsilon_{\gamma}$  for  $l \gg n$  is given by the first term proportional to  $m'$ . ls-splitting is then equal to  $\Delta \varepsilon_{\gamma} \approx \gamma \cdot \Delta E_{rot}$ , where  $\gamma = \varepsilon/m$ ,  $\Delta E_{rot}$  - distance between neighbouring rotation levels (with coinciding signs of  $\vec{l} \cdot \vec{s}$ ). As is known in quasiclassical limit  $\Delta E_{rot}$  is equal to rotation frequency  $\omega$ . So the result obtained coincides in the relativistic limit with the expression for Thomas correction in eq.(2).

For exponentially growing potentials the series in eq.(5) can be summed explicitly.

For the cases considered so far the standard definition of  $\gamma$ -factor for circular motion is correct if the size of localization area  $\Delta r$  is not small as compared to  $1/m(r)$ . Otherwise fermion mass should be substituted by the effective mass  $m_{eff} \sim 1/\Delta r$  and correspondingly

$\gamma$ -factor should be defined as  $\gamma_{eff} = \varepsilon/m_{eff}$ . This situation takes place, for instance, for massless fermion confined in spherical cavity. Inside the cavity Dirac equation has the form  $\hat{p} \psi = 0$ . Confining boundary

condition is /8,9/

$$i n_{\mu} \delta_{\mu} \psi = \psi. \quad (7)$$

This boundary condition breaks  $\gamma_5$  -invariance as it should be for scalar confinement. We are interested in the energy splitting of levels described by wave functions /10/

$$\psi_+ = \mathcal{N}_+ \begin{pmatrix} R_l \mathcal{J}_{j_+, l} \\ -R_{l+1} \mathcal{J}_{j_+, l+1} \end{pmatrix}, \quad \psi_- = \mathcal{N}_- \begin{pmatrix} R_l \mathcal{J}_{j_-, l} \\ -R_{l-1} \mathcal{J}_{j_-, l-1} \end{pmatrix}.$$

$R_l$  - spherical Bessel functions,  $\mathcal{J}_{j, l}$  - spherical spinors.  $\psi_+$  and  $\psi_-$  correspond to the total angular momenta  $j_{\pm} = l \pm 1/2$  and energies  $\varepsilon_{\pm}$ , respectively. Boundary condition (7) leads to the equations for energies

$\varepsilon_{\pm}$  :

$$R_{l-1}(\varepsilon_- R) = -R_l(\varepsilon_- R), \quad (9)$$

$$R_{l+1}(\varepsilon_+ R) = R_l(\varepsilon_+ R). \quad (10)$$

Solutions of these equations for large  $l$  are

$$\varepsilon_+ = \frac{1}{R} [l + C_m l^{1/3} + \mathcal{O}(1)], \quad C_m \approx 0.809 \quad (11)$$

$$\varepsilon_- = \frac{1}{R} [l + C_0 l^{1/3} + \mathcal{O}(1)], \quad C_0 \approx 1.856 \quad (12)$$

Energy difference increases for large  $l$  according to

$$\varepsilon_- - \varepsilon_+ = \frac{1}{R} C l^{1/3}, \quad C = C_0 - C_m,$$

the level with  $\vec{s}$  parallel to  $\vec{l}$  having lower energy. The distance between rotation levels as is seen from the same formula is equal to

$$\Delta E_{rot} = \Delta \varepsilon_+ = \Delta \varepsilon_- \approx 1/R.$$

Thus, for large  $l$   $\varepsilon_- - \varepsilon_+ \gg \Delta E_{rot}$ . The same inequality took place for Thomas correction in the string model, eq. (2). The analogy with the string can be traced further. To do that let's define effective  $\gamma$  -factor for massless fermion confined within cavity. Using properties of Bessel

functions it is easy to see, that the wave function is localized within rather thin layer near the surface. The size of the layer  $\Delta r \sim R/\ell^{2/3}$ , hence the effective fermion mass is  $m_{eff} \sim \ell^{1/3}/R$ . Fermion energy  $\epsilon_f \sim \ell/R$ , and so effective  $\gamma$ -factor is equal to  $\gamma = \epsilon_f/m_{eff} \sim \ell^{1/3}$ . It is seen now that spin-orbit splitting is  $\gamma$  times larger than distance between rotation levels.

Thus, relativistic quantum mechanics reproduces quasiclassical result for 1s-splitting caused by Thomas precession.

Let us stress one more time, that in relativistic limit  $\Delta E_T \gg \omega = \Delta E_{rot}$ . In that sense Thomas precession represents nonperturbative effect.

Let us consider now orbitally excited mesons. Because of the Thomas precession of quarks spins particle on  $\rho$ -trajectory with quantum numbers  $J^P$ ,  $P = (-1)^J$  has lower mass than its partner on  $\pi$ -trajectory with the spin  $J-1$  and the same parity. To estimate the effect we need to know  $\gamma$ -factor for the string end. For high orbital excitations  $\gamma \sim J^{1/4}$ , therefore, let's say, for  $J \sim 10$  1s-splitting is of order of distance between two neighbouring points on one and the same trajectory.

Numerical predictions of the model for masses of orbitally excited qq-mesons ( $q = u$  or  $d$ ) are shown in Fig.1 in comparison with experimental data. Parameters  $m_q$  and  $v$  have been fixed by position of two points on trajectory 1,  $m_q = 340$  MeV,  $(2\pi v)^{1/2} = 1.07$  GeV. As there are no dependences on isospin, particles with  $T = 0$  and  $1$  have equal masses. Quantum numbers of resonances on trajectory 1 are  $J^{PC} = 2^{++}, 3^{--}, 4^{++} \dots$ . Number of particles on the trajectory 2 is twice as large, here  $J^P = 1^+, 2^-, 3^+, \dots$  and  $C = +1$  or  $-1$ . In particular,  $\rho$ -excitations must lie on trajectory 1, and excitations of  $\pi$ -type - on trajectory 2. According to experimental data the tendency for "inverse" order of levels is seen. There is a certain optimism in the last statement because the data available

need to be clarified. It is more interesting, of course, to have experimental data on  $\bar{\pi}$  -trajectory for  $J > 3$ .

Equations (3) can be obviously generalized for different quark masses. Introducing one more parameter  $m_s$ , strange quark mass, enables to calculate  $K$  and  $K^*$  -trajectories. The results are shown in Fig. 2 in comparison with experimental data. It is seen that the model predictions are in agreement with experimental data for high spins. Of course, it is also desirable to have more precise data on  $K$  -trajectory.

Discrepancy of model predictions with experiment for small  $J$  is explained by the fact, that besides Thomas precession there exist another essential spin effects due to the presence of vector (for example, Coulomb) interaction. To estimate contributions of different spin forces let us use potential approach. Let  $\mathcal{E}(r)$  be the sum of scalar and vector potentials. (In nonrelativistic limit string is equivalent to lineary rising scalar potential  $\propto r$  /11/). Then to the first order in  $1/m^2$  the effective potential, depending on spins, can be presented

$$\begin{aligned}
 V_{eff} = \mathcal{E} - a \left( \frac{\vec{s}_1}{2m_1} + \frac{\vec{s}_2}{2m_2} \right) \vec{\ell} + b \left( \frac{\vec{s}_1}{2m_1} + \frac{\vec{s}_2}{2m_2} + \frac{\vec{s}_1 + \vec{s}_2}{m_1 m_2} \right) \vec{\ell} + \\
 + c \frac{1}{m_1 m_2} \hat{T} + d \vec{s}_1 \vec{s}_2,
 \end{aligned}
 \tag{13}$$

where

$$\hat{T} = \frac{(\vec{\ell} \vec{s})^2 + \frac{1}{2} (\vec{\ell} \vec{s}) - \frac{1}{3} \ell^2 s^2}{(2\ell+3)(2\ell-1)}, \quad \vec{s} = \vec{s}_1 + \vec{s}_2.$$

Here  $m_1$  and  $m_2$  - masses of quarks. In what follows spin-spin forces will not be taken into account because we consider nonzero orbital angular momenta. General formalism of calculation of functions a,b,c,d in QCD was developed in Ref./12,13/.  $a(r)$  is determined by scalar potential; functions b,c,d - by vector potential.

Proceeding from general form of potential (13) we can estimate contributions of separate terms to the masses of  $P$ -wave analogs of light mesons and then to predict, for instance, spin effects for mesons made of light and heavy quarks.

Similar model-independent analysis was made recently in Ref./14/. For that purpose we will use experimental data on  $P$ -wave strange mesons  $K_1$  (1280) and  $K_1$  (1400) representing mixture of  $^3P_1$  and  $^1P_1$ -levels with mixing angle  $\theta \approx 56^\circ$  /15/, and  $K_2^*$  (1430) with quantum numbers of  $^3P_2$ -state. Let us rewrite eq.(13) in the form

$$V_{eff} = \varepsilon + \alpha (\vec{s}_2 - \vec{s}_1) \vec{\ell} + \beta (\vec{s}_2 + \vec{s}_1) \vec{\ell} + \gamma \hat{T}. \quad (14)$$

$\varepsilon$ ,  $\alpha$ ,  $\beta$  and  $\gamma$  are now understood as matrix elements of the corresponding operators. Then

$$\mu(^3P_2) = \varepsilon + \beta - \frac{1}{2} \gamma.$$

Mass matrix of axial mesons has the form

$$\begin{pmatrix} \varepsilon - \beta + \frac{1}{6} \gamma & \alpha \sqrt{2} \\ \alpha \sqrt{2} & \varepsilon \end{pmatrix}. \quad (15)$$

Eigenvalues  $\mu_1$  and  $\mu_2$  of this matrix are masses of physical states.  $\alpha$  is straightforward expressed in terms of experimental data

$$|2\sqrt{2} \alpha| = (\mu_2 - \mu_1) \sin 2\theta$$

Omitting details we write down the answer for matrix elements

$$\alpha \approx 45 \text{ MeV}, \quad \beta = 50.65 \text{ MeV}, \quad \gamma = 0.50 \text{ MeV} \quad (16)$$

Uncertainties in these estimates are due to experimental errors. Estimates of matrix elements of the original potential (13) depend on quark masses  $m_1 = m_q$  and  $m_2 = m_s$ . For  $m_s = (1.3+1.5) m_q$  spin-orbit contributions of scalar and vector potentials are comparable (see also Ref./16/). When  $J$  increases the size of the system gets larger and spin forces due to vector interaction vanishes more rapidly than the contribution of scalar interactions.

(For linearly rising scalar potential and Coulomb-like vector potential we have  $a \sim 1/r$ ,  $b \sim 1/r^2$ ). This should lead to the "flip" of sign of spin-orbit splitting. Experimental data do not contradict such interpretation (see Figs. 1, 2). However, it is highly desirable to have information on  $\pi$  and  $K$ -trajectories for  $J > 3$ .

Let us consider now  $P$ -wave mesons made of heavy and light quarks, for example,  $b\bar{u}$ . For estimate we put  $m_2 \rightarrow \infty$ . Then matrix elements (which we write with index  $\infty$ ) satisfy equations

$$\beta_{\infty} = -\alpha_{\infty}, \quad \gamma_{\infty} = 0,$$

and mass matrix of axial mesons has the form

$$\begin{pmatrix} \varepsilon_{\infty} + \alpha_{\infty} & \alpha_{\infty}\sqrt{2} \\ \alpha_{\infty}\sqrt{2} & \varepsilon_{\infty} \end{pmatrix} \quad (17)$$

It is easy to see that mixing angle is fixed:

$$\tan 2\theta_{\infty} = 2\sqrt{2}, \quad \theta_{\infty} \approx 35^\circ$$

Masses of  ${}^3P_2$  and  ${}^3P_0$ -states in that case are equal to

$$\mu({}^3P_2) = \varepsilon_{\infty} - \alpha_{\infty}, \quad \mu({}^3P_0) = \varepsilon_{\infty} + 2\alpha_{\infty}.$$

As a result, relative position of four  $P$ -wave states looks approximately as shown in Fig. 3. The splitting of pairs of degenerate particles is equal to  $3\alpha_{\infty}$ .

Thus, the inverse order of levels for mesons with  $m_2 \gg m_1$  is expected already starting from  $P$ -wave. Analogous conclusion was made in Ref. /17/.  $\alpha_{\infty}$  can be estimated from eq. (16) if the ratio of radii of  $s\bar{q}$  and  $b\bar{q}$ -mesons is known. For  $(R_{s\bar{q}}/R_{b\bar{q}})^2 \sim 2$  spin-orbit splitting  $3\alpha_{\infty} \sim 50 + 100$  MeV.

For charmed mesons large corrections arise from taking into account finite  $C$ -quark mass /18/. However, for  $D$ -like excitations inverse order of levels is also expected to take place for lower  $J$  than in mesons made of quarks with equal masses.

In conclusion let us stress one more time the importance for experimental investigation of the problem of

high spin hadrons spectroscopy. It may provide us with the information on spin effects, which are defined by the particular character of interaction between quarks at large distances. If we accept quasiclassical approach of QCD-string then spin effects occur to be large and rather unusual. Energetically preferable orientation of spins corresponds to positive  $\vec{L}\vec{S}$ . Magnitude of spin-orbit splitting is comparable to the mass difference of two neighbouring particles on one and the same trajectory. From the model independent analysis based on QCD it can be concluded that in mesons made of light quarks the "flip" of sign of spin-orbit term happens for  $J > 3$ . For mesons constructed of light and heavy quarks these effects should take place for lower spins.

Besides investigations of meson spectroscopy it would be highly desirable to have more accurate data on baryon trajectories /19/.

#### References

1. Nambu Y. - Phys.Rev., 1974, D10, 4262.
2. Chodos A., Thorn C.B. - Nucl.Phys., 1974, B72, 509;  
Johnson K., Thorn C.B. - Phys.Rev., 1976, D13, 1934.
3. Barbashov B.M., Nesterenko V.V. - "Relativistic string model in hadron physics". Energoatomizdat, Moscow, 1987.
4. Pisarski R.D., Stack J.D. - Preprint FERMILAB-PUB-86/122-T, 1986.
5. Borodulin V.I., Pluschai M.S., Fronko G.P. - Preprint IHEP 86-205, 1986.
6. Kobzarev I.Yu., Martemyanov B.V., Schepkin M.G. - Yadern.Fiz., 1986, 44, 475.
7. Martemyanov B.V., Schepkin M.G. - Yadern.Fiz., 1987, 45, 296.
8. Chodos A. et al. - Phys.Rev., 1974, D9, 3471.
9. Logunov V.N., Martemyanov B.V. - Yadern.Fiz., 1979, 29, 815.
10. Berestetskii V.B., Lifshits E.M., Pitaevskii L.P. -



"Relativistic quantum theory". V.I., Moscow, 1968.

11. Buchmuller W. - Phys.Lett., 1982, 112B, 479.
12. Eichten E., Feinberg F.L. - Phys.Rev., 1981, D23, 2724.
13. Gromes D. - Z.Phys., 1984, G26, 401.
14. Olson M.G., Suchyta C.J. - Phys.Rev., 1987, D35, 1738.
15. Daum C. et al. AOCMOR Collaboration - Nucl.Phys., 1981, B187, 1.
16. Krivoruchenko M.I. - Pis'ma JETP, 1983, 38, 146.
17. Schnitzer H.J. - Nucl.Phys., 1982, B207, 131.
18. Godfrey S., Isgur N. - Phys.Rev., D32, 189, 1985.
19. Kobzarev I., Kondratyuk L., Martemyanov B., Schepkin M. - Preprint ITEP 86-67, 1986.

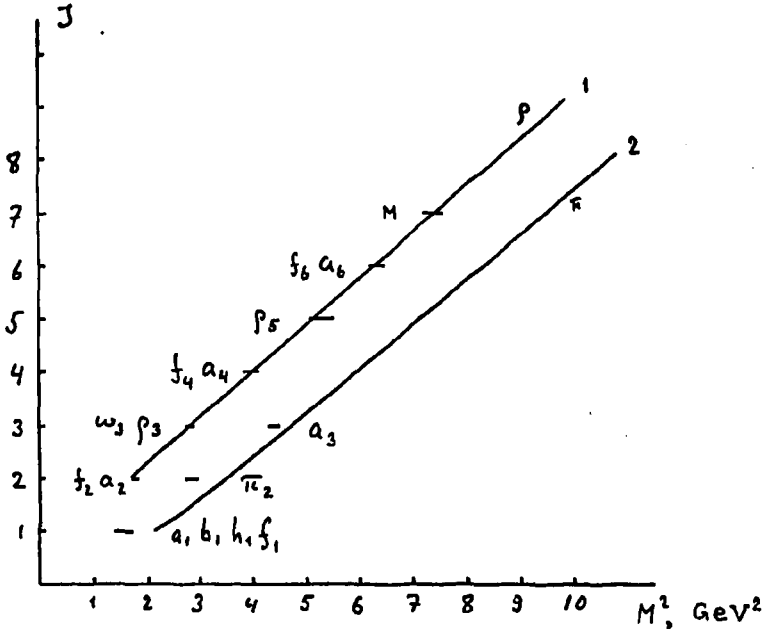


Fig. 1

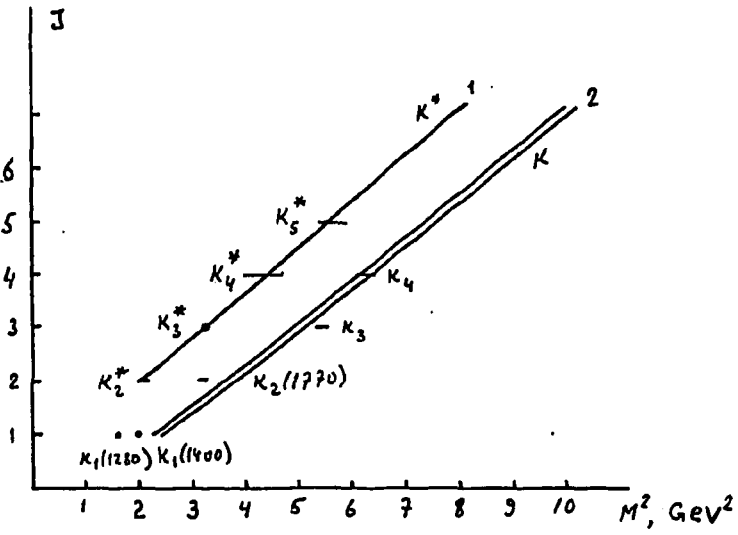


Fig. 2

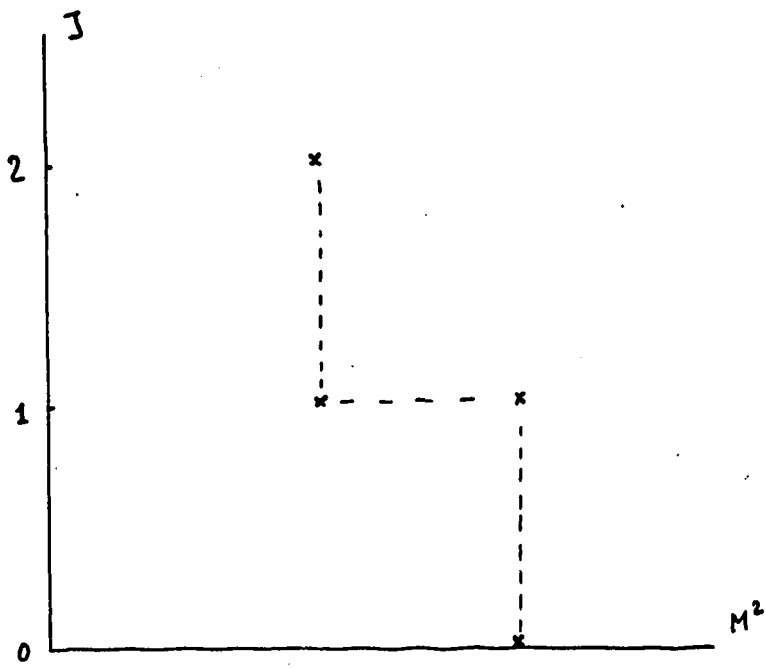


Fig. 3

# DECAYS OF GLUONIUM IN THE GENERALIZED QUARK MODEL OF SUPERCONDUCTIVITY TYPE

M. Nagy

Institute of Physics of the Electro-Physical Research Centre,  
Slovak Academy of Sciences, 842 28 Bratislava, Czechoslovakia

M.K. Volkov

Laboratory of Theoretical Physics,  
Joint Institute for Nuclear Research, Dubna, USSR

## Abstract

In the generalized quark model of superconductivity type (GQMST), obtained by the introduction of gluonium into a quark model with four quark interactions<sup>1</sup>, the calculations of  $G(\epsilon')$  decays into  $2\pi$ ,  $2K$  and  $2\eta$  are performed.

One of the motivations for construction of GQMST was the problem of the description of scalar mesons in the framework of quark model, namely the interpretation of  $S^*(975)$  and  $\epsilon(1300)$  states (in the new notation  $f_0(975)$  and  $f_0(1300)$ , respectively). It is difficult to answer, in the framework of pure quark models, why the  $\epsilon(1300)$  state, consisting mainly of light quarks, is heavier than  $S^*(975)$  state, consisting mainly of the strange quarks. The next question is connected with the problem of existence of the third isoscalar meson which should be lighter than 1 GeV. The existence of this meson (well known as  $\sigma$ -meson) has been predicted many years ago in the framework of phenomenological chiral sigma models.

It was shown<sup>2</sup>, that in the GQMST the three scalar states ( $\epsilon(550)$ ,  $S^*(1070)$  and  $\epsilon'(1200)$ ) appeared in natural way. These three isoscalar states arising in the scalar sector were identified with mesons in following way.

The first resonance consisting mainly of light u and d quarks and possessing the large width of the decay into  $2\pi$  equal to its mass, i.e. it is difficult to observe. This resonance is a good candidate for the role of the well known  $\sigma$ -particle.

The second resonance is close to the scalar meson  $S^*(975)$  and it consists almost completely of the s-quarks; however, owing to the small admixture of the gluonium, this resonance decays into  $2\pi$  with the decay width corresponding to the experimental value.

Finally, the last resonance is almost completely defined by the gluonium. This state possesses the properties close to the  $\epsilon(1300)$  meson. It decays mainly into  $2\pi$  with the decay width not contradicting the last experimental data<sup>3,4</sup>, with smaller probability also into  $2K$  and its decay into  $2\eta$  is suppressed. A qualitatively reasonable picture expressing the existence of three such states is in the agreement with experimental data.

The inclusion of the gluonia into the quark model of superconductivity type<sup>1</sup> have been carried out in the scheme proposed in papers<sup>5,6</sup>. We have obtained the following expression for the Lagrangian describing the interaction of the gluonium field  $G$  with quarkonium fields (of scalar and pseudoscalar mesons)<sup>2</sup>

$$\begin{aligned} \Delta\mathcal{L} = & -H_0 e^{4G/f_g} \left( 1 \eta_{\frac{f_g}{G}} + \frac{G}{f_g} \right) + \quad (1) \\ & + (e^{2G/f_g} - 1) \left\{ (m_U^2 - \frac{m_\pi^2}{2Z}) \left[ (\vec{\pi}^2 + \eta_U^2)Z + (\sigma_U - Z^{1/2}f_\pi)^2 \right] \right. \\ & \left. + (m_S^2 - \frac{m_\eta^2}{2Z}) \left[ \eta_S^2 Z + (\sigma_S - Z^{1/2}f_S)^2 \right] + \left[ (\frac{m_U + m_S}{2})^2 Z - \frac{m_K^2}{2} \right] K^2 \right\}, \end{aligned}$$

where  $H_0 = \frac{b}{8} G_0$ ,  $b = \frac{11}{3} N_C - \frac{2}{3} N_f$  ( $N_C = 3$  is the number of colours,  $N_f = 3$  is the flavour number),  $G_0 = \langle 0 | \frac{\alpha_s}{\pi} G_{\mu\nu}^a G_a^{\mu\nu} | 0 \rangle$  is the gluon condensate for which we use following value  $G_0 = 0.012 \text{ GeV}^4$  according to<sup>7</sup>,  $f_\pi = 93 \text{ MeV}$ ,  $f_S = 1.28 f_\pi$  are meson decay constants,  $Z = 1.4$  is the constant occurring from the inclusion

$\pi$ - $A_1$  transitions<sup>1</sup>, ( $m_{\eta_s} = 700$  MeV,  $m_U = 200$  MeV,  $m_s = 455$  MeV). In the Lagrangian (1) there are three new uncertain parameters  $G$ ,  $f_g$  and  $m_G$  (gluonium mass). They have been fixed by choosing<sup>2</sup> three conditions giving as a result  $f_g = 212$  MeV =  $2.28 f_\pi$  and  $m_G = 1.16$  GeV. In the corresponding Lagrangian<sup>2</sup> there appear the nondiagonal terms containing  $G \sigma_U$  and  $G \sigma_S$

$$\mathcal{L}(G\sigma_U, G\sigma_S) = - \frac{2G}{Z^{1/2} f_g} \left[ (2m_U^2 Z - m_\pi^2) f_\pi \sigma_U + (2m_S^2 Z - m_{\eta_s}^2) f_s \sigma_S \right] \quad (2)$$

The direct decay of the gluonium  $G(\epsilon')$  into  $2\pi$ ,  $2K$  and  $2\eta$  is allowed by

$$\begin{aligned} \mathcal{L}(G\pi^2, GK^2, G\eta^2) = & \frac{G}{f_g} \left\{ (2m_U^2 Z - m_\pi^2) \vec{\pi}^2 + \left( \frac{(m_U + m_s)^2}{2} Z - m_K^2 \right) \vec{K}^2 + \right. \\ & \left. + \left[ (2m_U^2 Z - m_\pi^2) \sin^2(\varphi - \varphi_0) + (2m_S^2 Z - m_{\eta_s}^2) \cos^2(\varphi - \varphi_0) \right] \eta^2 \right\} \end{aligned} \quad (3)$$

where we have taken into account the mixing

$$\eta_U = \eta' \cos(\varphi - \varphi_0) - \eta \sin(\varphi - \varphi_0) \quad (4)$$

$$\eta_S = \eta' \sin(\varphi - \varphi_0) + \eta \cos(\varphi - \varphi_0)$$

with mixing angle  $\varphi - \varphi_0 = -53^\circ$ .

The  $G(\epsilon') \rightarrow 2\pi$  decay goes in the direct way as well as via the intermediate  $\sigma_U$  state and for the total amplitude we obtained as a result<sup>2</sup>

$$\Gamma_{G \rightarrow 2\pi}^{\text{tot}} = f_g^{-1} (2m_U^2 Z - m_\pi^2) \left[ 1 + \frac{(2m_U)^2}{m_G^2 - m_{\sigma_U}^2} \right] G \vec{\pi}^2 \equiv \tilde{g} G \vec{\pi}^2 \quad (5)$$

and the corresponding decay width is

$$\Gamma_{G \rightarrow 2\pi} = 3(8\pi m_G)^{-1} \tilde{g}^2 (1 - 4m_\pi^2/m_G^2)^{1/2} = 150 \text{ MeV} \quad (6)$$

in agreement with the experimental data<sup>3,4</sup>. The amplitude of

the  $G(\epsilon') \rightarrow 2K$  decay, following from the Lagrangian (3), leads to the width<sup>2</sup>

$$\Gamma_G \rightarrow 2K = 30 \text{ MeV} \quad (7)$$

which is in qualitative agreement with experiment<sup>3</sup>. The process being taken into account via intermediate  $\sigma_S(S^*)$  state increases twice the value in question.

For the amplitude of the direct  $G(\epsilon') \rightarrow 2\eta$  decay we get

$$\begin{aligned} \Gamma_G \rightarrow 2\eta = f_g^{-1} \{ (2m_U^2 Z - m_\pi^2) \sin^2(\varphi - \varphi_0) + \\ + (2m_S^2 Z - m_\eta^2) \cos^2(\varphi - \varphi_0) \} g\eta^2 = \tilde{g}G\eta^2 \end{aligned} \quad (8)$$

which leads to the width

$$\Gamma_G \rightarrow 2\eta = (8\pi m_G)^{-1} \tilde{g}^2 (1 - 4m_\eta^2/m_G^2)^{1/2} = 7.5 \text{ MeV} \quad (9)$$

So far, there are no reliable experimental values for the decay width of this process. However, there is some evidence that decay was seen as claimed by PDG<sup>3</sup>.

As a whole, the picture we have obtained<sup>2</sup> is in agreement with the experiment. GQMST offers thus some other possibilities in investigation of gluonium properties.

#### REFERENCES

1. Volkov M.K. - a) Sov. Journ. Particles and Nuclei, 1986, 17, p.433 (in Russian); b) Ann. Phys., 1984, 157, p.282.
2. Nagy M. et al. - JINR Rapid Comm., No 25-87, Dubna, 1987, p.11.
3. Particle Data Group - Phys. Lett., 1986, 170 B.
4. Alde D. et al. - Nucl. Phys., 1986, B269, p.485.
5. Lánik J. - Phys.Lett., 1984, 144B, p.439; Ellis J., Lánik J. - ibid., 1985, 150B, p.289; 1986, 175B, p.229.
6. Lánik J. - JINR Rapid Comm., No 20-86, Dubna, 1986, p.10.
7. Shifman M.A. et al. - Nucl. Phys., 1979, B117, pp.385,448.

## YANG-MILLS PROPAGATORS IN BACKGROUND FIELDS

H. J. Kaiser

Institut für Hochenergiephysik der AdW, Berlin-Zeuthen, DDR

K. Scharnhorst

Sektion Physik der Humboldt-Universität Berlin, DDR

E. Wieczorek

Institut für Hochenergiephysik der AdW, Berlin-Zeuthen, DDR

In a Euclidean Yang-Mills theory with  $a$ , for the moment, unspecified gauge group (structure constants  $f^{abc}$ ), gauge parameter  $\alpha$ , and background field  $B_\mu^a(x)$  we calculate the gauge resp. ghost propagators  $G_{\mu\nu}^{ab}(x,y,\alpha)$  resp.  $G^{ab}(x,y)$  by inverting the kernels

$$\begin{aligned} K_{\mu\nu}^{ab} &= (D_\mu^2 \delta_{\mu\nu} + (\frac{1}{2}\alpha - 1) D_\mu D_\nu)^{ab} + 2g f^{abc} F_{\mu\nu}^c(x) \\ K_x^{ab} &= (D_x^2)^{ab} \end{aligned} \quad (1)$$

where  $D_\mu^{ab}(B) = \delta^{ab} \frac{\partial}{\partial x_\mu} + g f^{abc} B_\mu^c(x)$

making use of

$$K_{\mu\nu}^{ab}(\alpha) G_{\mu\nu}^{bc}(x,y,\alpha) = -\delta^{ac} \delta_{\mu\nu} \delta(x-y), \quad K_x^{ab} G^{bc}(x,y) = -\delta^{ac} \delta(x-y). \quad (2)$$

It is possible to express the gauge propagator for arbitrary  $\alpha$  in terms of the special propagator for  $\alpha=1$

$$\begin{aligned} G_{\mu\nu}^{ab}(x,y,\alpha) &= G_{\mu\nu}^{ab}(x,y,1) + (1-\alpha) U_{\mu\nu}^{ab}(x,y) \\ U_{\mu\nu}^{ab}(x,y) &= \int dz G_{\mu\alpha}^{ac}(x,z,1) \left( \frac{D_\mu D_\alpha}{z} \right)^{cd} G_{\lambda\nu}^{db}(z,y,1). \end{aligned} \quad (3)$$

To verify (3) we use the identity (valid if  $D_\mu^{ab} F_{\mu\nu}^b = 0$ )

$$D_\mu^{ab} \left\{ \delta_{\mu\nu} (D^2)^{bc} + (\frac{1}{2}\alpha - 1) (D_\mu D_\nu)^{bc} + 2g f^{bcd} F_{\mu\nu}^d \right\} = \frac{1}{2} (D^\nu D_\nu)^{ac}$$

and the functional equations with respect to  $y$

$$\begin{aligned} D_\mu^{ab} G_{\mu\nu}^{bc}(x,y,\alpha) D_\nu^{cd} &= -\alpha \delta^{ad} \delta(x-y) \\ D_\mu^{ab} G_{\mu\nu}^{bc}(x,y,\alpha) &= -\alpha G^{ab}(x,y,\alpha) D_\nu^{bc}. \end{aligned}$$



Now we specify the YM theory to the gauge group  $SU(2)$  (i.e.  $f^{abc} = \epsilon^{abc}$ ) and a constant homogeneous magnetic background field in the colour 3 direction

$$B_{\mu\nu}^a(x) = -\frac{1}{2} F_{\mu\nu}^c x_\nu, \quad F_{\mu\nu}^c = \epsilon_{\mu\nu}^c \delta^{c3} B. \quad (4)$$

We use the notation

$$\begin{aligned} x_1^2 &= x_1^2 + x_2^2 & \delta_{\mu\nu}^\perp &= \begin{pmatrix} 1 & & & \\ & 1 & & \\ & & 0 & \\ & & & 0 \end{pmatrix}, & \delta_{\mu\nu}^\parallel &= \begin{pmatrix} 0 & & & \\ & 0 & & \\ & & 0 & 1 \\ & & & 0 \end{pmatrix} \\ x_{\mu'}^2 &= x_3^2 + x_4^2 \\ \tilde{X}_\mu &= \epsilon_{\mu\nu}^\perp x_\nu & \epsilon_{\mu\nu}^\perp &= \begin{pmatrix} 0 & 1 & 0 & 0 \\ -1 & 0 & 0 & 0 \\ 0 & 0 & 0 & 0 \\ 0 & 0 & 0 & 0 \end{pmatrix} \\ \delta_{\perp}^{ab} &= \delta^{a1} \delta^{b1} + \delta^{a2} \delta^{b2} \end{aligned}$$

We diagonalize the kernels

$$\begin{aligned} K_{\mu\nu}^{ab} &= \delta_{\mu\nu}^\perp (D^2)^{ab} + 2gB \epsilon_{\mu\nu}^\perp \epsilon^{ab3} \\ K^{ab} &= (D^2)^{ab} = \Delta \delta^{ab} - \left(\frac{gB}{2}\right)^2 x_1^2 \delta_1^{ab} + gB (x_1 \partial_2 - x_2 \partial_1) \epsilon^{ab3} \end{aligned}$$

in colour and space-time indices and arrive at the problem to invert the operators

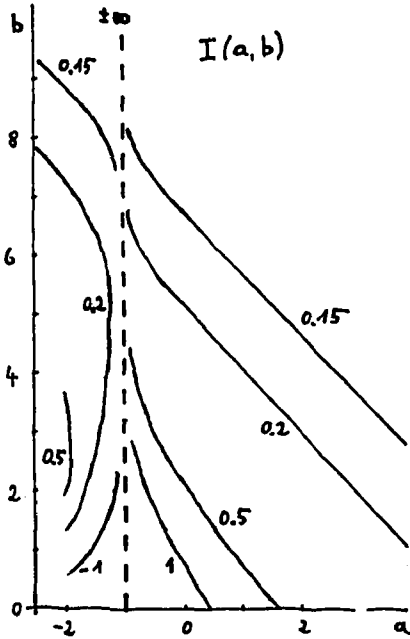
$$h^\pm = -\Delta + \left(\frac{gB}{2}\right)^2 (x_1^2 + x_2^2) \mp i gB (x_1 \partial_2 - x_2 \partial_1)$$

as well as  $h_{\pm 2gB}^+$  and  $h_{\pm 2gB}^-$ . After separating the  $x_{3,4}$  dependence by means of a Fourier transformation we obtain 2-dimensional harmonic oscillator Hamiltonians and calculate from their eigenfunctions and (infinitely degenerate) eigenvalues the inverses

$$[h^\pm(x, y)]^{-1} = \frac{1}{gB} e^{\pm i\varphi(x, y)} \int \frac{d^2 k}{(2\pi)^2} e^{ik(x-y)} I(a, b) \quad (5)$$

and analogous expressions for  $(h_{\pm 2gB})^{-1}$  involving  $I(a_{\pm 2}, b)$  instead. In writing down (5) we have used the notation

$$a = \frac{k_1^2}{gB}, \quad b = \frac{k_2^2}{gB}, \quad \varphi(x, y) = \frac{gB}{2} (x_1 y_2 - x_2 y_1). \quad (6)$$



The function  $I(a, b)$  has the integral representations

$$I(a, b) = \int_0^{\infty} \frac{d\tau}{\cosh \tau} e^{-a\tau - b \tanh \tau} \quad (\text{Re } a > -1)$$

$$= e^{-b} \int_0^{\infty} \frac{d\tau}{\cosh \tau} e^{-a\tau} [e^{b(1-\tanh \tau)} - 1 - e^{-2\tau}] + \frac{2e^{-b}}{a+1} \quad (\text{Re } a > -3).$$

$I(a, b)$  has a tower of poles as can be seen from its expression in terms of Laguerre polynomials

$$I(a, b) = 2e^{-b} \sum_{r=0}^{\infty} \frac{(-1)^r L_r(2b)}{a+2r+1} \quad (8)$$

In  $x$ -space we have the dependences  $(\lambda = gBx_+^2/2, \mu = gBx_-^2/2)$

$$D^0(x) = \frac{1}{gB} \left( \frac{d^4 k}{(2\pi)^4} e^{ikx} I(a, b) \right) = \frac{gB}{4\pi^2} \int_0^{\infty} \frac{d\tau}{\tau \sinh \tau} e^{-\frac{\lambda}{\tau} - \mu \tanh \tau}$$

$$= \frac{gB}{4\pi^2} e^{-\mu} \sum_{r=0}^{\infty} L_r(2\mu) K_0(2\sqrt{(2r+1)\lambda}) \sim \frac{gB}{8} \pi^{-3/2} \lambda^{-1/4} e^{-2\sqrt{\lambda} - \mu} \quad (\lambda \rightarrow \infty)$$

$$D^\pm(x) = \frac{1}{gB} \left( \frac{d^4 k}{(2\pi)^4} e^{ikx} I(a \pm 2, b) \right)$$

$$D^0 = \frac{D^+ + D^-}{2}, \quad D^m = \frac{D^+ - D^-}{2}.$$

More details about the long- and short-distance behaviour of  $D^0$ ,  $D^+$ , and  $D^-$  are derived in /4/.

The propagators for  $\alpha=1$  are finally

$$G^{ab}(x, y) = \phi^{ab}(x, y) D^0(x-y) + \frac{1}{4\pi^2 |x-y|^2} \delta^{a3} \delta^{b3}$$

$$G_{\mu\nu}^{ab}(x, y, \lambda) = \phi^{ab}(x, y) [\delta_{\mu\nu}^0 D^0(x-y) + \delta_{\mu\nu}^\perp D^P(x-y)] + \tilde{\phi}^{ab}(x, y) \varepsilon_{\mu\nu}^\perp D^m(x-y) + \frac{1}{4\pi^2 |x-y|^2} \delta^{a3} \delta^{b3} \delta_{\mu\nu}.$$

Where the phase factors

$$\phi^{ab}(x, y) = \delta_1^{ab} \cos \varphi(x, y) + \epsilon^{ab3} \sin \varphi(x, y), \quad \tilde{\phi}^{ab} = \phi^{ac} \epsilon^{cb3} \quad (11)$$

involve  $\varphi(x, y)$  defined in (6).

The large-distance behaviour of the gauge propagator is

$$G_{\mu\nu}^{ab}(x, y, 1) \sim \frac{1}{8\pi^{1/2}} (\frac{1}{2}B)^{-4} [(x_{11}-y_{11})^2]^{-1/4} [\phi^{ab}(x, y) \delta_{\mu\nu}^{\perp} + \tilde{\phi}^{ab}(x, y) \epsilon_{\mu\nu}^{\perp}] \times \\ e^{-i\sqrt{\frac{1}{2}B(x_{11}-y_{11})^2} - \frac{1}{4}B(x_{11}-y_{11})^2} + \frac{\delta^{a3} \delta^{b3} \delta_{\mu\nu}}{4\pi^2 (x-y)^2} \quad (12)$$

To recognize that the integral expression  $U_{\mu\nu}^{ab}$  in (3) is well-defined we need besides (12) the relation

$$D_{\mu}^{ab} [\phi^{bc}(x, y) \delta_{\mu\nu}^{\perp} + \tilde{\phi}^{bc}(x, y) \epsilon_{\mu\nu}^{\perp}] e^{-\frac{1}{4}B(x_{11}-y_{11})^2} H_0^{(1)}(\sqrt{\frac{1}{2}B(x_{11}-y_{11})^2}) = 0 \quad (13)$$

which holds due to the structure of the phase factors.

To evaluate  $U_{\mu\nu}^{ab}$  we use partial integration to let  $D_{\mu}^{ce}$

operate on  $G_{\mu\nu}^{ac}(x, z, 1)$ , apply the relations

$$\phi^{ab}(x, z) \phi^{bc}(z, y) = -\tilde{\phi}^{ab}(x, z) \tilde{\phi}^{bc}(z, y) = \phi^{ac}(x-y, z)$$

$$\phi^{ab}(x, z) \tilde{\phi}^{bc}(z, y) = \tilde{\phi}^{ab}(x, z) \phi^{bc}(z, y) = \tilde{\phi}^{ac}(x-y, z)$$

and 
$$\frac{\partial}{\partial z_{\perp}^2} D^{\rho}(z) + \frac{\partial B}{2} z_{\perp}^{\perp} D^{\rho}(z) = \frac{\partial}{\partial z_{\perp}^2} D^{\sigma}(z)$$

$$\frac{\partial B}{2} z_{\perp}^{\perp} D^{\rho}(z) + \frac{\partial}{\partial z_{\perp}^2} D^{\rho}(z) = -\frac{\partial B}{2} z_{\perp}^{\perp} D^{\sigma}(z)$$

with the result

$$U_{\mu\nu}^{ab}(x, y) = \int dz \{ \phi^{ac}(x-y, z) \mathcal{L}_{\mu} P_{\nu}(\xi, \eta) + \tilde{\phi}^{ac}(x-y, z) \mathcal{L}_{\mu} P_{\nu}(\xi, \eta) \} \\ - \delta^{a3} \delta^{b3} \int \frac{d^4 k}{(2\pi)^4} e^{ik(x-y)} \frac{z_{\mu} \eta_{\nu}}{k^4}$$

where

$$P_{\nu}(\xi, \eta) = \left( \frac{\partial}{\partial \xi_{\nu}} - i \frac{\partial B}{2} \tilde{\xi}_{\nu} \right) D^{\rho}(\xi) \left( \frac{\partial}{\partial \eta_{\nu}} + i \frac{\partial B}{2} \tilde{\eta}_{\nu} \right) D^{\rho}(\eta), \quad \xi = x-z, \quad \eta = z-y. \quad (14)$$

It is easy to show that for real  $fg$

$$\begin{aligned}
(\partial_x \phi^{ab}(x-y, z) f(x-z) g(z-y) &= \phi^{ab}(x, y) R_0 Q + \tilde{\phi}^{ab}(x, y) \tilde{R}_0 Q \\
(\partial_x \tilde{\phi}^{ab}(x-y, z) f(x-z) g(z-y) &= -\phi^{ab}(x, y) \tilde{R}_0 Q + \tilde{\phi}^{ab}(x, y) R_0 Q \\
Q &= (\partial_\gamma e^{i \frac{q^2}{2} \not{x}} \not{f} f(\not{t}) g(\not{\eta}), \quad \chi = \frac{t-y}{2}.
\end{aligned}
\tag{15}$$

Using these relations we get

$$\begin{aligned}
U_{\mu\nu}^{ab}(x, y) &= \phi^{ab}(x, y) R_0 Q_{\mu\nu}(x-y) + \tilde{\phi}^{ab}(x, y) \tilde{R}_0 Q_{\mu\nu}(x-y) \\
&= \int_{\sigma^2} \int_{\sigma^2} \left( \frac{d^4 k}{(2\pi)^4} e^{ik(x-y)} \frac{\hat{\mu} \hat{\nu}}{k^4} \right)
\end{aligned}
\tag{16}$$

with  $Q_{\mu\nu}(x-y)$  given in terms of  $P_{\mu\nu}(\not{t}, \not{\eta})$  from (14)

$$Q_{\mu\nu}(x-y) = (\partial_\gamma e^{i \frac{q^2}{2} \not{x}} \not{f} P_{\mu\nu}(\not{t}, \not{\eta}), \quad \not{t} = \frac{x-y}{2} + \not{\chi}, \quad \not{\eta} = \frac{x-y}{2} - \not{\chi}.
\tag{17}$$

In the expressions (14), (16), (17) we have now a convenient form which provides a starting point to construct a compact integral representation for and to study the analytic properties of the general gauge propagator  $G_{\mu\nu}^{ab}(x, y, \alpha)$  in a constant homogeneous background field.

A short summary of calculations of the 2-loop contributions to the imaginary part of the effective potential in terms of the background field propagators will be published in the Proceedings of the XXI International Symposium Ahrenschoop/Sellin 1987.

### References

- /1/ J. Ambjorn, R.J. Hughes, Ann. Phys.(NY) 145(1983)340
- /2/ W. Dittrich, M. Reuter: Effective Lagrangians in Quantum Electrodynamics, Springer-Verlag, Berlin 1985
- /3/ H.J. Kaiser, K. Scharnhorst, E. Wieczorek Proc. IX Int. Sympos. Ahrenschoop 1986
- /4/ H.J. Kaiser, K. Scharnhorst, E. Wieczorek Preprint PHE 87-9, Berlin-Zeuthen 1987

CRITICAL EXACTLY SOLVABLE MODELS AND CONFORMAL FIELD THEORY

V.V. Bazhanov

Institute for High Energy Physics,  
Serpuukhov, Moscow Region, USSR

**Abstract.** The eigenvalues of the transfer matrix of the generalized RSOS model are exactly calculated. From the consideration of the thermodynamics of the quantum system on the one-dimensional chain connected with the RSOS model, we calculate the central charges of the effective conformal field theories describing the critical behaviour of the model in different regimes.

The underlying algebraic structure of the 8-vertex model is a deformation of the universal enveloping algebra of  $sl(2)/\mathbb{Z}$ . From this point of view, the original 8-vertex model<sup>2,3</sup> corresponds to the spin  $s=1/2$  representation. The authors of<sup>4</sup> developed a method (called the fusion procedure) to construct the vertex models corresponding to the arbitrary spin representations. The generalized 8-vertex models obtained in this way were considered in ref.<sup>5</sup>.

In refs.<sup>6,7</sup> it has been shown that one can associate the ordinary 8-vertex model (of the spin  $s=1/2$ ) with a series of integrable RSOS (Restricted Solid-on-Solid) models which are of considerable interest due to their non-trivial critical behaviour.

Recently Date et al<sup>8</sup>, using the fusion procedure, have obtained integrable generalizations of the RSOS model of ref.<sup>7</sup>, corresponding to the "higher spin" 8-vertex models. The fluctuating variables in these models are integer "heights"  $\{\ell_i\}$ , assigned to sites of a square lattice. The Boltzman weights are non-vanishing only if

$$(\ell_i - \ell_j - L)/2 \in \{0, 1, \dots, L\}, \quad (1)$$

$$1 \leq \ell_i \leq r-1, \quad (2)$$

$$L < \ell_i + \ell_j < 2r-L, \quad (3)$$

where  $L=p$  for a horizontal pair of adjacent sites  $(i, j)$ ,  $L=q$  for a vertical one;  $p, q, r$  ( $r \geq \max(p, q) + 2$ ) are positive integers characterizing the model. Moreover there are two more parameters  $\hat{q}$  and  $v$  (as usual,  $v$  enters Yang-Baxter equations,  $\hat{q}$  is related to the modulus of elliptic functions, parametrizing the weights).

Note, that the generalized RSOS model is closely related to its vertex counterpart, the generalized 8-vertex model. Indeed, using the results from<sup>8</sup>, one can show that it can be considered as a "higher spin" 8-vertex model with some special boundary conditions.

In this paper, we present several exact results for the generalized RSOS model.

Using some specific properties of the Boltzman weights we obtain a system of functional equations which allows to calculate exactly the spectrum of the transfer-matrices  $T^{p, q}(v)$ . As usual, the eigenvalues are determined through the solutions of a system of transcendental equations. We show that up to an overall normalization and a shift of the parameter  $v$  the spectra of the transfer-matrices  $T^{p, q}, T^{p, q'}, T^{p', q}, T^{p', q'}$ , where  $p+p'=r-2, q+q'=r-2$  coincides. This means, that all physical characteristics of the model (e.g., such as critical exponents) should not change under independent transformations  $p \rightarrow r-2-p, q \rightarrow r-2-q$ .

The model becomes critical when  $\hat{q}=0$ . In this case there are two physically distinct regimes at  $p=q$

$$i) 0 \leq v \leq r/r; \quad ii) -\hat{r}/2 + \hat{r}/r \leq v \leq 0. \quad (4)$$

In work<sup>/9/</sup> Belavin, Polyakov, Zamolodchikov have developed a conformal bootstrap program to classify possible types of a universal critical behaviour and to calculate critical exponents. According to this approach, the critical behaviour of a two-dimensional statistical system at a second order transition point is described by some unitary<sup>/10/</sup> conformal field theory, specified by a value of the central charge of the (Virassoro) algebra of the conformal transformations. The parameters of this conformal theory can be extracted from the information about the spectrum of the transfer-matrix of the statistical system<sup>/11-13/</sup>.

At present, a number of conformal field theories are been constructed, in which the spectrum of the conformal dimensions is known exactly (see, e.g.<sup>/9, 10, 14-16/</sup>).

Returning to the RSOS model under consideration, define a (local) hamiltonian

$$H^p \approx \frac{d}{dv} \ell_{NT}^{p,p}(v) \Big|_{v=0} \quad (5)$$

of a one-dimensional quantum RSOS model on a chain of  $N$ -sites. In the critical case hamiltonian (5) has a gapless spectrum with the linear dispersion law in the vicinity of the Fermi level  $\xi(p) = v_F |p - p_F|$ . The value of the central charge  $c$  of the corresponding conformal field theory may be calculated<sup>/11-13/</sup>, on the one hand, from the leading finite-size correction to the ground state energy of hamiltonian (5) for the periodic boundary conditions

$$E_0 = N \epsilon_0 - \frac{\pi c v_F}{6N} + O\left(\frac{1}{N^2}\right) \quad (6)$$

and, on the other hand, from the low-temperature asymptotics of the specific free energy of the quantum system with hamiltonian (5) at  $N \rightarrow \infty$

$$\begin{aligned} \text{Tr} \langle e^{-\beta H} \rangle &= e^{-\beta N F(\beta)}, \\ F(\beta) &= \epsilon_0 - \frac{\pi c}{6v_F} \beta^{-2} + O(\beta^{-2}), \quad \beta \gg 1, \end{aligned} \quad (7)$$

where  $\beta = T^{-1}$  is an inverse temperature.

We take the second way and investigate the thermodynamics of the quantum RSOS model. In doing this, we use some hypothesis on the types of allowed string solutions to the transcendental equations, determining the spectrum of hamiltonian (5) within a thermodynamical limit. We verify our hypothesis for the cases  $p=1, r=3$  (completely ordered model) and  $p=1, r=4$  (Ising model), when the eigenvalues may be calculated exactly at finite  $N$  and suppose, that it is valid in a general case. In particular, this hypothesis leads to the true asymptotics of the dimension of the space of states of the quantum RSOS model, when  $N \rightarrow \infty$ .

The results for the central charges for two critical regimes (4) are of the form

$$1) c = \frac{3p}{p+2} \left(1 - \frac{2(p+2)}{r(r-p)}\right); \quad 1) c = 2 - \frac{6}{r}. \quad (8)$$

Both expressions are symmetric respect to the transformation  $p \rightarrow r-2-p$ , discussed above.

Note, that calculations with formula (6) should give the same values of the central charges. Using the method of ref.<sup>/17/</sup> one can show that it is indeed so for the case  $p=1$ , of regime 1). Moreover, we numerically establish this correspondence for several values of  $p$  and  $r$  in the regime 1). Moreover, we numerically establish this correspondence for several values of  $p$  and  $r$  in the regime 1). These results confirm our hypothesis used for the derivation of eq. (8).

The basic results of the talk were obtained in collaboration with N.Yu. Reshetikhin. The author is grateful to him.

### References

1. E.K.Sklyanin. - Funk. anal. prilozh. 16 (4), 27 (1982); 17 (4), 34, 1983.
2. R.J.Baxter. - Ann. Phys. 70, 193 (1972).
3. L.D.Faddeev, L.A.Takhtadjan. - Sov. Math. Uspekhi 34, 13 (1979).
4. P.P.Kulish, N.Yu.Reshetikhin, E.K.Sklyanin. - Lett. Math. Phys. 5, 393 (1981).
5. I.V.Cherednik. - Funk. anal. prilozh. 19 (1), 89 (1985);  
Yad. Fiz. 36, 549 (1982).
6. R.J.Baxter. - Ann. Phys. 76, 25 (1973).
7. G.E.Andrews, R.J.Baxter, P.J.Forrester. - J. Stat. Phys. 35, 193 (1984).
8. E.Date, M.Jimbo, T.Miwa, M.Okado. - Lett. Math. Phys. 12, 209 (1986).
9. A.A.Belavin, A.M.Polyakov, A.B.Zamolodchikov. - J. Stat. Phys. 34, 763 (1984); Nucl. Phys. B241, 333 (1984).
10. D.Friedan, Z.Qiu, S.Shenker. - Phys. Rev. Lett. 52, 1517 (1984).
11. J.L.Cardy. - Nucl. Phys. B270, 166 (1986).
12. H.W.Blötte, J.L.Cardy, H.P.Nightingale. - Phys. Rev. Lett. 56, 742 (1986).
13. I.Affleck. - Phys. Rev. Lett. 58, 746 (1986).
14. D.Friedan, Z.Qiu, S.Shenker. - Phys. Lett. B251, 37 (1985).
15. V.A.Fateev, A.B.Zamolodchikov. - ZhTF, 89, 380 (1985); *ibid.* 90, 1553 (1986).
16. V.A.Fateev, A.B.Zamolodchikov. - Teor. Mat. Fiz., 71, 163 (1987).
17. N.M.Bogoliubov, A.G.Izergin, N.Yu.Reshetikhin. - Pis'ma v ZhETF 44, 405 (1986).

A NON-RELATIVISTIC MODEL OF TWO-PARTICLE DECAY: RESONANCE  
AND BOUND STATES

J. Dittrich<sup>1</sup>, P. Exner<sup>1,2</sup>

<sup>1</sup>Nuclear Physics Institute of CSAS, Řež, Czechoslovakia

<sup>2</sup>Lab. Theor. Phys., JINR, Dubna, USSR

With the aim to verify some general properties of unstable particles on a simple solvable quantum mechanical model, a spinless particle decaying into two lighter particles is considered. The model is similar to the Lee [1] and Friedrichs [2] ones. The meromorphic structure of reduced resolvent [4], decay law [5], mutual scattering of two light particles [6] and the existence of bound states [6] are studied. A sample of results is presented here. Further details, proofs and references are given in [3 - 6].

1. The Model

After separating the center-of-mass motion, the relative motion part of the model acquires the following form. The space of states

$$\mathcal{H} = \mathbb{C} \oplus L^2(\mathbb{R}^3)$$

contains the subspaces  $\mathcal{H}_u = \mathbb{C}$  of undecayed unstable particle and  $\mathcal{H}_d = L^2(\mathbb{R}^3)$  of decay products, corresponding to the relative motion of two light particles. The Hamilto-



nian in the momentum representation acts on the state  $\psi \in \mathcal{X}$  as

$$H_g \psi = \begin{pmatrix} E & g(\hat{v}, \cdot) \\ g\hat{v}(\vec{p}) & \frac{\vec{p}^2}{2m} \end{pmatrix} \begin{pmatrix} \mathcal{L} \\ \hat{\psi}(\vec{p}) \end{pmatrix} = \begin{pmatrix} E\mathcal{L} + g(\hat{v}, \hat{\psi}) \\ \mathcal{L}g\hat{v}(\vec{p}) + \frac{\vec{p}^2}{2m} \hat{\psi}(\vec{p}) \end{pmatrix}$$

where  $E > 0$  is the energy released in the decay,  $m$  the reduced mass of the decay products, and  $g$  the coupling constant. The function  $\hat{v}$  determining the interaction is assumed to satisfy the following conditions:

- i)  $\hat{v}(\vec{p}) = v_1(|\vec{p}|)$  with  $\hat{v}_1 \in L^2(\mathbb{R}^+, p^2 dp)$   
(rotational symmetry)
- ii) defining  $v_2(p) = |\hat{v}_1(p)|^2 p$  and  $v_3(\lambda) = v_2(\sqrt{2m\lambda})$ , the function  $v_3$  can be holomorphically extended into a neighbourhood of real positive semiaxes in the complex plane;
- iii)  $\hat{v}_1(\sqrt{2mE}) \neq 0$  ;
- iv)  $|\hat{v}_1|^2 \leq C_1$  ,  $v_2 \leq m C_1$  ,  $|v_2'| \leq C_1$  ,  $m |v_2''| \leq C_1$   
for some constant  $C_1$  .

## 2. Reduced Resolvent, Decay Law and Scattering

The reduced resolvent is defined as

$$R_u(z) = E_u (H_g - z)^{-1} E_u = r_u(z) E_u \quad (z \in \mathbb{C} \setminus \mathbb{R}^+)$$

where  $E_u$  is the projection onto the subspace  $\mathcal{X}_u$  in  $\mathcal{X}$ . The function  $r_u$  can be analytically continued from the upper half-plane into a complex neighbourhood  $\Omega$  of  $E$ . For a suf-

ficiently small coupling constant  $g$ , the continued function  $r_u^{\Omega}$  has in  $\Omega$  just one singularity - a simple pole at  $Z = Z_p(g)$  with  $\text{Im } Z_p(g) < 0$ .

The decay law  $P(t) = |u(t)|^2$  is given by the function  $u(t)$  defined by the relation

$$E_u e^{-iH_g t} \begin{pmatrix} 1 \\ 0 \end{pmatrix} = \begin{pmatrix} u(t) \\ 0 \end{pmatrix} .$$

For a sufficiently small  $g$ , the inequality

$$|u(t) - A e^{-iZ_p t}| \leq \frac{Cg^2}{t} , \quad (1)$$

$$A = [1 - g^2 G'_\Omega(Z_p)]^{-1}$$

holds for  $t > 0$  with a constant  $C > 0$  independent of  $g$ .

Function  $G_\Omega$  is the analytic continuation of

$$G(Z) = 4\pi \int_0^\infty \frac{|\hat{V}_1(p)|^2 p^2 dp}{Z - \frac{p^2}{2m}}$$

from upper complex half-plane into  $\Omega$ . Inequality (1) shows that the decay law is approximately exponential with the width given by  $\text{Im } Z_p = O(g^2)$  in the region of times comparable with  $(\text{Im } Z_p)^{-1}$ .

The mutual scattering of two light particles is well defined since the wave operators  $\Omega_\pm$  can be shown to exist and be complete (i.e.  $\text{Ran } \Omega_\pm = \text{Ran } P_{ac}(H_g)$ ); if  $\hat{V}_1$  has piecewise continuous derivative, they are also asymptotically complete (i.e.  $\sigma_{\text{sing}}(H_g) = \emptyset$ ). The R-matrix can be written as

$$R(\vec{p}, \vec{p}') = 2\pi i m g^2 |\hat{v}_1(p)|^2 p r_u^a \left( \frac{p^2}{2m} \right) \quad (2)$$

where  $\vec{p}$  and  $\vec{p}'$  are the initial and final momenta. We see that the scattering is isotropic and that the analytically continued S-matrix has the same pole as the reduced resolvent. The presence of the pole  $Z_p$  leads to the resonance behaviour of the cross-section and s-wave phase shift.

### 3. Bound States

The following statements about the existence of bound states (eigenstates of  $H_g$ ) can be shown assuming  $g \neq 0$ .

i)  $\epsilon > 0$  is an eigenvalue of  $H_g$  if and only if

$$\hat{v}_1(\sqrt{2m\epsilon}) = 0$$

and

$$\epsilon = E + 4\pi g^2 \int_0^\infty \frac{|\hat{v}_1(p)|^2 p^2 dp}{\epsilon - \frac{p^2}{2m}}$$

ii)  $\epsilon = 0$  is an eigenvalue of  $H_g$  if and only if

$$\int_0^\infty \frac{|\hat{v}_1(p)|^2}{p^2} dp < \infty$$

and

$$E = 8\pi g^2 m \int_0^\infty |\hat{v}_1(p)|^2 dp$$

iii) There is at most one bound state with a negative energy; it exists if and only if

$$g^2 > g_{cr}^2 = E \left[ 8\pi m \int_0^\infty |\hat{v}_1(p)|^2 dp \right]^{-1}$$

## References

- [1] Lee T. D., Phys. Rev. 95(1954)1329.
- [2] Friedrichs K. O., Commun. (Pure and) Appl. Math. 1(1948)361.
- [3] Dittrich J., Exner P., Czech. J. Phys. B37(1987)503.
- [4] Dittrich J., Exner P., Czech. J. Phys. B37(1987)1028.
- [5] Dittrich J., Exner P., preprint JINR E2-86-750, Dubna 1986.
- [6] Dittrich J., Exner P., preprint JINR E2-87-599, Dubna 1987.

THE TRIPLE PROBLEM OF CONVERGENCE IN THE PERTURBATION  
EXPANSIONS WITH NON-DIAGONAL PROPAGATORS;

M. Znojil<sup>a/</sup>, M. F. Flynn<sup>b/</sup> and R. F. Bishop<sup>b/</sup>

<sup>a/</sup> Nucl. Phys. Institute, Řež, Czechoslovakia

<sup>b/</sup> UMIST, Manchester, United Kingdom

Let us consider the standard perturbation theory of the Rayleigh-Schrödinger type, with the Hamiltonian split

$$H = H_0 + g H_1 \quad /1/$$

and pair of ansatzs

$$E = E_0 + g E_1 + g^2 E_2 + \dots \quad /2/$$
$$|\psi\rangle = |\psi_0\rangle + g |\psi_1\rangle + \dots$$

Their insertion in the Schrödinger equation  $H|\psi\rangle = E|\psi\rangle$  leads to a RS hierarchy of relations

$$H_0 |\psi_0\rangle = E_0 |\psi_0\rangle \quad /3/$$

and

$$H_0 |\psi_k\rangle + H_1 |\psi_{k-1}\rangle = E_0 |\psi_k\rangle + \dots + E_k |\psi_0\rangle \quad /4/$$

with  $k = 1, 2, \dots$

In a textbook spirit, we may interpret  $E_1, E_2, \dots$  as abbreviations,

$$E_n = \frac{1}{\langle \psi_0 | \psi_0 \rangle} \langle \psi_0 | (H_0 | \psi_n \rangle + H_1 | \psi_0 \rangle - E_n | \psi_n \rangle), \dots \quad /5/$$

and, inserting them in /4/, eliminate formally also the wavefunction corrections,

$$| \psi_n \rangle = \frac{1}{E_n - H_0} (H_0 | \psi_0 \rangle - E_n | \psi_0 \rangle), \dots \quad /6/$$

In this way, perturbation theory may be interpreted as a reduction of the full problem to its simplified version /3/.

The "simplicity" of  $H_0$  is usually specified as a possibility of its complete diagonalisation. In the modified RS /MRS/ approach<sup>1</sup>, the "simplicity" of  $H_0$  is weakened: in a given "unperturbed" basis  $|0\rangle, |1\rangle, \dots$ , we admit all operators  $H_0 = T + |0\rangle g \langle 0|$  with a free parameter  $g$  and "invertible" matrix  $T$ , i.e., with such a matrix that we may obtain also an explicit form of the operator  $R$  /with, say,  $R = 1/(E_0 - T)$  where  $E_0$  is a function of  $g$ /.

The main MRS idea is simple - we have noticed that an explicit knowledge of  $R$  and  $V$  specifies already all the corrections /5/ and /6/, while a presence of a free parameter  $g$  enables us also to get rid of the eigenvalue problem /3/<sup>1</sup>. Indeed, we may write, in an explicit manner,

$$| \psi_0 \rangle = R | 0 \rangle g \langle 0 | \psi_0 \rangle, \quad \langle 0 | \psi_0 \rangle \neq 0 \quad /7/$$

$$g = g(E_0) = 1 / \langle 0 | R(E_0) | 0 \rangle.$$

In practice, it is useful to write  $g = g(E_0)$  and treat  $E_0$  as a free parameter itself.

There is one important reason for using non-diagonal  $T$  in the split /1/ - we may make  $H - H_0$  as small as necessary for a good convergence of the expansions /2/. There is a price to be paid of course - we must guarantee a quick practical convergence also in a transition  $T \rightarrow R$  and in the corresponding MRS forms of prescriptions /5/ and /6/.

### 1. The $T \rightarrow R$ convergence.

The simplest way how to define  $R$  is a brute-force numerical inversion of the truncated matrices  $N \times N$ . In Ref.<sup>1</sup>, the related  $N \rightarrow \infty$  convergence has been reduced to a continued-fractional convergence, by means of a restriction of  $T$ 's to tridiagonal matrices. In Ref.<sup>2</sup>, this procedure has been extended to  $2s+1$  - diagonal  $T$ 's. An alternative, purely non-numerical type of the  $T \rightarrow R$  transition<sup>3</sup> represents one of the possible final solutions of this problem - we may reconstruct any trial  $T'$  into an "invertible" one simply by its fixed-point re-arrangement  $T' = T + \text{corrections}$ . Numerically, this has been illustrated elsewhere<sup>3</sup> - we may only summarize here that there are no problems with the first,  $N \rightarrow \infty$  type of convergence in practice, since its "residuum" may simply be incorporated in the perturbation itself.

## 2. The intermediate-summation convergence.

Each MRS contribution, say,  $E_k$ , is defined as a RS-type sum over intermediate states. Each insertion of R represents a single summation in the RS formalism - here, the summation goes over the two /left and right/ indices. The related "additional" convergence problem may again be eliminated in the same manner as above - we may modify the input unperturbed propagator  $R'$  /general matrix/ and use its  $2t+1$  - diagonal part only,  $R' \rightarrow R'/t$ ,  $t < \infty$ . Again, the related modification of  $T' \rightarrow T'/t$  (= a general matrix now) is, in effect, again a mere re-definition of the perturbation.

The numerical tests of the above idea may again be found elsewhere<sup>4</sup> and illustrate, for the cut-offs  $t$  decreasing from infinity, an emergence of the RS-type asymptotic-series divergence, especially for small  $t$  (= 0 or 1) ~~in~~ an opposite setting, the analysis of the  $t \rightarrow \infty$  limit supports a hypothesis of the MRS convergence - see Table 1 here, which lists the "optimal orders" /giving the optimal asymptotic-series MRS results/for anharmonic oscillators as analysed in Ref.<sup>4</sup>.

---

Table 1. An "optimal order"  $N_0$  as a function of  $t$ .

$t$	0	1	3	5	7
$N_0$	2	2	4	6	10



3. The numerical indications of the MRS convergence of energies.

For any coupling  $\lambda$  of anharmonicity  $x^4$ , we may choose H with another coupling  $\lambda_0$  as a matrix T. For a broad range of  $\lambda_0$ , we obtain results exemplified here in Figure 1.

A similar pattern is obtained also for the very broad range of parameters  $E_0$ . For the variable  $\lambda_0$  we obtain the dependence illustrated here in Figure 2 for  $\lambda = 1$ .

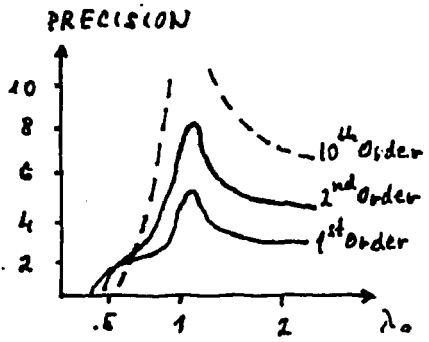


Fig. 2

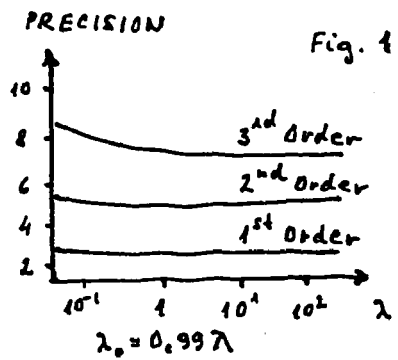


Fig. 4

We may see that the  $\lambda_0 < 1$  part of the latter Figure is a curve with an inflection point which is almost order-independent. - We believe that the MRS con-

vergence is very good for  $\lambda_0 > \lambda^{(\text{inflection})}$  and conjecture that  $\lambda_0^{(\text{inflection})} \leq 1$  is a "natural" boundary of the convergence domain, or at least of a domain of a reliable use of the MRS asymptotic series.

Références.

- 1/ M. Znojil, Phys. Rev. A 35 /1987/ 2448.
- 2/ - " - , Dubna, JINR communication E5 - 87 - 634.
- 3/ ibid., E4 - 87 - 655, 4/ ibid., E4 - 87 - 667.

Remarks on angular distributions of muon pairs  
in high energy hadronic collisions

Mikuláš Blažek

Institute of Physics, EPRC, Slovak Academy of Sciences,  
842 28 Bratislava, Czechoslovakia

Experimental investigation of the hadronic production of muon pairs brought just recently very interesting results. In the present contribution the angular distributions of these muons are studied. It is shown that a simple approach involving coherent state expansions allows to obtain a closed expression for the angular distributions under consideration. It generalizes the well known expressions like the "naive" Drell-Yan and the lowest order QCD angular distribution of dimuons arising from decays of virtual photons and  $Z^0$ 's. The influence of the parity violating terms is mentioned too.

1. Introduction. An early analysis of the angular distribution of muons in the dimuon rest system led to the "naive" Drell-Yan model [1] with

$$d\sigma/d\cos\vartheta d\varphi \sim 1 + \lambda \cos^2\vartheta \quad (1)$$

where  $\lambda = 1$  and  $\vartheta$  characterizes the polar angle. (In accordance with other approaches also our analysis is performed in the Collins-Soper reference frame [2] where the effects of smearing and nuclear reinteractions are minimal.)

If the transverse momentum  $p_T$  of dimuons is not negligible, the cylindrical symmetry of (1) is broken and dependence on the azimuthal angle  $\varphi$  appears,

$$d\sigma/d\cos\vartheta d\varphi \sim 1 + \lambda \cos^2\vartheta + \mu \sin 2\vartheta \cos\varphi + (\nu/2) \sin^2\vartheta \cos 2\varphi. \quad (2)$$

Especially, if it is assumed that in hadronic collisions the dileptons arise from decays of virtual photons and  $Z^0$ 's at large mass and finite transverse momentum, the angular distribution of the form (2) is obtained in the lowest order

---

Contribution to the Hadron Structure '87 Conference, Smolenice,  
Czechoslovakia, November 16-20, 1987

QCD and the Weinberg-Salam model with three fermion generations [3]. The right hand side of (2) is influenced only by the parity conserving terms.

The NA 10 Collaboration has taken data at the CERN SPS Collider and it studied the production of muon pairs of high mass by high-intensity negative pion beams of 140, 194 and 286 GeV/c off deuterium and tungsten targets. The analysis of the angular distributions of the muons in the dimuon rest frame already published for the 194 GeV/c data [4] has been refined and extended to the 140 and 286 GeV/c data [5]. In this respect the conclusions of ref. [6] can be shortly formulated as follows: (i) the parameter  $\lambda$  in (1) is observed to be essentially constant and close to unity, at all three energies, (ii) the parameter  $\mu$  is found to be compatible with zero, (iii) the parameter  $\nu$  is observed to increase markedly with  $p_T$ , in clear disagreement with the perturbative QCD prediction [7]; (iv) then the Callan-Gross relation

$$1 - \lambda = 2\nu \quad (3)$$

established for the perturbative QCD is evidently not satisfied by the data of ref. [6] and (v) the angular distributions of muon pairs produced off the deuterium target at 286 GeV/c are in excellent agreement with those produced off tungsten, indicating that this discrepancy (mentioned in (iv)) is not due to a nuclear effect.

Those conclusions call for generalization of rel. (2). In the next sections we show that such a generalization can be obtained in a simple approach involving the coherent state expansions.

2. Angular distributions in terms of coherent states. In the present approach we apply the coherent state expansions as they were treated essentially by Glauber [8] and Lachs [9].

First of all, the conclusion (v) of the preceding section leads us to the assumption that in the phase space the number of emitting centers (or modes) depends (if at all) only very weakly on the kind of the nucleus. With respect to the results obtained on the deuterium we shall deal only

with one emitting cell (mode). We assume that the one-mode field (1) is a mixture of stochastic and coherent states [8] with  $\langle n_T \rangle$  being the average number of stochastically produced secondaries and  $\langle n_C \rangle \equiv |\beta|^2$  corresponds to the coherently produced ones; the parameter  $\beta$  is the complex eigenvalue of the coherent field [8], [9]. The average value of the total (charged) multiplicity  $\langle n \rangle = \langle n_T \rangle + \langle n_C \rangle$ ; and (ii) it gives rise to secondary particles whose x-, y- and z-coordinates are correlated (in the phase space).

In the one-dimensional case [9] the probability to observe the coordinate  $q$  is given by  $P(q) = \int P(\alpha) |\langle \alpha | q \rangle|^2 d^2\alpha$  where for the mixed field  $P(\alpha) = [1/(\pi \langle n_T \rangle)] \exp[-|\alpha - \beta|^2 / \langle n_T \rangle]$  and

$$|\langle \alpha | q \rangle|^2 = \text{const.} \exp\left\{-\left[(q - b \cdot \text{Re} \alpha) / (\sqrt{2} \cdot \sigma)\right]^2\right\}. \quad (4)$$

With respect to that one-dimensional case (4), now the corresponding three-dimensional Gaussian distribution is involved containing the dispersions  $\sigma_j$ , the parameters  $b_j$  characterizing the non-centralities and the correlation matrix  $\rho_{j,k}$  (always  $j, k = 1, 2, 3$ ) where  $\rho_{j,k} = \rho_{k,j}$  and  $\rho_{j,j} \equiv 1$  (we put  $\rho_{12} = \rho_{23} = \rho_{31} \equiv \rho$ ).

Introducing the spherical coordinates,

$$x = r \sin \vartheta \cos \varphi, \quad y = r \sin \vartheta \sin \varphi, \quad z = r \cos \vartheta$$

and performing the necessary integrations we obtain eventually the marginal probability in angular variables  $(\cos \vartheta, \varphi)$  in the following exact form,

$$d\sigma / d\cos \vartheta d\varphi = \text{const.} (2g_1)^{-3/2} [\exp(v^2/4)] \cdot D_{-3}(v \equiv g_2 / (2g_1)^{1/2}). \quad (5)$$

In rel. (5),  $D_{-3}(v)$  is the function of the parabolic cylinder. It holds,

$$[D_{-3}(v)] \exp(v^2/4) = 2^{-3/2} \cdot [\sqrt{\pi} \cdot F(3/2, 1/2, v^2/2) - 2\sqrt{2} \cdot v \cdot F(2, 3/2, v^2/2)] \quad (6)$$

where  $F(a, b, u)$  is the degenerate (confluent) hypergeometrical function,

$$F(a, b, u) = 1 + \frac{a}{b} u + \frac{a(a+1)}{b(b+1)} \frac{u^2}{2!} + \dots$$

The functions  $g_1$  and  $g_2$  in (5) are given as follows,

$$a) \quad g_1 = a_{00} \left( 1 + \sum_{n=1}^5 \epsilon_n v_n \right) / 2 \quad (7)$$

where

$$\begin{aligned} v_1 &= \cos^2 \vartheta, & v_2 &= \sin^2 \vartheta \cos 2\varphi, & v_3 &= \sin 2\vartheta \cos \varphi, \\ v_4 &= \sin^2 \vartheta \sin 2\varphi, & v_5 &= \sin 2\vartheta \sin \varphi \end{aligned} \quad (8)$$

and

$$\epsilon_1 = (2a_{33} - a_{11} - a_{22}) / a_{00}, \quad \epsilon_2 = (a_{11} - a_{22}) / a_{00}, \quad (9)$$

$$\epsilon_3 = -2a_{13} / a_{00}; \quad \epsilon_4 = -2a_{12} / a_{00}, \quad \epsilon_5 = -2a_{23} / a_{00}$$

with  $a_{00} = a_{11} + a_{22}$ . In (9),

$$a_{jj} = (1 + \rho) / [2\sigma_j^2(1 - \rho)(1 + 2\rho)] - f_j^2 / A,$$

$$a_{jk} = \rho / [2\sigma_j \sigma_k (1 - \rho)(1 + 2\rho)] + f_j f_k / A, \quad \text{with } j \neq k$$

and

$$f_j = \left\{ (b_j / \sigma_j) - [\rho / (1 + 2\rho)] \cdot \sum_{k=1}^3 (b_k / \sigma_k) \right\} / [2\sigma_j (1 - \rho)],$$

$$A = \langle n_T \rangle^{-1} + \left\{ \left[ \sum_{k=1}^3 (b_k / \sigma_k)^2 \right] + \rho \left[ \sum_{k=1}^3 (b_k / \sigma_k) \right]^2 \right\} / [2(1 - \rho)(1 + 2\rho)].$$

The angular functions  $v_n$  ( $n=1, \dots, 5$ ), from (8), entering (7) represent the parity conserving terms, i.e. they do not change the sign under the transformation

$$\vartheta \rightarrow \vartheta' = \pi - \vartheta, \quad \varphi \rightarrow \varphi' = \varphi + \pi; \quad (10)$$

b) the function  $g_2$  in (5) is given as follows,

$$g_2 = -2(a_1 l_1 + a_2 l_2 + a_3 l_3) \quad (11)$$

where

$$l_1 = \sin \vartheta \cos \varphi, \quad l_2 = \sin \vartheta \sin \varphi, \quad l_3 = \cos \vartheta \quad (12)$$

and

$$a_j = f_j \cdot \text{Re} \beta / (\langle n_T \rangle A). \quad (13)$$

The angular functions (12) represent the parity violating terms (they change sign under the transformation (10)). If

they do not vanish, their even powers -appearing through the even powers of the variable  $v$  in rel.(5)- contribute also to the parity conserving part. The normalization factor "const" in rel.(5) can be expressed in terms of the parameters  $a_j$  and  $a_{jk}$ ; we don't give here its explicit form.

3. Application of rel.(5) to the data of the NA 10 Collaboration [4],[5],[6],[10]. From the analysis [4] we know that the parity violating terms are very small; we put all  $a_j = 0$ , i. e.,  $\varepsilon_2 = 0$ . Then

$$d\delta/d\cos^2\varphi \sim (\varepsilon_1)^{-3/2} . \quad (14)$$

Now, let us assume that the summation in  $\varepsilon_1$ , rel.(7), satisfies the following condition,

$$\left| \sum_{n=1}^5 \varepsilon_n v_n \right| < 1. \quad (15)$$

Then

$$d\delta/d\cos^2\varphi \sim 1 + \sum_{n=1}^5 (-3/2)\varepsilon_n v_n . \quad (16)$$

All NA 10 analyses conclude that not only the parameter  $\mu$  (in the present approximation,  $\mu = (-3/2)\varepsilon_3$ ) is compatible with zero but also the parameters  $\varepsilon_4$  and  $\varepsilon_5$  do so. Therefore we can write,

$$d\delta/d\cos^2\varphi \sim 1 + (-3/2)\varepsilon_1 v_1 + (-3/2)\varepsilon_2 v_2 \quad (17)$$

where  $v_1, v_2$  and  $\varepsilon_1, \varepsilon_2$  are given by (8) and (9), respectively.

In our approach, rel.(17) is obtained from (5) if there is no correlation in the phase space ( $\rho = 0$ ) and all three Gaussian distributions are central (all  $b_j = 0$ ). In this case the coefficients  $\varepsilon_1, \varepsilon_2$  contain two parameters, say  $(\sigma_1/\sigma_3)^2 \equiv S_1$  and  $(\sigma_2/\sigma_3)^2 \equiv S_2$ . If they are independent there is no Callan-Gross relation. However, if they are related by the relation  $S_2 = (6 + M.S_1)/13$  then the relation (3) is satisfied.

Moreover, if  $\sigma_1^2 = \sigma_2^2 = \sigma_0^2$  then the cylindrical symmetry appears (in (2) also  $v = 0$ ); now the Drell-Yan distribution (1) is obtained with  $\sigma_0^2 = 2\sigma_3^2$ .

If only the parity violating terms vanish (e.g. due to  $\text{Re}\beta \sim 0$ ), the angular distribution is given by (14) or (16). Those expressions contain five coefficients,  $\varepsilon_n$  ( $n=1, \dots, 5$ ). In this case, with the assumption like  $b_1 = b_2 = b_3 \equiv b_0$  and  $\sigma_1 = \sigma_2 \equiv \sigma_0$  we meet five free parameters, namely  $\varphi$ ,  $\langle n_T \rangle$ ,  $b_0$ ,  $\sigma_0$ ,  $\sigma_3$ .

Let us retain the parity violating terms in (5). If they are small and the condition (15) is satisfied then their presence in the angular distribution is manifested by the terms like  $\cos\vartheta$ ,  $\sin^2\vartheta \cos\varphi$ ,  $\sin^2\vartheta \sin\varphi$ ,  $\cos^2\vartheta$  etc (and moreover they will influence also the coefficients multiplying the parity conserving terms as it is seen in (5)). In this way one can conclude about the presence of the parity violation.

Relation (16) can be applied also to the description of the muon-proton data obtained by the EMC Collaboration, ref.[11].

**4. Conclusion.** We showed that the application of the coherent state expansions allows to derive the expression for the angular distribution of the muon pairs (5) which generalizes the Drell-Yan distribution (1) as well as the one obtained in the lowest order QCD (2). This generalized distribution can be applied also in the cases when the Callen-Gross relation (3) is not satisfied.

#### R e f e r e n c e s :

- [1] S.D. Drell and T.M. Yan, Phys. Rev. Lett. 25 (1970) 316.
- [2] J.C. Collins and D.E. Soper, Phys. Rev. D 16 (1977) 2219.
- [3] M. Chaichian, M. Hayashi and K. Yamaguchi, Phys. Rev. D 25 (1982) 130.
- [4] S. Falciano et al., (NA 10 Collab.), Z. Phys. C 31 (1986) 513.
- [5] M. Guanziroli et al. (NA 10 Collab.): Angular distributions of muon pairs produced by negative pions on tungsten (contribution No. 270 to the Int'l Symp. on Lepton and Photon Int's at High Energies, Hamburg, July 1987).

- [6] H. Suter : Recent results of NA 10 experiment on the hadronic production of muon pairs (contribution to the Int'l Europhysics Conference on High Energy Physics, Uppsala, June-July 1987).
- [7] P. Chiappetta and M. Le Bellac, Z. Phys. C 32 (1986) 521.
- [8] R. Glauber, Phys. Rev. 131 (1963) 2766.
- [9] G. Lachs, Phys. Rev. 138 (1965) B 1012.
- [10] V. L. Telegdi (NA 10 Collaboration): Drell-Yan process, angular and  $p_T$  distributions. (Proc. Int'l. Europhysics Conference on High Energy Physics, Bari, July 1985; p. 477).
- [11] M. Arneodo et al., Z. Phys. C 34 (1987) 277 .



## ENTROPY IN THE MULTIPARTICLE PRODUCTION

V. Šimák

Inst. of Physics, Czech. Acad. Sci.,  
Na Slovance 2, CS 180 40 Prague, Czechoslovakia

M. Šumbera and I. Zborovský

Nucl. Phys. Inst., Czech. Acad. Sci.,  
CS 250 68 Řez near Prague, Czechoslovakia

Experimental results from the CERN SPS Collider have considerably changed our understanding of asymptotic behavior of multiparticle production/1/. Multiplicity distributions of particles in the full phase space and also in different rapidity windows are usually analysed using the statistical moments/1-4/, their energy dependence being interpreted in terms of KNO scaling /5/ and its possible violation/1,2,8,9/.

In the present contribution we would like to point out and exploit a different strategy/6/. We introduce a new quantity characterizing charged particle multiplicity distributions - entropy /7/:

$$S = - \sum P(N) \ln P(N) \quad (1)$$

Let us mention some properties of this quantity:

(i) The entropy describes a general pattern of independent particle emission. Total entropy produced from  $\nu$  statistically independent phase space regions (e.g. Poisson distributed clans or superclusters /8/) is equal the sum of entropies of individual sources

$$S = S_1 + S_2 + \dots + S_\nu.$$

Hence, for correlated sources with known entropy, their total entropy can be used to evaluate correlation strength among them.

(ii) Contrary to the statistical moments the entropy is invariant under arbitrary distortion of multiplicity scale (i.e. different shapes of multiplicity distribution can have the same value of entropy). For instance the entropy calculated from charged and negative particles data in the full phase space give the same value of S.

(iii) There is a simple relation between S, average multiplicity  $\langle N \rangle$  and KNO function  $\psi(z)$ :

$$S = \ln \langle N \rangle + H/2 \quad (2)$$

where

$$H = - \int \psi(z) \ln(\psi(z)) dz \quad (3)$$

is the entropy of KNO function  $\psi(z)$ , normalized

$$\int \psi(z) dz = \int z \psi(z) dz = 2. \quad (4)$$

(iv) There exists a natural bound:

$$S - \ln(\langle N \rangle / 2) \leq 1 \quad (5)$$

which follows from the maximization of the entropy  $H$  within the class of KNO functions fulfilling usual normalization conditions (4) given above.

Entropy in full phase space.

Experimental situation concerning evolution of the entropy with c.m.s. energy  $\sqrt{s}$  for pp,  $\bar{p}p$ ,  $\gamma p$ ,  $n-p$ , K+p, K-p, inelastic interactions /1-4,9/ is presented in fig.1. Increase of entropy with energy seems to be approximately similar for all hp interactions and reveals a universal asymptotic linearity with  $\ln s$ :

$$S = 0.4 \ln \sqrt{s} + 0.8 \quad (6)$$

In addition to this, when expressed as a function of a maximum rapidity of produced hadrons  $Y_m = \ln(\sqrt{s})/m_\pi$ :

$$S = (0.417 \pm 0.005) Y_m \quad (7)$$

This suggests, that in hh collisions the entropy per unit of rapidity  $S/Y_m$  is universal and the energy independent quantity.

The observed behaviour of entropy together with limiting property (5) puts severe restriction on the energy dependence of both  $\langle N \rangle$  and  $\Psi(z)$  of charged particles. We illustrate this statement in fig.2. Experimental data up to  $\sqrt{s} = 900$  GeV are yet far from saturation of the bound

$$-\int \Psi(z)/2 \ln(\Psi(z)/2) dz = S - \ln(\langle N \rangle/2) \leq 1 \quad (8)$$

Approximate energy independence of  $\Psi(z)$  (early KNO scaling) is violated by Collider data, but the behaviour of multiplicity at still higher energies must be governed by the upper bound (8). Consequently the onset of ultimate multiplicity scaling is expected in a few TeV region (fig.2). Furthermore either the entropy  $S$  must slow down, violating (7), or the average charged multiplicity  $\langle N \rangle$  must grow faster with the energy than the present parametrization of the data indicates /1/. In the later case extrapolation of (7) to the asymptotic region gives:

$$\langle N \rangle \sim s^{0.14 \pm 0.02}$$

Using the FNAL /10/ and ISR /11/ data on multiplicities of charged or negative particles from pd, p $\bar{p}$ ,  $\bar{p}p$  inelastic interactions we try to extend the observed regularity to the case of high energy collisions of lightest nuclei (fig.3). Agreement with the universal hp curve is surprisingly good and helps to fill the gap between pp ISR and pp Collider data (for calculation of  $Y_m$  we have used the total c.m.s. nucleus-nucleus energy).

Entropy in rapidity windows.

Data on multiplicity distributions in central intervals of centre-of-mass (pseudo) rapidity  $|y| < y_c/3, 4, 12$  may be used to study the evolution of entropy with the central rapidity window width  $y_c$  starting from a very small central windows up to  $Y_m$ . Charge conservation, which restricts the multiplicities of

charged particles in the full phase space to their even values and makes entropies, calculated from data on negative and charged particles equal to each other, is no more applicable when discussing the windowing data. At present only one set of experimental data exists on multiplicity distributions of both negative and charged particles in different rapidity intervals (at  $\sqrt{s} = 22 \text{ GeV}$  /3,4/). We have studied the dependence of entropy on  $y_c$  using these data. Contrary to the entropy of negative particles, the entropy of charged ones reveals a non monotonic behaviour with  $y_c$ . This may be understood as a result of long range correlations between oppositely charged particles which manifest themselves in full phase space. Supposing that particles are produced via neutral clusters consisting of two oppositely charged hadrons /13/, one can, with the help of information from the first three moments of the multiplicity distribution of charged particles /14/, extract the multiplicity distribution of negative ones for Collider data, too.

The dependence of  $S$  on the central rapidity window width  $y_c$  is not linear contrary to its dependence on  $Y_m$ . Extension of energy independence of ratio  $S/Y_m$  into a smaller rapidity intervals is nevertheless possible. The data, when plotted in the form  $S(y_c)/Y_m$  versus a reduced rapidity  $\xi = y_c/Y_m$ , indeed reveal a satisfactory scaling behaviour (fig.4).

From fig.4 it follows that the entropy reaches its full phase space value quite early, for  $\xi > 0.5$ ; a remarkable fact, bearing in mind that first two moments of multiplicity distribution are still noticeably changing /3,12/ within this region. Thus the entropy production in fragmentation region seems to be negligible.

For semiinclusive rapidity distributions the scaling in reduced rapidity  $\xi$  has been proposed a long ago /15/. Its connection with observed violations of KNO scaling has been revived recently from the point of view of clusters /16/. Original arguments in favor of this scaling law were based on Feynman's analogy between statistical properties of (one dimensional) fluid contained inside finite volume and distribution of produced particles in rapidity space. The longitudinal geometric scaling /15/ states that this distribution of particles does not change with external volume  $Y_m$  provided we use instead of rapidity  $y$  its reduced value  $\xi$  to label particle's position inside the volume. Such type of selfsimilarity need not be generally true for any fluid. On the other hand an extensive character of both the volume and the entropy of the fluid guarantees that entropy of the multiplicity distribution should be always a homogenous function of its volume  $y_c$ :

$$S(\lambda y_c) = \lambda S(y_c). \quad (9)$$

Taking  $\lambda = 1/Y_m$  we get the scaling law of fig.4.

#### ----- Particle density in the central region. -----

To study consequences of the above regularity for particle production in the central region we present in fig.5 dependence of  $S$  on  $\langle N \rangle$  for windows with  $\xi < 0.25$ . For these small rapidity intervals all energy dependence of  $S$  is within a reasonable

accuracy given entirely by its dependence on  $\langle N \rangle$ . Analytical expression

$$S = \ln(\langle N \rangle) + (\langle N \rangle + 1) \ln(1 + 1/\langle N \rangle) \quad (10)$$

valid for the entropy of geometrical distribution, represent also a good approximation of the data. Given the values of  $y_c$  and  $Y_m$  one can, using the entropy scaling (fig.4), predict  $S$  and hence (from fig.5) also the average charged multiplicity and particle density in the central region at Collider energies/17/ and beyond (fig.6).

In conclusion, we would like to stress the general character of observed empirical regularities in entropy, which underlines once again the statistical character of multiparticle production in soft hadronic collisions.

#### References

- /1/ UAS Collab., G.J. Auner et al., Phys.Lett. B138(1984)394, ibid B167(1986)476.
- /2/ UAS Collab., G.J. Auner et al., Phys.Lett. B160(1985)199.
- /3/ NA22 Collab., M. Adamus et al., Phys.Lett. B177(1986)239.
- /4/ W. Meyers, Ph.D. Thesis, Nijmegen 1987.
- /5/ Z. Koba, H. B. Nielsen and P. Olesen, Nucl. Phys. B40(1972)317.
- /6/ V. Šimák, M. Šumbera and I. Zborovský, Proc. Int. Europhysics Conf. on High Energy Physics, Uppsala, Sweden, June 1987.
- /7/ A. Wehrl, Rev. Mod. Phys. 50(1978)221.
- /8/ A. Giovannini and L. Van Hove, Z. Phys. C30(1986)391; V. Šimák and M. Šumbera, Czech. J. Phys. B36(1986)1267.
- /9/ R. Szwed, G. Wrochna and A.K. Wroblewski, preprint IFD/3/87-Warsaw.
- /10/ S. Dado et al., Phys. Rev. D20(1979)1589.
- /11/ W. Bell et al., Phys.Lett. B128(1983)349.
- /12/ UAS Collab., G.J. Auner et al., Phys.Lett. B160(1985)239.
- /13/ K. Fialkowski and H.I. Miettinen, Phys.Lett. B43(1973)61; T.T. Chou and C.N. Yang, ibid B135(1984)175.
- /14/ P. Carruthers and C.C. Shih, Phys.Lett. B165(1985)209.
- /15/ A.J. Buras and J. Dias de Deus, Nucl. Phys. B78(1974)445.
- /16/ J. Dias de Deus, Phys.Lett. B178(1986)301.
- /17/ UAS Collab., G.J. Auner et al., Z. Phys. C33(1986)1.

#### Figure Captions

Fig.1 Entropy of the charged particles multiplicity distributions (eq.1) for pp,  $\bar{p}p$  (a) and  $\bar{\pi}p$ ,  $\bar{\pi}+p$ , K-p, K+p (b), inelastic data/1-2,9/. Full line corresponds to eq.7.

Fig.2 Energy development of the entropy of KNO function  $\psi(z)$  (calculated from  $S = -\ln(\langle N \rangle)$ ). Shaded corridor corresponds to  $S$  and  $\langle N \rangle$  parametrizations given by eq.7 and of ref.1, respectively. Region with arrow indicates our prediction of the onset of multiplicity scaling in the few TeV region.

Fig.3 Summary of the energy dependence of hadron induced inelastic interactions (from fig.1) together with data on high energy nuclear interactions/11,12/.

Fig.4 Entropy as a function of the width of the (pseudo)rapidity window  $y_c$  for  $\sqrt{s} = 22 \text{ GeV}/3/$  and  $546 \text{ GeV}/12/$  rescaled by  $Y_m$  (eq.9).

Fig.5 Entropy of the negative particles in the central rapidity window ( $|\eta| < 0.25$ ). The curve corresponds to the entropy of the geometrical distribution (eq.10).

Fig.6 Predicted density of charged particles for two values of reduced rapidity  $\eta$  as a function of c.m.s. energy. The data points correspond to ISR and Collider experiments from ref.17.

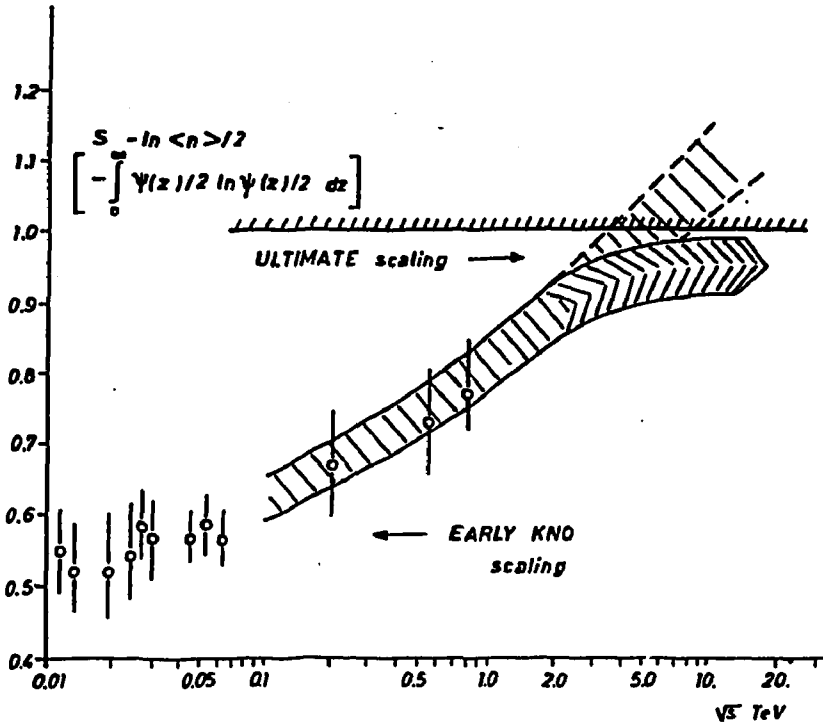


Fig. 2.

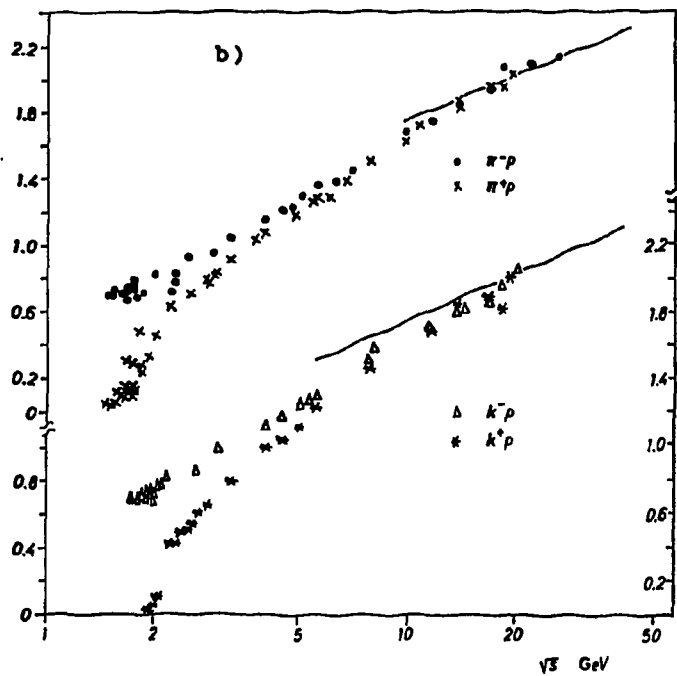
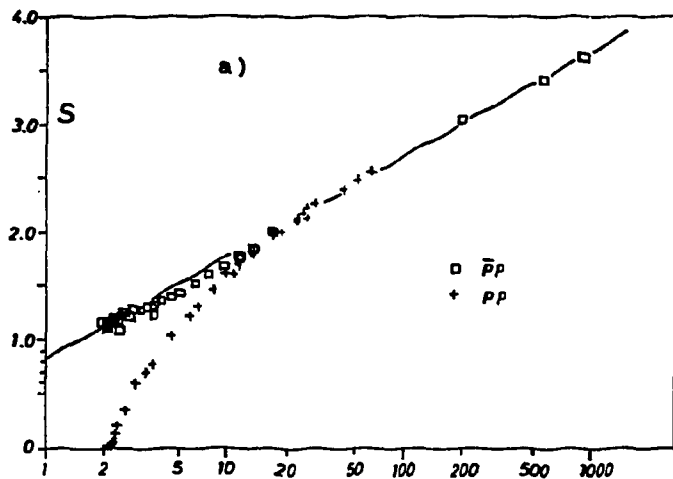
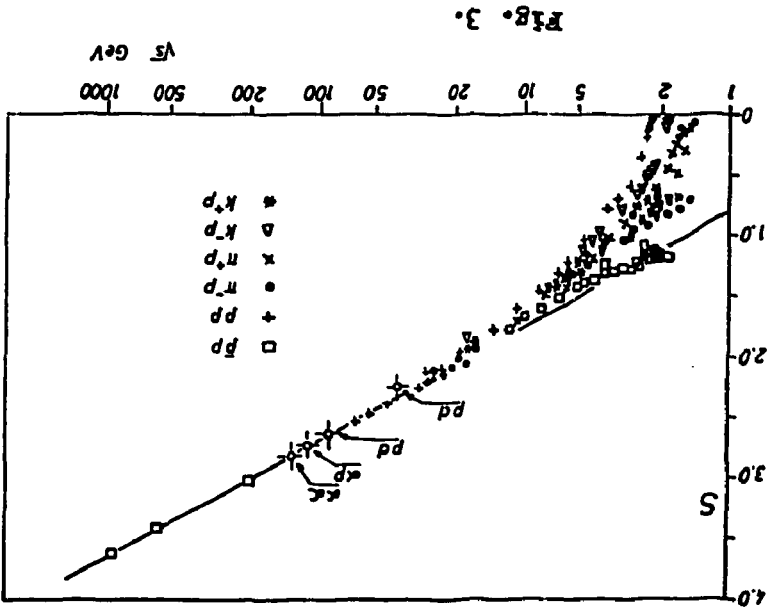
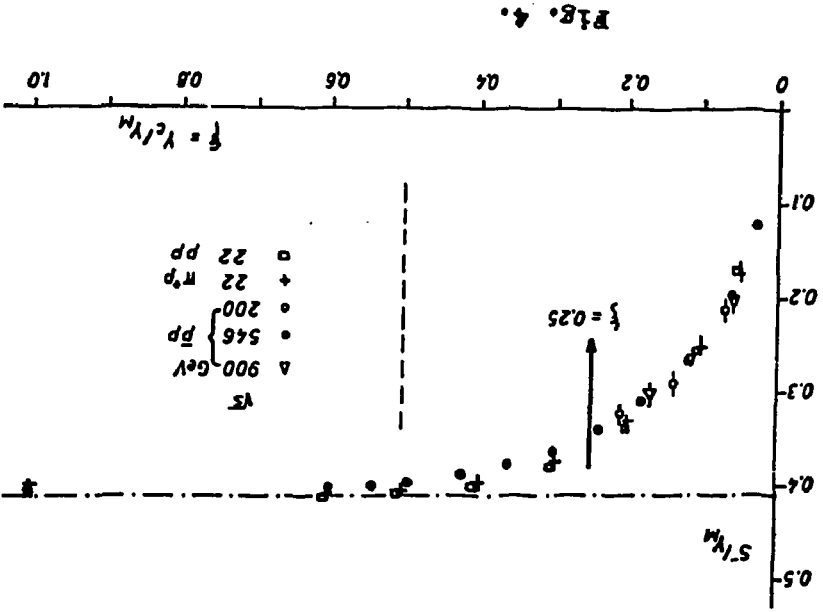


Fig. 1a, 1b.



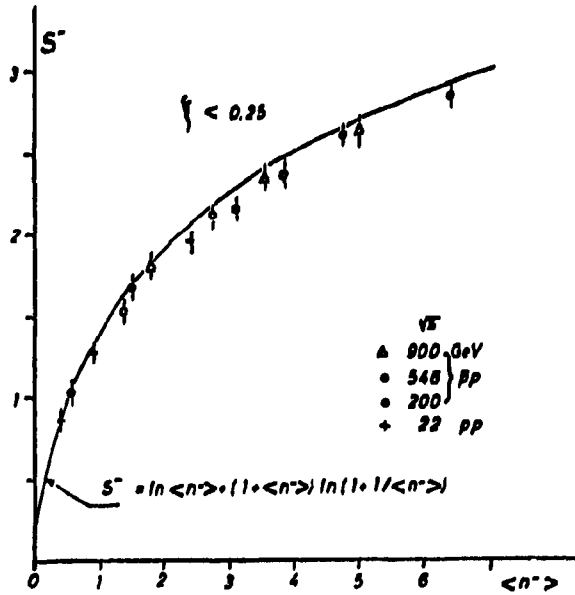


Fig. 5.

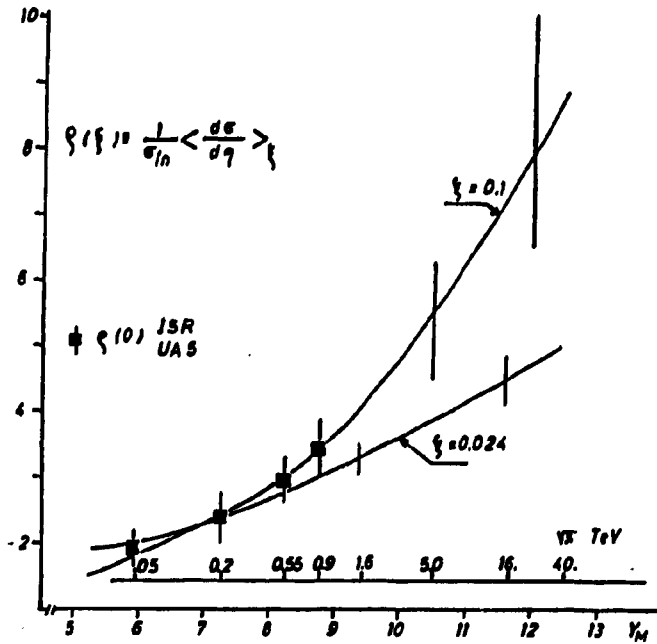


Fig. 6.



Coherence, Chaos and Entropy Scaling in High Energy  
Collisions

M. Plümer, S. Raha\* and R.M. Weiner

High Energy Physics Group, University of Marburg  
Mainzer Gasse 33, D-3550 Marburg, Fed.Rep. of Germany

\*On leave from Saha Institute of Nuclear Physics,  
Calcutta, India

The remarkable recent finding<sup>1)</sup>, that the experimental multiplicity distributions of charged secondaries produced in pp- and p $\bar{p}$ -collisions exhibit "entropy-scaling" in a range of CM-energies between  $\sqrt{s} = 19$  GeV and  $\sqrt{s} = 900$  GeV, has raised considerable interest and attention. For symmetric rapidity intervals  $|y| < y_0$ , the authors of ref. 1 have calculated the entropies

$$S(y_0, s) = -\sum_n P(n, y_0, s) \ln P(n, y_0, s) \quad (1)$$

from the respective data on multiplicity distributions  $P(n, y_0, s)$ , and when they plot  $S(y_0, s)/y_{\max}$  against the scaled rapidity variable  $\xi = y/y_{\max}$  ( $y_{\max} = \ln(\sqrt{s}-2M_N/m_\pi)$ ), they find that for the above-mentioned range of  $\sqrt{s}$  all points lie on one curve. As will be shown below, a calculation of the entropy via eq. (1) relies on two implicit assumptions: (i) the density matrix  $\rho$  of the system does not have any off-diagonal elements in the particle number representation, and (ii) all particles are emitted by one source which is described by a negative binomial (n.b.) multiplicity distribution. Since these assumptions are not expected in general to hold it appears necessary to calculate the entropy under different assumptions. Among other things the fact that we are dealing with a quantum system suggests that non-diagonal terms of  $\rho$  are important. Furthermore there exist indications, that the negative binomial fit does not work at large  $y$  and therefore more than one source exists. For these reasons we have computed the entropy in a two-component model<sup>2)</sup>, which does not rely upon assumptions (i) and (ii) and replaces the poorly understood  $s$ - and  $y$ -dependences of the n.b. parameter by a heuristically appear-

ling interpretation of coherent and chaotic sources. We show that in the context of this model the entropy scaling reflects itself in a scaling behaviour of the mean multiplicities and rapidity distribution of the chaotically produced particles, and we write a master equation for the rapidity dependence of the chaotic multiplicity distribution.

The entropy of a system characterized by a density matrix  $\rho$  is

$$\rho = - \text{Tr} (\rho \ln \rho) \quad (2)$$

For instance, consider the case of  $k$  independent sources described by density matrices  $\rho_i$ , i.e.

$$\rho = \rho_1 \otimes \rho_2 \otimes \dots \otimes \rho_k \quad (3)$$

Then the multiplicity distribution and the entropy are given by

$$P(n_1, \dots, n_k) = \prod_{i=1}^k P_i(n_i) = \prod_{i=1}^k \langle n_i | \rho_i | n_i \rangle \quad (4)$$

$$S = \sum_{i=1}^k S_i, \quad S_i = - \text{Tr}(\rho_i \ln \rho_i) \quad (5)$$

where  $n_i$  is the multiplicity from the  $i$ -th source. Only if all the  $\rho_i$  are diagonal in the  $n_i$ -representation,  $S$  can be calculated from the multiplicity distribution:

$$\langle m_i | \rho_i | n_i \rangle = \delta_{m_i n_i} P_i(n_i) \quad (i = 1, \dots, k) \quad (6)$$

$$S = - \sum_{\{n_i\}} P(n_1, \dots, n_k) \ln P(n_1, \dots, n_k)$$

In general the  $\langle m_i | \rho_i | n_i \rangle$  will not necessarily vanish; e.g., in the case of one coherent source,  $\rho = |\alpha\rangle\langle\alpha|$ , where  $|\alpha\rangle$  is an eigenstate of the annihilation operator,  $a|\alpha\rangle = \alpha|\alpha\rangle$ , one has

$$P(n) = \frac{|\alpha|^{2n}}{n!} e^{-|\alpha|^2}, \quad S = 0 < - \sum_n P(n) \ln P(n) \quad (7)$$

i.e. eq. (1) does not hold.

However, even in the case described by eq. (6), where the off-diagonal elements do not play a role, when one has more

than one source eq. (1) may not be applied to the convolution

$$\tilde{P}(n) = \sum_{\{n_i\}} P(n_1, \dots, n_k) \delta_{n, \sum n_i}, \text{ since}$$

$$S = - \sum_{\{n_i\}} P(n_1, \dots, n_k) \ln P(n_1, \dots, n_k) > - \sum_n \tilde{P}(n) \ln \tilde{P}(n) \quad (8)$$

We shall now proceed to apply that formalism to the above-mentioned two-component model. The multiplicity distributions of the chaotically and coherently produced particles,  $P_{ch}(n_{ch})$  and  $P_c(n_c)$ , are given by a Planck-Polya and a Poisson distribution, respectively, and since the sources are assumed to be independent,  $P(n_{ch}, n_c) = P_{ch}(n_{ch}) \cdot P_c(n_c)$ . Thus, the model has two parameters, the total mean multiplicity  $\langle n \rangle$  and the chaoticity  $p = \langle n_{ch} \rangle / \langle n \rangle$ ; for a given  $\sqrt{s}$  and a given rapidity interval, they can be determined by fitting the first two moments of the measured multiplicity distribution. It has been shown<sup>2)</sup> that at fixed  $\sqrt{s}$   $p$  decreases when one goes from the center to the wings of the rapidity range; at fixed rapidity,  $p$  increases with  $s$ .

Since the entropy of a coherent state is zero (cf. eq. (7)), we find

$$S(y_c, s) = S_{ch}(y_c, s) = (\langle n_{ch}(y_c, s) \rangle + 1) \ln (\langle n_{ch}(y_c, s) \rangle + 1) - \langle n_{ch}(y_c, s) \rangle \ln \langle n_{ch}(y_c, s) \rangle \quad (9)$$

In figure 1, for data obtained at  $\sqrt{s} = 21.5 \text{ GeV}^3)$ ,  $200 \text{ GeV}^4)$ ,  $546 \text{ GeV}^5)$  and  $900 \text{ GeV}^4)$  we have plotted  $S(y_c, s)/y_{max}$  against  $\xi = y_c/y_{max}$ . Clearly, we find the same type of scaling as in ref. (1), but with a different scaling function  $F(\xi) = S/y_{max}$ . Eq. (9) then implies a scaling behaviour of  $\langle n_{ch}(y_c, s) \rangle$ , that is to say it depends on  $y_c$  and  $s$  through the variable  $u \equiv y_{max} \cdot F(\xi)$  only; in the limit of large  $\langle n_{ch}(y_c, s) \rangle$ , we have

$$\langle n_{ch}(y_c, s) \rangle = \frac{1}{\alpha} \left( \frac{\sqrt{s}}{m_\pi} \right)^{F(\xi)} \quad (10)$$

and for the rapidity distribution

$$\frac{dn_{ch}}{dy} = F'(\xi) \cdot \frac{1}{e^{\left(\frac{\sqrt{s}}{m_{\pi}}\right)^2}} F(\xi) \quad (11)$$

It is noteworthy that for the entire rapidity range eq. (10) together with the observed  $F(1) = 0.46$  implies that  $\langle n_{ch} \rangle \propto s^{0.23}$ , which is not far off the  $s^{1/4}$  behaviour predicted in the Landau model.

Eq. (11) shows that, if the entropy scaling will persist at higher  $\sqrt{s}$ ,  $\frac{dn_{ch}}{dy}$  will (asymptotically) develop two distinct symmetric maxima that move away from the center. In figure 2, where  $\frac{dn_{ch}}{dy}$  as calculated from the data has been plotted, one may already see the onset of such behaviour, though at these energies the values of  $\langle n_{ch}(y_c, s) \rangle$  are not yet large enough for eqs. (10), (11) to be good approximations.

As a further consequence of the scaling behaviour of  $\langle n_{ch}(y_c, s) \rangle$  expressed in eqs. (10), (11),  $P_{ch}(n_{ch}, y_c, s)$  can be shown to satisfy the master equation

$$-\frac{\partial P(n, y_c)}{\partial y} = F'(\xi) \{ (n+1) P(n+1, y_c) - n P(n, y_c) \} \quad (12)$$

Changing variables from  $y_c$  to  $t = y_{max} - y_c$ , one finds that (12) describes something like an absorption process;  $t$  plays the role of time coordinate: as the system evolves in time, the particles initially present (at  $t=0$ ) are absorbed (or decay),  $F'(\xi)dt$  gives the "time"-dependent probability for a particle to be absorbed in the interval  $(t, t+dt)$ . It is a challenging task to ascribe some physical meaning to the master equation (12).

In conclusion we see that the scaling behaviour found in ref. 1 is recovered in the present approach, with the difference that the entropy refers now to the chaotic part of the system which has more direct implications for the investigation of thermal equilibrium. The fact that the entropy is concentrated in the central rapidity region confirms the observation of ref. 2 that the chaotic source dominates the same rapidity range. Furthermore new predictions for the rapidity

distribution of the chaotic component are made and a master equation for this component is derived.

### References

- (1) V. Šimák, M. Šumbera and I. Zbhorovsky, Proc. of the Europhysics Conference 1987 at Uppsala, to appear.
- (2) G.N. Fowler et al., Phys.Rev.Lett. 57, 2119 (1986).
- (3) NA22 Collab., M. Adamus et al., Phys.Lett. B177, 239 (1986).
- (4) UA5 Collab., C. Fuglesang et al., Proc. of the XVII. Int. Symposium on Multiparticle Dynamics at Seewinkel, ed. M. Markytan et al., World Scientific, p. 553.  
UA5 Collab., G.J. Alner et al., Phys.Lett. 167B, 476 (1986).
- (5) UA5 Collab., G.J. Alner et al., Phys.Lett. 121B, 209 (1983);  
UA5 Collab., G.J. Alner et al., Phys.Lett. 160B, 193 (1985).

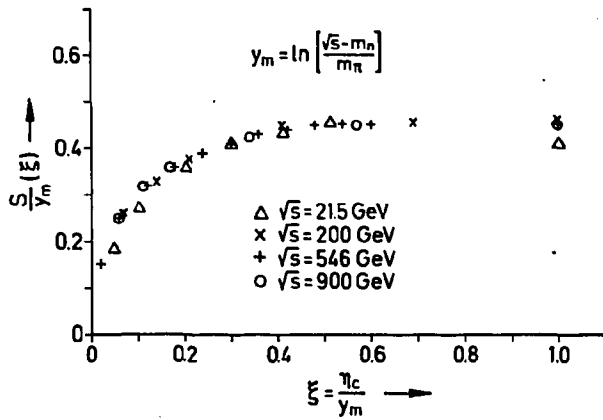


**Figure 1**

Entropy scaling found by applying the two component model to data

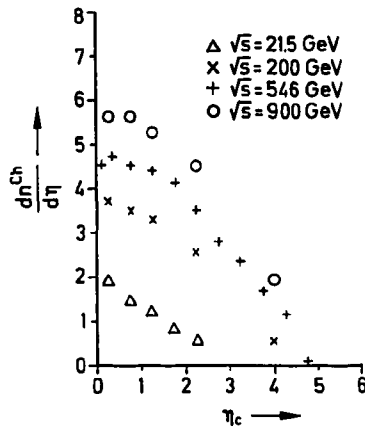


**Figure 2**

Pseudo-rapidity distributions of chaotically produced particles

# LONG-RANGE CORRELATIONS IN HADRON-NUCLEUS INTERACTIONS

Presented by  
**PIOTR MALECKI**  
*Institute of Nuclear Physics, Kraków*

November 15, 1987

## 1 Abstract

An analysis of correlations in rapidity of charged particles produced in proton and antiproton interactions on hydrogen, argon and xenon at 200 GeV/c is presented. Positive, long-range correlations were observed in interactions on heavy targets. The dependence of rapidity correlations between forward and backward hemispheres on number of projectile collisions is discussed.

## 2 Introduction

The study of correlations among particles produced at various rapidity regions reveals the mechanisms of particle production. Many experiments show strong positive short-range correlations corresponding to clustering of particles over regions of about one unit in rapidity. In particular, correlations between particles emitted at the central rapidity region are dominated by these short-range correlations. On the contrary, correlations which extend over a longer range in rapidity are observed in hadron-hadron reactions only above energies of the ISR (above  $\sqrt{s} \approx 30$  GeV) [1].

It has been suggested that long-range correlations might be much stronger in hadron-nucleus interactions than in hadron-hadron scattering at the same energy per nucleon [2]. Interactions of hadrons with nuclei, as commonly described, are assumed to proceed via independent collisions of a projectile or its constituents with constituents of the target. These multiple collisions result in an abundant production of particles in the backward hemisphere while, in the forward hemisphere only a small excess of particles is observed in comparison to the corresponding hadron-hadron collisions. At presently available energies this excess extends to about one unit in rapidity from a cms rapidity of zero [3]. To analyze mutual relations of multiplicities of different rapidity regions, which are characteristic for nuclear target interactions, an appropriate selection of rapidity intervals is necessary [2].

The correlation strength between the multiplicities in two rapidity intervals ( $y_{B1}, y_{B2}$ ), ( $y_{F1}, y_{F2}$ ) is often measured with the slope  $b$  of the following linear relation:

$$\langle N_B \rangle = a + bN_F \quad (1)$$

where

- $\langle N_B \rangle$  is the average value of multiplicity in the interval ( $y_{B1}, y_{B2}$ )

- $N_F$  is the multiplicity in the interval  $(y_{F1}, y_{F2})$ .

In the present analysis the estimation of the parameter  $b$  is given for full unbiased samples of events of  $p - Ar$ ,  $p - Xe$ ,  $\bar{p} - Ar$  and  $\bar{p} - Xe$  reactions. A sample of hadron-nucleus events corresponds to a distribution of the number of collisions  $\nu$ , average of which is usually estimated by:

$$D = \frac{A\sigma_{hN}}{\sigma_{hA}}$$

where

- $A$  is the atomic number
- $\sigma_{hN}$  and  $\sigma_{hA}$  are the cross sections for a hadron  $h$  interacting with a nucleon or nucleus, respectively.

*A* estimation of a shape or a width of the distribution of  $\nu$  is the matter of models. In our earlier publication [4] we have discussed certain model calculations [5] of the distribution of  $\nu$  in relation to a number of slow identified protons  $N_p$ , observed in an individual event. It was shown that a sample of events with fixed number of  $N_p$  corresponds to a narrower distribution of the number of collisions  $\nu$  than the full unbiased sample. We refer to this model estimation also here to test the dependence of the correlation strength on the dispersion of the  $\nu$  distribution. It seems to be obvious to interpret the origin of the long-range correlations in h-nucleus interactions as a consequence of the fact that a sample of h-A events consists of a mixture of events of different number of collisions and, consequently, a different particle production in forward and backward directions.

In the following section a brief description of the experimental data and analysis is given. The results are presented and discussed in Sect. 4, followed by concluding remarks.

### 3 Data and analysis

The data on proton and antiproton interactions with hydrogen, argon and xenon nuclei at 200 GeV/c used for the present analysis were collected in the NA5 experiment at CERN SPS. The details of the experimental set-up and the reconstruction procedure can be found in our earlier publications [3,6].

For the following analysis we have selected the test rapidity intervals:

$$(y_{D1}, y_{D2}) = (0.75, 1.75) \quad (y_{F1}, y_{F2}) = (3.25, 4.25)$$

as suggested in [2]. (The values are given in the laboratory system, in which the rapidity  $y=3.028$  corresponds to a cms rapidity of zero for p-p scattering at 200 GeV/c.) Introducing a gap of 1.5 units in rapidity between the intervals one expects to eliminate considerably the contribution of short range correlations. On the other hand, selected intervals seem to be far enough from phase space limits and effects of the intra-nuclear cascade are eliminated to a large extent [3]. As a matter of fact the proper choice of intervals is crucial: it was shown [3] that for the interval  $(y_{F1}, y_{F2})$  chosen further in the forward region, where the density of particles does not vary considerably with the number of collisions and is very small, the long-range correlations are unmeasurable.



## 4 Results

The values of the slope  $b$  - the result of a linear regression of scatter plots of events on the  $N_p$ ,  $N_B$  plane - are shown in Table 1. for all analyzed reactions. (For completeness, the results for our own data on elementary  $p-p$  and  $\bar{p}-p$  interactions are also given.)

	$b$		$b$
$p-p$	$-.01 \pm .01$	$\bar{p}-p$	$.00 \pm .01$
$p-Ar$	$.28 \pm .04$	$\bar{p}-Ar$	$.35 \pm .04$
$p-Xe$	$.41 \pm .04$	$\bar{p}-Xe$	$.44 \pm .04$

Table 1. Slope  $b$  for full samples of events.

The observed correlation strengths are large for interactions on argon and xenon as suggested [2] and negligible for the elementary interactions.

A similar analysis has been performed for sub-samples of events characterized by the multiplicity of slow identified protons  $N_p$ . As mentioned above, sample of events with fixed  $N_p$  may be associated with the distribution of  $\nu$  which is narrower than for the full unbiased sample [4]. To study the dependence of the strength of long-range correlations on the  $\nu$  distribution we have calculated the slope  $b$  for samples of events of a different contents of  $N_p$ . The sample of events with  $N_p = 0$  corresponds to the narrowest  $\nu$  distribution, a sample with  $N_p = 0$  and 1 corresponds to the wider one and so on. The detailed model calculations can be found in [4]. E.g. the sample of  $p-Xe$  events with  $N_p = 0$  corresponds to the distribution of  $\nu$  with the average 1.56 and the dispersion .95 while the  $\nu = 3.32$  and dispersion equals 2.20 for the full sample. Fig. 1 shows the dependence of the slope  $b$  on the number  $N_p^c$  by which we denote the highest  $N_p$  contained in the sample. A strong dependence of  $b$  on  $N_p^c$  is observed for all analyzed reactions.

Finally, we apply the model calculations of ref. [4] to relate  $N_p^c$  scale to the dispersion of the combined  $\nu$  distribution for each sample. As illustrated in Fig. 2, slopes for  $p-Ar$  and  $p-Xe$  interactions, which can now be plotted together, show a similar and strong dependence on the dispersion squared of the distribution of the number of collisions. This confirms an intuitive interpretation of the origin of long-range correlations in hadron-nucleus collisions at energies at which no such correlations are observed for elementary interactions.

## 5 Conclusions

Large positive long-range correlations among particles produced at various rapidity regions in proton and antiproton interactions with argon and xenon nuclei at 200 GeV/c were observed. This observation confirms the earlier theoretical predictions [2]. The strength of these correlations, measured with the slope of the relation (1), depends on the distribution of the number of slow identified protons contained in the analyzed sample of events. With certain model assumptions such a distribution may be related to the distribution of the number of projectile collisions  $\nu$  inside the target nucleus. It was shown, in the framework of these assumptions, that the wider

is the distribution of  $\nu$  the stronger are correlations.

## 6 Acknowledgments

We thank A. Capella for suggesting this investigation.

## References

- [1] K. Alpgård et al., Phys. Lett. 123B (1983) 361; see also refs. therein.
- [2] A. Capella, J. Tran Thanh Van, Long range rapidity correlations in hadron - nucleus interactions. Orsay preprint LPTHE - 83/10 (1983).
- [3] C. de Marzo et al., Phys. Rev. D26 (1982) 1019.
- [4] C. de Marzo et al., Phys. Rev. D29 (1984) 2476.
- [5] B. Andersson, I. Otterlund and E. Stenlund, Phys. Lett. 73B (1978) 343.
- [6] F. Dengler et al., Z. Phys. C - Particles and Fields 33 (1986) 187.

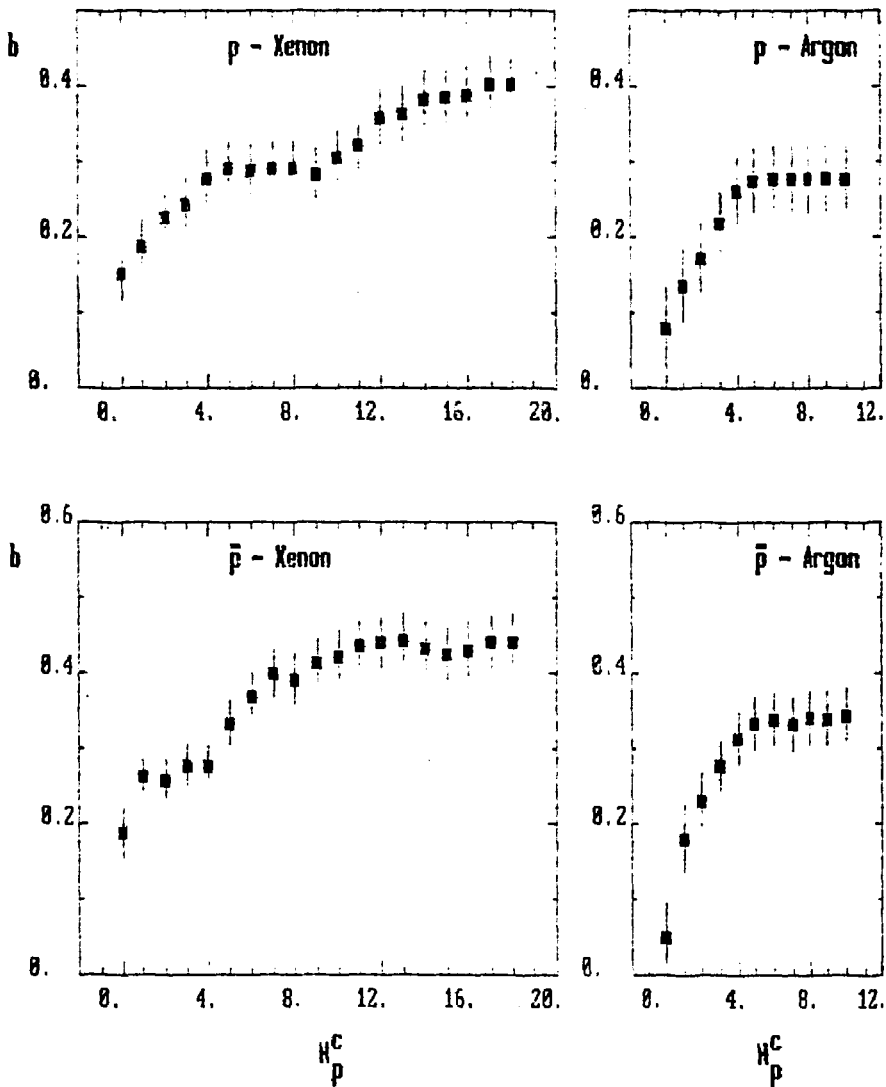


Fig. 1. Values of the slope  $b$  for samples with different number of slow protons.

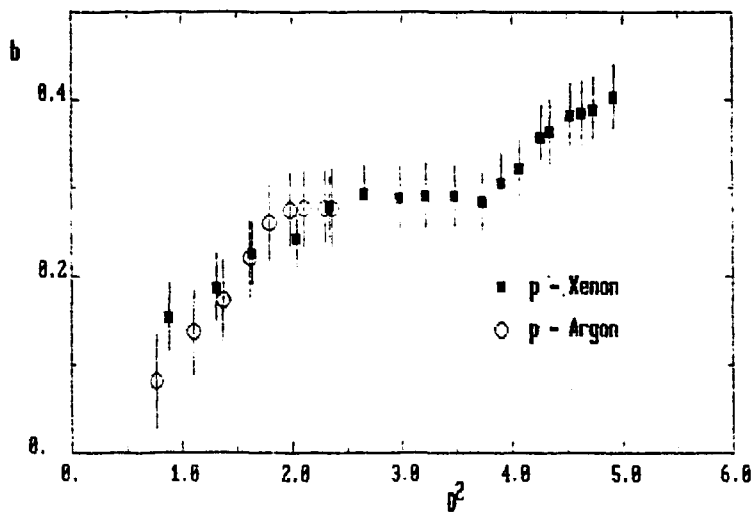


Fig. 2. Slope  $b$  as a function of the dispersion of the number of collisions.

## Transverse energy distributions in hadron - nucleus and nucleus - nucleus collisions

J. Ftáčnik

Department of Theoretical Physics, Comenius University  
842 15 Bratislava, Czechoslovakia

Recently we can observe raising interest in the search of quark - gluon plasma. The existence of plasma is predicted by QCD (for review see [1]), but it is not known, whether high enough energy densities can be reached in heavy ion collisions. Several dedicated experiments [2,3] have already published first results on transverse energy distributions in collisions of  $O^{16}$  with various heavy targets at 60 and 200 GeV/nucleon. In attempt to distinguish in  $E_T$  distributions possible QCD plasma formation signature from conventional physics we have developed a simple non-plasma model for calculation of  $E_T$  distributions in hadron - nucleus and nucleus - nucleus collisions.

Our simple model aims to describe the qualitative features of  $E_T$  distributions in the absence of plasma formation. In this model we assume the total  $E_T$  of the event to be built up by the independent contributions of nucleon - nucleon collisions. Each of these nucleon - nucleon collisions is supposed to be similar to proton - proton collisions at the same energy in what concerns rapidity distribution of produced hadrons and their transverse energy distribution. After fixing the parameters of the model using data in central rapidity region (where we don't expect the contribution from cascading) we underestimate  $E_T$  distributions in target fragmentation region. This we interpret as the evidence for the contribution of cascading which we have to include into our model.

The calculation of  $E_T$  distributions in our model is based on the determination of three probability distributions. At the beginning we have to determine the total number of nucleon - nucleon collisions  $N$  at the given impact parameter  $b$  of the colliding nuclei  $P(N | b)$ . This is mostly the question of geometry of the collision. We combine geometrical considerations with ideas motivated by Glauber model. Knowing the number of nucleon - nucleon collisions we can estimate the probability for the production of the total number of hadrons  $n_h$  (both charged and neutral)  $P(n_h | N)$ . Here we use the similarity of nucleon - nucleon collisions with p-p collisions and the simple assumption about energy losses in consecutive collisions of projectile nucleons. Finally knowing the total number of produced hadrons in the given rapidity interval we need only to determine the probability for the production of total transverse energy in the given event  $P(E_T | n_h)$ . This probability is calculated from the probability distribution of  $E_T$  for one produced hadron. Knowing all three probabilities we only need to integrate their product over all possible impact parameters and sum over all values of  $N$  and  $n_h$  to

obtain the differential cross section

$$\frac{d\sigma}{dE_T} = \int db^2 \sum_{N, n_h} P(E_T | n_h) P(n_h | N) P(N | b) \quad (1)$$

We will now describe the actual calculation of the differential cross section.

### Proton - nucleus collisions

#### • $P(N | b)$

Calculation of the number of nucleon - nucleon collisions  $N$  at the given impact parameter of the proton  $b$  is motivated by Glauber model and is based on simple geometrical picture. We estimate  $N$  as the number of nucleons in the target nucleus being present in the tube "seen" by the incoming proton with the base area equal to the total inelastic cross section of nucleon - nucleon collision  $\sigma_{nn}$ . The expression for the probability  $P(N | b)$  then reads

$$P(N | b) = \binom{A}{N} \left[ \frac{N_A(b)}{A} \right]^N \left[ 1 - \frac{N_A(b)}{A} \right]^{A-N} \quad (2)$$

where  $N_A(b) = \sigma_{nn} \int ds \rho_A(s, b)$  and for the density of nucleons we take standard Wood - Saxon parametrisation

$$\rho_A(r) = \frac{\bar{\rho}_A}{1 + \exp((r - R_A)/d)}$$

with  $\bar{\rho}_A$  being the normalisation constant and parameters  $d = 0.54 \text{ fm}$ ,  $R_A = 1.19A^{1/3} - 1.61A^{-1/3} \text{ fm}$ . For nucleon - nucleon cross section we use the value  $\sigma_{nn} = 25 \text{ mb}$ .

#### • $P(n_h | N)$

For the estimation of the production of hadrons we need to calculate the average number of produced hadrons  $\bar{n}_h$ . For the number of produced hadrons we use negative binomial distribution

$$P(n_h | N) = \binom{n_h + k - 1}{n_h} x^{n_h} (1 - x)^k \quad (3)$$

where  $x = \bar{n}_h / (\bar{n}_h + k)$ . From the data on proton - nucleus scattering [4] we fix the value  $x = 0.3$ . For the calculation of  $\bar{n}_h$  we have to estimate energy losses in consecutive collisions of proton with nucleons of target. We use simple geometrical filter  $E_n = (1 - u)E_{n-1}$  where  $E_n$  is the energy of the projectile after the  $n$  collisions with target nucleons. The probability distribution for  $u$  is  $P(u) = \alpha u^{\alpha-1}$ ,  $\alpha = 2$ . In each proton - nucleon collision we expect the rapidity distribution of produced hadrons to be equal to pp collisions at the same energy. For the rapidity distribution  $d\bar{n}_h/dy$  we use parametrisation [5]

$$\frac{d\bar{n}_h}{dy} = 3.15(1 - x)^{2.5}(1 - x_-)^6$$

where  $s = m_T/(E+p) \exp(y)$ ,  $s_- = m_T/m_N \exp(-y)$ ,  $m_T = 0.4 \text{ GeV}$ . The average number of produced hadrons in given rapidity region is obtained by integration of the sum of such distributions for all proton - nucleon collisions.

•  $P(E_T | n_h)$

For the calculation of transverse energy produced in proton - nucleus collision we use the phenomenologically successful expression for one particle  $E_T$  distribution

$$P^{(1)}(E_T) = \frac{E_T}{T^2} \exp(-E_T/T)$$

with  $\langle E_T \rangle = 2T$ ,  $T = 0.2 \text{ GeV}$ . For  $n_h$  produced hadrons we are able to perform convolutions analytically with the resulting distribution

$$P(E_T | n_h) = \frac{1}{T(2n-1)!} e^{E_T/T} \left(\frac{E_T}{T}\right)^{2n_h-1} \quad (4)$$

Using Eq.(1) for the fit to the NA 35 data on  $E_T$  distribution in p-Au collisions at 200 GeV we have fixed our most important parameters  $\sigma_{nn} = 25 \text{ mb}$  and  $\alpha = 2$ . Data were taken in the rapidity interval  $2.2 < y < 3.8$  corresponding to central rapidity region. The result of the fit can be seen on Fig.1. Using the same set of parameters we have performed the calculation for target fragmentation region data of Helios collaboration on p-Pb collisions at the same energy for the rapidity interval  $-0.1 < y < 2.9$ . We interpret the discrepancy between the model and the data as the indication for the substantial contribution of cascading to the  $E_T$  distribution. We intend to include cascading into our model in the near future.

### Nucleus - nucleus collisions

•  $P(N | b)$

For nucleus - nucleus collisions the calculation of the total number of nucleon - nucleon collisions is much more complicated than for proton - nucleus collisions. We are using simple Gaussian probability distribution

$$P(N | b) = \frac{1}{\sqrt{2\pi D^2}} \exp\left[-\frac{(N - \bar{N})^2}{2D^2}\right] \quad (5)$$

around some mean value  $\bar{N}$  (we take also  $D^2 = \bar{N}$ ). For mean value  $\bar{N}$  at given impact parameter  $b$  we are again using "tube" approach. We approximate  $\bar{N}$  as the sum of products of the mean number of nucleons in all possible tubes in nucleus A and corresponding tubes in nucleus B  $\bar{N} = \int d^2s / \sigma_{nn} N_A(\vec{s}) N_B(\vec{b} - \vec{s})$  where  $\vec{s}$  is the impact parameter of the tube within the nucleus A.  $N_A$  and  $N_B$  are again mean numbers of nucleons in corresponding tubes given by expressions  $N_A(\vec{s}) = \sigma_{nn} \int dx \rho_A(x, \vec{s})$  and  $N_B(\vec{b} - \vec{s}) = \sigma_{nn} \int dx \rho_B(x, \vec{b} - \vec{s})$ . The density of nucleons is again parametrized by Wood - Saxon parametrization for nuclei with  $A > 15$ .

•  $P(n_h | N)$

For the total number of produced hadrons we are using the approach described already for proton nucleus collisions. For  $P(n_h | N)$  we use negative binomial distribution in the form of Eq.(3). The only difference is connected with the fact that nucleons from nucleus B are interacting with several nucleons from the projectile nucleus A. After interacting once nucleon from nucleus B starts to move in the direction of projectile. Therefore it has smaller relative velocity with respect to the next incoming nucleon from nucleus A. This causes shifts toward positive values of the beginning of the rapidity plateau of produced hadrons in consecutive interactions of nucleon from nucleus B. Taking this detail into account we can repeat all the reasoning presented for proton - nucleus collisions.

•  $P(E_T | n_h)$

For this distribution we can again derive the parametrisation in Eq.(4) using the same arguments.

Using the same set of parameters used already for proton - nucleus case we are able to fit the data of NA 35 collaboration on  $E_T$  distribution in  $^{16}O - Pb$  collisions at 200 GeV/nucleon in the central rapidity region (see Fig.3). On Fig.4 we compare our model with the data of Helios collaboration for  $^{16}O - W$  collisions with the same energy, but in the target fragmentation region. Both rapidity intervals correspond to quoted in proton - nucleus case. We again clearly see the need for some additional mechanism of  $E_T$  production in target fragmentation region - in our opinion it is cascading.

We have shown that the recent data on  $E_T$  distributions in heavy ion collisions can be understood as the sum of the contributions of individual nucleon - nucleon collisions. This strongly indicates, that up to now we have not observed the creation of QCD plasma. However, we have found evidence for the substantial contribution of cascading in the target fragmentation region.

#### Acknowledgements

The work presented here was done in collaboration with J. Pišút and N. Pišútová. I want to express to both of them my gratitude for the most pleasant collaboration. I am indebted also to V. Černý, M. Mojiš and P. Lichard for numerous valuable discussions.

#### References

- [1] L. McLerran, Phys. Rep. **88** (1982) 379
- [2] NA - 35 Collaboration, A. Bamberger et al., Phys. Lett. **B184** (1987) 271
- [3] Helios Collaboration, T. Åkesson et al., preprint CERN - EP/87 - 176, Subm. to Zeit.f.Physik C
- [4] C. De Marzo et al., Phys. Rev. **D26** (1982) 1019 and Phys. Rev. **D29** (1984) 2476
- [5] K. Kinoshita, A. Minaka and H. Sumiyoshi, Prog. Theor. Phys. **63** (1980) 928



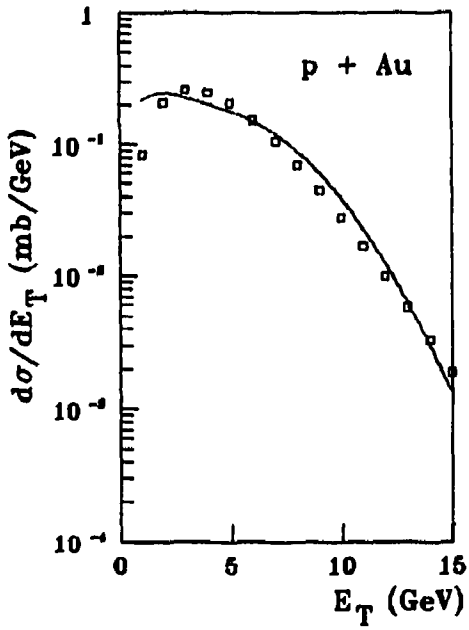


Fig.1

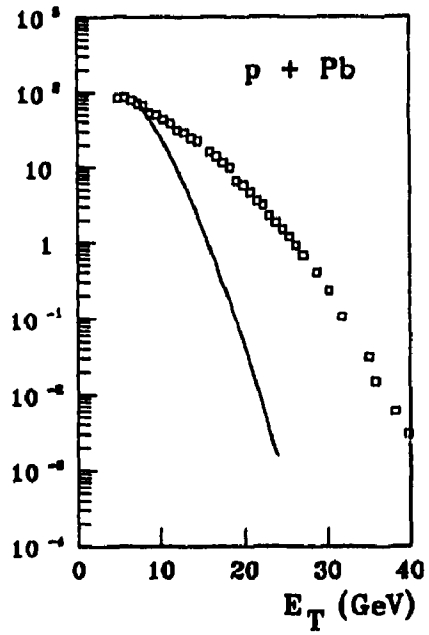


Fig.2

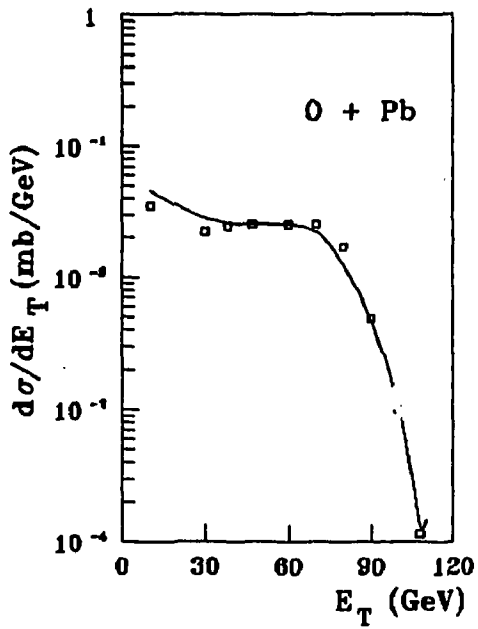


Fig.3

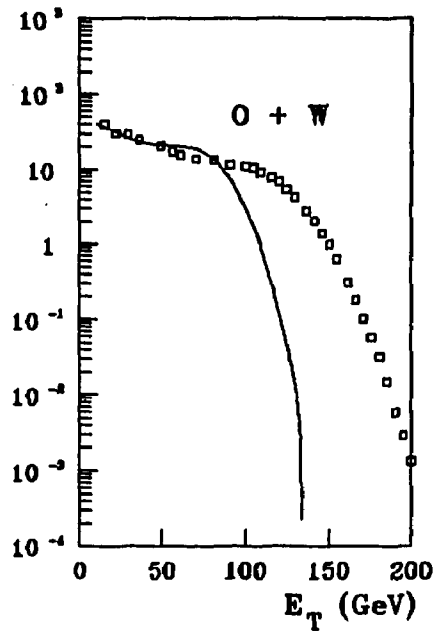


Fig.4

# CHARGED PARTICLE MULTIPLICITY DISTRIBUTIONS AT 200 GeV AND 900 GeV

The UA5 Collaboration  
Bonn-Brussels-Cambridge-CERN-Stockholm  
presented by  
B. Åsman  
Inst. of Physics, Univ. of Stockholm  
Vanadislav. 9, S - 113 46 Stockholm, Sweden

## ABSTRACT

Moments for corrected charged multiplicity distributions in limited regions of phase space are given. An accidental scaling of the multiplicity distributions is seen in the pseudorapidity interval less than 0.5 in absolute value. Negative binomial distributions are shown to fit multiplicity distributions in all pseudorapidity intervals at 200 GeV and in small intervals at 900 GeV. The values of the parameter  $k$  for the fitted negative binomial distributions are given.

## INTRODUCTION

The KNO scaling law [1] which was derived using Feynman scaling [2] states that the normalized charged particle multiplicity distribution should become energy independent at very high energies if plotted in the variable  $z = n/\langle n \rangle$ . Although Feynman scaling was known not to hold at ISR energies (20-63 GeV) the concept of KNO scaling was nevertheless very successful for energies up to 63 GeV. However, the UA5 collaboration showed that at 546 GeV [3] the scaling properties were broken. Furthermore the UA5 collaboration showed that the multiplicity distribution of charged particles at 546 GeV could be successfully described with the negative binomial distribution [4]. This distribution is given by:

$$P(n; \bar{n}, k) = \binom{n+k-1}{k-1} \left[ \frac{\bar{n}/k}{1+\bar{n}/k} \right]^k \left( \frac{1}{1+\bar{n}/k} \right)^k$$

It only has two free parameters  $\bar{n}$  and  $k$ , where  $\bar{n}$  is the mean of the distribution. It was shown that the negative binomial did not only fit the multiplicity distribution in full phase space but also in different pseudorapidity intervals and in pp collisions at various energies [5]. The negative binomial distribution has after that been fitted to multiplicity distributions obtained with different beams and at various energies [6,7]. In this contribution the results on the multiplicity distribution obtained in proton-antiproton collisions at 200 GeV and 900 GeV will be discussed.

## THE DETECTOR

The UA5 detector was well suited for the study of charged particle multiplicity distributions. The charged particles were detected in two large streamer chambers, one placed above, the other below the beam pipe. The geometrical acceptance of the chambers was about 95% in the pseudorapidity range  $|\eta| < 3$  falling to zero at  $|\eta| = 5$ . The spatial resolution of the tracks was very good. No magnetic field was used, so the tracks were straight and easy to measure. The streamer chambers were triggered by scintillation counter hodoscopes at each end. For the sample analysed here, a minimum bias trigger which excluded most single diffractive events but recorded about 95% of the non single diffractive events was used. For a description of the detector see ref. [8,9]. The results presented here are based on about 3800 events at 200 GeV and about 6500 events at 900 GeV.

## THE CHARGED PARTICLE MULTIPLICITY DISTRIBUTION

The corrected charged particle multiplicity distributions were determined for full phase space and for a set of symmetric intervals defined by the pseudorapidity cut  $\eta_c$  from 0.5 to 2.0 in steps of 0.5. One small central interval for which  $\eta_c$  is 0.25 is also added. The results in full phase space at c.m. energies of 200 GeV and 900 GeV confirm the UA5 finding at 546 GeV that KNO scaling is not observed in the

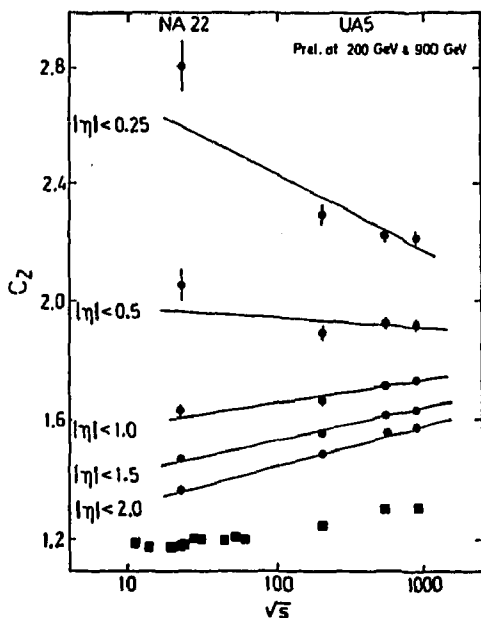


Fig. 1. The  $C_2$ -moment for the charged particle multiplicity distributions found in full phase space [10] and in different  $\eta$ -intervals plotted [4,7] versus the centre of mass energies. The  $C_2$ -moments in full phase space are plotted as squares. The straight lines are fits to the  $C_2$ -moments in the various  $\eta$ -intervals.

non single-diffractive component. In fig. 1 the  $C_2$ -moment in various  $\eta$ -intervals has been plotted versus the centre of mass energy. For comparison NA22 data [7] and earlier published UA5 data [4] are given in the figure. The definition of C-moments is  $C_n = \langle z^n \rangle$ , where  $z = n/\langle n \rangle$ , from which follows that KNO scaling implies energy-independent  $C_n$  moments. In full phase space this is approximately true below 62 GeV but not above 200 GeV. As can be seen the  $C_2$ -moment increases with energy not only for multiplicity distributions in full phase space but also for multiplicity distributions in large pseudorapidity intervals. In very small intervals however, the  $C_2$ -moment decreases with energy. This shows, since  $C_2 - 1 = (D/\langle n \rangle)^2$  where  $D$  is dispersion, that the multiplicity distributions are getting relatively broader when the energy is increasing, in large  $\eta$ -intervals but in small  $\eta$ -intervals the distributions are getting relatively more narrow with increasing energy. It is also seen that the  $C_2$ -moment increase with decreasing  $\eta$ -intervals at all energies. The lines shown in the figure are fitted straight lines to the  $C_2$ -moments in each pseudorapidity region. The slope of the lines is plotted versus the size of the pseudorapidity region in figure 2. In this figure the corresponding slopes for the  $C_3$ -moments are also shown. As can be seen in the figure, the slope is zero in the pseudorapidity region  $|\eta| < 0.5$ . This indicates an accidental scaling in that region, for c.m. energies between 22 GeV and 900 GeV.

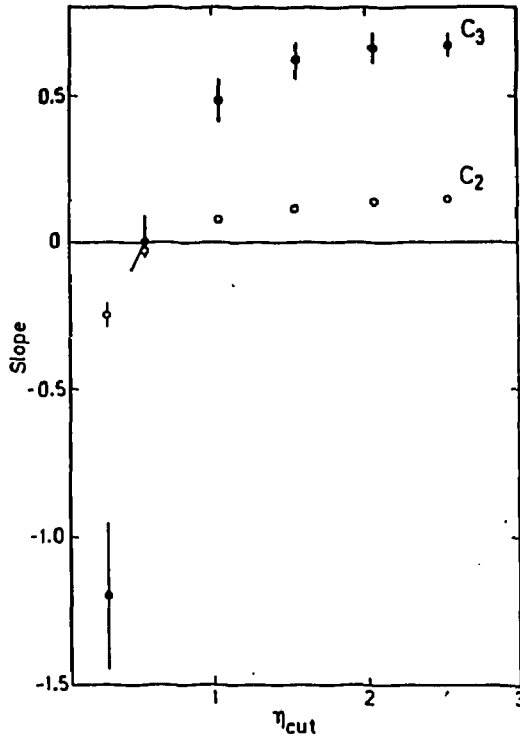


Fig. 2. The slope of the straight lines given in figure 1 plotted versus the  $\eta$ -interval  $\eta_{cut}$  where  $|\eta| < \eta_{cut}$ . The corresponding slopes for  $C_3$  are also given.

## THE NEGATIVE BINOMIAL DISTRIBUTION

The negative binomial distribution has been fitted to multiplicity distributions in regions of pseudorapidity centred around zero. In all pseudorapidity intervals the fits are good at 200 GeV. At 900 GeV the fits are good in small  $\eta$ -intervals but not in large intervals. In the large intervals the fits are still good in the high multiplicity tail. However, for e.g. the region  $|\eta| < 5.0$  at multiplicities around 20 the data exceed the curve while in the multiplicity region of about 35 the curve exceeds the data. This unexpected bad fit in large  $\eta$ -intervals at 900 GeV lead to further investigations of possible systematic errors. A comparison between multiplicity distributions measured at our different laboratories with different equipments showed that all the measuring machines give consistently the same result. No asymmetry between the multiplicity distribution in the upper chamber and in the lower chamber or between the multiplicity distribution in the forward and backward region has been found. There is no contamination of events at the energy of 200 GeV in the event sample at 900 GeV. The events occur on the same film and are labeled 200 resp. 900 GeV. If the labeling should have malfunctioned during the run a contamination of lower multiplicity events at 200 GeV could have been mistaken as 900 GeV data. However, an independent test exists since the level of the beam was slightly shifted between two the different energies. No contamination was found. The conclusion is that we have not found any systematic error that causes the deviation between the negative binomial distribution and data. In figure 3 the

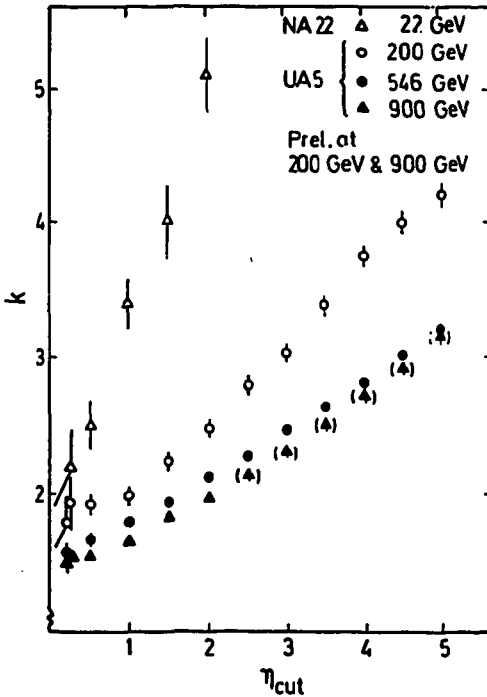


Fig. 3. The value of the parameter  $k$  plotted versus  $\eta_{\text{cut}}$ , where  $|\eta| < \eta_{\text{cut}}$  for data at 22 GeV [7], 200 GeV, 546 GeV [4] and 900 GeV. If the value is given in parenthesis the fit is not good.

fitted  $k$  values are given for 200 GeV, 546 GeV and 900 GeV. If the value is given in parenthesis the fit is not good. For comparison also NA22 [7] data are given. The parameter  $k$  increases almost linearly with increasing pseudorapidity interval at all energies and it decreases with energy.

#### SUMMARY

At all energies investigated the multiplicity distributions are getting relatively wider (the dispersion divided by the mean multiplicity is increasing) when the  $\eta$  interval is made smaller.

In most  $\eta$  intervals the multiplicity distributions are getting relatively broader with increasing energy. However, in the smallest  $\eta$  interval ( $\eta_c < 0.05$ ) they are getting relatively more narrow with increasing energy.

The negative binomial distribution fits data in all pseudorapidity intervals at 200 GeV and in small intervals at 900 GeV.

#### REFERENCES

- [1] Z. Koba, H.B. Nielsen and P. Olesen, Nucl. Phys. **B40** 317 (1972).
- [2] R.P. Feynman, Phys. Rev. Lett. **23** 1425 (1969).
- [3] G.J. Alner et al., Phys. Lett. **138B** 304 (1985).
- [4] G.J. Alner et al., Phys. Lett. **160B** 193 (1985).
- [5] G.J. Alner et al., Phys. Lett. **160B** 199 (1985).
- [6] M. Derrick et al., Phys. Lett. **168B** 299 (1986).  
M. Derrick et al., Phys. Rev. **D34** 3304 (1986).  
M. Arnedo et al., Z. Phys. **C35** 335 (1987).  
M. Dengler et al., Z. Phys. **C33** 187 (1986).
- [7] F. Meijers, Thesis, University of Nijmegen.  
M. Adamus et al., Phys. Lett. **177B** 239 (1986).  
M. Adamus et al., Z. Phys. **C32** 475 (1986).
- [8] UA5 Collab G.J. Alner et al., Phys. Rep. **154** 5,6 (1987).
- [9] G.J. Alner et al., Z. Phys. **C32** 153 (1986).
- [10] V.V. Ammosov et al., Phys. Lett. **42B** 519 (1972).  
H.B. et al., Nucl. Phys. **B110** 300 (1976).  
W.M. Morse et al., Phys. Rev. **D15** 66 (1977).  
S. Barish et al., Phys. Rev. **D9** 2689 (1974).  
A. Firestone et al., Phys. Rev. **D10** 2080 (1974).  
C. Bromberg et al., Phys. Rev. Lett. **31** 1563 (1973).  
J. Whitmore et al., Phys. Rep. **10C** 273 (1974).  
A. Breakstone et al., Phys. Rev. **D30** 528 (1984).

# New Results on Proton Structure Functions from Deep Inelastic Muon Scattering at High $Q^2$

Bologna - CERN - Dubna - Munich - Saclay Collaboration

presented by W. Lohmann  
 Institut fuer Hochenergiephysik, Zeuthen, DLR

**Abstract:** New results on the proton structure functions  $F_2(x, Q^2)$  and  $R = \sigma_L / \sigma_T$  measured in a high statistics deep inelastic muon-hydrogen scattering experiment are presented. The analysis is based on  $2 \times 10^6$  events recorded at beam energies of 100, 120, 200 and 280 GeV. The kinematic range covered is  $.06 < x < .8$  and  $7 \text{ GeV}^2 < Q^2 < 260 \text{ GeV}^2$ . The observed scaling violations are compared to predictions of perturbative QCD. They allow to determine the QCD mass scale parameter  $\Lambda$  and to estimate the distribution of gluons in the proton.

The one-photon exchange deep inelastic muon-proton cross section can be written as

$$\frac{d^2\sigma}{dx dQ^2} = \frac{4\pi\alpha^2}{Q^4 x} \left\{ 1 - y + \frac{y^2 Q^2}{4E^2} + \frac{y^2 E^2 + Q^2}{2E^2(R(x, Q^2) + 1)} \right\} F_2(x, Q^2)$$

where  $E$  is the energy of the incident beam,  $Q^2$  the squared four momentum transfer carried by the virtual photon and  $x$  and  $y$  are the Bjorken scaling variables.  $F_2(x, Q^2)$  is the proton structure function and  $R = \sigma_L / \sigma_T$  is the ratio of absorption cross sections for virtual photons of longitudinal and transverse polarization.  $F_2$  and  $R$  contain all the information about the structure of the nucleon obtainable from unpolarized lepton-proton scattering.

The data was collected at the CERN SPS muon beam with a high luminosity spectrometer which is described elsewhere [1]. It consists of 8 segmented iron toroids of 5m length magnetized close to saturation. Eight 5m long liquid hydrogen targets are located in front of the apparatus and in the central bore. Muons scattered in the target are deflected into the spectrometer iron. Each magnet module is instrumented with ring-structured trigger counters and 8 planes of MWPC for coordinate measurements. The resolution of the spectrometer, limited mainly by multiple scattering and effective chamber resolution, is  $\sigma_p/p = 10\%$  and  $\sigma_{Q^2}/Q^2 = 8\%$ , almost constant over the kinematic region.

The momentum of the incident muons was measured with a spectrometer consisting of an airgap magnet and four scintillator hodoscopes upstream of the apparatus.

The analysis is based on  $2 \times 10^6$  events after all cuts, recorded at beam energies of 100, 120, 200 and 280 GeV. The

data sample and kinematic ranges are summarized in table 1.

Table 1. The data sample

Beam energy (GeV)	x range	Q <sup>2</sup> range (GeV/c <sup>2</sup> )	Number of events
100	.06-.80	7- 80	570000
170	.06-.80	8-106	420000
200	.06-.80	16-150	800000
280	.06-.80	26-260	190000

In view of the high statistical accuracy of the data a big effort was invested into the calibration of the apparatus in order to reduce the systematic errors to a similar level. As a summary the accuracy reached for the main sources of systematic errors will be given. More details can be found in ref. /2/.

- calibration of the incident energy  $\Delta E/E < 1.5 \times 10^{-3}$
- calibration of the scattered muon momentum  
magnetic field  $\Delta B/B < 2 \times 10^{-3}$   
energy loss  $\Delta E_{\text{loss}}/E_{\text{loss}} < 10^{-2}$
- normalization, absolute  $< 3\%$   
relative  $< 1\%$
- corrections for the finite resolution  
of the spectrometer  $\Delta \sigma/\sigma < 5 \times 10^{-2}$

Particular effort has been devoted to the muon energy loss and the spectrometer resolution. The energy loss was measured in a dedicated experiment and simulated taking into account the stochastic nature of all contributions /3/. The momentum resolution of the spectrometer was measured in special runs with beams directed into the magnets.

In order to isolate the one-photon exchange cross section, corrections for higher order processes have to be applied to the measured cross section. We used the formulae by Bardin et al. /4/, which contain

- vacuum polarization by leptons and quarks
- lepton current processes up to order  $\alpha^2$
- hadron current processes of order  $\alpha^3$
- contributions from  $\gamma$ -Z interference

The error on the structure functions from uncertainties of the radiative corrections was estimated to be less than 1 %.

The comparison of cross sections at different beam energies allows to determine R by minimizing the  $\chi^2$  of the four data sets with respect to each other. This is done separately for each x-bin assuming R to be independent of Q<sup>2</sup>. The result is shown in fig. 1. Also shown is an earlier measurement of the EMC experiment /5/. At  $x > 0.25$ , the measured values are small and compatible with zero. At small x, the data shows a rise well described by the QCD prediction (solid curve). R<sub>000</sub> was used to compute the F<sub>2</sub> at the four different beam energies. Their excellent agreement, especially at large x, is a powerful cross-check of the systematics /2/. The final F<sub>2</sub> from the combined data sets is shown in fig. 2 together with the EMC data and with the SLAC-MIT results from electron proton scattering at low Q<sup>2</sup> /5/. The agreement with the EMC data



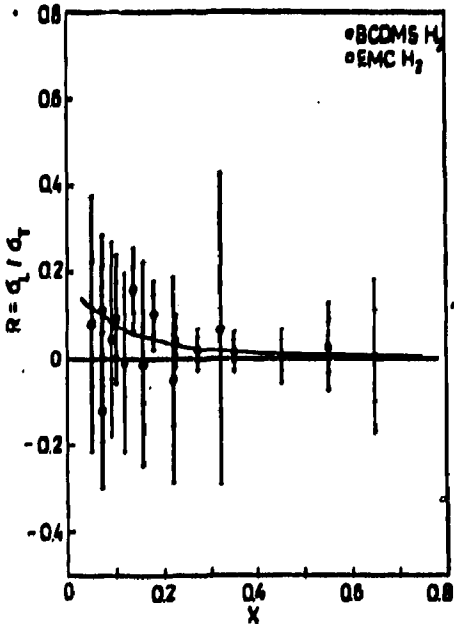


FIG. 1

is poor especially at small  $x$  where the  $F_2$  measured in this experiment is larger by up to 20%. The SLAC-MIT results fit well to our data without any normalization factor.

The data exhibits a clear deviation from Bjorken scaling. In the framework of perturbative QCD [7] scaling violations are due to the  $Q^2$  evolution of quark and gluon distributions which can be described by the Altarelli-Parisi equations. Our measurement is extended to large  $Q^2$  and  $x$  and therefore well suited for a precise test of the evolution equations. To fit the evolution equations to the experimental data we employed two methods [8,9] which have been

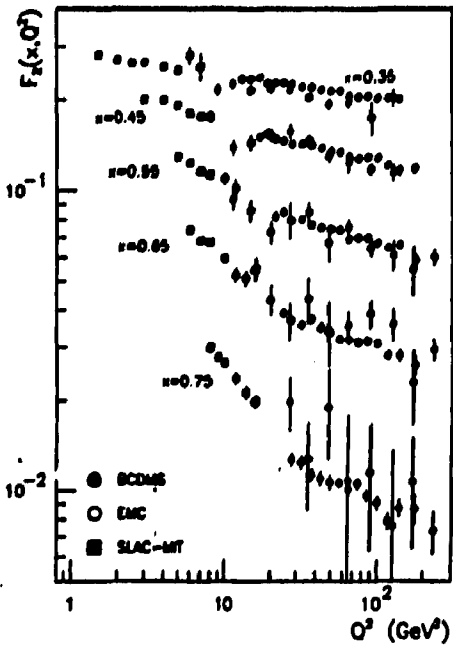
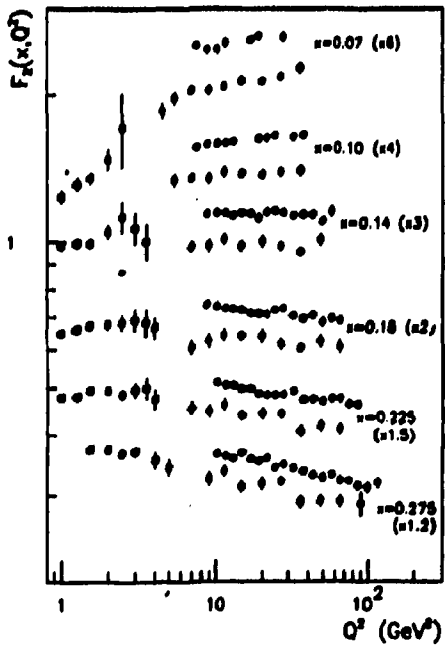


FIG. 2

developed within our collaboration. They allow to fit the flavour singlet and nonsinglet evolution equations both in a

leading order (LO) perturbation expansion and in a next-to-leading order expansion in the  $\overline{MS}$  renormalization scheme.

The region of  $x \geq .275$  and  $Q^2 > 20 \text{ GeV}^2$  was used in the non-singlet approximation where the gluon distribution is ignored. The results of these fits are summarized in table 2.

Table 2 : Results of non-singlet fits

	$\Lambda_{Lo}$	$\chi^2/DOF$	$\Lambda_{\overline{MS}}$	$\chi^2/DOF$
ref /8/	$182 \pm 20$	169/180	$211 \pm 22$	169/180
ref /9/	$184 \pm 20$	170/180	$201 \pm 20$	168/180

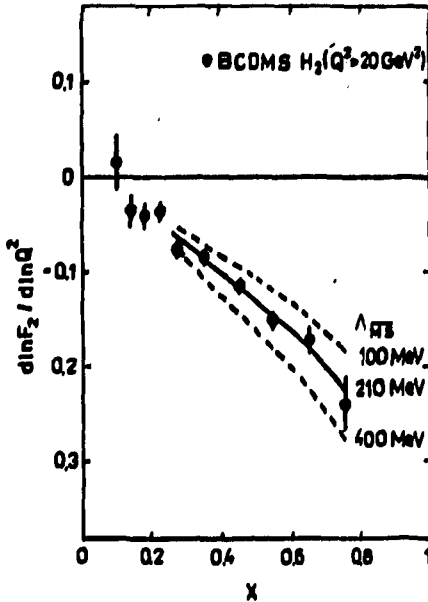


FIG.3

dependence of the  $F_2$  which is not predicted by the theory. A more stringent test is obtained by comparing the  $x$ -dependence of the scaling violations observed in the data to the one expected from the QCD evolution. This is the only prediction of perturbative QCD for deep inelastic scattering which can be tested experimentally. The nonsinglet case is shown in fig. 3 where the logarithmic derivatives  $d \ln F_2(x, Q^2) / d \ln Q^2$  are compared to the next-to-leading order predictions for  $\Lambda_{\overline{MS}} = 210 \text{ MeV}$ . The measured  $x$ -dependence of the scaling violations in fig. 3 is in excellent agreement with the predicted one within statistical errors.

For the QCD analysis over the full  $x$  range of the data, the proton structure function is decomposed into a singlet (S) and a nonsinglet (NS) part as //

$$F_2(x, Q^2) = 5/18 F_2^S(x, Q^2) + 1/6 F_2^{NS}(x, Q^2)$$

where  $F_2^{NS}$  and  $F_2^S$  follow different  $Q^2$  evolutions. All data points at  $Q^2 > 10 \text{ GeV}^2$  are used in the fits. The gluon momentum is parametrized as  $xG(x, Q^2) = A(\eta+1)(1-x)^\eta$  at  $Q_0^2 =$

Our best estimate for the QCD mass scale parameter at next-to-leading order is

$$\Lambda_{\overline{MS}} = 210 \pm 20 \text{ (stat.) MeV}$$

corresponding to a strong coupling constant of

$$\alpha_s = 0.1874 \pm 0.003 \text{ (stat.)}$$

at  $Q^2 = 100 \text{ GeV}^2$ . The detailed evaluation of the systematic error on  $\Lambda$  has not yet been completed, but it is expected to be similar to that of our carbon target measurement ( $\Delta\Lambda = 60 \text{ MeV (syst.)}/2$ ).

Conventionally,  $\Lambda$  has been determined from global GCD fits to  $F_2(x, Q^2)$ , which do not, however, constitute a sensitive test of QCD. The  $\chi^2$  of such fits describe mainly the agreement with the

5 GeV<sup>2</sup> and is allowed to evolve with Q<sup>2</sup>. From energy-momentum sum rule, A equals the fraction of the total proton momentum carried by gluons and is found to be A = .45 at Q<sup>2</sup> = 5 GeV<sup>2</sup>.

The results for A and η from two different methods [8,9] are given in table 3.

Table 3. Results of singlet + nonsinglet QCD fits to F<sub>2</sub>(x,Q<sup>2</sup>) at x ≥ 0.07 and Q<sup>2</sup> ≥ 10 GeV<sup>2</sup>

	Λ Lo	η Lo	x <sup>2</sup> /DOF	Λ NS	η NS	x <sup>2</sup> /DOF
ref. [8]	196±19	5.2±1.5	281/282	214±19	10.3±1.5	282/282
ref. [9]	183±25	5.4±1.3	269/277	195±20	8.9±1.5	270/277

The results for A are in good agreement with those of the nonsinglet fits. The measured scaling violations are compared in fig.4 to next-to-leading order fits for different values of η and show again very good agreement with the theoretical prediction. The gluon distribution has been determined for the first time from singlet fits in next-to-leading order QCD. As can be seen from fig. 5, it is significantly softer than in leading order, which also explains the observed weak dependence of A on η.

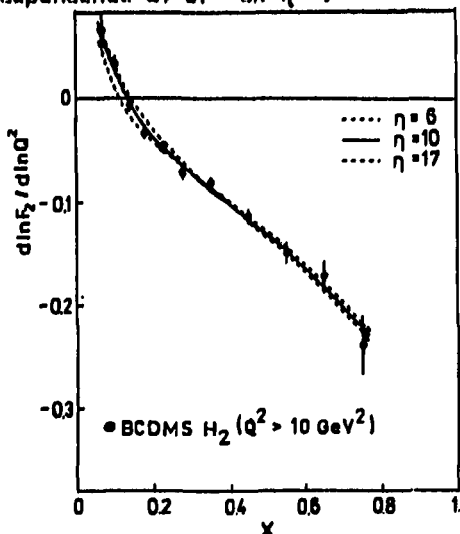


FIG 4

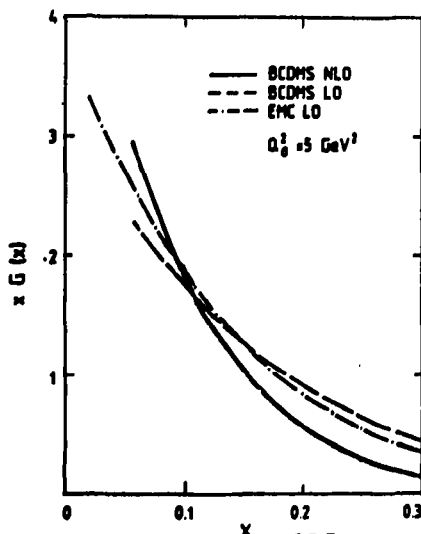


FIG 5

#### References

- /1/ BCDMS, A.C. Benvenuti et al., Nucl. Instr. Meth. 226 (1984) 330.
- /2/ BCDMS, A.C. Benvenuti et al., Phys. Lett. 195B (1987) 91 and 97.
- /3/ BCDMS, R. Kopp et al., Z. Phys. C 28 (1985) 171;
- W. Lohmann et al., CERN 85-03 (Yellow Report).
- /4/ A.A. Akhundov et al., Sov. J. Nucl. Phys. 26 (1977) 660;
- A.A. Akhundov et al., Preprint JINR E2-86-104, Dubna 1986.
- /5/ EMC, J.J. Aubert et al., Nucl. Phys. B259 (1985) 189.
- /6/ A. Bodek et al., Phys. Rev. D20 (1979) 1471.
- /7/ G. Altarelli, Phys. Rep. B1 (1982) 1.
- /8/ M. Virchaux and A. Ouraou, Preprint D.PhPE 87-15.
- /9/ V.G. Krivokhizhin et al., Z. Phys. C

# SCALAR GLUEBALL INDICATION IN PION SCATTERING <sup>†</sup>

D. Krupa

Institute of Physics of the Electro-Physical Research Centre,  
Slovak Academy of Sciences, 842 28 Bratislava, Czechoslovakia  
V.A. Meshcheryakov, Yu.S. Surovtsev  
Laboratory of Theoretical Physics,  
Joined Institute of Nuclear Research, 141 980 Dubna, USSR

## Abstract

The production  $\pi\pi \rightarrow K\bar{K}$  s-wave amplitude calculated from the  $\pi\pi \rightarrow \pi\pi$  s-partial wave scattering amplitude by means of the coupled channel formalism indicates the importance of coupling of channels above 1.2 GeV. The possible interpretation of partial wave singularities supposed to be due to the lightest glueball is given.

There are several independent theoretical indications<sup>1</sup> that the lightest glueball should be the state with no spin and positive parity, and that it should have the mass between 0.5 and 2.0 GeV. The natural way to see such state is to look at the  $I=0$ , s-wave  $\pi\pi$  scattering. The Particle Data Group<sup>2</sup> lists two such states -  $f_0(975)$  and  $f_0(1300)$ , previously called as  $S^*$  and  $\epsilon$ , respectively. Since there was a lot of controversy concerning the nature of these states we have done a new attempt to establish these mesons from the data on s-wave  $\pi\pi$  scattering<sup>3</sup>.

Because the  $S^*$  mass is very close to the  $K\bar{K}$  production threshold energy, above which there is a large coupling of the  $\pi\pi$  and  $K\bar{K}$  channels, we have used the 2x2 S-matrix coupling together  $\pi\pi$  and  $K\bar{K}$  channels:

$$S = \begin{pmatrix} S_{11} & S_{12} \\ S_{21} & S_{22} \end{pmatrix} \quad \begin{matrix} 1 - (\pi\pi) \\ 2 - (K\bar{K}) \end{matrix}$$

In order to describe the  $\pi\pi$  scattering data the analytical continuation of the S-matrix to the unphysical sheets

<sup>†</sup>Talk presented at the Hadron Structure'87 conference.

in the  $s$  variable was used where  $s$  is the total centre of mass energy squared. Each elastic resonance is parametrized by four zero-pole pairs as the result of this continuation. Their position is determined just by two parameters corresponding to the mass and to the width of resonance. The first two zeros are placed on the first sheet complex plane symmetrically around the real  $s$ -axis. The second pair is at the same position on the fourth sheet. The poles are also at same positions in  $s$  variable but they are placed on the second and the third sheet. However, due to the absorptive effects the zero-pole pairs on the third and the fourth sheets are shifted relatively to those on the first and the second sheet<sup>4</sup>.

The  $\pi\pi$  S-matrix element can then be easily parametrized by a suitable rational form. In order to take into account the Riemann sheet structure generated by unitarity we write this rational form in a new variable

$$z = \frac{k_1(s) + k_2(s)}{k_1(4m_K^2)} \quad (2)$$

defined by the centre of mass momenta

$$k_1(s) = \frac{1}{2}(s-4m_\pi^2)^{1/2} \quad \text{and} \quad k_2(s) = \frac{1}{2}(s-4m_K^2)^{1/2} \quad (3)$$

in the  $\pi\pi$  and  $K\bar{K}$  channels, respectively.

By this means a very good and effective description of all  $\pi\pi \rightarrow \pi\pi$  s-wave data from  $\pi\pi$  threshold energy up to 1.89 GeV was achieved. Moreover, the two other coupled S-matrix elements for processes  $K\bar{K} \rightarrow K\bar{K}$  and  $\pi\pi \rightarrow K\bar{K}$  were predicted from the  $\pi\pi$  data assuming the validity of 2x2 S-matrix unitarity. Our prediction of the  $\pi\pi \rightarrow K\bar{K}$  production process is shown in Fig.1 and Fig.2 where the absolute value of phase of the  $S_{12}$  matrix element is compared with experimental data.<sup>5-7</sup> This comparison shows the remarkable agreement with the data up to 1.2 GeV. For higher energies there is deviation of the predicted values and the experimental ones. This means that the 2x2 S-matrix unitarity is violated at these higher energies

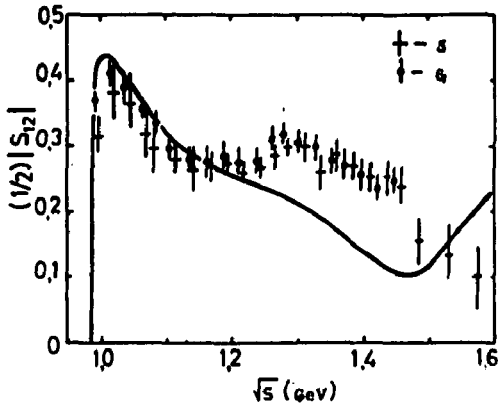


Fig. 1

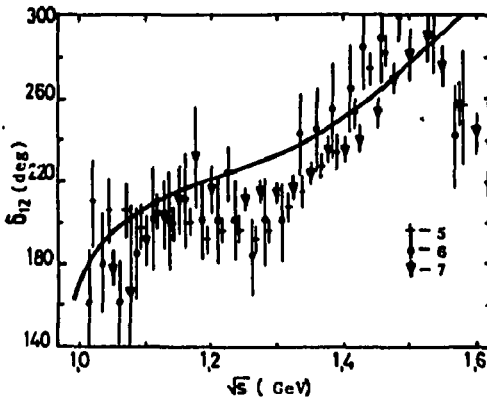


Fig. 2

and that in order to achieve more realistic results the  $\gamma\gamma$  coupled channel should be also taken into account at least. This would result in  $3 \times 3$  S-matrix coupled channel calculation. Having these three coupled channels the  $\pi\pi$  scattering amplitude analyticity structure requires to consider more complicated Riemann sheet structure consisting of eight connected Riemann sheets. The elastic resonance will now be described by eight instead of four zero-pole pairs at the same complex-conjugate points in the s-variable on all eight Riemann sheets.

In the January issue of this year CERN Courier<sup>8</sup> there appeared an article about interesting analysis of Au, Morgan and Pennington in which they analyse the scalar glueball sector including the new CERN ISR double pomeron exchange data on  $pp \rightarrow pp\pi\pi$  and  $ppK^+K^-$  processes<sup>9</sup>. Their conclusion is that a single narrow resonance is not enough to fit the data and they find as much as three different states in the 1GeV energy region.

Their analysis is based on the coupled channel K-matrix approach. The advantage of this approach is that the K-matrix does not have the right-hand cuts generated by unitarity and

therefore one does not need to bother about the complicated Riemann sheet structure. However, after identifying the resonances by means of the K-matrix one is still interested in placing them into an appropriate Riemann sheet of the S-matrix in order to interpret them properly.

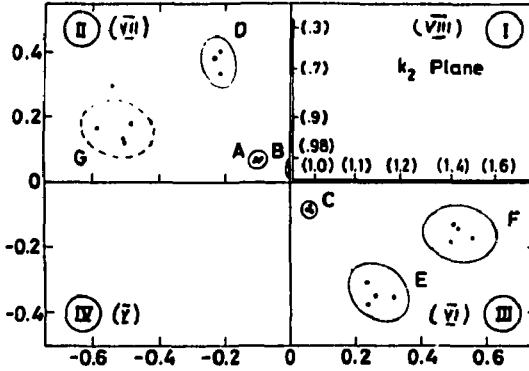


Fig.3

The S-matrix poles found by Au and collaborators in Fig.3. They are displayed in the  $k_2(s)$  complex plane. In different solutions the poles were placed in the regions of the complex  $k_2$  plane denoted as A through G. One can see how these poles reproduce the

symmetry pattern that a pole on the 2nd sheet has a counter-part image pole on the 3rd sheet. The average pole positions and the couplings of the corresponding resonances to  $\pi\pi$  and  $K\bar{K}$  channels are in the following table:

Position	Name	Couplings		Sheet
		$g$	$g_K$	
A = 1.001 - 0.026i	$S_1(991)$	0.22	0.28	II
C = 0.985 - 0.020i				III
D = 0.87 - 0.381i				VII
E = 0.94 - 0.351i	$\epsilon(900)$	0.52	0.27	VI
F = 1.42 - 0.231i				II
G = 1.42 - 0.221i	$\epsilon(1430)$	0.58	0.16	III
B = 0.988	$S_2(988)$	0.02	0.35	L-H.C.

Table 1.

They have very interesting interpretation.  $S_1$  is interpreted as the glueball,  $S_2$  is interpreted as the  $K\bar{K}$  molecule and  $\xi(900)$  is a broad state where, all three states together reproduce the old  $S^*$  phenomenon.

What can we say to these interesting results in view of our approach? First, we have not found any need of other states beside the narrow  $S^*$  in the 1GeV energy region. But we have not analysed such rich amount of data and namely, we have not analysed the CERN ISR data as they did and which make essential contribution to their analysis. Second, we came to the conclusion that in order to have a reliable results above 1.2 GeV one has to perform the  $3 \times 3$  coupled channel analysis. In Ref.9 the data up to 1.6 GeV were analysed.

We can therefore ask the question what would happen if the poles in terms of the K-matrix would be projected onto the S-matrix with 8 Riemann sheets ( corresponding to  $3 \times 3$  coupled channels ) instead of the 4 sheets? Would not the poles denoted as D and E fall on the VII-th and VI-th sheet as they are denoted in Table 1 and also in Fig.3 in brackets? But that would mean that all four poles A,C,D and E describe the same one physical resonance.

The pole denoted as B with coupling to  $K\bar{K}$  but not to  $\pi\pi$  channels could simply simulate the  $K\bar{K}$  background coming for instance from the left-hand cut which starts at  $s = 4(m_K^2 - m_\pi^2)$ , i.e. just below the  $K\bar{K}$  threshold where it was found. This pole does not appear in the  $\pi\pi$  channel S-matrix element since it is located almost on the  $\pi\pi$  channel physical region, i.e. on the s variable real axis, and so it is cancelled by the corresponding zero approaching the same position from the I-st sheet. Therefore it is not seen in our analysis<sup>10</sup>.

Though our arguments concerning interpretation of these poles are rather tentative we hope that interesting results of Au et al. will stimulate further research both experimental as well as theoretical in order to clarify the scalar mesons physics.



## References

1. A.Palano, Preprint CERN-EP/87-92  
F.Couchat, Orsay Preprint LAL 87-40  
J.Lánik, Dubna Preprint JINR E2-87-483
2. Particle Data Group, Phys.Lett. 170B April 1986
3. D.Krupa, V.A.Meshcheryakov, Yu.S.Surovtsev,  
Yad.Fiz. (Sov.Jour.Nucl.Phys.) 43 (1986) 231
4. D.Krupa, V.A.Meshcheryakov, Yu.S.Surovtsev,  
Problems on High Energy Physics and Field Theory, p.335-344,  
Moscow, "Nauka", 1987, Ed. M.V.Saveliev
5. A.B.Wicklund et al., Phys.Rev.Lett. 45 (1980) 1469  
D.Cohen et al., Phys.Rev. D22 (1980) 2595
6. A.D.Martin, E.N.Ozmutlu, Nucl.Phys. B158 (1977) 520
7. A.Etkin et al., Phys.Rev. D25 (1982) 1786
8. M.Albrow, CERN Courier 27 (1987) 16
9. K.L.Au, D.Morgan, M.R.Pennington, Phys.Rev. D35 (1987) 1633
10. D.Krupa, V.A.Mashcheryakov, Yu.S.Surovtsev,  
Bratislava Preprint FU-87/09, Submitted to Czech.Jour.Phys.

INVESTIGATION OF (e,e') SCATTERING ON ELECTRON  
SYNCHROTRON AT YEREVAN PHYSICS INSTITUTE

D.S. Bagdasaryan, G.B. Kazaryan,  
H.G. Mkrtchyan, I.A. Troshenkova

Yerevan Physics Institute, Markarian St. 2,  
375036, Yerevan, Armenia, USSR

Abstract

Experimental cross sections of the (e,e') scattering on  ${}^6\text{Li}$ ,  ${}^9\text{Be}$ ,  ${}^{12}\text{C}$  and  ${}^{28}\text{Si}$  nuclei in the region of quasi-elastic peak and  $\Delta$ -resonance at  $0.1 \leq q^2 \leq 0.5 \text{ GeV}^2/c^2$  have been reported. Theoretical calculations in the nucleus shell model reproduce successfully experimental spectra. In the quasi-elastic peak region the results for  ${}^9\text{Be}$  and  ${}^{12}\text{C}$  show a good Y-scaling behaviour.

It is well known that at a given energy of the incident electron,  $E$ , and at sufficiently large transferred three-dimensional momenta,  $\bar{q} > 400 \text{ MeV}/c$ , in electron scattering energy spectra at  $E'$  close to  $E$  one may observe a characteristic peak corresponding to elastic scattering of the electron on the nucleus nucleon, the so-called quasi-elastic peak. With increasing transferred energy (or virtual photon energy  $\omega = E - E'$ ) the next peak appears which may be compared to the resonance pion production on the bound nucleon of nucleus.

As shown by the recent (e,e') experiments, particularly by the experiments /1,2/ on the separation of contributions of the transversely and longitudinally polarized photons on nuclei, systematical measurements, especially in the region of quasi-elastic peak and  $\Delta$ -resonance, at higher energies and  $\bar{q}$ , respectively, remain an urgent problem so far. Of great interest is as before the study of  $A$  and  $q^2$  dependence of the extent of the excess of experimental cross sections over theoretical calculations in the region between quasi-elastic and

### $\Delta$ -peaks.

On the extracted electron beam of the Yerevan synchrotron there have been carried out measurements on  $(e, e')$  scattering on  ${}^6\text{Li}$ ,  ${}^9\text{Be}$ ,  ${}^{12}\text{C}$  and  ${}^{28}\text{Si}$  nuclei in the region of quasi-elastic peak and  $\Delta$ -resonance in the initial electron energy range  $(1.0 - 2.1)$  GeV and  $\Theta = 15.5^\circ - 20^\circ$ .

The layout of the magnetic elements of the spectrometer and detecting equipment is shown in Fig. 1. Slowly ejected electrons with  $\Delta E/E \sim \pm 0.5\%$  and intensity  $\sim 5 \times 10^9 e^-/c$  were focused to remote-controlled targets. The beam monitoring was realized with a secondary-emission monitor and a Gauss quantummeter with an accuracy no worse than  $\sim 2\%$ . The beam position and sizes were monitored by flag indicators.

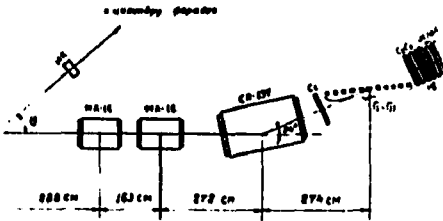


Fig. 1

Scattered electrons were registered at  $\Theta \geq 15.5^\circ$  with a magnetic spectrometer consisting of two MA-16 type quadrupole lenses and an CN-137 type vertically deflecting magnet. The detecting equipment of the spectrometer may be functionally divided into three parts: the aperture counters ( $C_1 - C_3$ ), the electron identification system ( $dE/dX$ ) and the pulse hodoscope consisting of 11 (or 17) scintillation counters. The spectrometer pulse capture was up to 17%, angular acceptance  $\sim (1.9 - 0.75)$  msterad, depending on the value of angular collimation of scattered electrons ( $\pm 2.5^\circ$  or  $\pm 1^\circ$ ); the spectrometer momentum resolution was  $\sim \pm 0.5\%$ .

The absolute calibration of the set-up was realized by comparison of measured spectra of elastic  $ep$ -scattering (by the method of subtraction of  $\text{CH}_2$  and C spectra) with calculated ones.

More detailed information on the experimental set-up and its calibration technique one can find in Ref./3/.

The main source of the background are the electrons pro-

duced from the process  $\gamma \rightarrow e^+e^-$  and nonsuppressed  $\pi$ -mesons.

The level of random coincidences at  $\sim 5 \times 10^9$   $e^-$ /sec beam intensity and  $\sim 0.5$  msec ejection time was less than  $\sim 2\%$ . The background from the beamline residual gas was determined by measurements without target and did not exceed  $\sim 1\%$ . Contributions from the  $\gamma \rightarrow e^+e^-$  process and from nonsuppressed  $\pi$ -mesons were estimated by measurements at the spectrometer reverse polarity. The background made up  $\sim (2-5)\%$  in the quasi-elastic peak region and reached  $\sim (5-10)\%$  in the  $\Delta$ -resonance region.

Some experimental data obtained at Yerevan Physics Institute for  ${}^6\text{Li}$ ,  ${}^9\text{Be}$ ,  ${}^{12}\text{C}$  and  ${}^{28}\text{Si}$  nuclei are presented in Fig.2.

The errors indicated in Fig.2 include only statistical (3-5)% ones and those connected with the determination of the set-up efficiency. The systematical errors, due to the beam monitoring and normalizing factors, make up  $\sim 10\%$ .

The results have shown that for all the nuclei there is observed a characteristic peak of quasi-elastic scattering whose width increases with atomic number of nucleus. Also another peak was observed, corresponding to the  $\Delta$ -resonance production.

Theoretical curves represent a sum of contributions from the quasi-elastic peak and  $\Delta$ -resonance and are calculated in the shell model under assumption that the cross section on the nucleus is a noncoherent sum of cross sections on individual nucleons. The model parameters obtained in Ref./4/ were used. Calculations on the shell model, in general, reproduce successfully experimental spectra. To compare experimental results with calculations, radiative distortions corresponding to experimental conditions were introduced into theoretical cross sections.

The accounting of radiative corrections was realized by the method worked out by Mo and Tsai /5/.

The  $\Delta$ -resonance maxima are strongly smoothed by Fermi-motion of nucleons. The overlap of the threshold region of  $\pi$ -meson production with the "tail" of quasi-elastic peaks

imitates the shift of the  $\Delta$ -resonance maximum towards the quasi-peak by 20-30 MeV.

In the quasi-elastic peak maximum the cross section normalized by the number of nucleons decreases with increasing atomic number of the nuclei. While in the region of  $\Delta$ -resonance maximum the cross section normalized by the number of nucleons within the experimental errors does not depend on the atomic number.

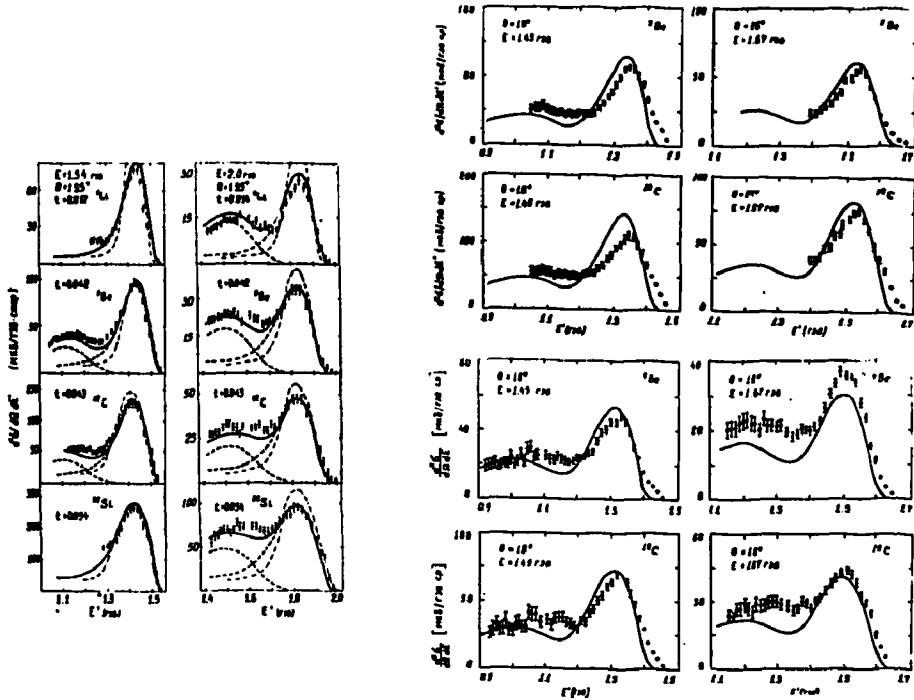


Fig. 2

For further analysis it is necessary to subtract from measured spectra the "tail" contributions of the process of elastic scattering of electrons on nuclei at  $E \leq 1.45$  GeV as well as to remove radiative distortions.

The extraction of nonradiative cross sections is connected with measurements at  $\Theta = \text{const}$  and different initial energies  $E$ , while the requirement  $q^2 = \text{const}$  (the necessary con-

dition for the separation of  $R_L$  and  $R_T$ ) is provided by the change of the angle. To match these programs, the search for the optimal plan of measurements is necessary for a given set-up.

In Ref./6/, by means of mathematical modelling of spectra of the  $(e, e')$  process in the region of quasi-elastic scattering and  $\Delta$ -isobar production, there has been worked out a method to obtain from initial experimental material data free from radiative distortions.

It was shown that at the Yerevan set-up the measurement program aimed at separation of longitudinal and transverse components of the cross section of  $(eA)$  interaction is quite real. Ibidem the practical aspects of the realization of such investigations at energies of initial electrons  $E \geq 1$  GeV are considered.

The given series of measurements was carried out with account of namely these programs.

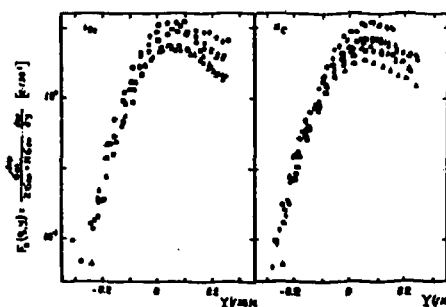


Fig. 3. Experimental points refer to:  $\Delta(\blacktriangle)$  - 1.45 GeV,  $16^\circ(18^\circ)$ ;  $\square(\blacksquare)$  - 1.67 GeV,  $16^\circ(18^\circ)$ ;  $\circ(\bullet)$  - 1.93 GeV,  $16^\circ(18^\circ)$ ;  $\diamond(\blacklozenge)$  - 2.13 GeV,  $16^\circ(18^\circ)$ .

Fig. 3 shows results of our measurements of  $(e, e')$  reactions in the quasi-elastic peak region, processed in accordance with the Y-scaling concept /7/.

#### References

- /1/ Barreau P. et al. Nucl.Phys., 1983, v.402, p.515.
- /2/ Marchand C. et al. Phys.Lett., 1985, v.153B, p.29.
- /3/ Bagdasaryan D.S. et al. Sov. J. PTE, 1986, N.5, p.36.
- /4/ Aznauryan I.G., Troshenkova I.A. Yad.Fiz., 1986, v.43, p.342.
- /5/ Mo L.W., Tsai Y.S. Rev.Mod.Phys., 1969, v.41, N.1, p.205.
- /6/ Mkrtchyan H.G., Troshenkova I.A. VANT, 1986, iss.4(30)1-96.
- /7/ West G.B. Phys.Rep., 1975, v.18, p.263.

## HIGH ENERGY HADRON SCATTERING IN FORWARD DIRECTION

V. Kundrať, M. Lokajíček  
Institute of Physics, CSAV, Prague

D. Krupa  
Institute of Physics SAV, Bratislava

In the high-energy elastic differential cross section experiments with unpolarized particles the quantity which is measured is the counting rate  $\Delta N(t)$  (i.e. the number of counts per second per small interval  $\Delta t$  of four-momentum transfer squared). This counting rate is normalized to the differential cross section  $\frac{d\sigma}{dt}$  in the following manner /1/

$$\Delta N(t) = L \frac{d\sigma}{dt} ; \quad (1)$$

the normalization factor  $L$  is the luminosity for colliding beams.

Theoretically, the differential cross section is given by the absolute square of the total elastic amplitude  $F(s,t)$  which is the complex function of the CMS energy  $\sqrt{s}$  and  $t$ . It means that one can determine only the module of the total amplitude from the experimental data.

Let us confine ourselves to the case of the hadron-hadron or hadron-nucleus elastic scattering. The differential cross section is being determined for  $-t \in (10^{-3} - 10^{-2}, 1. - 15.) \text{ GeV}^2$ ; i.e. the measured interval covers: the region where pure nuclear scattering with the amplitude  $F^N$  predominates and also the region where the Coulomb amplitude plays a significant role and which can be exactly calculated within the framework of QED. Therefore the total amplitude  $F$  can be decomposed into two components

$$F = F^C + F^N. \quad (2)$$

Evidently, only the module of the nuclear component  $F^N$  can be determined from experiment; its phase being introduced by expression

$$F^N(s,t) = i |F^N(s,t)| e^{-i} f(s,t), \quad (3)$$

remains completely unknown function of  $s$  and  $t$ . Do we need to know it?

The answer is yes. The reason is that instead of studying the properties of elastic scattering in the  $t$ -variable one can investigate it in the impact-parameter space  $b$  using the Fourier-Bessel transform

$$h(s, b) \sim \int_{-\infty}^{\infty} \sqrt{-t} d\sqrt{-t} F^N(s, t) J_0(b\sqrt{-t}), \quad (4)$$

where  $J_0(x)$  is the Bessel function of zero order. The absolute square  $|h(s, b)|^2$  of the image of the nuclear component gives us the distribution of elastic scattering in the impact parameter space which tells us something about the range of nuclear forces acting between colliding hadrons.

Physically, two kinds of this distribution are of great interest. The first one called central has its maximum at  $b=0$  and decreases with increasing  $b$  in such a way that  $\langle b^2 \rangle$  remains small. In this case one uses for the nuclear component  $F^N$  the amplitude with dominant imaginary part in a rather great interval of  $t$  around  $t=0$  and vanishing at the dip. The real part which smoothly increases with increasing  $|t|$  is introduced in order to obtain the non-zero value of  $\frac{dG}{dt}$  at the dip. However, it means that one uses the amplitude with slowly varying phase  $f(s, t)$  being taken practically as constant. After performing the Fourier-Bessel transform (4) to such an amplitude one unavoidably obtains the central distribution of elastic scattering which has very important logical consequences. Firstly, the protons in "head-on" collisions must be rather transparent, which seems to be a "puzzle" /2/. Secondly, there is a discrepancy in the description of diffraction scattering, if elastic scattering is central, since the inelastic diffraction, being produced by a similar production mechanism, is being always described by the peripheral profiles /3/.

The second kind of distribution called peripheral can be characterized by a rather large value of  $\langle b^2 \rangle$  and has its maximum at some positive value of  $b$  or at least a broad plateau. It can be obtained if one has rather strong increase of  $f(s, t)$  with increasing  $|t|$  in such a way that  $\text{Im } F^N(s, t) = 0$  at  $|t| \lesssim 0.1 \text{ GeV}^2$  /4/.



Comparing it with the previous case one uses again the amplitude with dominant imaginary part but now only for very small values of  $|t|$ . There is, of course, a great difference in physical consequences and basic assumptions. It is evident that the mentioned troubles related to the first kind of central behaviour can be removed if one regards the elastic scattering as peripheral process. Moreover, the arguments leading to the "old-type" amplitude and giving the central distribution are based fully on asymptotic properties and can be hardly justified at present energies, which all lead to the conclusion that all elastic collisions should be peripheral /5/. Therefore, we prefer the peripheral picture of elastic scattering for which the strong  $t$ -dependence of the phase is crucial.

One of the methods which could in principle decide between the mentioned two possibilities is the interference between the Coulomb and nuclear components of the total amplitude. Let us mention, first, the case of  $pp$  scattering. The currently used analysis /6-8/ uses for the total amplitude the following form

$$F(s,t) = \frac{\alpha e}{t} f_p^2(t) e^{i\alpha\phi} + \frac{\sigma_{tot}}{4s} p \sqrt{s} (\rho+i) e^{Bt/2} . \quad (5)$$

The first term in (5) corresponds to the Coulomb component; here  $\alpha = 1/137$  is the fine structure constant,  $f_p(t) = \left(\frac{0.71}{0.71-t}\right)^2$  is the conventional proton dipole form factor and

$\alpha\phi = -\ln((-Bt/2) + \delta)$  is the total West-Yennie phase with Euler constant  $\delta = 0.577$ . The second term describes the nuclear component where  $B$  is the diffraction slope,  $\sigma_{tot}$  the total cross section and  $\rho$  is the ratio of the real to imaginary parts in the forward direction. Thus, applying this formula to the differential cross section data one can determine the values of free parameters  $\sigma_{tot}$ ,  $B$  and  $\rho$ .

However, formula (5) is valid, provided three assumptions are fulfilled:

- (i) spin effects can be neglected,
- (ii) there is the characteristic exponential  $t$ -dependence of the nuclear component in the interference region,

(ii) there is the same  $t$ -dependence of the real and imaginary parts of nuclear components.

The first two assumptions seem to be fully justified /9-11/. The third assumption means that the  $t$ -dependence of the phase is neglected, but there are no reasonable arguments for it. If we want to obtain peripherality of elastic scattering the phase  $\xi(s, t)$  must be strongly  $t$ -dependent. Therefore, conventional formula (5) cannot be used. Instead of it one has to use the modified Cahn's approach /10/ (see /11/)

$$F(s, t) = \frac{\alpha s}{t} r_p^2(t) + F^N(s, t) \cdot \left\{ 1 - i\alpha \int_{-\infty}^0 dt' \ln \frac{t'}{t} \frac{d}{d\vartheta} \left[ r_p^2(t') \frac{F^N(s, t')}{F^N(s, 0)} \right] \right\} \quad (6)$$

with the nuclear component

$$F^N(s, t) \sim e^{Bt/2 - i \xi(s, t)} \quad (7)$$

and with the following parametrization of the phase

$$\xi(t) = \xi_0 + \xi_1 \left| \frac{t}{t_0} \right|^{\alpha} e^{\gamma t} + \xi_2 \left| \frac{t}{t_0} \right|^{\lambda}, \quad t_0 = 1 \text{ GeV}^2; \quad (8)$$

here  $\xi_0, \xi_1, \alpha, \gamma, \xi_2, \lambda$  are the free parameters which can be in principle energy-dependent. The form of used parametrization (8) is based on our previous results /4/ and allows the peripheral as well as central distribution.

We have applied it to the case of the  $pp$  elastic scattering for seven different values of  $p_{lab} = 100 - 2081 \text{ GeV}/c$  (for details see /11/. We have performed two types of the fits: first one with the parameters  $\xi_1 = \xi_2 = 0$ , which corresponds to the case of constant  $\varrho = \tan \xi_0$ . The results are in Table 1. In the second type of the fits the parameters  $\xi_1$  and  $\xi_2$  were allowed to change. Under some constraints leading to peripherality (for details see /11/) we obtained nearly the same values of  $\chi^2$  distributions as in the previous case (see Table 1) with slightly modified values of  $\sigma_{tot}$ ,  $B$  and  $\rho$  (for the values of other free parameters see also /11/. The obtained peripherality is characterized

by the quantity  $\sqrt{\langle b^2 \rangle} = 1.6 - 1.9$  fm which is much greater than in the case of the constant phase ( $\sqrt{\langle b^2 \rangle} = 0.66 - 0.69$  fm). Due to the same level of  $\chi^2$  values we regard the results of both the fits as indistinguishable experimentally.

The second investigates type of elastic scattering is the case of  $p\text{-}^4\text{He}$  process at  $p_{\text{lab}} = 200$  GeV/c. Again the conventional analysis /12/ uses a similar formula as (5)

$$F(s, t) = \frac{2\alpha s}{t} f_p(t) f_{\text{He}}(t) e^{i\phi} e^{\frac{Ct}{4}} p \sqrt{s} (\rho+i) e^{(Bt+Ct^2)/2} \quad (9)$$

where

$$f_{\text{He}}(t) = (1 - (2.56t)^6) e^{11.70t} \quad (10)$$

is the  $^4\text{He}$  electromagnetic form factor. Formula (9) is valid under similar assumptions as in the case of  $pp$  scattering and leads to the central distribution. The peripherality can be again obtained if one admits the strong  $t$ -dependence of the phase. In this case instead of Eq. (9) one must use for the total amplitude analogically to Eq. (6)

$$F^{N+C}(s, t) = \frac{2\alpha s}{t} f_p(t) f_{\text{He}}(t) + F^{\text{Nu}}(s, t) \cdot \left\{ 1 - 2i\alpha \int_{-\infty}^0 dt' \ln \frac{t'}{t} \frac{d}{dt'} \left[ f_p(t') f_{\text{He}}(t') \frac{F^{\text{Nu}}(s, t')}{F^{\text{Nu}}(s, 0)} \right] \right\} \quad (11)$$

where the nuclear amplitude is

$$F^{\text{Nu}}(s, t) \sim e^{(Bt+Ct^2)/2 - i \xi(s, t)} \quad (12)$$

and the phase is parametrized as

$$\xi(t) = \xi_0 + \xi_1 \left| \frac{t}{t_0} \right|^{\alpha} e^{\nu \left| \frac{t}{t_0} \right|^{\beta}} + \xi_2 \left| \frac{t}{t_0} \right|^{\alpha}, \quad t_0 = 1 \text{ GeV}^2 \quad (13)$$

Again two types of fits (the first one with constant phase and the second one giving the peripherality) have been performed. The preliminary results can be found in Table 1. The obtained peripherality is characterized by  $\sqrt{\langle b^2 \rangle} = 2.9$  fm, while in the case of constant phase  $\sqrt{\langle b^2 \rangle} = 1.22$  fm. Both the fits exhibit the same value of  $\chi^2$  and are experimentally indistinguishable

again. The corresponding peripheral distribution (together with that one which belongs to  $pp$  scattering at  $p_{lab} = 1487 \text{ GeV}/c$ ) is shown in Fig. 1.

On the basis of our results we can conclude: the concept of peripherality is in a full agreement with the experimental interference data. But we must admit that the analysis of these data cannot decide between the two different pictures of high-energy elastic scattering. The preference should be given to the peripheral interpretation due to logical reasons. The doubts concerning the dominance of imaginary part are also supported by the last experiments at CERN Collider giving an unexpectedly large value of  $Q$  for  $\bar{p}p$  scattering /13/.

### References

- /1/ Block M.M., Cahn R.N.: Rev.Mod.Phys. 57 (1985), 563
- /2/ Giacomelli G., Jacob M.: Phys.Rep. 55 (1979), 1
- /3/ Giovannini A. et al.: Rivista Nuovo Cimento 2 (1971), 1
- /4/ Kunderát V., Lokajíček M Jr., Lokajíček M.: Czech.J.Phys. B31 (1981), 1334
- /5/ Kunderát V., Lokajíček M., Krupa D.: in Elastic and Diffractive Scattering at the Collider and Beyond, Proceedings of the First Workshop, Blois, France, 1985, edited by B.Nicolescu and J.Tran Thanh Van (World Scientific, Singapore, 1986), p.301
- /6/ Amaldi U. et al.: Phys.Lett. 66B (1977), 390
- /7/ Burq J. et al.: Nucl.Phys. B217 (1983), 285
- /8/ Amos N. et al.: Nucl.Phys. B262 (1985), 689
- /9/ Martin A.: Phys.(Paris) Colloq. 46 (1985), C2-727
- /10/ Cahn R.N.: Z.Phys.C15 (1982), 253
- /11/ Kunderát V., Lokajíček M., Krupa D.: Phys.Rev. D35 (1987), 1719
- /12/ Bujak A. et al.: Phys.Rev. D23 (1981), 1895
- /13/ Bernard D. et al.: CERN preprint CERN/EP 87-147

Type	Fit I					Fit II			
	$P_{lab}$ (GeV/c)	$\sigma_{tot}$ (mb)	B (GeV <sup>-2</sup> )	$\phi$	$\chi^2/DF$	$\sigma_{tot}$ (mb)	B (GeV <sup>-2</sup> )	$\phi$	$\chi^2$
pp	100	38.43	11.78	-0.096	81.15/69	38.49	11.74	-0.090	81.44
	150	38.73	12.03	-0.038	74.61/64	38.73	11.86	-0.040	75.14
	250	39.26	12.03	-0.043	43.70/60	39.29	11.94	-0.039	43.72
	300	39.47	12.16	-0.035	63.18/56	39.53	12.08	-0.035	62.89
	1063	41.88	13.10	+0.056	59.70/53	41.93	13.10	0.061	51.84
	1487	42.38	13.11	0.075	45.51/37	42.38	13.10	0.082	43.06
	2081	43.49	13.14	0.086	30.58/30	43.82	13.20	0.089	28.70
p- <sup>4</sup> He	200	122.69 C=-24.93 (GeV <sup>-4</sup> )	33.03	0.027	44.40/40	122.18 C=-36.34 (GeV <sup>-4</sup> )	32.60	0.021	45.55

Table 1.

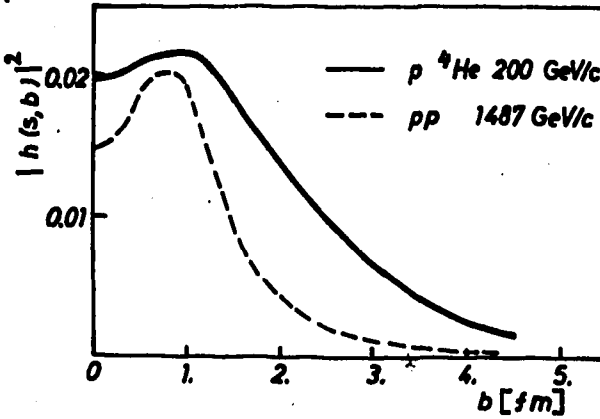


Fig. 1

# A MODEL OF MASSIVE NEUTRINOS WITH A CONSERVED LEPTON NUMBER<sup>1</sup>

W. Grimus  
Institut für Theoretische Physik  
Universität Wien

## ABSTRACT

We consider a left-right symmetric model with the standard assignments of fermion and scalar fields which possesses a strictly conserved lepton number.

---

<sup>1</sup>Supported in part by "Jubiläumsfonds der Österreichischen Nationalbank", Project Nr. 2765.

## 1. INTRODUCTION

In many extensions of the standard model neutrinos are massive. We know from experiment that neutrino masses must be much smaller than those of their charged counterparts [1]. In models with only Dirac mass terms this fact is hard to understand. Since neutrinos are electrically neutral they can also have Majorana mass terms. If in such a theory there is a heavy scale small neutrino masses are obtainable via the seesaw mechanism. However, this mechanism usually creates a large hierarchy among the light neutrino masses and the cosmological bound

$$\sum_{\nu_{light}} m_{\nu} \lesssim 100 \text{ eV} \quad (1)$$

is difficult to satisfy if  $m_{\nu_e}$  is of the order eV. Therefore one has to make the  $\nu_{\mu}$  and  $\nu_{\tau}$  sufficiently unstable to circumvent the bound (1). This requires in general the introduction of additional fields.

Here we want to discuss a three generation left-right symmetric model [2]<sup>2</sup> which has a strictly conserved lepton number of the Zel'dovich-Konopinski-Mahmoud (ZKM) type [3]. It contains a light Dirac and a light Majorana neutrino. Moreover, the seesaw mechanism is effective despite of the existence of Dirac neutrinos, the cosmological bound (1) can naturally be satisfied with the right-handed scale in the TeV range and there are no additional fields in the model other than the minimal set which is required by the gauge group  $SU(2)_L \times SU(2)_R \times U(1)_{B-L}$  and its spontaneous breakdown to  $U(1)_{em}$  [4]. Therefore we call it a minimal left-right symmetric model (MLRM).

## 2. THE MODEL

The Yukawa interaction of the leptons in the MLRM is given by

$$\mathcal{L}_Y = -\bar{\psi}_L G_1 \Phi \psi_R - \bar{\psi}_L G_2 \tilde{\Phi} \psi_R + \psi_L^T C^{-1} G_L i \sigma_2 \Delta_L \psi_L + \psi_R^T C^{-1} G_R i \sigma_2 \Delta_R \psi_R + h.c. \quad (2)$$

where the lepton doublets transform as

$$\psi_L \sim (1/2, 0, -1), \quad \psi_R \sim (0, 1/2, -1)$$

and the Higgs scalars as

$$\Phi \sim (1/2, 1/2, 0), \quad \Delta_L \sim (1, 0, 2), \quad \Delta_R \sim (0, 1, 2)$$

<sup>2</sup>See Ref. [2] also for further references.

under the gauge group. These scalars comprise the set of Higgs scalars in the MLRM apart from fields<sup>3</sup> which appear only in the potential and which are necessary to obtain spontaneous CP violation and a small vacuum expectation value of  $\Delta_L$  at most in the eV range. If this were not the case the mass of the electron neutrino would be too large as can be seen from the mass matrix.

After spontaneous symmetry breaking the neutrino mass term is obtained as

$$\mathcal{L}_{\nu \text{ mass}} = \frac{1}{2} \omega^T C^{-1} \mathcal{M}_\nu \omega + h.c. \quad \text{with} \quad \omega = \begin{pmatrix} \nu_L^C \\ \nu_R \end{pmatrix} \quad (3)$$

being the right-handed neutrino fields and

$$\mathcal{M}_\nu = \begin{pmatrix} \sqrt{2} u_L^c G_L^c & M_D \\ M_D^T & \sqrt{2} u_R G_R \end{pmatrix} \quad \text{with} \quad M_D = \frac{1}{\sqrt{2}} (v G_1 + w^* G_2) \quad (4)$$

the neutrino mass matrix. The vacuum expectation values are given by

$$\langle \Phi \rangle_0 = \frac{1}{\sqrt{2}} \begin{pmatrix} v & 0 \\ 0 & w \end{pmatrix}, \quad \langle \Delta_{L,R} \rangle_0 = \frac{1}{\sqrt{2}} \begin{pmatrix} 0 & 0 \\ u_{L,R} & 0 \end{pmatrix}. \quad (5)$$

From a consideration of the  $K^0 \bar{K}^0$  system the mass of the predominantly right-handed charged gauge boson  $W_2$  and therefore also the value of the  $|u_R|$  should be at least in the few TeV range [5]. Henceforth we shall assume that we can neglect  $u_L$ . Furthermore, one has to impose the condition  $\det G_R \neq 0$  for the seesaw mechanism to be operative. Otherwise, there would be light neutrinos with masses of the order of those of their charged partners.

The three generation model we want to discuss is given by the Yukawa coupling matrices

$$G_{1,2} \text{ diagonal}, \quad G_L = G_R = \begin{pmatrix} 0 & g & 0 \\ g & 0 & 0 \\ 0 & 0 & h \end{pmatrix}. \quad (6)$$

This model can be obtained in two ways from symmetry requirements:

- i) Imposing the usual left-right symmetry and a strictly conserved lepton number.

The usual left-right or parity symmetry gives the condition

$$G_{1,2}^\dagger = G_{1,2}, \quad G_L = G_R. \quad (7)$$

<sup>3</sup>In the simplest case one can take a pseudoscalar gauge singlet.



Apart from a case with extensive fine tuning in the charge lepton sector there is a unique way to impose a lepton number under the condition  $\det G_R \neq 0$ , namely

$$\psi_{L,R1} \rightarrow e^{i\alpha} \psi_{L,R1}, \quad \psi_{L,R2} \rightarrow e^{-i\alpha} \psi_{L,R2}, \quad \psi_{L,R3} \rightarrow \psi_{L,R3}. \quad (8)$$

This transformation gives rise to the model (6) with the conserved lepton number  $\tilde{L} = L_1 - L_2$  of the ZKM type. This symmetry remains intact after the spontaneous breakdown of the gauge group because the Higgs fields have zero lepton number.

ii) Imposing a generalized left-right or parity symmetry.

A generalized left-right or parity transformation is given by

$$\begin{aligned} \psi_L(x) &\rightarrow U_P \gamma^0 \psi_R(\bar{x}) & \Delta_L(x) &\rightarrow -\Delta_R(\bar{x}) & \Phi(x) &\rightarrow \Phi^1(\bar{x}) \\ \psi_R(x) &\rightarrow V_P \gamma^0 \psi_L(\bar{x}) & \Delta_R(x) &\rightarrow a_L \Delta_L(\bar{x}) \end{aligned} \quad (9)$$

with  $|a_L| = 1$ ,  $\bar{x} = (x^0, -\vec{x})$  and the gauge bosons transforming in the usual way. The unitary matrices  $U_P$ ,  $V_P$  act in flavour space. Such a transformation leaves the gauge part of the Lagrangian invariant but induces restrictions on the Yukawa sector. For the simplest case  $U_P = V_P = 1$  and  $a_L = -1$  they are given by Eq. (7). One can show that there is a unique case giving restrictions on all three generations. This case coincides with the Yukawa couplings of Eq. (6). The simplest way to realize it is by choosing

$$U_P = 1, \quad V_P = \begin{pmatrix} i & & \\ & -i & \\ & & 1 \end{pmatrix}, \quad a_L = -1. \quad (10)$$

Thus one can regard the generalized parity transformation (10) as the reason for the appearance of the lepton number  $\tilde{L} = L_1 - L_2$ .

Considering the neutrino mass matrix of our model it is obvious that it decays into a Dirac part with non-trivial  $\tilde{L} = L_1 - L_2$

$$\mathcal{M}_\nu^{(D)} = \begin{pmatrix} 0 & 0 & a & 0 \\ 0 & 0 & 0 & b \\ a & 0 & 0 & d \\ 0 & b & d & 0 \end{pmatrix} \quad \text{with} \quad m_{\nu_D} \simeq \left| \frac{ab}{d} \right|, \quad m_{N_D} \simeq |d| \quad (11)$$

and a Majorana sector ( $\tilde{L} \equiv 0$ )

$$\mathcal{M}_\nu^{(M)} = \begin{pmatrix} 0 & c \\ c & e \end{pmatrix} \quad \text{with} \quad m_{\nu_M} \simeq \left| \frac{c^2}{e} \right|, \quad m_{N_M} \simeq |e|. \quad (12)$$

$\nu_D, \nu_M$  denote the light Dirac and Majorana neutrinos, respectively, whereas  $N_D, N_M$  denote the heavy ones with masses of the order of the  $W_2$  mass.

Using the cosmological bound (1) and taking  $a, b, c$  of the order of the corresponding charged lepton masses one gets bounds on  $m_{N_D}$  and  $m_{N_M}$ , respectively. For the three possibilities to choose  $\tilde{L}$  the lowest bounds are obtained by taking  $\tilde{L} = L_e - L_\tau$ . Thus one gets, e.g.,  $m_{\nu_M} \sim m_\mu^2/m_{N_M} \sim 10 \text{ keV}/m_{N_M}(\text{TeV})$  which requires  $m_{N_M} \gtrsim 100 \text{ TeV}$  to satisfy (1). A right-handed scale of such an order, however, virtually excludes any left-right effects at low energies, e.g. in  $K^0 \bar{K}^0$ .

Fortunately, one can find a further symmetry, namely a generalized CP transformation [6] which does not destroy the relations (6) but sets  $G_1 = 0$ . In this way one can easily see that

$$m_{\nu_D} \simeq \left| \frac{w}{v} \right|^2 \frac{m_e m_\tau}{m_{N_D}} \lesssim \frac{10 \text{ eV}}{m_{N_D}(\text{TeV})}$$

$$m_{\nu_M} \simeq \left| \frac{w}{v} \right|^2 \frac{m_\mu^2}{m_{N_M}} \lesssim \frac{100 \text{ eV}}{m_{N_M}(\text{TeV})}$$
(13)

because  $|w/v|^2$  is naturally of the order  $(m_b/m_t)^2 \lesssim 10^{-2}$ . Now the cosmological bound is easily satisfied with  $m_{N_D}, m_{N_M}$  in the few TeV range.

### 3. RESULTS AND PHENOMENOLOGY

- i) The model has a light Dirac neutrino  $\nu_D$  associated with both the electron and the tau, and a light Majorana neutrino  $\nu_M$  coupled to the muon.  $m_{\nu_D}$  and  $m_{\nu_M}$  are both "naturally" in the eV range. "Natural" means that  $m_{\nu_D}$  and  $m_{\nu_M}$  are related to the masses of the charged leptons and the gauge boson  $W_2$  by a symmetry. The mass of  $W_2$  is assumed to be in the few TeV range as suggested by consideration of the  $K^0 \bar{K}^0$  system. There is also a heavy Dirac neutrino  $N_D$  and a heavy Majorana neutrino  $N_M$  with masses of the order of the  $W_2$  mass.

The most remarkable feature of this model is the fact that all light neutrinos can have masses of the same order in contrast to the usual seesaw mechanism. With the right-handed scale in the few TeV range the cosmological bound on the light neutrino masses is automatically satisfied.

- ii) The model possesses a conserved lepton number  $\tilde{L} = L_e - L_\tau$  of the ZKM type. Thus, classifying the leptons according to  $\tilde{L}$  we have

$$e^-, \tau^+, \nu_D, N_D \quad \text{with} \quad \tilde{L} = 1$$

and

$$\mu^\pm, \nu_M, N_M \quad \text{with} \quad \bar{L} = 0.$$

For three generations this is essentially the unique possibility of assigning a lepton number in the MLRM.

iii) As a consequence of the conserved lepton number the processes  $\mu \rightarrow e\gamma$ ,  $\mu \rightarrow eee$ ,  $e^- \mu^+ \rightarrow \mu^- e^+$ ,  $\mu e$ -conversion,  $K^+ \rightarrow \pi^- e^+ e^+$ , neutrinoless double  $\beta$  decay  $(Z, A) \rightarrow (Z + 2, A) + e^- + e^-$ , neutrino oscillations etc. are all forbidden.

iv) Among the allowed processes we have  $e^- \rightarrow \tau^+$  conversion which is, however, of second order in the weak interactions with additional suppression factors. The probability of getting  $\tau^+$  instead of  $e^-$  in  $\nu_D$ -scattering is of the order  $(m_{\nu_D}/m_\tau)^2 < 10^{-9}$  for neutrinos coming from  $\pi_{e2}$ ,  $K_{e2}$  decays.

At high energies the heavy neutrinos can be produced which decay like  $N_D \rightarrow e^- W_{1,2}^+$ ,  $\tau^+ W_{1,2}^-$  and  $N_M \rightarrow \mu^\pm W_{1,2}^\mp$ . Thus one could have characteristic signatures such as  $e^- p \rightarrow \tau^+ X$  and  $pp \rightarrow e^+ \tau^+ X, \mu^+ \mu^+ X$  with  $X$  being purely hadronic.

At low energies the only obvious test of the present model seems to be the determination of the  $\nu_D$  mass.

## REFERENCES

- [1] See, e.g., H.-J. Gerber, *Lepton Properties*, to appear in the Proc. of the International Europhysics Conference on High Energy Physics, Uppsala (Sweden), 1987.
- [2] G. Ecker, W. Grimus and M. Gronau, *Nucl. Phys.* **B279** (1987) 429.
- [3] Ya.B. Zel'dovich, *Doklady Nauk USSR* **86** (1952) 505;  
E.J. Konopinski and H. Mahmoud, *Phys. Rev.* **92** (1953) 1045.
- [4] J.C. Pati and A. Salam, *Phys. Rev.* **D10** (1975) 275;  
R.N. Mohapatra and J.C. Pati, *Phys. Rev.* **D11** (1975) 566 and 2558;  
R.N. Mohapatra and G. Senjanović, *Phys. Rev. Lett.* **44** (1980) 912;  
*Phys. Rev.* **D23** (1981) 165.
- [5] G. Beall, M. Bander and A. Soni, *Phys. Rev. Lett.* **48** (1982) 848;  
G. Ecker and W. Grimus, *Nucl. Phys.* **B258** (1985) 328.
- [6] G. Ecker, W. Grimus and H. Neufeld, *Nucl. Phys.* **B247** (1984) 70.

SPONTANEOUS CP VIOLATION AND NEUTRAL  
FLAVOUR CONSERVATION IN  $SU(2)_L \times U(1)$ <sup>1</sup>

H. Neufeld  
Institut für Theoretische Physik  
Universität Wien

---

<sup>1</sup>Supported by "Jubiläumsfonds der Österreichischen Nationalbank", Project Nr. 2766.

## 1. GENERAL CP TRANSFORMATIONS

In the standard model [1] with a single Higgs doublet CP violation [2] occurs through the Kobayashi-Maskawa (KM) mechanism [3] for at least three quark generations ( $n_G \geq 3$ ). The hard CP breaking is achieved through complex Yukawa couplings and manifests itself only in the mixing matrix of the charged current interaction. Higgs exchange conserves CP and flavour in a natural way.

However, the standard model does not offer any explanation why some Yukawa couplings should be complex. An attractive alternative is provided by the concept of spontaneous CP violation (SCPV) suggesting a common origin of gauge and CP symmetry breaking. In this case one has to find the general conditions that a given Lagrangian is CP invariant (before spontaneous symmetry breaking). As an explicit example I will discuss a model based on the gauge group  $SU(2)_L \times U(1)$  with an arbitrary number  $n_H$  of Higgs doublets

$$\Phi_\alpha = \begin{bmatrix} \varphi_\alpha^+ \\ \varphi_\alpha^0 \end{bmatrix}, \quad 1 \leq \alpha \leq n_H. \quad (1.1)$$

The weak eigenfields of the quarks are denoted by

$$q_{iL} = \begin{bmatrix} p_i \\ n_i \end{bmatrix}_L, \quad p_{iR}, \quad n_{iR}, \quad 1 \leq i \leq n_G. \quad (1.2)$$

The existence of generations is now an important point. Prior to spontaneous symmetry breaking these generations are completely undistinguishable. The same is, of course, true for the scalar fields where we have  $n_H$  identical copies of Higgs doublets. So, a general CP transformation [4,5,6] is given by<sup>2</sup>

$$\begin{aligned} q_L(x^0, \vec{x}) &\rightarrow V_L C q_L^*(x^0, -\vec{x}), \\ p_R(x^0, \vec{x}) &\rightarrow V_R^p C p_R^*(x^0, -\vec{x}), \\ n_R(x^0, \vec{x}) &\rightarrow V_R^n C n_R^*(x^0, -\vec{x}), \\ \Phi_\alpha(x^0, \vec{x}) &\rightarrow V_{H,\alpha\beta} \Phi_\beta^*(x^0, -\vec{x}), \end{aligned} \quad (1.3)$$

with the Dirac charge conjugation matrix  $C$ .  $V_L$ ,  $V_R^p$  are  $n_G$ -dimensional unitary matrices in generation space and  $V_H$  is an  $n_H$ -dimensional unitary matrix in the space of scalar doublets. There is a priori no reason to prefer certain  $V_L$ ,

<sup>2</sup>The gauge fields transform in the standard way.

$V_R^{p,n}, V_H$ . Of course, a lot of freedom in the choice of these CP matrices is really redundant because under a basis transformation we have

$$\begin{aligned} V_L &\rightarrow A_L^\dagger V_L A_L, \\ V_R^p &\rightarrow A_R^{p\dagger} V_R^p A_R^p, \\ V_R^n &\rightarrow A_R^{n\dagger} V_R^n A_R^n, \\ V_H &\rightarrow A_H^\dagger V_H A_H, \end{aligned} \quad (1.4)$$

with unitary  $A_L, A_R^{p,n}, A_H$ . One may even have the suspicion that one can always choose a basis transformation in such a way that  $V_L, V_R^{p,n}, V_H$  are transformed into unit matrices recovering the usual CP transformations. We have recently shown [7] that this is in general not the case: although  $V_L, V_R^{p,n}, V_H$  may be brought to certain real standard forms, the resulting matrices are in general non-diagonal.

Quarks and scalars are allowed to interact through Yukawa terms in the Lagrangian,

$$-\mathcal{L}_Y = \sum_{\alpha=1}^{n_H} (\bar{q}_L \Gamma_\alpha \Phi_\alpha n_R + \bar{q}_L \Delta_\alpha \tilde{\Phi}_\alpha p_R) + h.c., \quad (1.5)$$

with  $\tilde{\Phi}_\alpha = i\sigma_2 \Phi_\alpha^*$ . Nontrivial CP invariance will constrain the Yukawa couplings  $\Gamma_\alpha, \Delta_\alpha$  in a possibly more severe way than simple CP transformations ( $V_L = V_R^{p,n} = 1_{n_G}, V_H = 1_{n_H}$ ) which enforce real Yukawa couplings. In a certain sense, CP may act like a discrete horizontal symmetry, although generalized CP is in general not equivalent<sup>3</sup> to the combined action of the simple CP transformations and a horizontal symmetry.

To demonstrate the non-triviality of generalized CP, let me mention the following example for  $n_G = n_H = 2$ :

$$V_L = V_R^{p,n} = \begin{bmatrix} 0 & 1 \\ -1 & 0 \end{bmatrix}, \quad V_H = 1_2. \quad (1.6)$$

In this model neutral flavour conservation (NFC) in the Higgs sector is enforced [6] in a nontrivial way without constraining the Cabibbo angle. This is known to be impossible [8] via a horizontal symmetry.

<sup>3</sup>Applying general CP twice always yields a horizontal symmetry, which may, however, be trivial.

## 2. NEUTRAL FLAVOUR CONSERVATION (NFC)

Spontaneous symmetry breaking leads to quark mass matrices

$$M_p = \sum_{\alpha=1}^{n_H} \Delta_{\alpha} v_{\alpha}^*, \quad M_n = \sum_{\alpha=1}^{n_H} \Gamma_{\alpha} v_{\alpha}, \quad (2.1)$$

with  $v_{\alpha} = \langle \varphi_{\alpha}^0 \rangle_{vac}$ . The weak eigenfields  $p, n$  are related to the mass eigenfields  $u, d$  by unitary transformations

$$p_{L,R} = U_{L,R}^p u_{L,R}, \quad n_{L,R} = U_{L,R}^n d_{L,R} \quad (2.2)$$

leading to the mixing matrix

$$K_L = U_L^{p\dagger} U_L^n. \quad (2.3)$$

In the basis of the physical quark fields  $u, d$  the Yukawa couplings are given by

$$\hat{\Gamma}_{\alpha} = U_L^{p\dagger} \Gamma_{\alpha} U_R^n, \quad \hat{\Delta}_{\alpha} = U_L^{p\dagger} \Delta_{\alpha} U_R^p. \quad (2.4)$$

In general,  $\hat{\Gamma}_{\alpha}$  and  $\hat{\Delta}_{\alpha}$  will be non-diagonal inducing flavour changing neutral Higgs exchange. Instead of invoking large enough neutral Higgs masses one can impose the condition that  $\hat{\Gamma}_{\alpha}, \hat{\Delta}_{\alpha}$  are diagonal. The simultaneous diagonalizability of the Yukawa matrices through (2.4) is called NFC in the Higgs sector [9].

We have studied [6] the consequences of the joint requirements of SCPV and NFC within the framework of the  $SU(2)_L \times U(1)$  multi Higgs model. For  $n_G = 3$ , SCPV in its general form and NFC were shown to yield a CP conserving mixing matrix if phenomenological constraints are taken into account.

For  $n_G \geq 4$ , SCPV and NFC admit complex mixing matrices [6,10,11]. We have completely analyzed the consequences of NFC together with real Yukawa couplings (simple CP invariance). Contrary to a widespread belief [12], the mixing matrix violates CP in general. If it does so, some of its matrix elements must be equal in absolute magnitude. Only if there are no such relations between matrix elements, the mixing matrix must conserve CP. For a specific ansatz we have also performed a detailed phenomenological investigation [10].



## REFERENCES

- [1] S.L. Glashow, Nucl. Phys. **22** (1961) 579;  
S. Weinberg, Phys. Rev. Lett. **19** (1967) 1264; A. Salam, Proc. 8th Nobel Symposium, Aspenåsgården, 1968, ed. N. Svartholm (Almqvist and Wiksell, Stockholm, 1968) 367.
- [2] For recent reviews, see:  
W. Grimus, Univ. of Vienna preprint UWThPh-1987-10, to appear in Fortschritte der Physik;  
G. Ecker, Univ. of Vienna preprint UWThPh-1987-33, to be published in the Proc. of the Conference on Phenomenology of High Energy Physics, Trieste, July 20 - 22, 1987; eds. J.C. Pati and Q. Shafi, World Scient. Publ. Co.
- [3] M. Kobayashi and T. Maskawa, Progr. Theor. Phys. **49** (1973) 652.
- [4] G. Ecker, W. Grimus and W. Konetschny, Nucl. Phys. **B191** (1981) 465.
- [5] G. Ecker, W. Grimus and H. Neufeld, Nucl. Phys. **B247** (1984) 70.
- [6] H. Neufeld, W. Grimus and G. Ecker, Univ. of Vienna preprint UWThPh-1987-21, to be published in Journal Mod. Phys. A.
- [7] G. Ecker, W. Grimus and H. Neufeld, J. Phys. **A20** (1987) L807.
- [8] R. Gatto, G. Morchio and F. Strocchi, Nucl. Phys. **B163** (1980) 221.
- [9] S.L. Glashow and S. Weinberg, Phys. Rev. **D15** (1977) 1958;  
E. Paschos, Phys. Rev. **D15** (1977) 1966;  
L.T. Trueman, F. Paige and E. Paschos, Phys. Rev. **D15** (1977) 3416.
- [10] G. Ecker, W. Grimus and H. Neufeld, Phys. Rev. **B194** (1987) 251.
- [11] M. Gronau, A. Kfir, G. Ecker, W. Grimus and H. Neufeld, Technion preprint TECHNION-PH-87-26, to be published in Phys. Rev. D.
- [12] G.C. Branco, Phys. Rev. Lett. **44** (1980) 504.

## On quark masses in (Q $\bar{Q}$ ) potential models

K. Lewin, G. B. Motz

### 1. Nonrelativistic (Q $\bar{Q}$ ) potentials

The heavy quarkonia occurring as families of narrow resonances can be successfully described as bound states of heavy quark-antiquark pairs. In nonrelativistic Schrödinger theory with a local, central potential the mass spectrum of a quarkonium family is computed by

$$M_n(Q\bar{Q}) = 2m_q + E_n(m_q, V), \quad (1)$$

$$\left[ -\frac{1}{2m_q} \Delta + V(r) \right] \psi_n(r) = E_n \psi_n(r) \quad (2)$$

The correct (Q $\bar{Q}$ ) potential  $V(r)$  has so far not been determined from first principles. Therefore we are referred to a variety of more or less theoretically motivated flavourinvariant (Q $\bar{Q}$ ) potentials which describe the experimentally observed levels  $M_n(Q\bar{Q})$  of the  $c\bar{c}$  and  $b\bar{b}$  systems with surprising accuracy. There exist both successful pure phenomenological potentials<sup>[1,2]</sup> and QCD-motivated potentials taking into account the known asymptotic behaviour of the static (Q $\bar{Q}$ ) potential in QCD for large and short distances and choosing the behaviour in the intermediate region  $0,1 \text{ fm} \leq r \leq 1 \text{ fm}$  ad hoc<sup>[3-7]</sup> (see Table 1).

The open parameters of the potentials are adjusted to describe the  $\Psi$  and  $\Upsilon$  spectroscopies remarkably well. According to the equations (1) and (2) the static quark masses  $m_b$  and  $m_c$  appear in this approach as additional fit parameters. They differ for various potential models as shown in Table 2.

### 2. The b and c quark masses

Whereas the heavy quark masses obtained within a definite potential model depend obviously on the structure and the special parameters of the chosen potential, the mass differences  $m_b - m_c$  are much better constrained (comp. Table 2). This remarkable model independence of the heavy quark mass

Table 1

Examples of (QQ) potentials

Potential  $V_i$

Potential parameters

$$V_1(r) = A + B r^\alpha \quad A = -6,31 \pm 0,6 \text{ GeV} \quad , \quad \alpha = 0,126 \pm 0,02 \quad [1]$$

$$B = 5,22 \pm 1,0 \text{ GeV}$$

$$V_2(r) = -b r^{-1/2} + a r^{1/2} \quad a = 1,15 \text{ fm}^{-1/2} \text{ GeV} \quad [2]$$

$$b = 0,41 \text{ fm}^{1/2} \text{ GeV}$$

$$V_3(r) = -\frac{k}{r} + ar \quad k = 0,494; \quad a = 0,173 \text{ GeV}^2 \quad [3]$$

$$V_4(r) = (k+ar)^2 F(t) \quad k = 0,216 \pm 0,20 \quad [4]$$

$$F(t) = 1 + \sum_{n=1}^N c_n \sin(4\pi n t) \quad a = 0,0649 \pm 0,02 \text{ GeV}^2$$

$$t = \frac{1}{1+r} \quad c_1 = 1,827 \pm 1,67$$

$$c_2 = 0,541 \pm 0,23$$

$$c_3 = 0,336 \pm 0,39$$

$$V_5(q^2) = -\frac{4}{3} \frac{125}{33-24f} \cdot \frac{1}{q^2} \cdot \frac{1}{\ln(1+q^2/\Lambda_e^2)} \quad , \quad \Lambda_e = 0,375 \quad [5]$$

$$V_6(r) = -\frac{16\pi}{25} \cdot \frac{1}{r f(r)} \left[ 1 + \frac{28E + 53/75}{f(r)} - \frac{462 \ln f(r)}{625 f(r)} \right] + a\sqrt{r} + c \quad , \quad \Lambda = 0,4 \text{ GeV} \quad [6]$$

$$a = 0,70 \text{ GeV}^{3/2}$$

$$b = 4,99$$

$$c = -0,81 \text{ GeV}$$

$$f(r) = \ln \left[ \frac{1}{(1r)^2} + b \right]$$

$$V_7(r) = -\frac{g(\Lambda r)}{r} + r(c_1 + c_2 r) e^{-r/r_0} + ar \quad , \quad a = 0,18 \text{ GeV}^2 \quad [7,8]$$

$$c_1 = -1,35$$

$$c_2 = 1,15$$

$$r_0 = 0,57 \text{ GeV}^{-1}$$

$$\Lambda = 0,4 \text{ GeV}$$

difference  $m_b - m_c$  has been mentioned already by other authors [4,9,10,11]

Table 2

The masses  $m_b$  and  $m_c$  in different potential models

Potential [Ref.]	$m_c$ (GeV)	$m_b$ (GeV)	$m_b - m_c$ (GeV)
$V_1$ [1]	1,76	5,14	3,38
$V_2$ [2]	1,80	5,20	3,40
$V_3$ [3]	1,35	4,77	3,42
$V_4$ [4]	$1,36 \pm 0,17$	$4,77 \pm 0,15$	$3,41 \pm 0,02$
$V_5$ [5]	1,50	4,91	3,41
$V_6$ [6]	1,41	4,83	3,42
$V_7$ [7,8]	1,58	4,99	3,41

To study the interdependence between a given potential  $V_1(r)$  and the fitted mass  $m_{Q_i}$  belonging to it we start with a potential  $U_{Q_i}$  in the following general form containing explicitly the mass terms:

$$U_{Q_i}(r) = 2 \mu_{Q_i}(s_1^{(i)}, \dots, s_{n_1}^{(i)}) + V_1(r; s_1^{(i)}, \dots, s_{n_1}^{(i)}) \quad (3)$$

Here the index  $i$  denotes again the type of the corresponding flavour independent potential  $V_1$  characterized by its general dependence on the interquark distance  $r$ . The  $n_1$  parameters  $s_1^{(k)}$  occurring in  $V_1$  are adjustable to fit the energy levels  $M_n(Q\bar{Q})$  of the charmonium and bottonium systems together with the mass parameters  $m_{Q_i}$ :

$$M_n(U_{Q_i}) = 2 \mu_{Q_i} + E_n^i(U_{Q_i}) \quad (4)$$

$$\left[ -\frac{1}{\mu_{Q_i}} \Delta + U_{Q_i}(r) \right] \psi_{Q_i}^i(r) = M_{Q_i}(U_{Q_i}) \psi_{Q_i}^i(r) \quad (5)$$

To compare potential models of this kind it seems to be necessary and reasonable in the Schrödinger theory that the quark masses have to be independent of the structure and parameters of the chosen potential  $V_1$ :

$$\mu_{a_i}(s_i^{(1)}, \dots, s_i^{(u)}) = \mu_a, \quad (a = b, c). \quad (6)$$

This leads to a correlation among the parameters, f. i.

$$s_i^{(u)} = f_{a_i}(s_i^{(1)}, \dots, s_i^{(u-1)}), \quad (7)$$

and the potentials  $U_{a_i}$  would obtain the form

$$U_{a_i} = 2\mu_a + W_{a_i}(r, s_i^{(1)}, \dots, s_i^{(u-1)}) \quad (8)$$

where

$$W_{a_i}(r, s_i^{(1)}, \dots, s_i^{(u-1)}) = V_i(r, s_i^{(1)}, \dots, s_i^{(u-1)}, f_{a_i}(s_i^{(1)}, \dots, s_i^{(u-1)})). \quad (9)$$

Flavour-independence of the potentials  $W_1$  needs

$$f_{a_i}(s_i^{(1)}, \dots, s_i^{(u-1)}) = f_i(s_i^{(1)}, \dots, s_i^{(u-1)}) \quad (10)$$

Equation (10) follows, however, from equ. (7) under the condition that

$$\mu_{b_i}(s_i^{(1)}, \dots, s_i^{(u)}) - \mu_{c_i}(s_i^{(1)}, \dots, s_i^{(u)}) = \Delta \mu \quad (11)$$

is model and parameter independent. For the potentials of Table 1 this is fulfilled. To ensure this mass condition, it is useful, to consider one of the parameters  $s_i^{(k)}$  (e.g.  $s_i^{(u)}$ ) as an additive constant term  $V_0$  in the potential  $V_1$  [8, 12] which facilitates the variation of the quark masses  $\mu_{a_i}$  in the fits [12].

We conclude that the constancy of the quark mass differences  $\mu_{b_i} - \mu_{c_i}$  appears as a condition to fit the charmonium and bottomonium spectra with flavour invariant potentials  $V_1$  and

unique b and c quark masses.

### References

1. Martin, A.  
Phys. Lett. 93 B, 338 (1980), Phys. Lett. 100 B, 511 (1981)
2. Song Xiaotong, Lin Hefen, Z. Phys. C 34, 223 (1987)
3. Eichten, E., Gottfried, K., Laus, K. D., Yan, T. M.  
Phys. Rev. D17, 3090 (1978), Phys. Rev. D 21, 203 (1980)
4. Miller, K. J., Olsson, M. G., Phys. Rev. D 25, 2383 (1982)
5. Richardson, J. L., Phys. Lett. 82 B, 272 (1979)
6. Kühn, J. H., Ono, S., Z. Phys. C 21, 395 (1984)  
C 24, 404 (E) (1984)
7. Hagiwara, K., Jacobs, S., Olsson, M. O., Miller, K. J.,  
Phys. Lett. 130 B, 209 (1983)
8. Hagiwara, K., Martin, A. D., Peacock, A. W.,  
Z. Phys. C 33, 135 (1986)
9. Bertlmann, R. A.; Martin, A., Nucl. Phys. B 168, 111  
(1980)
10. Martin, A.; Richard, J. M., CERN-TH 4584/86
11. Olsson, M. G., Phys. Lett. 139 B, 417 (1984)
12. Schmitz S. et al., Phys. Rev. D36, 484, (1987)

# UNITARITY BOUNDS FOR HIGH-ENERGY SCATTERING IN MANY DIMENSIONS

Masud Chaichian

Department of High Energy Physics, University of Helsinki,  
Siltavuorenpenger 20C, SF-00170 Helsinki, Finland

and

Jan Fischer

Institute of Physics, Czechoslovak Academy of Sciences,  
Na Slovance 2, CS-18040 Prague 8, Czechoslovakia

There has been recently an increasing interest in the high-energy behaviour of string scattering amplitudes. It is a rather complex problem which combines both short and long distance physics, and apparently combines them in a different way than it does in strong interactions. During the last year, remarkable progress has been made in correlating the string theory with the general properties of scattering amplitude. Soldate /1/ investigated the high-energy unitarity of the partial-wave expansion of a closed four-scalar tree amplitude in flat space-time of a general dimension  $D \geq 6$ , and gave a general argument that such partial-wave amplitudes would violate unitarity at sufficiently high energy. Gross and Mende /2/ and Amati, Ciafaloni and Veneziano /3/ studied the high-energy behaviour of the string and the superstring amplitudes respectively and found dominating contributions in different kinematic regions. Muzinich and Soldate /4/ looked into the behaviour of string amplitude by summing multiple Reggeized graviton exchange in the eikonal approximation.

I will give a short report on our contribution to this development, which we made in the same period /5/. We obtain an upper bound on the high-energy behaviour of the elastic scattering amplitude imposed by unitarity and analyticity in higher-dimensional space-time. We first show that the methods of Froissart /6/ and Martin/7/ can be generalized to any space-time dimension. Assumptions are analogous; let us mention that analyticity of the elastic scattering amplitude in the complex  $\cos\theta$  plane in an ellipse with foci at  $\cos\theta = \pm 1$  is essential. We calculate explicitly the high-energy bounds for forward and non-forward scattering in the flat space-time of a general dimension  $D$ .

If  $N$  is the number of on-mass-shell particles involved, the number of independent kinematical variables is  $N(N-3)/2$  and  $(D-1)N - D(D+1)/2$  for  $N \leq D$  and  $N \geq D$  respectively. In particular, this number equals 2 for  $N=4$  (elastic scattering) and any  $D \geq 3$ ; we therefore define  $s$ ,  $t$  and  $u$  in the usual way.

The partial-wave expansion of the four-scalar elastic scattering amplitude in  $D$  dimensions has the form

$$F(s, t) = s(s) \sum_{\ell=0}^{\infty} (N_{\ell}^{\lambda})^{-1} C_{\ell}^{\lambda}(t) C_{\ell}^{\lambda}\left(1 + \frac{t}{2k^2}\right) f_{\ell}(s), \quad (1)$$

where

$$\lambda = (D-3)/2, \quad (2)$$

$$s(s) = 2 \Gamma(D/2-1) (16\pi)^{D/2-1} s^{2-D/2}, \quad (3)$$

$$N_{\ell}^{\lambda} = \frac{2^{1-2\lambda} \pi \Gamma(\ell+2\lambda)}{\ell! (\ell+\lambda) \Gamma^2(\lambda)}, \quad (4)$$

$$C_{\ell}^{\lambda}(t) = \frac{\Gamma(\ell+2\lambda)}{\ell! \Gamma(2\lambda)} \quad (5)$$

and the Gegenbauer polynomials  $C_{\ell}^{\lambda}(x)$  can be represented in the following form:

$$C_{\ell}^{\lambda}(x) = M(\ell, \lambda) \int_0^{\pi} \left(x + \sqrt{x^2-1} \cos\varphi\right)^{\ell} (\sin\varphi)^{2\lambda-1} d\varphi, \quad (6)$$

$$M(\ell, \lambda) = \frac{\Gamma(\ell+2\lambda) \Gamma(\lambda+1/2)}{\sqrt{\pi} \Gamma(\ell+1) \Gamma(2\lambda) \Gamma(\lambda)}. \quad (7)$$

They are obtained in (1) by integrating over irrelevant angles from the generalized spherical functions which span the representation space of the  $SO(D-1, 1)$  group corresponding to unitary irreducible representations of its maximal compact subgroup. The normalization is such that

$$|f_{\ell}(s)| \leq 1. \quad (8)$$

Using the integral representation (6) we can derive, in analogy with Martin's result /7/ for  $D=4$ , the following lower bound on  $C_{\ell}^{\lambda}(x)$  (see ref. /5/ for details):



$$C_{\ell}^{\lambda}(x) \cong M(\ell, \lambda) u^{\ell} \int_0^{\varphi_0} (\sin \varphi)^{2\lambda-1} d\varphi \quad (9)$$

for any  $\varphi_0$ ,  $0 < \varphi_0 < \pi$ , where  $u = (x + \sqrt{x^2 - 1} \cos \varphi_0)^{\ell}$ .

We shall now assume that, for  $s$  fixed, the amplitude  $F(s, t)$  is analytic in  $\cos \theta$  in a region  $G$  containing the segment  $[-1, +1]$ . Then, in analogy with the  $D=4$  case, the expansion (1) will converge inside the largest ellipse contained in  $G$  and having the foci at  $\cos \theta = \pm 1$  (see /8/, theorem 9.1.1). Let  $1+2R/s$  be the semimajor axis of the ellipse, where  $\sqrt{R}$  is the smallest (true or effective) mass of the theory. Then we use the bound (9) to obtain the following inequality for the imaginary part  $A(s, t)$  of  $F(s, t)$ :

$$A(s, t) > \delta(s) \int_0^{\varphi_0} (\sin \varphi)^{2\lambda-1} d\varphi \sum_{\ell=0}^L C_{\ell}^{\lambda}(\varphi) M(\ell, \lambda) u^{\ell} / N_{\ell}^{\lambda} \quad (10)$$

where  $L = L(s)$  makes the partial-wave expansion of  $A(s, 0)$  maximal if  $a_{\ell} = \text{Im } f_{\ell}$  are chosen such that  $a_{\ell} = 1$  for all  $0 \leq \ell \leq L$  and  $a_{\ell} = 0$  for all  $\ell \geq L+2$ .

Further steps of the derivation include the determination of the high-energy behaviour of the inequality (10) for a general energy dependence of  $L$ , which is unknown. Details are discussed in ref. /5/. The resulting high-energy bound on  $A(s, 0)$  is

$$A(s, 0) \leq K_1 s (\ln s)^{D-2} \quad (11)$$

where the constant in front of the energy dependence depends on the dimension  $D$ , on the quantities  $R$  and  $\varphi_0$  and on the power of the general polynomial bound which is assumed to hold for  $A(s, t)$  in the ellipse. If  $D$  is equal to 4, this formula gives the high-energy behaviour of the Froissart-Martin bound for forward scattering in the Minkowski space.

In a similar way, methods of obtaining high-energy bounds on the non-forward scattering amplitude can be generalized to an arbitrary number of dimensions  $D \geq 3$ . The Gegenbauer polynomials obey, similarly as the Legendre polynomials, a bound which for  $\ell$  high enough and  $\theta$  fixed gives

$$C_2^\lambda(x) < K_2 l^{\lambda-1} / \theta^\lambda$$

where  $x = \cos\theta$  and  $K_2$  is again a constant. This estimate can be used in the imaginary part of (1) to give

$$A(s, t) < K_3 s^{(7-D)/4} (\ln s)^{(D-1)/2} \theta^{(3-D)/2} \quad (12)$$

for sufficiently high  $s$ . Choosing  $D=4$  and replacing  $\theta$  by  $\sin\theta$ , we obtain the Froissart-Martin bound at fixed angle in the case of Minkowski space.

It is interesting to observe that while the bound (11) becomes looser with increasing  $D$ , the factor  $s^{(7-D)/4}$  on the right-hand side of (12) makes the fixed-angle bound particularly stringent with increasing  $D$ . On the other hand, if  $t$  is kept negative and fixed near forward scattering, (12) takes the form

$$A(s, t) < K_4 s (\ln s)^{(D-1)/2} |t|^{(3-D)/4} \quad (13)$$

Also this bound coincides for  $D = 4$  with the well-known fixed- $t$  high-energy bound.

To discuss the results obtained, let us consider elastic scattering of two scalar particles in  $D$ -dimensional flat space-time in tree approximation. The physical interpretation of this example is not straightforward; its relevance to string theory is shortly discussed below.

It has been pointed out in ref. /1/ that this amplitude violates partial-wave unitarity at sufficiently high energies. Indeed, due to the graviton term, the scattering amplitude in tree approximation will be dominated by  $s^2/t$  for  $t$  near 0 and  $s \rightarrow \infty$ ; thus, the  $\ell$ -th partial wave corresponding to this term will rise unboundedly with increasing energy.

This term also violates our bounds (11) and (13), and even if the graviton-exchange term is replaced by the massive spin-2 boson term  $s^2/(t-m^2)$  the violation takes place (note that this latter choice is more appropriate because our bounds were obtained under the assumption that the partial-wave expansion converges outside the physical interval of  $\cos\theta$ ).

Since strings are dominated by Regge trajectories at tree level, it is of interest to discuss the behaviour of typical Regge terms. We can easily check that a Reggeized massive boson exchange term violates (11) for any intercept greater than 1, and also (13) at least in an interval  $t \in (-\mathcal{L}, 0)$ , where  $\mathcal{L}$  is a positive number.

The violation of the bounds (11), (12) and (13) by the closed-string four-scalar amplitude in tree approximation is not surprising for various reasons. While the exact amplitude could well be unitary, one can hardly expect its tree approximation separately to satisfy the unitarity condition. But tree approximation is widely used as guidance for general considerations; it is therefore of interest to know to what extent it is consistent with general principles. Our result suggests that the string perturbation expansion about flat space-time is strongly coupled at high energies (see a similar conclusion /1/ in a different context). Further, the dominance of Regge trajectories assumed in string theory represents another approximation which may lead to further unitarity violations. Finally, the assumed finite mass gap can be relevant to string theories only in a rough approximation; one can argue, for instance, that the amplitude is, for physical reasons, smooth in  $\cos\theta$ , especially in higher dimensions, due to phase space suppression; this indicates that the singularities of the exact amplitude cannot be too strong. Further analysis can elucidate these problems; see also a more detailed discussion in ref. /5/.

- /1/ M.Soldate, Partial-wave unitarity and closed string amplitudes, FERMILAB-PUB-86/149-T
- /2/ D.J.Gross and P.F.Mende, The high energy behaviour of string scattering amplitudes, PUPT-1062, June 1987
- /3/ D.Amati, M.Ciafaloni and G.Veneziano, Superstring collisions at Planckian energies; CERN-TH.4782/87
- /4/ I.J.Muzinich and M.Soldate, High-energy unitarity of gravitation and strings; FERMILAB-Pub-87/114-T
- /5/ M.Chaichian and J.Fischer, Higher-dimensional space-time and unitarity bound on the scattering amplitude; Helsinki, HU-TFT 87-29, July 1987
- /6/ M. Froissart, Phys.Rev. 123(1961) 1053
- /7/ A.Martin, Phys.Rev. 129(1963)1432; Nuovo Cim. 42(1966)930
- /8/ G.Szego, Orthogonal Polynomials; Colloquium Publications Vol. XXIII, American Math. Society, New York, 1959
- /9/ A.Martin, F.Cheung, Analyticity Properties and Bounds of the Scattering Amplitudes; Gordon and Breach, Inc., 1970

**SUPERSTRING-INSPIRED LEFT-RIGHT SYMMETRIC MODELS**

A.R.Kereselidze, A.G.Liparteliani, G.G.Volkov  
 Institute for High Energy Physics,  
 Serpukhov, Moscow Region, USSR

Of all known superstring theories, the heterotic d=10 theory with  $E_8 \times E_8$  gauge group<sup>1/</sup> appears to be the most phenomenologically viable. The requirement of unbroken  $N=1$  supersymmetry (SUSY) in four dimensions suggests<sup>2/</sup>, that internal six dimensions form the Ricci-flat, Kähler manifold  $K$  with  $SU(3)$  group of holonomy (Calabi-Yau manifold). The embedding of the spin connection in the  $SU(3)$  subgroup of one  $E_8$ , breaks the latter down to  $E_6$ . Matter fields left massless after compactification are chiral  $N_g$  generations of 27 representations of  $E_6$  (see table 1) and  $b_{1,1}$  copies of  $(27, \bar{27})$ ,  $b_{1,1} \geq 1$  being the Betti-Hodge number of manifold  $K$ . If  $K$  admits a discrete symmetry  $G$  that acts freely<sup>2,3/</sup> then instead of  $K$  we can consider the multiply connected manifold  $K/G$  with reasonably small number of generations;  $N_g = 1/2 [\chi(K)/N(G)]$ ,  $\chi(K)$  being the Euler characteristic of  $K$  and  $N(G)$  number of elements of  $G$ . For example, superstring theory formulated on  $K_0/G$ , where  $K_0$  is Calabi-Yau manifold with  $\chi = 200$  and

$b_{1,1} = 1$  defined as the subspace of  $CP^4$  with  $\sum_{i=1}^5 x_i^5 = 0$ , and admitting<sup>2/</sup> a discrete symmetry group  $G = Z_5 \times Z_5$ , will have 4 generations. For such multiply connected manifolds the nontrivial Wilson-loop operators

$$U_g = \exp i \left\{ \sum_j \lambda_j H_j \right\} \quad (1)$$

can give rise to "flux breaking" of  $E_6$  down to some subgroup  $V$  satisfying  $[V, U_g] = 0$  (Hosotani mechanism<sup>3/</sup>). In eq. (1)  $H_j$  are the elements of the Cartan subalgebra of group  $E_6$ . The requirement of unbroken  $SU(3) \times SU(2)_L$  group fixes  $\lambda_j$  as;  $\lambda = [-c, c, a, b, c, 0]$ .

In the case of  $b_{1,1} = 1$  light fields from  $b_{1,1} (27, \bar{27})$  surviving after flux breaking are those components of  $27$  for which  $U_g |27\rangle = |27\rangle$  and the corresponding copies in  $27^3/$ . Such fields we will denote by subscript  $s$ .

Recently the great deal of interest have arisen the manifolds constructed by Yau<sup>5/</sup>, which gives the models with three generations. The simplest of them with  $b_{1,1} = 6$  is determined as the cubic polynomials in the space  $CP^3 \times CP^3$  and admits the discrete symmetry group  $G = Z_3$ . The Hosotani mechanism breaks  $E_6$  down to  $SU(3) \times SU(3)_L \times SU(3)_R$  which is the group of unification in four dimensions. Fields left light after flux breaking are 6 copies of  $SU(3)_C$ -singlets and 4 copies of color fields.

The further  $F$  and  $D$  flat breaking of gauge symmetry  $V$  at an intermediate scale of order  $O(10^{14-15})$  GeV is possible, provided after "flux breaking" there are left light fields from  $b_{1,1} (27, \bar{27})$ , which are singlets under standard model.

$E_6$  is not the only existing symmetry group left unbroken after compactification. The possibility<sup>4/</sup> of constructing stable irreducible, holomorphic  $SU(5)$  or  $SU(4)$  vector bundles over some Calabi-Yau manifolds, result the  $SU(5)$  or  $SO(10)$  gauge groups respectively in four dimensions. So it is natural to consider left-right symmetric models in such theories with  $SO(10)$  group of unification. The flux breaking of  $SO(10)$  is analogous to  $E_6$ -breaking, with  $\lambda = [-2e, 0, c, -e, e]$  and the low energy spectra in four dimensions;  $N_g = 16 + 5(16 + \bar{16}) + 5 \cdot 10$ ,  $N_g$ ,  $\bar{5}$  and  $10$  being the non-negative integers defined by the topological properties of inertial manifold. In Table 1 we give diagonal elements of Wilson loop for  $E_6$  and  $SO(10)$  case, together with fields on which they act.

In the present paper we consider several left-right symmetric models inspired by superstrings and the possibility for existence of low-lying scale of right-handed symmetry breaking ( $M_R \sim 10^3 - 10^5$  GeV).

The analysis of the parameters  $\sin^2 \theta_w$  and  $M_X$ , using one-loop renormalization group equations for gauge couplings of the standard  $SU(3)_C \times SU(2)_L \times U(1)_Y$  symmetry shows, that in the case of  $V \subset SU(2)_L \times SU(2)_R$  symmetry (with  $b_{1,1} \gg 1$ ) the scale  $M_R$  must be very high:  $M_R \gg 10^{14}$  GeV, as in  $E_6$  (see table 2) so in  $SO(10)$ -models (see table 4). In the calculations we have assumed that group  $E_6$  was broken down to subgroup  $SU(3)_C \times SU(2)_L \times SU(2)_R \times U(1)_L \times U(1)_R$  via flux mechanism (conditions  $b=3c$  and  $a=2c$  in eq. (1)). One can see from table 1, that light fields from  $b_{1,1} (27+\bar{27})$ , in this case, are  $H_a$  and  $E_a^c$ , forming the representation  $H_a (1, 2, 2)$  and the SM singlet field  $N_a (1, 1, 1)$  together with their mirror components from  $\bar{27}$ . At the scale  $\langle M_R \rangle = 10^{15}$  GeV the group  $U(1)_L \times U(1)_R$  will break down to  $U(1)_{B-L}$ , and the "new" fields  $D, D^c, E$  and  $E^c$  will acquire masses  $O(10^{15}$  GeV). After flux breaking of  $SO(10)$  down to  $SU(3)_C \times SU(2)_L \times SU(2)_R \times U(1)_{B-L}$ , light fields from  $\bar{5} (16+\bar{16})$  ( $\xi=1$ ) are  $L_{RS}$  and  $L_{RS}^c = \begin{pmatrix} \nu \\ e \end{pmatrix}$  together with their "mirror" partners from  $\bar{16}$ , and from  $\xi 10$  ( $\xi=2$ ) fields  $H$  and  $E^c$ , forming representation  $H (1, 2, 2)$ . As for the  $E_6$  model with  $b_{1,1} > 1$  the VEV  $\langle M_R \rangle = 10^{15}$  GeV breaks  $[SU(3)]^3$  down to  $SU(3)_C \times SU(2)_L \times SU(2)_R \times U(1)_{B-L}$ . The further symmetry breaking leads to the standard model with three generations and is the same as in  $SO(10)$ -symmetric case. In  $E_6$ -models with  $b_{1,1}=1$ , with the existing Higgs content it is impossible to break  $SU(2)_R$  symmetry at such a high scale, at the same time leaving unbroken  $SU(2)_L$  and supersymmetry. In addition the neutrino mass problem is left unsolved in this model. The existence of right-handed doublet  $L_{RS}$  in  $SO(10)$ -models with  $b_{1,1}=1$ , and  $E_6$ -models with  $b_{1,1} > 1$  opens the possibility for the solution of both these problems, but  $M_R$ -scale remains high:  $M_R \gg 10^{14}$  GeV (see table 4). The situation will totally change if after flux breaking of  $E_6$  and  $SO(10)$  only the  $U(1)_{T_{3R}}$  part of  $SU(2)_R$ -symmetry is left unbroken. In this case we can obtain permissible values of  $\sin^2 \theta_w$  and  $M_X$  for a quite big range of  $M_R$ , and even the right-handed scale close to  $10^3$  GeV is possible (see tables 3, 5).

Table 1. Matter fields and corresponding Wilson loop diagonal elements

Fields	$\begin{pmatrix} u \\ d \end{pmatrix} = \psi$	$u^c$	$d^c$	$\begin{pmatrix} \nu \\ e \end{pmatrix} = L$	$\nu^c$	$e^c$
$U_6$ for $E_6$	$\exp(i-c)$	$\exp(i-b-a)$	$\exp(i-a-c)$	$\exp(ib)$	$\exp(-a-c)$	$\exp(a-b-2c)$
$U_6$ for $SO(10)$	$\exp(ie)$	$\exp(-c-e)$	$\exp(c-e)$	$\exp(-3e)$	$\exp(3e-c)$	$\exp(c+3e)$

Fields	$\begin{pmatrix} E^c \\ E^- \end{pmatrix} = \bar{E}$	$\begin{pmatrix} E^+ \\ E^0 \end{pmatrix} = \bar{E}^c$	$D$	$D^c$	$N$
$U_6$ for $E_6$	$\exp(i2c-a)$	$\exp(i(c+a-b))$	$\exp(i2c)$	$\exp(c-b)$	$\exp(i(b-3c))$
$U_6$ for $SO(10)$	$\exp(ie)$	$\exp(-ie)$	$\exp(-i2e)$	$\exp(i2e)$	-

**Table 2.**  $M_X$  and  $\sin^2\theta_w$  values in the case of  $SU(3)_C \times SU(2)_L \times SU(2)_R \times U(1)_L \times U(1)_R$ . All scales in tables are given in GeV.

$M_R$	$m_B$	$M_X$	$\sin^2\theta_w$
$10^3$	$10^3$	$9.4 \cdot 10^{20}$	0.295
$10^5$	$10^3$	$1.0 \cdot 10^{20}$	0.285
$10^8$	$10^3$	$5.7 \cdot 10^{18}$	0.271
$10^{10}$	$10^3$	$8.0 \cdot 10^{17}$	0.281
$10^{14}$	$10^4$	$1.2 \cdot 10^{16}$	0.241
$10^{15}$	$10^4$	$4.4 \cdot 10^{15}$	0.238

**Table 4.**  $\sin^2\theta_w$  and  $M_X$  values for  $SU(3)_C \times SU(2)_L \times SU(2)_R \times U(1)_{B-L}$  gauge symmetry

$M_R$	$m_B$	$M_X$	$\sin^2\theta_w$
$10^3$	$10^2$	$1.6 \cdot 10^{17}$	0.313
$10^6$	$10^2$	$7.6 \cdot 10^{16}$	0.295
$10^8$	$10^4$	$2.5 \cdot 10^{16}$	0.278
$10^{11}$	$10^4$	$1.2 \cdot 10^{16}$	0.260
$10^{14}$	$10^4$	$5.4 \cdot 10^{15}$	0.241
$10^{15}$	$10^4$	$4.2 \cdot 10^{15}$	0.238

**Table 3.**  $M_X$  and  $\sin^2\theta_w$  values for of  $V = SU(3)_C \times SU(2)_L \times U(1)_{T_{3R}} \times U(1)_L \times U(1)_R$  (condition  $a+c=0$  in eq. (1)).

$M_R$	$m_B$	$M_X$	$\sin^2\theta_w$
$10^3$	$10^2$	$3.8 \cdot 10^{16}$	0.216
$10^3$	$10^3$	$5.3 \cdot 10^{16}$	0.210
$10^4$	$10^3$	$1.9 \cdot 10^{16}$	0.218
$10^6$	$10^3$	$2.3 \cdot 10^{15}$	0.234
$10^9$	$10^4$	$1.4 \cdot 10^{14}$	0.252
$10^{12}$	$10^4$	$1.8 \cdot 10^{13}$	0.272

**Table 5.**  $\sin^2\theta_w$  and  $M_X$  for  $SU(3)_C \times SU(2)_L \times U(1)_{T_{3R}} \times U(1)_{B-L}$

$M_R$	$m_B$	$M_X$	$\sin^2\theta_w$
$10^3$	$10^2$	$1.43 \cdot 10^{13}$	0.234
$10^3$	$10^3$	$1.34 \cdot 10^{13}$	0.231
$10^4$	$10^3$	$1.7 \cdot 10^{13}$	0.230
$10^5$	$10^3$	$2.3 \cdot 10^{13}$	0.235
$10^{10}$	$10^3$	$9.0 \cdot 10^{13}$	0.245
$10^{14}$	$10^3$	$2.7 \cdot 10^{14}$	0.258

#### References

1. D.J.Gross et al. - Phys. Rev. Lett., 54 (1985) 502.
2. P.Candelas et al. - Nucl. Phys., B258 (1985) 46.
3. E.Witten. Nucl. Phys., B258 (1985) 75;  
Y.Hosotani, Phys. Lett., 126B (1983) 309.
4. E.Witten. Nucl. Phys., B268 (1986) 79.
5. T.-S.Yau. In: Argon Symposium on Anomalies, Geometry and Topology. (World Scientific 1985).

P. Möbius

Department of Physics, Technical University of Dresden, GDR

## 1. Introduction

In the preceding lectures enough motivations were given to study nonlinear field equations and to look especially for exact solutions. They are of great importance for further modelling, because they bear in general new notions being more adequate to describe the behaviour of the excitations in such systems. A typical example is the "soliton", a stable excitation moving with constant velocity without deformation through the system. It is advantageous to look at first for a rough classification of special nonlinear field equations having some physical importance. A good starting point is the nonlinear superposition principle and it is useful to divide the equations into those, for which general rules for superposition can be formulated and in to the ones where no statements can be made /1/. In the case of soliton physics it means to split the corresponding equations into two types, the first one, where there is only elastic scattering of solitons, being called "integrable field equations" and the second one with inelastic scattering where additional decaying wave tracks or solitons can occur. In the last time new methods of solution have been developed for the case of integrable field equations in (1+1)-space-time dimensions, e. g. the "method of spectral transform" (MST) and the "direct iterative method" (DIM), involving considerable knowledge of the procedures known for linear problems. Surprisingly a great variety of exactly soluble nonlinear field equations were discovered providing a new basis for starting already with a "neighbouring" nonlinear problem as the "first approximation". These exact results gave us also a more extensive insight into the foundation of physics, providing even a new point of view for the treatment of problems in classical physics even in classical mechanics.

## 2. Integrable systems of classical mechanics.

In the case of classical mechanics "integrable systems" play a preferred role, because there a number of reliable statements are possible about the time evolution of the system. In the case of Hamiltonian systems with  $f$  degrees of freedoms integrable systems are defined in the following way: Given a Hamiltonian  $H(p_1 \dots p_f, q_1 \dots q_f)$ , where  $f$  is finite, there exist  $f$  globally conserved quantities  $I_i(p, q)$ , i. e.  $\dot{I}_i(p, q) = 0$ , obeying in the framework of Poisson brackets the following relations /2/

$$\{H, I_i\} = 0 \quad i = 1 \dots f, \quad \{I_i, I_j\} = 0 \quad 1 \leq i, j \leq f, \quad (1)$$

i. e. being in involution. Then action-angle variables can be introduced and the motion be described as occurring on a  $f$ -dimensional torus. Now it can be shown, that all systems of Hamiltonian mechanics, describable by a  $(f \times f)$ -matrix  $M(t)$ , where the time evolution is given by a similarity transformation

$$M(t) = B^{-1}(t) M(0) B(t), \quad (2)$$

are integrable systems obeying the equations of motion

$$\dot{M}(t) = [M, A] \quad \text{with} \quad B^{-1}(t) \dot{B}(t) = A(t) \quad (3)$$

being essentially equivalent to the Hamiltonian equations. But now the quantities

$$\text{Sp}M(t)^k = \text{Sp}M(0)^k \quad k = 1 \dots f, \quad (4)$$

are time-independent and can serve as constants of motion. They are in many cases homogeneous functions of the momenta  $p_i$  of degree  $k$ , the coefficients depending on the coordinates  $q$ . An interesting example is the "Toda-system" /2/ of 3 particles with the Hamiltonian (1)

$$H(p, q) = 1/2 (p_1^2 + p_2^2 + p_3^2) + e^{(q_1 - q_2)} + e^{(q_3 - q_2)} + e^{(q_3 - q_1)} - 3 \quad (5)$$

describing in the first approximation 3 one-dimensional har-



monically coupled particles and having 3 conserved quantities  $I_1 = p_1 + p_2 + p_3$ ,  $I_2 = H$ ,  $I_3 = 1/3(p_1 + p_2 - 2p_3)(p_2 + p_3 - 2p_1)(p_3 + p_1 - 2p_2) + (p_1 + p_2 - 2p_3)e^{q_1 - q_2} + (p_2 + p_3 - 2p_1)e^{q_2 - q_3} + (p_3 + p_1 - 2p_2)e^{q_3 - q_1}$  which are in involution.

The idea is now to extend this procedure to field equations in (1+1)-space-time dimensions.

### 3. Infinite dimensional integrable systems

The question is if a straightforward extension of the notion of an integrable system to the case of an infinite number of degrees of freedom is possible, i.e. if field equations exist, having an infinite set of conserved quantities. Surprisingly there exists a number of nonlinear evolution and wave equations in (1+1)-space-time dimensions having this property, admitting solitary solutions, sometimes even N-soliton solutions. At the first glimpse nonlinear integrable field equations should obey the following requirements /3/:

- i. Existence of solitary solutions.
- ii. Existence of N-soliton solutions (  $N = 1, 2 \dots \infty$  ).
- iii. Existence of nonlinear superposition functions.

Now it can be shown, that the existence of N-soliton solutions is equivalent to the existence of N-1 conservation equations and this is connected with the fact of elastic scattering of solitary excitations. The third condition about nonlinear superposition functions is related to a construction of Bäcklund-transformations /4/. The standard example for the treatment of bell-solitons is the Korteweg-de Vries equation

$$\frac{\partial U}{\partial t} + c \frac{\partial U}{\partial x} + bU \frac{\partial U}{\partial x} + a \frac{\partial^3 U}{\partial x^3} = 0, \quad (6)$$

while the one for kink-solitons is the sine-Gordon equation

$$\frac{1}{c^2} \frac{\partial^2 U}{\partial t^2} - \frac{\partial^2 U}{\partial x^2} + k^2 \sin U = 0. \quad (7)$$

For both equations /5/ it is possible to give closed

expressions for the N-soliton solution incorporating a nonlinear superposition rule for solitary excitations and to construct an infinite set of conservation equations

$$\frac{\partial D_n}{\partial t} + \frac{\partial F_n}{\partial x} = 0, \quad (n = 1, 2, 3 \dots) \quad (8)$$

where the  $D_n$  are densities and the  $F_n$  are flows, expressible as polynomials in the field and its derivatives /5/. The equations (6) and (7) can serve as representatives for "integrable nonlinear field equations" in (1+1)-space-time dimensions. At least two different methods are known to solve the Cauchy-problem for them, one being the method of spectral transform (MST), the other is the direct iterative method (DIM). But already a nonlinear wave equation of the type

$$\frac{1}{c^2} \frac{\partial^2 U}{\partial t^2} - \frac{\partial^2 U}{\partial x^2} + V'(U) = 0 \quad (9)$$

is only integrable if the field potential  $V(U)$  obeys the relation /5/

$$V''(U) = \pm k^2 V(U).$$

The question naturally arises, what are the essential differences between integrable and non-integrable nonlinear field equations. What is the reason that in the first case general methods can be formulated to solve them and general results are obtained in (1+1)-space-time dimensions, while in the second case there is at the moment no hope for general statements? A partial answer is related to the fact, that a connection can be established between special nonlinear field equations and infinite-dimensional Lie algebras, reflecting the existence of an infinite number of conservation equations.

#### 4. Infinite-dimensional Lie algebras

In the following chapter the basic physical motivations to construct and apply infinite-dimensional Lie algebras are given.

In the case of finite-dimensional semi-simple Lie algebras we introduce a set of generators of infinitesimal transformations obeying the commutation relations

$$[L_i, L_j] = if_{ijk}L_k \quad 1 \leq i, j, k \leq p, \quad (11)$$

where  $p$  is the dimension of the algebra and  $f_{ijk}$  are the totally antisymmetric structure constants. So we have a universal set of generators for the whole system. But sometimes it is desirable to have generators, depending on an abstract coordinate or parameter, to combine the principles of symmetry and locality. It is preferable to introduce instead of a continuous parameter  $\xi$  via  $\xi \rightarrow \xi^n$  a dependence of the generators only on the discrete values  $n$  in the following way

$$L_i \rightarrow L_i(\xi) \rightarrow L_i(\xi^n) \rightarrow L_i^n. \quad (12)$$

Looking e. g. for  $SU(2)$  this means

$$L_1 = \frac{1}{2} \begin{pmatrix} 0 & 1 \\ 1 & 0 \end{pmatrix} \rightarrow L_1(\xi^n) = \frac{1}{2} \begin{pmatrix} 0 & \xi^n \\ \xi^n & 0 \end{pmatrix} = L_1^n,$$

$$L_2 = \frac{1}{2} \begin{pmatrix} 0 & -1 \\ 1 & 0 \end{pmatrix} \rightarrow L_2(\xi^n) = \frac{1}{2} \begin{pmatrix} 0 & -1 \xi^n \\ 1 \xi^n & 0 \end{pmatrix} = L_2^n$$

$$L_3 \rightarrow L_3(\xi^n) = L_3^n,$$

providing the commutation relations

$$[L_i^m, L_j^n] = if_{ijk}L_k^{m+n}, \quad 1 \leq i, j, k \leq p, \quad n, m = 0, \pm 1, \pm 2, \dots, \quad (13)$$

written already in a general form. The relations (13) represent the so-called "loop algebra" (Schlaufenalgebra) having already an infinite set of generators  $L_i^n$ . But as opposed to the finite dimensional semi-simple Lie algebra it is possible to add a central extension operator  $\hat{1}$  to (13) in the form

$$[L_i^n, L_j^n] = if_{ijk}L_k^{m+n} + 2m \delta_{m, -n} \delta_{ij} \hat{1} \quad (14)$$

whose permitted values of  $\hat{1}$ , the "central charges" enrich the structure of the algebra.

It is advantageous to add a derivation operator  $D$  leading to the so-called "affine untwisted Kac-Moody algebra" of the form

$$[L_i^m, L_j^n] = if_{ijk} L_k^{m+n} + 2m \delta_{m,-n} \delta_{ij} \hat{1}, \quad 1 \leq i, j, k \leq p; m, n = \dots (15a)$$

$$[\hat{1}, L_i^n] = 0, \quad [\hat{1}, D] = 0, \quad [D, L_i^m] = mL_i^m. \quad (15b)$$

The representations of (15) for  $1 \neq 0$  are infinite-dimensional. But it is nevertheless possible to introduce an invariant scalar product or metric in the standard way. Assuming  $L_i^0$  are the generators of the ordinary underlying Lie algebra (11) obeying

$$Sp(L_i^0, L_j^0) = 2\delta_{ij} \quad (16)$$

we try to extend this relation by assuming that even for infinite-dimensional matrices the following trace relations for products of matrices are valid /6/

$$Sp(AB) - Sp(BA) = 0, \quad Sp([A, B]C) + Sp(B[A, C]) = 0. \quad (17)$$

Applying (17) to combinations of the generators of (15) the following results can be obtained

$$Sp(L_i^m L_j^{-n}) = 2\delta_{ij} \delta_{mn}, \quad Sp(DL_j^m) = 0, \quad Sp(D\hat{1}) = 1, \\ Sp(\hat{1}, L_j^m) = 0, \quad Sp(\hat{1}^2) = 0. \quad (18)$$

So the two-dimensional subspace of  $\hat{1}$  and  $D$  is orthogonal to the infinite-dimensional space spanned by the generators  $L_j^m$ . Assuming at the moment that

$$Sp D^2 = x \quad (19)$$

is an unknown quantity the diagonalization of the two-dimensional subspace leads the secular equation

$$\begin{vmatrix} -\lambda & 1 \\ 1 & x-\lambda \end{vmatrix} = 0, \quad \lambda^2 - \lambda x - 1 = 0, \quad \lambda_1 \lambda_2 = -1, \quad (20)$$

providing that independent of the value of  $x$  one eigenvalue  $\lambda_1$  is negative leading to an "indefinite metric". This justifies the name Lorentzian metric and cast the bridge to "vertex operator construction". It is possible to choose

$$Sp D^2 = 0.$$

To this algebra we associate a Virasoro algebra constructed in analogy to (12) by

$$T \rightarrow T(\xi) = \xi^{n+1} \cdot \frac{d}{d\xi} \rightarrow T^n$$

fulfilling the commutation relations

$$[T^m, T^n] = (m - n) T^{m+n}$$

which again can be complemented by a central operator in the following way

$$[T^m, T^n] = (m - n) T^{m+n} + \frac{k}{12} m(m^2 - 1) \delta_{m,-n} 1, \quad (21)$$

where the quantity  $k$  can take on special values. For several physical applications it is worthwhile to take the semi-direct product of the Kac-Moody and Virasoro algebra in the following way

$$[T^m, L_j^n] = -L_j^{m+n}. \quad (22)$$

An interesting problem is now to look for the permitted values of the C-numbers  $l$  and  $k$  and their interrelations, depending surely on the considered physical systems. There are at least 3 distinct fields of applications:

1. To integrable nonlinear evolution equations with solitary excitations, where  $l = 0$ . The corresponding field equations can be derived with the help of Lax pairs constructed from elements of the Kac-Moody algebra.
2. To two-dimensional spin-lattice systems, like e. g. the Ising model, where  $k = \frac{1}{2}$ , permitting to calculate the critical exponents, being connected with the eigenvalues of  $T^0 \geq 0$  for unitary representations.
3. To conformal quantum field theory in (1+1)-space-time dimensions, where many interesting problems can be treated.

I hope, I could demonstrate with this short introduction the fascinating perspectives of combining common properties of special nonlinear field equations with infinite-dimensional Lie algebras.

## References

- /1/ Möbius, P., Czech. J. Phys. B 37 (1987) 1041.
- /2/ Thirring, W., Lehrbuch der Math. Physik Bd. 1: Klassische Dynamische Systeme. Springer-Verlag, Wien-New York, 1977.
- /3/ Clarkson, P., Physics D 18 (1986) 209.
- /4/ Felsager, B., Geometry, Particles and Fields. Odense University Press, 1981.
- /5/ Eilenberger, G., Solitons. Springer Series in Solid State Sciences, Vol. 19, Springer-Verlag, Berlin-Heidelberg-New York-Tokyo, 1983.
- /6/ Olive, D. I., Kac-Moody Algebras: An Introduction for Physicists. Imperial /TP/84-85/14.

## Phase transitions of W-condensation in the hot Universe

H. Pérez-Rojas \*

Institute of Physics, EPRC, Slovak Academy of Sciences

R. González

Institute of Cybernetics, Mathematics and Physics, Cuban Academy of Sciences

### INTRODUCTION

In its very well known paper [1] Linde proved that condensation of W-bosons may be induced by fermion density at zero temperature. In more recent papers [2], one of us (H.P.R) with O.K. Kalashnikov studied the problem of induced W-Bose-Einstein condensation at finite temperature. It was found that the critical lepton density to start the phase transition of W-condensation decreases with temperature down to  $T_c$ , the symmetry restoration critical temperature, which becomes also a critical temperature for W-condensation. In [2] only lepton number and total electric charge were considered to be conserved. Later [3], Ferrer, de la Incera and Shabad investigated the same problem by using a different method than the one used in [2], and introducing the additional condition of weak neutral charge conservation. Their phase diagram is not in agreement with that of [2], and a later calculation made by Kalashnikov and H.P.R [4] by using the unitary gauge, gave phase diagrams different from that of [3] and in agreement with [2].

One of the consequences of the introduction of the neutral weak charge is the appearance of a divergent term, which express the charge of the vacuum acquired through the symmetry breakdown mechanism. This charge depends on the weak neutral chemical potential, and its simple deletion, as was made in [3] and [4] is not a gauge invariant renormalization

---

\*On leave from Institute of Cybernetics, Mathematics and Physics, Cuban Academy of Sciences

procedure, and it may be the source of the disagreement in results of the above mentioned papers.

In the present paper we deal again with the W-condensation induced by fermion density at finite temperature. We shall start from the Weinberg-Salam Lagrangian in which the first generation of quarks is also included. The distinct feature as compared with [3], [4] is that we propose a gauge invariant subtraction procedure of the divergent weak neutral charge of the scalar sector. This leads to a high temperature phase diagram very close to that of [2].

### I. The Lagrangian and the partition functional

The Lagrangian of the present model has the form:

$$\begin{aligned}
 \mathcal{L} = & -\frac{1}{4} G_{\mu\nu}^i G_{\mu\nu}^i - \mathcal{F}_{\mu\nu} \mathcal{F}_{\mu\nu} - \bar{\Psi}_L \gamma_\mu (\partial_\mu - i\frac{g}{2} \tau^i W_\mu^i + i\frac{g'}{2} B_\mu) \Psi_L \\
 & - e_R \gamma_\mu (\partial_\mu + ig' B_\mu) e_R - \bar{Q}_L \gamma_\mu (\partial_\mu - i\frac{g}{2} \tau^i W_\mu^i - i\frac{g'}{6} B_\mu) Q_L \\
 & - \bar{u}_R \gamma_\mu (\partial_\mu - i\frac{2}{3} g' B_\mu) u_R - \bar{d}_R \gamma_\mu (\partial_\mu + i\frac{2}{3} g' B_\mu) d_R \\
 & - \left| (\partial_\mu - i\frac{g'}{2} \tau^i W_\mu^i + i\frac{g'}{2} B_\mu) \phi \right|^2 - \frac{\lambda^2}{4} (\phi^\dagger \phi - a^2) \quad (1) \\
 & - \lambda_1 (\bar{\Psi}_L \phi e_R + \bar{e}_R \phi^\dagger \Psi_L) - \eta_1 (\bar{Q}_L \phi u_R + \bar{u}_R \phi^\dagger Q_L) \\
 & - \eta_2 (\bar{Q}_L \phi d_R + \bar{d}_R \phi^\dagger Q_L)
 \end{aligned}$$

where  $G_{\mu\nu}^i$  and  $\mathcal{F}_{\mu\nu}$  are respectively the non-abelian SU(2) and the abelian field tensors built from  $W_\mu^i$  and  $B_\mu$  respectively. All abbreviations in (1) are usual and many other details connected with this model may be found in [2], [5]. It is convenient to point out here that the spinor doublets are



$$\psi_L = \frac{1}{2}(1-\gamma_5)(\nu) \quad Q_L = \frac{1}{2}(1-\gamma_5)(u) \quad (2)$$

and the singlets

$$i_R = \frac{1}{2}(1+\gamma_5)l \quad \text{where } l = e, u, d \quad (3)$$

We use in (1) Euclidean metric and this means that  $\partial_4 = -i\partial_0$ ,  $W_4 = -iW_0$ ,  $B_4 = -iB_0$   $\gamma_\mu\gamma_\nu + \gamma_\nu\gamma_\mu = 2\delta_{\mu\nu}$   
 Finally the scalar field is defined as

$$\phi = \frac{1}{\sqrt{2}} \left\{ \begin{pmatrix} 0 \\ \xi \end{pmatrix} + \begin{pmatrix} i h_1 + h_2 \\ \sigma - i h_3 \end{pmatrix} \right\}, \quad \tilde{\phi} = i\tau_2 \phi \quad (4)$$

where  $\xi \neq 0$  is the symmetry breakdown parameter.

By following the method of Refs. [4][5], we may introduce the chemical potentials  $\mu_1, \mu_2, \mu_3, \mu_4$  as factors of the Noether conserved charges which account respectively for the electric charge, lepton number, weak neutral charge and baryon number. These products are used to write the density matrix

$$\rho = e^{-\beta(\mathcal{H}_0 - \sum_{i=1}^4 \mu_i N_i)} \quad (5)$$

From (5) we get the partition functional

$$\mathcal{Z} = N(\beta) \int \exp \left[ - \int_0^{\beta} \int_{\mathcal{M}} \mathcal{L}_{eff} \right] \prod_{l,m} \mathcal{D}B^m \mathcal{D}\psi^l \mathcal{D}\gamma^l \prod_{j=0}^3 \delta(G_j) \text{Det } \mathcal{M} \quad (6)$$

where  $m$  stands for all Bose and  $l$  for all Fermi fields,  $G_j = 0$  are the gauge conditions and  $\mathcal{M}$  the Faddeev-Popov matrix, which may be incorporated to  $\mathcal{L}_{eff}$  through adequate ghost fields. The introduction of  $\mu_1, \mu_3$  in (5) leads to the fact that the gauge fields acquire nonzero vacuum expectation values

$$\langle W_4^3 \rangle = \frac{i}{g} (\mu_1 - \mu_3 \frac{2 \cos^2 \theta}{\cos 2\theta}), \quad \langle B_4 \rangle = \frac{i}{g'} (\mu_1 + \mu_3 \frac{2 \sin^2 \theta}{\cos 2\theta}) \quad (7)$$

where  $\mu_1$  and  $\mu_3$  appear as displacements of the derivatives, i.e.

$$\mathcal{L}_{\text{eff}} = \mathcal{L} \left\{ \begin{array}{l} W_4^3 \Rightarrow W_4^3 + \langle W_4^3 \rangle \\ B_4 \Rightarrow B_4 + \langle B_4 \rangle \\ \partial_\nu \ell \Rightarrow (\partial_\nu - \mu_2 \delta_{\nu 4}) \ell \\ \partial_\nu q \Rightarrow (\partial_\nu - \mu_4 \delta_{\nu 4}) q \end{array} \right. \quad (8)$$

where  $\ell = \nu, e_L, e_R, q = u_{L,R}, d_{L,R}$

The chemical potentials of leptons, quarks and  $W$ 's are:

$$\begin{aligned} \mu_{eL} &= \mu_1 + \mu_2 + \mu_3, & \mu_{eR} &= \mu_1 + \mu_2 + \mu_3 \frac{2 \sin^2 \theta}{\cos 2\theta} \\ \mu_\nu &= \mu_1 + \frac{\mu_3}{\cos 2\theta}, & \mu_{uL,R} &= -\frac{2}{3} \mu_1 + \mu_4 + \mu_3 \frac{\alpha_{L,R}}{3 \cos 2\theta} \\ \mu_{dL,R} &= \frac{1}{3} \mu_1 + \mu_4 + \frac{\beta_{L,R}}{3 \cos 2\theta} \mu_3, & \mu_W &= \mu_1 - \mu_3 \frac{2 \cos^2 \theta}{\cos 2\theta} \end{aligned} \quad (9)$$

where

$$\alpha_L = 3 \cos^2 \theta - \sin^2 \theta, \quad \alpha_R = -4 \sin^2 \theta$$

$$\beta_L = -(3 \cos^2 \theta + \sin^2 \theta), \quad \beta_R = 2 \sin^2 \theta$$

and among others the chemical equilibrium equations are satisfied

$$\mu_{eL} + \mu_{\bar{\nu}} = \mu_{W^-}, \quad \mu_{dL} = \mu_{uL} + \mu_{W^-} \quad (10)$$

We must point out here that the neutral charge which should be obtained from  $\partial V / \partial \mu_3$  (where  $V = \beta'(\ln Z)$ ) in the one-loop approximation contains a  $\mu_3$  dependent vacuum term which is divergent and comes from the infinite weak neutral charge of the vacuum.

(This is due to the contribution of the scalar term and may be understood even in the simple case of the  $U(1)$  self-inter-

acting charged scalar field  $\phi = \frac{1}{\sqrt{2}}(\xi + \sigma + i\eta)$  with symmetry breaking parameter when a chemical potential  $\mu$  (the analog of  $\mu_3$ ) is introduced. As the masses of  $\sigma$  and  $\eta$  are different (even in the one-loop approximation), this gives a  $\mu$ -dependent vacuum contribution to the thermodynamic potential which is divergent.

Even more, when using other gauges than the unitary ( $\hbar_{1,2,3=0}$ ) the otherwise massless Goldstone bosons acquire a  $\mu_3$ -dependent mass and they are not properly cancelled by the ghost terms. The latter, on the contrary, suppress<sup>45</sup> extra degrees of freedom of the gauge vector field terms.

A gauge invariant way of removing the infinite vacuum term may be obtained by adding to the exponent  $\mathcal{H} - \sum_i \mu_i N_i$  in (5) adequate counterterms. If we take the  $U(1)$  scalar charge counterterm  $C \{ [(a - i\frac{g}{2} z^i W_A^i - i\frac{g'}{2} B_A) \phi]^\dagger \phi - \phi^\dagger [(a + i\frac{g}{2} z^i W_A^i + i\frac{g'}{2} B_A) \phi] \}$  we get that for  $C = \mu_3 / \cos 2\theta$ , the infinite weak neutral charge term is removed, and in the one-loop approximation, the Goldstone bosons are cancelled by the ghost terms. We must emphasize here that although we refer to the one-loop approximation, in order to ensure that the Goldstone boson masses vanish we must introduce two-loop corrections to the scalar masses; this is necessary also in order to have the thermodynamic potential and the charges defined in the scalar mass shell at any  $T$  (see below).

## 2. The Thermodynamic Potential and Equilibrium Equations

We shall adopt the gauge conditions

$$\begin{aligned} \partial_\nu W_\nu - g\frac{\hbar}{2} \pm &= 0 \\ \partial_\nu Z_\nu + \sqrt{g^2 + g'^2} \frac{\hbar_3}{2} &= 0 \\ \partial_\nu A_\nu &= 0 \end{aligned} \tag{11}$$

where  $\hbar^\pm = (\hbar_1 \mp i\hbar_2)$

$$\partial_\nu^\pm = \partial_\nu \pm \mu_\nu \delta_{4\nu}$$

After substitution in (6) we get in the one-loop approximation (after the removal of the divergent term) the effective

potential per unit volume [5]

$$V = \frac{\lambda^2}{8} \xi^4 - \frac{a^2 \xi^2}{4} + \Omega(a^2, \beta, \mu_i, \xi). \quad (12)$$

From V we get the equation for the minimum of the effective potential with respect to  $\xi^2$

$$\frac{\partial V}{\partial \xi^2} = \frac{\lambda^2 \xi^2}{4} - \frac{a^2}{4} + \frac{\partial \Omega}{\partial \xi^2} = 0, \quad (13)$$

as well as the conservation of electric and weak neutral charges

$$\frac{\partial V}{\partial \mu_{1,3}} = \frac{\partial \Omega}{\partial \mu_{1,3}} = 0, \quad (14)$$

and the conservation of leptons  $l$  and baryons  $b$

$$\frac{\partial V}{\partial \mu_2} = \frac{\partial \Omega}{\partial \mu_2} = -l, \quad \frac{\partial V}{\partial \mu_4} = \frac{\partial \Omega}{\partial \mu_4} = -\frac{b}{3}. \quad (15)$$

Eq. (13) may be understood as a temperature-dependent renormalization of the mass parameter  $a^2$ , i.e. it is equivalent to write

$$\frac{\lambda^2 \xi^2}{4} - \frac{a^2(T)}{4} = 0 \quad (16)$$

where  $a^2(T) = a^2 - 4 \partial \Omega / \partial \xi^2$ .

In what concerns to eqs. (14) and (15), to have scalar on-shell masses we must also replace  $a^2 \rightarrow a^2(T)$ , which is equivalent to correct such masses by the two-loop terms in  $\Omega$ . This ensures the complete fulfillment of the Goldstone theorem and of the Higgs mechanism. In this way equations (14) and (15) become exactly expressed in terms of the spectra of the particles involved. We shall write only the asymptotic limit, i.e. for  $\mu_i, m_i \ll T$  we have

$$\lambda^2 \xi^2 - a^2 + \frac{\alpha T^2}{12} = 0 \quad (13')$$

$$\frac{T^2}{54} [10\mu_W + 11\mu'_3 - 6\mu_4] + T^2 \mu_W + \frac{T^2}{6} (\mu_{e_L} + \mu_{e_R}) = 0$$

$$\frac{T^2}{54} [(1 - 10 \cos 2\theta) \mu_W + 22 \sin^2 \theta \mu'_3 - 12 \sin^2 \theta \mu_4] - 2 \cos^2 \theta T^2 \mu_W + \frac{T^2}{6} [(\mu_{\nu} + \mu_{e_R}) - \cos 2\theta (\mu_{e_R} + \mu_{e_L})] = 0 \quad (14)$$

and

$$\frac{T^2}{6} (\mu_{e_L} + \mu_{e_R} + \mu_{\nu}) = \ell; \quad \frac{T^2}{9} (-\mu_W - 2\mu'_3 + 6\mu_4) = \frac{b}{3}$$

where  $\alpha \approx (3\lambda^2 + 6e^2(1 + 2 \cos^2 \theta / \sin^2 2\theta))$  (we have neglected the fermion masses for simplicity) and  $\mu'_3 = \mu_3 / \cos 2\theta$ . The resulting critical equation is

$$\left(\ell - \frac{b}{12}\right)^2 = K \alpha \frac{m_W^2}{m_\sigma^2} T^4 (T_0^2 - T^2) \quad (17)$$

where  $K \sim 1/3$ . For  $T > T_c$  it is estimated as  $\ell^2 \sim T^4 (T^2 - T_c^2)$ . The condensate is present in the region bounded by both curves in the  $\ell, T$  plane.

We see that the high temperature W Bose-Einstein condensation phenomenon is produced and follows again the qualitative behaviour described in [2]. The validity of (17) is restricted to the region in between the chiral and Higgs symmetry restoration temperatures where quarks are considered as free. (The inclusion of the colour fields require a separate consideration). Nevertheless, if in our universe  $\ell \gg b$ , then (17) may have a wider range of validity, as discussed in (2).

#### REFERENCES

- (1) A.D. Linde, Phys. Lett. 86B (1979), 39
- (2) H. Perez Rojas and O.K. Kalashnikov, *Kratkie Soob. po Fizike* (Lebedev Institute Reports, Allerton Press) N 2 (1986) 23; Nucl. Phys. B 293 (1987) 241
- (3) E. Ferrer, V. de la Incera and A.E. Shabad, Phys. Lett. B 185 (1987) 407.
- (4) O.K. Kalashnikov and H. Perez Rojas, Preprint ICIMAF, Cuban Acad. of Sci. (1987) (Subm. to Mod. Phys. Lett.A)
- (5) H. Perez Rojas, Dr.Sc. Dissertation, Havana-Bratislava, 1987

ON THE GEOMETRY OF GROUP SPACE OF THE GROUP OF MOTION  
OF THREE-DIMENSIONAL QUADRATIC FORM

I. Lukáč

Institute of Physics of Electro-Physical Research Centre  
Slovak Academy of Sciences, Bratislava

It is useless to stress once again the significance and exceptional role of the continuous groups in theoretical physics. The simplest groups of this type are the rotation group  $SO(3)$  in three-dimensional euclidean space and the group of similar transformations in three-dimensional pseudoeuclidean space -  $SO(2,1)$ -group. Properties, characteristic features and representations of these groups were discussed in many articles, monographs and text-books (e. g. <sup>1-5</sup>). Both these groups possess three-parametrical group space and conserve some quadric - in the first case it is a sphere  $(z^1)^2 + (z^2)^2 + (z^3)^2 = 1$ , in the second one it is a hyperboloid  $(z^1)^2 - (z^2)^2 - (z^3)^2 = 1$ . The quadratic forms mentioned above, of course, have been obtained from some general quadric by means of transformations of an affine group using the classification under corresponding invariants <sup>6</sup>. Therefore it is natural to make an attempt to consider the group of transformations of some general quadratic form in three-dimensional euclidean space

$$c_{1k} z^1 z^k = 1, \quad 1, k = 1, 2, 3 \quad (1)$$

with nine (arbitrary) real coefficients  $c_{1k}$ . We shall call such group of transformations, i. e. the group of matrices  $D_k^1(x)$  depending on the set of three parameters  $x = (x^1, x^2, x^3)$  which fulfil the condition

$$c_{1j} D_k^1(x) D_1^j(x) = c_{k1}, \quad \det |D_k^1(x)| = 1,$$

as the group of motion of three-dimensional quadric and we shall denote it as  $SQ(3)$ . Such approach to the transformations of general quadrics will allow us to demonstrate the utility of application of tensor methods in the group theory. Note the correct and successive introduction of tensor indices e. g. for  $SO(3)$ -group is impossible <sup>7</sup>. Certainly, we are able to make

the classification under an affine (or centred-affine) group and corresponding invariants in all the final formulae.

The concrete form of transformation matrix  $D_j^1(x)$  depends on the choice of a set of parameters  $x^1, x^2, x^3$ . It is necessary to note that each choice of the parametrization determines the certain coordinate system in the group space and, of course, the different parametrizations correspond to the different coordinate systems. Really, the different parametrizations are mathematically (group-theoretically) equivalent but from the physical point of view they lead to the different sets of observables (i. e. to the different complete sets of quantum numbers) which correspond to the different (and non-equivalent) physical problems. We have no place to discuss it in detail here.

For the present case we shall use the Cayley's parametrization of the transformation matrix  $D_j^1(x)$  which can be written in a symbolic form as  $D = (C - A)(C + A)^{-1}$  <sup>8</sup>. The symmetrical matrix  $C$  has elements  $c_{ik}$  and  $A$  is an antisymmetrical matrix with elements  $a_{ik} = -a_{ki}$  which can be expressed (especially for three-dimensional space) by means of a vector  $x^k$  in the form  $a_{ij} = e_{ijk}x^k$  ( $e_{ijk}$  is a covariant completely antisymmetrical tensor).

After some bulky but not very complicated calculations one can find the explicit form of transformation matrix  $D_j^1(x)$  as a function of three parameters  $x^1, x^2, x^3$  ( $-\infty < x^k < \infty$ ):

$$D_j^1(x) = R_x^{-1} \cdot \left[ (2c_0 - R_x)\delta_j^i + 2u_j x^i + 2c_0 c^{ik} e_{kjm} x^m \right]. \quad (2)$$

The following notations were used here:

$$c_0 = \det |c_{ik}| \neq 0, \quad u_j = c_{jk} x^k, \quad c^{ik} c_{kj} = \delta_j^i, \\ R_x = \det |c_{ik} - a_{ik}| = c_0 + u_j x^j = c_0 + c_{ik} x^i x^k.$$

Now having the explicit form of  $D_j^1(x)$  it is easy to convince that the relations written below take place:

$$D_j^1(0) = \delta_j^i, \quad \det D_j^1(x) = 1, \quad e_{ijk} D_p^i(x) D_q^j(x) D_r^k(x) = e_{pqr}, \\ D_j^1(x) x^j = x^i, \quad D_j^1(x) u_i = u_j, \quad c_{ij} D_k^i(x) D_l^j(x) = c_{kl}, \quad (3) \\ D_j^1(x) D_k^j(-x) = \delta_k^i, \quad D_j^1(-x) D_k^j(x) = \delta_k^i.$$

Note should be taken that the matrix  $D_j^i(-x)$  represents an inverse transformation to the transformation of  $D_j^k(x)$ .

It is well-known what crucial role plays the composition of parameters in the theory of continuous groups <sup>9, 10</sup>, and therefore we shall try here very briefly to show how one can get such relation for the matrices of type (2). If we make two successive transformations with the sets of parameters  $x$  and  $y$  we get some new transformation with the set of parameters  $z$  according to the formula:

$$D_k^i(z) = D_j^i(y) D_k^j(x). \quad (4)$$

In order to obtain the composition of parameters for SQ(3) it is necessary to solve the matrix equation (4) in regard to  $z = \langle y, x \rangle$ . It turned out that it can be done rather simply. For this purpose we use the relation (see (3))

$$D_j^i(z) z^j = z^i$$

which can be rewritten by means of (4) and (3) in the form

$$\left[ D_k^j(y) - D_k^j(-x) \right] z^k = 0.$$

Multiplying this equation from the left side in turn by  $u_j = c_{jk} x^k$  and  $v_j = c_{jk} y^k$  (we consider this operation as a scalar product of a covariant and a contravariant vectors) we obtain two equations determining  $z$

$$u_j \left[ D_k^j(y) - \delta_k^j \right] z^k = 0, \quad v_j \left[ \delta_k^j - D_k^j(-x) \right] z^k = 0. \quad (5)$$

The system of equations (5) means that the contravariant vector  $z^k$  is perpendicular to two covariant vectors  $A_m$  and  $B_n$

$$A_m = u_j \left[ D_m^j(y) - \delta_m^j \right], \quad B_n = v_j \left[ \delta_n^j - D_n^j(-x) \right].$$

Now it is obvious that the vector  $z^k$  has to have the form:

$$z^k = \text{const } e^{kmn} A_m B_n. \quad (6)$$

The unknown constant in (6) can be determined from (4) by means of taking the trace what leads to the relation

$$R_z = R_x R_y (c_0 - c_{1k} x^1 x^k)^{-1}.$$

Finally, one can get a very simple, nice and useful explicit form for the composition of parameters of the group of motion of three dimensional quadric:



$$z^i = \langle y, x \rangle^i = \frac{c_0 (x^i + y^i) - e^{ijk} c_{jm} x^m c_{kn} y^n}{c_0 - c_{pq} x^p x^q} \quad (7)$$

From the composition formula (7) obviously follows:

$$\langle x, y \rangle^i \neq \langle y, x \rangle^i, \quad \langle 0, x \rangle^i = x^i, \quad \langle y, 0 \rangle^i = y^i, \quad \langle x, -x \rangle^i = 0.$$

The explicit form of the law for the composition of parameters allows now to get all the characteristics of the SQ(3) group and its group space like generators, structure constants, frames, metric tensor etc. Having only very limited volume of this contribution we shall restrict ourselves here by the enumeration of the corresponding formulae:

a) Generators  $J_i$  of SQ(3)

$$J_i = -1/2 \left( \frac{\partial z^k}{\partial y^i} \right)_{y=0} \partial_k = -1/2 c_0 \left[ c_0 \partial_i + u_1 (x^k \partial_k) + c_0 c^{kj} e_{kil} x^l \partial_j \right], \quad \partial_k = \partial / \partial x^k.$$

b) Structure constants  $c_{ij}^m$  of SQ(3)

$$c_{ij}^m = -1 \left( \frac{\partial^2 z^m}{\partial x^i \partial y^j} \right)_{x=y=0} = -1 e_{ijk} c^{km}.$$

Hence, the commutation relations of SQ(3) have the form:

$$[J_i, J_j] = -1 e_{ijk} c^{km} J_m.$$

c) Casimir's operator  $C^{(2)}$  for SQ(3)

$$C^{(2)} = 1/2 c_0 c^{ik} (J_i J_k + J_k J_i) = 1/2 c_0 e^{ijk} J_i J_j J_k = 1/4 R_x \left[ c_0 c^{ik} \partial_i \partial_k + (x^i \partial_i) (x^k \partial_k) + 1 \right].$$

d) Frames  $T_k^m(x)$  of the group space of SQ(3)

$$T_k^m(x) = 2 \left( \frac{\partial y^m}{\partial z^k} \right)_{z=x} = 2 c_0 (\delta_k^m - c^{mj} e_{jki} x^i) / R_x.$$

e) Metric tensor  $g_{ik}$  of the group space of SQ(3)

$$g_{ik} = c_{mn} T_i^m(x) T_k^n(x) = 4 (R_x c_{ik} - u_1 u_k) / R_x^2, \quad g_{ij} g^{jk} = \delta_i^k, \\ g^{ik} = R_x (c_0 c^{ik} + x^i x^k) / 4 c_0, \quad g_0 = \det |g_{ik}| = 64 c_0^2 / R_x^4.$$

f) Christoffel's symbols of the group space of SQ(3)

$$\Gamma_{kl,m} = 1/2 (\partial_k g_{lm} + \partial_l g_{km} - \partial_m g_{kl}) = -(u_k g_{lm} + u_l g_{km}) / R_x, \\ \Gamma_{kl}^i = g^{ij} \Gamma_{kl,j} = -(u_k \delta_l^i + u_l \delta_k^i) / R_x.$$

g) Riemann's tensor of curvature of the group space of  $SQ(3)$

$$R^i_{jkl} = \partial_k \Gamma^i_{jl} - \partial_l \Gamma^i_{jk} + \Gamma^i_{rk} \Gamma^r_{jl} - \Gamma^i_{rl} \Gamma^r_{jk} = \\ = 1/4 (\varepsilon_{jl} \delta^i_k - \varepsilon_{jk} \delta^i_l), \quad R_{ijkl} = 1/4 (\varepsilon_{ik} \varepsilon_{jl} - \varepsilon_{il} \varepsilon_{jk}).$$

h) Ricci's tensor and the curvature of the group space of  $SQ(3)$

$$R_{ik} = R^j_{ijk} = 1/2 \varepsilon_{ik}, \quad R = g^{ik} R_{ik} = 3/2 > 0.$$

One can continue this list of formulae, of course, but it doesn't add some new essence into the developed tensor methods. All the details of these calculations will be published elsewhere. It should be emphasized only that the more interesting results can be obtain in some analogical consideration of four-dimensional real, three-dimensional complex or some other (e. g. symplectic) quadratic forms.

1. Biedenharn, L. C., Louck, J. D.: *Angular Momentum in Quantum Physics*. Addison-Wesley Publ. Comp., Reading, Massachusetts 1981.
2. Wigner, E. P.: *Group Theory and Its Application to the Quantum Mechanics and Atomic Spectra*. Academic Press, New York-London 1959.
3. Barut, A. O., Rączka R.: *Theory of Group Representations and Applications*. PWN - Polish Scientific Publishers, vol. 1 and 2, Warszawa 1977.
4. Gel'fand, I. M., Minlos, R. A., Shapiro, Z. Ya.: *Representations of the Rotation and Lorentz Groups*. Moscow 1953 (in russian).
5. Varshalovich, D. A., Moscalev, A. N., Khersonskii, V. K.: *Quantum theory of Angular Momentum*. Moscow 1975 (in russian).
6. Korn, G. A., Korn, T. M.: *Mathematical Handbook for Scientists and Engineers*. McGraw-Hill Book Comp., New York-Toronto-London 1961.
7. Lukáč, I.:  $SO(3)$ -Group Space as a Riemannian Space. In: *Bi-annual Report 1984-1985 of the Institute of Physics of EPRC, Slov. Acad. Sci., Bratislava 1986*, p. 22.
8. Turnbull, H. W.: *The Theory of Determinants, Matrices and Invariants*. Dover Publ. Inc., New York 1960.
9. Eisenhart, L. P.: *Continuous Groups of Transformations*. Princeton 1933.
10. Chebotarev, N. G.: *Theory of Lie's Groups*. Moscow-Leningrad 1940 (in russian).

# PROMPT GAMMA PHYSICS: RECENT EXPERIMENTAL RESULTS

M. Bonesini \*

Sesione INFN, Milano - Italy

## 1. Introduction

The production of prompt gammas (or direct photons) offers a good testing ground for hadron constituent dynamics in high  $p_T$  collisions [1]. To first order in  $\alpha_s$ , the Born terms responsible for the process are: the annihilation diagram  $q\bar{q} \rightarrow \gamma g$  (dominant in  $p\bar{p} \rightarrow \gamma X$  and important in  $\pi^- p \rightarrow \gamma X$  reactions at large  $X_T$ , where  $X_T = 2p_T/\sqrt{s}$ ) and the QCD Compton diagram  $qg \rightarrow \gamma g$  (dominant in  $\pi^+ p \rightarrow \gamma X$  and  $pp \rightarrow \gamma X$  reactions). These graphs produce a clear event structure: an isolated high  $p_T$  direct photon recoiling against a quark or gluon jet together with two spectator jets (beam/target fragments). This naive picture is complicated however by higher order corrections ( $O(\alpha_s^2)$ ), the quark bremsstrahlung that provides not isolated gammas, the intrinsic parton  $k_T$  smearing and possible higher twist effects.

Since the first published results from experiment R412 at ISR [2], there had been a growing interest in prompt gamma studies. Now we have an active second generation fixed target program with incident  $\pi^\pm, p, \bar{p}$  both at Cern SPS (NAS, NA24, WA70 and UA6) and Fermilab Tevatron (E705, E706) and new results from Cern  $p\bar{p}$  collider (UA1, UA2). Recent results from Cern ISR (AFS, R110) on  $p\bar{p}, p\bar{p}$  interactions have already been published, but some analysis must still be completed. The  $p\bar{p}$  collider data, in the low  $X_T$  range .03-.13, complement the kinematical domain of fixed target ( $X_T \approx .3-.6$ ) and ISR data ( $X_T \approx .1-.35$ ). The advantage of fixed target experiments is the possibility of probing direct gamma production with a variety of projectiles and targets, in a wide kinematical range, thus allowing the separation of QCD annihilation and Compton processes. For example, the difference  $\sigma(\pi^- p \rightarrow \gamma X) - \sigma(\pi^+ p \rightarrow \gamma X)$  isolates the annihilation diagrams. For more details see [1]. Here we stress only that:

- a prompt gamma is directly detectable in the final state (without any jet reconstruction algorithm) and its kinematics (angle and energy) may be measured with good precision
- a fragmentation model is not required to make a comparison with theory (now available as next-to-leading log calculation [3]). Theoretical calculations of inclusive direct gamma cross sections are claimed to be at a 20 % level, so that we may hope in a quantitative test of perturbative QCD.
- prompt gamma production is either accompanied by gluon emission or initiated by a gluon, thus providing a way to investigate gluon structure functions (S.F.) and fragmentation functions.

However, the detection of a prompt gamma signal is a difficult experimental task :

- cross sections are low, compared for example to jet production ( $\sigma_\gamma/\sigma_{jet} \approx 3 \times 10^{-4}$  for  $p_T \geq 30$  GeV/c, as determined from UA2).
  - there is a large background from neutral meson decays into gammas ( $\pi^0 \rightarrow \gamma\gamma, \eta^0 \rightarrow \gamma\gamma, \dots$ ). At low  $p_T$ , if one gamma escapes the apparatus or has a too low energy, the other gamma may fake a direct photon. At high  $p_T$ , the two gammas from a  $\pi^0 \rightarrow \gamma\gamma$  decay may not be resolved ("coalescing"), thus simulating a single "fake" direct gamma.
- Additional backgrounds are due to hadrons misidentified as e.m. showers ( $K_S^0, n, \dots$ ) and to the bremsstrahlung of high energy muons, accompanying the beam particles in fixed target experiments. The  $\mu$  halo background is relevant at high  $p_T$ , but may be rejected using veto counters or timing and angular cuts.
- having very steep cross sections as a function of  $p_T$ , a small uncertainty in the energy scale ( $\sim 1\%$ ) may result in a large normalisation error ( $\sim 10\%$ ).

\* Hadron Structure 87 Conference, Smolenice, November 1987.

## 2. Experiments and Data Analysis

Two different experimental techniques are used to detect a prompt gamma signal. In the former ("direct method") events are reconstructed on an event by event basis. Position and energy of incident gammas are measured in a fine grain, wide geometrical acceptance e.m. calorimeter. Trigger showers are paired with any other shower in the calorimeter, looking for  $\pi^0$  or  $\eta^0$ . Unpaired showers are considered as single photon candidates. This method is well suited for the study of the structure of direct gamma events, as compared, for example, to high  $p_T$   $\pi^0$  events, but is limited at high  $p_T$  due to the coalescing of showers from a  $\pi^0$  decay [NA3 [5], WA70 [6], NA24 [7], UA6 [8]].

The latter ("statistical method") is used instead when the spatial resolution of the available e.m. calorimeters does not allow to separate high  $p_T$   $\pi^0$ ,  $\eta^0$  and single  $\gamma$ . An isolated e.m. shower is requested with some additional cuts to distinguish statistically between  $\gamma$ 's and  $\pi^0$ 's. One criterium ("conversion method") exploits the different conversion probability in a preshower detector for  $\pi^0 \rightarrow \gamma\gamma$  and single  $\gamma$ 's (UA2 [9]). Others use the difference in shower pattern for  $\pi^0$ 's and  $\gamma$ 's, such as cluster width (R110) or longitudinal sampling (UA1). While the "direct method" allows a better control over most of the backgrounds and is compulsory when the ratio  $\gamma/\pi^0$  is small, where the "statistical method" is dominated by systematic errors, the "statistical method" has no intrinsic upper limit to the  $p_T$  values that may be studied.

A list of recent experiments is shown in table 1. While the first convincing evidence for prompt gamma production came from ISR experiments, the bulk of new results now come from Cern fixed target experiments and  $p\bar{p}$  collider (mainly UA2). As good summaries of new UA2 results are available [9], in the rest of this talk I will briefly review only results from fixed target experiments, in the  $X_T$  range 0.3-0.6.

Final results are available from experiments NA3[5], NA24[7] and WA70 [6], while UA6 has presented only preliminary results on part of the final statistics for the  $p\bar{p}$  sample [8]. The Fermilab experiments are still in data taking. While experiment NA3 uses an isoscalar Carbon target and experiments NA24, WA70 use a liquid  $H_2$  target, UA6 uses a novel design molecular hydrogen jet target, put in a straight section of the SPS.

A typical set-up, from experiment WA70 at Cern Sps, is shown in figure 1. A high intensity, unseparated hadron beam at Cern SPS ( $p_{lab} = 280 \text{ GeV}/c$ ) hits a 1 meter long  $H_2$  target in the middle of a magnetic spectrometer ( $\Omega'$  at Cern), equipped with MWPC and Drift Chambers for charged tracks and vertex reconstruction. The photon detector is a lead-liquid scintillator sandwich of 24  $X_0$  thickness, segmented in depth to give informations on the longitudinal development of showers. The active elements, made of 2m long extruded teflon tubes, containing liquid scintillator, are arranged orthogonally in channels 1.07 and 2.14 cm wide. A timing system (TOF) is used to resolve spatial ambiguities (Y/Z matching of shower profiles).

To obtain sufficient spatial resolution, the NA3 and NA24 experiments use in addition to their e.m. calorimeters (taken from old set-ups) a fine grain photon detector. NA3 uses a shower chamber at about 5  $X_0$  into the calorimeter, with strip and pad readout on the cathode planes, while NA24 uses a 9.6  $X_0$  additional e.m. calorimeter made of a lead-proportional tubes sandwich. The UA6 photon detector is made interleaving lead plates with 1 cm proportional tubes (alternate x-y readout). All experiments trigger on the energy deposition in the photon detector.

All fixed target experiments (WA70, NA3, NA24, UA6) consider as direct gamma candidates photons outside the  $\pi^0$  and  $\eta^0$  mass peaks. The quoted resolutions for  $\pi^0$  ( $\eta^0$ ) mass are 13 (38) MeV for NA3, 10 (29) MeV for WA70, 16 (30) MeV for NA24 and 20 (35) MeV for UA6. Due to the good calorimetric spatial resolutions ( $\sigma_x \sim 1 \text{ mm}$ ), the requirement that the trigger shower points back to the interaction vertex allows a good rejection of  $\mu$  halo events. Timing requirements may improve this rejection and avoid also pile-up events. The fine transverse granularity (up to 1 cm in WA70 experiment) allows also cuts on the transverse shower width, rejecting coalescing showers from  $\pi^0$  decays.

The overall efficiency correction (geometrical acceptance, trigger efficiency, e.m. pattern recognition and analysis efficiencies) and the background subtraction are performed using M.C. simulations.

Results on direct gamma production are usually limited by statistics (sensitivity of the order of  $1 \text{ pb}^{-1}$  are needed to extend the study of direct gammas to high  $p_T$  and systematic errors, mainly due to:

- uncertainty in luminosity monitoring ( $\sim 5\%$ )
- uncertainty in background subtraction ( $\sim 20\%$ ), strongly  $p_T$  dependent
- uncertainty in the calorimeter energy scale ( $\sim 20\%$ )

### 3. Recent Experimental Results

All fixed target experiments (NA3, WA70, NA24, UA6) present results on the cross section ratio  $\gamma/\pi^0$ , that is less sensitive to systematic errors and the invariant cross section  $E \times d^3\sigma/dp^3$  as a function of  $p_T$  [5],[6],[7],[8]. Results as a function of  $X_F$  or  $y_{cm}$  are presented from WA70 and NA24 experiments. While WA70 presents its results in a fine  $X_F - p_T$  grid, NA24 has only results versus  $y_{cm}$  for  $\pi^- p$  interactions where the sensitivity is higher. Having obtained the inclusive cross sections in a fine  $X_F - p_T$  grid, the WA70 collaboration has obtained also a phenomenological parametrisation of direct gamma and high  $p_T$   $\pi^0$  production.

Comparison with theory is done usually in the framework of perturbative next-to-leading-log QCD, where the scale ambiguity is removed using an optimisation method, such as the Principle of Minimal Sensitivity of Stevenson and Politzer [4]. Duke-Owens S.F. are used, where Duke-Owens set 1 corresponds to a soft glue and a value  $\Lambda_{\overline{MS}} = 200 \text{ MeV}$ , while Duke-Owens set 2 has  $\Lambda_{\overline{MS}} = 400 \text{ MeV}$  and a hard glue [10].

The cross section ratios  $\gamma/\pi^0$  from experiments WA70, NA24 and UA6, as a function of  $p_T$  are shown in figure 2. A clear signal is evident. The solid line indicates a QCD theoretical prediction, using next-to-leading log calculations from [2] for direct gamma production and the Lund fragmentation model for high  $p_T$   $\pi^0$  production, with optimised scales and set 1 of Duke-Owens S.F.

The reactions  $p\bar{p} \rightarrow \gamma X$  and  $\pi^- p \rightarrow X$ , in the studied  $X_T$  range, are dominated by annihilation diagrams and may be used to determine  $\Lambda$ , as the used S.F. are well known. The invariant cross section  $E d^3\sigma/dp^3(\pi^- p \rightarrow \gamma X)$  as a function of  $p_T$  and  $X_F$  (from WA70 experiment at Cern Sps) is shown in figure 3. Next-to-leading-log QCD predictions from [2] are shown, using Duke-Owens set 1 (solid line) or set 2 (dashed line) and optimised scales. Similar results from experiment NA24 ( $\pi^- p \rightarrow \gamma X$ ) and UA6 ( $p\bar{p} \rightarrow \gamma X$ ) are shown in figure 4. The resulting ratio Data/QCD predictions, for  $\pi^- p$  interactions in WA70 and NA24 experiments, using DO set 1, is shown in figure 5. The agreement between theory and experiments is quite good. The difference in direct gamma cross sections from incident  $\pi^-$  and  $\pi^+$ , which arises mainly from annihilation diagrams, is shown in figure 6 (WA70). Here the two sets of predictions differ in the assumed value of  $\Lambda$ , where again the value  $\Lambda_{\overline{MS}} = 200 \text{ MeV}$  is preferred.

The QCD Compton graph  $g\bar{g} \rightarrow g\gamma$  dominates the reactions  $\pi^+ p \rightarrow \gamma X$  and  $p\bar{p} \rightarrow \gamma X$  and may be used to extract informations on the shape of the gluon S.F.  $G(x)$ . For  $p\bar{p} \rightarrow \gamma X$ , figure 7 shows the invariant cross section  $E d^3\sigma/dp^3$  as a function of  $p_T$  for the Cern SPS experiments NA3, NA24, WA70 and as a function of  $X_F$  for WA70. Over a fine  $X_F - p_T$  grid, in the framework of next-to-leading-log QCD with optimised scales, WA70 data are compatible with theory using Duke-Owens set 1 (soft glue) :

$$\Lambda = 200 \text{ MeV}/c \quad x \cdot G(x) \simeq (1 + 9x)(1 - x)^6$$

while Duke-Owens set 2 (hard glue) is excluded :

$$\Lambda = 400 \text{ MeV}/c \quad x \cdot G(x) \simeq (1 + 9x)(1 - x)^4$$

These results are confirmed by  $\pi^+ p$  data, shown as ratio Data/prediction versus  $p_T$ , using Duke-Owens set 1 in figure 8 and by the ratio  $\sigma(\pi^+ p \rightarrow \gamma X)/\sigma(p\bar{p} \rightarrow \gamma X)$ , which is not affected by systematic errors in the absolute normalisation, see figure 9.

### 4. Conclusions.

A clear direct  $\gamma$  signal is seen in a large  $X_T$  range from different experiments. All the new results from fixed target experiments on inclusive direct gamma cross sections, as well the ones from  $p\bar{p}$  collider, are in agreement with theory over a wide energy range at a 20 % level, in the framework of next-to-leading-log QCD with optimised scales. A soft glue with  $\Lambda_{\overline{MS}} = 200 \text{ MeV}/c$ , corresponding to Duke-Owens set 1 S.F. [10] seems strongly favoured.

New results may be expected from a detailed analysis of the event structure for direct gammas, that has been made for  $p\bar{p}$  interactions at ISR and is in progress for  $p\bar{p}$ ,  $\pi^\pm p$  interactions at fixed target (WA70) and also from the forthcoming Fermilab experiments (E705, E706), that will cover an  $X_T$  region corresponding to ISR data.

**References**

- [1] T. Ferbel and W.R. Molson, *ReV. Mod. Phys.* **56**, 161(1984)  
J.F. Owens, *ReV. Mod. Phys.* **59**, 465(1987)
- [2] P. Darriulat et al., *Nucl. Phys.* **B110**, 365(1976)
- [3] P. Aurenche et al., *Phys. Lett.* **140B**, 87(1984)  
P. Aurenche et al., *LPTHE Orsay 87/30*  
P. Aurenche et al., *Nucl. Phys.* **B286**, 509(1987)
- [4] P.M. Stevenson, *Phys. ReV.* **D23**, 2916(1981)  
H.D. Politser, *Nucl. Phys.* **B194**, 493(1982)
- [5] J. Badier et al., *Z. Phys.* **C30**, 45(1986)
- [6] L. Bachmann et al., *CERN/SPSC/80-108*(1980)  
M. Bonesini et al., *Nucl. Instr. and Meth.* **A261**, 471(1987)  
M. Bonesini et al., *CERN-EP/87-185*(1987)  
M. Bonesini et al., *CERN-EP/87-222*(1987)
- [7] C. De Marso et al., *Phys. ReV.* **D36**, 16(1987)
- [8] A. Bernasconi et al., *CERN-EP/87-120*(1987)
- [9] J.A. Appel et al., *Phys. Lett.* **B176**, 239(1986)  
P.H. Hansen, proceedings of the EPS Conference, Uppsala, 1987
- [10] D.W. Duke and J.F. Owens, *Phys. ReV.* **D20**, 49(1984)  
J.F. Owens, *Phys. ReV.* **D30**, 943(1984)

EXPERIMENT	$\sqrt{s}$	$X_1$	PHOTON DET.	HADRON MEAS.	METHOD
NA3 $\pi^+C$ $\pi^-C$ pC	19.4	0.3-0.5	scintillator/lead calorimeter+ shower counter	magnet spectrometer, cerenkov	direct CERN SPS
NA24 $\pi^-p$ $\pi^+p$ pp	23.7	0.3-0.6	prop. tube/lead+ scintillator/lead calorimeters	hadron calorimeter	direct CERN SPS
WA70 $\pi^-p$ $\pi^+p$ pp	23.0	0.3-0.6	liquid scintillator/ lead calorimeter	$\Omega$ spectrometer	direct CERN SPS
UA6 $p\bar{p}$ pp	24.3	0.3-0.6	prop. tubes/lead calorimeter	magnet spectr., dE/dx transition radiation	direct CERN SPS
UA1 $p\bar{p}$	630	0.03-0.13	scintillator/lead calorimeter	hadron calorimeter	isol.+longit. samplings CERN $SppS$
UA2 $p\bar{p}$	630	0.03-0.13	prehower+ scint./lead calor.	hadron calorimeter	isolation+ conv.prob. CERN $SppS$
R110 pp	63	0.1-0.35	lead glass+ MWPC	magnet spectrometer	isolation+ cluster shape CERN ISR

Table 1

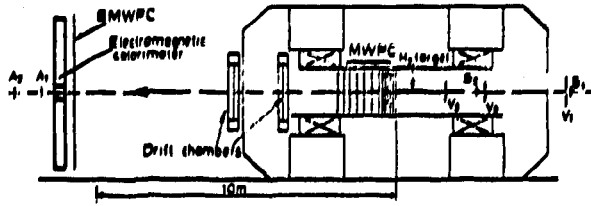


Fig. 1a - WA70 experimental set up

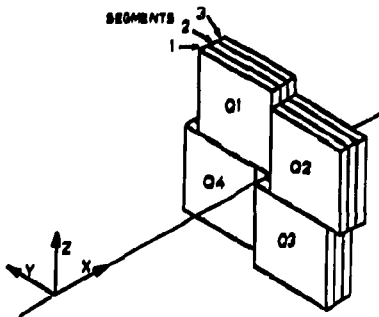


Fig. 1b - WA70 e.m. calorimeter

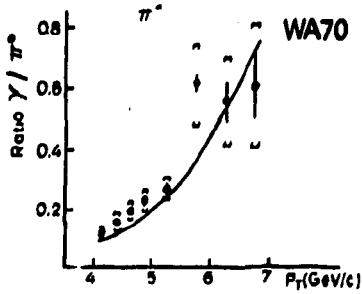
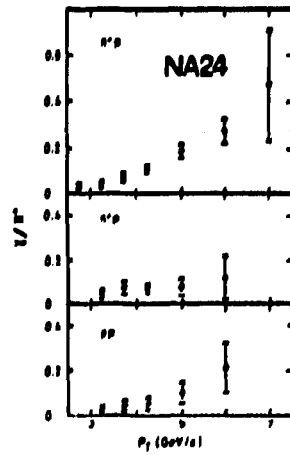
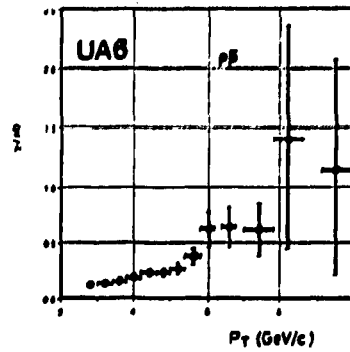


Fig. 2 - Ratio  $\gamma/\pi^0$  vs  $p_T$  with different incident beams



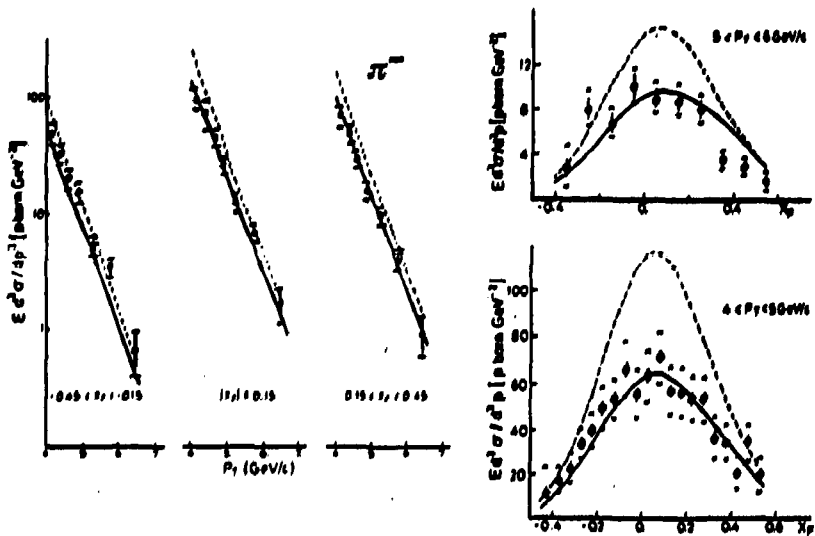


Fig. 3 - Invariant cross section for  $\pi^- p \rightarrow \gamma X$  vs  $p_T$  and  $X_p$  (WA70)

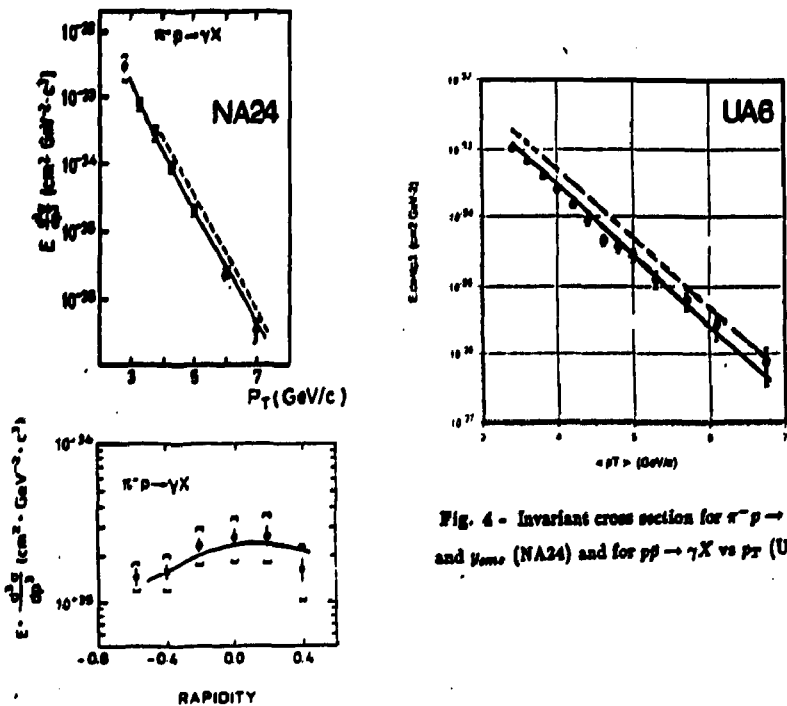


Fig. 4 - Invariant cross section for  $\pi^- p \rightarrow \gamma X$  vs  $p_T$  and  $\eta_{\text{cm}}$  (NA24) and for  $pp \rightarrow \gamma X$  vs  $p_T$  (UA6)



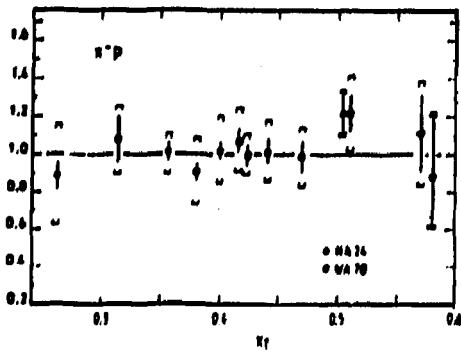


Fig. 5 - K-factor for  $\pi^- p \rightarrow \gamma X_T$  vs  $X_T$

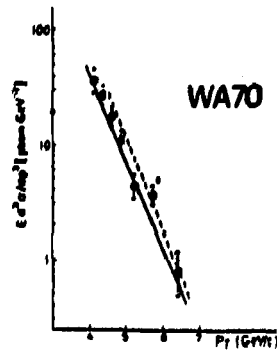


Fig. 6 -  $\sigma(\pi^- p \rightarrow \gamma X) - \sigma(\pi^+ p \rightarrow \gamma X)$  vs  $p_T$

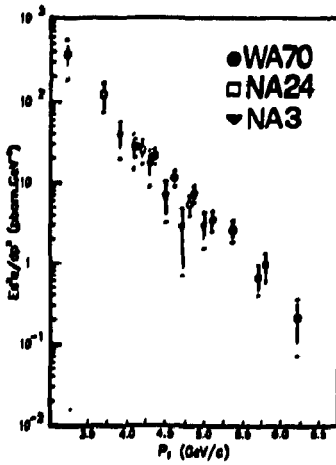


Fig. 7 - Invariant cross section for  $pp \rightarrow \gamma X$  vs  $p_T$  and  $X_T$

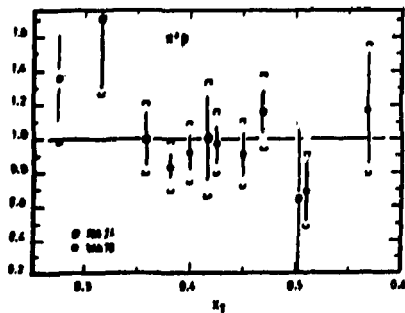
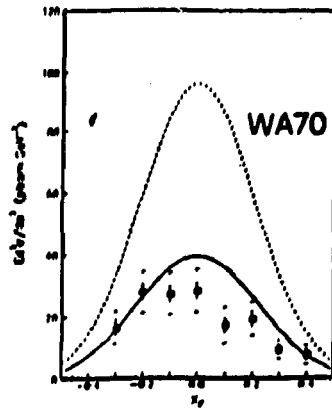


Fig. 9 - K-factor for  $\pi^+ p \rightarrow \gamma X$  vs  $X_T$

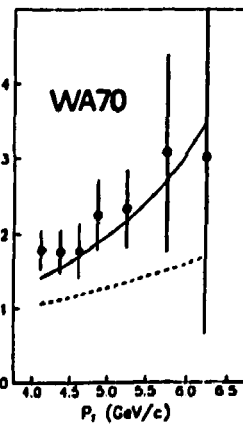


Fig. 10 -  $\sigma(\pi^+ p \rightarrow \gamma X) / \sigma(pp \rightarrow \gamma X)$  vs  $p_T$

## Author Index

- Asman B., 289  
Bagdasaryan D.S., 305  
Bazhanov V.V., 244  
Bender C.M., 40  
Bialas A., \*\*\*  
Bishop R.F., 252  
Blažek M., 257  
Bonesini M., 362  
Campostrini M., \*\*\*  
Chaichian M., 334  
Cronström C., \*\*\*  
Derado I., \*\*\*  
Dittrich J., 247  
Ecker G., 145  
Efimov G.V., 210  
Efremov A.V., 133  
Exner P., 247  
Faber M., 175  
Feilmair W., 175  
Fischer J., 334  
Flynn M.F., 252  
Fodor Z., 202  
Ftáčnik J., 284  
Gorishny S.G., 180  
González R., 350  
Greensite J., 25  
Grimus W., 317  
Haroutunian R., \*\*\*  
Hasenfratz P., \*\*\*  
Ivanov A.N., \*\*\*  
Ivanov M.A., 210  
Kaiser H.J., 239  
Kataev A.L., 180  
Kazaryan G.B., 305  
Kereselidze E.R., 339  
Kolář P., 218  
Krupa D., 299, 310  
Kummer W., 11  
Kundrát V., 310  
Kutschera M., 123  
Lang C.B., 166  
Larin S.A., 180  
Laurson M.L., 171  
Levchenko B.B., 118  
Levin E.M., 95  
Lewin K., 329  
Liparteliani A.G., 339  
Lohmann W., 294  
Lokajíček M., 310  
Lukáč I., 357  
Malecki P., 278  
Markum H., 175  
Meshcheryakov V.A., 299  
Mkrtchyan H.G., 305  
Mobius P., 342  
Motz G.B., 329  
Muller-Preussker M., 171  
Nagy M., 235  
Neufeld H., 324  
Nikolaev N.N., \*\*\*  
Pauli H.-C., \*\*\*  
Pavlenko O., \*\*\*  
Perez-Rojas H., 350  
Perlt H., \*\*\*  
Petrov V.K., 158  
Pišút J., 70  
Pišútová N., 70  
Plumer M., 272

Raha S., 272  
Ramello L., 60  
Ryskin M.G., 95  
Salmhofer M., 166  
Scharnhorst K., 239  
Schepkin M., 223  
Schöberl F., 192  
Schmakov S.Yu., 85  
Surovtsev Yu.S. 299  
Šzwed J., \*\*\*  
Šimák V., 264  
Šumbera M., 264  
Tripiccione G., \*\*\*

Troshenkova I.A., 305  
Turbiner A.V., 51  
Turko L., 198  
Uzhinskii V.V., 85  
Volkov G.G., 339  
Volkov M.K., 235  
Weiner R.M., 272  
Wieczorek E., 239  
Wosiek J., \*\*\*  
Závada P., \*\*\*  
Zborovský I., 264  
Zinoviev G.M., 158  
Znojil M., 252

\*\*\* Oral presentation only.

## List of Participants

### AUSTRIA

G.Ecker, Vienna  
M.Faber, Vienna  
W.Feilmair, Vienna  
W.Grimus, Vienna  
W.Kummer, Vienna  
H.Neufeld, Vienna  
M.Pilch, Graz  
M.Salmhofer, Graz  
F.Schöberl, Vienna

### CUBA

H.C.Pérez-Rojas, Habana

### FINLAND

C.Cronström, Helsinki

### FRANCE

C.Charlot, Palaiseau  
R.Haroutunian, Villeurbanne

### FRG

I.Derado, Munich  
H.-C.Pauli, Heidelberg  
M.Plümer, Marburg

### GDR

B.Jozefíni, Berlin  
H.-J.Kaiser, Zeuthen  
W.Lohmann, Zeuthen  
P.Möbius, Dresden  
G.Motz, Berlin  
M.Müller-Preussker, Berlin  
H.Perlt, Leipzig

### HUNGARY

Z.Fodor, Budapest

### ITALY

M.Bonesini, Milan  
M.Campostrini, Pisa  
L.Ramello, Turin  
R.Tripiccione, Pisa

### POLAND

A.Bialas, Cracow  
E.Bialas, Cracow  
P.Górnicki, Warsaw  
A.Kotański, Cracow  
M.Kutschera, Cracow  
P.Malecki, Cracow  
J.Szwed, Cracow  
L.Turko, Wroclaw  
J.Wosiek, Cracow

### SWEDEN

B.Åsman, Stockholm

### SWITZERLAND

P.Hasenfratz, Bern

### USA

C.M.Bender, St. Louis  
J.Greensite, S. Francisco

USSR

V.V.Bazhanov, Serpukhov  
A.V.Efremov, Dubna  
A.N.Ivanov, Leningrad  
M.A.Ivanov, Dubna  
A.L.Kataev, Moscow  
B.B.Levchenko, Moscow  
E.M.Levin, Leningrad  
H.G.Mkrtchyan, Yerevan  
N.N.Nikolaev, Moscow  
O.Pavlenko, Kiev  
V.K.Petrov, Kiev  
M.Schepkin, Moscow  
S.Schmakov, Dubna  
A.V.Turbiner, Moscow  
G.G.Volkov, Serpukhov

G.Martinská, Košice  
M.Mojžiš, Bratislava  
M.Nagy, Bratislava  
M.Noga, Bratislava  
A.Nogová, Bratislava  
I.Novák, Bratislava  
Š.Olejník, Bratislava  
J.Pišút, Bratislava  
N.Pišútová, Bratislava  
P.Prešnajder, Bratislava  
V.Šimák, Prague  
E.Truhlík, Řež  
P.Závada, Prague  
M.Znojil, Řež

CZECHOSLOVAKIA

M.Bednař, Prague  
M.Blažek, Bratislava  
T.Blažek, Bratislava  
J.Boháčik, Bratislava  
V.Bužek, Bratislava  
V.Černý, Bratislava  
J.Dittrich, Řež  
A.Z.Dubničková, Bratislava  
J.Fischer, Prague  
J.Ftáčnik, Bratislava  
L.Hlavatý, Prague  
J.Hošek, Řež  
P.Kolář, Prague  
A.Košinárová, Bratislava  
D.Krupa, Bratislava  
V.Kundrát, Prague  
R.Lietava, Bratislava  
P.Lichard, Bratislava  
I.Lukáč, Bratislava

# **Hadron Structure '87**

**Proceedings  
of the Conference  
Smolenice  
November 16—20, 1987**

**Physics and  
Applications  
Vol. 14**

**Editori: D. Krupa  
Zodpovedný redaktor: S. Luby**

**Vydal: Fyzikálny ústav CEFV SAV, 842 28 Bratislava**

**Formát: B/5**

**Náklad: 400 výtlačkov**

**Počet strán: 376**

**Vytlačilo: Malotirážne stredisko VEDY,  
vydavateľstva Slovenskej akadémie vied  
v Bratislave.**

**Do tlače schválené Edičnou radou SAV, č.88/87  
zo dňa 6.X.1987**

**In the series Physics and Applications  
the Proceedings of the following con-  
ferences have been published:**

**Vol. 1. Hadron Interactions at Low  
Energies, Smolenice 1973  
Edited by D. Krupa and J. Pišút**

**Vol. 2. High Energy Particle Interactions,  
Smolenice 1975  
Edited by D. Krupa and J. Pišút**

**Vol. 3. Hadron Constituents and  
Symmetries, Smolenice 1976  
Edited by J. Lánik and M. Noga**

**Vol. 4. Hadron Structure as Known from  
Electromagnetic and Strong Interactions,  
High Tatras 1977  
Edited by S. Dubnička**

**Vol. 5. Amorphous Metallic Materials,  
Smolenice 1978  
Edited by P. Duhaj and P. Mraško**

**Vol. 6. Neutron Induced Reactions,  
Smolenice 1979  
Edited by I. Ribanský and E. Běták**

**Vol. 7. Quantum Chromodynamics,  
Smolenice 1980  
Edited by A. Nogová**

**Vol. 8. Low Radioactivities,  
High Tatras 1980  
Edited by P. Povinec and J. Krištiak**

**Vol. 9. Transport Properties of Solids,  
Smolenice 1981  
Edited by E. Majková and E. Mariani**

**Vol. 10. Neutron Induced Reactions,  
Smolenice 1982  
Edited by P. Obložinský**

**Vol. 11. Physics at Secondary School,  
Račková dolina 1983  
Edited by A. Nogová and J. Pišút**

**Vol. 12. Hadron Structure '83,  
Smolenice 1983  
Edited by I. Lukáč**

**Vol. 13. Low-Level Counting and  
Spectrometry, Bratislava, 1985  
Edited by P. Povinec**